Polymeric Materials for Electronics Packaging and Interconnection

John H. Lupinski, EDITOR
General Electric Company

Robert S. Moore, EDITOR
Eastman Kodak Company

ACS Symposium Series

M. Joan Comstock, *Series Editor*

1989 ACS Books Advisory Board

Foreword

The ACS SYMPOSIUM SERIES was founded in 1974 to provide a
medium for publishing symposia quickly in book form. The
format of the Series parallels that of the continuing ADVANCES
IN CHEMISTRY SERIES except that, in order to save time, the
papers are not typeset but are reproduced as they are submitted
by the authors in camera-ready form. Papers are reviewed under
the supervision of the Editors with the assistance of the Series
Advisory Board and are selected to maintain the integrity of the
symposia; however, verbatim reproductions of previously pub-
lished papers are not accepted. Both reviews and reports of
research are acceptable, because symposia may embrace both
types of presentation.

Preface

POLYMERS PLAY AN INCREASINGLY IMPORTANT ROLE in the construction of integrated circuitry (IC) and electronic devices. Future trends in electronics include continuing efforts toward further miniaturization and the manufacture of ever more complex structures. These trends require exceptional materials that are relatively easy to process. Polymers do have an advantage over ceramics and other inorganic materials because of easier processing conditions.

Advanced polymeric materials and methods of polymer processing are clearly necessary for advanced ICs and electronic devices. The versatility of organic chemistry and polymer chemistry provides for an almost unlimited number of variations in polymer structure, thus allowing the preparation of polymer compositions that are tailor-made for particular applications. *Polymeric Materials for Electronics Packaging and Interconnection* covers many aspects relating to the development of novel polymeric materials and processes. Included, for instance, are the preparation of polymer compositions, determination of their physical and chemical properties, and testing of their performance in actual devices. The emphasis is on chemistry and materials science rather than circuitry, its electrical capabilities, or its design characteristics. Efforts have been made to correlate the chemical structure of polymers with their performance in devices under widely varying conditions.

JOHN H. LUPINSKI
General Electric Company
Corporate Research and Development Center
Schenectady, NY 12301

ROBERT S. MOORE
Eastman Kodak Company
Research Laboratories–82
Rochester, NY 14650–2104

May 6, 1989

Chapter 1

Polymeric Materials for Electronics Packaging and Interconnection

An Overview

John H. Lupinski[1] and Robert S. Moore[2]

[1]General Electric Company, Corporate Research and Development Center, Schenectady, NY 12301
[2]Eastman Kodak Company, Research Laboratories–82, Rochester, NY 14650–2104

An overview of the driving forces for the increased importance of packaging and interconnection to progress in electronics is presented, with emphasis on the influence and importance of the role of polymers. Relevant information on market values for components is included, where appropriate. In addition, trends in interconnection and packaging, their combined role, and their market size are discussed. Examples are given in which plastic packaging can lead to substantial reductions in packaged IC cost. An extensive overview of polymer applications is presented, with special emphasis on thin films, protective gels, rigid encapsulants, and printed wiring board materials and processes. The chapter also indicates why the symposium and the book are timely and important, especially for those interested in the chemical aspects of these materials.

From a number of standpoints, progress in electronics is becoming critically dependent on electronic packaging and interconnection. The ability to achieve fast clock rates, sufficient heat dissipation, uniform and appropriate electrical impedance, and high reliability and performance of packages, to name a few, are key requirements for which interconnection and packaging play increasingly important roles. In fact, it is projected that by 1995 the value added by packaging and interconnection will exceed that of the integrated circuit chips themselves in many more applications than occurs even today (1).

Although a number of organizations and symposia have dealt with packaging, and to some extent with polymers, virtually none have emphasized the synthetic and physical chemistry aspects of these systems. For those reasons, we felt it was especially

important to address the role of polymers in electronic packaging and interconnection.

The symposium and this book have enabled us to assemble the results of research by experts in polyimides and related materials, polymeric encapsulants, gels, and printed wiring board (PWB) substrates, with emphasis on the chemical aspects of these materials.

The market for polymeric and polymer-related materials is significant and is expanding. For example, Rose Associates estimates the 1988 worldwide market just for encapsulation resins at $412M (156M pounds), with projected growth to $616M (236M pounds) by 1990 (2).

Polymer Characteristics

Polymers have unique versatility for many packaging applications in that their mechanical properties can be tailored, giving materials ranging from rubber-like gels with dramatic changes in modulus with temperature, to hard solids with almost no changes at all. Moreover, electrical properties can be varied to achieve, within limits, desired values of dielectric constant, low ionic conductivity, etc. Key concerns today often center on the ability to achieve simultaneously the desired mechanical and electrical properties, a difficult task. The ability to tailor the coefficient of thermal expansion, CTE (also often abbreviated TCE) to match that of the substrate or of other components is a subject of considerable interest.

Trends in Interconnection and Packaging

The earliest kinds of interconnection involved solder joints; later, wire bonding and dual in-line (DIP) phenolic-molded packages were developed. In fact, the DIP continues to be the most commonly used package. In a DIP (see Figure 1) the IC chip (shown here encapsulated) is connected by wire bonding to the two rows of package leads which are then inserted in holes in the PWB for subsequent soldering. The lead spacing, being 100 mils, limits the DIP's effective use to devices 64 leads or less. In a DIP, most IC's are encased in plastic, but ceramic materials are also available.

Figure 1 also shows the small outline IC package (SOIC), which was developed to reduce package size. This package has leads on 50 mil centers, and hence is about one-half the size of the DIP. The SOIC is available with "J-lead" and "gull wing" leads for surface mounting (see below).

The need for accommodating a higher number of leads resulted in development of chip carriers with contact pads on four sides. The example shown in Figure 2 is leadless, but several lead formats, including the gull wing and J-lead configurations shown in Figure 3, are available. The chip carrier is designed for mounting on the board surface rather than for through-hole mounting (see below). Chip carriers are available in premolded or postmolded
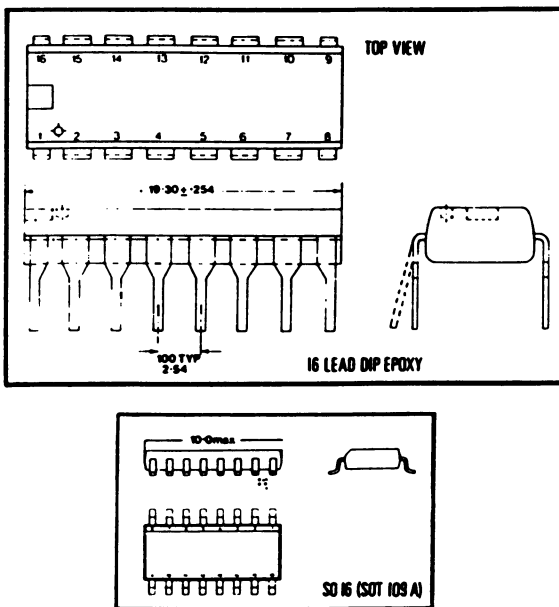
Figure 1. Example of current IC packages. (Reproduced with permission from Ref. 4. Copyright 1988 BPA [Technology and Management, Ltd.].)
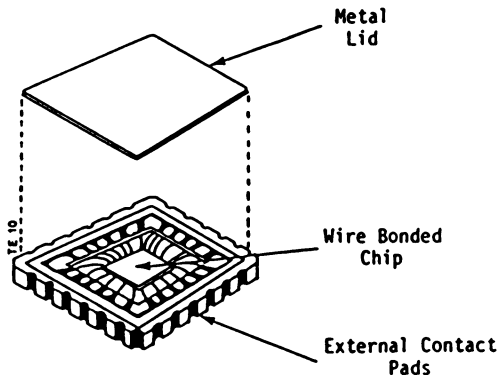

Figure 2. Conventional chip carrier. This example with a lid is for hermetic applications. (Reproduced with permission from Ref. 4. Copyright 1988 BPA [Technology and Management, Ltd.].)

plastic versions, e.g., the plastic, leaded chip carrier. Chip carriers are also available in ceramic versions for hermetic applications.

Figure 4 shows an example of a pin grid array (PGA), developed to accommodate IC's with 84 or more pins. The original PGA's were ceramic packages, but several techniques are now used to produce them in plastic. The PGA's can be through-hole mounted on the printed wiring board, or can be socketed and surface mounted.

All of the historic techniques, methods, and packages are still in use. More recent technology includes a variety of IC packages, both polymeric and ceramic, for housing IC chips, and the use of tape automated bonding (TAB) technology to gang bond an inner set of leads to an IC (and subsequently the outer set of leads to the next level of interconnection). Figure 5 shows an example of TAB technology in which an IC chip has been gang bonded to the TAB inner leads. Subsequently, the etched fingers are excised from the TAB tape to form the outer leads, which are then bonded to pads on the substrate. The TAB tape often uses a polymeric layer to support the leads.

In general, through-hole mounting is giving way to components mounted and interconnected on the PWB surface (surface-mounted components) due to lower cost and closer spacing of components, etc. Other trends include direct encapsulation of IC's with silicone, epoxy, and other encapsulants and gels. A more detailed discussion of the various package types is beyond the scope of this chapter. Further information can be found in a number of references (1,3-6), and in trade journals such as Semiconductor International or Solid State Technology.

The hierarchy of interconnection is typically as follows: Zero level--interconnection of elements on the IC chip itself. This level of interconnection is intrinsically part of the chip design. First level--connection of the IC chip to the next-higher level, usually an IC package, either by wire bonding or, more recently, by TAB.

Second level--connection of the IC package to the printed circuit board. A key alternate route is direct mounting of the chip on the board, saving one level of interconnection. The chips are protected by the use of gel ("blob top") coatings of polymeric encapsulants applied directly to the IC chip.

The succeeding third and higher levels involve connection of boards to subsystems or mother boards and, finally, to the system and its power outlets, etc.

Multi-chip modules, in which chips are attached with TAB directly to an interconnection substrate, typically silicon or aluminum nitride or other ceramics, represent an emerging technology. The module interconnect circuits are generated with IC fabrication technology, but at a relatively modest level of resolution. Typically, as shown in Figure 6, the substrates can include power and ground planes plus one or more signal planes, and low dielectric constant interlayer materials such as polyimides. These modules, which have feature sizes ca. 5 to 50 μm, and which are mounted directly on the PC board or serve as the board itself,
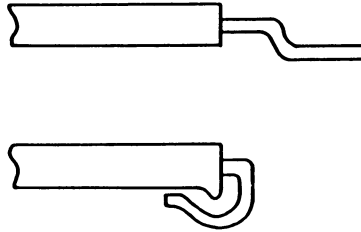
Figure 3. Details of two types of leads for leaded chip carriers: gull wing, above; J-lead, below. (Reproduced with permission from Ref. 4. Copyright 1988 BPA [Technology and Management, Ltd.].)

Top View   Bottom View   End View

Thick Film
Multilayer
Interconnection from
Chip Pad to Pins
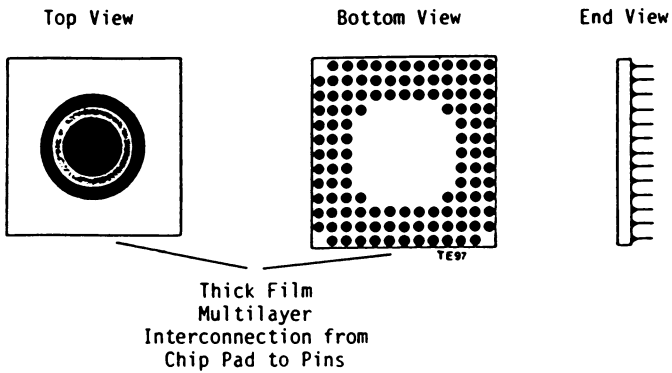
Figure 4. Pin grid array. (Reproduced with permission from Ref. 4. Copyright 1988 BPA [Technology and Management, Ltd.].)
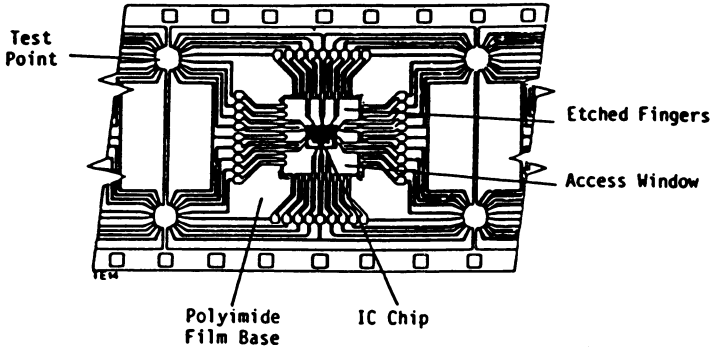
Figure 5. Tape   automated   bonding   system.   (Reproduced   with
permission   from   Ref.   4.   Copyright   1988   BPA
[Technology and Management, Ltd.].)

**Typical Thin Film Multilayer
Package Structure**
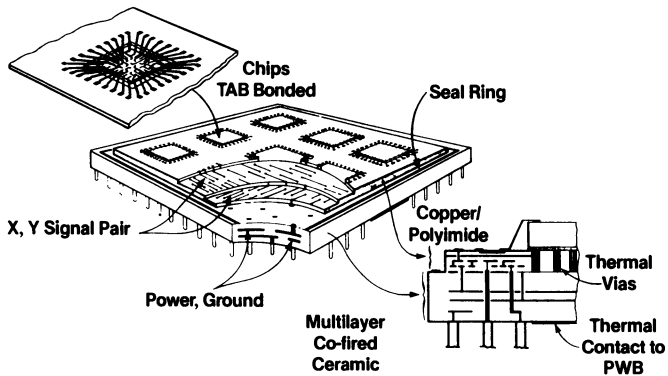
Figure 6. Multichip module system.   (Courtesy of Honeywell, Inc.)

are coming into rapid use. In fact, a market of $6B ($6 x 10^9) by 1995 is projected for the substrate and its interconnection (3).

Polymeric substrate materials in use include highly filled phenolic and epoxy resins for rigid printed circuit boards, polyimides and polyesters for circuit substrates as well as for more general applications, special foamed poly(tetrafluoroethylene) polymers and copolymers, foamed composite materials of the latter, special epoxy fiberglass composites, and polyimide support layers for TAB. In addition, epoxies and silicone polymers are used increasingly in applications as encapsulants, as humidity and environmental barriers within packages, and as packaging materials themselves.

The magnitude of the applications for polymeric substrates has been estimated (in tons) for 1987 on a worldwide basis as: phenolic resin, 78K; epoxy resin, 130K; polyester fiber, 1,010; polyimide film, 235; molding compounds, 330; polymers for high-frequency applications, 300; and high-temperature polymers, 1,440 (4).

Driving Forces. The driving forces in electronic packaging and interconnection today are cost, performance, and physical space limitations. Over time, performance demands are causing dramatic increases in the number of functions or components on a chip, resulting in significant increases in the number of leads per chip as shown in Figures 7 and 8. In fact, for many years the number of functions per chip has doubled every one to two years. Figure 8 also shows that the average pin count per IC has tended to increase more rapidly for in-house manufacturers than for merchant suppliers.

However, these average values can, in fact, be misleading for two reasons: First, as shown in Figure 9, the number of I/O pins (or leads) per chip varies significantly depending on the device type and/or device complexity. With the present increase of 25 percent per year for gates for gate arrays, some sources estimate that the number of leads per chip for gate arrays will exceed 200 by 1992. Second, the average value is misleading because it is heavily weighted by the very large number of low-lead count devices (16 to 18 leads). In fact, estimates by BPA (Technology and Management, Ltd.) (5) suggest that by 1995 of all leads (about 3.9T [3.9 x 10^{12}] total leads worldwide), 50 percent will originate on chips with over 60 leads, and 25 percent will originate on chips with over 100 leads, a most interesting forecast. Thus, a very large number of the interconnections will originate on high-lead count devices.

To achieve compact design in order to meet speed requirements (especially at high-lead count), fine spacing of leads, e.g., 2-mil wide leads on 4-mil centers, or less will be required. The delicate nature of such leads and their close spacing will impose severe constraints on the amount of allowable thermally induced stress (or strain) generated by an encapsulant or by a package due to differences in the TCE. Similarly, substrates will need to maintain dimensional stability, dielectric constant values, planarity, etc., to much finer tolerances than in the past.

IC DENSITY TRENDS
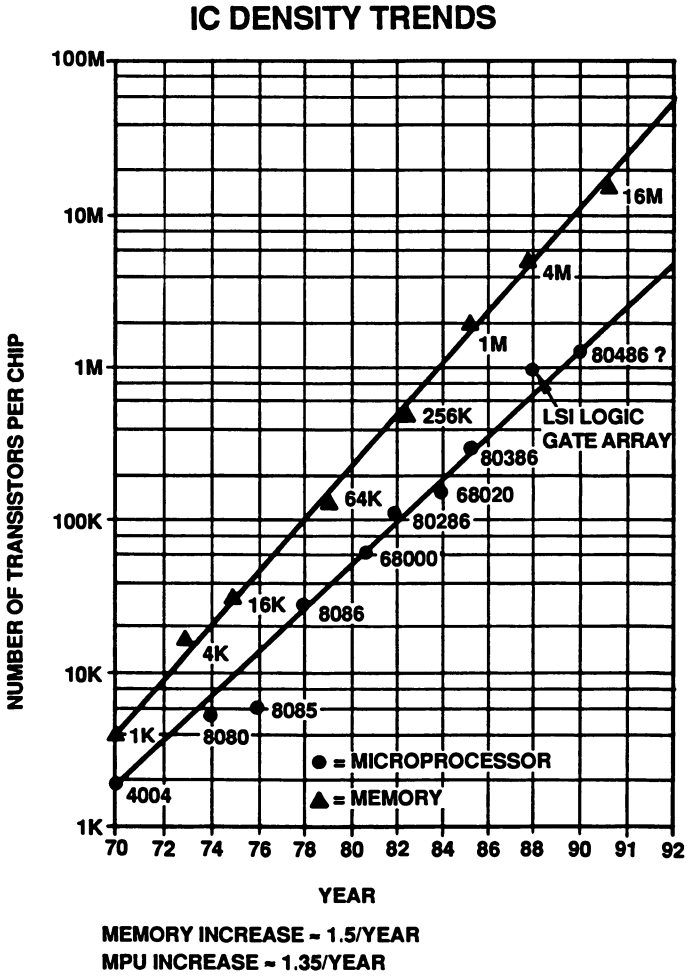
Figure 7. Number of transistors per chip. The memory size in bits is given for each memory chip data point. The chip model number is designated for each microprocessor chip data point. (Reproduced with permission from ref. 50. Copyright 1989 Integrated Circuit Engineering Corporation.)
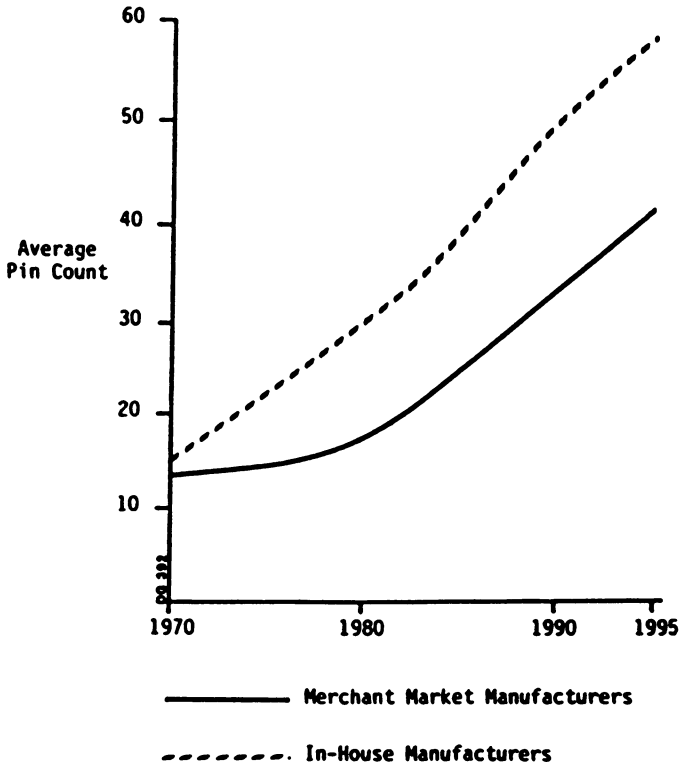
Figure 8. Number of leads per IC. (Reproduced with permission from Ref. 1. Copyright 1986 BPA [Technology and Management, Ltd.].)
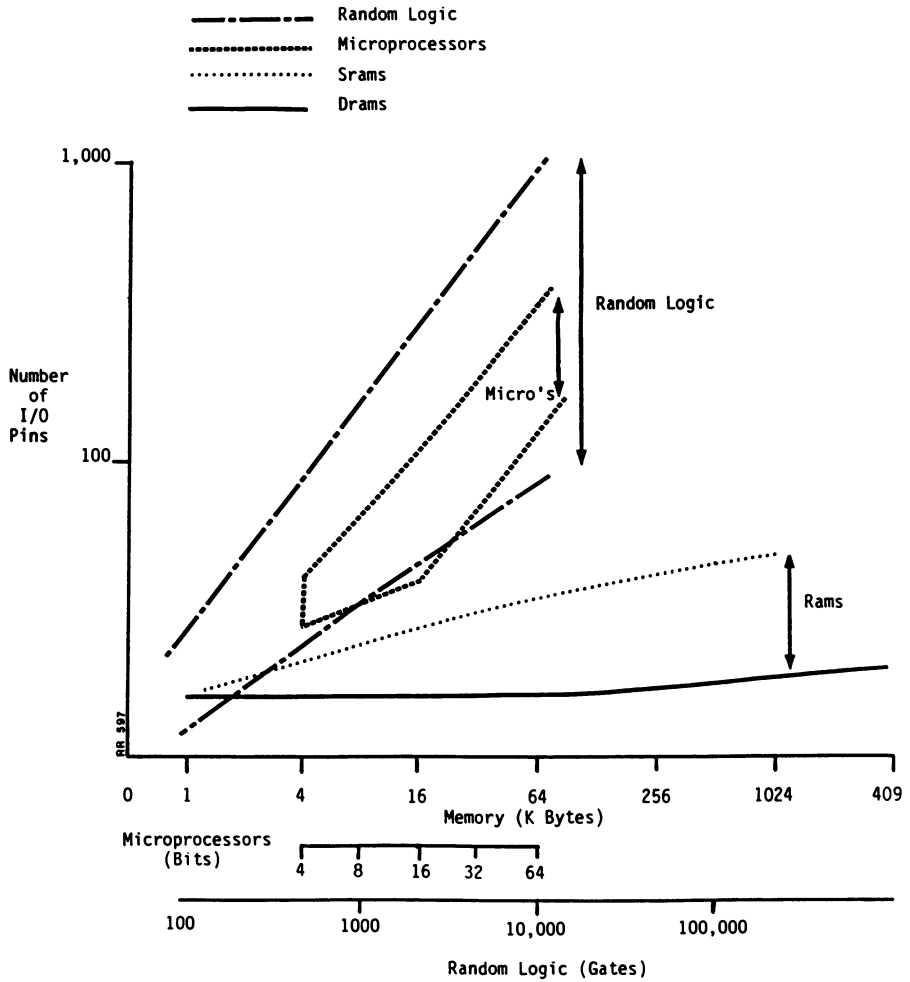
Figure 9. Digital circuit pin out increase with IC complexity.
(Reproduced with permission from Ref. 1. Copyright 1986
BPA [Technology and Management, Ltd.].)

Roles of Packaging and Interconnection

The general functions of packaging and interconnection are to transform basic electronic elements into optimized hardware systems that are manufacturable, functional, and reliable. It is a challenge, of course, to achieve these goals without a decrease in overall system performance. The process includes assembly at each step, as well as design, manufacture, and performance characterization of the package (6). In particular, packaging (and interconnection) provides mechanical and environmental protection, electrical interconnection and, in principle, proper heat dissipation. More details on this subject are beyond the scope of this chapter, but are available through a number of sources, such as the National Technical University Course in Basic Electronic Packaging Engineering (6).

Market Projections for Packaging and Interconnection

Market projections for packaging and interconnection can be put in perspective by looking first at the size and growth trends for electronic equipment in general. In 1987 the electronic equipment market on a worldwide basis, including the non-free-world market, (7) was about $613B (current dollars, forecasted exchange rates). It is projected (7) to grow to over $1T by 1992. In the U.S., the current (1987) market (7) of about $210B is becoming a significant part of the $3.8T GNP and, thus, is influenced by national and international economic factors. For reference, according to ElectroniCast Corp. (8), 1987 U.S. production of non-IC components (relays, switches, connectors and sockets, capacitors, resistors, and printed circuits) totaled about $12B. In comparison, IC's (digital plus linear), including the package, totaled about $11B (Jardine, L. J., ElectroniCast Corp., personal communication, 1988).
 The predominant market segment for electronic equipment on a worldwide value basis (1986) is computers, followed by products for government/military markets, then industrial/instrument, communications, and consumer sectors. In the U.S. the trend is similar, although the consumer market is a lower percentage (9).
 For digital IC's in the U.S., the predominant driving force in terms of IC value is clearly computers, followed by communications (Jardine, L. J., ElectroniCast Corp., personal communication, 1988). While military applications in the U.S. drive specific aspects of the technology, they are a small part of the overall digital IC usage.
 A typical classification of package types by units and value is given in Table I on a worldwide basis (2). Note that plastic dual in-line packages (PDIP) account for the majority of the market, followed by ceramic DIP, small outline IC (SOIC) packages, and plastic, leaded chip carriers (PLCC). It should also be noted, however, that the percent of PDIP units (which are inserted through the circuit board) will decline over time, reflecting the concerted move to surface-mount technology and its associated packaging.

Table I.   Worldwide   IC   leadframe   forecast

(Plated Values)

		1987	1988	1989	1990	1991
PDIP	B Units	24.6	25.3	26.1	26.9	27.7
	M $	482	490	475	457	443
CERDIP	B Units	1.7	1.8	1.8	1.9	1.9
	M $	40	42	43	44	45
SOIC	B Units	2.2	5.9	10.3	13.9	16.0
	M $	30	82	150	208	240
PLCC	B Units	0.6	1.6	3.2	4.4	5.0
	M $	10	28	58	84	95
Total IC Frames	B Units	31.5	34.6	41.4	47.1	50.6
	M $	562	642	726	793	823
Total All Frames	B Units	62.5	68.6	77.4	86.1	93.6
	M $	772	865	962	1039	1078

Source: Reproduced with permission from ref. 2.
Copyright 1988 Rose Associates.

The value of the U.S. printed wiring board market is estimated at \$4.4B to \$4.7B for 1987; growth is projected at 17.5 percent for 1988. Laminates used to produce these boards had a value of about \$840M to \$890M (including about \$130M to \$140M of "prepreg" [resin-impregnated woven glass, cloth, or paper]) (10, 11).

The value of finished flexible circuits in the U.S. was about \$350M (10) to \$400M (12) in 1987, the world market being about \$1B, with Japan accounting for about \$400M, according to William Jacobi & Associates (12). Laminates for flex circuits in the U.S. for 1987 were about 77 percent polyimide on a value basis, but 48 percent on an area basis (compared to 52 percent for polyester) (13). These ratios are atypical of worldwide usage, the values there for polyimide being 59 percent and 27 percent, respectively (13). Clearly, the latter probably reflects low-cost consumer applications, whereas (12) the U.S. market is about 50 percent military applications. In 1988, the U.S. market was expected to grow about 20 percent (12).

The worldwide market value for gels and encapsulants, although considerably smaller than even the flex circuit market value, is increasing in importance. As noted earlier (2), encapsulants are expected to grow on a worldwide basis from \$412M (1987) to reach \$616M in 1990.

Cost Savings with Polymers

As one example in the value-added chain, it is clear that a significant cost saving can be obtained if ceramic packages can be replaced by plastic packages, and/or if protective encapsulants can be used directly on the IC chip, especially at high lead counts. Sharenow, for example, has estimated (14) for IC devices for which device size is bond-pad limited, that for 300-lead devices, the packaged device cost can be reduced from \$120 (ceramic pin grid array [PGA], hermetic seal, wire bonded, 6-mil pad centers) to \$95 (TAB bonded, 5-mil pad centers) to \$64 (TAB bonded, 4-mil pad centers) to \$30 (encapsulated, nonhermetic, TAB bonded, chip on board, 4-mil pad centers). At 150 leads, he estimated that packaged IC device cost can be reduced from \$27 (ceramic PGA, hermetic, wire bonded, 7-mil pad centers) to \$16 (plastic pin grid array, nonhermetic, wire bonded, 7-mil centers) to \$8.70 (plastic quad flat pack [PQFP] nonhermetic, wire bonded, 7-mil pad centers) to \$7.47 (PQFP, nonhermetic, TAB bonded, 4-mil centers) to \$5.00 (encapsulated, nonhermetic, TAB bonded, chip on board, 4-mil pad centers).

Note that packaging and interconnection can be an appreciable fraction of the total packaged IC cost, and that the package technology can strongly influence yielded IC cost through the ability to space leads on a finer pitch, which results in both an IC of smaller total size and a higher number of good die per wafer.

Future Directions

Trends in overall technology are toward IC's that are faster, that
have higher lead counts, and that consume more power. These trends
require more demanding tolerances for uniformity of impedance.   In
turn, these factors are leading to the connection of chips with
multi-chip modules, increased use of TAB, highly specialized
substrates tailored to the customer's needs, customized packages,
and three-dimensional molded interconnects. Such trends will lead
to the creation of additional value added in the packaging and
interconnection areas.   This will enhance the opportunity to
introduce new polymer materials with special attributes on a
custom-design basis, with functions and performance being key
considerations as opposed to price alone.

General Technical Comments

Application of polymers in electronic devices requires development
of specially designed materials and techniques for their
manipulation and processing. Because little can be borrowed from
existing   processing   techniques   for   inorganic   semiconductor
materials, the applications of polymers in electronic devices are
going through their own developmental phases.
     Polymers   are   seldom   pure,   single,   component   systems.
Typically, there is a range of molecular weights, and there may be
differences in the way the monomer units are linked together in a
polymer chain.   In some cases there are head-to-head as well as
head-to-tail bonds between monomeric units within the same polymer
chain, and there may be branching. Since polymer properties are
also dependent on thermal history, moisture content, and end
groups, a methodology had to be developed to obtain reliable and
reproducible test results even in the light of the many variations
normally found in "pure" polymers. For instance, a lot of time had
to be devoted to learning how to obtain reproducible results when
measuring electrical properties of polymers (Senturia, S. D.,
Massachusetts   Institute   of   Technology,   personal   communication,
1988).   This book presents an overview of current progress in many
of these areas, and references are also made to pertinent related
work published elsewhere (e.g., 15,16).
     The use of polymers in electronics can be grouped into four
categories:

     1. Thin films
     2. Protective gels
     3. Rigid bulk encapsulants
     4. Printed circuit board materials

     Typically, polyimides play a dominant role in thin film
applications, while silicones are selected almost exclusively for
soft gel applications.   Epoxies are used in the majority of
encapsulant   and   printed   circuit   board   applications.   Each

application has its own set of specific requirements, and a multidisciplinary approach is needed to solve all the problems.

Most applications of polymers in electronic packaging have a number of common requirements. Most pervasive is the moisture issue, but other important requirements are low dielectric constant, low dielectric losses (dissipation factor), and good adhesion to various substrates and metallizations. With the exception of the gels, generally high glass transition temperatures are preferred, and matching the coefficients of thermal expansion of the polymers with those of the inorganic materials of the circuitry appears to be a never ending challenge. Equally important is long-term chemical stability over widely varying temperatures and humidity conditions. Various aspects of these issues will be given in this introductory chapter.

Moisture

It is well known that in the presence of moisture, ionic impurities, and electric fields, the delicate integrated circuitry is very vulnerable to corrosion. Since no polymer is impermeable to moisture, it is impossible to completely exclude moisture from the packaged device.

It is most important to minimize the ionic impurity levels since cations interfere with the electrical performance of the devices, and anions, such as chloride and bromide, act as catalysts in the promotion of corrosion under the influence of moisture. The disastrous effects are reached by the following events. Metal surfaces such as aluminum are always covered with a thin, native protective oxide layer. However, under device operating conditions, that is, in the presence of moisture, chloride ion contaminants, and electric fields, the chloride ions are able to penetrate through the oxide layer and attack the aluminum metal, forming aluminum chloride compounds. These compounds hydrolyze to give hydroxides and to regenerate mobile chloride ions, which will start another corrosive attack on the remaining aluminum. Bromide ions function in the same manner. Thus, the corrosion of aluminum is largely determined by the availability of moisture. Given the permeability of most polymers, an almost unlimited amount of moisture will be available. Corrosion of the Al will continue until large parts of the metallic conductors have been converted to nonconducting corrosion products, and the device will fail because of open electrical connections. The chemistry of aluminum corrosion is very complex and will not be described in detail in this chapter. However, the reader may consult some selected literature references (17–22).

For good protection of delicate circuitry against the influence of moisture, polymers with the following characteristics are needed: low ionic impurity content, low moisture absorption, and good adhesion to substrates.

Dielectric Properties

The dielectric constants of polymers are strongly influenced by
their chemical structure. Generally, molecules with more polar
groups have higher dielectric constants. Polymers with very low
dielectric constants (<3) such as polyethylene and polytetrafluoro-
ethylene, do not always meet the combined thermal and mechanical
requirements for application in electronic devices, nor do they
have desirable adhesive characteristics. Polyimides with much
better thermal and mechanical properties have dielectric constants
between 3 and 4. Efforts to combine the desirable features of the
fluoro polymers with those of the polyimides have been successful
in that the resulting compositions have dielectric constants equal
to or smaller than 3 without sacrificing too much of the thermal
and mechanical properties of the polyimides (23).
    Generally, polymer films are good electrical insulators.
However, low concentrations of mobile, electrically charged species
such as ions may be present and give rise to some degree of
electrical conductivity, especially in the presence of moisture and
under the influence of electric fields.
    While polymers are very good electrical insulators in direct
current situations, dielectric losses occur under the influence of
alternating current conditions. This is caused by the fact that
molecular dipoles will align themselves with the alternating
electric field, thus absorbing energy from the electric field. At
temperatures below the glass transition temperature, T_g, where
the polymer matrices are rigid, the interactions between the
dipoles and the external field are limited. However, at higher
temperatures, increased molecular motions facilitate the
interaction between dipoles and the external field, thus absorbing
more energy. In the extreme, this leads to a thermal runaway where
the rising temperature of the sample facilitates additional energy
absorption from the field, causing a further rise in temperature,
and so on. At temperatures near the T_g, steep increases in
dielectric losses occur.

Thermal Properties

Another parameter which changes drastically at or near the T_g is
the coefficient of thermal expansion (CTE). Typically, the CTE of
a polymer above its T_g is about three to four times as large as
it is below its T_g. At low temperatures, CTE's of unfilled
polymers are in the $5.0-9.0 \times 10^{-5}/°C$ range, filled epoxies are
approximately $2.0 \times 10^{-5}/°C$, and a material such as Si has a CTE
of about $2.5 \times 10^{-6}/°C$. Clearly, upon thermal cycling, a large
discrepancy in CTE's of the materials in a packaged device will
lead either to delamination (when the adhesion between the various
components is weak) or to stresses on the device (when the adhesion
between components is strong). The stresses may deform or crack a
device. Another undesirable situation resulting from CTE mismatch
occurs when two conductor layers are separated by a dielectric
(polymer) interlayer. Usually, such conductor layers are

electrically connected through metallized holes, or via's, through
the dielectric layer. If expansion causes the thickness of the
dielectric layer to exceed the length of the via, there is a risk
of breaking the electrical connections between the layers of
circuitry in the via, thus rendering the device inoperative.
Relatively low CTE's have been realized in polymers in which the
polymer chains can be oriented in a parallel direction (24-26).

Thin Films

As indicated earlier in this chapter, polyimides play an important
role as thin film dielectrics in interconnections. An overview of
polyimide chemistry can be obtained from references 27 and 28. For
electronic applications, good adhesion of polymers to the circuitry
materials is important to provide good moisture resistance. The
diffusion of moisture in polyimides has been described in
reference 29. Fully imidized polyimide homopolymers often show
poor intrinsic adhesive properties. To overcome this shortcoming,
silane-based adhesion promoters can be used or, alternatively, a
thin layer of a fusible fluorocarbon polymer is first bonded to the
polyimide film. This fluorocarbon polymer serves as a hot melt
adhesive when the polyimide film is laminated to a substrate at
elevated temperature and pressure. Often polyimide films can be
obtained by deposition of the corresponding polyamic acid followed
by imidization at higher temperature. In this case, some of the
polar amic acid groups may provide better adhesion to the
substrate. In yet another approach to improve the adhesion of
polyimides, polysilicone-imide copolymers have been prepared. The
silicone moieties can be introduced by means of the diamines or the
dianhydrides. It is interesting to note that the improved adhesive
characteristics are found only in a rather narrow composition
region (ratio of silicone to polyimide). Of the various approaches
to improve the adhesive features of polyimides, the conversion to
polysilicone-imides appears to be very attractive because, in
addition to improved adhesion, the silicone-imide copolymers have a
lower dielectric constant and lower moisture absorption than the
polyimide homopolymer.
    Reliable methods of measuring the adhesive bond strength
between the dielectric coating (film) and the various substrates
are needed to determine the performance of the film or the
coating. Often the adhesion is tested in an indirect way: simply
by exposing the samples to accelerated test conditions, e.g., high
humidity and high temperature, until failure. Direct measurement
of the adhesive bond strength has been performed in various
manners. The simplest of these is the "tape test". In this test,
the coating is scribed in parallel in two directions which are at
90° to one another. In this fashion, a number of small squares of
coating are formed. Subsequently, adhesive tape is pressed over
the scribed area. After pulling the tape off, the remaining
squares are counted and those numbers are compared with similar
results obtained with other films. A word of caution is in order
because, in some cases, it has been observed that the adhesive on

the tape was virtually unable to bond to certain polymer coatings, erroneously suggesting excellent adhesion of the coating to its substrate. What was measured, however, was the lack of adhesion of the adhesive tape to the coating rather than the adhesion of the coating to its substrate. Recently an alternate, direct method was refined by Senturia and co-workers and described in more detail in this book. See also reference 30 for additional adhesion studies.

Protective Gels

This area is dominated by silicones. Variations in chemical composition allow formulations to vary from very soft gels (almost liquids) to elastomeric compositions to hard solids. In this class of materials, we find applications for thin coatings, as well as for bulk encapsulation. Silicones in electronic applications are always cross-linked. One of their major advantages is that they exert only minor stress on chips, wires, etc. (31). Among their disadvantages are low mechanical strength and high permeability to moisture. Because of their weak mechanical properties, devices covered with silicone gels are further protected from the environment by enclosure in metal or ceramic containers that are closed by lids which are soldered or glued on.

Rigid Bulk Encapsulants

These resins are typically applied by transfer molding over IC devices that are wire bonded to lead frames. The transfer molding compositions are primarily based on epoxy resin chemistry. Silicone-based transfer molding compounds are being replaced by epoxies due to the higher cost of the silicones and the continuously improving performance of the epoxies. Transfer molding is the process of choice because transfer molding compounds, as a result of their low molecular weight, provide for much needed low viscosity at the time that the liquid resin surrounds the delicate IC structure, in particular its wire bonds. Wire sweep (deformation of the wire configuration) would readily occur with a resin with a high melt viscosity. Thermoset melt flow studies were reported by Blyler et al. (32) and by Manzione et al. (33). Important requirements that these encapsulants have to meet are: (1) low melt viscosity and rapid cure, (2) low stress on IC devices (that is, low CTE's), (3) good adhesion to devices (which leads to good moisture protection), (4) low impurity levels, and (5) low flammability.

Typical transfer molding compositions for encapsulation of electronic devices are mixtures of an epoxy novolac resin, a phenolic resin hardener, a catalyst, large amounts of inorganic filler (e.g., SiO_2), flame-retardant ingredients, internal lubricants, carbon black, and sometimes other additives such as getters to trap ionic impurities (34,35), corrosion-protection materials, and stress-relief ingredients.

These formulations are quite reactive, and all current commercial transfer molding resins require refrigeration to about 4°C during shipping and storage. To prevent moisture pick-up during use, the materials have to be brought to ambient temperatures prior to opening the container. Although the refrigeration and thermal equilibration prior to use are cumbersome, these materials and processes have been widely accepted throughout the electronics industry. Two chapters in this book are devoted to developmental molding compositions which are sufficiently stable so that they can be stored and shipped without refrigeration.

Earlier in this chapter, it was indicated that the presence of halide ions (e.g., Cl^- and Br^-) is undesirable because they tend to promote the corrosion of parts of the IC. Low-flammability requirements for these encapsulants are realized through the use of brominated epoxy resins in combination with antimony oxide (Sb_2O_3). For some time the brominated epoxies have been suspected as a possible source of Br^- ions. Since it is difficult to achieve low flammability for these encapsulants without the bromine-containing species, efforts have been made to arrive at bromine-containing flame retardants of greater hydrolytic stability so that the flame retardant does not inadvertently diminish the corrosion protection these encapsulants are expected to provide.

The comments about moisture, ionic impurities, and electric fields made earlier in this chapter apply to encapsulants for electronic devices as well (36). Efforts have been made to improve the moisture resistance of encapsulated IC's. In one such approach, the epoxy transfer molding compound is coated over circuitry previously coated with a polysilicone-imide (37). The evaluation of new encapsulants is based largely on their performance under extreme humidity conditions. With the continuing improvements in encapsulant performance, the test conditions have become more severe. For instance, several years ago, encapsulated devices were tested at 85°C and 85% relative humidity and bias. As the protection provided by the encapsulants improved, the time for testing became very long. Usually, the failure rate is taken as the time needed for 50% of the samples to fail. Simply by reducing the level of ionic impurities and hydrolyzable halogen compounds in the transfer molding resins, 50% failure levels could be reached only after hundreds, if not thousands, of hours of testing at 85°C and 85% RH. Gradually, the testing time was shortened by increasing the temperature. Testing a suitable device at 145°C, 85% RH and bias in a pressure chamber can reduce the time for 50% failure to a few hundred hours with the currently available commercial materials (19,38,39).

In another critical test, the device is subjected to repeated thermal cycling to determine if a mismatch in CTE's of the various device components would result in failure. In this test, a number of devices (~25) are taken through thermal cycles between −65°C and +150°C. A cycle consists of a few minutes at the temperature

extremes and rapid transfer from one temperature chamber to the other. With high-quality encapsulants, devices can be taken through 1,000 cycles without any failures at all.

After transfer molding at 1,000 psi and about 180°C, the encapsulant, because of its larger CTE, tends to shrink more than the IC when the whole device cools to ambient temperatures. As the IC features become smaller and smaller, they also become more fragile and more vulnerable to damage by the stresses of the shrinking encapsulant. There are currently two different approaches to arrive at low stress materials. In the first approach, the resin is filled with a compressible, rubber-like powder (40). Upon shrinkage of the bulk resin, the compressible, rubber-like particles absorb some of the stress, thus reducing the stress to which the IC is exposed. In the second approach, the brittleness of the cross-linked epoxy novolac resin is diminished by chemically modifying the epoxy novolac with silicone groups, which can be viewed as stress relievers at the molecular level (41).

Stress in packaged electronic devices has been the subject of several recent studies (42-44). Clearly, the differences between the CTE's of polymers and of inorganic materials are sufficiently large to provide for a continuing challenge, especially as the IC's to be packaged become larger while their individual features become smaller.

Printed Wiring Board Materials and Processes

While a detailed discussion of printed wiring boards is well beyond the scope of this chapter, a few general concepts and remarks can be presented.

In the typical manufacturing process for a rigid laminate (the precursor to the PWB), paper or a glass cloth web is treated with a resin, then dried, cut (this is the prepreg sheet), stacked to give the desired thickness, covered with copper foil (one or both sides), and is then laminated and cured to give a rigid thermoset. The dielectric resin materials are generally thermosets, although thermoplastic materials are also used. To form circuit conductor paths, or "traces," a circuit pattern is formed on a resist layer and the laminate is then etched, or else copper is "plated up" additively. The electrical pathway between layers (for a multilayer board) is formed by drilling and then plating a thin layer of copper on the hole walls. These holes may serve either as connections or as mounting holes for through-hole mounted devices.

Multilayer boards are formed by adding unetched, single-sided laminates on either side of an etched single or multilayer laminate by using an interface of partially cured resin and (usually) glass mats. In the mass-lamination approach, large arrays of boards can be produced, although the technique is usually limited to about ten layers.

Materials for rigid laminates include paper-phenolic (the original material), paper-epoxy, and glass-epoxy. Composite laminates, which contain two or more types of reinforcing

materials, include both polyester and epoxy resin composites. Newer materials under evaluation include polyimides, poly(cyanurates), poly(tetrafluoroethylene) (PTFE), and foamed PTFE. Detailed discussion can be found elsewhere (45).

Much of the newer technology is driven by the needs for low dielectric constant and controlled impedance, a low dielectric constant being an advantage of foamed materials. Clearly, dimensional stability is becoming increasingly important for printed wiring boards.

Flexible printed wiring laminates usually contain (but are not limited to) either a polyimide or a polyester [usually poly(ethylene terephthalate)] with copper conductors. These laminates are prepared in sheets or by roll-to-roll lamination, usually by means of an adhesive. Alternatively, direct fusion without an adhesive is used. Recent developments include the use of alternative substrate materials such as poly(ether sulfones), additive plating of copper, and casting of a polymer directly on the copper foil web.

Three-dimensional interconnects can be prepared through several processes, some of which use directly molded circuit boards. These boards use a variety of materials such as polysulfones, poly(ether sulfones), poly(ether imides), poly(aryl sulfones), poly(phenylene sulfides), fluorinated ethylene propylene copolymers, and aromatic polyamides (46). Three basic routes to creating trace (or track) systems are used: mold first, add traces later; mold-in the trace pattern, add conductors later; and mold and "circuitize" simultaneously (46). Generation of traces is achieved by a variety of methods. Examples of these methods include: screen printing of conductive inks (for route one); a double-shot molding process which produces a track system by using two resins, one catalyzed to enable selective plating of copper (for route two), and transfer of a polymer thick film circuit into the molding tool (for route three) (46).

Discussions of directions in board technology suggest that the classic epoxy fiberglass "FR-4" board will dominate for some time (47). However, trends in materials and technology indicate that usage will include 3-D molded boards, provided volumes are large enough (50K to 100K pieces) to justify the costs of the molds (48). The ability to form actual 3-D circuits will further enhance the potential of this technology, as would the use of polymer thick film printed resistors and conductors (48).

The trends toward more functionality per board, finer lines and spaces, shorter run lengths per design, and faster turnaround are driving board manufacturers to seek new methods of producing boards without sacrificing quality and yield. If possible, these new methods need to be compatible with existing board materials. As a consequence, direct-to-board imaging (of a polymeric photoresist to define circuit traces) has become an intriguing area of increasing interest. Recently, technological advances have been reported for systems which use computer-driven laser imaging. Although such approaches obviate the need for producing a phototool

(e.g., a photographic film that is used for subsequent imaging of the photoresist), many of these approaches have not yet demonstrated yield enhancement for finer lines. A new system under development uses a laser-exposed, liquid crystal light-valve (LCLV) projection system to expose the resist, and suggests an interesting alternative (49). In this system, heat from a low-power diode laser is used to form light-scattering regions in the liquid crystal layer. Light incident on these regions is scattered away from the projection lens, and appears as a dark image on the display screen (49).

Conclusion

Polymers are playing increasingly important roles in packaging and interconnection as the versatility of being able to customize their mechanical and electrical properties becomes better established and more well known. The rest of this book presents specific chapters on polymeric materials and their applications in this field. In reading them it is hoped the reader will keep in mind the increasingly important roles of these materials, their consequent market value, and their place in the hierarchy of electronic packaging and interconnection.

Literature Cited

1. BPA (Technology and Management, Ltd.), Compass Programme; 1986.
2. Rose, D. J. Rose Associates, Los Altos, CA, presentation SEMI Information Services Seminar, January 1988.
3. Sage, M. G. BPA News, Spring 1988, p 2.
4. BPA (Technology and Management, Ltd.), Circuit Substrates; 1988, p 23.
5. BPA (Technology and Management, Ltd.), idem, p 72.
6. Johnson, B. C.; Hamilton, D. J. Basic Electronic Packaging Engineering, University of Arizona (National Technical University Course), 1985.
7. Anavy, R. A. Electronic Outlook Corp., San Francisco, CA, Economic and Electronic Industries Outlook--U.S. and World Overview, Implications for Hybrids, presentation Hybrid Marketing Research Council, The Institute for Packaging and Connection of Integrated Circuits (IPC), June 1988.
8. Electronic Business, 1988, July 1, p 37.
9. Reference 4, p 9.
10. Henderson, E.; Loeb, W. E. Electronic Industry Outlook, presentation Technical/Marketing Research Council (T/MRC), IPC, June 1988, pp 13, 15.
11. Analysis of the Market for Rigid Printed Wiring Boards for 1987, T/MRC, IPC, June 1988.
12. Socolovsky, A. Electronic Business, 1988, May 1, pp 106-108.
13. Reference 4, pp 41, 42.

14. Sharenow, B. Tape Automated Bonding High Lead Count Cost Analysis, Proc. Technical Program, NEPCON West, 1988 (written subsequently).
15. Proc. Electr. Packaging and Corrosion in Microelectronics, Nicholson, M. E., Ed.; ASM International: 1987.
16. Salmon, E. R. Encapsulation of Electronic Devices and Components; Marcel Dekker: New York and Basel, 1987.
17. Olberg, R. C.; Bozarth, J. L. Microelectronics and Reliability 1976, 15, 601.
18. Taylor, D. F. IEEE Trans. Electr. Insul. 1984, EI-19, 288.
19. Gallace, L.; Rosenfield, M. RCA Review 1984, 45, 249.
20. Padmanabhan, R. IEEE Proceedings of the 35th Electronic Components Conference, 1985, p 309.
21. Wada, T.; Higuchi, H.; Ajiki, T. Journal of the Electrochemical Society 1986, 133, 362.
22. Comizzoli, R. B.; Frankenthal, R. P.; Milner, P. C.; Sinclair, J. D. Science 1986, 234, 340.
23. St. Clair, A. K.; St. Clair, T. L.; Winfree, W. P. Polymeric Materials Science and Engineering, 1988, 59, 28.
24. Hofer, D. C.; Swanson, S.; Volksen W. Proceedings/Abstracts of the Interdisciplinary Symposium on Recent Advances in Polyimides and Other High Performance Polymers, July 1987, Reno, NV.
25. Hofer, D. C. Proceedings/Abstracts of the Interdisciplinary Symposium on Recent Advances in Polyimides and Other High Performance Polymers, July 1987, Reno, NV.
26. Numata, S.; Kinjo, N. Polymer Engineering and Science 1988, 28, 906.
27. Proceedings/Abstracts of the Interdisciplinary Symposium on Recent Advances in Polyimides and Other High Performance Polymers, July 1987, Reno, NV.
28. Proceedings/Abstracts of the Third Intern. Conf. Polyimides, November 1988, Ellenville, NY.
29. Denton, D. D.; Day, D. R.; Priore, D. F.; Senturia, S. D.; Anolick, E. S.; Schneider, D. J. Electronic Materials 1985, 14, 119.
30. Buchwalter, L. P.; Lacombe, R. H. Proceedings/Abstracts of Third Intern. Conf. on Polyimides, November 1988, Ellenville, NY, p 138.
31. Shoraka, F.; Gealer, C. A.; Bettez, E. Semiconductor International, October 1988, p 110.
32. Blyler, L. L.; Bair, H. E.; Hubbauer, P.; Matsuoka, S.; Pearson, D. S.; Poelzing, G. W.; Progelhof, R. C.; Thierfelder, W. G. Polym. Eng. Sci. 1986, 26, 1399.
33. Manzione, L. T.; Poelzing, G. W.; Progelhof, R. C. Polym. Eng. Sci. 1988, 28, 1056.
34. Ainger, F. W.; Brettle, J.; Dix, I.; Goosey, M. T. In Polymers in Electronics; Davidson, T. Ed.; 1984 ACS Symposium Series No. 242; American Chemical Society: Washington, D.C. 1984, p 31.

35. Sameshima, R.; Tanimoto, S.; Tanake, K.; Koshibe, S.; Kakei, M. <u>Proceedings Electron Components Conference</u>, 1987, p 181.
36. Belani, J.; Cathers, L.; Malladi, D. <u>Proceedings of the Sixth International Electronics Packaging Conference</u>, 1986, p 713.
37. Collins, W. R.; Powell, D. B. <u>IEEE Proceedings of the 35th Electronic Components Conference</u>, 1985, p 14.
38. Malik, S. K.; Gunn J. E.; Camenga, R. E. <u>Proceedings of the IEEE International Test Conference</u>, 1983, p 790.
39. Charles, S. <u>Australian Telecommunication Research</u> 1986, <u>20</u>, 39.
40. Nakamura, Y.; Tabata, H.; Suzuki, H.; Iko, K.; Okubo, M.; Matsumoto, T. <u>J. Appl. Pol. Sci.</u> 1986, <u>32</u>, 4865.
41. Saito, N.; Nakajima, N.; Ikushima, T.; Kanagawa, S.; Takahashi, T. <u>Polymeric Materials</u> 1987, <u>57</u>, 558.
42. Guan, D. Y.; Gukelberger, T. F.; Cahoon, E. C.; Joseph, T. W.; Snowdon, J. M. <u>Proceedings of the 36th Electronic Components Conference</u>, 1986, p 107.
43. Turner, T.; Wendel, K.; <u>23rd Am. Proc. Reliab. Phys. Symp.</u>, 1985, p 142.
44. Groothuis, S.; Schroen, W.; Murtuza, M. <u>Annu. Proc. Reliab. Phys. (Symp.)</u>, 1985, p 184.
45. Reference 4, pp 125-138.
46. Reference 4, pp 210-213.
47. Martel, M. L. <u>Circuits Manufacturing</u> 1989, <u>29</u>, 31.
48. Tuck, J., idem, 39.
49. Holihan, S. K.; Bergstrom, N. <u>PC Fab</u>, January 1989, pp 77-79.
50. "IC Density Trends," A Report on the Integrated Circuit Industry; Integrated Circuit Engineering Corp. (ICE), 1989.

Chapter 2

Cure Studies of PMDA-ODA- and BTDA-ODA-Based Polyimides by Fluorescence Spectroscopy

Eric D. Wachsman[1], Peter S. Martin[2], and Curtis W. Frank[2]

[1]Department of Materials Science and Engineering, Stanford University, Stanford, CA 94305
[2]Department of Chemical Engineering, Stanford University, Stanford, CA 94305

The effect of thermal curing on the morpholgy and conformation of PMDA-ODA and BTDA-ODA polyimides is investigated using fluorescence spectroscopy. These polyimides are found to exhibit intrinsic fluorescence. This fluorescence arises as a result of excitation in either of two spectral bands. Emission from a single chromophore is observed and the two excitation bands are described in terms of both an intra- and an inter-molecular charge transfer complex (CTC). The intra-CTC is ascribed to rotation around the imide nitrogen-phenyl bond. The inter-CTC arises as a result of the increase in aggregation associated with a more ordered phase. The emission intensity from excitation of the inter-CTC band increases linearly with reciprocal intermolecuar spacing.

Aromatic polyimides have gained wide popularity as dielectric materials in a variety of applications in the manufacturing of electronic circuits due to their thermal, mechanical and electrical properties. Most notable among these applications are as interlayer dielectrics in multilevel VLSI circuits and in multilevel inter-connects, as well as in the packaging of integrated circuits. Aromatic polyimides have glass transition temperatures in excess of 400 °C, excellent toughness and elongation properties and dielectric constants comparable to that of inorganic dielectrics, about 3.5. An important feature relative to these applications is their ability to planarize the topography when spun on as the soluble precursor polyamic acid. The subsequent intramolecular condensation reaction to form the heterocyclic imide is typically a thermal "curing" process.

Thermal "curing" is not only necessary for completion of the imidization reaction but is also responsible for elimination of any solvents and the water condensation by-product. In addition, "curing" is responsible for any thermally activated change in morphology and any associated change in material properties. The effect of curing on the material properties of polyimide can be seen both in the reduction in dielectric constant and the increase in Tg with degree of cure. Here the "degree of cure" is qualitatively related to the degree of aggregation associated with the final cure temperature.

A method for determination of the final degree of cure is necessary in order to obtain repeatable material properties while processing polyimide for integrated circuits. FTIR can be used for the determination of the extent of the imidization reaction by monitoring the reduction in absorption by the carboxyl groups in polyamic acid and the increase in absorption by the imide groups in polyimide. Since the imidization reaction is essentially complete for polyimide cured at temperatures less than 250 °C, little additional structural information can be obtained from FTIR for polyimide subjected to higher temperatures. X-ray diffraction can be used to monitor the degree of cure, for polyimide cured above 250 °C, as polyimide undergoes molecular reorientation with cure so as to obtain localized regions of ordered aggregates (1). This technique, however, is not practical as an in-situ measurement of the degree of cure.

In a previous investigation (2) we demonstrated that Du Pont PI-2555 polyimide fluoresces and that the intensity of the fluorescence depends on the degree of cure, for polyimide annealed at temperatures in excess of the point where the imidization reaction is essentially complete. Unfortunately, the PI-2555 was misidentified in that paper as PMDA-ODA, whereas we have recently learned that it is a BTDA-ODA/MPD type polyimide and that PI-2545 is in fact based on the PMDA-ODA structure (3). These structures as well as those of the other polyimides investigated are shown in Figure 1. This difference in the chemical structure of the dianhydride fragment has minimal impact on the conclusions drawn in that investigation, as will become apparent in the present paper. The inclusion of MPD as a minor component also has a negligible affect. We will show that UV irradiation of polyimide results in an intrinsic fluorescence for which the intensity and emission wavelength strongly depend on the cure temperature. We propose that the change in the fluorescence is due to a change in the microenvironment of the chromophore associated with a higher degree of aggregation. Recently, Dickinson and Sung (4) have shown that fluorescence spectroscopy can also be used to monitor the extent of reaction for the formation of a 6FDA-NDA polyimide from 5,5'-[2,2,2-trifluoro-1-(trifluoromethyl) ethylidene]bis-1,3-isobenzofurandione (6FDA) and 1,5-naphthyl diamine (NDA). Thus, fluorescence spectroscopy has the potential of monitoring the extent of the entire polyimide process, from polyamic acid through formation of the most ordered polyimide film.

<u>Sample Preparation</u>

Fluorescence spectra of polyimide as a function of thermal history for two of the most common commercially available polyimide precursors, Du Pont PI-2545 and PI-2555, were obtained. These precursors are polyamic acids formed from the polycondensation reaction of pyromellitic dianhydride (PMDA) and oxydianiline (ODA), PI-2545, and from 3,3',4,4'-benzophenone tetracarboxylic dianhydride (BTDA) and ODA, PI-2555. Meta-phenylenediamine (MPD) is also present in PI-2555 as a minor component (3). Its presence has a negligible affect on the results of this study, other than a possible broadening of the spectral band ascribed to the rotation of the imide-phenyl bond, and hence will not be discussed further.

Twelve samples of each type of polyimide were prepared by spinning the polyamic acid precursor on 3" quartz wafers followed immediately by thermal imidization of the films. Half of the samples of each type of polyimide were cured supported and the other half were cured unsupported. A 14% solution of the PI-2545 polyamic acid and a 19% solution of the PI-2555 polyamic acid in 1-methyl-2-

PMDA-ODA

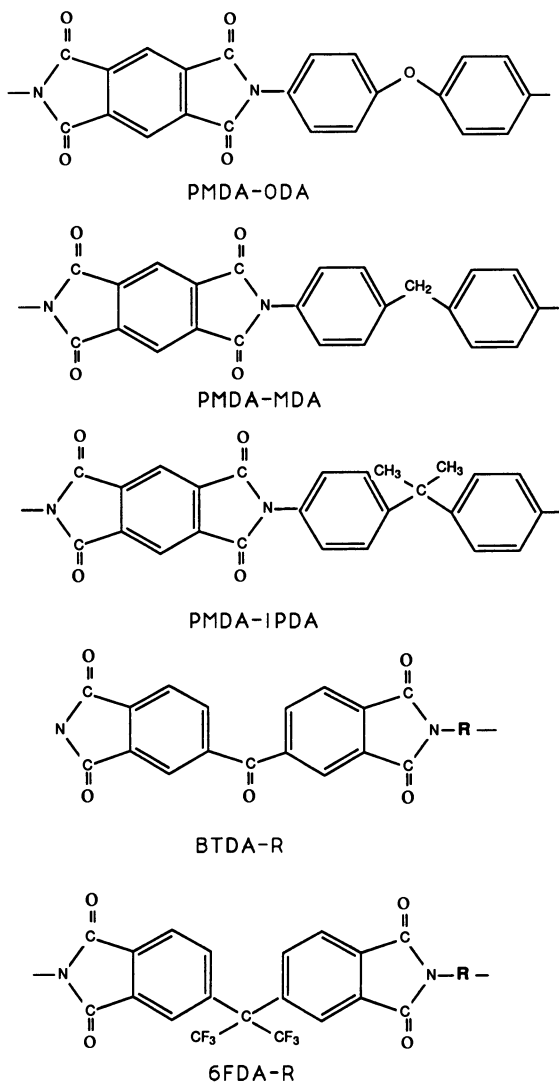PMDA-MDA

PMDA-IPDA

BTDA-R

6FDA-R

Figure 1. Structures of the various polyimides investigated in this study.

pyrrolidinone was spun on for 60 seconds. The films that were cured supported on wafers were spun at 3000 rpm resulting in about 3 to 4 micron thick films after imidization. Thickness of the films was ascertained using a Tencor Alphastep on similarly prepared samples that had been photolithographically delineated prior to imidization. The films that were cured unsupported were spun at 500 rpm; their exact thickness is not known but it is a factor of two to three greater than that of the films spun on at the higher speed. Relative emission intensity can be compared either between all of the films that were cured supported or between those cured unsupported. The reduction in film thickness (densification) upon thermal curing does not change the total number of polyimide chains in each sample. Furthermore, at the wavelengths investigated the optical path is much greater than the film thickness.

The samples all received initial thermal treatments of 142 °C for 30 minutes, in the range of a typical B-stage cure. The samples that were cured unsupported were then peeled from their wafers. All of the films then received a 200 °C cure for 1 hour to essentially complete the imidization reaction. They were then cured in successive 50 °C increments for 30 minutes each. All of the thermal treatments were in an inert nitrogen atmosphere except for the first 142 °C bake, which was in air. For the supported PI-2555 cure study thermal treatment up to 350 °C was performed in a convection oven and the 400-450 °C samples were prepared by subsequent heating in a Thermco Minibrute furnace. For the PI-2545 and the unsupported PI-2555 cure studies all of the thermal treatments, up to 400 °C, were performed in a convection oven.

We also investigated the effect of the chemical structure of the diamine and dianhydride moieties on fluorescence. This included investigation of less flexible, more bulky groups for the ether linkage in the diamine moiety of PMDA-ODA as well as substitution of 5,5'-[2,2,2-trifluoro-1-(trifluoromethyl)ethylidene]bis-1,3-isobenzofurandione (6FDA) for the dianhydride. Several polyimide films were supplied by Dow Chemical: PMDA-ODA, PMDA-methylene dianiline (MDA), PMDA-isopropylidene dianiline (IPDA), 6FDA-ODA, 6FDA-MDA and 6FDA-IPDA; their structures are shown in Figure 1. All of the precursor polyamic acids were synthesized as described in (5). The films were then prepared by casting the precursor on a glass substrate with a doctor blade followed immediately by an 80 °C bake in nitrogen for 1 hour. The films were then removed from their substrates and cured free-standing at 250 °C in vacuum for 15 hours. The resulting films were on the order of 25 microns thick. One of the 6FDA-IPDA films was subsequently annealed at 310 °C in nitrogen for 7 hours. The intermolecular spacing of these films was determined by X-ray diffraction (6).

The absorption and fluorescence spectra of zone refined PMDA, sublimed BTDA and sublimed ODA model compounds in dioxane were obtained in order to identify the chromophores responsible for fluorescence of the polyimide films.

Fluorescence Analysis

A Spex Fluorolog 212 spectrophotometer was used for recording the emission and excitation spectra of the polyimide films and the model compounds. The slit width used for the films was 2 mm and for the model compounds was 1 mm. Excitation and emission spectra were subsequently normalized with respect to the lamp intensity fluctuations by dividing each spectrum by that obtained with a Rhodamine-B standard solution. Absorption spectra were obtained with

a Cary 210 uv-visible spectrophotometer. All of the spectra were obtained at room temperature in air.

Results

<u>Cure Study - Supported Films</u>. Fluorescence excitation spectra were measured for each of the PI-2555 and PI-2545 films in the cure study by monitoring the intensity of the strongest emission peak, 590 nm for PI-2555 and 610 nm for PI-2545, while scanning the excitation wavelength. The excitation spectra of PI-2555 have been presented previously (2). The excitation spectra of supported PI-2545 are shown in Figure 2. Several features of the spectra of both polyimides change with increasing cure temperature. The first of these is the intensity, which increases dramatically with cure temperature. The excitation spectra of both commercial polyimides consist of two primary bands. The first "short-wavelength" band is broad and unstructured. It is centered at about 350 nm for PI-2555 and about 380 nm for PI-2545. The second "long-wavelength" band is centered at about 490 nm for both polyimides. While the short-wavelength band remains broad and relatively featureless, the long-wavelength band becomes structured with increasing cure temperature. The structured band is composed of several peaks, which are presented for the highest cure temperature of each polyimide in Table I. In addition, the intensity of the structured band increases relative to that of the unstructured band with cure.

Table I. Excitation and Emission Maxima (nm) for Supported
PI-2555 (450 °C cure) and PI-2545 (400 °C cure)

	PI-2555	PI-2545
<u>Excitation Bands</u>		
"Short-Wavelength"	352*	380*
"Long-Wavelength"	427, 465, 486*	430, 463, 490*
	509 & 532	& 519
<u>Emission Band</u>		
Peaks	560, 590	610
Shoulders	500, 530, 630	570

*Excitation wavelength corresponding to maximum emission, λmax.

The emission spectra of PI-2555 obtained with 352 nm and 486 nm excitation wavelengths have been presented previously (2). The emission spectra of PI-2545 obtained with 490 nm excitation are shown in Figure 3. Similar spectra are observed for 380 nm excitation. The emission maxima of the highest cure temperature sample of each polyimide are presented in Table I. The emission intensity increases with cure temperature for both sets of emission spectra from both polyimides. In addition, the emission intensity from excitation of the long-wavelength band increases relative to that from excitation of the short-wavelength band with cure temperature for both polyimides.
    Excitation and emission spectra of both polyimides exhibit initial shifts in spectral maxima over the 200 to 300 °C range. The excitation maxima of both polyimides blue shift about 10 nm over this temperature range. For PI-2555 samples cured between 200 and 450 °C, excitation at both 352 and 486 nm results in a red shift with cure of 630 cm^{-1} for the 560 nm emission peak and 590 cm^{-1} for the 590 nm
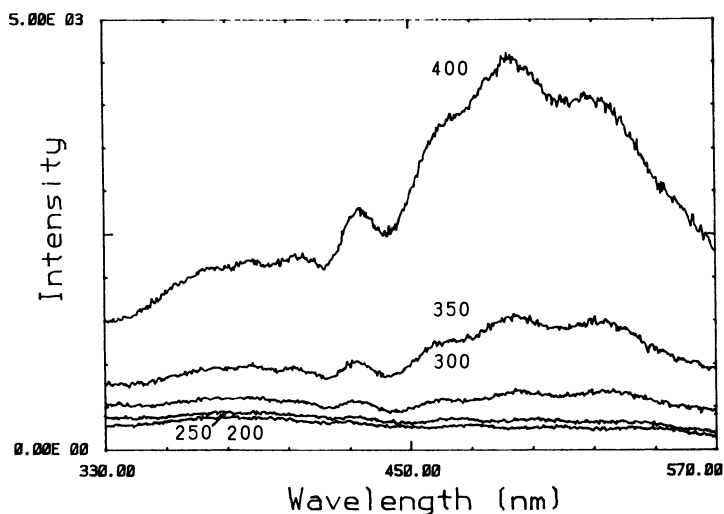
Figure 2. Excitation spectra of PI-2545; 610 nm emission intensity as a function of excitation wavelength and cure temperature. The numbers by the curves refer to the highest cure temperature in °C.
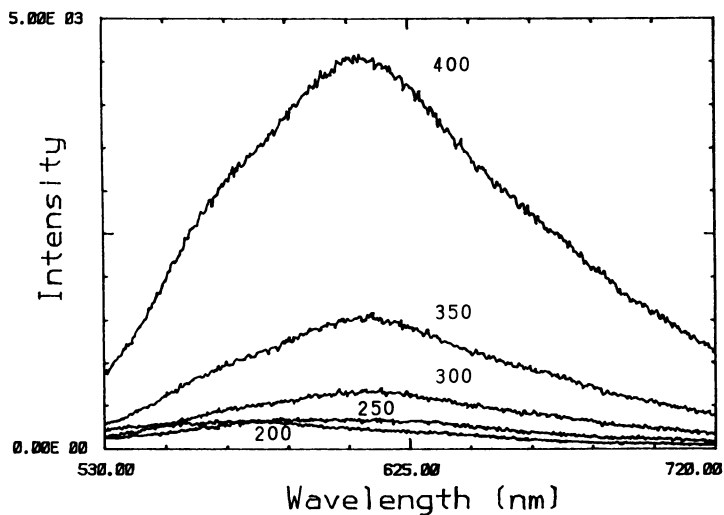

Figure 3. Emission spectra of PI-2545 as a function of cure temperature for 490 nm excitation.

emission peak. However, the spectrum of the 250 °C cured sample
appears to be anomalously displaced relative to the spectra of the
200 and 300 °C cured samples. Similarly, the emission maximum of 200
°C cured PI-2545 is 572 nm; however, for samples cured at 300 °C and
above the emission maximum is 610 nm with a shoulder in the 570 nm
range. These initial shifts in spectral maxima may be attributable to
further extent of the imidization reaction, similar to the results of
Dickinson and Sung (4).

The emission intensity of the BTDA-ODA based polyimide is more
than two orders of magnitude greater than that of the PMDA-ODA based
polyimide for similar thermal treatment. This is significant since
the relative emission intensity of the BTDA and PMDA model compounds,
for the same concentration, is reversed. An Arrhenius plot of the
normalized intensity of 560 nm emission from PI-2555 and 610 nm
emission from PI-2545 for both excitation bands of each polyimide is
shown in Figure 4. The slope for the unstructured band of PI-2555
gives an apparent activation energy of 6.3 kcal/mole and the
structured band results in an activation energy of 10.9 kcal/mole.
For PI-2545 the unstructured band has an activation energy of 7.3
kcal/mole and the structured band has an activation energy of 12.4
kcal/mole. These activation energies are relatively small, on the
order of bond rotation energies. The lower activation energies for
the BTDA-ODA polyimide are consistent with the increased flexibility
of the chain due to the addition of the carbonyl linkage in the
pyromellitimide moiety.

Cure Study - Unsupported Films. The effect of stress on the
morphology and hence the fluorescence spectra of polyimide is evident
by comparing the excitation spectra of films cured supported with
those cured unsupported. In Figure 5 are the excitation spectra of
the 400 °C cured samples from the cure studies of unsupported PI-2555
and PI-2545. The structure apparent in the spectra of the supported
films is almost nonexistent in the spectra of the unsupported films.
The center of the bands for these films, given in Table II, is
essentially the same as in the supported films; however, the relative
intensity of the short-wavelength band to the long-wavelength band is
significantly reduced in the unsupported films. Similarly, the
centers of the emission bands are essentially unchanged and the
emission spectra of unsupported films also show a lack of structure
as compared to those of supported films.

Table II. Excitation and Emission Maxima (nm) for 400 °C Cured
Unsupported PI-2555 and PI-2545 Films

Polyimide	Short-Wavelength Band	Long-Wavelength Band	Emission
PI-2555	359	432 & 500	580
PI-2545	375	433 & 517	616

The apparent activation energies for the short- and long- wavelength
excitation bands of unsupported PMDA-ODA are 7.3 and 12.8 kcal/mole,
respectively, essentially identical to that of the the supported
films. The activation energy associated with the short-wavelength
band of BTDA-ODA was reduced to 5.0 kcal/mole as compared to 6.3
kcal/mole, for the unsupported and supported films respectively. By
contrast, the activation energy associated with the long-wavelength
band increased from 10.9 kcal/mole to 12.9 kcal/mole, for the
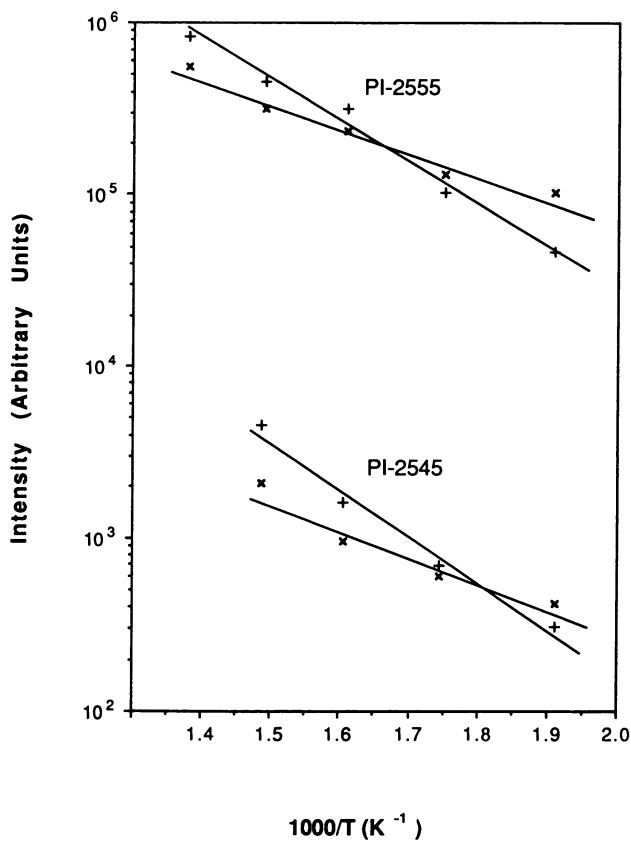supported and unsupported films respectively.

Figure 4. Arrhenius plots of the emission intensity of supported PI-2545 and PI-2555, from irradiation in the short-wavelength (x) and long-wavelength excitation band (+), as a function of cure temperature.

Structural Effects. Excitation and emission spectra of the PMDA
based polyimide films obtained from Dow were measured. The
fluorescence intensity decreases in the order: PMDA-ODA > PMDA-MDA >
PMDA-IPDA, as the ether linkage is replaced with more bulky, less
flexible linkages. X-ray diffraction data, provided by Dow, also show
that this is the order of increasing intermolecular distance, d. The
wavelength of the excitation maximum also shifts to higher energy
with reduced flexibility and increased bulkiness of this linkage.
These results are tabulated in Table III below.

Table III. Intermolecular Distance (d), Relative Emission
Intensity, Excitation λmax and Emission λmax of Various Polyimides

Polyimide	d (Å)	Intensity	Excitation (nm)	Emission (nm)
PMDA-ODA	4.7	2.83×10^4	515	604
PMDA-MDA	4.9	1.36×10^4	500	552
PMDA-IPDA	5.1	1.15×10^4	490	558
6FDA-IPDA	5.7	5.14×10^4	466 & 480	537
6FDA-IPDA*	5.2	1.37×10^5	466 & 480	540

* After 310 °C cure.

The effect of an additional 310 °C cure on the emission
intensity and intermolecular spacing of a 6FDA-IPDA film, as compared
to a 250 °C cured 6FDA-IPDA film, is also shown in Table III. The
intensity of the 310 °C cured sample is significantly greater than
that of the 250 °C cured sample. This behavior is identical to that
observed in the cure study of the commercial polyimide films.
Furthermore, this increase in intensity corresponds to a decrease in
intermolecular distance, as shown by the data in Table III, analogous
to the trend observed with the PMDA films. Finally, this extra cure
appeared to result in a more ordered film as is evident by the
addition of two minor diffraction peaks corresponding to 3.4 and 2.1
Å (d).
     In Figure 6 are the excitation spectra of a selection of some
of the synthesized PMDA and 6FDA based polyimide films supplied by
Dow. One can see the added structure in the long wavelength region of
the excitation spectra of 6FDA based polyimides as compared to the
relatively featureless excitation spectra of similarly prepared PMDA
based polyimides. Similar to the comparison between BTDA-ODA and
PMDA-ODA emission intensity, the intensity of 6FDA-IPDA is a factor
of five greater than that of PMDA-IPDA for similar thermal treatment
and an order of magnitude greater for similar intermolecular spacing.

Model Compounds. The excitation spectra of the PMDA and BTDA model
compounds, as a function of concentration, are shown in Figures 7a
and 8a, respectively. Their corresponding absorption spectra, at
fixed concentration for two different absorbance scales, are shown in
Figures 7b and 8b, respectively. A small absorption peak
corresponding to the excitation maximum is apparent upon expansion of
the absorbance scale for both of the compounds. The emission spectra
of these compounds are shown in Figure 9. The positions of the
excitation maxima, the corresponding red edge maxima of the minor
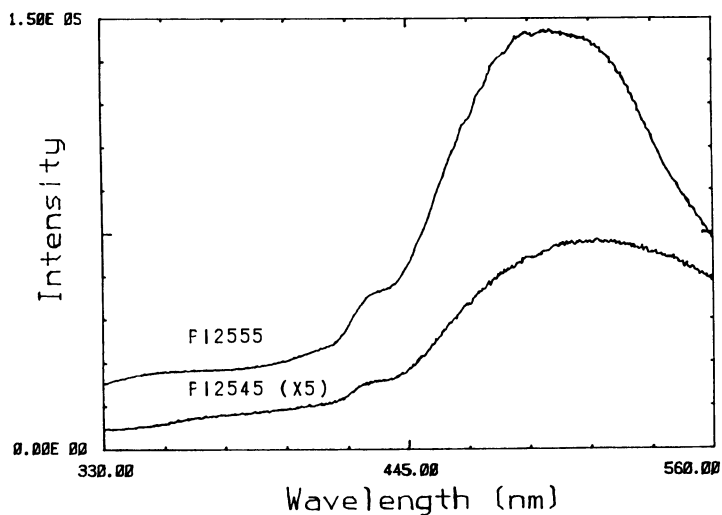absorption peak and the emission maxima are tabulated in Table IV.

Figure 5. Excitation spectra of 400 °C cured unsupported films. 580 nm emission intensity and 616 nm emission intensity as a function of excitation wavelength for PI-2555 and PI-2545, respectively.
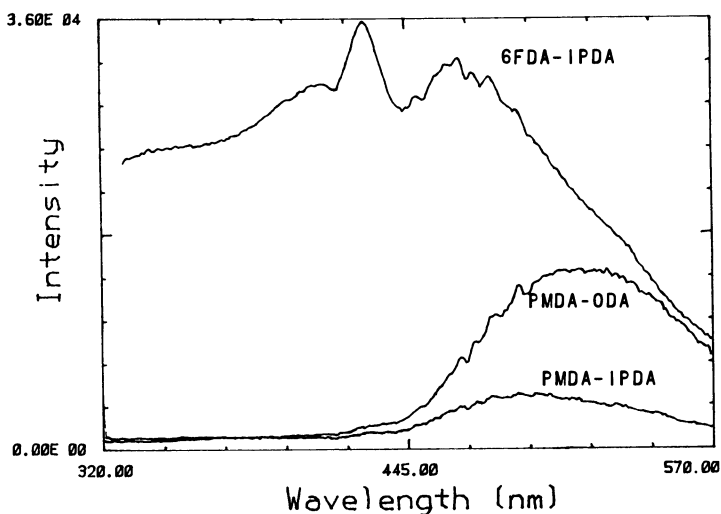

Figure 6. Excitation spectra of synthesized PMDA and 6FDA based polyimides with same cure history indicating effect of flexibility of diamine on relative intensity of PMDA-ODA vs PMDA-IPDA; and effect of flexible dianhydride on spectral structure and relative intensity of PMDA-IPDA vs 6FDA-IPDA.
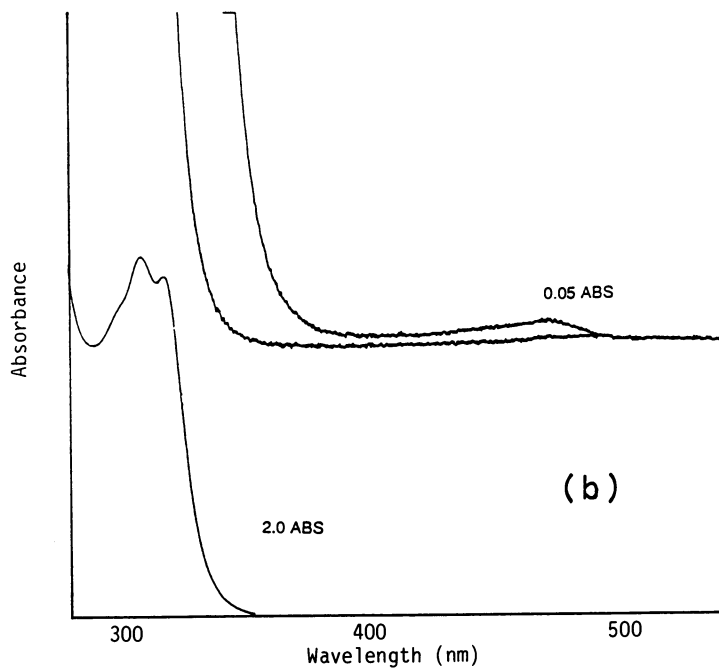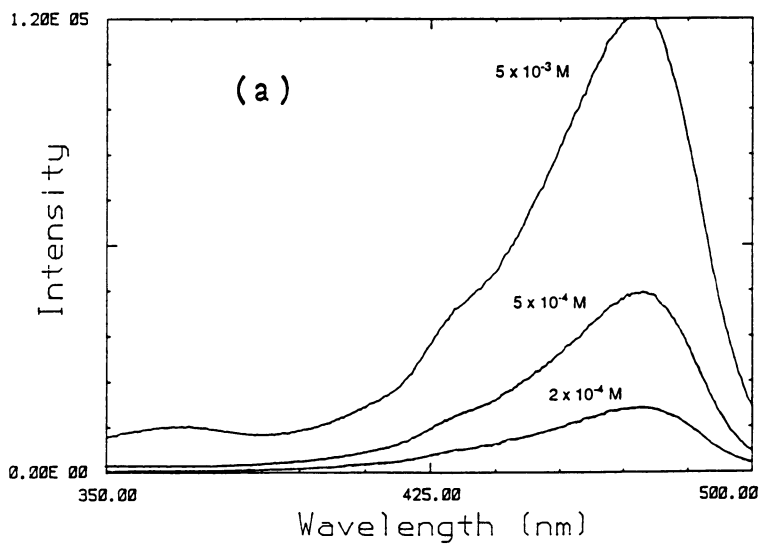
Figure 7. a)Excitation spectra as a function of concentration of PMDA in dioxane. b) Absorption spectrum of 5x10^{-4} M PMDA in dioxane for 2.0 and 0.05 relative absorbance full scale (ABS).
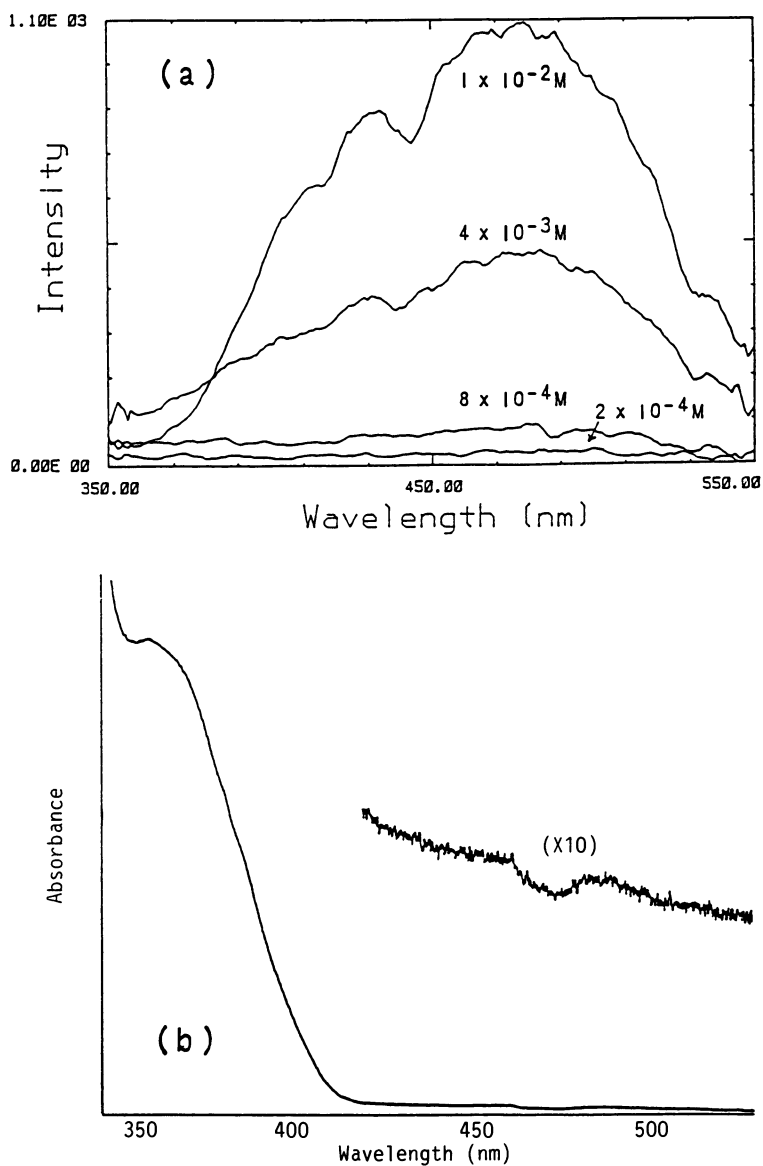
Figure 8. a) Excitation spectra as a function of concentration of BTDA in dioxane. b) Absorption spectrum of 10^{-3} M BTDA in dioxane for 0.2 and 0.02 relative absorbance full scale.
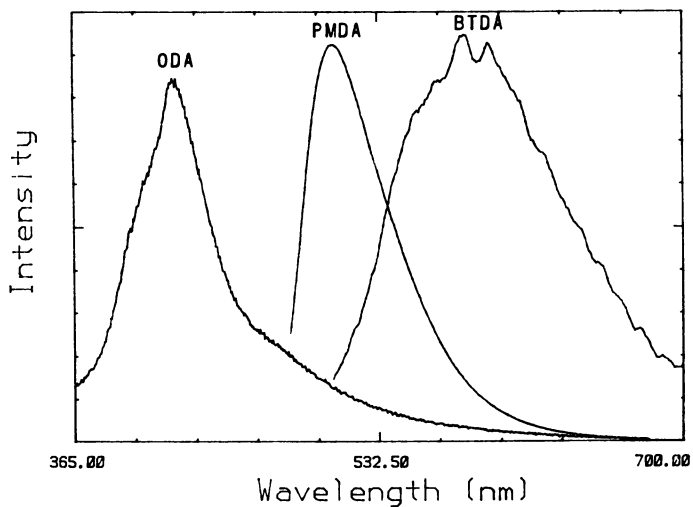
Figure 9. Emission spectra of ODA, PMDA and BTDA in dioxane. Full scale intensity is different for each compound: ODA, 2.0×10^4; PMDA, 2.5×10^5; BTDA, 1.2×10^3.

Table IV. Model Compound Spectral Maxima (nm)

Compound	Absorption	Excitation	Emission
PMDA	475	430 & 475	508
BTDA	490	431, 466, 479 & 489	580 & 593
ODA (10^{-6} M)	250 & 305	250 & 305	360
ODA (10^{-2} M)	250 & 305	350	420

The excitation and absorption spectra of ODA as a function of concentration are shown in Figures 10a and 10b, respectively. At low concentration, of about 10^{-6} M, the excitation maxima correspond to the absorption maxima; however, as the concentration is increased the excitation maxima red shift while the absorption maxima remains constant. At a concentration of ~10^{-2} M there is a single excitation peak with total self absorption for all wavelengths below 350 nm. The red edge absorption, excitation and emission band positions of ODA are summarized in Table IV.

Discussion

The objective in Part A is to identify the chromophores responsible for the fluorescence spectra of the films in the cure study. In Part B we will review the literature with respect to the aggregation and degree of ordering of polyimide with cure in order to interpret the change in fluorescence of the films with respect to changes in the morphology of polyimide with cure. In Part C we will relate the difference in spectra between supported and unsupported films to the effect of stress on morphology.

A. Assignment of Spectral Features. In comparing the absorption spectra of these polyimides to the excitation spectra obtained in this investigation it is apparent that fluorescence is obtained from excitation at the far red portion of the absorption spectrum. This is in agreement with our model compound studies. For the spectral region of interest our absorption spectra compare favorably with the spectra available in the literature (7,8). The ultraviolet spectroscopic properties of PMDA-ODA have been investigated by both Ishida et al (7) and Barashkov et al (8). Both groups describe a broad featureless absorption peak extending out as a "tail" to around 500 nm; Ishida observes that this peak is centered at 378 nm. We have found that excitation of the strong absorption maxima at wavelengths less than 340 nm results primarily in non-radiative decay. By contrast, excitation in this long wavelength "tail" or band results in the strongest emission. Thus, we will focus on the literature pertinent to description of this ~380 nm absorption band.

In a study of model compounds Ishida (7) showed that the tail is intrinsic to the pyromellitimide moiety and that the center of the peak associated with the tail became red shifted with the degree of conjugation provided by the substituents at either end of an N,N'-pyromellitimide. The absorption maximum red shifted from 345 nm to 356 nm in going from cyclohexyl to phenyl substitution and further to 371 nm with substitution of phenoxyphenyl. Furthermore, upon aromatic substitution the imide nitrogen changed its electronic character from tetrahedral- sp^3 to planar- sp^2. This shift of the absorption maximum to longer wavelength is consistent with an increase in electron delocalization afforded the pyromellitimide moiety with aromatic
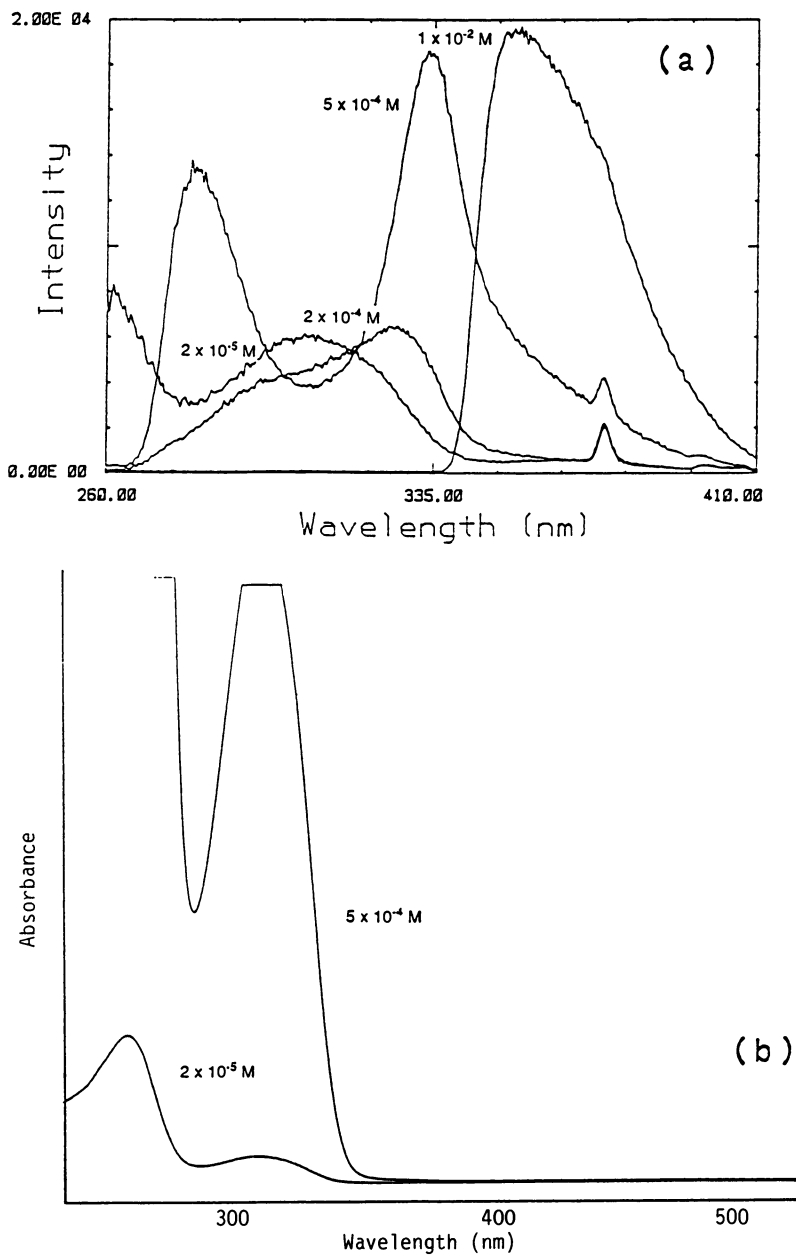
Figure 10. a) Excitation spectra as a function of concentration of ODA in dioxane. b) Absorption spectra as a function of concentration of ODA in dioxane, 2.0 relative absorbance full scale.

substitution. Conjugation of this type is maximized when the aromatic rings are coplanar with the pyromellitimide structure, thus allowing π-orbital overlap from the aromatic substituent to the pyromellitimide group. In addition, such an aromatic substituted pyromellitimide has the potential of forming a charge transfer complex between the aromatic substituent and the pyromellitimide. Thus the long wavelength absorption tail might be a single broad band, indicative of the loose binding nature of the ground state in a charge transfer complex (9). This concept will be expanded upon after discussion of the emission spectra. In our cure study, the short-wavelength excitation band of PI-2545 (PMDA-ODA) is 381 nm and corresponds both in position and shape to the absorption band described by Ishida for the pyromellitimide moiety in PMDA-ODA. Our observed short-wavelength excitation band for PI-2555 (BTDA-ODA) is centered at 350 nm. This blue shift, from PI-2545 to PI-2555, may be due to the reduction in conjugation of the BTDA moiety as compared to the PMDA moiety when the two phenyl rings of BTDA are rotated out of planarity at the center carbonyl.

Since the absorption spectra of our samples are identical in the region of interest, greater than 340 nm, to that reported by the above authors, it is reasonable to conclude that the observed fluorescence of the commercial polyimides is not due to an extrinsic chromophore. This is confirmed by the observed fluorescence of the polyimides supplied by Dow. Barashkov et al (8) observed fluorescence from the PMDA-ODA polyamic acid precursor and an N,N'-diphenyloxide pyromellitimide model compound, but did not observe polyimide fluorescence. Similarly, Dickinson and Sung (4) observed fluorescence from the polyamic acid precursor of 6FDA-NDA but did not observe any fluorescence from the polyimide. However, Dickinson and Sung report a decrease in emission intensity for illumination at the absorption maximum, where we have found the fluorescent response to be at a minimum, indicating that they may not have investigated excitation at the red edge of the absorption spectrum.

An excitation spectrum is analogous to an absorption spectrum and can hence be similarly used to identify the absorbing chromophores. The observed excitation spectra of PMDA, BTDA and ODA can thus be used to elucidate the PMDA-ODA and BTDA-ODA polymer excitation spectra. Although PMDA and BTDA are dianhydrides rather than diimides, the n->π* transition from delocalization of the nitrogen lone pair to the carbonyl in the diimide, as described by Matsuo (10) for the case of N-substituted maleimides, should be similar in nature to that of delocalization of the oxygen lone pair to the carbonyl in the dianhydride. The fact that the excitation λ_{max} of PMDA, BTDA and concentrated ODA are red shifted with respect to the absorption maxima is consistent with the excitation spectra of PMDA-ODA and BTDA-ODA. In addition, the total self absorption of short wavelength illumination in concentrated ODA might explain the lack of fluorescence from short wavelength illuminated polyimides made from ODA.

Early absorption work was done by Matsuo (10) and Nurmukhametov et al (11) but we refer to more recent work by Ishida et al (7), who assigned the 300-330 nm absorption band of PMDA-ODA to a π->π* transition of the central phenyl ring and the long wavelength absorption band to an n->π* transition that red shifts and intensifies to a π->π* transition upon conjugation of the nitrogen atom with aromatic substitution.

In our model compound study we observe both a weak absorption band and a corresponding strong excitation band at 475 nm for PMDA

and 490 nm for BTDA, with no observable activity in the 350 to 380 nm range. For concentrated ODA the excitation spectrum, consisting of a single peak at 350 nm, is significantly red shifted relative to its absorption spectrum. However, neither absorption spectrum has a band corresponding to the ~380 nm band in PMDA-ODA. By contrast, Ishida's study of substituted pyromellitimides (7) reports only absorption peaks in the 345 to 371 nm range with a tail extending to longer wavelengths. This apparent lack of an absorption band attributable to either of our model compounds in the ~380 nm region can be explained by reference to Kotov et al (12) who found similar results and attributed this band to a charge transfer complex, CTC, in the polymer. Following Ishida, we also attribute PMDA-ODA absorption in the 370 - 380 nm range to a $\pi \rightarrow \pi^*$ transition of the aromatic substituted pyromellitimide moiety. This absorption range corresponds to our short-wavelength excitation band; thus we attribute excitation in this band to the same $\pi \rightarrow \pi^*$ transition. This band may arise due to the conjugation of an aromatic ring of the diphenyl ether moiety with the adjacent aromatic ring in the pyromellitimide moiety. This conjugation occurs when the two are coplanar, with sp^2 hybridization of the nitrogen electrons.

The long-wavelength excitation band can be attributed to an n-> π^* transition of the carbonyl groups of the pyromellitimide moiety. This syllogism is drawn both from experimental observations and the transition rules of photochemistry: (1) The excitation spectra of PMDA and BTDA model compounds correspond in position as well as some of the general structure to their respective polymers (i.e. the 430 and 475 nm peaks of PMDA as compared to the 430 and 467 nm peaks of supported PMDA-ODA, and the 431, 466 and 489 nm peaks of BTDA as compared to the 427, 465 and 486 nm peaks of supported BTDA-ODA). (2) The excitation spectra of these model compounds are devoid of any intensity in the short-wavelength region where, according to the above discussion, a conjugating substituent is necessary for the observed $\pi \rightarrow \pi^*$ transition. (3) n-> π^* transitions occur at longer wavelengths than $\pi \rightarrow \pi^*$ transitions. (4) n-> π^* transitions are symmetry forbidden and thus less strongly absorbing than $\pi \rightarrow \pi^*$ transitions (9), which may explain the small absorptivity of the model compounds and polyimides in the region of the long-wavelength excitation maxima. (5) An excitation spectrum of the intensity of the Raman lines associated with specific groups in PMDA-ODA (7) shows a decrease in intensity with wavelength, from 340 to 540 nm, for all of the groups except the carbonyls which increase and peak at about 490 nm corresponding to our long-wavelength excitation band.

The excitation spectrum of the synthesized PMDA-ODA film, Figure 5, which was cured unsupported is identical in terms of shape and position to that of the excitation spectra of the unsupported PI-2545 films, reaffirming that the observed fluorescence in PI-2545 is intrinsic to PMDA-ODA. Furthermore, by comparing the PMDA model compound spectrum with that of the synthesized PMDA-ODA film and the PI-2545 films that were cured unsupported one can confirm the assignment of the long-wavelength excitation band to the PMDA moiety. This conclusion is supported by the fact that all three spectra are similar both in shape, being broad and unstructured, and position, with maxima at around 500 nm.

In comparing the unsupported film excitation spectra of PI-2555 to that of PI-2545 one notices a hint of structure in the long-wavelength band of PI-2555, which can similarly be attributed to the BTDA moiety. It is important to note that the BTDA model compound spectrum has some structure to it in the region of this excitation

band. This structure is probably due to the ability of BTDA to rotate at the central carbonyl thus reducing the symmetry of the dianhydride. Evidence of this effect can be seen in a comparison of the excitation spectra of 6FDA and PMDA based polyimides. This indicates that this long wavelength spectral structure may be due to the addition of a flexible linkage in the otherwise similarly symmetric 6FDA based polyimides, thus having the ability of being electronically asymmetric. This may explain some of the structure in the excitation spectra of PI-2555 (BTDA-ODA), 6FDA based polyimides and the BTDA model compound that is not observed in either the PMDA based polyimides or in the PMDA model compound.

If we accept the proposal that absorption in the short-wavelength excitation band results in a π->π* transition and in the long-wavelength excitation band results in a n->π* transition, then the resulting emission could be due to a single π*->π transition of the pyromellitimide moiety. Excitation of either the short- or long-wavelength excitation bands in either PI-2545 or PI-2555 results in a similar emission spectrum for each. This similarity in emission spectra suggests that the emission chromophore is the same for both excitation wavelengths. Since we have shown that there are two different absorbing chromophores we conclude that some sort of charge transfer is invoked either prior to or during emission so as to obtain emission from a single chromophore. This is supported by the red shift of the polyimide emission spectrum as compared to that of the dianhydride and diamine moieties. Most notably, the emission λmax of PMDA-ODA is 610 nm as compared to 508 and 420 nm for PMDA and ODA, respectively. A CTC from a phenyl ring in the diphenyl ether moiety to the pyromellitimide moiety is reasonable given their electron donating and withdrawing properties, respectively.

Charge transfer complex formation in aromatic polyimides has been cited by a number of authors, including: (12,13). The absorption of a variety of individual dianhydride and diamine fragments, their complexes and the polyimides formed was measured and the conclusion was drawn that the long wavelength absorption tail, which corresponds to our short-wavelength excitation band, is due to the formation of a complex because the tail was only present in the presence of both donor and acceptor fragments (12). The conduction of a variety of polyimides was found to be a function of the electron affinity of the dianhydride acceptor, providing evidence for the donor-acceptor property of CTC formation (13).

The comparison of our model compound study with that of Ishida (7), suggests that excitation of the short-wavelength band results in charge transfer from the diamine moiety to the dianhydride moiety. An intramolecular CTC can occur when the pyromellitimide and diphenyl ether groups are coplanar. In such a configuration charge transfer can occur intramolecularly from the donor to acceptor fragments across the conjugated π-orbital network. The increase in emission intensity, from excitation in the short-wavelength band, with cure is then due to an increase in the population of the coplanar state. We have previously depicted this rotation around the nitrogen-phenyl bond to form the coplanar state (2). As intensity is proportional to population, the observed activation energy of emission from short-wavelength band excitation must be associated with rotation around the nitrogen-phenyl bond. Rotation of the amino-phenyl bond in N,N-dimethyl aminobenzonitrile has been shown to result in the formation of a twisted intramolecular charge transfer complex (14). This was investigated using fluorescence spectroscopy and found to have an activation barrier of ~7 kcal/mole in concentrated solution,

comparable to that found in this investigation. This local torsional rotation around the amino-phenyl bond is analogous to what we believe occurs with cure in polyimide. Moreover, the reported activation energy is in line with our observed thermal activation energy as well as with the expected heat of formation of a charge transfer complex, which is on the order of 5 kcal/mole (9).

As a separate activation energy was observed for each of the two excitation bands it is possible that there is a second change in conformation with cure associated with the long-wavelength excitation band and hence the dianhydride fragment. If a second CTC is formed that is intermolecular in nature then there might be two different morphologies. The increase in aggregation resulting in a decrease in the intermolecular distance between adjacent chromophores might then result in an increase in fluorescence of adjacent parallel chromophores. This parallel overlap of dianhydride and diamine moieties, in the ordered region of polyimide, has been depicted in the folded-chain structure of Isoda et al (15).

Evidence for an intermolecular CTC between adjacent parallel cromophores can be derived from the results of Kotov et al (12). If an intermolecular CTC between the diamine and dianhydride fragments is associated with emission from polyimide, then the emission intensity should increase with decreasing intermolecular distance. The emission intensity from excitation in the long-wavelength band of a series of PMDA based polyimide films, with differing flexibility of the central linkage in the diamine, linearly increases with increasing reciprocal intermolecular distance, Figure 11. This result is repeated with thermal treatment of 6FDA-IPDA and falls along the same line. Thermal treatment at 250 °C results in a 5.7 Å intermolecular spacing (d) and a subsequent 310 °C cure results in a reduction in d to 5.2 Å and a concomittant increase in emission intensity. Therefore, this reduction in intermolecular distance may result in the formation of an intermolecular CTC between adjacent chromophores that gives rise to an increase in emission intensity for excitation of the long-wavelength excitation band.

B. Molecular Ordering. The degree of aggregation of polyimide increases with cure. However, the morphology of the aggregated region is currently still a subject of controversy (15-20). A comparison of X-ray data to theoretical calculations (18) resulted in a theory for aromatic polyimide crystalline structures whereby the polyimide molecules orient themselves in parallel planar groups. Potential energy wells were calculated for rotation of main chain phenyl rings in and out of parallel alignment. These calculations indicated that, below a certain limit in oscillation amplitude, torsional oscillations of phenyl rings are mainly determined by the intramoleculer barrier for hindered rotation. However, as the packing density increases, intermolecular repulsion between adjacent rings becomes the dominant force. Furthermore, adjacent phenyl rings could undergo free rotation unhindered by intermolecular interactions if they were separated by an intermolecular distance of 6.6 Å or more. However, an intermolecular spacing of 5.2 Å would result in a barrier of 400 kcal/mole that would be prohibitive to phenyl rotation.

These values can be compared with the intermolecular spacing in the most highly ordered state reported in the literature, 4.7 to 4.9 Å (19), as well as the results for a variety of polyimides tabulated in Table III. This indicates that for highly ordered polyimide the rotational orientation of phenyl rings is fixed. The magnitude of the intermolecular spacing also requires that the adjacent phenyl rings associated with the diamine moiety be fixed coplanar with the imide
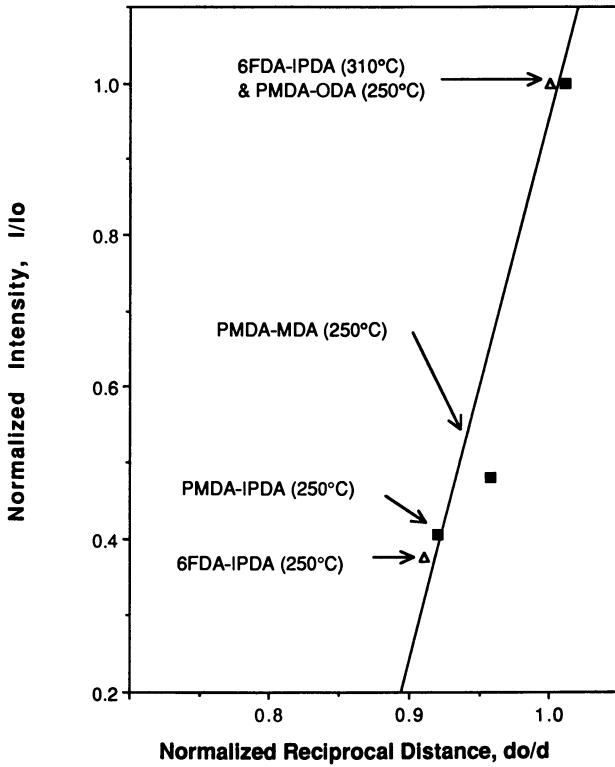
Figure 11. Normalized intensity as a function of normalized reciprocal distance for substituted PMDA polyimides and thermally treated 6FDA-IPDA.

moiety in highly ordered polyimide. However, there could be sufficient intermolecular spacing to allow rotation of phenyl rings around non-cyclic main chain bonds in disordered polyimide in solution, in the partially cured (< 200 °C cure) condensed state or in the amorphous region of a fully cured film.

Changes in the morphology of polyimide either as an amorphous to crystalline phase transition or as an increase in the localized aggregation of a mesomorphic phase can be fully described by conformational changes associated with the nitrogen-phenyl and ether linkages in PMDA-ODA and additionally the carbonyl linkage in BTDA-ODA. The increase in ordering of polyimide with cure has been associated with short-range changes in conformation. Due to the 109° bond angle in the ether linkage any rotation around the oxygen-phenyl bond would result in a change in the long-range ordering, unless cooperative rotation occurred along the chain. The pyromellitimide moiety, defined by the region across the acid dianhydride fragment from one nitrogen-phenyl bond to another, is a planar structure in PMDA-ODA. Cooperative rotation of the nitrogen-phenyl bonds on either end of this moiety results in a short-range (single segment) change in molecular ordering. The reduction in free energy of such a rotation to the planar conformation is twofold. First, the energy of conjugation, when the pyromellitimide moiety is coplanar with the phenyl rings on either side, is energetically favorable due to the electron delocalization made available by the π-orbital overlap in the coplanar structure. Second, rotation around the nitrogen-phenyl bond to form the coplanar structure allows closer packing of adjacent chains oriented in the same direction thereby obtaining a more ordered and lower energy state. This lower energy state is necessary in order to form the crystalline structure (19). Thus the emission intensity can be used as a local torsional probe of the nitrogen-phenyl bond to determine the relative population of the coplanar structure and in so doing infer the relative degree of ordering.

C. Supported Films. Sample preparation plays a large part in the morphology of polyimide and hence any reported analytical results. One consequence of sample preparation is that imposition of an external strain during cure can enhance the degree of ordering and impart a direction of orientation to the sample. Differing results may be obtained depending on whether the sample undergoes uniaxial strain (as in fibers), biaxial strain (from spinning on wafers) or if the sample is cured as a free standing film.

The in-plane ordering and biaxial stress of spun cast polyimide films is well documented (16,17,21) and so is the effect of stress on the electronic transitions (22,23). Iida et al (22) found that irradiation of polyimide at approximately 350 and 460 nm resulted in photoinduced current. Since these wavelengths correspond to the same excitation bands utilized in this investigation, it is quite possible that the fluorescence observed in the present study and the photogeneration of conduction electrons are related. Iida also found that the photocurrent strongly depended on the molecular ordering. Stretching of previously cured films at room temperature resulted in an increase in photocurrent and a reduction of molecular ordering, as determined by monitoring the intermolecular spacing with X-ray scattering. Wellinghoff et al (23) have shown that the phenoxyphenyl group, incorporated in polyimide and lying outside the crystalline region, will rotate around the nitrogen-phenyl bond in response to a tensile stress along the film plane. This rotation results in a change in the electron hybridization of nitrogen from sp^2 in the planar structure to that of sp^3 in the rotated structure. These

results indicate that the room temperature stretching of a previously cured polyimide films results in the reduction of molecular ordering and rotation of the nitrogen-phenyl bond away from the preferred orientation. It is possible that supported films cured under conditions of in-plane biaxial stress increase their degree of ordering since they are thermally able to relieve stress by segmental motion. By contrast, previously cured films stretched at room temperature reduce their degree of ordering to accommodate strain.

Comparison of the excitation spectra of supported and unsupported films suggests that the majority of the structure in the spectra of the supported films is due to the in-plane stress of the spun cast film. This stress may arise from the spinning process as well as the densification of the film during curing. The position of the long-wavelength band excitation maximum in the unsupported films corresponds to the far red peak in the excitation spectrum of the supported film. All of the spectral structure of this band at shorter wavelength from this peak can then be attributed to the change in conformation of the chain due to the in-plane stress.

The relative intensities of the two excitation bands can be used to suggest the morphology of the supported as compared to the unsupported films. The relative intensity of the short-wavelength excitation band, which we attributed to rotation of the nitrogen-phenyl bond, is much greater in the supported films than in the unsupported films. This indicates that the population of the coplanar state in the unsupported films is relatively much less than the conformation or morphology associated with the long-wavelength excitation band. Conversely, we conclude that the in-plane stress during curing results in an increase in the population of the coplanar conformation.

While the relative intensities of the two excitation bands of PMDA-ODA indicate that the morphology associated with the intermolecular CTC is preferred in unstressed films, the apparent activation energies of these films indicate no change due to stress. On the other hand, the two activation energies of unsupported BTDA-ODA diverged as compared to the activation energies of the supported films. This difference between the effect of stress on the apparent activation energies of PMDA-ODA and BTDA-ODA must be related to the ability of the central carbonyl of BTDA to rotate in order to accommodate stress.

The exact nature of the stressed conformation is not known but it may in some way relate to the two dimensional ordering of the supported films as compared to the isotropic morphology of the unsupported films.

Conclusions

Fluorescence spectroscopy can be used to monitor the degree of cure of polyimide. The observed increase in emission intensity, from illumination in the short-wavelength excitation band, with cure is due to the formation of an intramolecular CTC associated with coplanarization of the diamine and dianhydride fragments. Excitation of the dianhydride fragment, in the long-wavelength excitation band, results in fluorescence that is affected by the intermolecular distance associated with the increase in aggregation and may be due to the formation of an intermolecular CTC. An interesting result of this investigation is the apparent effect of stress on the excitation spectra of polyimide. This warrants further investigation.

Literature Cited

1. Russell, T. P. J. Polym. Sci. Polym. Phys. Ed., 1984, 22, 1105.
2. Wachsman, E. D.; Frank, C. W. Polymer, 1988, 29, 1191.
3. Springman, M. Semiconductor Materials Group, Du Pont, personal communication.
4. Dickinson, P.; Sung, C. S .P. ACS Preprints, Toronto, 1988.
5. O'Brien, K. C.; Koros, W.J.; Husk, G. R. J. Membrane Sci., 1988, 35, 217.
6. O'Brien, K. C. Dow Chemical USA, Walnut Creek Research Center, personal communication.
7. Ishida, H.; Wellinghoff, S. T.; Baer, E.; Koenig, J. L. Macromolecules, 1980, 13, 826.
8. Barashkov, N. N.; Semenova, L. I.; Nurmukhametov, R. N. Vysokomol. Soyed., 1983, A25, 1090.
9. Rao, C. N. R. Ultra-Violet and Visible Spectroscopy, 3rd Ed, Butterworth, London, 1975, Chapter 2; ibid., 164.
10. Matsuo, T. Bull. Chem. Soc. Jpn., 1964, 37, 1844; ibid., 1965, 38, 557.
11. Nurmukhametov, R. N.; Belaits, I. L.; Shigorin, D. N. Russ. J. Phys. Chem., 1967, 41, 1032.
12. Kotov, B. V.; Gordina, T. A.; Voischchev, V. S.; Kolninov, O. V.; Pravednikow, A. N. Vysokomol. Soyed., 1977, A19, 614.
13. Fainshtein, Y. B.; Igonin, L. A.; Lushcheikin, G. A.; Yemel'yanova, L.N. Vysokomol. Soyed., 1976, A18, 580.
14. Hayashi, R.; Tazuke, S.; Frank, C. W. Macromolecules, 1987, 20, 983.
15. Isoda, S.; Shimada, H.; Kochi, M.; Kambe, H. J. Polym. Sci. Polym. Phys. Ed., 1980, 13, 1293.
16. Russell, T. P.; Gugger, H.; Swalen, J. D. J. Polym. Sci. Polym. Phys. Ed., 1983, 21, 1745.
17. Takahashi, N.; Yoon, D. Y.; Parrish, W. Macromolecules, 1984, 17, 2583.
18. Krasnov, Y. P.; Stepanyan, A. Y.; Mitchenko, Y. I.; Tolkachev, Y. A.; Lukasheva, N. V. Vysokomol. Soyed., 1977, A19, 1566.
19. Kazaryan, L. G.; Tsvankin, D. Y.; Ginzburg, B. M.; Tuichiev, S.; Korzhavin, L. N.; Frenkel, S. Y. Vysokomol. Soyed., 1972, A14, 1194.
20. Milevskaya, I. S.; Baklagina, Y. G.; Sidorovich, A. V.; Korzhavin, L. N.; Lukasheva, N.V. Zh. Strukt. Khimii., 1981, May-June, 22, 42.
21. Elsner, G. J. Appl. Polym. Sci., 1987, 34, 815.
22. Iida, K.; Waki, M.; Nakamura, S.; Ieda, M.; Sawa, G. Jpn. J. Appl. Phys., 1984, 23, 1573.
23. Wellinghoff, S. T.; Ishida, H.; Koenig, J. L.; Baer, E. Macromolecules, 1980, 13, 834.

RECEIVED February 2, 1989

Chapter 3

Dynamic Fourier Transform–IR Analysis of Cure Reactions and Kinetics of Polyimides

Randy W. Snyder[1] and Paul C. Painter[2]

[1]IBM Corporation, Endicott, NY 13760
[2]Pennsylvania State University, University Park, PA 16802

A dynamic method for acquiring and treating infrared
spectroscopic data from the imidization of a number of
polyimide systems is presented. In situ FT-IR analysis
of polymer reactions is preferred when doing comparitive
studies on a number of polymer systems. For systems
where these reactions occur at relatively high tempera-
tures, it is often difficult to obtain good isothermal
data for determining kinetic parameters. Kinetic data
for several polyimide systems are shown and compared.

Polyimides are used extensively in the electronics industry as
dielectric and passivation layers in electronic devices. The curing
behavior of these systems is often an important consideration,
especially in situations where etching is performed at intermediate
cure levels. Infrared spectroscopy has proven to be useful for
following the level of imidization of polyimides (1-4). One of the
problems associated with performing kinetic studies on these systems
is the high temperatures that must be used for imidization to take
place. Isothermal studies are often tedious, with multiple samples
being required at each time / temperature combination due to the
additional curing that can occur during heating and cooling the
samples (5). Such time consuming tasks are inappropriate when
evaluating a number of polyimides (or other reacting systems) or
evaluating lot to lot variations. In situ infrared isothermal
studies are difficult to perform as accessories with sufficient
heating rates and rapid stability at high temperature are not
readily available.
     A method for determining kinetic parameters from dynamic
infrared data was developed to overcome the problems listed above
(4). Through the use of constant temperature ramps, appropriate
instrument software (6) (Sheen, C. W.; Snyder, R. W. Computers &
Chemistry, in press) and spreadsheet techniques the activation
energy and pre-exponential factor for any reacting system can be
obtained in a few hours. When performing this dynamic kinetic
analysis however there are some effects which must be accounted for

in order to correctly interpret the data. With polyimide systems
there is a temperature effect on the intensity of the 1780 cm-1
(imide) band that must be examined, and a correction in the area
data must be made to relate the data to a constant temperature (7).
        This paper shows the kinetic data for the imidization reaction
of several polyamic acids and polyamic acid derivatives. An
evaluation of the data with respect to polymer chain chemistry and
acid substitution is given.

Experimental

Thin film samples were prepared by spin coating 15% solutions of the
polyamic acids shown in Table I (structures are shown in Figure 1)
onto 13-mm X 2-mm NaCl disks using a spin coater running at 5000 RPM
for 30 sec. The samples were cured in an Accuspec Model 20 high
temperature cell, which utilizes a linear temperature programmer for
sample heating. A constant heating rate was achieved by setting the
initial temperature well below start of the reaction, the endpoint
on the temperature programmer to a high temperature (normally 550°C
is sufficient) and turning the programmer off after the reaction is
completed (approximately 250-300°C). Heating rates of 5°C/min were
utilized for the kinetic experiments. The actual temperature of the
sample was monitored using a K-type thermocouple, attached to the
heater element in the immediate vicinity of the sample, and a
Digi-Sense Thermocouple Thermometer.
        Infrared spectra were obtained on an IBM Instruments FT-IR/98
spectrometer utilizing 10 averaged scans at 4 cm-1 resolution and a
liquid nitrogen cooled MCT detector. Data collection was performed
utilizing the GC-IR software routines as described previously (6) or
using the standard collection routines which can collect four
spectra per minute. Peak areas were obtained using the MAXAREA
program which can determine endpoints for integration after input of
the peak maximum (Sheen, C. W.; Snyder, R. W. Computers & Chemistry,
in press). The band near 1780 cm-1, symmetric stretch of the imide
carbonyl, is normally used for following the progress of the
imidization reaction (see Figure 2). However, it has been shown
that this band is strongly influenced by temperature (7) (see Figure
3), so the band area for each spectrum was corrected to that which
would be measured at 25°C prior to kinetic calculations.
        The kinetic parameters may be calculated using the equation

$$\ln(-dC/dT) - \ln(C/m) = \ln(A) - Ea/RT \tag{1}$$

where m is the heating rate, C is one minus the concentration of the
absorbing species (1780 cm-1 band area), R is the gas constant and T
is the current temperature of the reaction. The -dC/DT values can
be determined from the slope of the lines between points in a plot
of the concentration of the reacting species versus temperature (see
Figure 4). The concentration, used for ln(C/m), is then the
concentration at the midpoint of the line. These values are then
plotted versus reciprocal temperature to obtain Ea and A (see Figure
5). Standard deviations for Ea were determined from scatter in the
data using a 95% confidence interval.

Figure 1. Polyamic acid structures and their derivatives.

Figure 2. Infrared spectra of PMDA/ODA polyimide at three stages of cure.
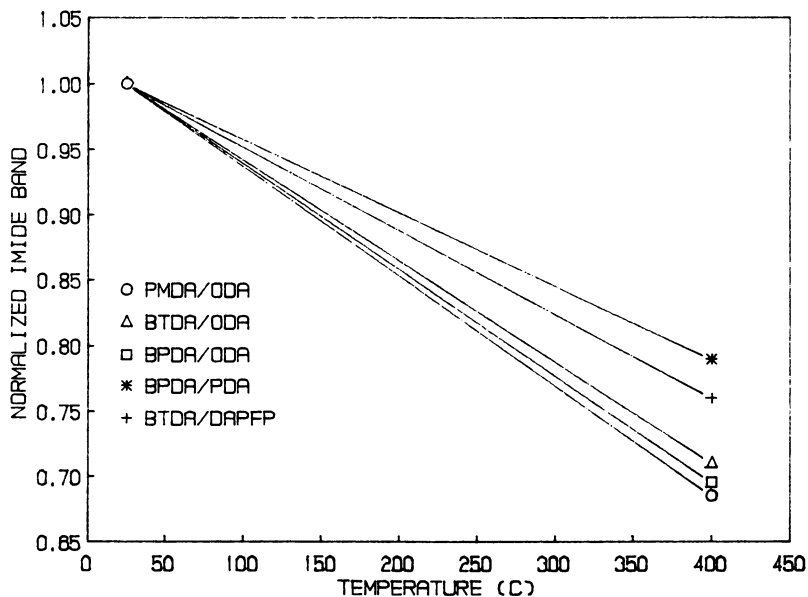
Figure 3. Plot showing the effect of temperature on the 1780 cm^{-1} band in several polyimides. The slope of the line appears to be affected by the structure of the amine.
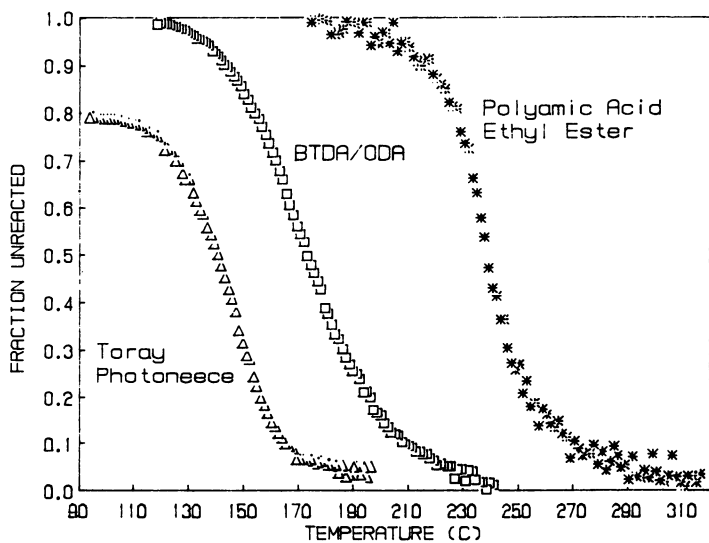
Figure 4. Plot of imide concentration versus temperature for Toray Photoneece, BTDA/ODA polyamic acid, and an ethyl ester of PMDA/ODA.

A recent re-evaluation of the data has shown that a better fit can be obtained using the equation for 2nd order reaction kinetics:

$$\ln(-dC/dT) - \ln(C^2/m) = \ln(A) - Ea/RT$$

(2)

(This fit can be seen in Figure 6.) Only small differences are observed between calculated parameters using the two equations. We have no chemical reason for assuming 2nd order kinetics for the imidization reaction, so we chose to calculate all kinetic parameters shown in this paper using the Equation 1. Work is in progress to address the descrepancy in the fit of the data.

Results and Discussion

Activation energies for the polyimide systems tested are shown in Table I, and the calculated reaction rates for imidization are included in Table II. There are some differences in the kinetic

Table I. Imidization Kinetic Parameters

POLYIMIDE	Ea (Kcal/mol)	ln(A) (min-1)
PMDA/ODA	28 ± 2	29.5
BTDA/ODA	22 ± 2	22.8
BPDA/ODA	16 ± 1	15.3
BPDA/PDA	14 ± 1	13.8
BTDA/DAPFP	21 ± 1	22.1
Toray Photoneece *	26 ± 1	29.7
PMDA/ODA Ethyl Ester	42 ± 2	40.3

* Toray Photoneece is a tertiary amine salt of BTDA/ODA polyamic acid.

Table II. Reaction Rate Constants for Polyimides (min-1)

POLYAMIC ACID	150°C	200°C	250°C
PMDA/ODA	2.2×10^{-2}	7.5×10^{-1}	12.9
BTDA/ODA	3.4×10^{-2}	5.4×10^{-1}	5.1
BPDA/ODA	2.4×10^{-2}	1.8×10^{-1}	0.9
BPDA/PDA	5.7×10^{-2}	3.3×10^{-1}	1.4
BTDA/DAPFP	5.6×10^{-2}	7.8×10^{-1}	6.6
Toray Photoneece	2.9×10^{-1}	7.7	108.0
PMDA/ODA Ethyl Ester	6.3×10^{-5}	1.2×10^{-2}	0.9
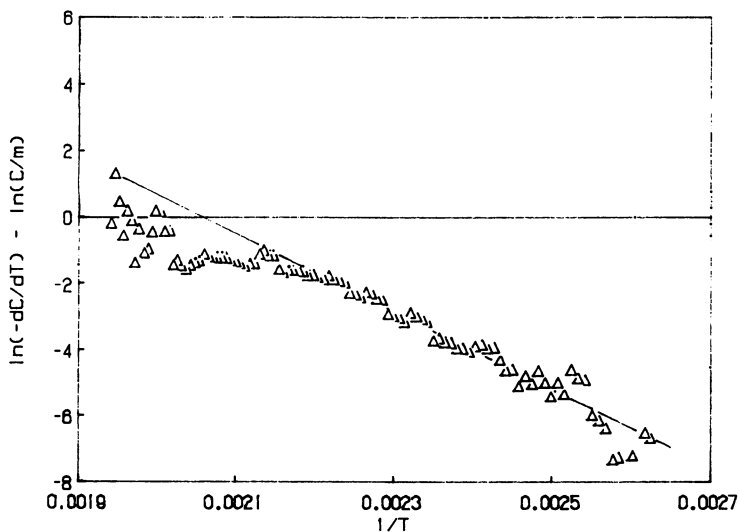
Figure 5. Plot of kinetic data for the curing of PMDA/ODA
polyimide using Eq. 1. The slope of the line yields Ea and ln(A)
is obtained from the intercept.
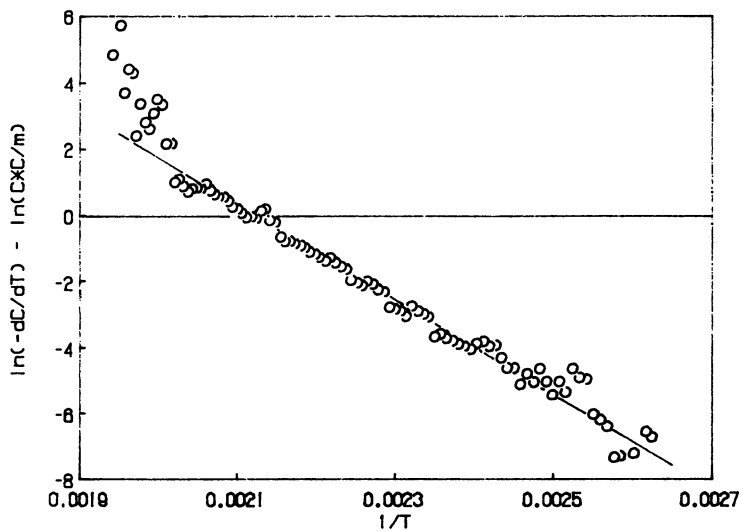
Figure 6. Plot of kinetic data for the curing of PMDA/ODA
polyimide using Eq. 2. The slope of the line yields Ea and ln(A)
is obtained from the intercept.

parameters for imidization of the different polyimides that appear
to be dependent on the structure of the dianhydride used to form the
polyimide. A change from PMDA/ODA to BPDA/ODA gives in a large
decrease in the activation energy. The effect of this decrease is
not obvious in the calculated reaction rate constants until higher
temperatures (> 200°C) are achieved, so it appears that it is
related to the flexibility of the polyimide structure. Most of the
variability is observed when changing dianydrides in the structures,
with very little change observed when the dianhydride remains
constant. Further work will have to be performed to more firmly
establish this correlation, but it seems plausible that such an
effect should occur as the flexibility of the chain could affect the
ability of the reacting species to interact.

The differences between the curing of the polyamic acids and
their tertiary amine salts or esters is even larger. The Toray
Photoneece photosensitive polyimide (which is a tertiary amine salt
of BTDA/ODA polyamic acid) begins reacting at much lower
temperatures and the reaction is completed faster during the
temperature ramp (see Table 2 and Figure 4). This effect is
consistent with work of Kruez et al. (1) on tertiary amine salts of
PMDA/ODA polyamic acid.

The effect of esterifying the polyamic acid on the cure rate is
opposite that of the amine salt. The imidization reaction requires
a much higher temperature than the polyamic acid, from which it was
derived, before it will begin. However, once the temperature is
reached where the reaction can begin, it does not require a the
large increase in temperature, as with the polyamic acid, to give a
relatively high reaction rate constant (see Table II). The slope of
the curve in Figure 4 for the ester is very high and this results in
the high calculated activation energy shown in Table I. This may be
the result of forcing the equilibrium of the reaction more heavily
towards the imide species by having a leaving group (ethanol) that
is less likely to react with the imide than the water given off by
the polyamic acid.

Both the amine salt and ester results are consistent with the
mechanism for imidization proposed by Kruez et al. (1) where it is
speculated that an intermediate species contains a carboxylate ion.
In the case of the amine salt, the ion is already present and not
much energy is required to cause ring closure. While with the ester
it would be much more difficult to form the carboxylate ion
intermediate and therefore the beginning of the reaction would be
somewhat slower.

CONCLUSIONS

The dynamic kinetics FT-IR method is an effective means of studying
high temperature curing reactions in polymers. Both the acid group
substitution and polymer backbone appear to have strong influences
on the rate of imidization in polyimides. The dianhydride used to
make the polymer appears to have a greater effect on the kinetics
than does the diamine.

Literature Cited

1. Kreuz, J. A.; Endrey, A. L.; Gay, F. P.; Sroog, C. E. <u>J. Polym.
   Sci.: Part A-1</u> 1966, <u>4</u>, 2607.
2. Denixov, V. M.; Kol'tsov, A. I.; Mikhailova, N. V.; Nikitin, V.
   N.; Bessonov, M. I.; Glukhov, N. A.; Shcherbakova, L. M. <u>Polymer
   Sci. USSR</u>, 1976, <u>18</u>, 1780.
3. Koton, M. M.; Meleshko, T. K.; Kudryavtsev, V. V.; Nechayev, P.
   P.; Kamxolkina, Ye. V.; Bogorad, N. N. <u>Polymer Sci. USSR</u> 1982,
   <u>24</u>, 791.
4. Snyder, R. W.; Sheen, C. W. <u>Appl. Spectrosc.</u> 1988, <u>42</u>, 655.
5. Snyder, R. W.; Sheen, C. W.; Painter, P. C. In <u>The Proceedings
   of the Symposium on Polymeric Materials for Electronic Packaging
   and High Technology Applications</u>, J.R. Susko, R.W. Snyder and
   R.A. Susko, Eds., The Electrochemical Society, Vol. 88-17, 1988,
   71.
6. Snyder, R. W.; Sheen, C. W. <u>Appl. Spectrosc.</u> 1988, <u>42</u>, 296.
7. Snyder, R. W.; Sheen, C. W.; Painter, P. C. <u>Appl. Spectrosc.</u>
   1988, <u>42</u>, 503.

Chapter 4

Polyimide Hydrolysis

Measurement by Fourier Transform–IR Spectroscopy

Coralie A. Pryde

AT&T Bell Laboratories, Murray Hill, NJ 07974

IR spectroscopy may be used to follow two reactions occurring in polyimides exposed to high temperatures and humidities: hydrolysis of the imide linkages and hydrolysis of residual anhydride end groups. The hydrolytic susceptibilities of several polyimides were measured at 90°C/95% R.H. Polymers based on benzophenone tetracarboxylic acid dianhydride (with either oxydianiline or m-phenylene diamine) appeared to undergo rather rapid hydrolysis initially, but the reaction had essentially halted by the time the measured imide content had decreased by 5-6%. Polymers based on 3,3',4,4'-biphenyl tetracarboxylic acid dianhydride (with p-phenylene diamine) and pyromellitic dianhydride (with oxydianiline) showed no significant imide hydrolysis. In all the polymers, the anhydride was hydrolyzed quite readily.

Because of their excellent thermal stability, polyimides are considered as strong candidates for use as interlevel dielectrics in a variety of advanced packaging applications. However, the actual dielectric properties of most standard aromatic polyimides are generally considered to be only just adequate for such uses. Therefore it is important to determine whether or not degradative reactions that might occur in processing or during use could cause any significant deterioration in these dielectric properties. One such question is whether or not polyimides are susceptible to any hydrolytic reactions during long-term use.

A number of reports (1,4) have demonstrated that, during the thermal cure of polyamic acids, dissociation to give free amine and anhydride end-groups competes with closure to the imide ring. Therefore, as indicated in Scheme I, polyimides exposed to high temperatures and humidities might be expected to undergo three different hydrolysis reactions: 1) hydrolysis of anhydride remaining after cure, 2) hydrolysis of imide rings and 3) hydrolysis of those polyamic acid units which remain after cure or are formed on imide hydrolysis. Previous studies (5,6) of polyimide hydrolysis have generally been based on changes in properties dependent on molecular weight, and thus have measured only the third reaction. The first two reactions are of concern, however, because they result in the formation of polar, hygroscopic groups which would be expected to degrade the dielectric properties of the polymer.

Measurements of the changes in both the imide (4) and the anhydride (1,2) concentrations by IR spectroscopy have already been reported. This paper will demonstrate another approach to using IR to measure anhydride contents and will then present results obtained during hydrolysis of thin films of five polyimides. The structures of the polyimides are shown in Table I. The effects of changes in the curing conditions will also be discussed.

EXPERIMENTAL

The polyamic acids were prepared in these laboratories using modifications of a standard preparation (7). Benzophenone tetracarboxylic acid dianhydride (BTDA), benzenetetracarboxylic acid dianhydride (pyromellitic dianhydride; PMDA), oxydianiline (ODA), 1,4-phenylenediamine (PDA) and 1,3-phenylenediamine (MPDA) were all obtained from Aldrich Chemical Co. The 3,3',4,4'-biphenyl tetracarboxylic acid dianhydride (BPDA) was obtained from Ube Chemical Company. The polyamic acids were prepared in N-methylpyrrolidinone (BTDA-ODA, BTDA-MPDA and BTDA with a 1:1 molar ratio of MPDA and ODA) or dimethyl acetamide (BPDA-PDA and PMDA-ODA).

The anhydride calibration curves were prepared by adding various amounts of the appropriate anhydride to polyamic acid solutions containing known concentrations of polymer. The films were spun onto NaCl plates or silicon wafers and cured at 200°C for 1 h.

In films prepared for hydrolysis, solutions of the polymers were spun onto either AgCl discs or double-polished silicon wafers using conditions designed to give thicknesses in the 1-3 micron range. The films were dried 1 h at 100°C (in air), then baked 1 h at 200°C and 1 h at 300°C (under nitrogen). Some samples were given a final cure at 400°C. Hydrolyses were carried out at 90°C/95% R.H. by placing the samples over a saturated solution of K_2SO_4 at 90 ± 2°C.

IR spectra were recorded on a Digilab FTS-60 Spectrometer equipped with a TGS detector. All spectra were collected using a resolution of 4 wavenumbers. Spectra of films on AgCl were obtained using 200 scans; those of films on silicon wafers were based on 400 scans. In each case, the spectra were recorded in the absorbance mode using a background obtained from the appropriate bare substrate. Interference from water vapor was minimized by purging the sample compartment for 15-20 minutes with dry nitrogen before beginning data collection. If necessary, corrections for remaining traces of water were made water by a scaled subtraction of a spectrum of water vapor.

RESULTS

Figure 1 shows the IR spectrum of a typical polyimide, BTDA-ODA:MPDA, after curing to 300°C on AgCl. The imide bands are seen at 1780, 1726, 1375 and 719 cm^{-1} in this polymer. The residual anhydride may be identified by the small peak at 1853 cm^{-1}. The peak at 1500 cm^{-1} due to one of the skeletal stretching modes of the aromatic rings has been found to provide a reliable internal standard (4).

Anhydride Hydrolysis

Hydrolysis of anhydride may be followed by measuring the decrease in the anhydride peak near 1850 cm^{-1}. Although the peak is extremely small, it can be expanded for measurement without any significant sign of interference from
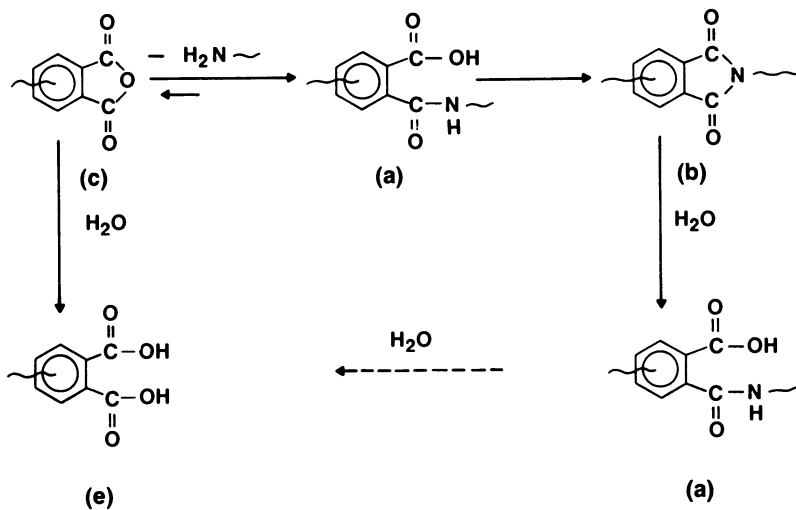
Scheme I. Polyimide curing and hydrolysis reactions.

Table I. Polyimide Structures

BTDA-ODA

BTDA-MPDA

BTDA-ODA: MPDA

PMDA-ODA

BPDA-PDA
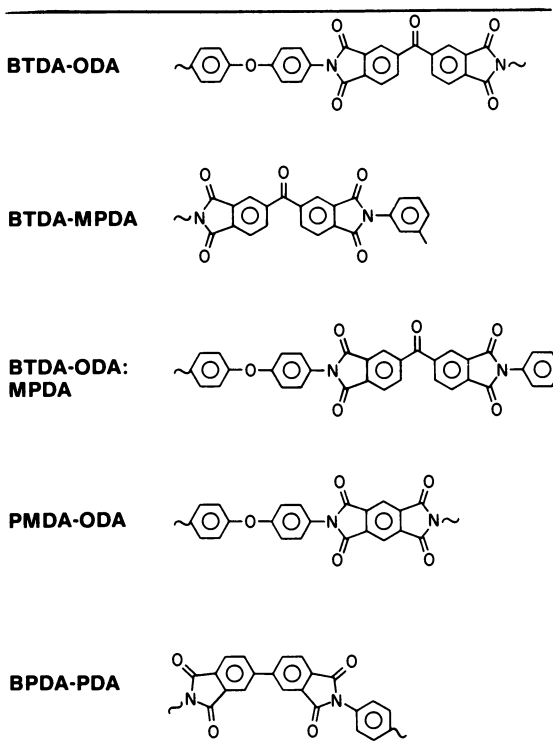
spectral noise. In all the polymers discussed here, only the amine moieties contribute to the 1500 cm^{-1} peak. Thus, for polymers prepared with approximately 1:1 amine:anhydride stoichiometry, the ratio of the 1850 cm^{-1} to the 1500 cm^{-1} band will provide a direct measure of the amount of free anhydride present in the polymer.

To determine the relationship between the size of the anhydride peak and the actual anhydride content, calibration samples were prepared which contained known amounts of anhydride added to the polyamic acid. Figure 2 shows the calibration curve for BTDA in BTDA-ODA. In this plot the data points fall in an essentially straight line. This indicates that, at these relatively high concentrations, the equilibrium formation of anhydride is strongly suppressed. At low concentrations of added anhydride, the equilibrium dissociation will be significant and the line will curve upward, as indicated by the point obtained with no added anhydride. Similar results were obtained for the other calibration curves. The extension of the straight line obtained for BTDA-ODA (Figure 2) intercepts the y-axis at a positive value, suggesting that this particular preparation deviates from 1:1 stoichiometry in that it contains a slight excess (about one percent) of anhydride.

For each calibration curve, the reciprocal of the slope of the line defined by the calibration points, i.e. the concentration divided by the IR absorption ratio, was determined. The values, R, found for this reciprocal slope in each of the polymers are given in Table II. The error limits suggested primarily reflect uncertainties in

Table II.   Anhydride Calibration Factors

Polymer	Calib. Substrate	Calib. Factor
BTDA-ODA	NaCl	450 ± 80
BTDA-MPDA	NaCl	110 ± 30
BTDA-ODA:MPDA	NaCl	250 ± 25
BTDA-ODA:MPDA	Si	215 ± 25
BPDA-PDA	NaCl	120 ± 20
BPDA-PDA	Si	100 ± 20
PMDA-ODA	NaCl	200 ± 70

the concentrations of anhydride in the calibration samples. Inaccuracies in weighing the components, impurities in the starting materials or deviations from 1:1 stoichiometry in the polymers could contribute to these uncertainties. In addition, however, if any anhydride is lost during heating of the films, this could significantly affect the measured absorbances. The values of R obtained on silicon are somewhat lower than those measured on NaCl. This may indicate that some anhydride is lost or destroyed when the films are heated to 200 ° C on NaCl.

Multiplying the observed anhydride/internal standard ratio in each cured film by the calibration factor gives an estimate of the initial anhydride content. As
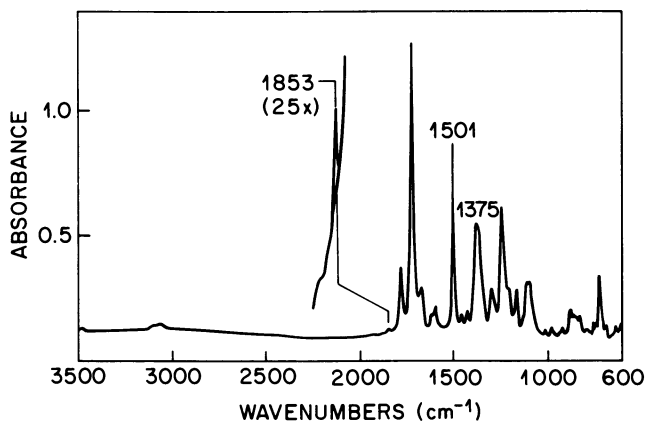
Figure 1.   IR spectrum of BTDA-ODA:MPDA copolymer cured to 300 ° C on AgCl.
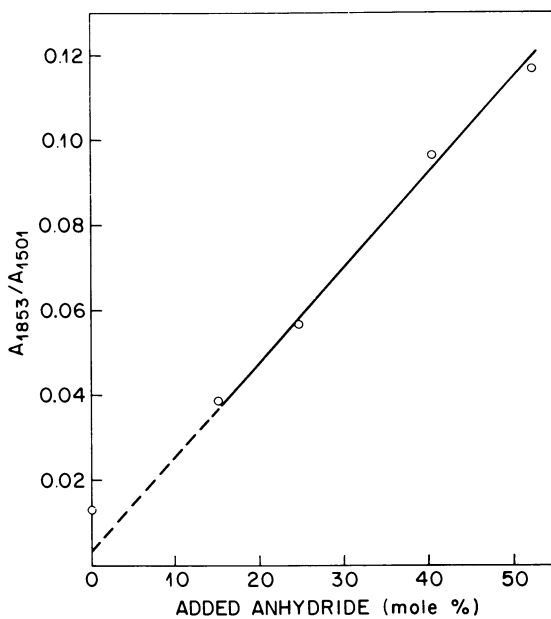
Figure 2.   Calibration data for BTDA in BTDA-ODA.

seen in Table III, the initial anhydride contents for a given polymer are dependent on the polymer components, the substrate used (higher contents are seen on the silicon substrates) and the cure conditions (curing to 400 °C significantly decreases the initial anhydride content). We would also expect that the anhydride contents would be affected by the backbone components present and by the stoichiometry of the particular preparation used. Although some of the preparations (eg. the BTDA-ODA:MPDA preparation used here) appeared to be very close to 1:1 in their stoichiometry, others deviated significantly. The preparation of BPDA-PDA used here, for instance, appeared to contain a significant excess of amine (perhaps as much as 10%). This will almost certainly lower the amount of residual anhydride observed.

Figure 3 shows changes in the anhydride concentrations in typical films on AgCl and silicon during hydrolysis. Although the exact rates of hydrolysis varied with the polymer used and the cure conditions, all the films gave generally similar results. In each case the hydrolysis is quite rapid and the anhydride is generally reduced to $\leq 25\%$ of its initial value within 100-200 h under these conditions. Essentially no anhydride was left in most of the samples after 400-600 h hydrolysis. The only exception was the sample of BPDA-PDA cured on silicon: about one-third of the initial anhydride content remained after 600 h hydrolysis.

Imide Hydrolysis

The imide peaks near 1780, 1370 and 730 cm^{-1} have all been used frequently to measure imide content. However, as was found recently, (4) both the 1780 and the 730 cm^{-1} peaks overlap anhydride absorption bands. Thus estimates of imide hydrolysis based on measurements of these bands would be considerably too large, particularly in the case of the 1780 cm^{-1} band. Therefore changes in imide concentration are best followed (2) by measuring the height of the imide peak at ~ 1370 cm^{-1} (see Figure 1) as a function of the height of the 1500 cm^{-1} internal standard. These normalized heights of this band, attributed to the C-N stretch (2) will be referred to here as the imide ratios. Readings taken on different spots on a given sample generally give imide ratios that agree well within one percent.

Figure 4 shows the changes in the imide band on hydrolysis for samples of two polymers, BTDA-ODA and PMDA-ODA. The samples of BTDA-ODA underwent a rapid decrease in the imide band during the first 24-48 h of hydrolysis. The reaction then slowed markedly. Samples cured to only 300 °C have a very slightly lower initial imide content and appear to hydrolyze somewhat more rapidly than those cured to 400 °C. However, as can be seen in Table II, the percentages of imide remaining after 600 h hydrolysis, based on the final *vs* initial imide ratios, are the same within experimental error.

The two other polymers based on BTDA showed patterns very similar to that of BTDA-ODA. The amount of imide remaining in each of these samples after prolonged hydrolysis is given in Table III. Again, the samples cured to 400 °C appeared to hydrolyze at a slightly lower rate. The data indicate some slight differences in rates depending on the final cure temperature (samples cured to 400 °C generally hydrolyze somewhat more slowly) and the substrate used (hydrolyses done on silicon were often somewhat slower than those on AgCl). Overall, however, the final degree of hydrolysis calculated for each sample does not seem to vary significantly with changes in substrate or cure conditions.

The data for PMDA-ODA shown in Figure 4 indicate a much lower susceptibility to imide hydrolysis. Here, the measured hydrolysis after 400 h is only $\sim 1\%$ based on the initial ratios. The sample cured to 400 °C appears to

Table III.   Summary of Cure Conditions and Hydrolysis Results

Polymer	Substrate	Cure Temp. (°C)	Init. Anh. Conc. (%)	Imide Hydrol. (%)	Hydr. Time (hr)
BTDA-ODA	Si	300°	7.6 ± 1.5	6.4	680
BTDA-ODA	Si	400°	5.1 ± 1.0	6.0	680
BTDA-ODA	AgCl	400°	0.4 ± 0.1	6.2	680
BTDA-MPDA	Si	300°	3.6 ± 1.0	6.1	680
BTDA-MPDA	Si	400°	2.1 ± 0.7	5.6	680
BTDA-ODA:MPDA	Si	300°	3.3 ± 0.5	4.8	485
BTDA-ODA:MPDA	AgCl	300°	3.0 ± 0.4	5.8	600
BTDA-ODA:MPDA	AgCl	400°	0.4 ± 0.1	5.8	600
BPDA-PDA	Si	300°	0.25 ± .05	0	600
BPDA-PDA	Si	400°	–	0	600
BPDA-PDA	AgCl	300°	0.2 ± .03	0	600
BPDA-PDA	AgCl	400°	–	0	600
PMDA-ODA	Si	300°	0.7 ± .25	1	400
PMDA-ODA	Si	400°	–	1	400

have a slightly higher imide content based on its initial imide ratio. Again, the curves suggest that this film hydrolyzes somewhat more slowly.

As seen in Figure 5, no significant changes (changes $\leq 0.5\%$) were seen in the imide ratios throughout 600 h hydrolysis for BPDA:PDA. The sample cured to 400 °C appears to contain about 3% more imide than the sample cured to only 300 °C.

DISCUSSION

The results given above indicate that, despite some variations in rate, anhydride end groups can all be classed as quite readily hydrolyzed. In contrast, the hydrolytic susceptibility of imide linkages varies much more with the polymer examined. BPDA-PDA showed no measurable imide hydrolysis whatsoever. In PMDA-ODA the amount of hydrolysis observed was small enough that we cannot eliminate the possibility that impurities in the anhydride component, rather than PMDA itself, resulted in the formation of hydrolyzable material. Of the polymers studied here, only those that contained BTDA as the anhydride component showed a marked susceptibility to imide hydrolysis. Even in this case, the data suggest that the reaction is limited in that only about 6-7% of the imide linkages appear to be susceptible to hydrolysis.

The reason for this pattern is not yet clear. As seen in the data presented in Table III, there is no strong correlation between the final cure temperature and the degree of hydrolysis after long-term exposure. Similarly, films of different thicknesses do not show significant differences in the amount of imide eventually hydrolyzed, suggesting that hydrolytic susceptibility is not related to surface effects. One possibility still under consideration is that different conformations of the benzophenone moieties result in different hydrolytic susceptibilities.

One conclusion that may be drawn from these results is that complete curing of polyimides (generally to 400 °C) will minimize possible hydrolytic damage in several ways. First, since it can be assumed in most cases that the bulk of the anhydride will be hydrolyzed after long-term exposure to humid conditions, the presence of any significant residues of anhydride would be expected to deleteriously affect the dielectric properties. As was seen in Table II, for a given substrate and polymer, curing to higher temperatures gave lower equilibrium anhydride concentrations.

Second, the samples of the BTDA-containing polymers cured to high temperatures appear to undergo imide hydrolysis somewhat more slowly. The differences obtained under the hydrolysis conditions used here are relatively small, but they could translate to significant differences in the time required to reach a given degree of hydrolysis among samples exposed to lower temperatures and/or humidities.

Finally, curing to higher temperatures should minimize the concentration of amic acid moieties remaining. The hydrolysis of these groups was not measured in this study, but it is generally believed that they are readily hydrolyzed. In any case, the presence of significant concentrations of these polar, hygroscopic species would, in itself, be expected to degrade the dielectric properties of the polymer. The concentrations of amic acids remaining after cure to 300 °C are not known, but may be equivalent to several percent. In BPDA-PDA, for instance, the 3% increase in imide on heating to 400 °C seems to be mostly attributable to conversion of moieties present as amic acids, since only a fraction of a percent of anhydride was present after the 300 °C cure. Even further imidization might be
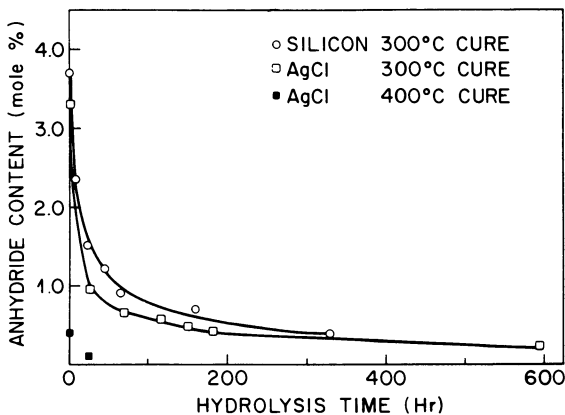
Figure 3. Anhydride hydrolysis in BTDA-ODA:MPDA.
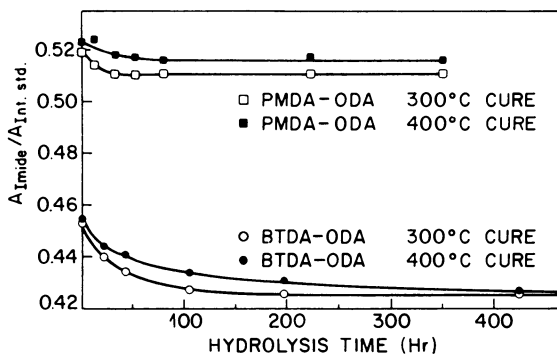
Figure 4. Imide hydrolysis in BTDA-ODA and PMDA-ODA.
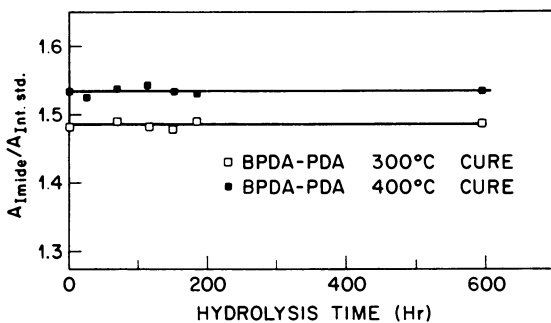
Figure 5. Imide Hydrolysis in BPDA-PDA.

observed on heating to higher temperatures, but it could be accompanied by some degradation in the less stable polyimides.

In BPDA-PDA, the only hydrolysis observed was of anhydride. If the samples are cured to at least 400 °C to minimize the residual anhydride, the bulk polymer should be quite stable to hydrolysis. In this material, then, the major remaining concerns about hydrolytic stability center on the polymer-substrate interfaces: whether possible polymer-metal interactions could result in the formation of hydrolytically unstable products and whether or not agents used to promote adhesion will retain their efficacy under humid aging.

CONCLUSIONS

IR spectroscopy provides a sensitive way of following two reactions in polyimides exposed to high temperatures and humidities: hydrolysis of anhydride end groups remaining after cure and hydrolysis of the imide linkages themselves. The anhydride moieties appear to be readily hydrolyzed in all cases. The results obtained for the imide linkages, in contrast, suggest that their hydrolytic susceptibility is influenced by the components of the polymer, particularly the anhydride component used. These results also indicate that thorough curing is essential to obtain maximum hydrolytic stability.

ACKNOWLEDGMENTS

REFERENCES

1. M. I. Bessonov, M. M. Koton, V. V. Kudryatsev and L. A. Laius, *Polyimides-Thermally Stable Polymers*: Consultants Bureau (Plenum Press): New York, 1987, pp 62-63.
2. P. R. Young, *SAMPE Preprints* **1985** *30* 889.
3. M.-J. Brekner and C. Feger, *J. Polym. Sci., Polym. Chem. Ed.* **1987** *25* 2479-91.
4. C. A. Pryde, to be published in *J. Polym. Sci., Polym. Chem. Ed.*
5. R. DeIasi and J. Russell *J. Appl. Polym. Sci.* **1971** *15* 2965-2974.
6. J. O. Punderson and J. F. Heacock, *International Wire and Cable Symposium Proceedings* **1985** 44-50.
7. W. R. Sorenson and T. W. Campbell, *Preparative Methods of Polymer Chemistry* Interscience: New York, 1968 p 170.

Chapter 5

Dielectric Characterization of Water in Polyimide and Poly(amide–imide) Thin Films

Allyson J. Beuhler, Neal R. Nowicki, and Joanne M. Gaudette

Amoco Chemical Company, Naperville, IL 60566

The effect of absorbed water on the low frequency dielectric properties of a series of polyimides and polyamide-imides was investigated. The polymers were prepared as solution cast thin films (25 microns) on glass. The dielectric constant and dielectric loss of the films were measured at 25°C (10kHz - 1 MHz) using a two-fluid cell technique after drying at elevated temperature, and after exposure to 40% relative humidity. The equilibrium water absorption and the dry and wet (40% relative humidity) dielectric constant increase with increasing amide content of the polymer. The effective polarizability of the absorbed water was calculated from the humidity induced change in the film dielectric constant using the Clausius-Mossotti equation. For polyimides, the absorbed water has a polarizability close to that of free water (μ_o = 1.9 Debyes (6.2 X 10^{-30} coulomb-meters), but this value decreases to $0.4\mu_o$ for polyamide-imides. This suggests that the water is weakly bound and can freely rotate in the polyimides, but is tightly bound or clustered in the polyamide-imides.

Aromatic polyimides have found extensive use in electronic packaging due to their high thermal stability, low dielectric constant, and high electrical resistivity. Polyimides have been used as passivation coatings, (1) interlayer dielectrics, (2) die attach adhesives, (3) flexible circuitry substrates, (4) and more recently as the interlevel dielectric in high speed IC interconnections. (5) High speed applications require materials with a combination of low dielectric constant, flat dielectric response versus frequency and low water absorption.

Commonly used high speed substrates such as polyethylene and polytetrafluoroethylene meet the low dielectric constant and low moisture requirements, but lack the thermal stability required

for these applications. Many high temperature polymers, such as polyimides and polyamide-imides, contain polar groups (permanent dipoles) which result in higher dielectric constants and increased moisture absorption.

The nature of the interaction between water and the polymers is important because absorbed water can adversely affect thermal, electrical and mechanical properties of the polymer. Moisture absorption increases the dielectric constant, (5,6) and dielectric loss, (7) and has been related to device reliability problems. (8) Water-induced plasticization causes hygroscopic expansion, lowering of Tg, and degradation of mechanical properties. (9)

Nuclear magnetic resonance (NMR), (10) differential scanning calorimetry, (11) and FTIR studies, (9) indicate that water can exist in both tightly bound and relatively free states, "bound water" being characterized by a nonfreezing component. Studies using dielectric measurements have shown that water molecules absorbed in thermoset epoxy resins exhibit 70-100% of their free state polarizability. (12) Based on a Clausius-Mossotti analysis of the moisture induced change in permittivity, Denton et al, (6) observed that water absorbed in device grade polyimide has a dipole moment nearly equal to that of free water.

In this paper we use dielectric measurements to calculate the polarizability of absorbed water in a series of aromatic polyimides and polyamide-imides. In the relatively non-polar polyimides, the absorbed water has a dipole moment close to that of free water (μ_o = 1.88 Debyes). This value drops to less than $0.4\mu_o$ for polyamide-imides. The decrease may be attributed to hydrogen-bonded water in the very polar polyamide-imides. In addition, the "group" dipole moment for amide is calculated and found to be greater than the dipole moment of free water.

Experimental
Polymer Films. Samples of DuPont KAPTON, Mitsubishi NOVAX, Ube UPILEX-S and General Electric ULTEM films were obtained from commercial sources. Chemical structures of the commercial polymers, as understood from the literature, are shown below.

O DuPont KAPTON
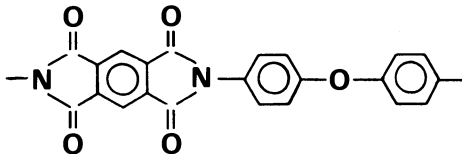
O General Electric ULTEM
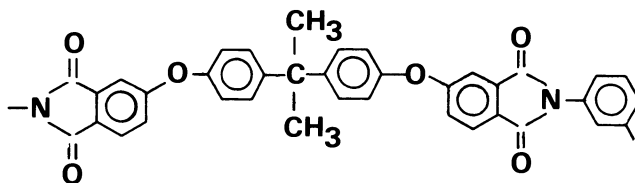
O   Ube UPILEX-S
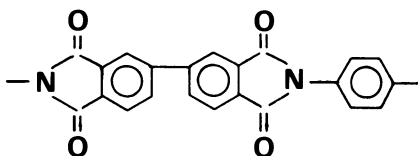
Experimental films were prepared from polyamic acid or polyamide-imide solutions in l-methyl-2-pyrrolidone (NMP) solvent by casting on soda-lime glass plates and curing in a forced air oven for one hour each at 80°C, 200°C, and 300°C. The resulting films were 25-50 microns thick.

The polyamic acid solutions were prepared by reacting an aromatic diamine and dianhydride in dry NMP for 8-24 hours, maintaining the reaction under dry nitrogen. In Table I, the experimental polyimide films prepared for this study are labelled as PI1 through PI12. The polyamide-imide solutions were prepared using an isocyanate route similar to that described in Reference 13. In Table I, the experimental polyamide-imides are labelled as PAI1 through PAI6. The dielectric constants and water absorption of both the polyimides and polyamide-imides were varied by changing the polymer structure. The polyimides are based on commercially available anhydrides PMDA, 6FDA, and BPDA. A general structure for the experimental TMA-based polyamide-imides is as follows:

O   Polyamide-imide (PAI)
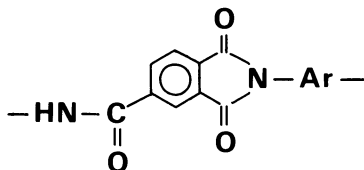
Dielectric Measurements

Dielectric measurements on thin films were made using a two-fluid cell technique as per ASTM D 150. The advantage of the two-fluid cell is that measurement of dielectric constant is independent of sample thickness, electrode spacing, and electrode area. Thin films can be stacked to increase testing accuracy. The reproducibility of the dielectric constant measurement using the two-fluid cell was ±2%.

Films designated as 0% RH were dried by heating in a nitrogen purged oven for 3 days at 250°C and then stored in a dry box prior to dielectric testing and weighing. Films designated as 40% RH were conditioned in a 40% RH humidity chamber until the film weight reached a steady state value. Figure 1 shows the

Table I - Polymer Data

Polymer	ϵ'(0%RH)	ϵ'(40%RH)	ρ(g/cm^3)	%H$_2$O(g/100g polymer) @ 40% RH
Polyamide-imides				
PAI-1	3.80	4.08	1.34	2.9
PAI-2	3.80	3.94	1.42	2.3
PAI-3	3.64	3.91	1.34	2.1
PAI-4	3.45	3.66	1.29	1.6
PAI-5	3.53	3.70	1.32	1.5
PAI-6	3.48	3.69	1.36	1.2
Commercial Polyimides				
KAPTON	3.00	3.20	1.45	1.0
UBE	3.07	3.28	1.48	0.7
Mitsubishi	2.81	3.00	1.38	0.5
ULTEM	2.97	3.08	1.30	0.4
Experimental Polyimides				
PI-1	3.14	3.42	1.26	1.2
PI-2	3.16	3.36	1.18	1.2
PI-3	3.22	3.38	1.40	1.1
PI-4	3.09	3.30	1.19	1.1
PI-5	3.18	3.27	1.28	1.0
PI-6	2.90	3.07	1.21	0.7
PI-7	2.70	2.80	1.34	0.6
PI-8	3.03	3.14	1.27	0.6
PI-9	2.72	2.80	1.35	0.6
PI-10	3.05	3.13	1.26	0.4
PI-11	2.95	3.06	1.30	0.4
PI-12	2.68	2.74	1.44	0.2

weight uptake water for a 50 micron thick film of sample PAI1. Equilibrium water uptake was obtained by taking the weight difference between 0% RH films and those conditioned at 40% RH. Typical humidity conditioning times prior to dielectric testing and weighing were 3-7 days. Polymer film densities were measured as per ASTM D 792.

Dielectric measurements for both the 0% RH films and films conditioned at 40% RH were made at room temperature over a range of frequency. The humidity induced change in the dielectric constant was independent of frequency from 10KHz to 1 MHz. Only the 1 MHz data is reported.

Results

Table I lists the experimentally measured dielectric constants at 0% and 40% RH, polymer densities, and the weight uptake of water per 100 g film at 40% RH for all the samples investigated. The polarizability of the absorbed water in the films was calculated using the Clausius-Mossotti equation (Equation 1) which relates macroscopic dielectric constant to molecular polarizability as follows:

$$\Sigma_i \; N_i \; P_i \; = \; \left[\frac{(\epsilon'-1)}{(\epsilon'+2)} \right] 3\epsilon_o \tag{1}$$

where P_i = polarizability of the ith component

N_i = number of dipoles/unit volume of the ith component

ϵ' = measured dielectric constant

ϵ_o = permittivity of free space

Letting p designate polymer and w water $\tag{2}$

$$\Sigma_i \; N_i \; P_i \; = \; N_p P_p + N_w P_w$$

In the water absorption experiment

$$\Sigma \; N_i P_i \; = \left[\frac{(\epsilon'-1)}{(\epsilon'+2)} \right] 3\epsilon_o \; \text{at 40\% RH}$$

and

$$N_p P_p \; = \left[\frac{(\epsilon'-1)}{(\epsilon'+2)} \right] 3\epsilon_o \; \text{at 0\% RH}$$

Substituting into Equation 2 gives the polarizability of the water component as

$$P_w \; = \; 3\epsilon_o \left[\frac{\frac{(\epsilon'-1)}{(\epsilon'+2)}_{40\%} \; - \; \frac{(\epsilon'-1)}{(\epsilon'+2)}_{0\%}}{N_w} \right] \tag{3}$$

The number of water dipoles per unit volume (N_w) is calculated
from the weight uptake water by

$$N_w = W\, N_o\, \rho/M$$

where W is the weight uptake water per g polymer, N_o is
Avogadro's number, ρ is the polymer density, and M the molecular
weight of water. The effective dipole moment of water (μ)
calculated for each polymer from $P_w = \mu^2/3kT$
plotted vs. the concentration of water is shown in Figure 2.

The polyimide samples are designated by squares and
polyamide-imides by open circles. The permanent dipole moment of
free water ($\mu_o = 1.88$ Debyes) is shown by the dashed line in
Figure 2. The dipole moment of the absorbed water molecules
varies from approximately 1.8 to 0.9 for the polyimides and from
1.1 to 0.7 for the polyamide-imides corresponding to fractional
polarizabilities of $1.0\mu_o$ -$0.4\mu_o$. The low values of μ ($<0.5\mu_o$) as
seen in all the amide-imide polymers and several of the
polyimides, indicate restricted mobility of the water molecules.
In the amide-imide polymers, we believe this is due to increased
water-polymer interactions such as hydrogen bonding. Other
evidence of hydrogen bonding in polyamide-imides is the
water-induced plasticization and Tg lowering frequently observed.
(14)

Figure 3 shows the dipole moment of absorbed water vs. ϵ'
measured at 0% RH. If ϵ'(0% RH) is viewed as a measure of
polarity of the polymer, μ is seen to decrease quite sharply
with increasing polymer polarity. A consequence of this
result is that $\Delta\,\epsilon$/% H_2O, the change in dielectric constant/%
H_2O will be higher for polymers with lower dielectric
constant.

The dipole moment of a selected functional group in the
polymer can also be calculated using the Clausius-Mossotti
equation. According to Van Krevelan, (15) the "effective
polarizability" of a functional group in the polymer is
calculated from the measured dielectric constant, the polymer
density and the number of moles of that group in the polymer
repeat unit. Using the data for the six polyamide-imides listed
in Table I, the effective polarizability of the amide group can
be determined from

$$\left[\frac{(\epsilon'-1)}{(\epsilon'+2)}\right]3\epsilon_o = (n_a P_a + n_r P_r)/V_t \tag{4}$$

where

n_a = # moles amide/polymer repeat unit
n_r = # moles other functional groups in polymer repeat unit
P_a = polarizability of amide group
P_r = polarizability of all groups other than amide

V_t = volume of repeat unit =

MW (molecular weight of polymer repeat unit)
ρ (polymer density)
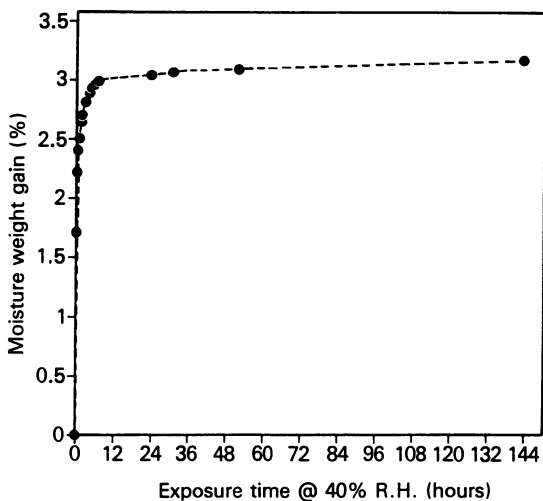
Figure 1. Moisture Weight Gain at 40% R.H. for Sample PAI1.
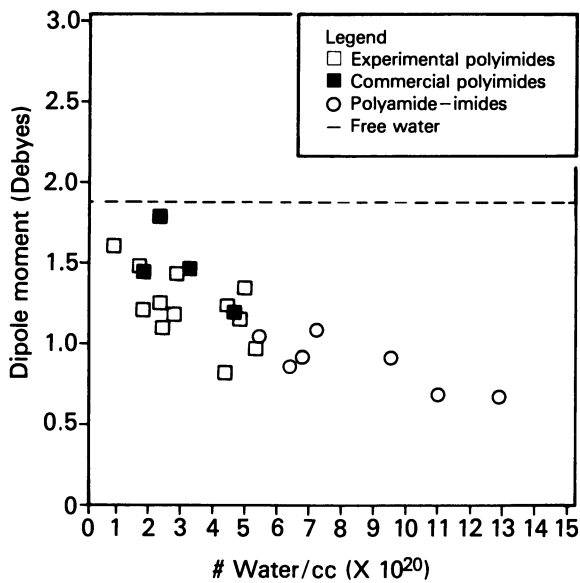
Figure 2. Water Dipole Moment as a Function of Concentration.
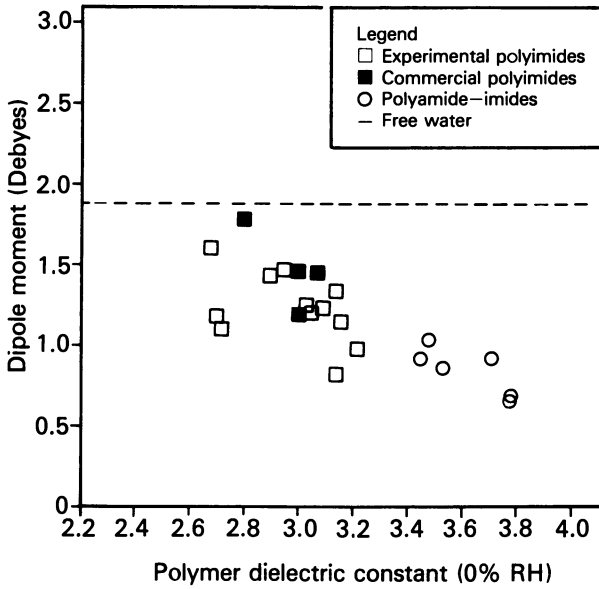
Figure 3. Dipole Moment of Absorbed Water vs. Polymer Dielectric Constant.
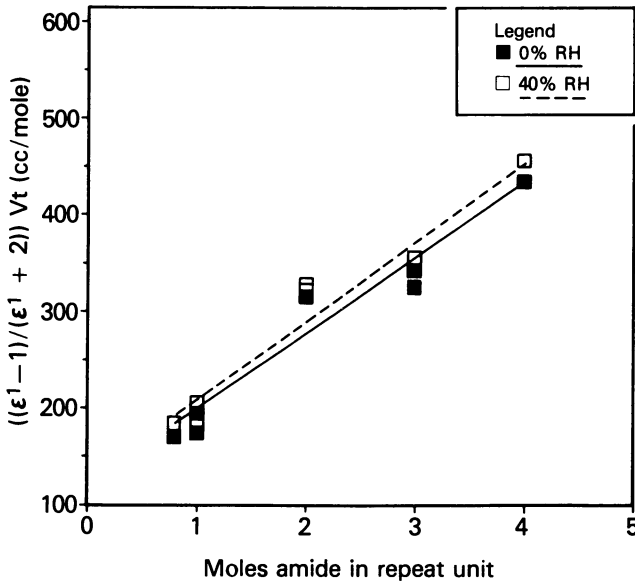
Figure 4. Polarization of Amide Group.

A plot of $[(\epsilon'-1)/(\epsilon'+2)]V_t$ vs. n_a is shown in Figure 4 for both the 0% and 40% relative humidity data. Assuming $n_a P_a \gg n_r P_r$, the slope of the plot yields the effective polarizability of the amide group. The dipole moment for the amide group, calculated from $\mu^2/3kT$ is 2.0 Debyes for the 0% RH data and 2.1 Debyes for the 40% RH data. These values are higher than the amide "group" dipole calculated by Van Krevelan, (15) 1.0 Debyes, but lower than the gas phase dipole moment of formamide, 3.7 Debyes. (16) The small increase in the amide dipole with the addition of water indicates that water mobility is hindered in the presence of the amide group.

Conclusions
Dielectric measurements were used to calculate the relative polarizability of absorbed water in a series of polyimides and polyamide-imides. The effective dipole moment of the absorbed water varied from 1.8 Debyes to 0.7 Debyes. This corresponds to 1.0 to 0.4 times the dipole moment of free water. The low values of μ indicate hindered dipole mobility which may be attributed to water hydrogen bonding with polar groups such as amide. μ is seen to decrease as the polarity of the polymer increases, suggesting that water exists in its free state in very non-polar polyimides, but the polarizability decreases due to water-polymer interactions as the polymer becomes more polar. No evidence is observed of distinct "bound" and "unbound" water phases.

The "group" dipole moment of the amide functional group is calculated from dielectric constant data and found to be 2.0 Debyes in dry polymer films and 2.1 Debyes in films conditioned at 40% RH. The small increase in "wet" films is consistent with the water absorption data indicating that the effective water dipole moment decreases in the presence of amide groups.

Literature Cited

1. Berger, R. G.; Gregoritsch, A. J. Induced Passivation Defect Study, Proceedings of 1975 IEEE Reliability Physics Symposium, 1975, Las Vegas, Nevada.

2. Mukai, K.; Saiki, A. IEEE Journal of Solid-State Circuits, August 1978, 4, SC-13.

3. Moghadam, F. K., "Development of Adhesive Die Attach Technology in Cerdip Package Materials Issue", Solid State Technology, 1984, 27, 149-157.

4. DuPont Technical Information Bulletin, "KAPTON-Summary of Properties", August 1982, No. E-50553.

5. R. Jensen, IEEE Transactions on Components, Hybrids, and Manufacturing Technology, December 1984, 4, CHMT-7.

6.   D. Denton, "Effects of Moisture Uptake on the Dielectric
      Permittivity of Polyimide Films", Proc. International
      Symposium on Moisture and Humidity, April 15-18, 1985, p 505,
      Washington, D.C.

7.   B. Bachman, 1st International SAMPE Electronics Conference,
      June 23-27, 1987, p 431.

8.   S. D. Senturia, Polymers for High Technology: Electronics and
      Photonics; American Chemical Society, Div. of Polymeric
      Materials: Science and Engineering, ACS Symposium Series,
      1987; p 346.

9.   Chatzi, E. G. Applied Spectrocopy, 1986, Vol.40, No. 6, 847.

10.   Dehl, R. E., J. Chem. Phys., 1968, 48, 831.

11.   S. Deodhar, Water in Polymers, ACS Symposium Series 127,
      Sept. 10-13, 1979, p 271.

12.   Aldrich, P. D., Polymer, 1987, 78, 2289.

13.   P. A. Bolon and T. B. Gorczyca, SPE Proceedings of the Second
      International Conference on Polyimides, 1978, p 129,
      Ellenville, N.Y.

14.   Amoco Chemical Corporation Bulletin TAT-35, TORLON
      Engineering Polymers/Design Manual.

15.   D. W. Van Krevelan, Properties of Polymers, Correlations with
      Chemical Structure, 1972, Elsevier Publishing, N.Y.

16.   CRC Handbook of Chemistry and Physics, 64th Edition, 1984,
      CRC Press, Inc., Boca Raton, Florida.

Chapter 6

Calculated Final-State Effects of the PMDA-ODA Polyimide X-ray Photoemission Spectrum

A. R. Rossi and B. D. Silverman

IBM Research Division, Thomas J. Watson Research Center, Yorktown Heights, NY 10598

X-Ray photoemission spectroscopy has been extensively utilized in probing surfaces and interfaces involving the technologically important class of polymers: the polyimides. We have previously shown that, within the Koopmans' approximation, the calculated core level positions can yield an accurate characterization of the relative positions of the chemically inequivalent atoms observed in the photoemission spectrum (XPS) of the PMDA-ODA polyimide. Whereas the *relative* positions agreed well with experiment, the *absolute* magnitudes of the calculated XPS peak positions were tens of electron volts above the measured values. To resolve this discrepancy, as well as to examine details involving the relative XPS peak positions, the carbon(C1s), nitrogen(N1s), and oxygen(O1s) ionization energies of the separate molecular units, pyromellitic diimide (PMDA) and hydroxyaniline, were calculated taking into account final state effects, and allowing for core hole relaxation. This technique is called the ΔSCF method since the ionization energy is calculated as a difference in energies between the neutral molecule and the resulting radical cation. The present calculations show that core-hole relaxation, treated in the ΔSCF approximation, shifts the calculated values of the photoemission peaks to within one electron volt of the observed peak positions. On the scale of relative shifts, the carbon 1s carbonyl peak was calculated within the Koopmans' approximation to lie 3 eV higher in binding energy relative to the main carbon 1s peak, while the present ΔSCF calculations yield a 4 eV separation between the main and carbonyl carbon C1s peaks. The observation of such an increased separation might reflect inter-chain bonding involving the carbonyl oxygen atoms.

Ab initio molecular orbital calculations have played a central role in the analysis and interpretation of X-ray photoemission data obtained on the PMDA-ODA polyimide surface [1-4]. The repeat unit of the PMDA-ODA polyimide is shown in Figure 1 and is constructed from planar pyromellitimide (PMDA) and diphenyl ether segments. An understanding of the XPS data and its relationship to the surface chemistry prior to the deposition of any metal is crucial with respect to the interpretation of changes in the XPS data which signify important metal-polymer chemistry that occurs upon formation of the interface.

At present, the analysis of films annealed in ultra-high vacuum has led one to infer that the surface of the PMDA-ODA polyimide approximates that expected for ideal bulk stoichiometry with, however, certain small but significant differences. This analysis has involved an examination of the relative shifts of the chemically inequivalent species of each of the elemental groups. For example, prior work[5] focussed attention on the small shifts of approximately one electron volt exhibited by the aromatic carbon atoms of the central benzene ring of the PMDA component. These shifts were calculated with respect to carbon 1s core level positions of atoms not conjugated with electron withdrawing species. Comparisons between calculated core level positions and photoemission data in the Koopmans' approximation, however, always required that the calculated peak positions be shifted to higher binding energy by tens of electron volts.

In X-ray Photoelectron Spectroscopy (XPS) an electron is ejected from a core level

$$P \;+\; h\nu \;\rightarrow\; P^{\dot{+}} \;+\; e^{-}$$

where P is a polymer and $h\nu$ is the incident radiation. The kinetic energy (KE) of the ejected photoelectrons is measured, $KE = h\nu - BE - \Phi$, and information about the chemical environment (chemical shifts) from the binding energy, BE (i.e. ionization energy, IE) of electrons, can be obtained when the workfunction, Φ, is known. The usual interpretation is to relate the peaks in the observed XPS spectrum to energy differences between the doublet ion (core hole) and ground state:

$$IE \;=\; E(P^{\dot{+}}) \;-\; E(P)$$

The SCF molecular orbitals of the neutral species, ψ_i , give rise to the ground state wavefunction, $\Phi(P) = |\psi_i|$, while the SCF orbitals of the positive ion for the core-hole state produce a doublet state wavefunction, $^2\Phi(P^+) = |\psi'_i|$. Koopmans' Theorem[6] assumes that there is no change in the molecular orbitals of the ground state and ionized species, $\psi_j = \psi'_j$, and that a vertical ionization energy can be obtained by the following expression:

$$IE^{KT} \;=\; E\,[^2\Phi_j^{KT}(P^+)] \;-\; E\,[\Phi(P)] \;=\; -\,\epsilon^{SCF}$$

where ϵ^{SCF} corresponds to the one-electron energy of a core orbital for the neutral molecule. When final state effects are included, calculations on both the neutral ground state and final ionized state are taken into account:

$$IE^{\Delta SCF} \;=\; E\,[^2\Phi_j(P^+)] \;-\; E\,[\Phi(P)]$$

These are called ΔSCF calculations since the energy difference between two SCF calculations is obtained. The relaxation energy, ΔE_{Rel} , is then defined as the difference between the ionization energy derived by Koopmans' Theorem and that obtained by a ΔSCF calculation:

$$\Delta E_{Rel} \;=\; IE^{KT} \;-\; IE^{\Delta SCF}$$

Since it is well known that final state effects or relaxation about the core hole can induce large shifts in the photoemission spectrum[7], these effects have been investigated within the framework of the ΔSCF approximation. The results of this investigation are described in the present paper.

Computational Details

All calculations were carried out with the MELD[8] series of programs. In particular, the RHFSCF program was specifically modified to enable the calculation of core hole states without variational collapse[9]. The PMDA and oxyaniline molecular units, Figure 2, were treated separately, largely because of molecular size and program limitations. These partic-
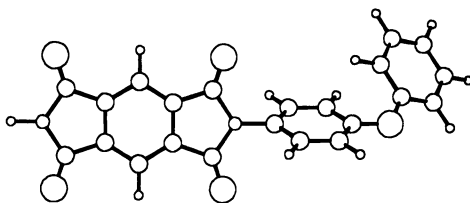
Figure 1. The full PMDA-ODA polyimide unit.
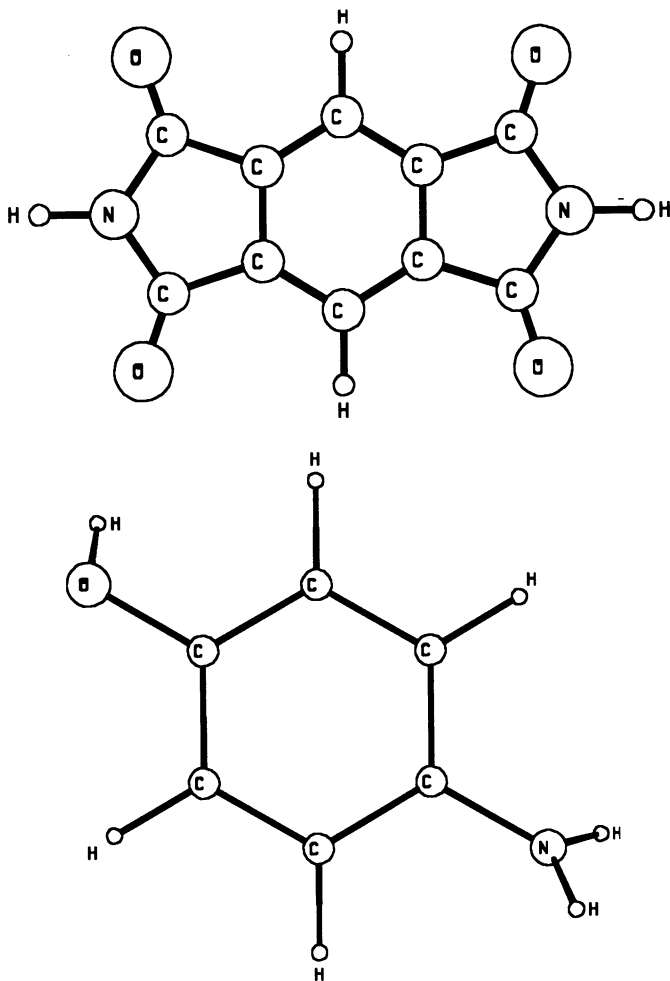
Figure 2. Top: the PMDA fragment. Bottom: the oxyaniline molecular unit.

ular molecular fragments were chosen for investigation since the calculated results obtained enabled us to reconstruct the XPS spectrum expected for the PMDA-ODA polymer. In addition, the calculations for each fragment were performed in reduced symmetry, i.e., the core holes were localized at single atomic sites, (C_s for PMDA and C_1 for hydroxyaniline), since previous calculations[10] have shown that lower energies are obtained for localized hole states.

The basis set employed in the present calculations included the Huzinaga[11] (9s,5p) for second row atoms and (4s) for hydrogen contracted to [3s,2p] and [2s], respectively following the scheme of Dunning and Hay.[12] The structural parameters for the PMDA and hydroxyaniline fragments were obtained from the X-ray study of 4,4'-bis(phthalimide) diphenyl ether[13], as well as from standard bond lengths and angles. For the hydroxyaniline fragment, all phenyl groups were chosen as idealized structures with all bond angles equal to 120° and C-C and C-H bond distances equal to 1.39 Å and 1.10 Å, respectively.

In order to compare the experimental and calculated core ionization energies, it is convenient to have a naming convention. This convention was discussed previously[6], but a brief review will be given here. The symbols Ar (arene) and Ph (phenyl) denote the benzene rings on the PMDA and hydroxyaniline fragments, respectively. Using this convention, C1s (Ar-X) represents a 1s ionization from a carbon atom situated in the benzene ring of the PMDA fragment where X = H, C=O indicating carbon bonded to either hydrogen or a carbonyl group. Thus, C1s(Ar-H) represents ionization from either of the two carbon atoms located in the central benzene of the PMDA fragment and connected to hydrogen atoms, while C1s(C-C=O) involves ionization from the remaining four carbon atoms of the central benzene which are bonded to C=O groups. C1s(C=O) represents the carbon 1s ionization energy for any of the carbonyl carbon atoms located in the PMDA fragment. Since the splitting is small, C1s (Ph-H) indicates ionization from any of the carbon atoms of the benzene located in the hydroxyaniline molecular fragment and bonded to hydrogen atoms. The remaining carbon ionizations for the hydroxyaniline fragment are given by C1s(Ph-N) and C1s(Ph-O), respectively. The N1s and O1s notations for both fragments then become obvious.

Results and Discussion

Computed XPS Spectrum

One problem in reconstructing the PMDA-ODA XPS photoemission spectrum from calculations on separate fragments arises because of differences in ionization energies of the PMDA fragment relative to the oxydianiline molecular unit. In other words, the electronic environment of the complete PMDA-ODA repeat unit changes when separate units are calculated. For example, previous calculations on a neutral PMDA-ODA molecule have yielded relative core level splittings to be ~ 0.5 eV greater than those obtained from calculations on the individual PMDA and oxydianiline units. This is presumably due to charge transferred from the ODA to PMDA segment. To correct such relative shifts in an approximate manner, the two calculated O1s ionization energies have been adjusted to correspond to the experimental splitting.

Comparison of Theory and Experiment

The calculated photoemission spectra for the PMDA-ODA repeat unit (obtained by adding the calculated results for the PMDA and hydroxyaniline units) for both the Koopmans' (dotted line) and ΔSCF (solid line) methods are compared to the experimental spectrum (triangles) in Figure 3. For comparison with experiment, each of the 1s ionization energies has been assigned equal intensity, Gaussian broadened by ~ 1 eV and then summed to yield a calculated energy distribution curve. The Koopmans' derived 1s ionization energies are tens of electron volts higher, relative to *both* the ΔSCF and experimental results. Examination of Figure 3 clearly shows that the effect of core-hole relaxation is responsible for, essentially, the major difference between the Koopmans' result and experiment. The carbon, nitrogen, and oxygen calculated ΔSCF photoemission peaks are now within 1.0 eV of the experimental

data. Even though the Koopmans' result is shifted significantly in absolute magnitude with respect to experiment, its' utility in interpreting photoemission data is generally recognized, since within each elemental grouping of photoemission levels, relaxation of inequivalent atoms yields comparable relaxation energies.
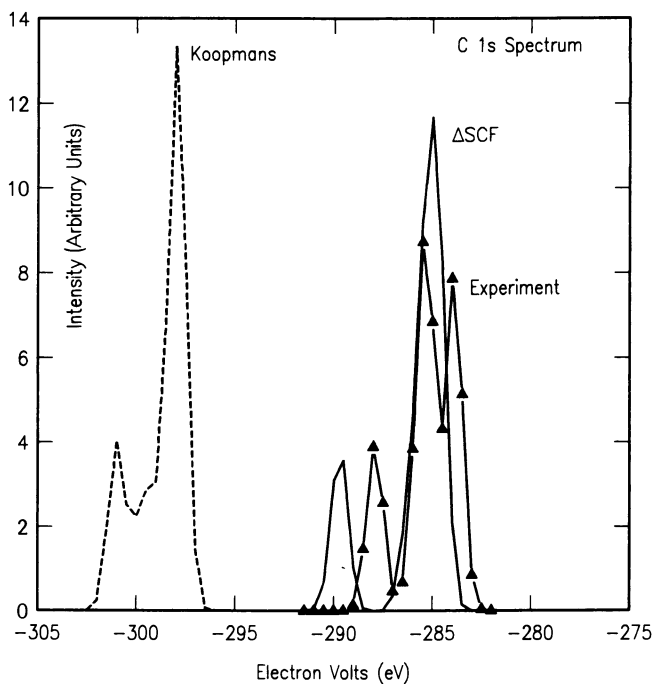
The experimental C1s spectrum[14] (connected triangles) along with the calculated (Koopmans'-dashed, ΔSCF-solid) broadened C1s spectra are given in Figure 4. The expanded scale in Figure 4 highlights the differences between the experimental spectrum of PMDA-ODA and the ΔSCF C1s values. It should be noted, however, that there is excellent agreement between the magnitude of the calculated and observed C1s spectrum. The Koopman's result on this scale is truly shown to be outside of the range of experiment. On a finer scale, there are differences between the ΔSCF and experimental values. The experimental peak at ~ 288 eV corresponds to the C1s(C=O) level and is approximately 1 eV lower binding energy that the calculated ΔSCF result. This difference is expected to arise from two factors. First, interchain coupling between carbonyl oxygen atoms and adjacent groups will decrease the carbon-oxygen bond order involving the carbonyl group, resulting in a shift of the carbonyl C1s core level to lower binding energy. Second, it is expected that the incomplete basis set describing the 1s orbital on the carbon atom can result in incomplete relaxation of the C(C=O) core hole. There is closer agreement between the main peak occurring at 285 eV and the ΔSCF results. The main peak, centered at 285 eV, has contibutions from the C1s(Ph-H) levels for the low-energy side, while the central and high-energy portions are derived from the C1s(Ar-H), C1s(Ar-C=O), and C1s(C-N) levels of the PMDA fragment. The absence of a double hump for the main peak of the calculated spectrum is primarily the result of values chosen to simulate the experimental broadening.
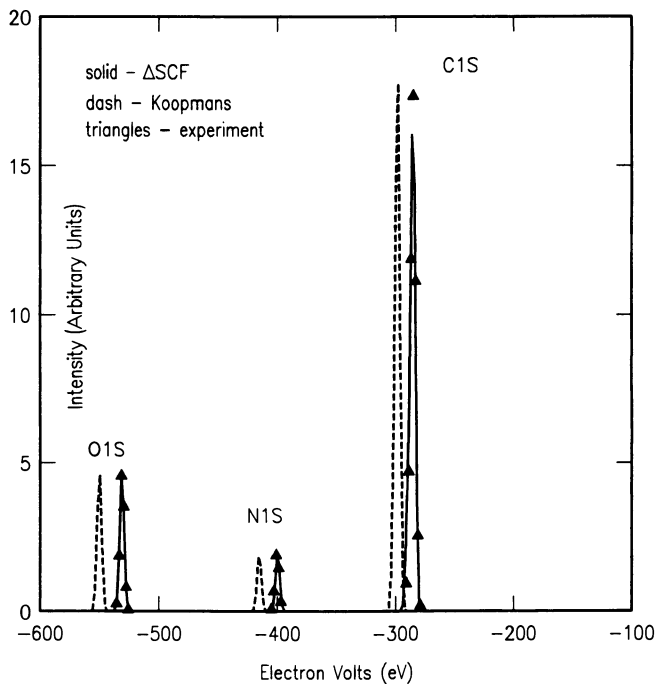
Figure 3.   The calculated photoemission spectra for the PMDA-ODA repeat unit for both Koopmans' (dotted line) and ΔSCF (solid line) and the experimental spectrum (triangles).

Figure 4.   The experimental C1s spectrum (connected triangles) and calculated
(Koopmans'-dashed, ΔSCF-solid) broadened C1s spectra.

Charge Shifts and Screening

To illustrate the screening process taking place upon core hole ionization, the electron population shifts between the neutral and ionized species will be examined. An electron density difference plot for the σ valence electrons is given in Figure 5 for the C1s(C=O) ionization process. Only σ electrons are shown in the plot since the electron density differences have been plotted in the nodal plane of the π molecular PMDA fragment. This plot illustrates that valence σ electron density moves from immediate regions surrounding the core hole (C(Ph), O(C=O), and N) to the C(C=O) atom. This increased electron density from surrounding atoms is the result of core hole relaxation which is driven by essentially, Coulomb forces. A similar shift of charge is also observed for the π system, but the amount of charge shifted is less than for the σ electrons. For the calculated core holes on the other atoms, the trend in neighboring atoms supplying electrons, as for case the of C1s(C=O), is maintained.
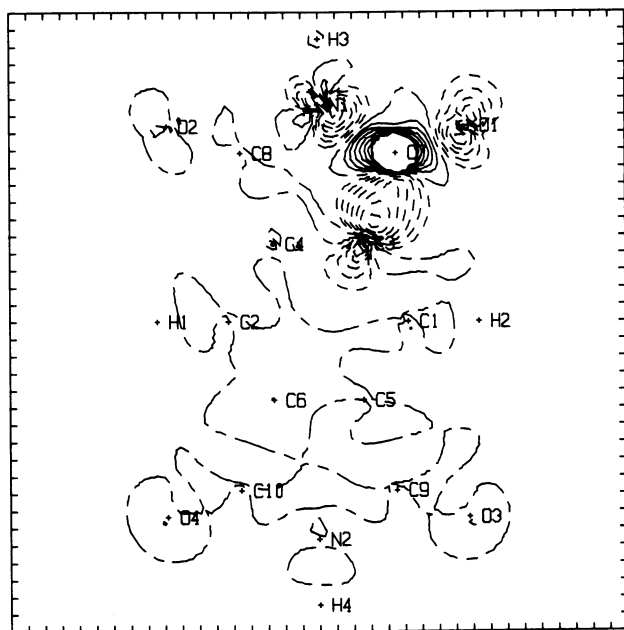
Figure 5. σ electron density difference plot for C1s(C=O) state of the PMDA segment. The dashed contour lines indicate removal of electronic charge relative to the neutral species. The solid lines specify increased electron charge with respect to the neutral PMDA fragment.

Summary

The agreement between the magnitudes of the core hole ionization energies calculated by the ΔSCF method and obtained from experiment is excellent. Differences, however, still remain when comparing experiment and theory to values within 1 eV. These differences are expected to be due to shortcomings in treating the actual polymeric environment, as well as to inherent limitations of the computational procedure. The Koopmans' results yield, as expected, very good *relative* splittings, but *absolute* ionization energies that are far from the experimental values.

Literature Cited

1. Hahn, P. O.; Rubloff, G. W.; Ho, P. S. *J. Vac. Sci. Technol.*, **1984**, A2, 756.

2. Silverman, P. N.; Sanda, P. N.; Ho, P. S.; Rossi, A. R. *J. Polym. Sci., Pol. Chem. Ed.*, **1985**, *23*, 2857.

3. Silverman, B. D.; Bartha, J. W.; Clabes, J. G.; Ho, P. S.; Rossi, A. R. *J. Polym. Sci., Pol. Chem. Ed.*, **1986**, *24*, 3325.

4. Rossi, A. R.; Sanda, P. N.; Silverman, B. D.; Ho, P. S. *Organometallics*, **1987**, *6*, 580.

5. Haight, R.; Silverman, B. D.; White, R. C.; Ho, P. S.; Rossi, A. R. *Mat. Res. Soc. Symp.*, **1988**, *108*, 233.

6. Koopmans T. *Physica*, **1934**, *1*, 104.

7. Ford, P. C.; Hillier, I. H. *J. Chem. Phys.* **1984**, *80*, 5664 and references therein.

8. Professor E. R. Davidson and co-workers, Department of Chemistry, Indiana University, Bloomington, Indiana 47405.

9. Hsu, H.; Davidson, E. R.; Pitzer, R. M. *J. Chem. Phys.* **1976**, *65*, 609.

10. Bagus, P. S.; Schaefer III, H. F. *J. Chem. Phys.*, **1972**, *56*, 224.

11. Huzinaga, S. *J. Chem Phys.* **1965**, *42*, 1293.

12. Dunning, Jr., T. H.; Hay, P. J. in *Modern Theoretical Chemistry.*; Schaefer, III, H. F., Ed.; Plenum Press: New York, 1976; Vol. 3, Chap. 1.

13. Takahashi, N.; Yoon, D. Y.; Parrish, W. *Macromolecules*, **1984**, *17*, 2853.

14. Haight, R.; White, R. C.; Silverman, B. D.; Ho, P. S. *J. Vac. Sci. Technol.*, **1988**, *A 6*, 2188.

Chapter 7

Effect of Diamic Acid Additives on Dielectric Constants of Polyimides

Diane M. Stoakley and Anne K. St. Clair

NASA Langley Research Center, Hampton, VA 23665–5225

The dielectric constants of commercially available polyimides used by the electronics industry range from approximately 3.2 - 4.0. Studies at NASA-Langley have established structure-property relationships in polyimides that provide a means of lowering dielectric constants by chemically altering the composition of polymer backbones to reduce chain-chain electronic interactions. That work has been extended to provide even further reductions in the dielectric constants of aromatic condensation polyimides by physically incorporating selected diamic acid additives into low dielectric constant polyimide systems. Polyamic acid resins containing 3 - 15 wt % of low molecular weight amic acid additives have been imidized and characterized. The dielectric constants of the resulting films ranged from 2.4 - 2.9, with minimal effect on the glass transition temperature and thermooxidative stability of the polymers.

Commercially available polyimides are being used increasingly by the electronics industry as high performance films and coatings. To be effective passivants and interlevel dielectrics they must be excellent insulators. The dielectric constants of commercial polyimides range from approximately 3.2 to 4.0, depending on the moisture content of the film and the measurement frequency. Studies conducted at NASA-Langley have established structure-property relationships in polyimides that provide a means of lowering their dielectric constants by chemically altering the composition of the polymer backbone to reduce chain-chain electronic interactions and by incorporation of fluorine atoms into the polymer molecular structure.[1]

That work has been extended to provide even further reductions in the dielectric constants of aromatic condensation polyimides by physically incorporating selected diamic acid additives into low dielectric constant polyimide systems. The monomer selection for the synthesis of these additives was based on the results of the Langley structure-property studies on lowering the dielectric constant of polyimides.[1]

The concept of synthesizing diamic acid additives and incorporating them into polyimides has previously been reported by NASA-Langley researchers in studies that were aimed at improving the processability of polyimides.[2-4] That work resulted in

increased melt flow in polyimides containing diamic acid additives and provided improved composite mechanical properties because of better composite consolidation.

Experimental

Materials

The aromatic diamines and dianhydrides used in the preparation of the polyamic acid resins and the diamic acid additives are listed in Figure 1. The 2,2-bis(3,4-dicarboxyphenyl)hexafluoropropane dianhydride (6FDA), 4,4'-oxydianiline (4,4'-ODA), and 3,3'-diaminodiphenylsulfone (3,3'-DDSO$_2$) were obtained from commercial sources. The remaining monomers were obtained as experimental materials as follows: (1) 4,4'-bis(3,4-dicarboxyphenoxy) diphenylsulfide dianhydride (BDSDA) from General Electric Corporate R&D Center; (2) 4,4'-oxydiphthalic anhydride (ODPA) from Occidental Chemical Corporation; (3) 2,2-bis[4(4-aminophenoxy)phenyl]hexafluoropropane (4-BDAF) from Ethyl Corporation and (4) 2,2-bis[4(3-aminophenoxy)phenyl]hexafluoropropane (3-BDAF) and 3,3'-oxydianiline (3,3'-ODA) from Mitsui Toatsu, Inc.

Dianhydrides

6FDA   BDSDA   ODPA

Diamines

3,3'-DDSO$_2$ BDAF   ODA
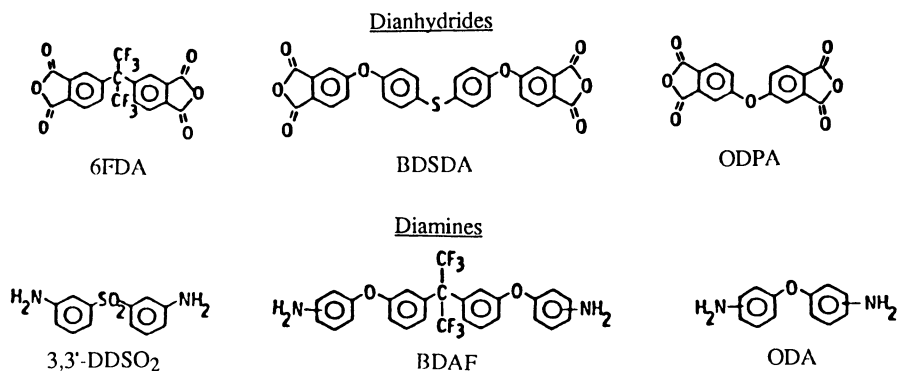
Figure 1. Monomers for polyimides and diamic acid additives.

Polyamic Acid Resins

Polyamic acid resins of BDSDA/4-BDAF, 6FDA/4-BDAF and 6FDA/3-BDAF were prepared in solution containing 15% solids (w/w) in N,N-dimethylacetamide (DMAc) by first dissolving the diamine in the DMAc in a flask flushed with dry nitrogen. The dianhydride was then added and the solution was mechanically stirred at room temperature for 4-5 hours. The inherent viscosities were 0.87 dl/g for BDSDA/4-BDAF, 1.10 dl/g for 6FDA/4-BDAF and 0.64 dl/g for 6FDA/3-BDAF.

Diamic Acid Additives

Six diamic acid additives were prepared by reacting 0.10 mol dianhydride with 0.20 mol aniline (An) or 0.10 mol diamine with 0.20 mol phthalic anhydride (PA) in a solvent mixture of one or more of N,N-dimethylformamide, N-methylpyrrolidinone and diglyme(2) at room temperature. The additives were precipitated into water. The chemical structures of the additives are shown in Figure 2.

6FDA-An   ODPA-An   3,3'-DDSO₂-PA

4,4'-ODA-PA   4-BDAF-PA
                     3-BDAF-PA
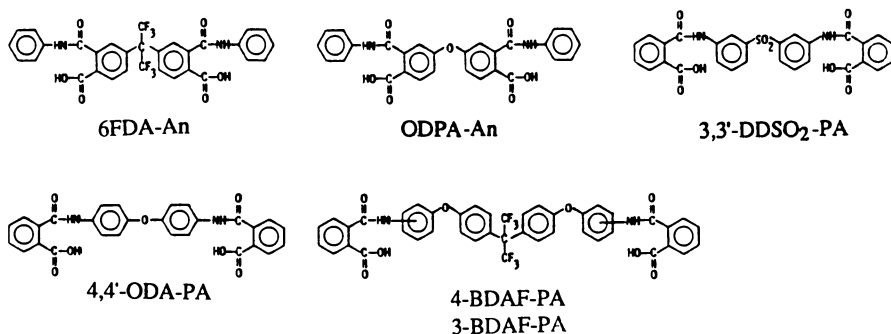
Figure 2. Diamic acid additives.

Polyimide Films

Control films of the polyamic acid resins were prepared by casting the solution of the
resin onto soda-lime glass plates using an aluminum blade with the gap set to obtain ~
1 mil cured film thicknesses. Films were placed in a low humidity box overnight, then
imidized by heating in a forced air oven for one hour each at 100°, 200° and 300°C.

Films containing the diamic acid additives were prepared by dissolving 3 - 15
weight percent (based on resin solids) of the additives into the polyamic acid solutions,
then casting and curing as above.

Characterization

Glass transition temperatures (Tgs) of the films were determined on a DuPont Model
943 Thermomechanical Analyzer (TMA) at a heating rate of 5°C/min. Thermo-
gravimetric analyses (TGA) were obtained in flowing air (15 cc/min) at a heating rate
of 2.5°C/min after an initial 30 min hold at 100°C. Dielectric constants of the films
were determined using a Hewlett Packard 8409C Automated Network Analyzer over
the frequency range of 8 - 12 GHz. The polymer films were desiccated overnight prior
to measurement. A stack of ten 1 mil thick film specimens were run on the network
analyzer at 26°C at 25 - 35% relative humidity to obtain the dielectric constant data.

Results and Discussion

Five diamic acid additives were added at varying concentrations to the polyamic acid
resin of BDSDA/4-BDAF. The properties of the resulting polyimide films are listed in
Table I. These additives were chosen because of their structural similarities to
monomers used to obtain low dielectric polyimides.(1) There was slight embrittlement
of the films containing 10 - 15 wt % additive as evidenced by the films breaking in the
film clamps in the 155 - 200°C range during TMA testing, although all of these films
were fingernail creasable. Additive concentrations higher than those listed gave films
that were noticeably embrittled and were therefore not tested. This embrittlement,
evident in the thin films, is not expected to be a problem when the resin is used in bulk
form. The effect of diamic acid addition on inherent viscosity and polymer molecular
weight has been determined in earlier studies.(3) The Tgs of the BDSDA/4-BDAF
films with 3 - 5 % additive were 4 - 16°C lower than the control. There was no loss in
thermooxidative stability.

Table I. Properties of BDSDA/4-BDAF Films Containing Diamic Acid Additives

Additive	Additive Conc., wt %	Tg by TMA, °C	TGA 10% wt. loss, °C	Dielectric Constant, 10 GHz
Control	--	217	517	2.84
6FDA-An	3	213	519	2.86
	5	207	530	2.85
	10	--(a)	529	2.80
	15	--(a)	507	2.73
ODPA-An	5	--(a)	521	2.65
3,3'-DDSO$_2$-PA	3	213	519	2.84
	5	203	516	2.84
	10	--(a)	500	2.71
4-BDAF-PA	5	208	520	2.61
	10	--(a)	515	2.59
3-BDAF-PA	5	201	521	2.71

(a)Film broke during testing

The dielectric constant at 10 GHz of the BDSDA/4-BDAF control film was 2.84.
Incorporation of the additives resulted in a lowering of the dielectric constant, in some
cases at the 5 wt % level and, in others, at the 10 - 15 wt % level. The most dramatic
reductions were achieved with the ODPA-An and 4-BDAF-PA additives which
resulted in films with dielectric constants in the range of 2.59 - 2.65.

  The data reproducibility was excellent as long as a single batch of control resin
was used for the studies so that variables such as monomer purity and polymer
molecular weight were controlled. In addition films were cast in a clean room to
minimize dust incorporation which can result in large errors in film thickness
measurements. Figure 3 shows the typical example and the worst case for dielectric
constant data variability on these films.

  An even lower dielectric polyimide was chosen as a second resin system for
screening the diamic acid additives. The 6FDA/4-BDAF control film had a dielectric
constant at 10 GHz of 2.53. As seen in Table II the effects on Tg and thermooxidative
stability of incorporating the additives into this resin system were comparable to those
seen in the BDSDA/4-BDAF films. However, not all of the additives screened were
effective in lowering the dielectric constant of the 6FDA/4-BDAF system. The ODPA-
An and 4-BDAF-PA additives that were most effective in the BDSDA/4-BDAF system
were also effective here, lowering the dielectric constant from 2.53 to 2.48. Even
more effective in the 6FDA/4-BDAF system was the incorporation of 4,4'-ODA-PA,
which had not been screened in the other resin. A 10 wt % concentration of 6FDA-An
provided still further reductions to 2.43.

  The ability of these additives to lower the dielectric constant appears limited as
the dielectric constant of the base resin is lowered even further. Screening of the
6FDA-An, ODPA-An, 4-BDAF-PA and 3-BDAF-PA additives in 6FDA/3-BDAF did
not result in any reduction in the dielectric constant of the base resin from its already

low value of 2.48 as is shown in Table III. In this resin system, however, three of the additives were not screened above a 5% (w/w) level because of film embrittlement. The 6FDA-An additive was screened at 10% (w/w), but did not result in any further lowering of the base resin's dielectric constant.
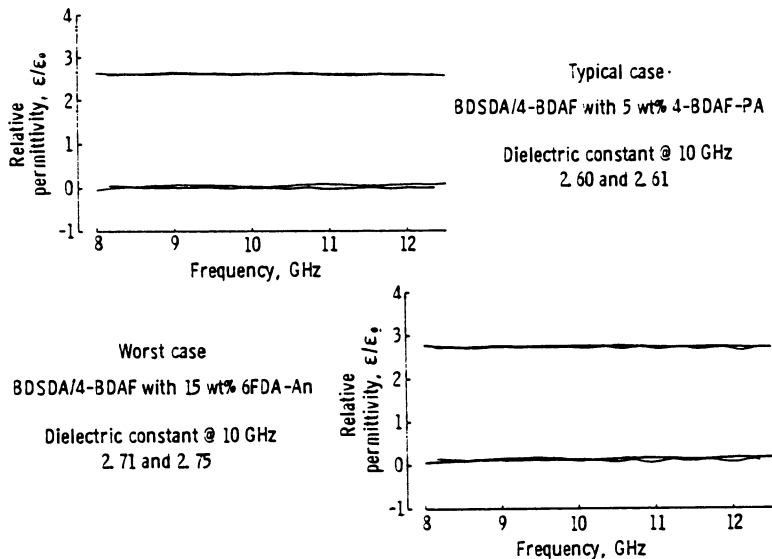
Figure 3. Dielectric constant data variability.

Table II. Properties of 6FDA/4-BDAF Films Containing Amic Acid Additives

Additive	Additive Conc., wt %	Tg by TMA, °C	TGA 10% wt. loss, °C	Dielectric constant, 10 GHz
Control	--	267	502	2.53
6FDA-An	3	257	507	2.56
	5	257	509	2.56
	10	--(a)	518	2.43
ODPA-An	5	--(a)	507	2.48
3,3'-DDSO$_2$-PA	3	252	506	2.50
	5	250	510	2.49
	10	--(a)	508	2.56
4,4'-ODA-PA	10	249	509	2.45
4-BDAF-PA	5	247	500	2.48
3-BDAF-PA	5	245	505	2.56

(a)Film broke during testing

Table III. Properties of 6FDA/3-BDAF Films Containing Diamic Acid Additives

Additive	Additive conc., wt %	Tg by TMA, °C	TGA 10% wt. loss, °C	Dielectric constant, 10 GHz
Control	--	218	505	2.48
6FDA-An	5	212	505	2.52
	10	--(a)	502	2.58
4-BDAF-PA	5	--(a)	495	2.59
3-BDAF-PA	5	213	510	2.55

(a)Film broke during testing

　　　　Two of the additives were also incorporated into a more conventional polyimide system, pyromellitic dianhydride (PMDA)/4,4'-ODA, to see if the diamic acid additives were effective in lowering the dielectric constant of a higher dielectric constant polyimide also. The evaluation was preliminary in that only two additives were screened at one concentration. As is shown in Table IV the dielectric constant was lowered, though not as significantly as in the BDSDA/4-BDAF system.

Table IV. Properties of PMDA/4,4'-ODA Films Containing Diamic Acid Additives
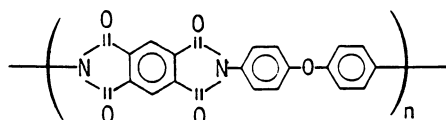
Additive	Additive conc., wt %	Tg by TMA, °C	TGA 10% wt. loss, °C	Dielectric constant, 10 GHz
Control	--	307	532	3.14
6FDA-An	10	308	523	3.02
4-BDAF-An	10	308	520	3.09

Conclusions

Selected diamic acid additives have been incorporated into low dielectric polyimide resins. Their addition resulted in a slight lowering of Tgs with no pronounced effect on thermooxidative stability. Dielectric constants have been significantly lowered by incorporating these additives - from 2.84 to 2.59 for BDSDA/4-BDAF films and from 2.53 to 2.43 for 6FDA/4-BDAF films. The effectiveness of the physical incorporation of these additives in reducing the dielectric constant of polyimides is limited as the dielectric constant of the base resin itself becomes very low.

References

1. St. Clair, A. K.; St. Clair, T. L.; Winfree, W. P. U.S. Patent Application 073542, 1987.
2. Stoakley, D. M.; St. Clair, T. L.; St. Clair, A. K.; Pratt, J. R.; Burks, H. D. ACS Polymer Preprints, 1986, 27(2), pp. 406-07.
3. Pratt, J. R.; St. Clair, T. L.; Burks, H. D.; Stoakley, D. M. SAMPE Symposium Preprints, 1987, 32, pp. 1036-50.
4. St. Clair, T. L.; Pratt, J. R.; Stoakley, D. M.; Burks, H. D. Proc. from the 3rd Intern'l Conf. on Polyimides, 1988, pp. 210-14.
5. Stoakley, D. M.; St. Clair, A. K. NASA Langley Invention Disclosure LAR 13902-1, 1987.

Chapter 8

Organic Dielectric Materials with Reduced Moisture Absorption and Improved Electrical Properties

D. L. Goff[1], E. L. Yuan[1], H. Long[1], and Herbert J. Neuhaus[2]

[1]Electronics Department, Experimental Station Laboratory, E. I. du Pont de Nemours and Company, Wilmington, DE 19880–0336
[2]Microsystems Technology Laboratories, Massachusetts Institute of Technology, Cambridge, MA 02139
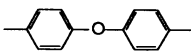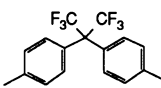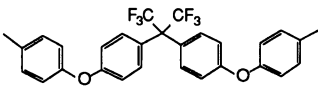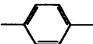
High performance polyimide films and coatings are finding increased use within the electronics industry for wafer, packaging, and board applications. The move toward increased circuit density and signal speed in these constructions has emphasized the need for identifying polyimide materials for interlayer dielectric applications which have dielectric constants < 3.0 and low levels of moisture absorption. Most commercially available aromatic polyimide chemistries have dielectric constants in the range of 3.0 to 4.0 and absorb between 2.5% to 4.0% by weight moisture. Also, the dielectric constant for a particular polyimide will vary with the amount of absorbed moisture. This tendency for polyimides to absorb moisture not only affects their electrical performance but also can place constraints on their processing utility in device fabrication. Two approaches to developing polyimide materials having reduced dielectric constants and lower levels of moisture absorption will be reported.

A reduction in the dielectric constant and level of moisture absorption can be achieved when fluorine is incorporated into an aromatic polyimide. One of the first commercially available fluorinated polyimides for electronic applications was produced by DuPont and is based on 2,2-bis(3,4-dicarboxyphenyl)hexafluoropropane dianhydride/oxydianiline (6FDA/ODA) backbone chemistry[1] (Table 1). Early work by DuPont in the area of fluorinated dianhydride and diamine monomers[2] also led to the development of a polyimide chemistry based on 2,2-bis(3,4-dicarboxyphenyl)hexafluoropropane dianhydride/2,2-bis(4-aminophenyl) hexafluoropropane (6FDA/6FDAM). The 6FDA/6FDAM polyimide is currently undergoing a renewed interest due to its excellent electrical properties (K=2.7) and low moisture absorption (<1.0%). However, its overall processing utility is somewhat limited due to poor mechanical properties and extreme solvent sensitivity.

In an effort to obtain a better property balance, the 6FDA/6FDAM polyimide was modified through the incorporation of aryl ether segments. The resulting 2,2-bis(3,4-dicarboxyphenyl)hexafluoropropane dianhydride/2,2-bis[4-(4-aminophenoxy)phenyl] hexafluoropropane (6FDA/BDAF) polyimide had a dielectric constant of 2.8 and a level of moisture absorption <1.0% (Table 1). Cured coatings of the 6FDA/BDAF polyimide displayed less solvent sensitivity toward NMP, ketones, THF, and diglyme

Table 1. 6FDA Based Polyimides

Polyimide (1)	Diamine (Ar)	Dielectric Constant (2)	% H$_2$O Absorbed	T$_g$ (°C)	T$_d$ (°C)
6FDA + ODA		3.00	1.5	300	525
6FDA + 6FDAM		2.70	<1.0	320	530
6FDA + BDAF		2.80	<1.0	260	520
6FDA + PPD		3.05	3.8	355	540

(1) Films (2 mil) were cast/cured under clean room conditions and dried prior to test.
(2) Measurements were taken at 1 KHz, 25°C, and 40% to 50% relative humidity.

as compared to the 6FDA/6FDAM polyimide based on visual inspection after 1 hour solvent exposure at room temperature. However, a significant reduction in T_g (260°C) was also observed which most likely is due to an increase in chain flexibility afforded by the aryl ether segments. A more rigid polymer backbone is realized in the 6FDA/ p-phenylene diamine (6FDA/PPD) polyimide and this is reflected in its higher T_g (355°C). However, the 6FDA/PPD polyimide had a dielectric constant of 3.05 and absorbed up to 3.8% by weight moisture.

The 6FDA/BDAF polyimide was modified using PPD in an effort to "stiffen" the polymer backbone and improve thermal performance (T_g). A better overall property balance was achieved in several of these 6FDA/BDAF/PPD copolyimides. A series of random copolymers was prepared in which the level of PPD was varied from 0% to 100% based on the total moles of diamine. The incorporation of PPD had little effect on the dielectric constant but did result in improved thermal performance and was accompanied by increased moisture uptake (Figures 1, 2, and 3). This behavior is consistent with the overall reduction in the amount of bound fluorine in the polymer backbone; however, additional work is required to establish a direct correlation. A reasonable property balance was realized over a range of 40 to 60 mole% PPD which displayed dielectric constants from 2.85 to 2.90, moisture absorption from 1.5% to 2.0%, and T_g from 280°C to 290°C. In addition, the 6FDA/BDAF/PPD copolyimides displayed somewhat less solvent sensitivity than the 6FDA/BDAF homopolymer as described above.

Polyimide-Teflon composites provide another approach for reducing the dielectric constant and level of moisture uptake in polyimide coatings. Our initial work involved the use of Teflon FEP and polyimides based on pyromellitic dianhydride/oxydianiline (PMDA/ODA) and 6FDA/ODA backbone chemistries. The Teflon FEP powder was dispersed in N-methylpyrrolidone (NMP) based solutions of the polyamic acid precursors of the PMDA/ODA and 6FDA/ODA polyimides. The resulting dispersions tended to settle on standing but were readily restored through mild agitation. When cured the coatings were opaque and exhibited a gradient of Teflon stratification with the greatest concentration of Teflon FEP at the surface of the coating. The incorporation of Teflon FEP afforded reduced dielectric constants and lower levels of moisture absorption as compared with the pure polyimides (Table 2).

Table 2. Polyimide-Teflon Composites

Composition	Teflon Wt%	Vol%	Dielectric Constant	% H_2O Absorbed	Tensile (PSI)	Elong (%)	E (KPSI)
Teflon FEP	100	100	2.15	< 0.5	3,000	300	70
PMDA/ODA	0	0	3.37	2.2	12,000	25	202
PMDA/ODA-Teflon FEP	35	26	---	---	8,200	20	178
	48	37	3.12	1.4	----	--	---
	60	49	3.01	1.1	7,700	21	150
	68	54	2.85	1.0	----	--	---
	73	63	---	---	5,500	11	140
6FDA/ODA	0	0	3.06	1.5	10,900	15	270
6FDA/ODA-Teflon FEP	38	28	---	--	7,300	9	192
	58	47	2.58	--	4,100	5	150
	68	54	2.50	--	3,800	5	140
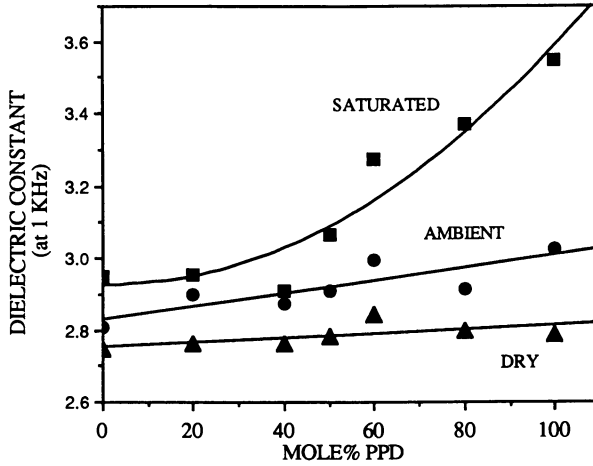
Figure 1. Dielectric constant vs. backbone chemistry for 6FDA/BDAF/PPD copolymers.
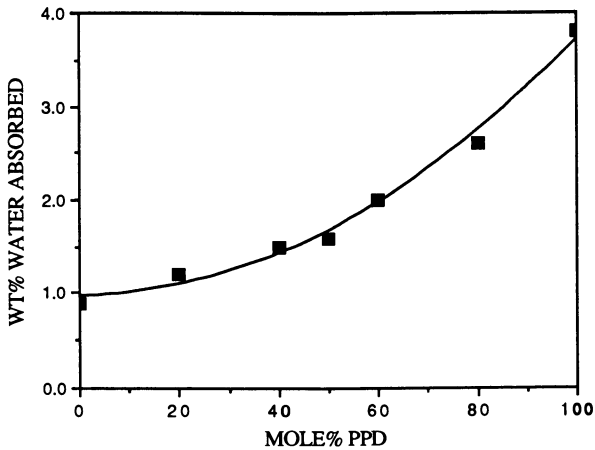
Figure 2. Water absorption vs. backbone chemistry for 6FDA/BDAF/PPD copolymers.
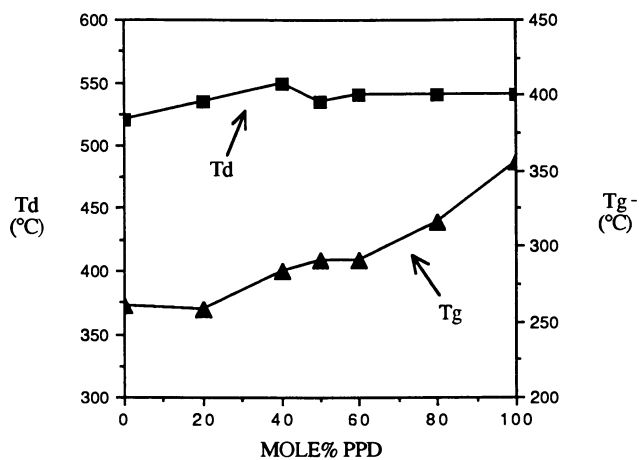
Figure 3. Thermal stability vs. backbone chemistry for 6FDA/BDAF/PPD copolymers.

However, as the level of Teflon FEP is increased, the mechanical properties of the composite are markedly decreased. A 60% by weight Teflon FEP loading is considered the useful limit, especially in the case of the 6FDA/ODA example. The dielectric constants for the composite coatings were determined using plane to plane capacitor test structure and were significantly lower than for the pure polyimides (Figure 4). The moisture absorption for several PMDA/ODA-Teflon FEP composites was determined by monitoring their capacitance change on exposure to ambients with varying moisture levels. The results showed that a two-fold reduction in the level of moisture absorption for PMDA/ODA can be achieved with a 60% by weight loading of Teflon FEP (Figure 5).

Experimental

The polyamic acid precursor solutions were prepared by the addition of the dianhydride to a solution of the diamine(s) in N-methylpyrrolidone (NMP) at 25°C under dry conditions.   The reactions were allowed to stir for 24 hours at room temperature following the dianhydride addition. The resulting polyamic acid solutions were pressure filtered to 1.0 μ (absolute), knife coated onto glass substrates (class 100 clean room), and thermally cured (350°C) to afford polyimide coatings of from 1 to 2 mils in thickness. The coatings were removed by soaking in water and then dried to constant weight in a vacuum oven (200°C). The dielectric constants were measured on film specimens using a Polymer Laboratories Dielectric Thermal Analyzer (DETA) at 25°C. The films had been metallized (top and bottom) with sputtered gold (200Å), and conditioned using water immersion (48 hours), ambient (40-60% R.H./48 hours), and oven dry (200°C/2 hours) immediately prior to test. Levels of moisture absorption were determined by gravimetric analysis of film samples which were conditioned using oven dry (200°C/2 hours) and water immersion (48 hours). Thermal analyses were performed using a DuPont Model 910 Differential Scanning Calorimeter (T_g) and a DuPont Model 990 Thermal Analyzer (T_d).

The Teflon dispersions were prepared by mixing Teflon FEP powder in NMP based solutions the polyamic acids. The dispersions were applied to glass or silicon wafer substrates by knife or spin coating techniques and thermally cured (120°C to 350°C) to imidize the polyamic acid and fuse the Teflon FEP fluorocarbon. The coated substrates were either characterized as prepared or the coatings were removed by soaking in water and the films dried to constant weight in a vacuum oven. The dielectric constants were determined using parallel plate capacitor micro test structures. The moisture absorption was determined by monitoring capacitance change on exposure to ambients with moisture levels between 0% and 50% R.H. and extrapolating to 100% R.H. The correlation between capacitance change in polyimide and water uptake has been demonstrated by Denton.[3,4] Mechanical properties were obtained for the free films using an Instron Model 1122.

Summary

Aromatic polyimides with dielectric constants < 3.0 and reduced levels of moisture absorption can be obtained by the incorporation of fluorine into the polymer backbone. However, this approach can also lead to a reduction in the thermal properties (T_g), and/or solvent resistance of the polymer. It has been found that the incorporation of paraphenylene diamine (PPD) into the 6FDA/BDAF polyimide affords copolymers having improved thermal performance and solvent resistance as compared with the parent homopolymer while maintaining a dielectric constant of 2.9 and moisture uptake < 2.0%. This approach can be considered as a possible alternative to the use of
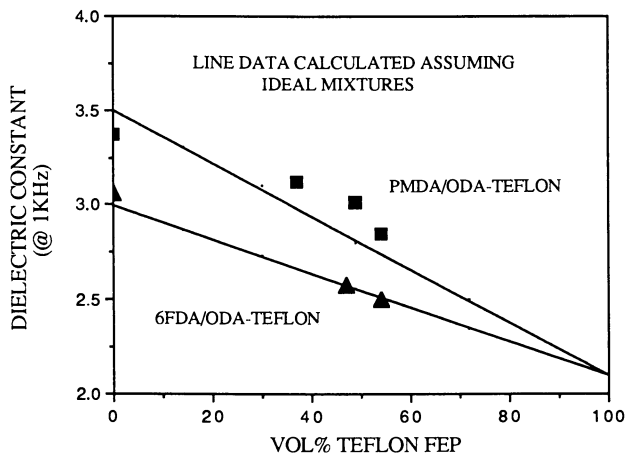
Figure 4. Dielectric properties for polyimide-Teflon composites.
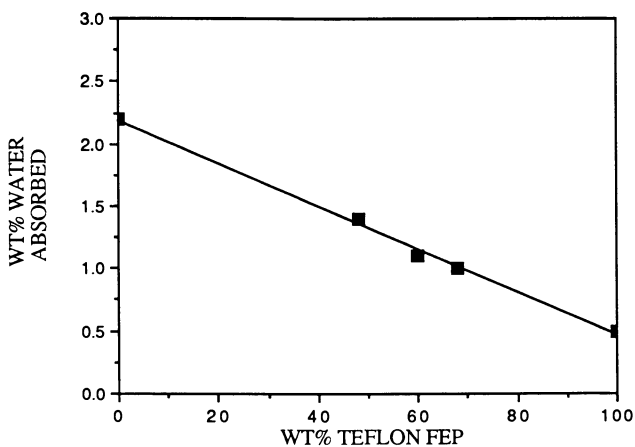
Figure 5. Water absorption vs. wt % Teflon for PMDA/ODA polyimide-Teflon composites.

crosslinked systems. It has also been demonstrated that Teflon FEP powder can be blended with polyamic acid solutions to yield dispersions which on cure provide polyimide-Teflon composite coatings having reduced dielectric constant and moisture absorption as compared with the pure polyimides.

Literature Cited

1. Rogers, F. E. U.S. Patent 3 959 350, 1976.

2. Coe, D. G. U.S. Patent 3 310 573, 1967.

3. Denton, D. D.; Camou, J. B.; Senturia, S. D. Proc. ISA Moisture and Humidity Conference, 1985, pp 505-513.

4. Denton, D. D. ; Priore, D. F.; Senturia, S. D.; Anolick, E. S.; Scheider, D. J. Elec. Mat. 1985, 14, 379-404.

Chapter 9

Synthesis and Characterization of the *t*-Butyl Ester of the Oxydianiline–Pyromellitic Dianhydride Polyamic Acid

F. M. Houlihan, B. J. Bachman, C. W. Wilkins, Jr., and Coralie A. Pryde

AT&T Bell Laboratories, Murray Hill, NJ 07974

Novel *t*-butyl esters of oxydianiline/pyromellitic dianhydride polyamic acid were prepared in good yield. The polymers were prepared with either meta or para repeating units. The cure behavior of these *t*-butyl esters was studied by IR, MS and TG analysis and was compared to that of both the parent polyamic acid and its methyl ester. It was found that a rapid deprotection of the *t*-butyl group occurs at around 200°C with liberation of free polyamic acid. Consequently, the cure behavior at 200°C of the *t*-butyl ester approaches that of the parent polyamic acid. Furthermore, the isomerism of the repeating units does not appear to have any detectable effect on the cure behavior of the polymer, although, meta isomerism appears to enhance solubility of the polymer in organic solvents.

Linear alkyl esters of polyamic acids have been prepared in the past.[1-8] Such esters are of interest because they are more stable in solution than the parent acids[4-7] and show little if any change in molecular weight with time. Unfortunately, the curing rates of linear alkyl esters are much slower than those of the corresponding acids (up to 60 times slower for the n-butyl ester).[4] In our work we sought to avoid this difficulty by synthesizing a polyamic ester capable of thermally liberating the free polyamic acid. Moreover, it was hoped that this type of approach would yield novel polyimide precursors with thermally removable bulky solubilizing groups. This could enable us to take advantage of the solubilizing effect of such groups during processing, giving access to low-boiling-point film-casting solvents, while ensuring that the final cured polyimide retains valuable physical properties. This work reports the synthesis of the *t*-butyl esters of the ODA/PMDA polyamic acids, and describes some preliminary physical properties of these materials. The *t*-butyl group (carbonate or ester) has been reported to thermally deprotect the hydroxyl group in styrene and polycarbonate-

based polymer systems. This precedent encouraged us to choose this type of protecting group for our application.[9–10]

EXPERIMENTAL

Materials and Characterization.

Elemental analyses were obtained from Galbraith Laboratories Inc. Polymer molecular weights were determined using a Waters Model 590 gel permeation chromatograph equipped with a Zorbax column, a Waters 410 differential refractometer, and a Waters Lambda-Max LC spectrophotometer. Molecular weights are given relative to polystyrene standards. NMR spectra were obtained on a Jeol 90Q FTNMR spectrometer, IR spectra were obtained on a Digilab FTS-60 FTIR spectrometer and mass spectra were obtained using an HP 5995C mass spectrometer with a direct insertion probe (DIP).

Preparation of the di–t–butyl Ester of Pyromellitic Acid.

Potassium t-butoxide, 20.60 g (184 mmoles), was added, while stirring under dry argon, to 20.00 g (91.69 mmoles) pyromellitic dianhydride dissolved in 400 mL of THF. After stirring overnight the resulting suspension was filtered-off, washed with THF and ether, and dried to give the potassium salt of the desired product. The salt was neutralized in aqueous solution with dilute HCl while keeping cold (10°C). The product was filtered, washed with distilled water, dried, and recrystallized several times from ethanol water. A total of 22.08 g (66% yield) of di-t-butylester was recovered in three crops of crystals. These crops consisted of 10.50 g of pure para isomer, 7.43 g of pure meta isomer, and a 50% mixture of the two isomers which constituted the remainder.

meta isomer:

Elemental analysis (C,H,0): found (58.98, 6.10, 35.29); calc (59.01, 6.05, 34.93).

IR (KBr, cm^{-1}): 3415, 2987, 2941, 1704, 1502, 1442, 1412, 1394, 1310, 1276, 1260, 1163, 1137, 1112, 927, 848, 796, 778.

H-1 NMR (ppm, DMSO D-6)*: 13.64 (broad s, 2H,OH acid); 8.05 (s, 1H, CH#6); 7.81 (s, 1H, CH#3); 1.65 (s, 18H, CH$_3$ t-butyl). *(For assignment see Scheme 1).

para isomer:

Elemental analysis (C,H,O): found (58.87, 6.04, 34.79); calc (59.01, 6.05, 34.93).

IR (KBr, cm^{-1}): 3570, 3001, 2982, 2935, 1728, 1704, 1502, 1442, 1422, 1369, 1306 1280, 1266, 1259, 1177, 1142, 917, 850, 803.

H-1 NMR (ppm, DMSO D-6)*: 13.64 (broad s, 2H, OH acid); 7.93 (s, 2H, CH#6,3); 1.65 (s, 18H, CH$_3$ t-butyl).* (for assignments see Scheme 1).

Formation of the Polyamic Acid Ester Derived From the para–di–*t*–butyl Ester of Pyromellitic Acid and ODA in NMP.

A solution was prepared under argon consisting of 0.7327 g (2 mmole) of para-di-*t*-butyl ester of PMDA, 0.4005 g (2 mmole) ODA, and 0.56 mL triethyl amine in solution in 2 mL NMP. The solution was cooled to -10°C and 1.6976 g (4 mmole) of N,N′-phenylphosphinobis[2(3H)-benzothiazolone] was added slowly. The reaction was kept at -10°C for 12 min and then allowed to return to room temperature, and stirred for 2 more hours. After diluting with 8 mL of NMP, the polymer solution was precipitated in 200 mL of methanol, filtered, washed with methanol and dried under vacuum for several days. In this way 0.83 g (79% yield) of tan polymer was isolated.

Molecular weight: Mw=18,000, Mn=11,000, D=1.6

Elemental analysis (C,H,N,O): found (66.56, 5.88, 5.30, 21.50); calc (67.91, 5.69, 5.27, 21.10).

IR: (KBr, cm^{-1}): 3320, 1722, 1679, 1607, 1512, 1407,1391, 1220, 1249, 1162, 1135, 1106.

H-1 NMR (DMSO D6, ppm)*: 10.63 (broad s, 2H, amide); 7.93 (s, 2H, H#6); 7.78 (d, 4H, H#2); 7.04 (d, 4H, H#3); 1.49 (s, H#11).* (for assignments see Figure 1b).

Formation of the Polyamic Acid Ester Derived From the meta–di–*t*–butyl Ester of Pyromellitic Acid and ODA in NMP.

The procedure was the same as in 2.1.2 except that the meta di-*t*-butyl ester of PMDA was used as a starting material. The workup differed in that the polymer was precipitated in a 50/50 mixture of methanol and water. In this way 0.87 g (82% yield) of tan polymer was recovered.

Molecular weight: Mw=20,000 Mn=7,000 D=2.8

Elemental analysis (C,H,N,O): found (66.63, 5.55, 5.22, 21.65); calc (67.91, 5.69, 5.27, 21.10).

IR: (KBr, cm^{-1}): 3320, 1722, 1685, 1605, 1407,1392, 1497, 1229, 1251, 1159, 1133, 1109.

H-1 NMR (DMSO D6, ppm)*: 10.62 (broad s, 2H amide); 8.13 (s, 1H, H#8); 7.78 (d, 4H, H#2); 7.60 (s, 1H, H#6); 7.04 (d, 4H, H#3); 1.43 (s, 18H, H#12).* (for assignments see Figure 1a).

Studies of Polymer Cure.

The Mass spectral curing studies were done by heating each sample of polymer in the **DIP** consecutively at 100°C, 200°C, and 350°C for 1 hour each. The extent of cure at 200°C was estimated by taking the ratio of the area for the peak at 200°C in the TIC (or the ion chromatogram of water or isobutene) to the combined area of the peaks at 200°C and 350°C. The samples for the IR curing study were spun from dimethylacetamide solutions of the polyamic acid or its esters onto NaCl

plates. The spun samples were dried at 110°C for about one hour, heated slowly to the cure temperature, allowed to remain at that temperature for one hour and then cooled. The degree of imidization then was calculated from the 1375 cm^{-1} imide peak (C-N stretch) using the 1501 cm^{-1} band (CH aromatic ring breathing) as an internal standard.[11] Thermogravimetry (TG) curing studies were performed on a Perkin-Elmer TGS-2 thermogravimetric analyzer interfaced with a System 4 microprocessor for temperature programming and a TADS Model 3700 data station for data acquisition and operational control. All measurements were obtained in N_2 with a gas flow rate of 30 cc per minute. Heating rates used for the dynamic study were 5 and 25°C/minute.

RESULTS AND DISCUSSION

Materials.

The synthetic pathway to arrive at the di-*t*-butyl esters of pyromellitic acid is shown in Scheme 1. These esters could not be made by the classical pathway used for the diester derived from linear alcohols.[8] The synthesis of the polyamic acid esters was accomplished by a procedure involving a direct coupling of a diester diacid monomer with an aromatic diamine (Scheme 2). A peptide coupling agent (N,N′-Phenylphosphino-bis [2(3H)-benzothiazolone], reported useful in the synthesis of aromatic polyamides[12] was used in this reaction. This approach not only had the advantage of avoiding conditions[8] that would cleave the *t*-butyl ester, but also decreased the number of steps needed to prepare the polymer. The polymerization with ODA was done with both the meta and the para isomer of the diacid diester and the solvents used were either NMP or THF. The yield of polymer ranged from 78 to 81%.

The t-butyl esters of ODA/PMDA polyamic acid retained the meta or para isomerism of the parent di-*t*-butyl ester diacid even on prolonged storage in DMSO solution. The identification of the isomers was based on the data provided by C-13 and H-1 NMR spectra. Figures 1a,b shows the two distinct C-13 NMR spectra given by the meta and para isomers. The polymer made up of meta units is soluble in low boiling solvents such as THF or glyme. In contrast, the polymer consisting of para units is soluble only in high boiling, polar solvents such as DMF and NMP. This difference in solubility cannot be accounted for by differences in molecular weight since the two polymers have similar molecular weights. This difference in solubility between para and meta polymers is probably related to the different shapes of the polymer molecules, which depend on the isomerism of the repeating units, and are accentuated by the steric bulk of the *t*-butyl group and its ability to disrupt interchain interactions. It has also been found that only partial meta isomerism (70%) is enough to give solubility of the polymer in low boiling point film casting solvents.

The same procedure was also extended to the n-butyl and methyl ester of the ODA/PMDA polyamic acid giving 79% and 84% yield respectively.
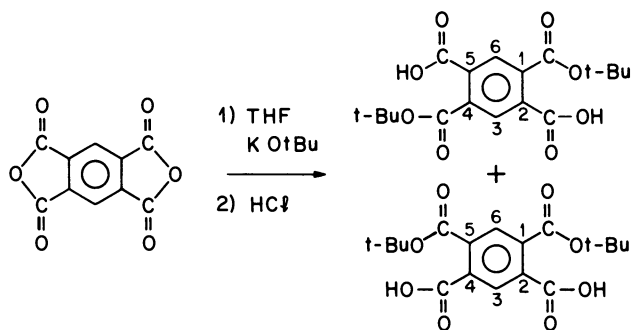
SCHEME 1
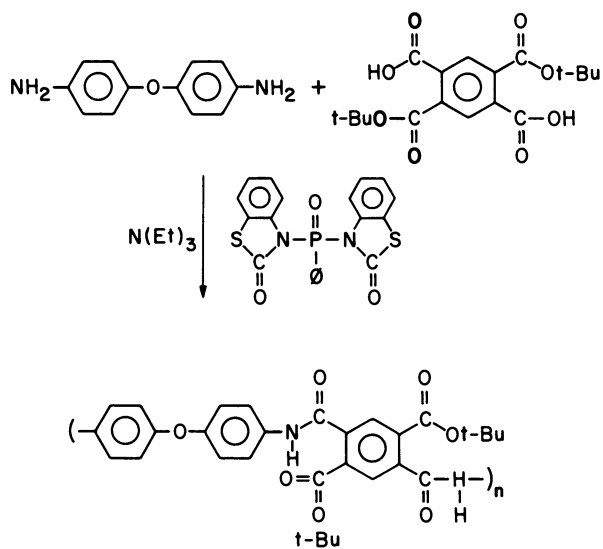
SCHEME 2

A) meta - tert - Bu ESTER OF POLYAMIC ACID
   OF ODA / PMDA
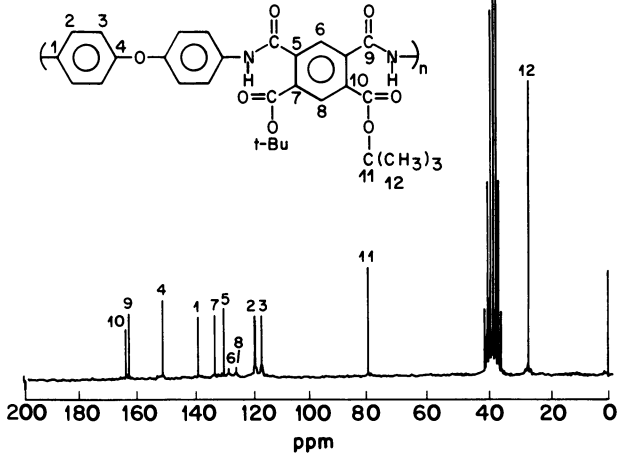
B) para - tert - Bu ESTER OF POLYAMIC ACID
   OF ODA / PMDA
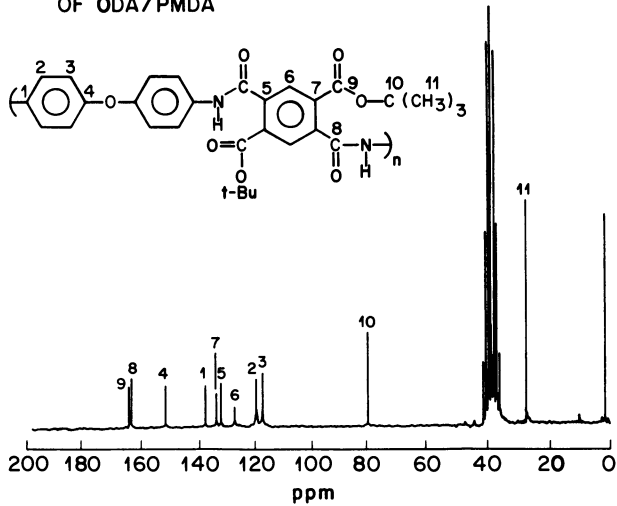
Figure 1. Carbon-13 NMR spectra of the two isomers of the t-butyl ester of the ODA/PMDA polyamic acid

Curing Behavior of Polymers.

Thermogravimetric Analysis.

Thermogravimetric (**TG**) and derivative thermogravimetric (**DTG**) curves obtained using a heating rate of 25°C per minute for ODA/PMDA polyamic acid and its esterified meta and para isomeric products are shown in Figure 2. It can be seen that the ODA/PMDA polyamic acid TG curve (Figure 2) has a broader region for weight loss. Figure 2 also shows the asymmetric shaped DTG curves for the isomeric esters compared with the symmetric curves obtained for the polyamic acid. Additionally, the maximum rate of reaction can been seen to occur earlier for the isomeric esters than for the polyamic acid. The asymmetric shaped DTG curves for the *t*-butyl ester could be explained by the presence of two simultaneously occurring reactions, namely, the deprotection of the carboxylic acid *t*-butyl group, which gives isobutene, and the imidization reaction, which generates water.

Table 1 summarizes the maximum rate of reaction, onset temperature, and weight loss percent at 495°C for the ODA/PMDA polyamic acid as well as the para and meta isomers. Additionally, a comparison of data obtained with and without solvent removal is provided.

Table 1. TG Analyses of ODA-PDA Polyamic Acid
and Its Esterified Products

Polymer	Heating Rate (°C per min)	Condition	Onset Temperature (°C)	Maximum Rate of Reaction (°C)	Weight Loss (Theory) %	Weight Loss (Actual) %
ODA-PMDA	25	Solvent	153	202	8.61	23.9
p-t-Bu Ester	25	Solvent	183	197	27.9	28.3
m-t-Bu Ester	25	Solvent	173	190	27.9	30.0
p-t-Bu Ester	5	Solvent	164	178	27.9	28.6
m-t-Bu Ester	5	Solvent	155	167	27.9	30.0
ODA-PMDA	5	Solvent Removed	150	187	8.61	12.1
p-t-Bu Ester	5	Solvent Removed	163	178	27.9	27.2
m-t-Bu Ester	5	Solvent Removed	164	202	27.9	28.3
Methyl Ester	5	Solvent Removed	176	217	15.3	16.9
n-Butyl Ester	5	Solvent Removed	193	247	27.9	29.0

The theoretical weight loss for the elimination of water, shown in Table 1, for ODA/PMDA polyamic acid is 8.61%. Contrast this with the actual weight loss obtained before and after solvent removal/drying of 23.9% and 13.1%, respectively. Although there are heating rate differences, the ODA/PMDA polyamic acid still exhibited a larger weight loss value before and after extraction/drying than predicted from the theoretical value.

Solvation of the polyamic acid by NMP could account for these larger weight losses. Conversely, both isomeric polyamic acid esters approached their theoretical weight loss of 27.9% regardless of solvent removal procedures.

The para-methyl diester of ODA/PMDA had a weight loss of 16.9% at 495°C
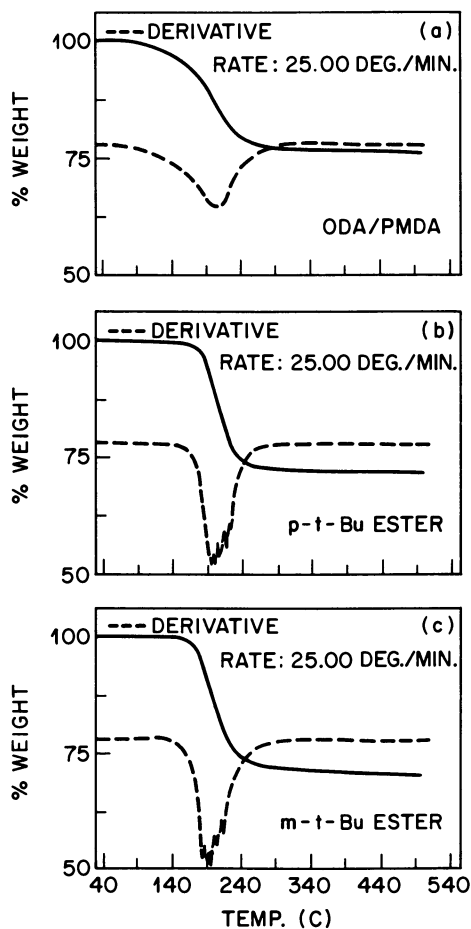
Figure 2. TG and DTG curves for the ODA/PMDA polyamic acid and the two isomers of the t-butyl ester.

compared to the theoretical value of 15.3%. Onset of weight loss for this polymer at a heating rate of 5°C/min was 177°C with a maximum rate of reaction at 217°C. As was the case for the polyamic acid samples the DTG for this polymer is symmetric. The methyl ester has a higher onset and maximum rate of reaction when compared to ODA/PMDA polyamic acid and its *t*-butyl esters, indicating that the *t*-butyl ester falls intermediate between ODA/PMDA polyamic acid and its methyl ester in ease of imidization. Since earlier work[5] had indicated that the n-butyl ester was far less susceptible to imidization than the methyl ester, this is a strong indication that the reaction does not proceed by the elimination of *t*-butanol since this process should be even harder to achieve than the elimination of n-butanol. Indeed, a TGA (5°C/min) of a sample of the n-butyl ester, confirmed that this material had a higher onset (193°C), and maximum rate of reaction than either the methyl or *t*-butyl ester. Figure 3 shows an isothermal TGA study which illustrates the drastic difference in the imidization rates for the t-butyl ester and the n-butyl ester. In this study a sample of polymer was heated at three temperatures (100, 200, 400°C) for an hour at each temperature. By comparing the weight loss at 200°C to that at the final cure temperature we could calculate the % imidization. Thus the n-butyl ester was found to have a much lower % imidization (46%) than was found for the *t*-butyl ester (93%).

IR Spectroscopy.

A IR study was made of the curing behavior of the parent ODA/PMDA polyamic acid compared to both the meta and para *t*-butyl esters. Samples heated to 200°C for 1 hour showed no significant differences in cure for either of the two esters as compared to PMDA/ODA polyamic acid: Analysis of all three samples showed $87\pm2\%$ imidization, based on results for sample given a final cure of 350°C. As can be seen in Figure 4a samples heated for 1 hour at 200°C give an IR spectrum very close to that of the parent polyamic acid cured under the same conditions (Figure 4b).

Mass Spectroscopic Analysis.

Mass spectroscopy showed that the products given off during the curing cycle were water and isobutene. As can be seen in Figure 5, the curing of the para-*t*-butyl ester can be followed by the total ion chromatogram (TIC) or, alternatively, the evolution of water and isobutene can be monitored separately by looking at their respective molecular ion chromatograms. Figure 5b,c shows that the liberation of water and isobutene from the polymer occurred simultaneously at 200°C and that isobutene was still being given off at 350°C. The extent of cure found by using either the total ion chromatograph or the ion chromatograph for the molecular ion of isobutene (87% and 88% respectively) is in good agreement with the values found in the FTIR curing study (88%). This suggests that, although the removal of the *t*-butyl group may be the rate determining step, this process is still rapid enough not to hinder significantly the amount of imidization occurring in an hour at 200°C. The meta isomer gives identical curing behavior consistent with the IR results. In contrast the n-butyl ester undergoes much less curing (43%) at 200°C (Figure 6a). Even the methyl ester, (Figure 6a), which is expected to cure more rapidly is much slower than the t-butyl ester (52%). As
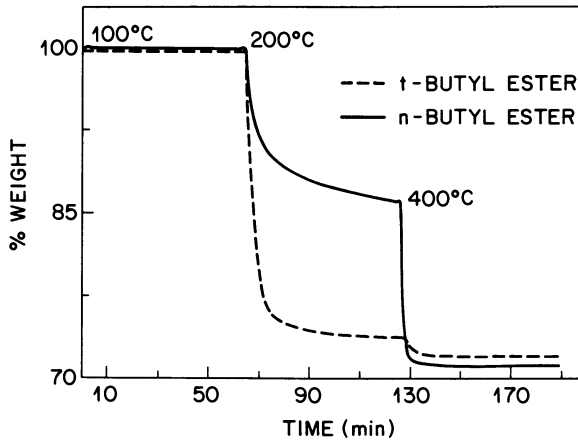
Figure 3. Isothermal TG study of the imidization of the t-butyl and n-butyl esters of the ODA/PMDA polyamic acid.
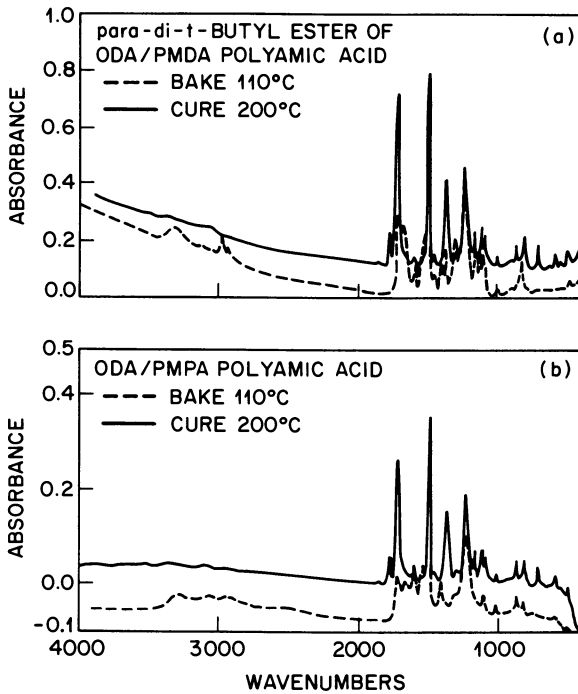
Figure 4. IR spectra for curing of ODA/PMDA polyamic acid and its t-butyl ester.
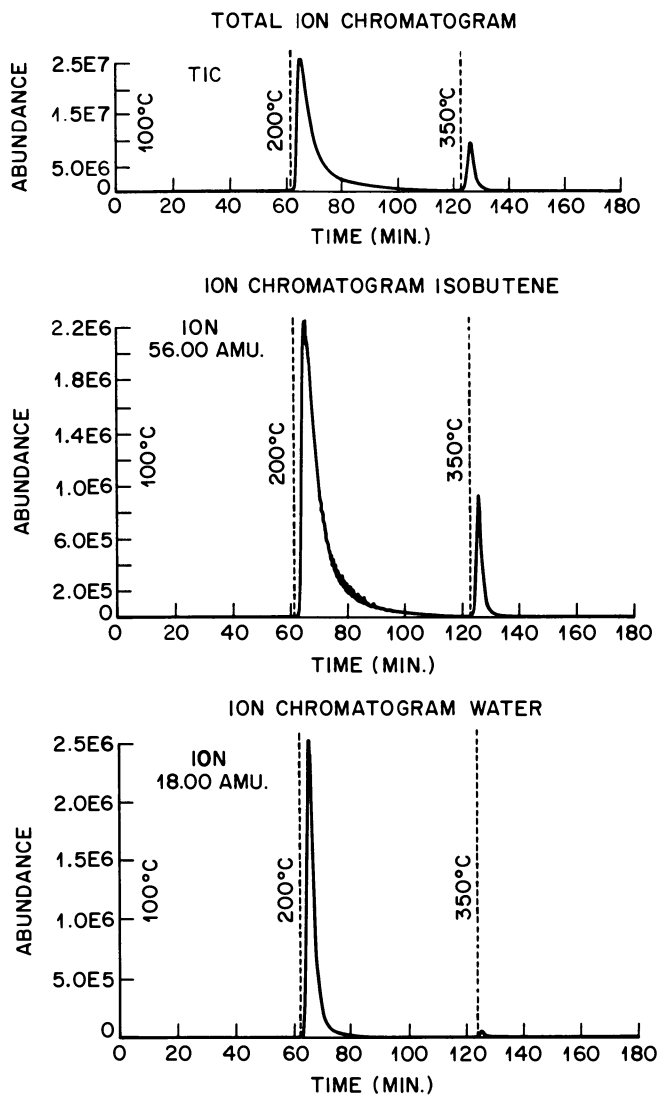
Figure 5.   Total ion chromatogram and ion chromatograms for isobutene and water taken during the curing of the para isomer of the t-butyl ester of the ODA/PMDA polyamic acid.

TIC OF n-BUTYL ESTER OF ODA/PMDA POLYAMIC ACID
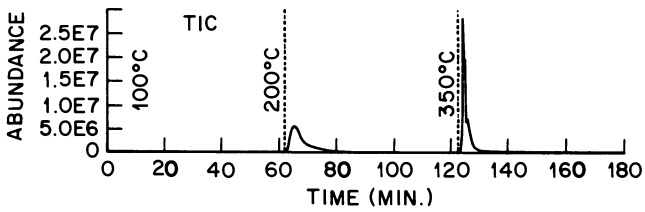
TIC OF METHYL ESTER OF ODA/PMDA POLYAMIC ACID
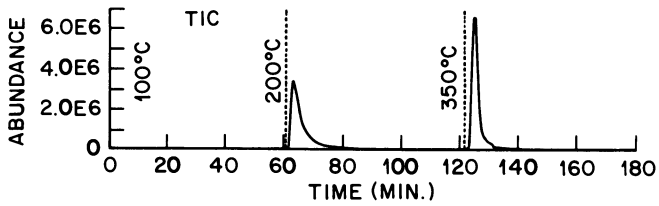
TIC OF t-BUTYL ESTER OF ODA/PMDA POLYAMIC ACID
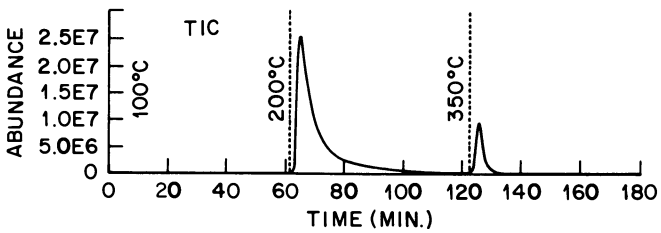
Figure 6. Total ion chromatogram taken during the curing of the t-butyl, n-butyl, and methyl esters of the ODA/PMDA polyamic acid.

expected, the products given off during the cure of the esters of linear alcohols are the corresponding linear alcohols.

CONCLUSIONS

We have shown that *t*-butyl esters of polyamic acids can be prepared in good yield and with acceptable molecular weights. The reaction has also been extended to other esters. Moreover, the *t*-butyl esters can be prepared as pure meta or para polymers, which show distinct differences in solubility. The curing behavior of these t-butyl esters has been shown to be similar to that of the parent polyamic acid and much faster than that for analogous linear esters. The cure of *t*-butyl ester has been shown to proceed by a more facile mechanism involving the liberation of a free polyamic acid rather than by a thermal elimination of alcohol. In future studies we will examine other bulky protecting groups capable of thermal removal.

REFERENCES

1. Kharkov, S. N.; Vinogradova, S. V.; Vygodskii, Ya. S.; Gerashchenko, Z. V. Vysokomol Soyed 1971, 13, 1190.

2. Kharkov, S. N.; Krasnov, Ye P.; Lavrova, Z. N.; Baranova, S. A.; Aksevova, V. P.; Chegolya, A. S. Vysokomol Soyed 1971, 13, 833.

3. Molodtsova, Ye. D.; Timofeyeva, G. I.; Pavlova, S. S. A.; Vygodskii, Y. S.; Vinogradova, S. V.; Korshak, V. V. Vysokomol Soyed 1977, 19, 346.

4. Nishizaki, S.; Moriwaki, T. Kogyo Kagaku Zasshi 1970, 73(8), 1970, 1873.

5. Nishizaki, S.; Moriwaki, T. Industrial Chemistry Magazine 1968, 71, 1559.

6. Kudryavtsev, V. V.; Koton, M. M.; Meleshko, T. K.; Sklizkova, V. P. Vysokomol Soyed 1975, A17 No. 8, 1764.

7. Koltsov, A. I.; Dauengauer, S. A.; Denisov, V. M.; Shibaev, L. A.; Sazanov, Yu N.; Bukina, M. K.; Koton, M. M. Doklady Akademii Nauk SSSR 1984, 278 No. 6, 1380.

8. Bessonov, M. I.; Koton, M. M.; Kudryavtsev, V. V.; Laius, L. A. Polyimides–Thermally Stable Polymers; Plenum Press, 1987.

9. Frechet, J. M. J.; Eichler, E.; Ito, H.; Willson, C. G. Polymer 1983, 24, 995; Ito, H.; Willson, C. G.; Frechet, J. M. J.; Farrall, M. J.; Eichler, E. Macromolecules 1983, 16, 510; Ito, H.; Willson, C. G.; Frechet, J. M. J. Proceedings SPIE Conference Santa Clara 1987. Ito, H.; Willson C. G.; Frechet, J. M. J. US Patent 4 491 628, 1985.

10. Frechet, J. M. J.; Bouchard, F.; Eichler, E.; Houlihan, F. M.; Izawa, T.; Kryozka, B.; Willson, C. G. Polymer Journal 1987, 19, 31.

11. Pryde, C. A. to be published J. Polym. Sci. Chem. Ed. 1988.

12. Ueda, M.; Mochizuki, A.; Hiratsuka, I.; Oikawa, H. Bull. Chem. Soc. Jpn. 1985, 58, 3291.

Chapter 10

Curing of Binary Mixtures of Polyimides

C. Feger

**IBM Research Division, Thomas J. Watson Research Center,
Yorktown Heights, NY 10598**

The cure of a BTDA-ODA/MPDA polyimide and 50:50 mixtures with PMDA-ODA are investigated using dynamic mechanical thermal analysis and TGA. Due to anhydride formation during storage and cure, exchange reactions leading to copolymer formation are possible. The mixtures show a curing behavior exhibiting the characteristics of both homopolymers. However, the cure behavior of each component is also influenced by the presence of the other. Thus the plasticization region is extended due to the presence of the flexible BTDA-ODA/MPDA. On the other hand, the more acidic PMDA-ODA polyamic acid catalyzes the imidization of the slower BTDA based polyamic acid. - Storage at room temperature allows for exchange reaction with longer storage times leading to more copolymer formation. Fast curing preserves the storage history whereas slow curing leads to additional copolymer formation. Variations in glass transition temperatures and the magnitude of the accompanying drops of the storage moduli are interpreted as indicating the various degrees of copolymer formation obtained through variations in storage conditions and cure schedules.

Recently Yokota et al. [1] reported the synthesis of polyimide blends which were obtained by solution mixing of the polyamic acid precursors and subsequent solid state imidization. In previous studies [2-4] it has been shown that polyamic acids in solution are capable to undergo exchange reactions with other amic acid compounds which might be present. Thus, changes in molecular weight distribution from an initially skewed to a normal distribution have been observed and attributed to such reactions [5]. Similarly, molecular weight changes of a polyamic acid have been observed in the presence of diamic acid model compounds [2]. These exchange reactions are assumed to proceed through reversal of the amic acid formation. In this reaction chain scission occurs under re-formation of anhydride and amine functionalities.

These can react again with each other or with any other suitable reactive group present.

The equilibrium of the reaction of amine with anhydride at room temperature is assumed to be far on the side of the amic acid [3]. This is indicated by the absence of anhydride bands in the IR spectra of polyamic acid films [6, 7]. Upon heating, however, the anhydride content in most polyimide films increases dramatically at the temperature where imidization occurs [3, 6, 7]. Again, the anhydrides are formed by a reversal of the amic acid formation. This time, however, anhydride formation is in competition with imidization: the imide is formed by nucleophilic attack of a carboxylic carbonyl group by the nitrogen of an amide group whereas the anhydride is formed by nucleophilic attack of the amide carbonyl group by the oxygen of the carboxyl group [6]. The formation of anhydrides makes exchange reactions possible. Thus, films which contain diamic acid model compounds become brittle upon heating [8, 9] which is attributed to lowering of the molecular weight due to exchange reactions. Due to the fact that in polyimides (contrary to model compounds) anhydride endgroups can not evaporate, further heating leads to diminishing anhydride concentrations; this observation is in agreement with the re-formation of amic acid and ultimate conversion to imide.

The evidence presented above indicates that exchange reactions via anhydride formation are occurring in homo-polyamic acid solutions, in solutions containing small interacting molecules, and during the solid state cycloimidization. Therefor, binary mixtures of polyamic acids should also exhibit such exchange reactions during storage in solution as well as during solid state cycloimidization. In both cases instead of a blend one would end up with a copolymer exhibiting different properties than the corresponding blend. The extent of such copolymerization will depend on miscibility of the polyamic acids in solution and in the solid.

In the following we have investigated a system consisting of PMDA-ODA and BTDA-ODA/MPDA polyamic acid/polyimide. PMDA-ODA is obtained by reaction of pyromellitic dianhydride (PMDA) with oxydianiline (ODA) whereas BTDA-ODA/MPDA is obtained reacting benzophenone - 3,3',4,4' - tetracarboxydianhydride (BTDA) and a 80:20 mixture of ODA and m- phenylenediamine (MPDA). PMDA-ODA polyimide has good thermal properties such as a high glass transition temperature and high thermal stability, and good mechanical properties such as high modulus, high elongation at break and little tendency to cracking. On the other hand it is plagued by adhesion problems to various substrates including itself; furthermore, given the opportunity it will pick up a considerable amount of water. These problems are alleviated in BTDA-ODA/MPDA polyimide which shows very good adhesion and less water up-take. However, its glass transition temperature is consider-

ably lower at around 310 °C. Blending of these two polyimides might lead to a material with superior properties then either one of them possesses in their pure form. The focus of this paper, however, is not on the ultimate properties of such binary mixtures but on the analysis of the cure by dynamic mechanical thermal analysis and the information such analysis yields with respect to possible exchange reactions.

Experimental

Both polyamic acid solutions (solvent: NMP with small amounts of hydrocarbon) were obtained from DuPont (Pyralin 5878 (PMDA-ODA) and Pyralin 2525 (BTDA-ODA/MPDA)). The solid contents are 15% in PI-5878 and 25% in PI-2525. (Pyralin 2555 which also consists of BTDA-ODA/MPDA behaves distinctly different in its curing behavior as well as in its behavior in blends with PMDA-ODA [10].) Blends were produced by mixing weighted amounts of polyamic acid solutions at room temperature for various lengths of time from about 10 minutes (the time needed for the schlieren to disappear) to up to 6 days. The latter time has been chosen arbitrarily. However, increasing the equilibration time does not lead to an increase in the effect described below. Films (thickness: .1 - .2 mm) were produced by doctorblading onto glass slides and immediate transfer into a vacuum oven preheated to 60 °C. They were measured the following morning.

All studies were performed under nitrogen (< 2ppm oxygen) using the single cantilever mode of the Polymer Labs DMTA at small deformation, 1 hz, and a heating rate of 5 or 0.5 °C/min.

Results and Discussion

The curing behavior of PMDA-ODA (Figure 1) has been analyzed previously [11]. The overall process is characterized by various physical and chemical steps: Decomplexation of the complex formed between NMP and polyamic acid [2, 3, 6]; plasticization of the material by the decomplexed NMP [11, 12]; evaporation of the solvent; cycloimidization accompanied by re-formation of anhydride and amine, a side reaction which leads to chain scission [2]; vitrification caused by solvent evaporation and imidization; and finally molecular ordering of the polyimide near and above the glass transition [11, 13, 14]. The particular features of all these processes are heating rate dependent (e.g. compare Figure 1.a and 1.b) [2, 6, 11].

Compared to PMDA-ODA the various processes occurring during the curing of BTDA-ODA/MPDA (Figure 2.a and b) are well separated. For a heating rate of 5 (0.5) °C/min they consist of the T_g of the complexed polyamic acid
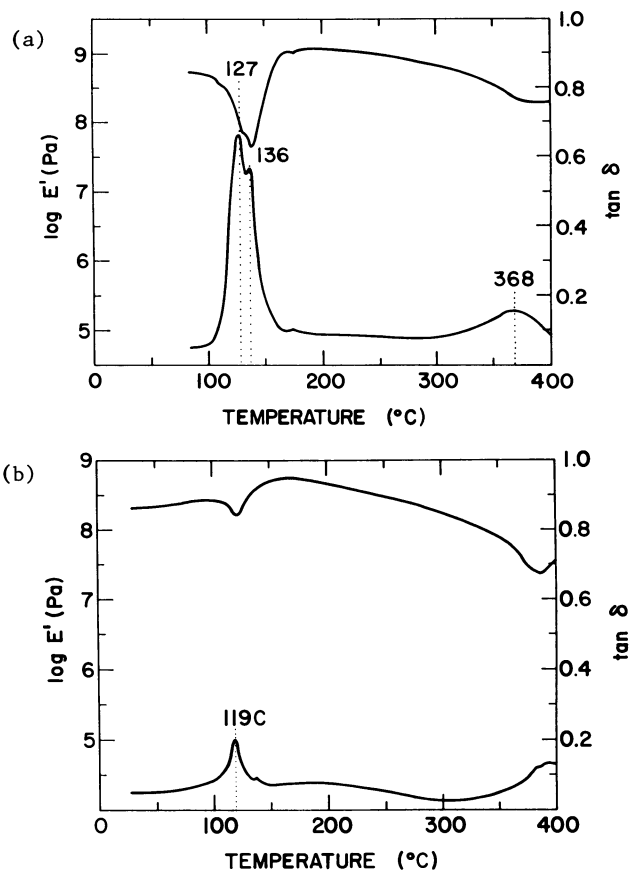
Figure 1. Dynamic mechanical spectrum (left: log E′(Pa), right: tan δ vs temperature (°C)) of the thermal cure of PMDA-ODA polyamic acid film at a.) 5 °C/min. and b.) 0.5 °C/min.
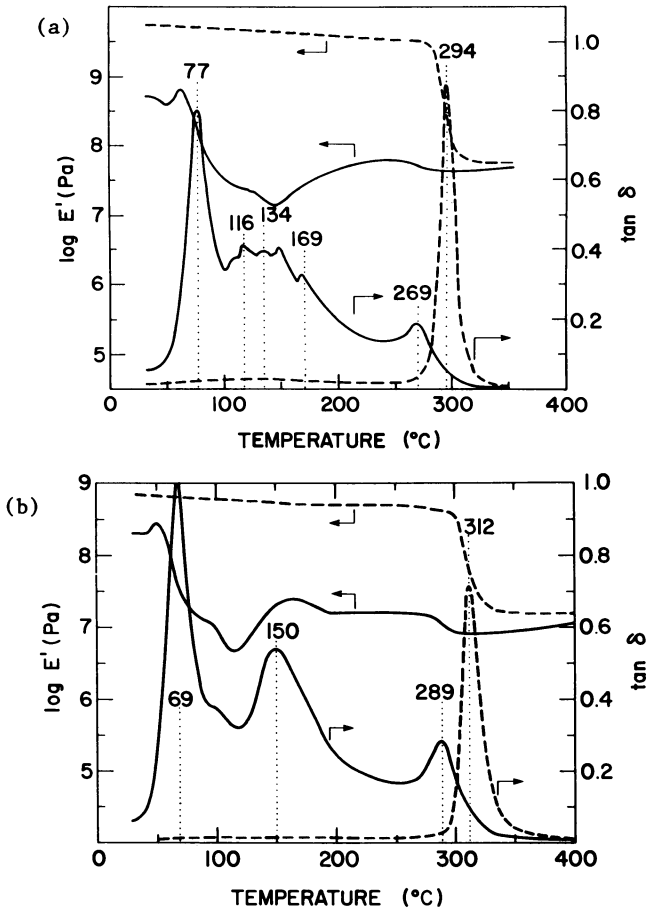
Figure 2.   Dynamic   mechanical   spectrum   of   the   thermal   cure   of BTDA-ODA/MPDA polyamic acid film at a.) 5 °C/min.   and b.) 0.5 °C/min. The dashed line represents the dynamic mechanical spectrum of the cured films measured at 5 deg. C/min.

at 78 (69) °C, an additional modulus drop due to the onset of the decomplexation followed by a modulus increase due to solvent loss at 125 (100) °C, (the glass transition of the uncomplexed polyamic acid which is observed only for the slow heating rate at around 175 °C), and the T_g of the partially imidized polymer at 269 (289) °C. As the TGA in Figure 3 shows (heating rate .5 °C/min) the loss of most of the solvent is separated from imidization which occurs only at high temperatures and proceeds above the T_g of the polyimide. Mass-spectrometry results indicate [15] that the high temperature loss is caused by loss of water and residual NMP. TGA and mass-spectrometry results indicate that BTDA-ODA/MPDA reacts slower than PMDA-ODA where solvent loss and water evolution occur simultaneously and are completed before 300 °C are reached [3]. The modulus of PI-2525 remains low after the initial drop despite the solvent evaporation. This behavior is observed even when the heating rate is lowered to 0.5 °C/min (Figure 2.b). The delayed modulus increase is attributed to the slow imidization but also due to slow formation of molecular ordering. The dynamic mechanical spectrum of the fully cured material (thin line in Figure 2.a and b) shows an increased glass transition compared to the one observed during the cure. The two heating rates however result in materials with differing glass transition: 295 °C at 5 °C/min and 312 °C at 0.5 °C/min. This is due to a thermally induced side reaction occurring in BTDA based systems. This reaction is yet not well understood but might involve radical formation at the BTDA carbonyl group [15]. Other thermal induced cross-linking mechanisms in polyimides have been proposed by J. Shouli et al. [16]. The increase in the glass transition temperature in the slower cured films is due to the longer times the sample is exposed to the temperatures at which the side reaction occurs. The increased high temperature exposure leads also to the increased skew in the tan δ peak accompanying the strong modulus drop at the glass transition [15].

The blend obtained by fast mixing of equal amounts of the two polyamic acid solutions shows a curing behavior at 5 °C/min (Figure 4) that exhibits characteristics of both homopolymers but also some changes. The initial modulus drop occurs at a higher temperature than in homo-BTDA-ODA/MPDA. After a short arrest the modulus continues to drop steeply at the temperature at which plasticization is observed in PMDA-ODA. The magnitude of the overall drop is larger than in any of the homopolymers alone. The modulus increase caused by imidization, however, occurs at a temperature about 30 °C higher than where it is found in pure PMDA-ODA. In the latter the modulus increase exceeds the starting modulus, whereas in the blend only about 50 % is recovered. This suggests that imidization occurs mostly at the PMDA units.

A well defined glass transition is observed at 318 °C. This is much higher than the 269 °C (Figure 2.a) seen during the 5 °C/min cure of pure PI-2525 but much lower than expected for PMDA-ODA (370 °C, Figure 1.a). On second
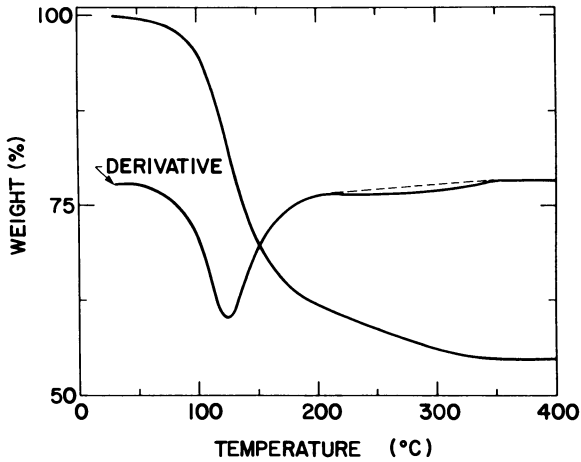
Figure 3.   Thermogravimetric   analysis   of   the   thermal   cure   of
BTDA-ODA/MPDA at 0.5 °C/min.
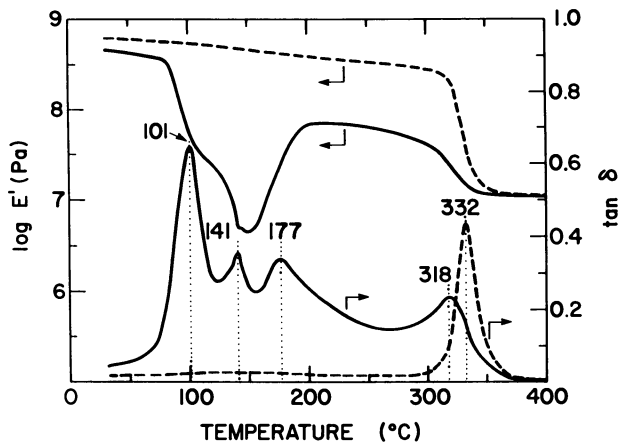
Figure 4.   DMTA spectrum of the 5 °C/min cure of a 10 minutes mixed
PMDA-ODA/BTDA-ODA/MPDA mixture (50:50).   Dashed lines as in Figure
2.

heating the glass transition becomes more pronounced and is found at a higher temperature (332 °C). This temperature increase is similar to the one observed on second heating of pure BTDA-ODA/MPDA. The glass transition temperature of the blend is about 40 °C above the one obtained with a similarly treated film of pure PI-2525.

The observation of well separated steps during imidization indicates a system that is at least micro phase separated (films produced from the blend are clear at all times). The retardation of the imidization modulus increase and the increased glass transition indicate, however, that at least partial phase mixing occurs. This is true particularly for samples mixed for extended periods of time.

The cure behavior of a mixture which equilibrated for 141 hours at room temperature (Fig.5) is compared to the one of samples which were mixed for only 10 minutes. Differences are observed in the decomplexation/imidization region and in the position of the glass transition temperature. In detail, these differences are as follows. The temperature at which the modulus drops is moved slightly to higher values. Although the modulus increase occurs at the same temperature as in the fast mixed samples, it increases to much higher values. The glass transition temperature during first heating is found to be about 15 °C higher than in the fast mixed sample; the modulus drop accompanying the glass transition is somewhat increased. On second heating, an increase of T_g by 13 °C is observed and again attributed to additional cure (imidization and side reaction) above the T_g during first heating.

The higher glass transition temperature in the long mixed samples indicates that during the room temperature equilibration some copolymerization occurs. This in turn leads to better mixing of the polyamic acids. Thus the presence of PMDA leads to acceleration of the imidization of BTDA which finds its expression in the more pronounced modulus increase during imidization in the equilibrated sample. Lavrov et al. [17] have shown that the addition of carboxylic acids to amic acids catalyzes the imidization reaction. Recently, Pyun et al. [18] have shown that in the solid state autocatalysis by the present amic acid is likely to accelerate the imidization. Due to the four electron withdrawing groups on the phenyl ring amic acids based on PMDA have higher acidity and higher reactivity [3] than the corresponding amic acids based on BTDA. The described behavior, then, indicates that in the more compatible sample the PMDA based amic acid catalyzes at least in part the imidization of the BTDA-ODA/MPDA.

The same effect as observed after prolonged mixing is obtained by slowly curing the fast mixed sample. Thus, a film made from the fast mixed blend but cured with a heating rate of 0.5 °C/min (thin line in Figure 6) shows the
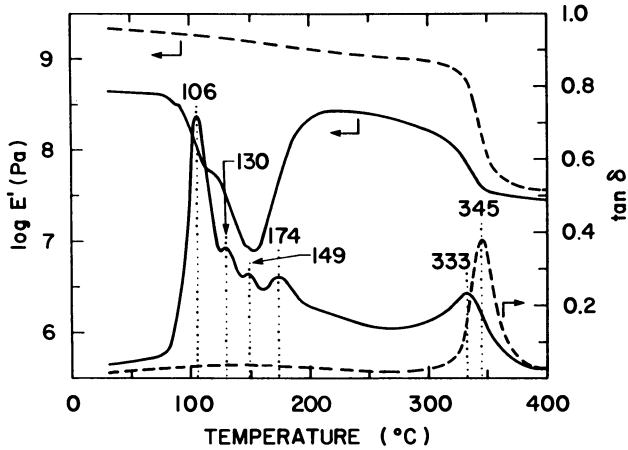
Figure 5. DMTA spectrum of the 5 °C/min cure of a PMDA-ODA/ BTDA-ODA/MPDA mixture (50:50) stored for 141 h at room temperature. Dashed lines as in Figure 2.
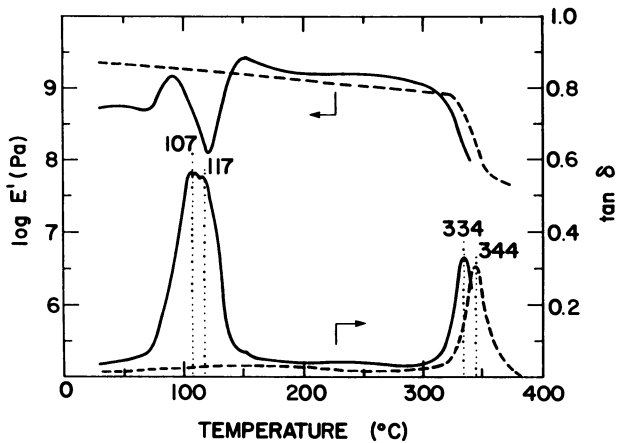
Figure 6. DMTA spectrum of the 0.5 °C/min cure of a 10 minutes mixed PMDA-ODA/ BTDA-ODA/MPDA mixture (50:50). Dashed lines as in Figure 2.

same behavior as the long mixed, 5 °C/min cured film (dotted line in Figure 5). This indicates that exchange reactions occur not only during the room temperature equilibration but also during cycloimidization. As explained above the exchange reaction involves anhydrides formed in competition with imides. The extent of the exchange during cycloimidization must be related to the reaction time, the anhydride concentration and their mobility. The anhydride concentration is not known. The reaction time and the mobility, however, are clearly related to the extent and duration of the plasticization during which most of the imidization occurs. Extent and duration of the plasticization depend strongly on the curing schedules. This has been shown previously [11].   It is also evident in the curing spectra of PMDA-ODA and BTDA-ODA/MPDA (Figures 1 and 2). In the considered mixtures this effect is particularly dramatic: As discussed above the fast mixed samples are at least somehow phase separated and the two amic acids imidize at different temperatures. Therefore, PMDA and BTDA anhydrides, respectively, occur in separate phases and at somewhat different times (temperatures). During fast cure little copolymer formation is expected. In the slow cure, however, further mixing (diffusion) can occur in the plasticized state which lasts for about 60 minutes in the 0.5 °C/min cure compared to only 10 minutes in the 5 °C/min cure. (The time for the exchange reaction to occur is taken to be the time between begin and end of the modulus increase which is attributed to cycloimidization.)

Following this reasoning it is not surprising that combining long equilibration time with slow cure leads to a material with the highest glass transition temperature (Figure 7). This material exhibits, furthermore, the highest modulus drop and the largest area under the tan δ peak accompanying the glass transition in the DMTA spectrum of the cure. This indicates that a greater portion of the material partakes in the process, i. e. phase mixing is more extensive.

Compared to the DMTA spectra of the slow cure of the homo-polymers two differences are striking: 1) Compared to PMDA-ODA (Figure 1.b) pronounced plasticization is observed due to the presence of the flexible BTDA based polymer. This leads to an increase in the imidization rate of PMDA compared to the slow cured homo-PMDA-ODA.   2) Compared to homo-BTDA-ODA/MPDA a much narrower plasticization region is found; the spectrum resembles fast cured PMDA-ODA. This is explained again as indication of the catalytic effect of the PMDA based amic acid on the imidization rate of the BTDA based system. Thus, both polyamic acids have an accelerating effect on the cycloimidization of each other in a slow cure.
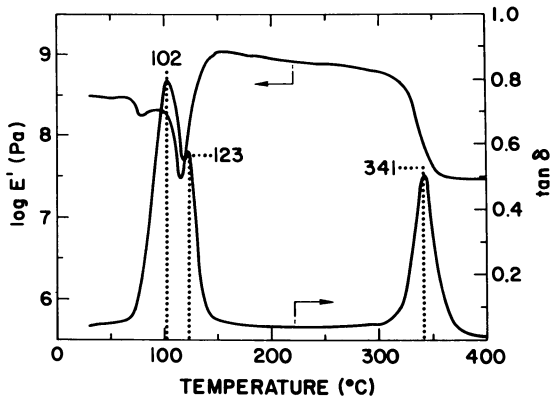
Figure 7.   DMTA spectrum of the 0.5 °C/min cure of a PMDA-ODA/
BTDA-ODA/MPDA mixture (50:50) stored for 141 h at room temperature.

Conclusion

The reverse reaction of the amic acid formation leads to anhydride formation during storage and cycloimidization. This opens a way for exchange reactions in mixtures of polyamic acids leading to copolymer formation. The exchange is slow during storage at room temperature. Thus mixtures cured shortly after mixing consist mainly of unchanged homopolymers as long as fast curing schedules are employed. Prolonged storage at room temperature leads to co-polyamic acids. In fast cures of such mixtures the composition at room temperature is mostly retained. Curing schedules which prolong the time during which imidization and thus anhydride formation occurs lead to increased co-polymerization. Thus, by changing the storage time and the curing schedule various materials can be realized.

The considered mixtures of PMDA-ODA and BTDA-ODA/MPDA show a curing behavior which exhibits certain characteristics of each homopolymer but also show that the curing behavior of each component is influenced by the presence of the other. Thus the plasticization region is extended due to the presence of the flexible BTDA-ODA/MPDA whereas the imidization of the latter is catalyzed by the more acidic PMDA-ODA polyamic acid. Various materials can be realized keeping the ratio of the starting materials constant but changing mixing and curing times. Thus, fast mixing and fast curing leads to a material which exhibits a relatively low glass transition temperature. Longer mixing or longer curing times lead to an increase in the glass transition temperature indicating better mixing due to the formation of probably quite blocky copolymer blends. Further copolymerization through long mixing times combined with a slow cure leads to even higher glass transition temperatures.

The results indicate that polyimides obtained from polyamic acid mixtures via thermal cure are extremely complex materials. To characterize the ensuing polymer structures fully will require extensive studies.

Acknowledgment

The author thanks G. Hougham for help with the TGA.

Literature Cited

1. Yokota, R.; Horiuchi, R.; Kochi, M. J. Polym. Sci., Part C 1988, 26, 215.

2. Brekner, M. J.; Feger, C. J. Polym. Sci., Polym. Chem. Ed. 1987 25 , 2479.

3. Bessonov, M. I.; Koton, M. M.; Kudryavtsev, V. V.; Laius, L. A. Polyimides, Thermally Stable Polymers Consultants Bureau: New York, 1987.

4. Walker, C. C. J. Polym. Sci., Polym. Chem. 1988 26 , 1649.

5. Metzger-Cotts, P.; Volksen, W. ACS Symp. Ser. 1984 242 , 227.

6. Brekner,M. J.; Feger, C. J. Polym. Sci., Polym. Chem. Ed. 1987 25 , 2005.

7. Pryde, C. A.; ACS PMSE Preprints 1988 29(2) , 219.

8. Stoakley, D. M.; St. Clair, A.; ACS PMSE Preprints 1988 29(2) , 33.

9. Feger, C.; unpublished results.

10. Feger, C.; to be published.

11. Feger, C. Polym. Eng. Sci. 1989 29 , in print.

12. Koton, M. M.; Meleshko, T. K.; Kudryavtsev, V. V.; Gofman, I. V.; Kuznetsov, N. P.; Dergacheva, Ye. N.; Bessonov, M. I.; Leonov, Ye. I.; Gorokhov, A. G. Polymer Sci. U.S.S.R. 1985 27 , 905.

13. Takahashi, N.; Yoon, D. Y.; Parrish, W.; Macromolecules 1984 17 ,2583.

14. Russell, T. P. Polymer Sci., Polym. Phys. Ed., 1984 22 , 1105.

15. Feger, C.; Molis, S.; Thomas, R. R.; Goldblatt, R. D.; to be published.

16. Shouli, J.; Ligang, Y.; Zikang, Z.; Zhiming, Z.; Qiyi, Z. Conf. Rec. 1985 Intl. Conf. Prop. Appl. Dielectr. Matls. 1985 2 , 583.

17. Lavrov, S. V.; Ardashnikov, A. Y.; Kardash, I. E.; Pravednikov, A. N. Polym. Sci. U.S.S.R. 1977 19 , 1212.

18. Pyun, E.; Mathison, R. J.; Sung, C. S. P.; accepted by Macromolecules

Chapter 11

Polyimides for Dielectric Layers

L. M. Baker[1], P. J. Brown, and J. L. Markham

AT&T Bell Laboratories, Engineering Research Center, Princeton, NJ 08540

The capability to layer interconnection levels is critical for many complex circuit designs. An organic polymer dielectric has several advantages over inorganic dielectrics in such applications. These advantages include a lower dielectric constant, ease of coating, and, in some instances, photodefinability. However, there are a number of material and processing constraints placed on the use of organic polymers. The polymer must be stable, metallizable, processable, and compatible with further processing steps. We selected a base polyimide for evaluation. The conditions of its preparation and imidization were characterized. The processing behavior was then correlated with the polymer characteristics. This work allowed identification of directions for further improvements to polyimides for dielectric applications.

The capability to layer interconnection levels is critical for many complex circuit designs. One particular application called for assembling devices on a silicon wafer with solder connections. The necessary interconnection density was obtained by using two signal layers above the power plane separated by a dielectric layer.(1)

In this application, organic dielectrics had some advantages over inorganic dielectrics. Firstly, the dielectric constant is generally lower. Most polymers have a dielectric constant in the range of 3.5, whereas inorganic materials typically have higher dielectric constants, although this varies with the particular material in question. A lower dielectric constant enhances switching speed and power dissipation while reducing noise. Since one of the major advantages of using silicon as the interconnection medium, as in this application, is increased switching speed, the dielectric constant of the insulator is especially important.

Secondly, the processing of organic polymers is simpler than processing inorganic dielectrics. Sputter deposition, frequently used for silicon dioxide, is slow and expensive, and the brittleness of the final glass makes the inorganics subject to voids and micro-cracking. The spun-on glasses, though more convenient to apply, are more prone to contamination than sputtered oxide, and the solutions can be unstable.

[1]Current address: AT&T Bell Laboratories, 1600 Osgood Street, North Andover, MA 01845

A major advantage of organic polymers is the possibility of photo-definition. The use of a photosensitive dielectric greatly simplifies processing by eliminating the application, processing, and removal of a separate photoresist. With the decrease in processing steps comes an increase in the yield of circuits.

A disadvantage of all organic dielectrics is the decreased thermal conductivity, which may result in localized overheating. Purity is another concern.

The ultimate goal here was to tailor the dielectric material to the particular requirements of this circuit. This paper describes the initial work done on a model polyimide resin toward this goal.

Experimental

Gel permeation chromatography (gpc) was performed on a Waters GPC-3 with a model 600 solvent delivery system, a 730 data module, a variable wavelength ultraviolet detector (uv), and a refractive index detector (RI). Calculations were made on the uv detector response with the wavelength set at 325 nm. Three μStyragel columns of porosities 10^5, 10^4, and 10^3 Å were used and calibrated with polystyrene standards. Injection size was 50-125μl of 0.05% solutions with a flow rate of 1.4 ml/min. The solvent was HPLC grade N-methyl pyrrolidone (NMP) obtained from Aldrich Chemical Co. buffered with 0.03 M LiBr and 0.03 M H_3PO_4.(2, 3)

Infrared spectra (IR) were taken on a Nicolet 7199 FT-IR. Thermal analyses were obtained on a DuPont 1090 thermal analyzer. Thermogravimetric analysis (TG) and differential scanning calorimetry (DSC) were performed at 10°C/min. heating rates under N_2. Reduced viscosity measurements (4) were made at 40°C in OC Ubbelohde viscometers. Values reported are the average of at least two measurements, which were within 0.2% of each other. Reduced viscosity is defined as follows:

$$\eta_{reduced} = \frac{\eta - \eta_0}{\eta_0 c}$$

η= flow measured in seconds
η_0= flow time of pure solvent
c = concentration in gm/ml

Solutions of polyimides were spin coated at 3000 rpm for 60 sec. onto silicon wafers which had been treated with DuPont VM 651 adhesion promoter. After coating, wafers were dried at 70°C on a hot plate. A Karl Suss proximity printer was used for imaging, and the wafers were developed in an APT spin-spray developer.

The polyamic acids were prepared from 3,3',4,4'-benzophenone dianhydride (sublimed) and 2,3,5,6-tetramethyl-1,4-phenylene diamine in Gold Label N,N-dimethyl formamide (DMF). All chemicals were obtained from Aldrich. A solution of the anhydride was added over 30 minutes to a solution of the amine with stirring under N_2 at room temperature at a net concentration of 15% solids. In general, a slight (1%) excess of the anhydride was needed to give maximum viscosity.

The polyimides were prepared chemically by adding the solution of the polyamic acid to excess acetic anhydride and pyridine in DMF with stirring under N_2. After stirring for 2 hours, the polyimide was precipitated with methanol and collected by suction filtration. The polymer was washed repeatedly with methanol and dried overnight in vacuo.

Results and Discussion

The model polyimide chosen for this study was the polymer derived from 3,3',4,4'-benzophenone tetracarboxylic dianhydride and 2,3,5,6-tetramethyl-1,4-phenylene

diamine (Figure 1). This polyimide was selected for several reasons bearing on processability, including stability, solubility, availability of starting materials, and photosensitivity. These properties are discussed in more detail in the following text.

Firstly, this is a polyimide with an aromatic backbone, and, therefore, possesses high thermal stability and resistance to many chemicals. The thermal stability was confirmed by TG (see Figure 2).

The polyimide is soluble in such solvents as NMP and DMF. Many polyimides are applied from solution as the polyamic acid. After evaporation of the solvent, the polyamic acid must be converted to the polyimide at high temperatures, typically greater than 350°C. This temperature is high enough to damage any active devices previously fabricated on the circuit. In addition, the film shrinks as a result of cooling from the cure temperature to room temperature, and this shrinkage is much greater for the polyimide than for the substrate. The film also shrinks during cure due to dehydration and cyclization. Shrinkage causes a reduction in thickness and generates stresses on the wafer. These stresses can warp the wafer to such an extent that it cannot be processed on standard equipment. A soluble polyimide, then, should avoid these problems.

Lastly, the polyimide has some inherent photosensitivity. The use of a photosensitive polymer requires fewer processing steps, which also implies an increased yield for the circuit. Ciba-Geigy announced the formulation of inherently photosensitive polyimides in 1985.(5) The use of an inherently photosensitive polyimide is attractive because no sensitizers are added to contaminate the final resin, no functionality is added which degrades the thermal and chemical resistance, and fewer volatiles are present to contaminate the resin or equipment than in some other approaches to photosensitive polyimides. Recent work has shown that these polyimides crosslink on irradiation through hydrogen abstraction by triplet benzophenone and subsequent coupling of the resultant radicals.(6)

Before beginning any processing study, a supply of reproducible material was needed. Since the polyimide is prepared from the polyamic acid with little or no chain extension during imidization, this means that the polyamic acid must be synthesized consistently. Preliminary lab experiments with benzophenone dianhydride and 4,4'-diaminodiphenyl ether had demonstrated conclusively that there is more to making a polyamic acid than simply mixing an anhydride and an amine. Early solutions were generally of low or highly variable viscosity and were not suitable for spin coating onto substrates. The literature contains many references to the preparation of polyamic acids, implicating many factors.(7) We examined several of the most commonly cited variables in a 20 run Plackett-Burman experimental design to arrive at the procedure given in the experimental section. These variables included order, method, and rate of addition; stoichiometry, purity, atmosphere, solvent, temperature, and concentration. The experimental design and the reduced viscosity results are given in the first table. The reduced solution viscosity was used as a quick, if indirect, indication of the molecular weight of the polyamic acid. Rate of addition was examined separately, with the reduced solution viscosity monitored over time. Also in a separate experiment, the stoichiometry had been varied over a wide range to verify the dependence of reduced viscosity on stoichiometry (Figure 3). Our findings were that the order, method, and rate of addition did not affect the final polyamic acid solutions. A slow rate of addition did minimize the initial large increase in viscosity and led to fewer viscosity fluctuations over time. Evidence has recently been presented which supports the idea that this viscosity decrease is due to equilibration of the molecular weight of the polymer.(3, 8) The use of a nitrogen atmosphere also improved stability without substantially affecting the solution. Since the polyamic acid solution viscosity varied over time and we were attempting to follow changes in viscosity as a function of factors affecting the preparation, it was important to
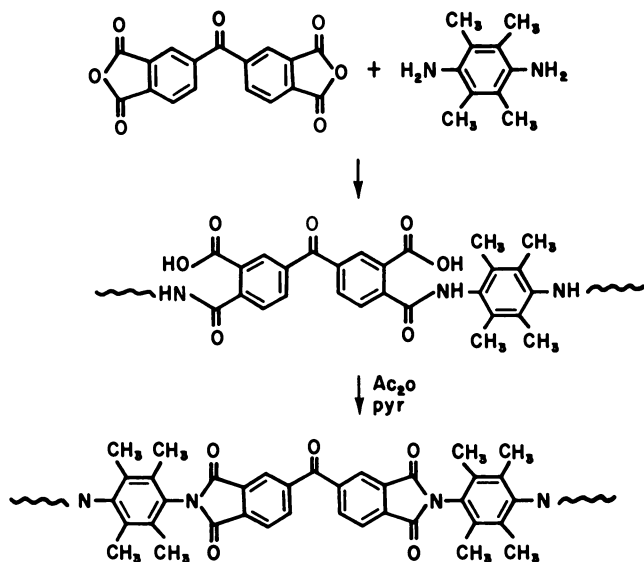
Figure 1.   Structure of model polyimide.
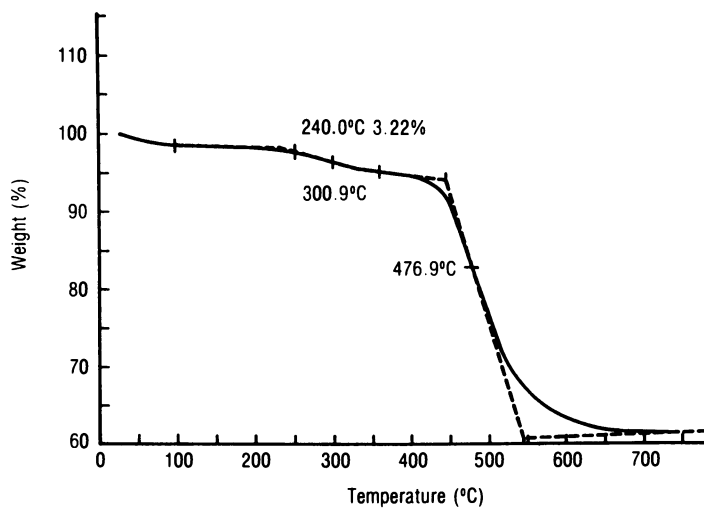
Figure 2.   TG of polyimide cured at 250°C.
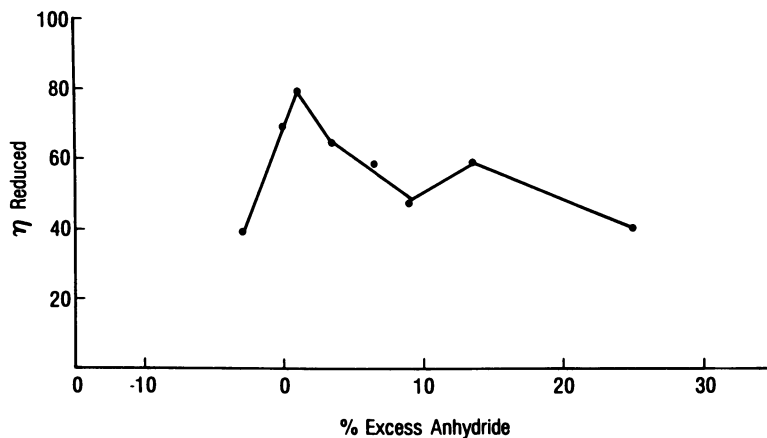
Figure 3. Reduced viscosity as a function of stoichiometry.

Table I. 20 Trial Plackett – Burman Experiment

Trial	Order of Addition (1)	Mode of Addition (2)	Stoich-iometry (3)	Solvent	% Solids (w:v)	T °C	Purity (4)	Atmos-phere	nreduced
1	H to M	Sol'n.	0.95	DMF	20	50	RG	N2	21
2	H to M	Solid	0.95	NMP	20	50	Pure	Air	61
3	M to H	Solid	1.05	NMP	20	50	RG	N2	46
4	M to H	Sol'n.	1.05	NMP	20	RT	Pure	Air	84
5	H to M	Sol'n.	1.05	NMP	5	50	RG	N2	96
6	H to M	Sol'n.	1.05	DMF	20	RT	Pure	N2	89
7	H to M	Sol'n.	0.95	NMP	5	50	Pure	N2	52
8	H to M	Solid	1.05	DMF	20	RT	Pure	N2	85
9	M to H	Sol'n.	0.95	NMP	5	RT	Pure	Air	66
10	H to M	Solid	1.05	DMF	5	RT	RG	Air	105
11	M to H	Sol'n.	0.95	DMF	5	RT	RG	N2	42
12	H to M	Solid	0.95	DMF	5	50	Pure	Air	90
13	M to H	Solid	0.95	DMF	20	50	RG	Air	22
14	M to H	Solid	0.95	NMP	20	RT	RG	N2	32
15	M to H	Solid	1.05	NMP	5	50	Pure	N2	146
16	M to H	Sol'n.	1.05	DMF	20	50	Pure	Air	38
17	H to M	Sol'n.	0.95	NMP	20	RT	RG	Air	23
18	H to M	Solid	1.05	NMP	5	RT	RG	Air	52
19	M to H	Sol'n.	1.05	DMF	5	50	RG	Air	74
20	M to H	Solid	0.95	DMF	5	RT	Pure	N2	53

Sum +	675								
Sum −	602								
Overall Sum	1277								
Difference	73								
Effect	7.3	−10.4	35.2*	4	−27.6*	1.6	10.5	−25.2*	−7.4
	X_{10}	X_{11}	X_{12}	X_{13}	X_{14}	X_{15}	X_{16}	X_{17}	X_{18}	X_{19}
Effect	−6	4.1	3.1	16.8	−9.1	12.2	5.6	18	3.4	−9.9

X_7, X_{10} − X_{19} Measures of experimental error

Average = 4.4

Minimum significant effect at 95% confidence limit = 23.9

Notes:

1. H to M: Anhydride added to amine; M to H: Amine added to anhydride.

2. Second reagent added as a solid or as a solution.

3. Ratio of amine to anhydride.

4. RG: Reagent grade.

take measurements at specified times for each solution. Stoichiometry was the major significant factor in the preparation of the polyamic acids. Purity of the reagents was a lesser factor, and this effect was also probably due to de facto changes in stoichiometry. The dependence on stoichiometry is to be expected, based on the relations developed by Flory.(9) The apparent effect due to concentration is consistent with polyelectrolyte effects (10) and may not be due to changes in molecular weight of the polyamic acid. The concentration was eventually decreased to 15% to insure complete dissolution of the anhydride. We assumed that results obtained with diaminodiphenyl ether would be directly applicable to the polymer made with tetramethylphenylene diamine. Solutions prepared with this procedure typically were pale yellow and stable for at least three weeks at room temperature, as followed by reduced viscosity measurements (Figure 4).

The next question addressed was the method of imidizing the polyamic acid. The polyamic acid can be thermally or chemically converted to the polyimide. (11) Thermal conversion was carried out at 250°C for 1 hour or at 250°C for 1 hour plus 400°C for 1 hour, and chemical dehydration was accomplished with acetic anhydride in pyridine. Conversion was monitored by IR, DSC, and TG. By IR spectroscopy, no differences were discernible in the imide region between samples cured at 250°C and those cured at 400°C. However, the band near 1780 cm^{-1} is subject to interference, and others have found the 1370 cm^{-1} band to be a more sensitive indication of imidization (Pryde, C. A.,J.Polym.Sci.,Chem.Ed., in press). Both DSC and TG showed an additional reaction in samples cured at 250°C only. Samples cured at 250°C only showed weight loss of 3-4% in the region of 300°C by TG (Figure 2) and endothermic peaks in the DSC at 280°C (Figure 5). Samples treated at 400°C showed no weight loss below decomposition temperatures (Figure 6) and no further peaks in the DSC (Figure 7). The chemically imidized material behaved in a comparable fashion to material cured at 250°C by TG and DSC (Figure 8). Polyimide prepared at 400°C was no longer soluble in organic solvents such as DMF and NMP. From the thermal and solubility data, it appears that the high temperature cure is necessary for complete or nearly complete imidization of the polyamic acid. Other processes, such as cross linking or molecular ordering, may also contribute to the decrease in solubility at high temperatures. These possibilities were not investigated. Again, such high temperatures in processing raise concerns about damage to active devices on the silicon substrate.

Chemical imidization was used for preparation of the polyimide for initial processing experiments, solely for reasons of convenience.

Three different lots of polyamic acid with different molecular weights were prepared and converted to the polyimide. Molecular weight data are given in Table II.

Table II. Molecular Weight Data		
Sample	**MW**	**MN**
High MW Polyamic Acid	127,000	44,000
High MW Polyimide	132,000	43,900
Medium MW Polyamic Acid	67,000	22,800
Medium MW Polyimide	63,000	26,300
Low MW Polyamic Acid	17,000	5000
Low MW Polyimide	20,000	10,600
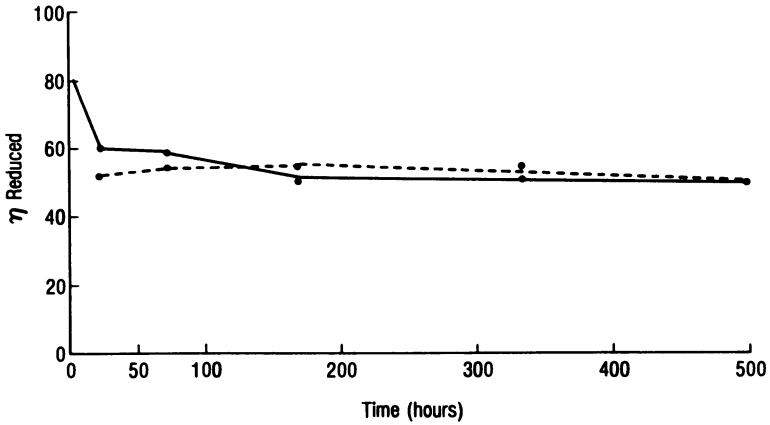
Figure 4. Reduced viscosity over time. Material stored at room temperature(-), and at 5°C (---).
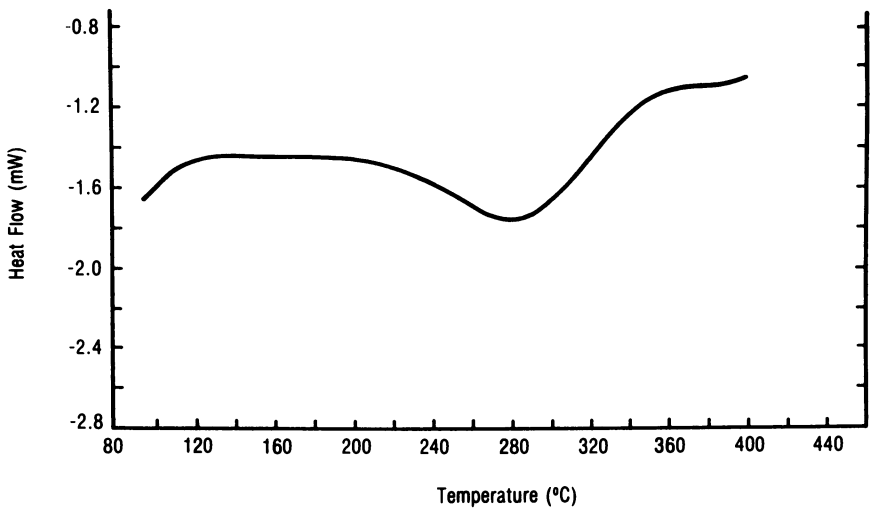
Figure 5. DSC of polyimide cured at 250°C.
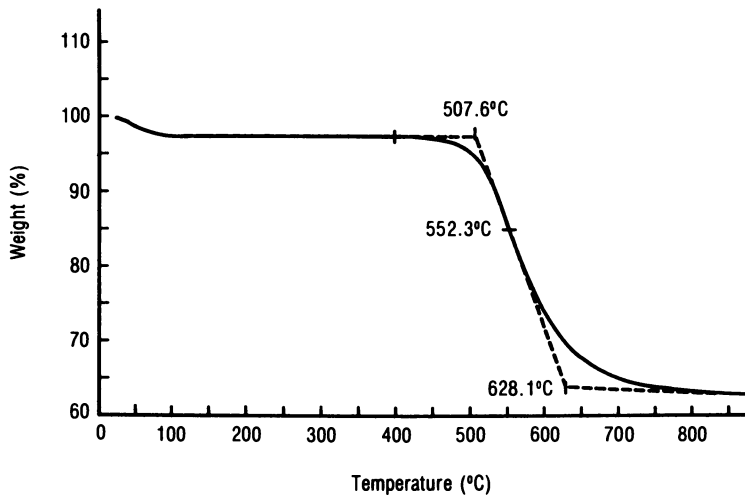
Figure 6.   TG of polyimide cured at 400°C.
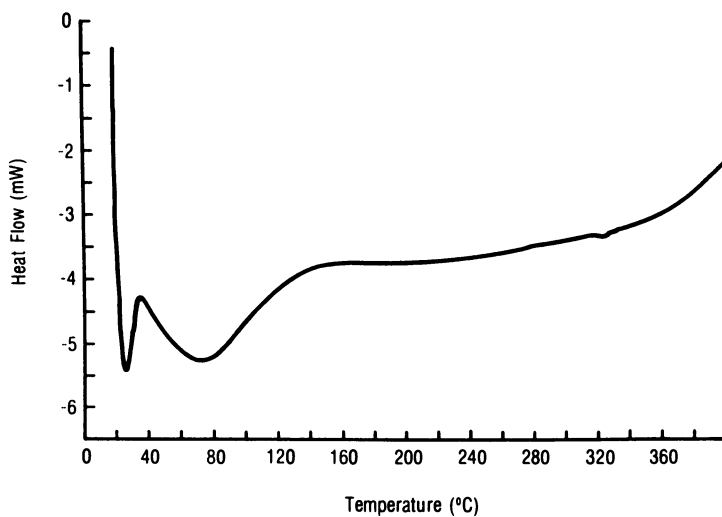
Figure 7.   DSC of polyimide cured at 400°C.

For the most part, the correlation is good between the values found for the polyamic acid and the corresponding polyimide. Even for the polyimides, it was essential to use the buffered mobile phase, again suggesting that there is a small amount of polyamic acid remaining after chemical dehydration. Reduced viscosity results reflect the molecular weight data. These results suggest that there is little branching occurring during chemical imidization.

The utility of the organic dielectric is improved if it can be applied to give a range of thicknesses. For instance, in this application with high speed circuits, controlled impedance is desirable. The impedance is related to the capacitance, which is determined by the distance between the signal plane and the ground plane (ie., the thickness of the dielectric layer). By using a thick dielectric as the first layer and thinner subsequent dielectric layers, the impedance can be approximately constant on all signal layers. The thickness depends on the spin speed, solids content of the solution, and molecular weight of the polymer, among other variables. The spin speed vs. thickness curve is shown for the medium molecular weight polyimide at 20% in NMP in Figure 9. For comparison, the low molecular weight polymer gives a 3.4μ coating at 1000 rpm, and the high molecular weight polyimide gives a 19.6μ thick film at the same speed.

The imaging and developing of the polyimide were strongly dependent on the molecular weight of the resin. The low molecular weight material could not be imaged. The coating uniformity and adhesion were poor. At the other extreme, the high molecular weight material gave the best films. Images were formed slowly (180 seconds), but developing was difficult. The medium molecular weight material showed the most promise. Adhesion and film uniformity were good. Imaging was again slow (180 sec.), but the material could be developed after 9 minutes in hot cyclopentanone. These results are summarized in Table III.

Table III. Processing Results		
Sample	**Imaging**	**Developing**
High MW Polyimide	Slow (180 sec.)	13 min. in hot cyclopentanone; lifting at edges
Medium MW Polyimide	Slow	9 min. hot cyclopentanone
Low MW Polyimide	No image	Washed off wafer in cyclopentanone/toluene(2:1)

Conclusions

Polyimides for use in electronics must be carefully selected and prepared to produce consistent materials with the desired properties. Furthermore, the impact of polymer processing on the circuitry must be carefully considered. In particular, the molecular weight of the polyimide resin must be controlled for successful application and imaging, which means that the molecular weight of the precursor polyamic acid must be controlled.

Although this polyimide from benzophenone dianhydride and tetramethyl phenylene diamine exhibits some photosensitivity, it is extremely slow. Profitable directions for improvement would be increasing the photospeed and the solubility in organic solvents. Other areas important for materials to be used as dielectrics include the coefficient of thermal expansion, the moisture uptake, and the dielectric constant.
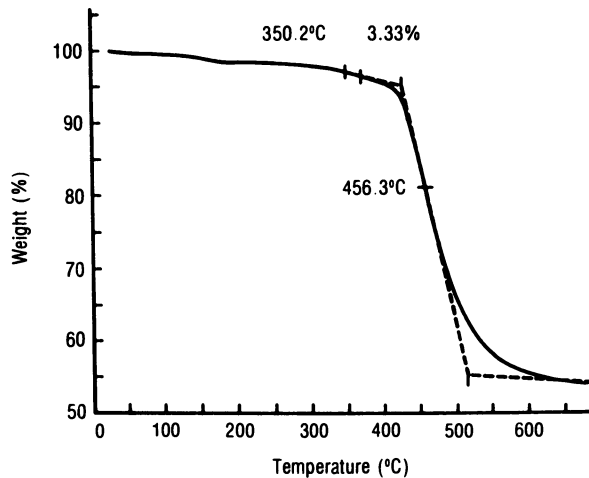
Figure 8.   TG of chemically imidized polyimide.
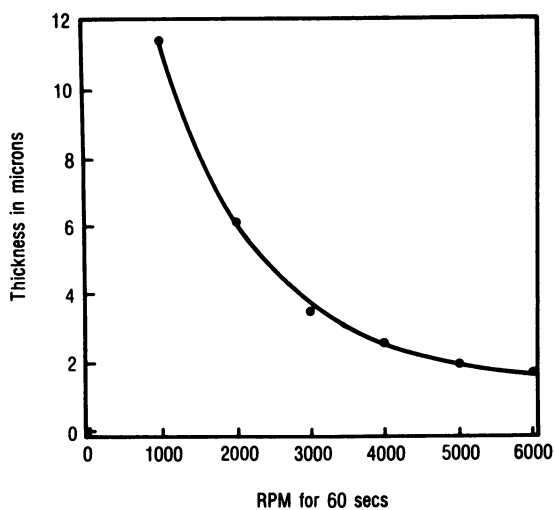
Figure 9.   Spin speed curve for 20% medium weight polyimide in NMP.

Literature Cited

1. Bartlett, C. J.; Segelken, J. M.; Teneketges, N. A., Proc. 37th Electronics Component Conference, 1987, p. 518.

2. Walker, C. C., Proc. 2nd International Conference on Polyimides, 1985, p. 426.

3. Walker, C. C., J. Polymer Sci.: Part A: Polymer Chemistry, 1988, 26, 1649.

4. Bikales, N. M., Characterization of Polymers; Wiley Interscience: New York, 1971; p. 5, 85.

5. Pfeifer, J.; Rohde, O., Proc. 2nd International Conference on Polyimides, 1985, p. 130.

6. Lin, A. A.; Sastri, V. R.; Tesoro, G.; Reiser, A.; Eachus, R., Macromolecules, 1988, 21, 1165.

7. Scroog, C. E., J. Polymer Sci.: Macromolecular Reviews , 1976, 11, 161.

8. Volksen, W.; Cotts, P. M., Polymers in Electronics; American Chemical Society: Washington, D. C., 1984; p. 227.

9. Flory, P. J., Principles of Polymer Chemistry; Cornell University Press: Ithaca, NY, 1953, p. 91–95.

10. Onyon, P. F., In Techniques of Polymer Characterization, Allen, P. W., Ed; Butterworths: London, 1959, pp. 171-206.

11. Harris, F. W., Proc. of the Interdisciplinary Symposium on Recent Advances in Polyimides and Other High Performance Polymers, 1987, p. 1.

Chapter 12

Siloxane Polyimides for Interlayer Dielectric Applications

P. P. Policastro, John H. Lupinski, and P. K. Hernandez

General Electric Company, Corporate Research and Development Center, Schenectady, NY 12301

The effect of processing conditions on molecular weight and thermal stability of siloxane polyimides prepared from α,ω-3 amino-propylpolydimethylsiloxane was investigated. Adhesion and dielectric properties were also studied. Siloxane polyimide copolymers were also prepared from the aromatic siloxane dianhydride 1,2-bis(4-phthalic anhydride)1,1,2,2-tetramethyl-disiloxane (1) and a variety of aromatic diamines. The copolymers obtained were analyzed by isothermal gravimetric analysis to determine stability relative to polyimide structures that did not contain subunits derived from monomer 1. Planarized coatings of the copolymers prepared from monomer 1 were readily obtained employing standard solution spin coating techniques, which were further characterized by peel adhesion testing. A high degree of adhesion of the coatings to silicon substrates was observed in the absence of surface priming agents after exposure to boiling water.

Current interest in siloxane polyimides is triggered by opportunities for such materials in military, aerospace and electronic applications as coatings, films, adhesives, molding compounds and composite matrix materials which are subject to demanding operating conditions. These polymers offer advantages such as excellent interlevel adhesion, plasma resistance, low water absorption, and stability at high temperatures.

Two synthetic approaches were used to prepare the materials discussed

in this report: (i) the two stage polyamide acid method (*1*) and (ii) solution imidization (*2*). Method (i) involves heating a polyamide acid film, formed by casting from a polar aprotic solvent, under inert atmosphere with a final cure temperature of 300°C. This procedure is applicable to systems in which the final polyimide product is insoluble in organic solvents. Polyimides which are soluble in organic solvents may be prepared as fully imidized polymers in solution at elevated temperature. The diamines and dianhydrides used in this study are illustrated in Figures 1 and 2.

Siloxane Polyimide With Intermediate Thermal Stability

SPI-100, a fully imidized aromatic-aliphatic siloxane polyimide, has been prepared in xylene/diglyme mixtures and in p-methylanisole. In the latter solvent, high molecular weight polymers are readily obtained. The extent of polymerization was determined by monitoring the relative intensities of absorption for the imide overtone band (3490 cm^{-1} in toluene) and the anhydride band (1860 cm^{-1} in chloroform). These polymers with higher molecular weight offer a significant advantage in peak use temperature over the low molecular weight material prepared in xylene/diglyme mixtures as is shown in Table I. The data suggest that high molecular weight SPI-100 can be used at temperatures up to 350°C in N$_2$ atmosphere.

Table I. Effect of Processing Conditions on Thermal Stability of SPI-100 in N$_2$

Process	M_n (g/mole)	IV (dL/g)	Temp. (°C)	1st 30 min	2nd 30 min	6 h
				Percent Weight Loss		
Xylene/diglyme	8000	0.25	400	19.3	5.9	32.1
"	"	"	350	2.7	3.7	19.3
Methylanisole	23000	0.44	400	3.4	1.9	16.9
"	"	"	350	0.2	0.2	4.0

Adhesive characteristics of thin SPI-100 films could not be measured directly because adhesive forces are generally larger than cohesive forces. To obtain some information on adhesion values, thin high molecular weight SPI-100 films on substrates were overcoated with about .1 mm of a commercially available polyimide (Product A) to provide greater cohesive strength than can be obtained with SPI-100 alone. The combined layers were then pulled in an Instron tester giving the results shown in Table II which also includes the values for commercial products A and B.

Adhesive characteristics for lower molecular weight SPI-100 on Si-oxide and nitride substrates are given in Table III.
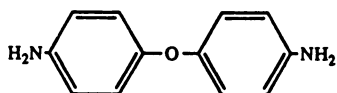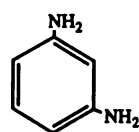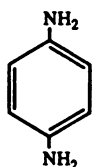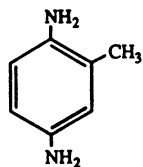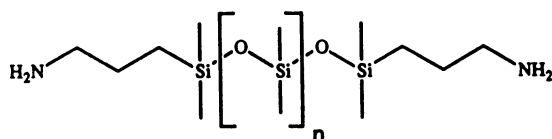
Figure 1.   Diamines Employed for the Preparation of Siloxane Polyimides.
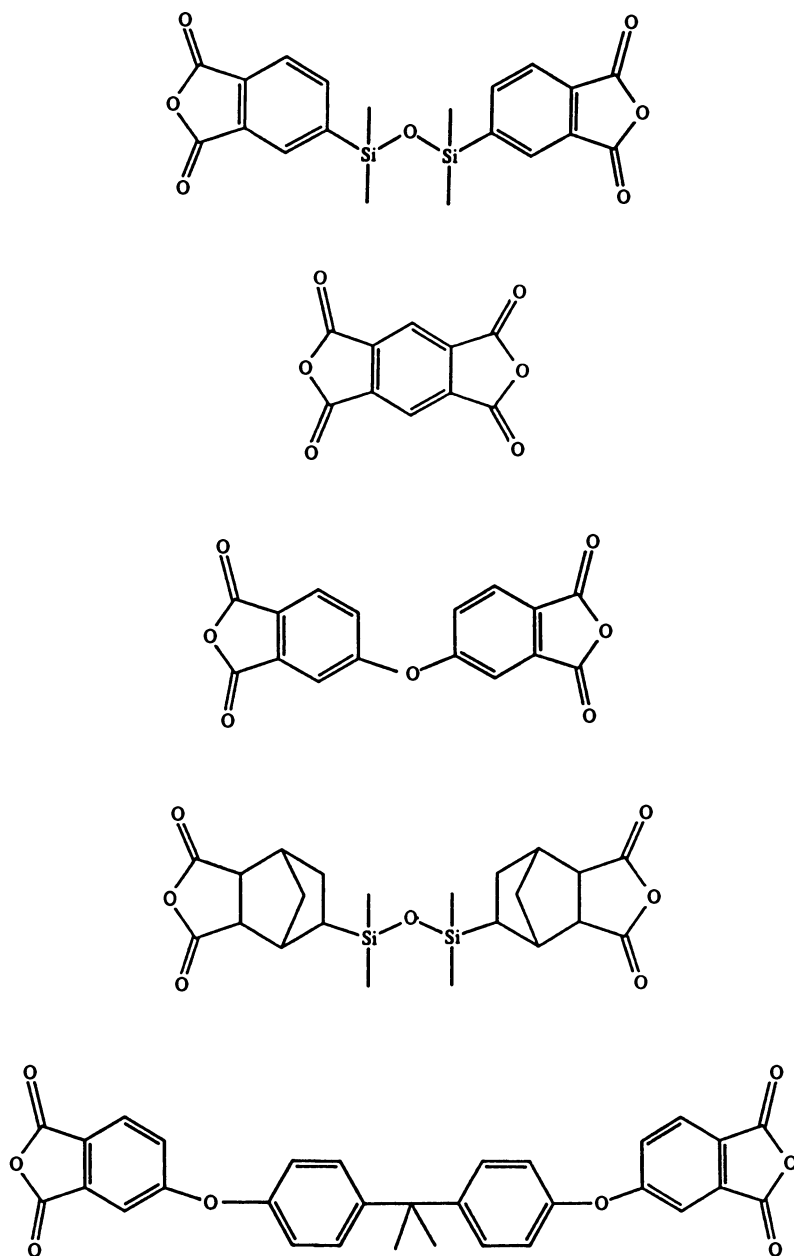
Figure 2. Dianhydrides Employed for the Preparation of Siloxane Polyimides.

Table II. Adhesion Values* of Polyimides

Polyimide Type	Adhesion Promoter	Film Thickness (mm)	Avg. Peel Strength (g/mm)
SPI-100 Overcoated with Product A	Not Required	.127	368**
Product A	Not Required	.025	101
Product B	Required	.013	18

* Silicon substrate.
**Cohesive failure without peeling.

Table III. Adhesion of Polyimides on Various Substrates

Polyimide Type	Substrate	Film Thickness (mm)	Avg.* Peel Strength (g/mm)
SPI-100 Standard + Product A	Si_3N_4 on Si Wafer	.76	288.0**
SPI-100 Standard + Product A	SiO_2 on Si Wafer	.76	298.0

* Average of 3 measurements.
**Cohesive failure without peeling.

Dielectric constant measurements were performed with an automatic Hewlett Packard (HP-4270A) capacitance bridge on 2.5 micron low molecular weight SPI-100 films on Al-wafers. A second Al-electrode was sputtered on to the polyimide and patterned with Shipley 1470 photoresist to provide a pattern of dots varying in diameter from .050 to .200 inches (1.3-5.1 mm) (see Figure 3).

Five measurements were made for each of the dot sizes. The averages for each size are given in Table IV.

Table IV. Dielectric Constant Measurements (100 kHz)

Diameter of Test Dot (mm)	5.08	2.54	1.91	1.52	1.27
Dielectric Constant*	2.677	2.692	2.734	2.683	2.721

* Overall Average 2.70.

Development of Highly Thermally Stable Siloxane Polyimides

A structure/property profile of polydimethylsiloxane imides such as SP-100 indicated that polydimethylsiloxane is the largest contributor to instability; it
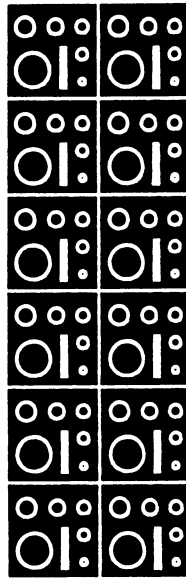
Figure 3. Pattern Used for Dielectric Constant Measurements. The diameter of the dots varies from .05 to .2 inches (~ 1.3 to 5.1 mm).

undergoes retropolymerization with evolution of volatile cyclic siloxanes. This was demonstrated by pyrolysis gas chromatography-mass spectroscopy in which a homologous series of cyclic siloxanes was detected upon heating at 375°C and above (Figure 4). The aliphatic linkages of bis(α-aminopropyl)tetramethyl-disiloxane (GAPD, Figure 1) also imparted instability to the system relative to the entirely aromatic control as determined by isothermal TGA studies.

A new reaction, referred to as "decarbonylative silylation" discovered by Rich (3), has made readily available the aromatic dianhydride disiloxane, PADS (4) (Figure 2). With the exception of a report by Babu (5), polyimides derived from PADS had not been described. Due to the aromatic nature of PADS, an improvement in thermal stability would be predicted compared to similar materials prepared from aliphatically linked disiloxanes. Three polyimides of comparable molecular weight were prepared from PADS, GAPD and 1,2-bis(5-norbornyl-2,3-dicarboxylicanhydride)-1,1,2,2,tetramethyl-disiloxane, (DiSiAn, Figure 2) (6). Examination of the respective polymer structures shows that all three materials contain diaryl ether units either derived from the diamine (4,4´-oxydianiline, ODA) or anhydride (4,4´-oxy(bis-phthalicanhydride), ODAN) components. These materials were evaluated for thermal stability by isothermal gravimetric analysis under air and nitrogen at several temperatures (Table V).

Table V. Isothermal Gravimetric Analysis of Siloxane Polyimides

Composition	Temperature (°C)	Atmosphere	% wt loss Δ 6 hours
PADS/4,4´-ODA	450	air	18
"	"	nitrogen	12
"	435	air	5
"	"	nitrogen	6
GAPD/ODAN	450	air	86
"	435	air	85
"	435	nitrogen	75
"	350	air	21
"	300	air	3
DiSiAn/4,4´-ODA	435	air	80
"	435	nitrogen	47

A significant improvement in thermostability was observed for the PADS containing copolymer as compared to the GAPD and DiSiAn containing materials. At 435°C under nitrogen, the PADS/ODA copolymer produced only 6% volatiles over six hours whereas the GAPD and DiSiAn containing materials lost 75
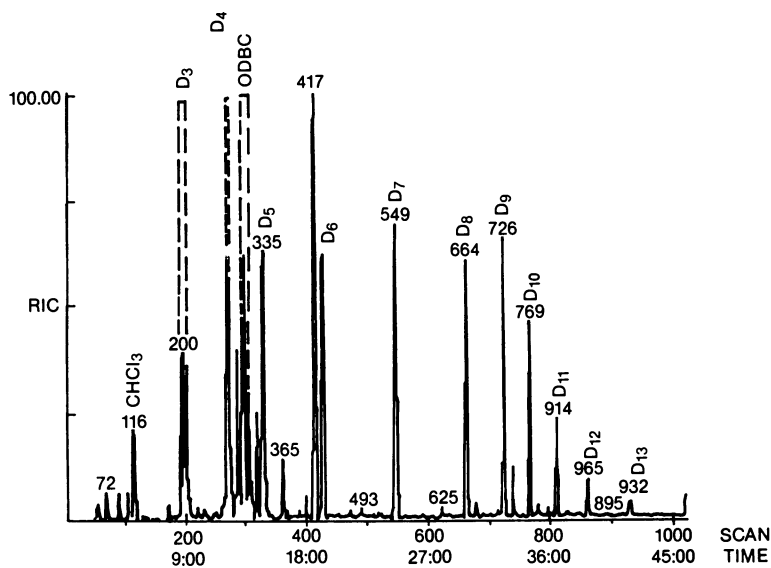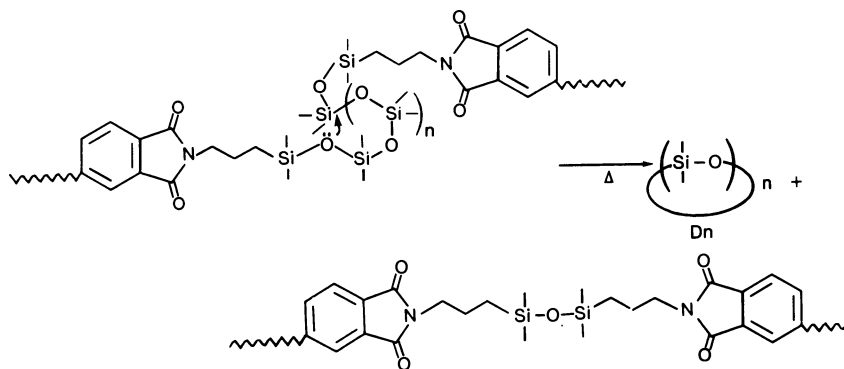
Figure 4. GC/MS of 450°C Pyrolysis Products of SPI 100.

and 47% of their weight, respectively, over the same period. Of additional importance is that the PADS containing material showed less sensitivity to an oxidative environment at 435°C than did the DiSiAn copolymer, which gave a much larger weight loss when the TGA was performed in air.

Because of the improved thermal stability for PADS containing polyimides vis a vis other available siloxane polyimides, a screening program to correlate properties such as T_g, solubility, thermal stability, adhesion properties, and water absorption characteristics to structure was undertaken. Several copolymers were prepared from diamines and co-dianhydrides. An ODAN/ODA copolymer in which 30 mole % PADS was substituted for ODAN, was prepared and TGA analysis at 450°C indicated that the material was the first siloxane containing polyimide identified that exceeded the established thermal stability criteria for interlevel dielectric applications. Stability and solubility of these materials as a function of PADS concentration is illustrated in Table VI.

Table VI.   Properties of PADS/ODAN/4,4´-ODA Siloxane Polyimide Copolymers

| PADS | ODAN | Tg | Thermo- | | p-methyl | |
mole%		(°C)	stability* (°C)	NMP**	anisole	chloroform
100	-	160	435	+	+	+
50	50	202	450	+	-	-
30	70	216	460	-	-	-
10	90	237	460	-	-	-
-	100	265	460	-	-	-

*   Temperature at which 1% wt loss/30 min occurs under nitrogen
    by isothermal gravimetric analysis.
**N-methylpyrrolidone.

Materials containing < 50 mole % PADS were insoluble in all common solvents including the polar aprotic variety, and thus were prepared by the two-stage method. A 1:1 ODAN/PADS composition could be prepared directly in NMP in reasonable molecular weight and of acceptable stability at 450°C. The polymer of PADS and ODA was soluble in common organic solvents such as o-dichlorobenzene (ODCB) and chloroform. This material, however, was stable only to 435°C. T_g's for this family of copolymers, as determined by DSC and TMA, ranged from 265°C for the ODA/ODAN material through 160°C for the ODA/PADS copolymer.

Both T_g and thermal stability of PADS/ODAN copolymers were increased when the ODA diamine component was replaced with m- or p-phenylenediamine (MPD, PPD) or a mixture of the two diamines (Table VII). A solvent resistant material prepared from PADS/ODAN/PPD/MPD 3:7:5:5 had a T_g of 260°C and exhibited outstanding thermal stability by TGA analysis, volatilizing less than 2 wt % per hour at 480°C under nitrogen.

Table VII. Thermal Stability of PADS Siloxane Polyimides

Composition		Max. Use Temp.* (°C)	T_g (°C)	T_m** (°C)
PADS/4,4′-ODA	1:1	435	160	-
PADS/MPD	1:1	435	160	-
PADS/PPD	1:1	435	180	350
PADS/BPADA/MPD	1:1:2	435	190	-
PADS/BPADA/MPD/PPD	1:1:1:1	435	205	-
PADS/BPADA/PPD	1:1:2	435	210	276
PADS/ODAN/MPD/PPD	3:7:5:5	480	260	-
PADS/PMDA/4,4′-ODA	3:7:10	460	320	-
PADS/PMDA/PPD	3:7:10	500	-	> 500

* Maximum use temperature defined by isothermal gravimetric analysis:
   ca. 1% wt loss/30 min at stated temperature under nitrogen.
** T_m = peak melting temperature.

A family of materials with even higher peak use temperatures (T_m ca. 510°C) was prepared through the copolymerization of PADS, pyromellitic dianhydride (PMDA), and PPD. A representative material was prepared with a molar ratio of 3:7:10 (PADS/PMDA/PPD). FTIR curing studies of this material coated to 1 micron thickness on a silicon wafer indicated that the extent of imidization does not increase above 300°C and is complete within levels of detection. This material did not suffer significant weight loss over short exposure periods (30 minutes) below 500°C.

Adhesion Studies

PADS containing siloxane polyimide compositions were evaluated for adhesion to silicon wafers according to the identical test protocol employed by Davis (7). As shown in Table VIII, these polymers had adhesive properties similar to the GAP derived siloxane polyimides; however, the PADS containing materials are of higher thermostability than the GAP derived materials. Thus, the PADS class of materials offers a balance of adhesive and thermal qualities not hitherto attainable.

Table VIII. Adhesion and Water Absorption of Polyimide

Materials Composition	Tg(°C)	Peel Test	Water Absorption
PADS/4,4′-ODA	160	Passes	<0.3%
PADS/4,4′-ODA/ODAN	220	"	"
PADS/ODAN/MPD/PPD	260	"	"
PADS/PMDA/4,4′-ODA	320	"	"
PADS/PMDA/PPD	(T_m = >500)	"	"
SPI-100	120	"	0.1

Adhesion for PADS-based siloxane polyimides was obtained over a range of comonomer compositions. The spun-on "PADS" coatings generally had to be annealed at 300°C to impart adhesion to silicon. In at least one series of copolymer compositions, the PADS content could be decreased to 10 mole % while maintaining adhesion to silicon as determined by the Tape Peel Test.

Water Absorption Studies

Dimensional stability, corrosion resistance and insulating properties of passivating and interlayer dielectric materials depend on ambient humidity conditions and water absorption characteristics of the polymer. The lowest possible water absorption is desirable for high electrical resistance, for prevention of swelling under humid conditions and to prevent corrosion of protected metal substrates. Polyimides typically absorb between 1 and 3% water when boiled for one hour under standard test conditions. Silicones, in contrast, although highly permeable to water vapor, absorb typically less than 0.3% by weight and have been well recognized for their encapsulating properties (8). Depending on composition, siloxane polyimides can have substantially improved water absorption characteristics. For example, SPI-100 which contains greater than 20% dimethylsilicone by weight, possesses water absorption properties similar to silicones. Improvement in water absorption characteristics for these materials comes at the expense of high temperature properties, however, thereby limiting their usefulness as interlayer dielectrics. On the other hand, PADS containing polyimides were shown to retain both low water absorption and high temperature capabilities. Water absorption for PADS polyimides was uniformly low at the 30 mole % PADS level, with no large effect observed across a range of copolymers which differed in diamine and codianhydride composition.

Characterization of Siloxane Polyimides

Characterization of the polymers was done by Gel Permeation Chromatography (GPC) which was performed on a Waters instrument equipped with a bank of μ-Styragel (trademark of Millipore Corporation) columns (chloroform eluent) and an ultraviolet (254 nm) detector. Reported molecular weights are relative to polystyrene standards. Isothermal Gravimetric Analysis and Differential Scanning Calorimetry (DSC) were performed on a Mettler TA3000 System. Reported thermal transitions were obtained via DSC analysis under nitrogen with a heating rate of 20°C/min.

General Procedure for 2 Stage Method for Preparation of Polyimides

To a flask containing enough NMP to produce a final polymer concentration of 20% solids was added at room temperature under nitrogen a quantity of diamine, followed proportionwise by an equimolar addition of dianhydride such that the reaction temperature did not exceed ca. 35°C. [On larger scale experiments (ca. > 0.25 moles) a cooling bath was employed to control the polymerization exotherm.] Upon complete addition of monomer, the contents were stirred for 4 hours until a homogeneous, high viscosity solution was obtained.

The polyamide-acid solution obtained was cast as a film (ca. .25 mm thick) onto a glass plate and dried for 12 hours at 80°C under vacuum (30 min). The resulting film was subjected to the following cure cycle under nitrogen on a hot plate monitored with a surface thermometer to effect imidization: 100°C (2 hours), 150°C (2 hours), 200°C (1.5 hours) and 300°C (1 hour). High T_g films (T_g > 300°C) were optionally cured for an additional 0.5 hours at a temperature of 480°C in an inert atmosphere oven to ensure imidization and removal of volatiles.

General Procedure for Solution Imidization

To a round bottom flask equipped with a modified Dean Stark trap, condenser, mechanical stirrer and nitrogen inlet, were added equimolar quantities of diamine and dianhydride as well as 0.5 wt % 4-N,N-dimethylaminopyridine and enough ODCB to provide an initial mixture containing 10% solids. The contents were heated for 6 hours at 180°C with azeotropic removal of water and distillation of ODCB such that the final polymer solution had a concentration of 20 to 25% solids. The polymer solution was cooled and precipitated twice into methanol, dried under vacuum (30 min) at 80°C for 12 hours and 170°C for 2 hours.

Acknowledgment

Literature Cited

(1)   Scroog, C. E; Endrey, A. L.; Abramo, S. V.; Berr, C. E.; Edwards, W. M.; Oliver, K. L. *J. Polym. Sci., A,* 1965, 3 (4), 1373.
(2)   See for example Takekoshi, T. and Kochanowski, J. E. U.S. Patent 3,991,004.
(3)   Rich, J.D. U.S. Patent 4,709,054.
(4)   Pratt, J.; Thames, S. *JOC* 1973, **38**, 4271.
(5)   Babu, G. N. in *Polyimides*; Mittal, K. L., Ed.; Plenum: New York, 1984; Volume 1, pp. 51-66.
(6)   Ryan, H.S. U.S. Patent 4,381,396.
(7)   Davis, G. C.; Heath, B. A.; Gildenblat G. in *Polyimides*; Mittal, K. L., Ed.; Plenum: New York, 1984; Vol. 2, pp. 847-869.
(8)   Davis, J. H. in *Plastics for Electronics*, Goosey, M. T., Ed.; Elsevier: New York, 1985; Chapter 3, pp. 67-98.

Chapter 13

Electrophoretic Deposition of Polyimides

Electrocoating on the Cathode

Stephen L. Buchwalter

IBM Research Division, Thomas J. Watson Research Center, Yorktown Heights, NY 10598

A method has been developed for applying polyimide films by cathodic electrophoretic deposition. This conformal method of coating metal substrates occurs from aqueous emulsions of the polymer dissolved in organic solvents. The chemistry of the process, involving an amine modification of soluble, pre-imidized polyimides, is characterized by infra-red spectroscopy, thermogravimetric analysis, and size exclusion chromatography. It is shown that the modification is eliminated during baking to regenerate the unmodified polyimide. Molecular weight of the polymer is little affected. The important parameters affecting film thickness are also investigated. It is found that the emulsions are well behaved electrocoating systems, *i.e.* a limiting thickness is reached after a few minutes at a given deposition voltage. The limiting thickness is found to depend linearly on voltage. Finally, the deposition characteristics are compared to that of the previously published anodic deposition of polyamic acid films.

Polyimide films have thermal and electrical properties which make them very useful for a number of applications in the electronics industry. (*1*) Conventional methods of applying polymer films, such as spraying, spin-coating and laminating can be used for polyimides; but these methods are more suitable for applying the films to essentially planar substrates. Electrophoretic deposition (*2*) is an important commercial method of applying polymer films to irregularly shaped metal articles, and adaptation of this method to polyimides could increase their utility significantly.

In fact there have been some reports of electrophoretic deposition of polyimides in the literature. Boldebuck, Lupinski and Fessler (*3*) developed a method of depositing polyamide-imides, and Lupinski, Boldebuck, McQuade and Flowers (*4*) applied it to the continuous coating of aluminum. Researchers from Westinghouse-- Phillips (*5*) and later Alvino, Fuller, and Scala (*6-8*)--reported the electrophoretic deposition of the polyamic acid precursor to a polyimide from a non-aqueous dispersion. This achievement has the advantage of using the polyimide from pyromellitic dianhydride and 4-aminophenyl ether (oxydianiline) in its readily available, soluble polyamic acid form. This particular polyimide is the one most widely used in the electronic industry because of its excellent combination of electrical, mechanical and thermal properties, and thus this method would be preferred over that of Lupinski *et al.*. The Westinghouse approach does have some disadvantages, however.

An important one is that deposition occurs on the anode, and it is known *(5)* that some metal is incorporated into the polymer film, presumably because oxidation of the substrate can compete with polymer deposition. Because of this problem of anodic metal dissolution, cathodic deposition of epoxy resins *(9-10)* was developed. A second disadvantage in using the polyamic acid is that the formulations used do not deposit an insulating film, and thus the film thickness is not self-limiting. Although this fact may allow quite thick films to be deposited, it also means that the film thickness is not uniform as it will depend on distance from the counter-electrode and other current density effects.

Contamination of the polyimide with metal ions is a serious concern with respect to the thermal and electrical properties of the finished films. Also, the ability to obtain uniform film thicknesses over irregular surfaces is one of the key advantages of electrophoretic deposition. It was these considerations that provided the impetus for the work reported in this paper.

Results and Discussion

Electrophoretic deposition is commonly done from an aqueous emulsion of the polymer. *(2)* In order to obtain such an emulsion, it is necessary to attach an optimum level of charged groups to the polymer. The optimum level generally falls in a fairly narrow range, with the lower limit constrained by emulsion stability and the upper limit constrained by efficiency in film deposition. Because the emulsion is stabilized by coulombic repulsion of the charged layers around the emulsion particles, it is readily seen that below a certain level of charged groups the emulsion, if formed at all, will rapidly revert to two separate phases. The explanation for the upper limit is more complex. The theory for the phenomenon of electrophoretic deposition *(2)* is schematically summarized in Figure 1 for cathodic deposition. The simultaneous electrolysis of water and polymer electrophoresis allows the polymer droplets to coalesce at the cathode because of the neutralization of the charges by the high local pH at the electrode surface. If the number of charges to be neutralized are too high, film deposition characteristics tend to become poor. A number of effects may contribute to the poor deposition. Bath conductivity is increased by an increase in charged groups, causing an increased current density. The latter can cause nucleation of gas bubbles which rupture the film. Also, the high level of charged groups are less completely neutralized, causing the film conductivity to be higher. High film conductivity reduces the tendency of the film to be self-limiting in thickness, and the film will not be uniform over the substrate. Finally, the rate of film re-dissolution can become a problem at higher charged group levels to the point that film deposition does not occur. The net result is that it is necessary that the chemistry of the polymer in question allow the number of charged groups to be adjusted to the optimum level.

This requirement has been met with soluble, pre-imidized polyimides. It has been found that secondary amines react quite readily with such polyimides in polar solvents such as N-methylpyrrolidinone or dimethylacetamide. The reaction was done initially with morpholine for a series of available pre-imidized polymers (see Table I). The reaction was easily followed by infra-red spectroscopy (IR) (see Figure 2), the imide carbonyl absorptions at 1780 and 1723 cm^{-1} being replaced by amide carbonyls at 1645 cm^{-1}. In addition, the aliphatic C-H absorptions at 2880 cm^{-1} were noted.

For the purposes of electrophoretic deposition, 1-methylpiperazine, a secondary-tertiary diamine, was chosen to attach a tertiary amine group to the polymer chain (see Figure 3). The stoichiometric ratio of amine to imide groups was adjusted in the range 0.25 to 0.65, and a ratio of 0.4 was found to be about optimum. The tertiary amine group was then available to be protonated with acid, forming the positively charged substituent requisite for emulsification and cathodic electrophoretic deposition. Both acetic acid and lactic acid were used successfully at a level stoichiometrically equivalent to that of the amine modifier.

The facile reaction of an aromatic imide with an amine seemed surprising, perhaps because
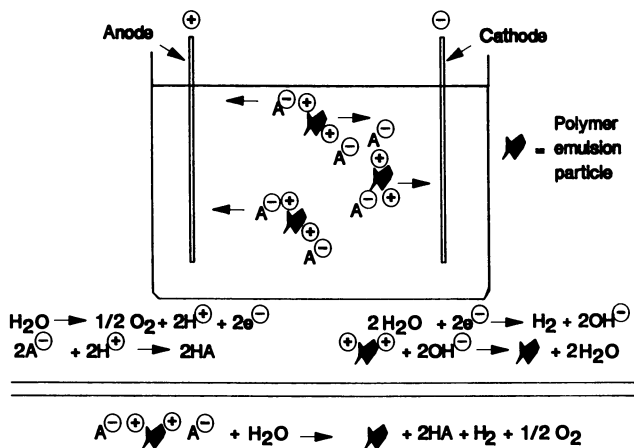
Figure 1. Schematic representation of electrophoretic deposition.

Wavenumber (cm⁻¹)
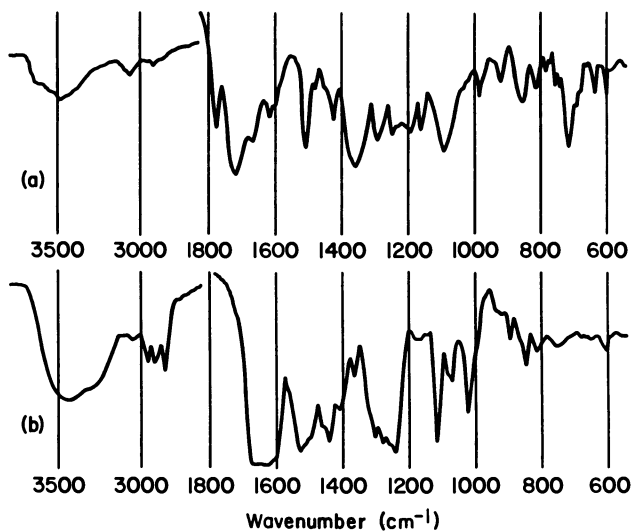
Figure 2. Infra-red spectra: a) Upjohn PI-2080; b) PI-2080 after reaction w/ excess morpholine.

TABLE I: Soluble Polyimides

Manufacturer	Polymer
Upjohn	PI-2080
M & T Chemicals	M & T 2065
M & T Chemicals	M & T 3500
M & T Chemicals	M & T 5000
Ciba-Geigy Corporation	Matrimid 5218 (XU-218)
National Starch and Chemicals Corporation	Thermid IP-630

the excellent thermal stability of polyimides gives one the impression that the polymers are chemically inert as well. There is precedent for such reactions in the chemical literature, however. Linde *(11)* reported reactions of alkylamines with aromatic imides in some work done to model the action of amine-functional adhesion promoters. Etching of polyimide with hydrazine *(12)* also constitutes precedence for the reaction in that hydrazine is a nucleophile that is similar to, albeit more aggressive than, an amine nucleophile.

The requirement of a controllable level of charged groups having been met, attention turned to the elimination of the amine modifier. In order to obtain the desirable properties of the polyimide, it was important that the modification be readily eliminated. At the outset, there was an indication in the literature that this would in fact be the case. In 1970, Delvigs and co-workers *(13)* reported the diethylamide derivative of a polyamic acid as an alternative precursor to polyimides. They provided IR evidence that the amine was eliminated thermally to form a polyimide indistinguishable from that obtained from the polyamic acid. In the present work, the elimination of 1-methylpiperazine was followed by thermogravimetric analysis (TGA), IR, and size exclusion chromatography (SEC).

Samples of Ciba-Geigy Matrimid 5218 modified with 1-methylpiperazine in N-methylpyrrolidinone/acetophenone were heated from room temperature to 500°C in the TGA instrument. Comparison of the observed weight loss to that expected based on loss of the known amount of solvent and amine showed excellent agreement (see Figure 4). Also shown is the TGA scan for the unmodified Matrimid 5218 solution, *i.e.* a solution identical to that of the modified polymer except that the amine modifier was replaced with an equal weight of additional solvent. Note that the two curves virtually coincide at high temperatures, *i.e.* after the amine is eliminated. This important point is brought out more clearly in Figure 5 in which the modified polymer and the control are subjected to TGA after a three-stage bake (1 hr each at 100, 250, and 350°C). The thermal stability of the polyimide is little affected by the amine modification. The small additional weight loss observed for the modified sample probably is a result of the elimination of the last traces of amine.

For the IR study, an electrodeposited film (see later) was dried at 100°, then stripped from the substrate by boiling in water for one minute. This free-standing film was convenient for recording IR spectra before and after heating at higher temperature. Films could not be removed from the substrate after the higher temperature bakes. The spectra obtained (Figure 6) corroborate the TGA results quite well. The reappearance of the imide absorptions on baking is readily seen, and there is a peak-for-peak correspondence between the spectrum for the modified polymer after baking and the control spectrum of the unmodified polymer. Based on the TGA and IR results, it is concluded that the amine modification is reversible, as is desired.

A further point of interest is the effect, if any, of the addition and elimination of amine on the molecular weight of the polyimide. An interesting experiment was devised to investigate this possibility. Samples of Matrimid 5218 were reacted in separate experiments with
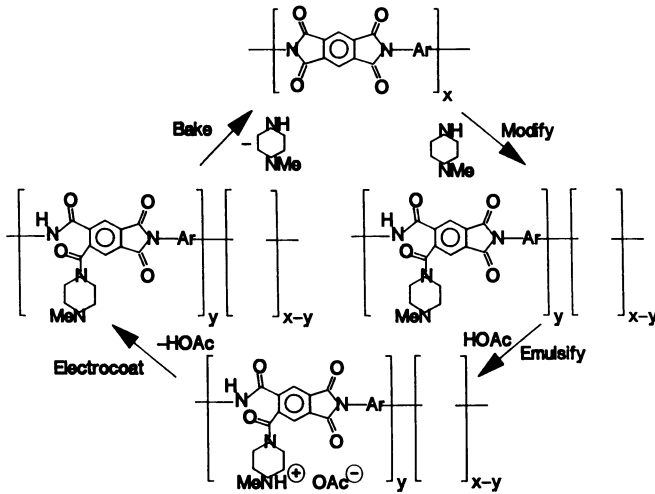
Figure 3. Reaction cycle for electrophoretic deposition of a polyimide.
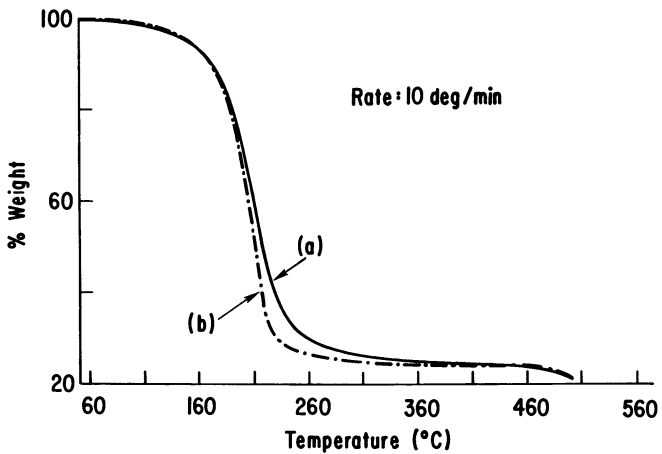
Figure 4. Thermogravimetric analysis: a) solution of amine-modified Matrimid 5218; b) solution of control Matrimid 5218 (see text).
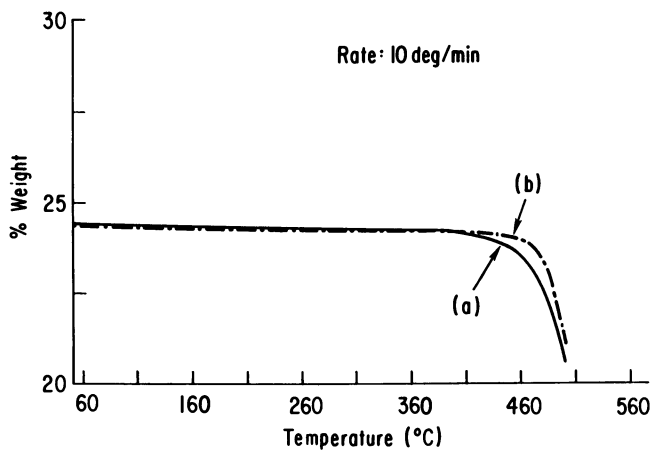
Figure 5. TGA after three-stage bake (see text): a) amine-modified Matrimid 5218; b) control Matrimid 5218.
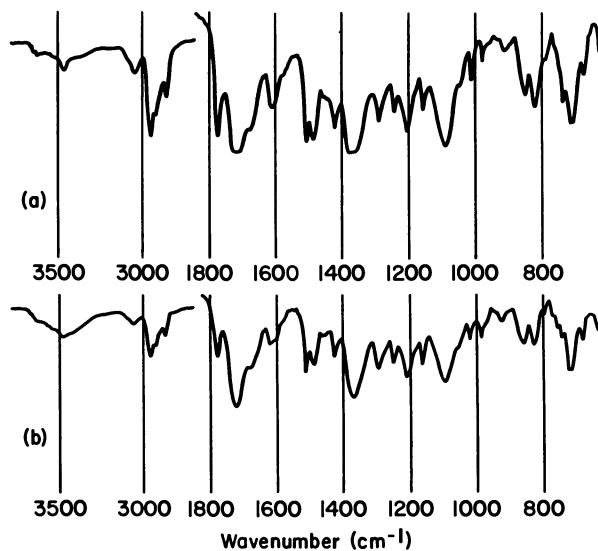
Figure 6. IR spectra: a) electrocoated Matrimid 5218 after curing; b) control Matrimid 5218.

morpholine, piperidine, and 1-methylpiperazine. Solutions of the modified polymers and a control solution of unmodified polymer were then analyzed by SEC using tetrahydrofuran. There was a sizable shift to smaller hydrodynamic volume for the modified polymers, as might be expected for increased intra-chain interactions brought about by the potential for hydrogen bonding. Elimination of the amines was then done by distillation of the dimethylacetamide (DMAC) solutions, with solvent replenishment, until no further amine could be seen in the distillate by gas chromatography. The polymer solutions were then re-analyzed by SEC. As shown in Figure 7, the hydrodynamic volume nearly recovers to its original value. An IR spectrum of the regenerated polymer was indistinguishable from that of a virgin sample.

The net change in hydrodynamic volume corresponds to as much as a 50% decrease in polystyrene molecular weight on the same column set but with toluene as solvent medium. Subjecting the control polymer to the elimination conditions caused no change in hydrodynamic volume. The explanation for the change may lie in a small amount of residual amine on the polymer causing increased intra-chain interactions, a small amount of hydrolysis to give amic acid groups, or some chain scission due to hydrolysis or the presence of trace amounts of primary amine in the secondary amine (none was detected by gas chromatography). At any rate, this change was observed in solution with excess amine. Even if this change reflects molecular weight degradation, it is expected that there will be considerably less opportunity for the amine to degrade the polymer during the reaction cycle for electrophoretic deposition (Figure 3), in which case less than one equivalent of amine is used and the elimination is done not in solution but in the polymer solid state.

The modification of the polyimide with 1-methylpiperazine attaches a pendant tertiary amine group to the polymer. This group is then available to generate an amine salt group upon the addition of acetic or lactic acid. It has been found that, with Matrimid 5218, addition of lactic acid to the solution of the modified polymer in NMP and a cosolvent allows a suitable emulsion to be formed by rapid agitation and slow addition of water. A number of cosolvents were used, but it was found that a water-insoluble solvent, such as acetophenone, was needed to deposit with the polymer and to promote good coalescence and flow in the film. A number of other formulation variables are available for optimizing the emulsion and the subsequent electrophoretic deposition. These include the the amounts of amine modifier, acid, and solvents, the degree of dilution (percent solids) of the emulsion, and the temperature, voltage and time of deposition. Although a detailed investigation of each of these variables has not been done, sufficient experimentation has been carried out to obtain some degree of optimization in each case. It is interesting that the result of this process gave parameters quite similar to those given by Beck (2) as optimum for other systems (see Table II).

TABLE II: Electrophoretic Deposition Parameters

Property	Beck's value (2)	This work
Meq ionic groups/g resin	1.0	1.35
Polymer molecular weight (daltons)	1,000-50,000	ca. 20,000
Polymer concentration	ca. 10%	4%
Degree of neutralization	35-90%	100%
Solvent (water/organic)	90/10	92/8
Current Density (mA/cm²)	1-5	0.75-8
Voltage (V)	50-400	85-150
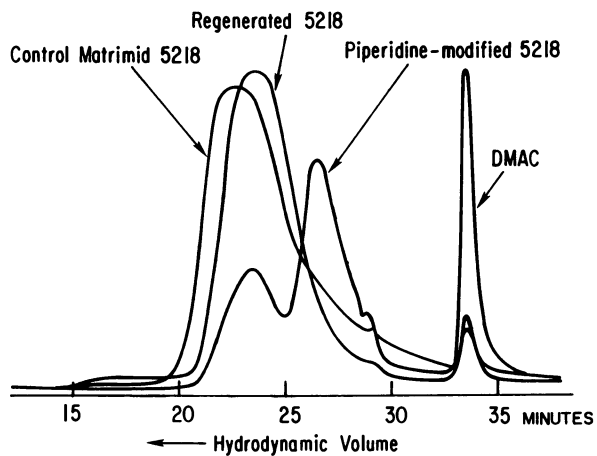
Figure 7. Size exclusion chromatography.

To establish the uniformity of the coatings, the deposition was done on aluminum test panels. After deposition and baking, a layer of metal was evaporated on top of the coating for visualization purposes; and the panels were cross-sectioned and potted in epoxy. Representative photomicrographs are shown in Figures 8 and 9. The film thickness is quite uniform on both sides. Only a single anode facing one side of the test panel was used (see Experimental), and thus the uniformity of the film thickness is a result of the tendency of the depositing film to insulate and not a result of uniformity in the electric field over the panel surface.

The film insulation also is revealed in the self-limiting characteristic of the deposition. This property was shown by stopping the constant voltage deposition after various times and measuring the film thickness. The rate of increase of thickness is rapid in the first 60 sec, but approaches some limiting value after 5 minutes (Figure 10). Pierce *(9)* has published a detailed analysis of film growth in some commercial electrophoretic deposition formulations, and the behavior shown in Figure 10 is very similar to that of the systems he studied. Pierce also reported that film thickness is linearly dependent on voltage, and this has been observed in the present case as well (Figure 11). This relation allows the film thickness to be controlled to some degree in order to meet the requirements of the application.

It is interesting to compare the electrophoretic deposition of the aqueous emulsions of this work to that of the non-aqueous emulsions of polyamic acids reported by Alvino, Scala, and Fuller. *(7)* In the present work, a few charged groups, 1.2 meq/g of polymer, are used to emulsify the polymer in a conductive medium, water. In the previous work, twice as many charged groups *ca.* 2.4 meq/g of polymer, are used in organic solvent, presumably much less conducting. Alvino *et al.* report some interesting coulombic yield measurements that indicate that deposition requires only one charge transfer for every 16-18 repeat units of the polymer. Since each repeat unit contains two carboxylic acid groups, one of which has been neutralized with amine, the deposited film must contain a large fraction of the charged groups originally there. Our own qualitative results with Alvino's formulation are consistent with a fairly conductive film being deposited from the non-aqueous emulsion. Test substrates coated in our experimental set-up using the Alvino emulsion had markedly different film thicknesses on the two sides of the substrate, with the side facing the cathode having roughly twice the thickness as the back side, as might be expected for a conductive film continuing to pass appreciable current. The film quality, however, was excellent; and there appeared to be no limit to film thickness. It seems clear that the non-aqueous, anodic method of Alvino *et al.* and the aqueous, cathodic deposition reported in this work are in fact complementary.

Experimental

General. Commercially available polyimides were used (see Table I). Solvents were reagent grade or better and were used as received. 1-Methylpiperazine (Aldrich Chemical Co.) was >99.9% pure. Lactic acid (Aldrich) was reduced to 50% by weight in water and refluxed for an hour to hydrolyze esters. IR spectra were recorded on a Perkin-Elmer Model 1430 spectrometer. Thermogravimetric analysis was done on a P-E System 4/TGS-2 instrument. Size exclusion chromatography was done on a Perkin-Elmer Series 3B equipped with the LC-75 spectrophotometric detector. The column set used consisted of P-E 0258-2134, 2133, and 2131 columns (pore sizes 10^3, 10^4, and 10^6 Å, respectively). For electrophoretic deposition experiments, a TCR Power Supply (Electronic Measurement Systems Inc.) was used. Temperatures are reported in °C throughout.

Reaction of Polyimides with Morpholine. For exploratory work, test tube solutions of the polymers in N-methylpyrrolidinone (10% by weight) were prepared. Morpholine at twice the polymer weight was added. After thorough mixing, the solutions were allowed to stand at room temperature for a day. The modified polymers were collected by precipitation in water, filtration, washing with more water, and drying *in vacuo* over phosphorous pentoxide for ten days. IR spectra were then recorded of KBr pellets containing the modified polymers. In
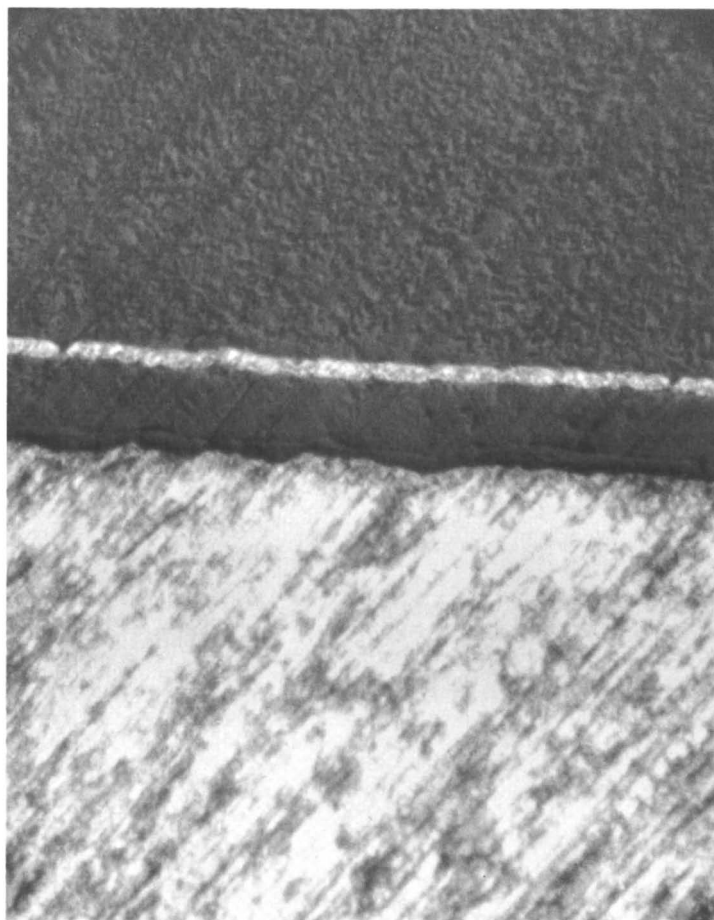
Figure 8. Cross-section of electrocoated film on aluminum.
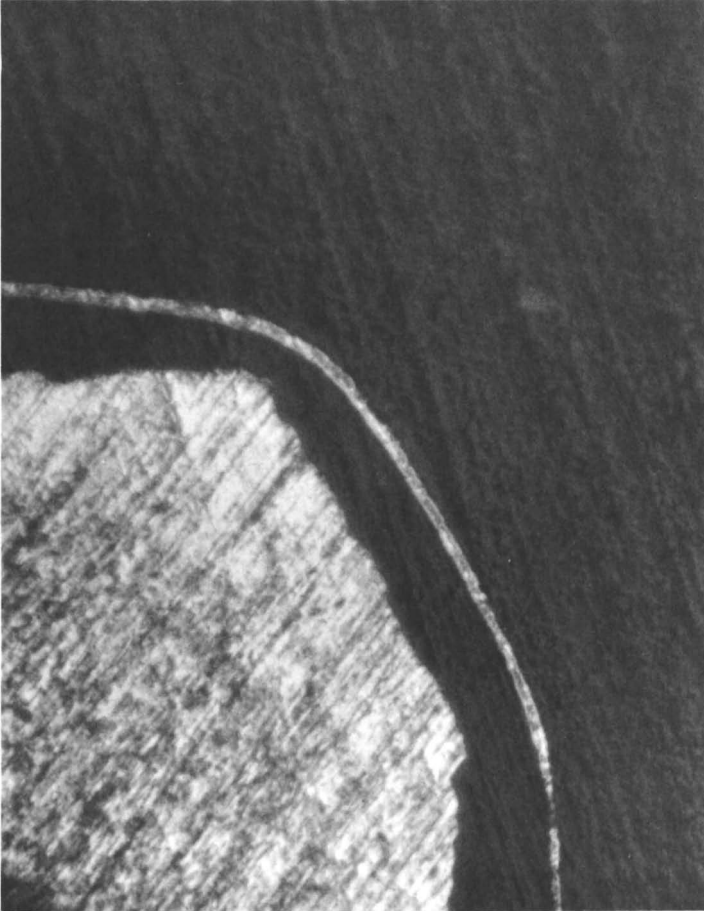
Figure 9. Cross-section of electrocoated film on aluminum (at edge).
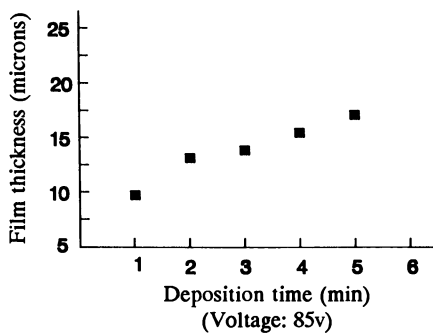
Figure 10. Film thickness *vs.* time.
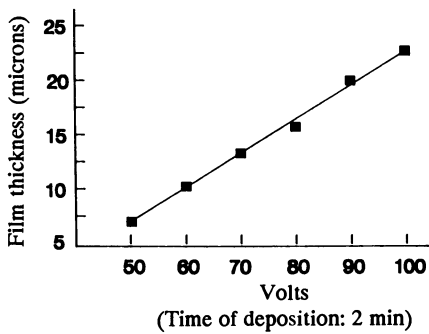
Figure 11. Film thickness *vs.* voltage.

each case, the imide absorptions were replaced by amide absorptions, as can be seen for PI-2080 in Figure 2.

Illustrative Example of Electrophoretic Deposition. Ciba-Geigy Matrimid 5218 (100 g) and 1-methylpyrrolidinone (200 g) were charged in a 500-ml reaction flask. The polymer was dissolved by stirring the mixture while warming to approximately 90°. A blanket of nitrogen was kept over the mixture. Once the polymer was completely dissolved (approximately 30 min), addition of a mixture of 12.04 g of 1-methylpiperazine and 100 g of acetophenone was begun. The addition was continued over about 90 min with vigorous stirring throughout. The temperature was kept at 85-95° during the addition. After the addition was complete, the mixture was stirred and warmed to 110° and held at that temperature for 2 hours. The resultant modified polymer solution was then used to prepare the electrophoretic deposition emulsion as detailed below.

To 88.3 g of the modified polymer solution was added 18.5 g of acetophenone and 4.9 g of 50% aqueous lactic acid. The mixture was stirred vigorously in a 500-ml stainless steel beaker while 488 ml of deionized water was added slowly. The stirred mixture became quite viscous as the gradual water addition continued, then thinned out as the addition of water was completed.

The translucent brown emulsion was placed in a constant temperature bath at 25° with stirring provided by a teflon stirbar and a submersible magnetic stirrer. Aluminum test pieces (100 mm x 45 mm) were placed into the emulsion along with a 9-mm diameter graphite rod. The latter was wrapped with teflon tape to reduce its surface area. The exposed area of the rod was approximately one-fifth of the area of the aluminum test piece. The distance between the rod and the test piece was ca. 60 mm. The rod and test piece were connected to a DC power supply as the anode and cathode, respectively. The voltage was turned up to 85 volts within 15 sec and held there for 2 min. The test piece was removed, rinsed rapidly in deionized water and placed in a warm (40°) dry chamber containing some acetophenone to impede the evaporation of same from the drying film. After 25 min, the test piece was removed from the chamber. Inspection showed a uniform, smooth coating still tacky with acetophenone.

The coating was baked in three steps. First, it was heated in a convection oven at 100° for six hours. The test piece was then transferred to a vacuum oven and heated under vacuum (ca. 10 torr) as follows: 250° for 4 hours, ramped to 350° over 3 hours, and heated at 350° for 45 min. The resultant smooth, dark brown coating had a thickness of 17 microns which was uniform front and back.

Acknowledgment

Literature Cited

1.   Sato, K.; Harada, S.; Saiki, A.; Kimura, T.; Okubo, T.; Mukai, K. *IEEE Trans. Parts, Hybrid and Packaging* 1973, 176.
2.   Beck, F. *Prog. Org. Coat.* 1976, **4**, 1.
3.   Boldebuck, E.; Lupinski, J.; Fessler, W. *Org. Coat. and Plast. Prepr.* 1976, **36**, 278.
4.   Lupinski, J.; Boldebuck, E.; McQuade, J.; Flowers, R. *Org. Coat. and Plast. Prepr.* 1976, **36**, 284.
5.   Phillips, D. *J. Electrochem. Soc.* 1972, **119**, 1645.
6.   Alvino, W.; Scala, L. *J. Appl. Polym. Sci.* 1982, **27**, 341.
7.   Alvino, W.; Scala, L.; Fuller, T. *J. Appl. Polym. Sci.* 1983, **28**, 267.

8. Scala, L.; Alvino, W.; Fuller, T. In *Polyimides: Synthesis, Characterization, and Applications*; Mittal, K., Ed.; Plenum Press: New York, 1984; Vol. 2, p 1081.
9. Pierce, P. *J. Coat. Tech.* 1981, **53**, 53.
10. Wismer, M.; Pierce, P.; Bosso, J.; Christenson, R.; Jerabek, R.; Zwack, R. *J. Coat. Tech.* 1982, **54**, 35.
11. Linde, H. *J. Polym. Sci. Polym. Chem. Ed.* 1982, **20**, 1031.
12. Jones, J. *J. Polym. Sci. C* 1968, **22**, 773.
13. Delvigs, P.; Hsu, L.; Serafini, T. *Polym. Lett.* 1970, **8**, 29.

RECEIVED March 10, 1989

Chapter 14

Accelerated Testing of Polyimide Coatings for Neural Prostheses

J. McHardy, D. I. Basiulis, G. Angsten, L. R. Higley, and R. N. Leyden[1]

Technology Support Division, Hughes Aircraft Company, El Segundo, CA 90245

The adhesion of polyimide insulator coatings to electronic materials was greatly enhanced by an alumina primer layer. Accelerated aging tests indicated that adhesion failure of alumina-primed polyimide coatings is unlikely to limit the functional life of in vivo electronics. Factors contributing to adhesion loss can be physical, chemical or electrochemical. Measurements used to evaluate the effect of these factors on adhesion included mechanical peel strength and electrochemical pore resistance. The tests showed dramatic improvements in the adhesion of polyimide coatings, even to noble metal substrates, when the substrate was first 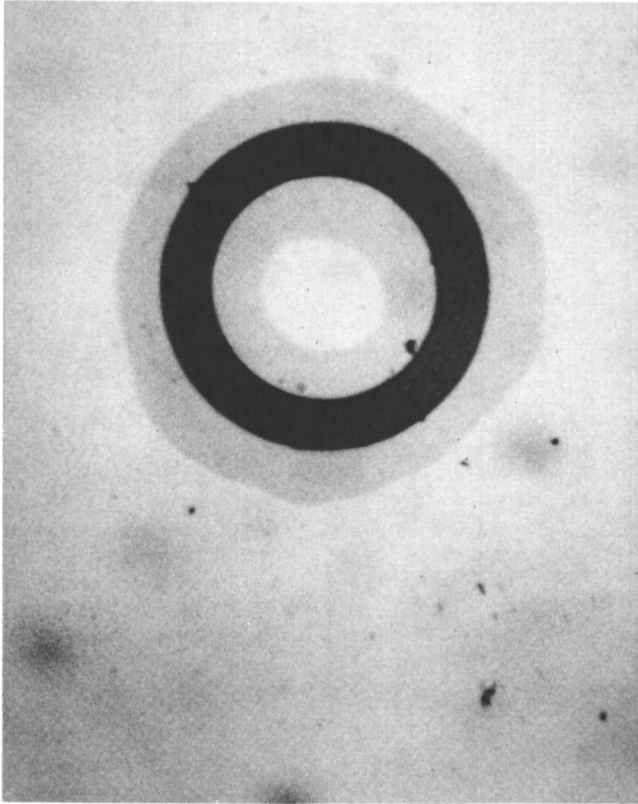treated with an aluminum chelate primer. Specimens survived for several weeks in boiling saline solution with no significant loss in adhesion strength. By comparison, unprimed specimens failed this test within a few hours. Applied voltage tests yielded similar distinctions: adhesion loss in primed specimens was induced only by treatments which attacked the underlying metal.

Electronic components of neural prostheses must survive and function under challenging conditions. They are exposed not only to the corrosive effects of saline fluids but also to natural foreign-body reactions. Hermetic packaging can delay the attack but it is not practical to seal the whole unit. The key to survival and reliable performance of neural implants is the selection of insulating materials that will neither harm the body nor be harmed by it.

In a non-hermetic package, the primary moisture barrier is typically a thin, (≤ 0.1 micron) inorganic passivation layer of silicon dioxide or silicon nitride. However, passivation layers cannot withstand physical handling and they are not resistant to saline exposure. Additional protection is needed in the form of organic polymer coatings.

[1]Current address: 3-D Systems, 12847 Arroyo Street, Sylmar, CA 91342

No organic coating is completely impermeable to water vapor but a tightly adhering one can block condensation of liquid water at the substrate surface. The protection afforded by a polymer coating is thus determined by the degree of adhesion maintained under adverse conditions. In this paper, we describe the use of accelerated tests for predicting long-term adhesion failure. Factors contributing to failure are physical (e.g., phase changes; temperature), chemical (e.g., salinity; pH), and electrochemical (e.g., metal dissolution; gas evolution). We have measured the effect of these factors on adhesion in terms of mechanical peel strength and electrochemical pore resistance.

EXPERIMENTAL

MATERIALS. The polyimide used in this study, PI-2555 and PIQ-13 (polyimide isoindoloquinazolinedione) were obtained from duPont and Hitachi, respectively. PIQ coupler, an aluminum chelate primer, was also obtained from Hitachi. The primer and polyimides were applied by spin coating. Test substrates included metallized glass slides, metal sheet, and 3-inch diameter silicon wafers.

Each substrate was cleaned on the spin coater by rinsing successively with acetone, isopropyl alcohol, and deionized water. It was then baked at 200°C for 10 minutes to remove water. When the PIQ Coupler was used, a 5ml volume of the solution was spun on at 4000 rpm for 30 seconds and then baked in air at 350°C for 30 minutes. The polyimide coatings were applied in three or four layers, each layer being spun on at 2500 rpm for 30 seconds and then prebaked at 110°C for 20 minutes. After the final coat, the wafer was heated in flowing nitrogen for 1 hour each at 100°C, 200°C, and 350°C. The coatings were applied either in a Class 100 clean room or in normal laboratory air. Microscopic inspection revealed fewer inclusions in the clean-room specimens but there was no appreciable improvement in their adhesion properties. When required, small openings were made in the polyimide by photolithography and oxygen-plasma etching (1).

ADHESION TESTING. We measured adhesion strength by adapting the peel test method of Saiki and Harada (2). In our method, test pieces were defined by scribing the film in a grid pattern of 1-cm squares separated by 2mm spaces. Thus, for a silicon specimen, a single 3-inch wafer yielded 21 possible peel sites. In a typical experiment, a specimen was subjected to a particular exposure (e.g., boiling saline) and removed at intervals for adhesion testing. A test site was selected at random and one edge of the polyimide square was carefully lifted with an Exacto knife. Tape was applied to the free edge so that it could be clamped in the upper jaw of a tensile tester (Instron Model 1125). The substrate was clamped in a horizontal position and the vertical force needed to maintain a peel rate of 5 mm/min was recorded. Results are quoted either as the maximum peel force or the average peel force during the test. The two parameters usually followed the same trend but the maximum peel force tended to be more reliable.

RESULTS

Peel test results are summarized in Tables I to III and graphed in
Figures 1-3. For the application of thermal and chemical stress,
specimens were immersed in 0.15M saline solution at a constant
temperature between $40^{\circ}C$ and $125^{\circ}C$. Exposures above $100^{\circ}C$
employed an autoclave. Tests at the upper temperatures were
terminated not because of adhesion loss but because of surface
erosion of the coatings. Spot checks on coating thickness with a
Dektak II instrument indicated average losses of up to 3 microns
(20-30%) after 7 days at $125^{\circ}C$. However, the thinning was
non-uniform: in a few spots, the coating appeared to have been lost
completely. Adhesion tests were also performed on unprimed
specimens but failure was very rapid. At all but the lowest
temperatures, the coatings suffered complete loss of adhesion within
a few hours.
    Our original intent was to measure adhesion loss as a function
of temperature, calculate an activation energy for the process and
then project the time to failure at body temperature. However, the
results indicate that adhesion loss in this system cannot be
characterized by a single rate parameter. in fact,as shown by
Figures 1-3, there was a distinct tendency for the peel strength to
pass through a minimum as a function of time. The tendency suggests
that at least two competing processes are at work.
    The initial drop in adhesion strength occurred rapidly, often in
a matter of hours. The drop may reflect a plasticizing effect of
moisture, similar to that observed in polymeric adhesives (4,5).
The effect, which is reversible, lowers the glass transition
temperature, T_g and the Young's modulus of the polymer. Because
our measurement of peel strength included the force needed to bend
the film through 90°, a decrease in Young's modulus of the film
would tend to lower the reading obtained. Surface analysis
following a peel test showed consistently that the separation
occurred between alumina and polyimide layers. It follows that the
rise in peel strength with prolonged heating in saline implied some
type of chemical change at this interface. Saiki and Harada (2)
showed that adhesion strength tended to increase with curing
temperature, suggesting that the bonding process may be incomplete
after the normal cure cycle. The upward trend in peel strength
observed after the initial drop may thus reflect a process of
continued bond formation between the polyimide and alumina layers.
For the application of electrical stress, a coated specimen was
immersed in a beaker of 0.15M saline solution at room temperature.
Electrical signals were applied between the specimen and a platinum
counter-electrode in the same solution. The test signal, generated
by means of a Pine Instruments RD4 potentiostat and an Hewlett
Packard HP 3301B function generator, was 0.5 kHz square wave.
Initial tests were performed at a fixed current amplitude of ±15mA.
Subsequently, potentiostatic voltage pulses were employed in which
the electrode potential of the test specimen was stepped at 500 Hz.
between predetermined limits with respect to the saturated calomel
reference electrode (SCE). The potential limits were selected in
each case to avoid visible gas evolution on the specimens. A

Table I.   Average Peel Strengths in gms/cm for PI 2555 Coatings on Alumina-Primed Titanium after Heating in Saline Solution

		DAYS OF EXPOSURE				
	TEMPERATURE	0.0	0.5	1.0	2.0	4.5
	100°C	487	451	449	361	464
	120°C	572	409	412	443	477

Table II. Maximum (or Average) Peel Strengths in gms/cm for Polyimide Coatings Applied in Laboratory Air to Alumina-Primed Silicon after Heating in Saline Solution

	DAYS OF EXPOSURE AT 100°C							
	0	0.17	2	9	14	24	44	60
PIQ-13	571(543)	400	433	531(518)	527	535(517)	527(494)	312(293)
PI 2555	574(494)	414	448	467(430)	541	553(545)	466(451)	555(539)

	DAYS OF EXPOSURE AT 125°C			
	0	0.17	2	9
PIQ-13	571(543)	339	439	550(500)
PI 2555	574(495)	363	301	329

Table III. Maximum (or Average) Peel strengths in gms/cm for Polyimide Coatings Applied in Clean Room Air to Alumina-Primed Silicon after Heating in Saline Solution

	DAYS OF EXPOSURE AT 80°C				
	0	5	10	17	46
PIQ-13	554(502)	475(455)	471(458)		520(510)
PI 2555	444(438)			394(376)	455(449)

	DAYS OF EXPOSURE AT 100°C		
	0	0.67	34
PIQ-13	381(376)	357(348)	417(410)
PI 2555	451(447)	360(356)	470(455)

	DAYS OF EXPOSURE AT 125°C				
	0	0.67	9	13	15
PIQ-13	486(479)	394(386)	403(393)	506(499)	381(365)
PI 2555	432(425)	363(357)	387(382)	369(360)	387(379)
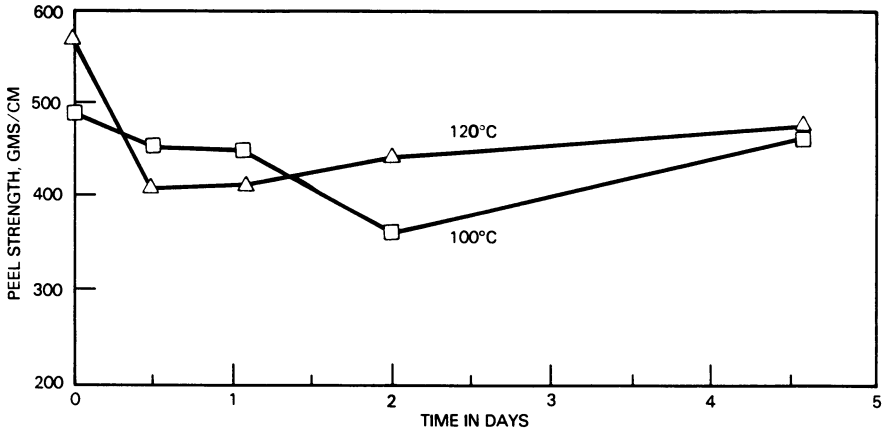
Figure 1.   Peel Strength of PI-2555 Coatings on Titanium After
             Exposure to Saline at 100°C and 120°C.
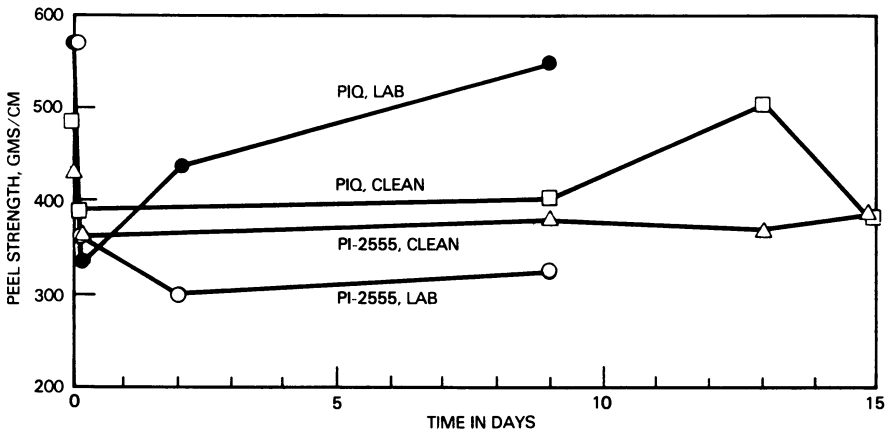
Figure 2.   Peel Strength of Polyimide Coatings on Silicon After
             Exposure to Saline at 125°C.
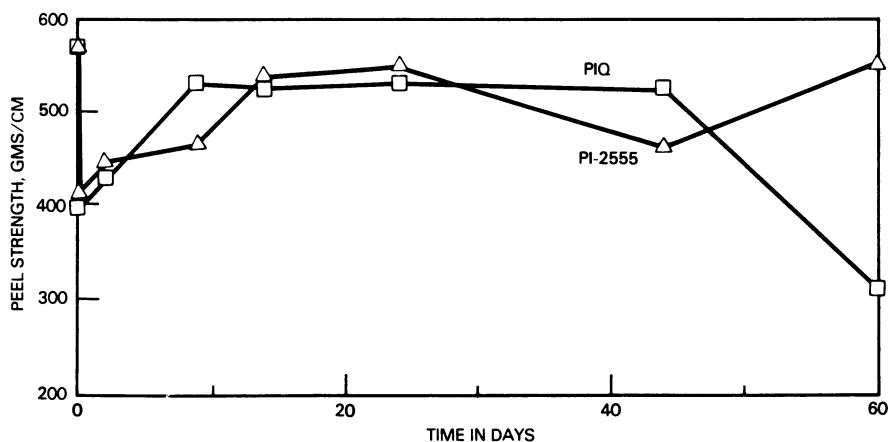
Figure 3.   Peel Strength of Polyimide Coatings on Silicon After
Exposure to Saline at 100°C.

gold-coated glass slide was primed, coated with polyimide, and
patterned with cross-shaped openings. The specimen was pulsed in
saline at ±15mA for 28 hours. Post-test inspection with a binocular
microscope showed that the gold itself had been dissolved,
undercutting the polymer around each opening. Pulse tests were then
applied to a platinum-coated specimen of similar design. Unlike the
gold specimen, the pulsing produced no evidence of undercutting.

     Changes in pore resistance measured by electrochemical impedance
spectroscopy (3) were consistent with the visual observations.
Plots of impedance vs. AC frequency on the gold specimen showed a
significant drop in pore resistance (reflecting enlargement of the
openings) whereas no changes in pore resistance was seen for the
platinum specimen.

     Similar specimens of PI 5555 on alumina-primed gold, tantalum,
or titanium, were subjected to potentiostatic pulses for 48 hours.
The potential limits were -0.3 to +1.0 volts vs. SCE for Ti and Ta,
and 0.0 to +1.0 for Au. Post-test inspection revealed discoloration
of the exposed tantalum and titanium areas but no apparent lifting
of the polyimide coating. However, when adhesive tape was applied
to the surface and peeled back, the polyimide was removed from the
edges around the cross-shaped openings. The gold specimen showed no
change in polyimide adhesion, although the metal had become visibly
etched. Scanning electron microscope (SEM) examination of the
tantalum specimen revealed that an oxide layer, several hundred nm
thick, had formed in the exposed areas. The oxides formed on
tantalum and titanium under pulsing conditions in saline are
evidently less protective than those formed in conventional
anodizing processes. Preanodization in 0.1 M H_3PO_4 did prevent
the attack in saline, but the anodizing voltage had to be kept very
low (1). As shown in Figure 4, anodization of a Ti specimen at 10
volts caused substantial undercutting of the polyimide.

CONCLUSIONS

The accelerated tests have shown dramatic improvements in the
adhesion of polyimide coatings, even to noble metal substrates, when

Figure 4.   Photomicrograph of Annular Opening (0.6 mm Outer
            Diameter) in PI-2555 Coating on Primed Ti Specimen
            Showing Undercutting Effect of a 10-volt Anodization.

the substrate was first treated with an aluminum chelate primer.
Specimens survived for several weeks in boiling saline solution with
no significant loss in adhesion strength. By comparison, unprimed
specimens failed this test within a few hours. Similarly, applied
voltage tests induced adhesion loss in primed specimens only under
conditions which attacked the underlying metal. We conclude that
adhesion loss in the alumina-polyimide coating system is unlikely to
be the life-limiting factor.

ACKNOWLEDGMENT

LITERATURE CITED

1. Leyden, R.N.; Basiulis, D.I. "Adhesion and electrical insulation of thin polymeric coatings under saline exposure", in <u>Biomedical Materials and Devices</u>, Hanker, J.S.; Giamarra, B.L., eds., MRS Symposia Proceedings, Materials Research Society, 1987; Vol. 110.
2. Saiki, A.; Harada, S. "New coupling method for polyimide adhesion to LSI surface", J. Electrochem. Soc. 1982, <u>129</u>, 2278-2282.
3. Kendig, M. <u>et al</u>. "The application of impedance spectroscopy to the evaluation of corrosion protection by inhibitors and polymer coatings", <u>CORROSION 85</u>, 1985, NACE, Houston, Texas, Paper 74.
4. Comyn, J. in <u>Durability of Structural Adhesives</u>, Kinlock, A.J., ed., Applied Science Publishers, London and New York, 1983; p. 94-98.
5. Emmerich, W.D.; Kaiserberger, E. in <u>High Tech - the Way into the Nineties</u>, Brunsch, K.; Golden, H.D.; Herkert, C.M., eds., Elsevier Science Publishers B.V., Amsterdam, 1986; p. 289-297.

Chapter 15

Conduction Transients in Polyimides

Herbert J. Neuhaus and Stephen D. Senturia

Microsystems Technology Laboratories, Massachusetts Institute of Technology, Cambridge, MA 02139

Space charge effects in electrical measurements of polymeric insulators have received considerable attention (1-7). In polyimide (PI) the formation of space-charge at the electrode under bias has been cited as a factor contributing to a space-charge modified Schottky barrier at the metal-PI contact (8), and mobile ionic impurities have been shown to give rise to measurement-history effects (9). Control of insulator space-charge is critical to reproducibility of electrical response measurements. In this paper, reproducible, history-free PI conduction transients are reported. At temperatures above 200°C the transients observed in PI films with Al cathodes have a characteristic peak, the time of which is a function of temperature, voltage, and ionic impurity concentration. Transient currents of this form have not been previously reported in PI films. No peak is observed when Au cathodes are used. A simple model has been formulated which explicitly couples the space-charge due to ionic polarization and electronic conduction (10). Ion and electron transport are modeled as hopping mechanisms. Numerical techniques are employed to compute the current-time transient response to a constant applied bias which is compared to data from PI samples containing controlled ion content.

PI, like many other insulating polymers, exhibits a complex transient response to an applied DC bias. The shape of the current-time transient varies with temperature. Figure 1 shows the PI transient current at several temperatures in Al-PI-Al parallel plate capacitors fabricated on Si substrates. The experimental method has been reported previously (11). The BTDA - MPDA/ODA PI (DuPont Pyralin PI-2555) contains 1 ppm Na by weight in the cured film (12), and the film thickness is 3.3 microns. The measurements are made in in dry N_2, and the PI films are dried before measurement by heat-treatment at 150°C for 30 min. The bias (100V) is applied directly to the lower Al electrode, and the upper electrode and guard ring are held at ground potential. The current from the upper electrode is measured with a pico-ammeter. Any surface currents are shunted around the pico-ammeter via the guard ring.
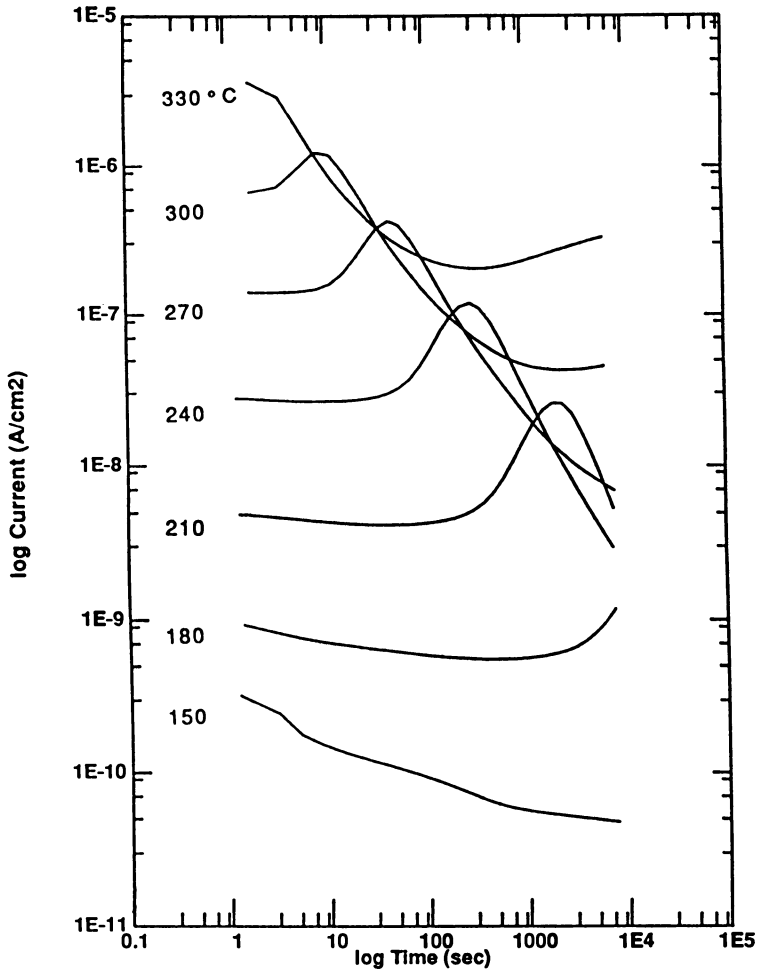
Figure 1. Transient currents in Al-PI-Al structure at various temperatures. The 3.3 micron film is a BTDA - MPDA/ODA PI, and is subjected to 100V. Al-PI-Al structure is used. Between each transient, the sample is discharged at 370°C for 10,000 sec. (Reproduced with permission from Ref. 10. Copyright 1989 M.I.T.)

History-effect problems are worsened at elevated temperatures. Wash-out of the transient structure occurs if the sample is not fully discharged between measurements. At a given temperature, discharge proceeds more slowly than charging. For this reason, the sample is heated to 370°C to discharge for 10,000 sec before each transient is recorded. This procedure results in stable and repeatable transient data.

At temperatures above 200°C the history-free transient has a characteristic peak, the time of which is a function of temperature, voltage, and ion concentration. No such PI transients have been previously reported. Near 200°C, the current is nearly constant for more than two hours before turning up to the peak.

The voltage dependence of the transient current in the as-received (1 ppm Na) material is shown in Figure 2 for voltages between 10 and 100V. Controlled introduction of Na has been used to prepare PI films containing 30 ppm Na. The method of Na-doping has been reported earlier (12). Figure 3 shows the voltage dependence of the transient current in the 30 ppm Na films. A direct comparison of the effect of Na is made in Figure 4 for the 10 and 100V data. The peak time is shorter for higher voltages and longer for higher Na levels. The current increases with voltage and Na concentration.

The charge under the current-time curves has been calculated by numerical integration and compared to the amount of charge due to Na ions. In Figure 4 the time at which the charge transported equals the Na charge is indicated by the arrows. At long times the total charge transported is much greater than the Na charge.

The transients in Al-PI-Au samples (Au upper electrode) are compared to Al-PI-Al data in Figure 5. The transient current in Al-PI-Al samples is polarity independent. In Al-PI-Au sample the transient peak is observed only for Al-cathode polarity, but the peak current is smaller than in the Al-PI-Al case. For the Au-cathode polarity no peak is observed within 10,000 sec, however, the current is not monotonically decreasing.

Model

The data show that true steady state conduction is established only on a time scale of days or longer, even at elevated temperatures. Therefore, examination of steady currents is a formidable task. A quantitative model of the transient response in PI would permit useful data collection on a shorter time scale.

The salient features of a model for the metal-PI-metal system are reviewed here. An exhaustive treatment has been given elsewhere (10). Electrical conduction is modeled as a two carrier system: positive mobile ions which are blocked at the electrodes, and electrons which may be injected or ejected at Al-PI contacts. The Al-PI contacts are represented as ideal ohmic contacts. This means (1) none of the applied voltage is dropped at the contact, and (2) an accumulation of injected electrons forms in the PI near the contacts. Such a contact corresponds to the insulator work-function being greater than that of the contacting metal. Since the work-function of Al (4.3 eV) is smaller than that of Au (5.1 eV), one expects the Al-PI contact to be a better electron injector than the Au-PI contact.

The behavior of such a system is easy to predict in the absence of mobile ions. Ohmic contacts and a high resistivity bulk give rise to a bulk-controlled or space-charge limited currents (13). A complete analysis of the space-charge limited transient current in insulating crystals has been given (14). The analysis in polymers is modified by the presence of mobile ionic impurities in two ways. First, in thermal equilibrium the bulk ion and electron concentrations must be
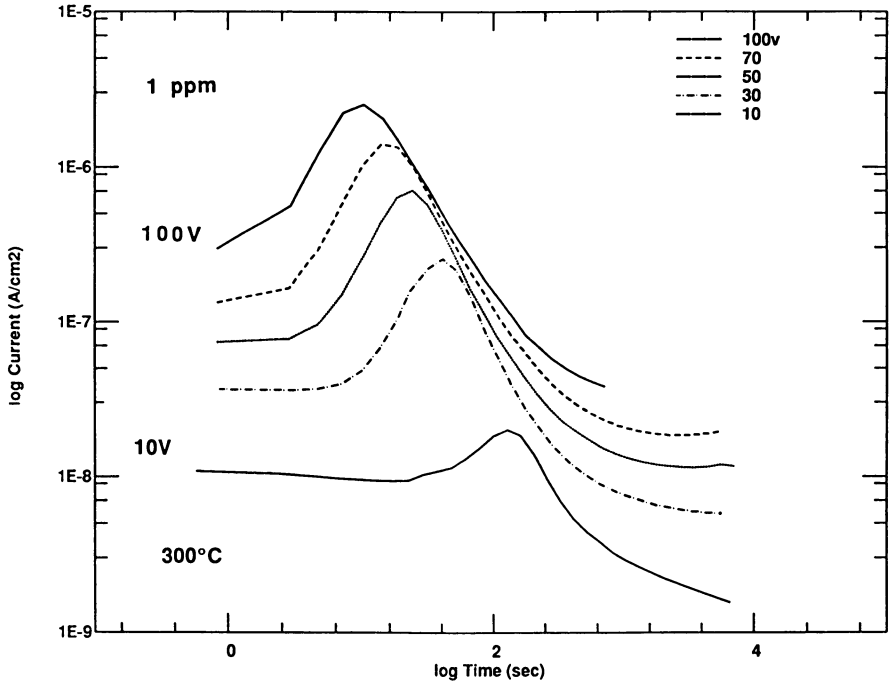
Figure 2. Variation of transient with voltage in as-received (1 ppm Na) films with Al electrodes. Temperature is 300°C. (Reproduced with permission from Ref. 10. Copyright 1989 M.I.T.)
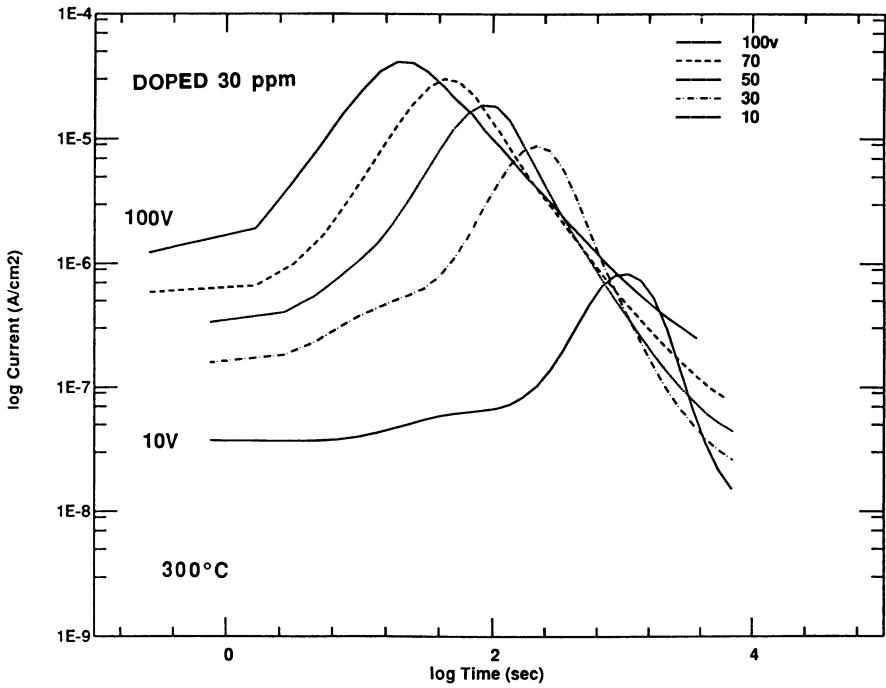
Figure 3. Variation of transient with voltage in films doped with 30 ppm Na and Al electrodes. Temperature is 300°C. (Reproduced with permission from Ref. 10. Copyright 1989 M.I.T.)
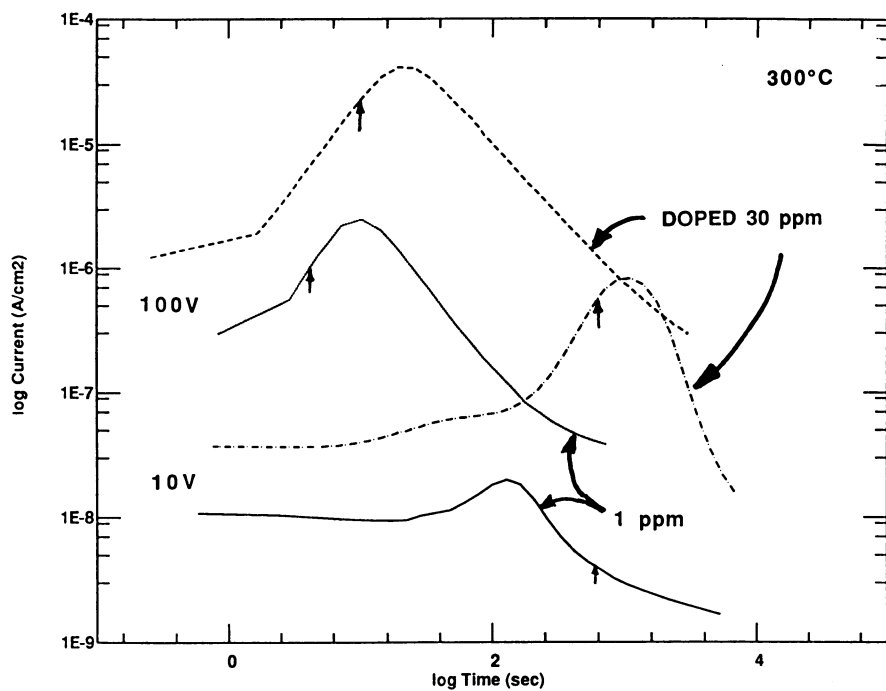
Figure 4. Comparison of voltage dependence in 1 ppm and 30 ppm films. Temperature is 300°C. The time at which the charge transported equals the Na charge is indicated by the arrows. (Reproduced with permission from Ref. 10. Copyright 1989 M.I.T.)
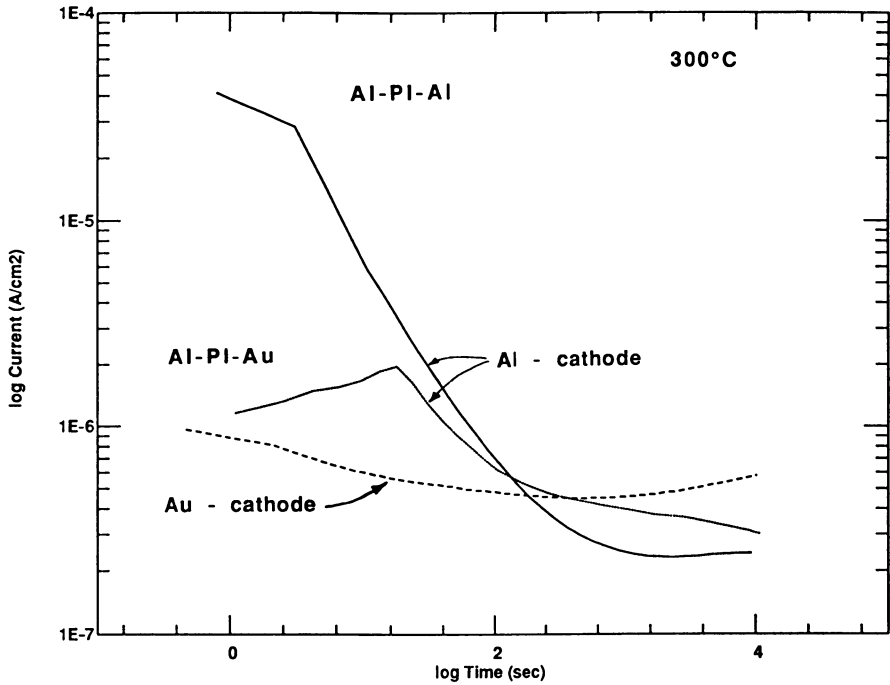
Figure 5. Comparison of transient currents in Al-PI-Al and Al-PI-Au samples. Current is polarity independent in Al-PI-Al samples. Two polarities are shown for Al-PI-Au samples. Au is upper (air side) electrode. Voltage is 100V and temperature is 300°C. (Reproduced with permission from Ref. 10. Copyright 1989 M.I.T.)

equal to ensure bulk neutrality. Second, the mobile ions drift under bias toward the cathode and modify the space-charge field in the PI. The result is a two-carrier, single-injection, ion-modified space-charge limited transient.

In the usual space-charge limited theory, electrons are injected into the insulator conduction band, and some of these electrons are immobilized in localized defect states. We have considered an alternate mechanism more appropriate to the polymer structure. Contact charge transfer studies in Polyethylene Terephthalate (PET) and other polymers (15-16) suggest that the electronic states accessible from metal contacts are localized molecular-ion states located deep in the forbidden energy gap. Charge transport is by hopping between localized states.

Carrier transport in the PI is calculated using a hopping formalism due to Iwamoto (17-18). The hopping formalism reduces to ordinary drift and diffusion in the limit of hopping length goes to zero. Electrons and ions move through two distinct sets of sites or wells, each with a characteristic potential height and hopping length. The potential barrier between wells is modified by the electric field near the wells.

We have considered only one species of ion and have assumed the total number of ions is fixed. The extensions to more general cases, such as more than one species or a temperature dependent ion concentration, are obvious. We have neglected the thermal or electron-hole pair contribution to conductivity.

The electric field in the film is calculated from the Poisson equation along with the constraint placed on the integral of the field by the fixed applied voltage. For each of a series of time steps, the carrier fluxes are calculated from the electric field and carrier concentrations. The time evolution of the system is calculated using fourth order Runge-Kutta integration of the carrier flux equations. Finite differences are used for spatial functions. The external current is given by the sum of injection and displacement currents.

Comparison of Calculated and Experimental Transients

The calculated current-time transient for Al-PI-Al are shown in Figure 6. The solid curve shows the behavior of the system if the ionic impurities are present but immobile. This corresponds to the space-charge limited transient in an insulating crystal with slow trapping (14). The behavior at short time is related to electron diffusion near the contacts, while the long time behavior is related to the propagation of the electronic space charge front across the film. Figure 7 shows the time-evolution of the total space-charge distribution. Initially, the insulator is neutral except near the contacts. As electrons are injected the net space-charge becomes increasingly negative. The steady-state distribution has the characteristic $x^{-1/2}$ dependence.

The dashed curve in Figure 6 includes the effect of mobile ions. The initial current is greater due to the ionic contribution, but the steady current is not affected. A comparison of Figs. 7 and 8 shows the differences in space charge distribution due to mobile ions migrating to the cathode.

With the simplified model described above, we may expect to reproduce only the gross features of the transient. Numerical agreement will require a more realistic model. As an example, Figure 9 compares the voltage dependence of both experimental and calculated transient currents. The shape of the model and experimental curves differ, but the variation with applied bias in both sets is similar.
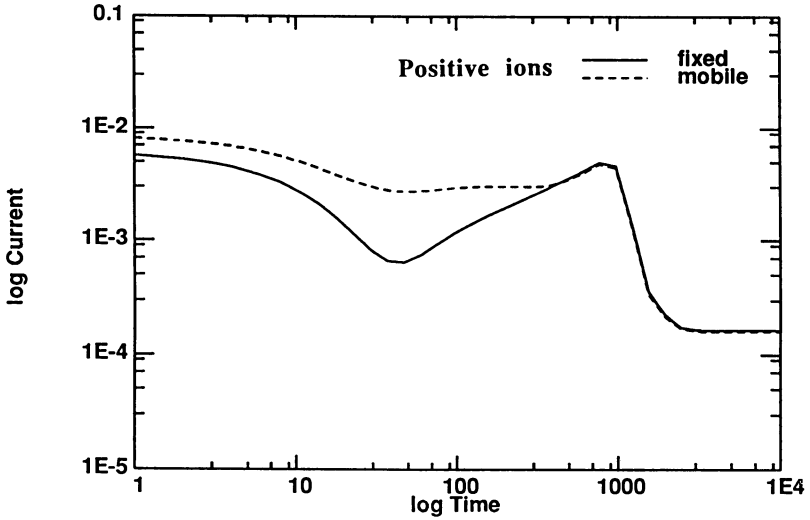
Figure 6. Calculated transient current. The conditions are: 100V, 1.0 micron thick, 1ppm Na by weight, 300°C, 50 electronic and 20 ionic wells.
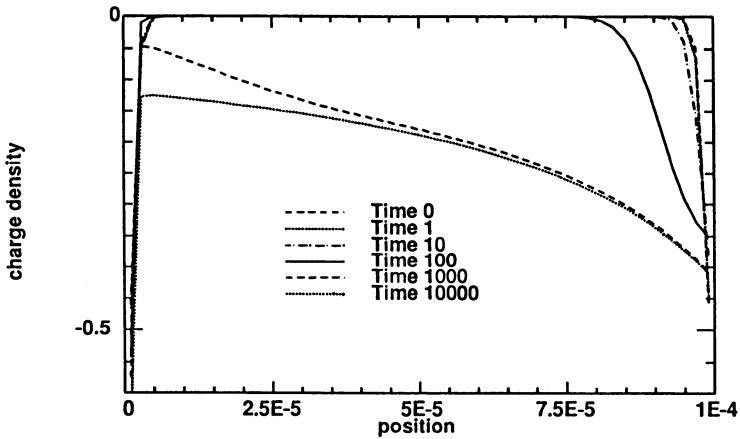
Figure 7. Calculated space-charge distributions at various times with fixed ions. Normalized times correspond to the time axis of Figure 1. (Reproduced with permission from Ref. 10. Copyright 1989 M.I.T.)
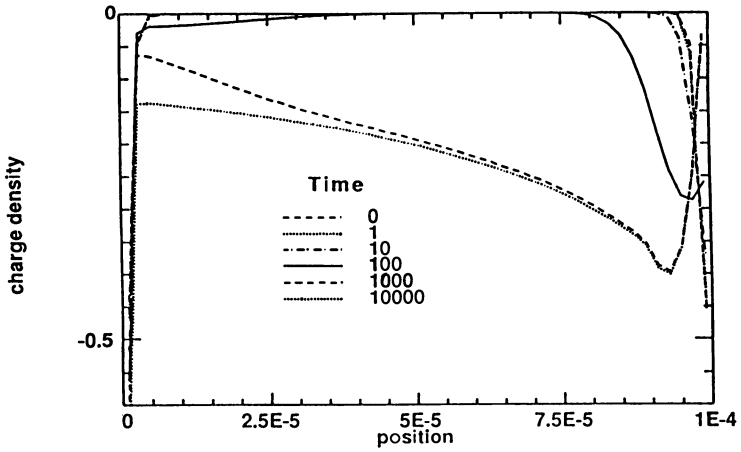
Figure 8. Calculated space-charge distributions at various times with mobile ions. (Reproduced with permission from Ref. 10. Copyright 1989 M.I.T.)
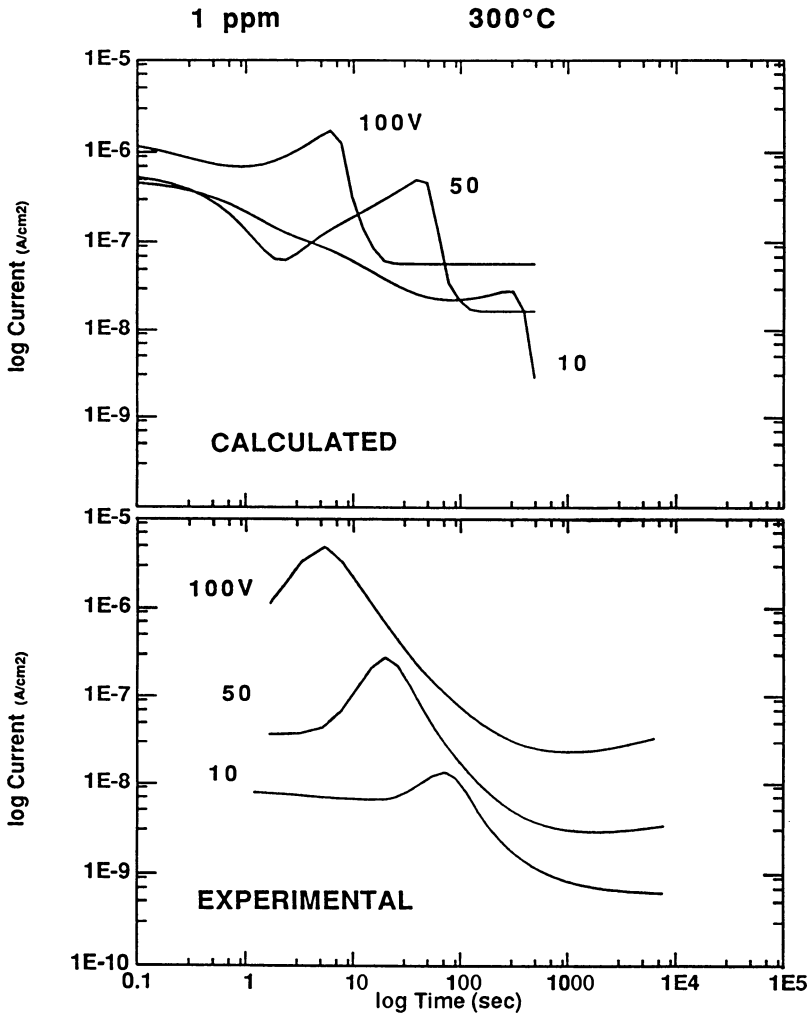
Figure 9. Comparison of transients at various voltages. The conditions are: 3.3 micron thick, 1ppm Na by weight, 300°C, 50 electronic and 20 ionic wells. Each transient starts with uniform ion and electron distributions, except near the contacts.

Discussion

PI Degradation. Because the transient measurements reported above are made at elevated temperatures, possible degradation of the PI must be considered. However, since the transient data are repeatable, we infer that the PI has not been significantly degraded during the bias-temperature exposure.

Electrode Metal. The fabrication sequence used for Al-PI-Al samples results in different histories for the upper and lower Al electrodes (11). In particular, the lower electrode is exposed to the PI cure cycle while the upper electrode is evaporated directly on to cured PI. However, the polarity independence of the transient current in the Al-PI-Al samples indicates that the two Al electrodes are electrically equivalent.

The Au-PI-Al samples are no longer symmetric. The observed behavior is consistent with electron injection at the Al-PI contact but not at the Au-PI contact. The increase in work function in Au over Al implies a less effective electron injector. When the Al is biased negatively, a peaked space-charge limited transient is observed, and when the Au is biased negatively, the transient has no peak.

Model. The comparison of theory and experiment in Figure 9 indicates that the simplified model can be used to calculate transients which agree with experiment in gross trends. The model permits quantitative analysis of bulk and contact space-charge effects in PI transient current measurements. In particular, this model is sufficient to calculate measurement-history effects due to mobile ions and bulk electronic space-charge (9). The relaxation of space-charge upon removal of the bias is intrinsically slower than its accumulation. Thus, the sample history is stored in the space-charge distributions. These results will be demonstrated in a future publication.

To improve the agreement between model and experiment, several enhancements to the model are possible. This model can be extended to include less idealized injecting Al-PI contacts, and Au-PI contacts can be simulated as blocking contacts. Also, a more detailed picture of the distribution of electronic states can be employed.

Implications. These results have an important implication concerning the use of Fourier analysis of DC transients in polymeric materials to extract the frequency-dependence of the dielectric response (19). In order for the principle of superposition to apply the electric field inside the material being measured must be time- and space-invariant. This critical condition may not be met in polymers which contain mobile ionic impurities or injected electrons. Experimentally, we can fix only the average of the electric field. Moreover, our calculations demonstrate that the bulk field is not constant in either time or space. Thus, the technique of extracting the dielectric response from the Fourier components of the transient response is fundamentally flawed because the contribution due to the formation of ionic and electronic space-charge to the apparent frequency-dependent dielectric response can not generally be separated from the dipole contribution.

Similarly, the application of isochronal analysis to transient data (20) assumes that the time dependence of the transient response is independent of the parameter being varied. For example, plotting current at a particular time against temperature yields useful data only if the transient proceeds at a rate independent of temperature. However, the example of Figure 1 and transients calculated from the model have features which would appear as peaks in an isochronal plot, yet are intrinsic to the conduction mechanism.

Conclusions

History-free, reproducible, transient currents are reported in as-received and Na doped PI films between 150 and 330°C. From a calculation of the total charge transported, purely ionic mechanisms can be ruled out, and an electronic conduction mechanism must be invoked. The electronic conduction is, however, modulated by the presence mobile ionic impurities. The current and total charge transported vary in proportion to the amount of Na ions in the film. Thus an ion/electron interaction in PI is postulated.

When the cathode is Al a peak is observed in the transient, but not when the cathode is Au. This observation is consistent with a space-charge limited transient due to electron injection from the smaller work-function Al electrode.

Ionic polarization and electron injection under bias result in a time-dependent, non-uniform electric field within the films. If complete discharge of the space-charge is not permitted between measurements, apparently non-reproducible transient behavior results from the space-charge field. Reproducibility is restored by high temperature discharge before each measurement.

A simple quantitative model for the metal-PI-metal system has been presented. The model was used to calculate space-charge modified conduction transients in PI. The calculated transients model the gross trends observed in experimental data. The effect of mobile ions is to change the shape of the current transient, but the steady current is not strongly dependent on ionic concentration. It has been shown that a detailed analysis of the formation of space-charge during electrical measurements is critical to the understanding of transient phenomena in insulating polymers.

Acknowledgments

Literature Cited

1. Lengyel, G. <u>J. App. Phys.</u> 1966, <u>37</u>, 807.
2. Lilly, A.; McDowell, J. <u>J. App. Phys.</u> 1968, <u>39</u>, 141.
3. Wintle, H. <u>J. App. Phys.</u> 1971, <u>42</u>, 4724.
4. Miyairi, K; Ieda, M. <u>Elec. Eng. Japan</u> 1976, <u>96</u>, 14.
5. Ko, A.; Hirsch, J. <u>Solid State Commun</u>. 1981, <u>39</u>, 215.
6. Lewis, T.J. <u>IEEE Trans. Elec. Insul.</u> 1984, <u>EI-19</u>, 210.
7. Ieda, M. <u>Int. Conf. Props. and App. Diel. Mat.</u>, 1986, p. 17.
8. Sessler, G.; Hahn, B.; Yoon, D. <u>J. App. Phys.</u> 1986, <u>60</u>, 318.
9. Neuhaus, H.; Feit, Z.; Smith, F.; Senturia, S. In
   <u>Recent Advances in Polyimide Science and Technology</u>; Weber,
   W.; Gupta, M., Eds.; Soc. of Plastic Eng.: Poughkeepsie, NY, 1987;
   p 362.
10. Neuhaus, H. Ph.D. Thesis, Mass. Inst. Tech., Cambridge, Mass, 1989.
11. Smith, F.; Neuhaus, H.; Senturia, S.; Feit, Z.; Day, D.; Lewis, T.J.
    <u>J. Elec. Mat.</u> 1987, <u>16</u>, 93.
12. Neuhaus, H.; Day, D.; Senturia, S. <u>J. Elec. Mat.</u> 1985, <u>14</u>, 379.

13. Lampert and Mark, <u>Current Injection in Solids</u>, Academic Press, New York (1970).
14. Many, A.; Rakavy, G. <u>Phys. Review</u> 1962, <u>126</u>, 1980.
15. Fabish, T.; Duke, C. <u>An. Rep.: Conf. Elec. Ins. Diel. Phenom</u>, 1977, p. 175.
16. Duke, C. <u>Mat. Sci</u>. 1984, <u>Vol. X</u>, 341.
17. Iwamoto, M.; Hino, T. <u>Elec. Eng. Japan</u> 1980, <u>100</u>, No. 2, 9. Translated from <u>Denki Gakkai Ronbushi</u> 1980, <u>100A</u>, 213.
18. Iwamoto, M.; Hino, T. <u>Elec. Eng. Japan</u> 1980, <u>100</u>, No. 3, 9. Translated from <u>Denki Gakkai Ronbushi</u> 1980, <u>100A</u>, 299.
19. Mopsik, F. <u>IEEE Trans. on Elec. Ins</u>. 1985, <u>EI-20</u>, 957.
20. Das-Gupta, D.; Brockley, R. <u>An. Rep.: Conf. Elec. Ins. Diel. Phenom</u>. 1977, p. 197.

Chapter 16

Polymer Insulating Layers for Multilayer Hybrid Circuits

L. M. Baker[1], J. L. Markham, and R. D. Small[2]

AT&T Bell Laboratories, Engineering Research Center, Princeton, NJ 08540

A new technology for the fabrication of hybrid circuits was developed which greatly enhances the circuit density. Multiple levels of circuitry are built up by alternating layers of an insulating polymer with the metallization. The polymer is a negative tone, photosensitive formulation developed within AT&T. Its final cure temperature is low enough to prevent degradation of devices, such as resistors, capacitors, and conductors, previously prepared on the substrate. The cured polymer is resistant to commonly used cleaning chemicals and to soldering conditions. It has good self-adhesion, as well as adhesion to ceramic and metal. The polymer performs satisfactorily in accelerated environmental tests. The polymer and its properties will be discussed in this paper.

Hybrid integrated circuits (HIC's) have been used widely for a number of years in switching and transmission equipment and in consumer products. A HIC consists of a ceramic substrate on which thin film resistors, capacitors, and conductors have been formed. Discrete active and passive devices are then bonded to the circuit by one of several techniques, such as soldering, thermal compression bonding, or die and wire bonding. This combination of circuitry types gave rise to the use of the term "hybrid." Circuitry can be placed on one or both sides of the substrate. In addition, the density of the circuitry can be increased by using a fired glaze dielectric to cross one conductor path over another. However, it is difficult to control the impedance of the line accurately or to achieve very high interconnection densities with cross-overs and cross-unders due to difficulties with line width control. In this respect, an organic dielectric has some advantages over an inorganic glaze. (1) An organic dielectric applied in a uniform thin film and appropriately patterned allows increased routing capability, flexibility, and density and, consequently, a reduction in circuit size. Distributed power and ground planes can be used, and the lower dielectric constant of the polymer results in reduced capacitance and conductance between lines.

There are several characteristics that would be desirable or essential in a polymeric dielectric for hybrid applications. A major consideration is compatibility with standard hybrid processing. This processing usually includes exposure of the substrates to various chemicals and to elevated temperature. Common processing chemicals to which the polymer should be resistant include trichloroethane, concentrated HCl, methylene chloride, methanol, and dilute hydrofluoric and sulphuric acids. The polymer must be thermally stable to soldering conditions, and, it is helpful if the T_g of the polymer is high enough to maintain dimensional stability. This is particularly important for reliability considerations, such as thermal cycling. On the other hand, the cure temperature of the polymer must not be so high as to damage any components present in previous

[1]Current address: AT&T Bell Laboratories, 1600 Osgood Street, North Andover, MA 01845
[2]Current address: Shipley Company, Inc., 2300 Washington Street, Newton, MA 02162

layers of metallization. A major improvement in processing would be achieved if a suitable dielectric were photodefinable, and, in order to build multiple layers of circuitry, the polymer must be metallizable.

Material Formulation

A survey of materials available at the time this development was undertaken revealed none that had the necessary thermal and mechanical properties and photosensitivity. The combination of chemical resistance and thermal stability with ease of processing suggested that a thermosetting polymer would be the likeliest candidate. Previous experience with triazine resins had demonstrated their superior electrical properties, chemical resistance, adhesion to a variety of substrates, and thermal stability. The T_g of unmodified triazine is generally around 250°C, depending on cure, and thermal decomposition starts above 450°C. These resins cure through reaction of pendant cyanate ester groups to form s-triazine rings (Figure 1). (2–4) Triazine can be processed much like bisphenol A epoxies, but has a higher crosslink density when thermally or catalytically cured. Because of the high crosslink density, cured triazine is quite brittle. It is not photosensitive. For this application, the triazine resin is modified with an acrylated acrylonitrile-butadiene rubber to improve resistance to cracking and thermal shock and to impart photosensitivity. Workers at Interez, Inc. used thermoplastic resins to modify triazines for improved fracture toughness in structural composite matrix applications. For their purposes, the butadiene-acrylonitrile rubbers were not satisfactory. (5) Here, however, fracture toughness and loss modulus are not as important as maintaining electrical performance and adding photosensitivity. Structural demands on the polymer are slight. The rubber does not react with the triazine resin, so an acrylated epoxy resin is added as a link between the rubber and the triazine. It is known that the cyanate ester reacts with epoxies to form oxazoline rings, and that the reaction is quite efficient (Figure 2). (6) Several other minor constituents are added to optimize properties. In addition to the photoinitiator (2,2-dimethoxy-2-phenylacetophenone), these include pigment, hardener (N-vinyl pyrrolidone), a photo-crosslinking agent (trimethylolpropane triacrylate), surfactant, and an adhesion promoter (glycidoxypropyl trimethoxysilane). The entire formulation is blended in a good solvent for all components. A generalized formulation is listed in Table I. (7) The structures of the components are shown in the Figure 3.

Table I. Polymer Formulation	
Ingredient	**Level**
Triazine Resin	40-65%
Rubber	0-30%
Acrylated Epoxy Resin	0-50%
N-vinyl pyrrolidone	0-12%
Trimethylolpropane triacrylate	0-8%
Glycidoxypropyl trimethoxysilane	0-5%
2,2-Dimethoxy-2-phenylacetophenone	0.5-3%
Pigment	0-1%
Surfactant	0-1%

The rubber and the triazine resin are immiscible, and are kept homogeneous prior to application through dissolution in a mutual solvent. As the solvent evaporates, the triazine and rubber separate into distinct domains, in a manner analogous to rubber modified epoxy resins. (8, 9) This domain structure is substantially frozen during photo-cure when the components containing acrylate and vinyl functionality undergo free radical polymerization. During subsequent thermal cure, the cyanate ester and epoxy groups polymerize to give a hard film. The cured polymer is resistant to organic solvents, but it is attacked by strong base and loses adhesion to the substrate on exposure to hot hydrogen peroxide.
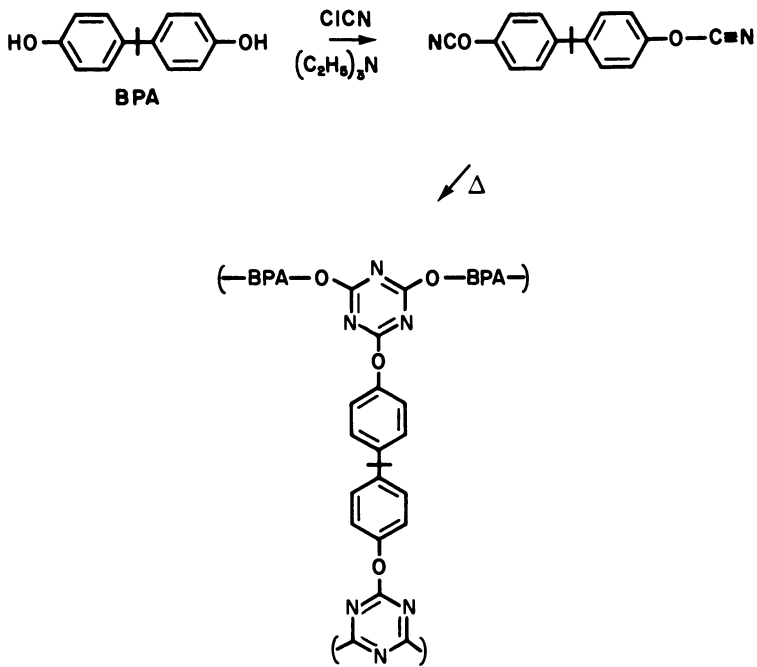
Figure 1. Polymerization of cyanate ester groups to form s-triazine rings.
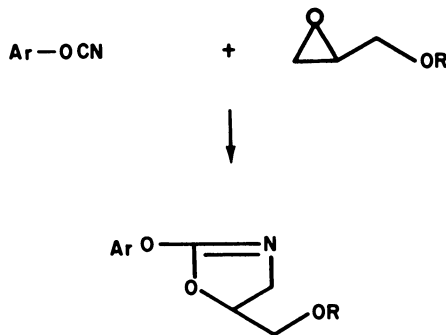
Figure 2. Reaction of cyanate ester with an epoxy to form an oxazoline ring.

$$\left(CH_2 = CHCO_2 CH_2\right)_3 C C_2 H_5$$

TMPTA

NVP

$$-CH_2 O CH_2 CH_2 CH_2 SI \left(O CH_3\right)_3$$

GPTMS

$$\left(OCH_3\right)_2$$
$$\phi C C \phi$$
$$\overset{\parallel}{O}$$
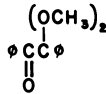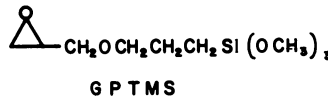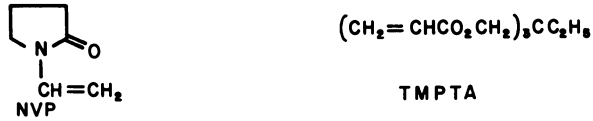
2,2 – Dimethoxy – 2 – phenylacetophenone
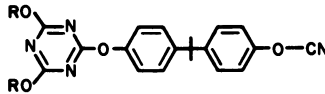
Triazine Prepolymer
Molecular Weight = 2000

$$O-BPA-OCH_2 \overset{OH}{CH} CH_2 O-\overset{\parallel}{C}-\left[(CH_2 CH=CHCH_2)_x-(CH_2 CH)_y\right]_z -\overset{\parallel}{C} OCH_2 \overset{OH}{CH} CH_2 OBPAOCH_2 \overset{OH}{CH} CH_2 O \overset{\parallel}{C} CH=CH_2$$

CH₂
CHOH
CH₂
O
C=O
CH=CH₂

Rubber

Acrylated Epoxy Resin
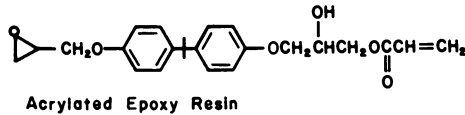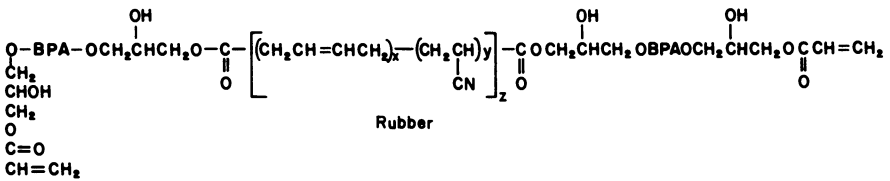
Figure 3. Chemical components used in the polymer formulation.

CERAMIC SUBSTRATE

CONDUCTORS AND RESISTORS

SPRAY PHOTOSENSITIVE
DIELECTRIC; BAKE

EXPOSE PATTERN
IN DIELECTRIC

DEVELOP PATTERN
IN DIELECTRIC; BAKE

THERMALLY CURE POLYMER

GASEOUS CLEAN;
SPUTTER CONDUCTORS

GENERATE CONDUCTOR
PATTERN
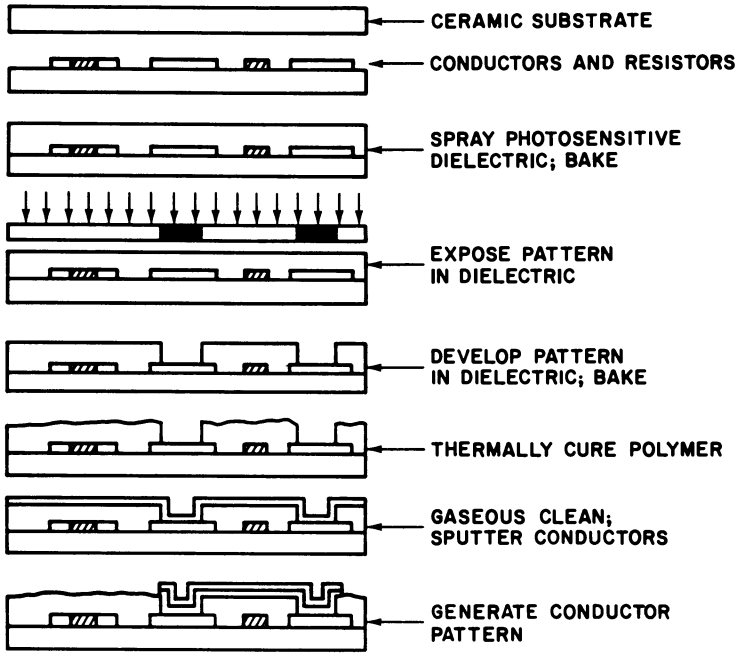
Figure 4. Schematic cross-section of POLYHIC fabrication process.

Due to the incorporation of the rubber, the thermal properties of the cured polymer are somewhat lower than those of the triazine alone. The thermal properties, along with the electrical properties, are given in Table II.

Table II. Properties of Cured Polymer	
Property	**Value**
T_g	150°C
Thermal Stability long term short term spikes	 180°C 210°C 300°C
Thermal Conductivity 90°C 125°C	 0.196 W/mK 0.209 W/mK
Dielectric Constant (ASTM D150)	3.61
Dielectric Strength (ASTM D149)	353 KV/cm at 25°C ambient humidity
Volume Resistivity (ASTM D257)	$>3.7 \times 10^{12}$ ohm-cm
Surface Resistivity (ASTM D257)	$> 4.25 \times 10^{12}$ ohm-cm

Results of accelerated testing of circuits prepared with this polymer as the dielectric layer are satisfactory. Circuits comprising two metallization and one polymer layer withstand a minimum of 500 cycles from -40 to +130°C with no loss of adhesion, cracking of the polymer, or open circuits. No mechanical or electrical failures occur during 1000 hours at 150°C in air, and the insulation resistance remains above 200 megohm during 500 hours at 85°C/85% RH/60 V (THB). Tantalum nitride resistors under the polymer change < 0.5% under these THB conditions.

Application

The polymer formulation is applied to the ceramic substrate, and the solvent is removed by a gentle bake to give a uniform film 2 mils thick. The polymer is patterned by exposure through a mask in a standard uv tool (off contact), and the unexposed regions are removed by solvent development. Polymer residues are cleared away in a plasma process. The polymer is then thermally cured at approximately 200°C. The polymer is treated with another plasma process to enhance the adhesion of the next level of metallization, which is applied by sputter deposition. The conductor layer is patterned using standard techniques and plated to the necessary thickness. (10) This process is represented schematically in Figure 4. Alternating layers of polymer and metal can be applied by repeating this process.

Typical circuits constructed with this procedure have 6 mil vias and 6 mil lines and spaces.

Conclusions

A novel, photodefinable, polymeric material was formulated to meet the needs of a particular circuit technology. Rubber modification of a thermoset resin with good thermal, chemical, and electrical properties generated a formulation that met stringent processing and reliability requirements.

Literature Cited

1. Shiflett, C. C.; et. al., Proc. International Symposium on Microelectronics, 1986.
2. Grigat, E.; Putter, R., Angew. Chem. 1967, 79, 219.

3. Ayano, S., Chem. Economy and Engineering Review 1978, 10, 1.
4. Graver, R.B., ACS Polymer Preprints 1986, 27, 491.
5. Shimp, D.A.; Hudock, F.A.; Bobo, W.S., Proc. InternationalSAMPE Technical Conference, 1986.
6. Shimp, D.A.; Hudock, F.A.; Ising, S.J., Proc. InternationalSAMPE Symposium, 1988.
7. Small, R.D., U. S. Patent 4,554,229.
8. Sultan, J.N.; Laible, R.C.; McGarry, F.J., Proc. Applied Polymer Symposium, 1971, 127.
9. Brown, P.J.; Markham, J.L., Proc. SPE ANTEC, 1988, 900.
10. DeForest, W.S., Photoresist Materials and Processes; McGraw-Hill: New York, 1975.

Chapter 17

Fabrication and Properties of Thermoset Films Derived from Bis-Benzocyclobutene for Multilayer Applications

S. F. Hahn, P. H. Townsend, D. C. Burdeaux, and J. A. Gilpin

Dow Chemical Company, M. E. Pruitt Research Center, Midland, MI 48674

The increase of the density of electronic circuits has been an area of active development over the past several decades. The primary reason for this interest is that the cost of an electronic component is roughly proportional to the total length of wire in the circuit[1]. The dielectric properties of materials used as insulators in multilayer interconnection structures determine the wiring density and total wire length in the finished part.

The use of tailored polymeric materials offers the potential for a significant reduction in the dielectric constant of the insulating layer. Polymers within the polyimide family have received significant attention for this application in the recent literature [2]. This paper reports on the use of new thermosetting polymers derived from bis-benzocyclobutene(bis-BCB) monomers[3,4] for use in multilayer electronic structures [5]. Figure 1 shows two monomers which show particular promise for electronic applications.These are ethylene-linked bisbenzocyclo-butene (BCB-1) and a di(vinylbenzocyclobutene) linked with a proprietary R group (BCB-2).

Chemistry of B-Staging and Film Deposition

Chemistry of Polymerization. Polymerization of bisbenzocyclobutene functional monomers is a thermal process which does not require catalysis and does not generate any volatile by-products. The polymerization is initiated by rearrangement of the hydrocarbon to give the highly reactive intermediate o-quinodimethane shown in Figure 2. This intermediate can undergo oligomerization with other o-quinodimethanes, or can be

reacted with a variety of unsaturated functional groups. The aromaticity of the benzene ring is restored after reaction of the intermediate o-quinodimethane. This produces a thermally stable polymer structure. Also, the polymer can be fully polymerized at 250°C in a relatively short time period (1 hour or less).

To cast the material as a thin film on a substrate, it is necessary to prepolymerize the monomer to an intermediate degree of conversion of the functional groups. The prepolymer can be handled either as a melt or in solution, and can be fully cured to the final thermoset after being cast as a film. Prepolymerization, or B-staging, is performed by heating the neat monomers to a temperature between 180°C and 195°C for 2 to 8 hours, depending upon the temperature. The extent of reaction can be determined from the reduction of the residual heat of reaction measured by differential scanning calorimetry (DSC)(6). Figure 3 shows a representative plot of the heat evolved during polymerization of BCB-1 while the temperature is increased to 350°C at 10°C/minute.

Since these monomers are multifunctional, the polymerization exhibits gel phenomena prior to complete conversion of the reactive functional groups. BCB-2 with 4 sites for polymerization, gels when 50% (as measured by DSC) of the polymerization exotherm has been depleted, while BCB-1 gels with the conversion of approximately 70% of the exotherm. The fully cured polymers are both crosslinked thermosets.

Prepolymer Solutions for Film Formation. The fabrication of microelectronic devices requires that relatively thin defect free films, generally 1 mm to 50 mm thick, be deposited on a supporting inorganic substrate. Optimal coatings derived from BCB-2 are prepared from prepolymers which are just below the (critical) gel point. These prepolymers are completely miscible with a variety of organic solvents such as xylene. The dissolved prepolymer can be cast onto a substrate by common spin and spray coating techniques. The viscosity of these solutions is critical to controlling coating thickness by either deposition technique.

Figure 4 shows the relationship between prepolymer content and viscosity for a xylene solution of BCB-2 prepolymer slightly below the gel point. Predictable coating thicknesses useful for multilayer structures were obtained from solutions with viscosities in the range of 10 cP to 150 cP.
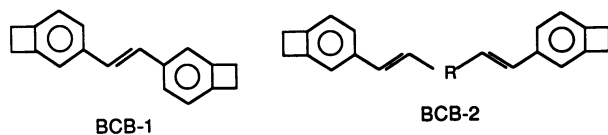
Figure 1. Bisbenzocyclobutene monomers used for the polymerization of thermoset films described in this work.
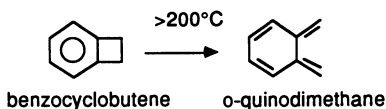
Figure 2. Thermal rearrangement of benzocyclobutene.
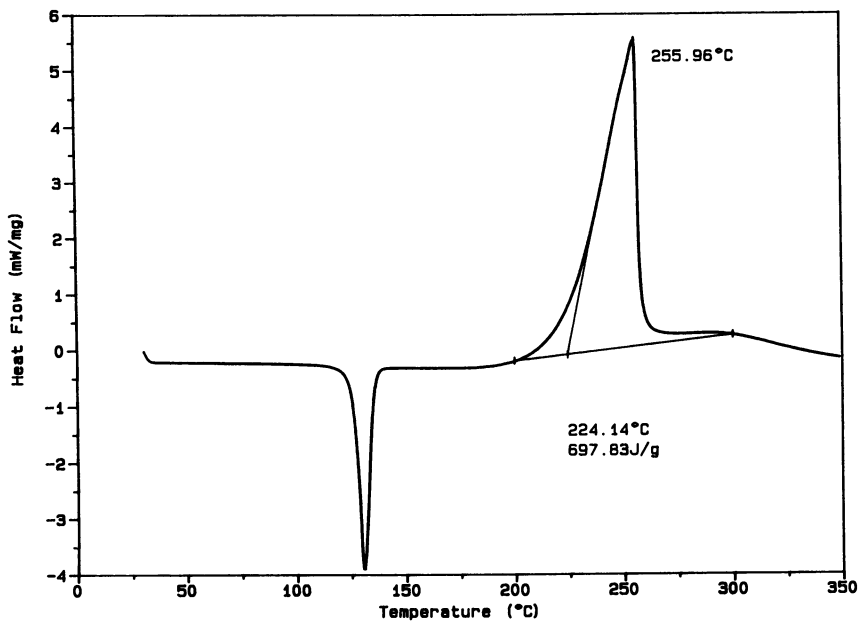
Figure 3. Heat evolved during polymerization of BCB-1 as a function of temperature.

Thermal Stability at Elevated Temperatures

Stability of the polymer at temperatures up to 400°C, as during the annealing of aluminum, is important for the use of the material in the fabrication of integrated circuits. Figure 5 shows thermogravimetricanalysis (TGA) of polymer prepared from monomer BCB-2 during heating at 10°C/minute in air and N_2. No weightloss occurs below 400°C in either environment. Isothermal weight loss is a more representative test of the ability of the polymer to withstand processing at a given temperature. Figure 6 shows the isothermal weight loss of the polymer derived from the BCB-1 monomer at 350°C. This polymer loses 0.7% of its weight after 1000 minutes at this temperature. Figure 7 shows the isothermal weight loss of the polymer derived from the BCB-2 monomer at 300°C and 350°C. Polymer prepared from BCB-2 loses ~0.5% of its weight at 300°C over 1000 minutes, and 4.5% at 350°C over that same time period in a nitrogen atmosphere. Figure 8 shows the isothermal weight loss of polymer prepared from BCB-2 when heated in an air atmosphere; at 350°C, the polymer loses about 1% by weight in 1000 minutes.

Electrical Properties of Freely Standing Films

Experimental. Films of B-staged BCB were coated on salt substrates by spray deposition and cured in air at 250°C for one hour. This cure period was determined from the minimum time necessary for the elimination of the reaction exotherm as measured by DSC. After the cure cycle the films were removed by dissolving the substrate in a water bath. The freely standing films so obtained were between 25 mm and 50 mm thick.

Samples for dielectric spectroscopy were prepared by sputtering 100 nm of Au in an Ar plasma onto both sides of the freely standing films. Disks 9.5 mm in diameter were punched out of the metallized films. These disks were used to measure both the dielectric permittivity with an HP 4192 Impedance Analyzer and the dissipation factor with a GenRad 1615-A Capacitance Bridge.

Samples used for dielectric breakdown measurements were not metallized. These films were placed between a copper plate and a 6.4 mm steel ball as electrodes.The voltage source was a Bertan Model 205A-10R Power supply driven by a ramp generator at 200 V/s.

Dielectric Permittivity Measurements. The dielectric permittivity of a material is a complex quantity, the real part of which is the dielectric
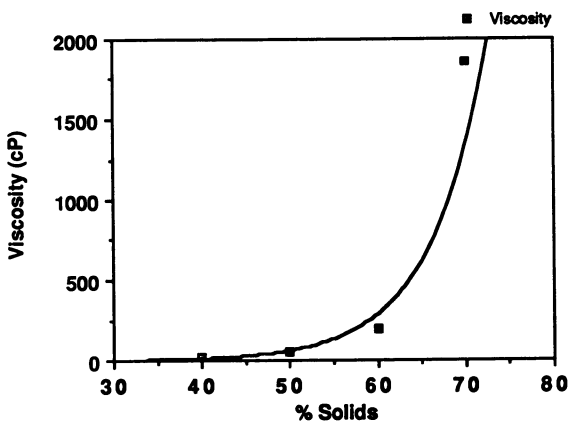
Figure 4.   Variation of solution viscosity as a
function of BCB-2 prepolymer in xylene.
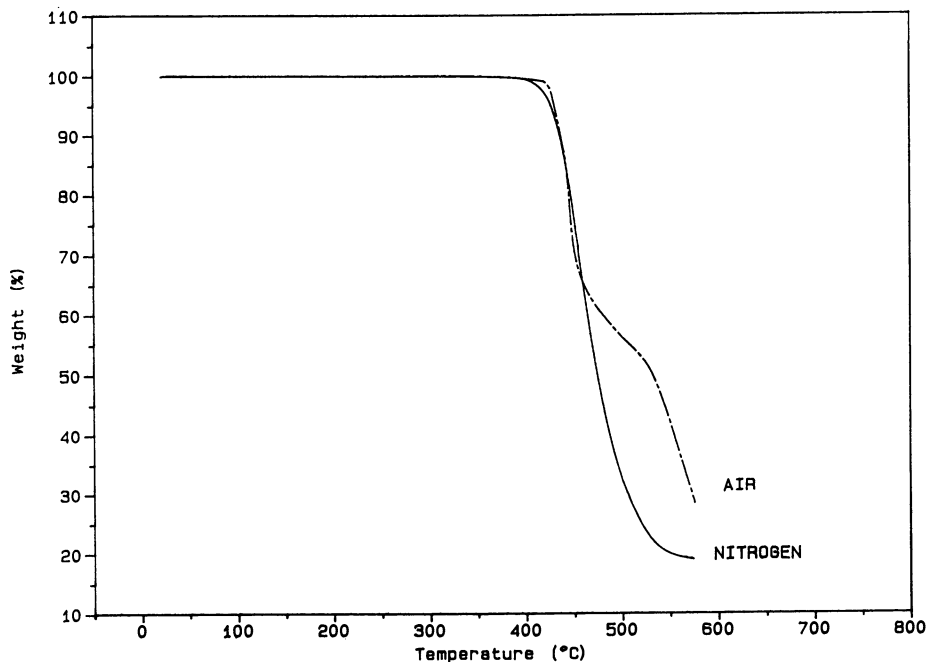
Figure 5.   Variation of weight change of fully cured
thermoset derived from BCB-2 monomer with temperature
measured by dynamic TGA in air and N$_2$.
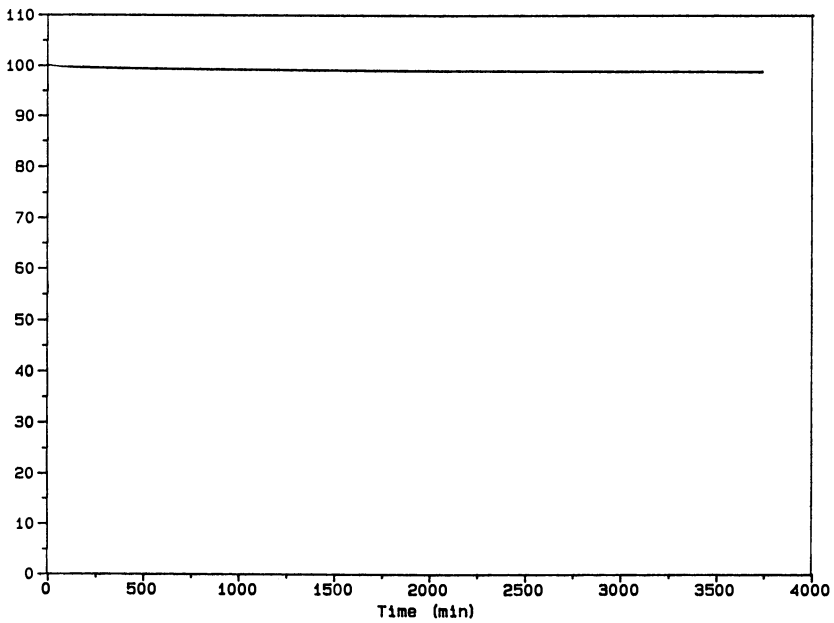
Figure 6.   Isothermal weight change of fully cured thermoset derived from BCB-1 monomer with time at 350°C in N_2.
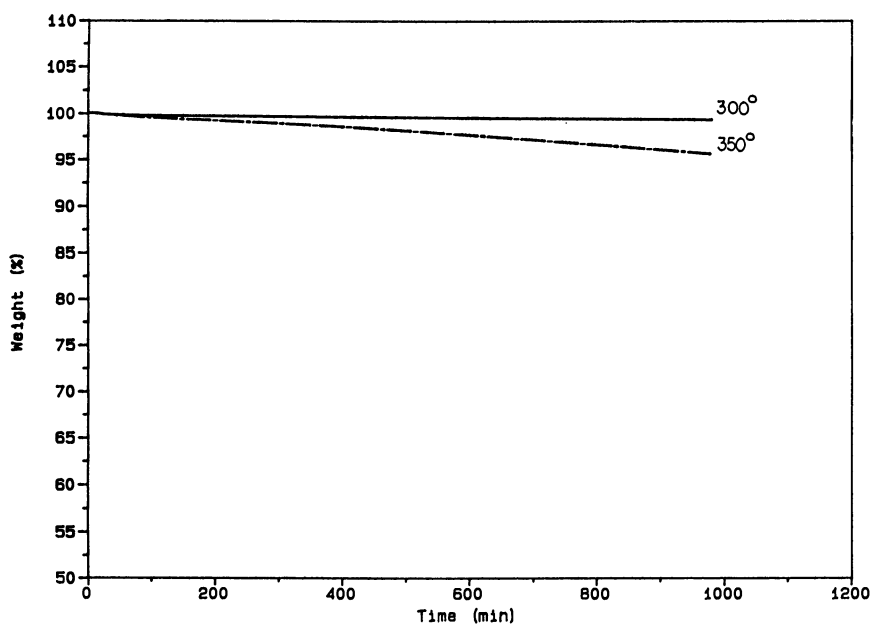
Figure 7. Isothermal weight change of fully cured thermoset derived from BCB-2 monomer with time at 300 °C and 350 °C in N_2.
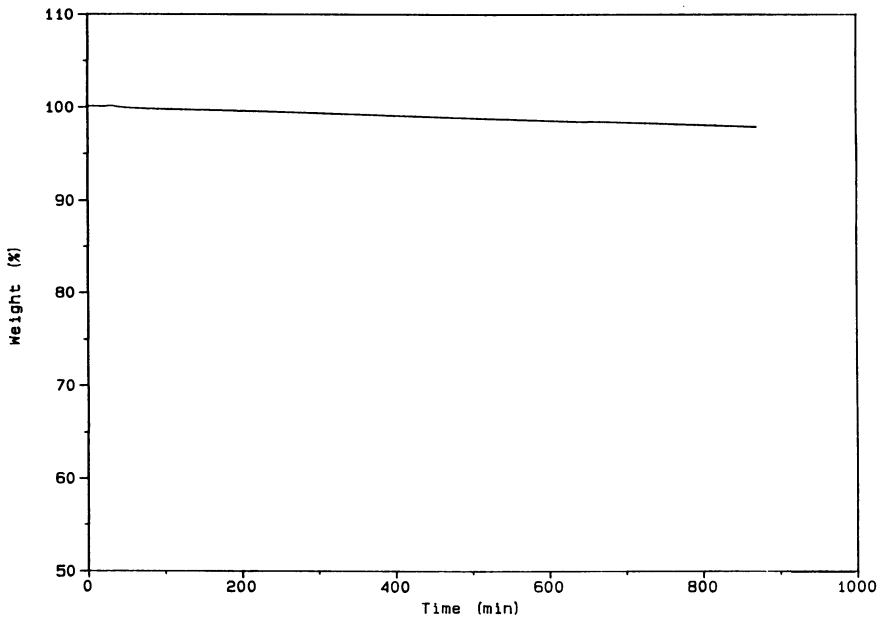
Figure 8.   Isothermal weight loss of fully cured thermoset derived from BCB-2 monomer with time at 350°C in air.

constant and describes the polarization response to an
applied field. The complex component of the
permittivity is a measure of the conductance and, so,
the energy loss in the material. The dissipation
factor, or loss tangent, is the ratio of the loss to the
dielectric constant. The reader is referred to one of
the standard texts for a more thorough discussion of
these quantities [7]. The relevance of these properties
to electronic circuits is that the signal propagation
velocity. The dissipation factor determines the amount
of signal attenuation during transmission along a trace
and, therefore, the amount of heat generated during
circuit operation.

Figure 9 shows the dispersion surface of a film
derived from the BCB-1 monomer during heating from room
temperature to 200°C. The dielectric constant was found
to be relatively flat over this surface with a value of
e_r ~2.65 $\pm$ 0.2. The uncertainty in th measurement was
due to the error in measuring the ratio of the sample
area to the thickness and is systematic over the entire
surface. The slight rise at 10 MHz is due to losses in
the experimental rig which could not be properly
subtracted out of the measurement. This flat response
over such a wide frequency range is characteristic of
non-polar polymers.

Figure 10 shows the dispersion surface of the
thermoset film derived from the BCB-2 monomer. The
dielectric constant was found to be relatively flat over
this surface with a value of e_r ~2.66 $\pm$ 0.1. The error
in this measurement was slightly less than indicated for
the previous figure because the sample dimensions were
more well defined. As in the previous figure, the
dielectric constant increases near 10 MHz because of
losses in the test leads.

Figure 11 shows the variation of the dissipation
factor with frequency for both of the thermoset films
measured at room temperature on a capacitance bridge.
The values are both below 0.001 at frequencies above 1.0
kHz. The use of the capacitance bridge was necessary for
this measurement because these values are well below the
normal resolution limit of the impedance analyzer.
Unfortunately, the bridge does not allow for measurement
at higher frequencies which are important for standard
circuit operation. However, the general observation is
that the dissipation factor continues to drop at higher
frequencies. This implies that the dissipation factor
for these two films should be well below 0.001 at
frequencies of 1.0 MHz and above.

The values in the two previous figures can be
compared to those of polyimide, which is currently used
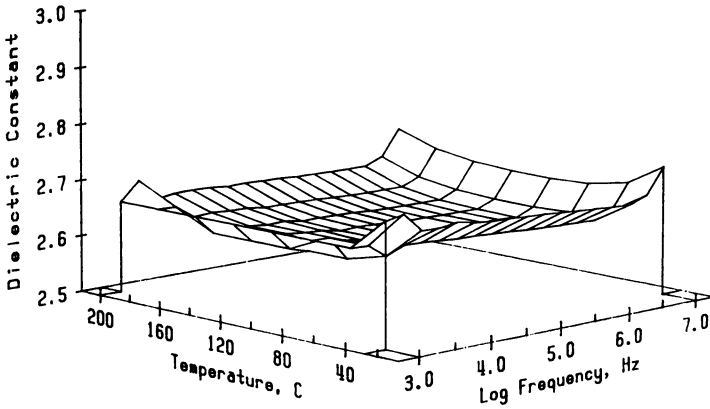
Figure 9.   Dispersion surface of dielectric constant of thermoset derived from BCB-1 monomer as a function of temperature.
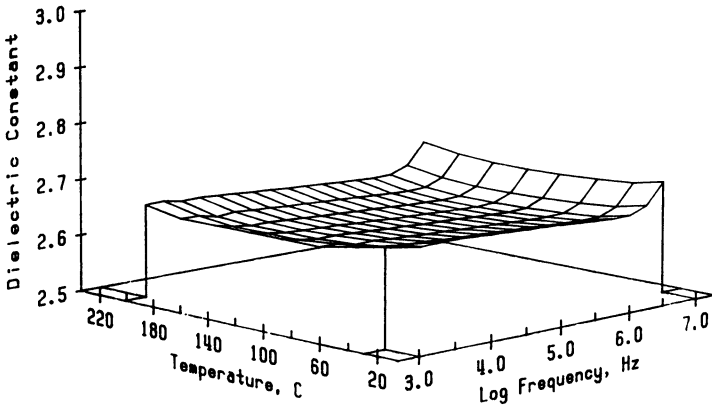
Figure 10.   Dispersion surface of dielectric constant of thermoset derived from BCB-2 monomer as a function of temperature.
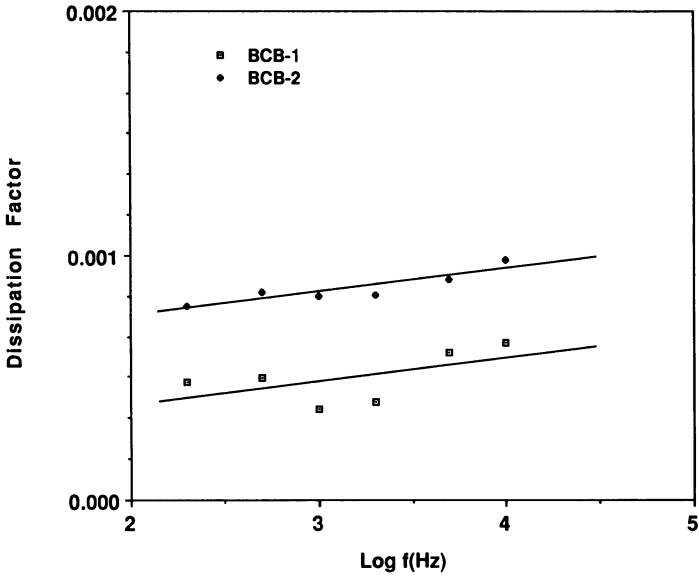
Figure 11. Frequency dependence of the dissipation factor of thermoset films derived from BCB-1 and BCB-2 monomers.

as an organic interlevel dielectric. The dielectric constant of polyimide is e_r ~3.5 and the dissipation factor is ~0.01[8]. The properties of both of the BCB films described in this work appear to offer substantial improvements in both the dielectric constant and dissipation factor in comparison to polyimide.

Dielectric Breakdown Measurements. The dielectric breakdown strength was measured on the freely standing BCB-2 films as described above. The breakdown strength was 2.5×10^6 V/cm for 22 mm thick films. This value is ~50% of the breakdown strength measured for 1.5 mm polyimide films on Si(8). However, the breakdown strength does not vary proportionally to the film thickness. The breakdown strength was also measured for 1.7 mm BCB-2 films deposited on a Si substrate. The value obtained from this measurement was 4.0×10^6 V/cm. The latter value was much closer to breakdown strengths observed in polyimide films of comparable thickness.

Summary

Polymers have been prepared from two new vinyl containing bisbenzocyclobutene monomers. These materials can be prepolymerized. The viscosity versus solids content for a representative prepolymer was described. Thin films of these polymers can be prepared by spin or spray coating xylene solutions of the prepolymer onto a supportive substrate.

The dielectric properties of two different thermoset films derived from bis-benzocyclobutene monomers were described. The dielectric constant was 2.65 + 0.1. The dissipation factor was below 0.001 above 1.0 kHz. These values are significantly lower than those reported for polyimide thin films. Therefore, the BCB films described in this work are attractive candidates for interlevel dielectrics in dense multilevel interconnection structures.

The dielectric breakdown strength of the BCB films was observed to be close to that reported for polyimide films of comparable thickness. The value of 4×10^6 V/cm appears to be acceptable for use in multilevel interconnection structures.

References

1.   Messner, G.; _IEEE Trans. Compon., Hybrids, and Manufac. Technol._ 1987, _CHMT-10_, 143
2.   See, for example, Wilson, A. M.; _Thin Solid Films_ 1981, _83_, 145

3. Kirchoff, R. A.; Baker, C. E.; Gilpin, J. A.; Hahn, S.F.; Schrock, A. K.; <u>Proc. 18th Int. SAMPE Conf.</u> 1985, 478-489

4. Tan, L.-S.; Arnold, F. E.; <u>ACS Polymer Preprints</u> 1985, <u>26</u>, 176 .

5. Johnson, R.W.; Phillips, T.L.; Hahn, S.F.; Burdeaux, D.C.; Townsend, P.H.; <u>Proceedings of the International Society for Hybrid Microelectronics</u> 1988,365.

6. Hurwitz, F.I.; Hyatt, L.H.; D'Amore, L.; Nguyen, H.X.; Ishida,H.; <u>Polymer</u> 1988, <u>29</u>, 184.

7. See, for example, <u>Dielectric Materials and Applications</u>; von Hippel, A.R.; The MIT Press, Cambridge, MA 1966

8. Rothman, L. B.; <u>J. Electrochem. Soc.</u> 1980, <u>127</u>, 2216

Chapter 18

Synthesis of Poly(arylene ether phenylquinoxaline)

James L. Hedrick and Jeff W. Labadie

IBM Research Division, Almaden Research Center, San Jose, CA 95120–6099

Poly(phenylquinoxalines), PPQ, have recently achieved commercial status since their first reports in the late sixties by Hergenrother and others (1,2). PPQ displays an excellent combination of properties including high T_g, thermal stability and low dielectric constant, and is an attractive candidate for high temperature insulators in the microelectronics industry (3). PPQ is generally synthesized through the condensation of an aromatic bis(o-diamine) with a bis(phenyl-α-dicarbonyl) compound (1-3). Both homopolymers and statistically random copolymers have been prepared, with T_gs ranging from 284 to 420°C depending on the combination of monomers used in the synthesis. Structures with lower T_gs generally contain ether linkages introduced through the bis(dicarbonyl) monomer (4). Alternatively, Hergenrother and co-workers (5) have prepared poly(arylene ether phenylquinoxalines) via nucleophilic aromatic substitution by the polycondensation of a difunctional phenolic hydroxyl monomer containing preformed quinoxaline rings with an activated dihalide (i.e., difluorodiphenyl sulfone, difluorobenzophenone, etc.). These structures are somewhat similar to poly(ether-imide) which is an excellent example of a high temperature polymer that has been favorably modified by the introduction of ether linkages (6). Tough ductile mechanical properties and good solution and melt processibility are typical characteristics of these materials (7).

As another means of preparing the quinoxaline-based analogue of the poly(ether-imides), we have investigated PPQ synthesis through a halo displacement approach. We surmised the electron deficient pyrazine component of the quinoxaline ring system would activate 6- or 7-halo substituents towards nucleophilic aromatic substitution. Facile displacement should occur at these positions since the pyrazine ring can stabilize the negative charge developed in the transition state through a Meisenheimer-like complex (I), analogous to conventional activating groups (e.g., sulfone, carbonyl) (8,9) (Scheme I). In our approach to poly(arylene ether-phenylquinoxalines), the quinoxaline ring is formed in the monomer synthesis, rather than in the polymerization, and the appropriately halo-substitued bis-quinoxaline is subjected to an aromatic displacement polymerization with various bisphenates.
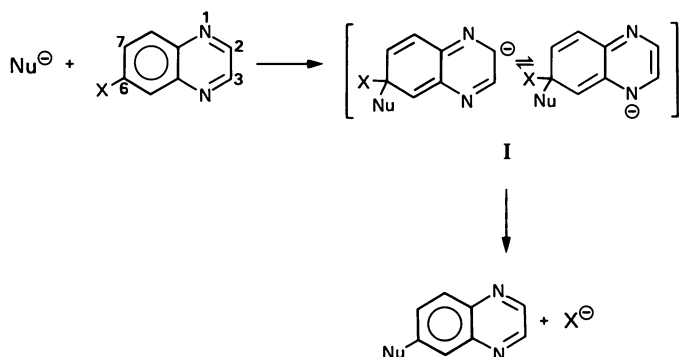
Scheme I

Experimental

4-Fluoro-o-phenylenediamine (ICN) was sublimed prior to use, and 1,4-bis(phenylglyoxalyl)benzene (IFP Enterprise), 1, was used without further purification. 2,3-diphenyl-6-fluoroquinoxaline, **2**, 6-(3-methylphenyl)-2,3-diphenylquinoxaline, **3**, and 1,4-bis(6-fluoro-3-phenyl-2-quinoxalinyl) benzene, **4**, were prepared and purified according to literature procedure (<u>10</u>). The bisphenols were obtained from Aldrich and recrystallized prior to use.

The polymers were synthesized by the standard NMP/K_2CO_3 procedure according to literature (<u>10,11</u>). Glass transition temperatures and thermal stability measurements (TGA) were performed on a Du Pont DSC 1090 instrument at heating rates of 10 and 5°C/min, respectively. Intrinsic viscosity measurements were determined using a Cannon- Ubbelhodhe dilation viscometer in NMP (25°C).

Results and Discussion

To demonstrate the feasibility of the quinoxaline activated poly(arylene ether) synthesis, a model reaction between 2,3-diphenyl-6-fluoroquinoxaline, **2**, and sodium cresolate was carried out in NMP (160°C) (Scheme II). Quantitative
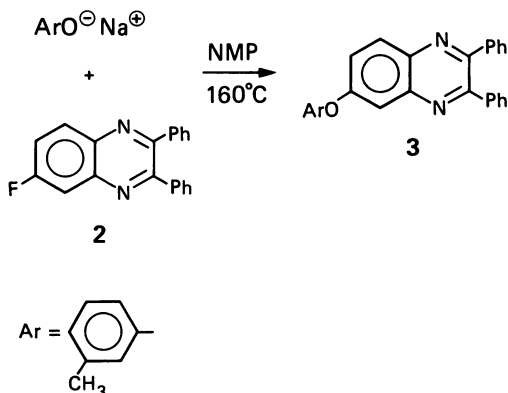
Scheme II

conversion of **2** was observed by HPLC (85:15 acetonitrile : water, μ-Bondapak- C18 column) with the formation of a single product with C, H, N analysis and spectral properties characteristic of the expected 6-(3-methylphenyoxy)-2,3-diphenyl quinoxaline, **3**. The model reaction demonstrated that the 6-fluoro group is readily displaced by phenates, as a result of activation by the adjacent pyrazine ring. Although nucleophilic displacement is known to occur at the 2- and 3-positions of quinoxalines (i.e., positions adjacent to nitrogen) (12), this represents the first example of nucleophilic aromatic substitution at positions in the fused benzene ring of these ring systems. The transformation occurred with high selectivity and was clearly suitable as a polymer-forming reaction.

The qunioxaline-activated poly(arylene ether) synthesis required the preparation of the appropriate bis(6-fluoroquinoxalinyl)-based monomer. This was carried out by the reacting of **1** with 4-fluoro-1,2-phenylenediamine in refluxing chloroform with trifluoroacidic acid as the catalyst. The resulting 1,4-(bis(6-fluoro-3-phenyl-2-quinoxalinyl) benzene (**4**) was isolated in 90% yield, and was recrystallized (ethyl acetate) to yield polymer grade monomer. Due to the nonselectivity of the quinoxaline formation, three isomers are possible (i.e., 6,6'-, 6,7'-, 7,7'- difluoro), analogous to the multiple isomeric phenylquinoxaline moieties formed in PPQ syntheses.

Polymerization of **4** with various bisphenols was carried out in the presence of K_2CO_3 in a NMP/toluene (2/1) mixture by the standard procedure (Scheme III) (11). In the initial stage of the polymerization, the water generated by the bisphenate formation was removed as an azeotrope with toluene. Upon completion of bisphenate formation and dehydration, the polymerization mixtures were heated to 180-190°C to effect the displacement reaction. In each case, polymer was attained within 24 hr as judged by the dramatic increase in viscosity.

Notably, high molecular weight poly(arylene ether-phenylquinoxalines) were formed using conventional polymerization conditions, whereas poly(ether-imide) synthesis requires milder conditions to avoid side reactions associated with the nitrite ion generated in the polymerization. The resulting polymer was coagulated in excess methanol. This general procedure was applied to a number of bisphenols affording high molecular weight materials, as indicated by the intrinsic viscosity measurements (Table 1). In contrast to conventional PPQ, the poly(arylene ether phenylquinoxalines) were soluble in NMP, a commonly used solvent for polymer processing in the microelectronics industry.

The glass transition temperatures ranged from 255 to 275 depending on the bisphenol used (Table 1). Interestingly, these values are 20-40°C higher than the poly(ether-imide) analogue, consistent with the expected affect of pendant phenyl groups. In addition, these materials demonstrated excellent thermal stability with polymer decomposition temperatures in excess of 450°C (Figure 1). Those structures based on Bisphenol-AF and dihydroxybenzophenone were the most thermally stable as judged by TGA.

Future work on poly(arylene ether-phenylquinoxalines) will focus on demonstrating the scope of materials possible by utilizing bisquinoxaline monomers derived from other bis(α-diketones) as well as other bisphenols. Further studies on the polymerization process will entail leaving group effects (i.e., chloro, nitro), ether interchange and molecular weight control. In addition, the mechanical and thermal properties will be investigated together with both the solution and melt viscosities.

Conclusions

The results demonstrate that quinoxaline-based poly(arylene ethers) can be synthesized via a halo displacement polymerization, where the fused pyrazine ring is the activating group. The polymerization provides a general method for preparing arylene ether-based PPQs where the structure of the arylene ether moiety is readily controlled by varying the bisphenol used analogous to the poly(ether-imide)
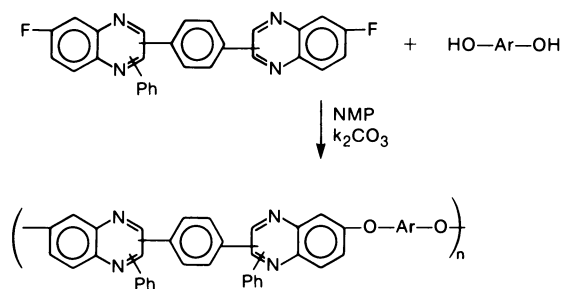
Scheme III

Table 1

Characteristics of Poly(arylene ether-phenylquinoxalines)

Ar	$[\eta]$ NMP 25°C (dl/gm)	Tg,* °C
C with CH₃, CH₃	1.20	255
C with CF₃, CF₃	1.20	255
C with Ph, Ph	1.45	270
SO₂	0.55	285

*DSC 10°C/min. heating rate
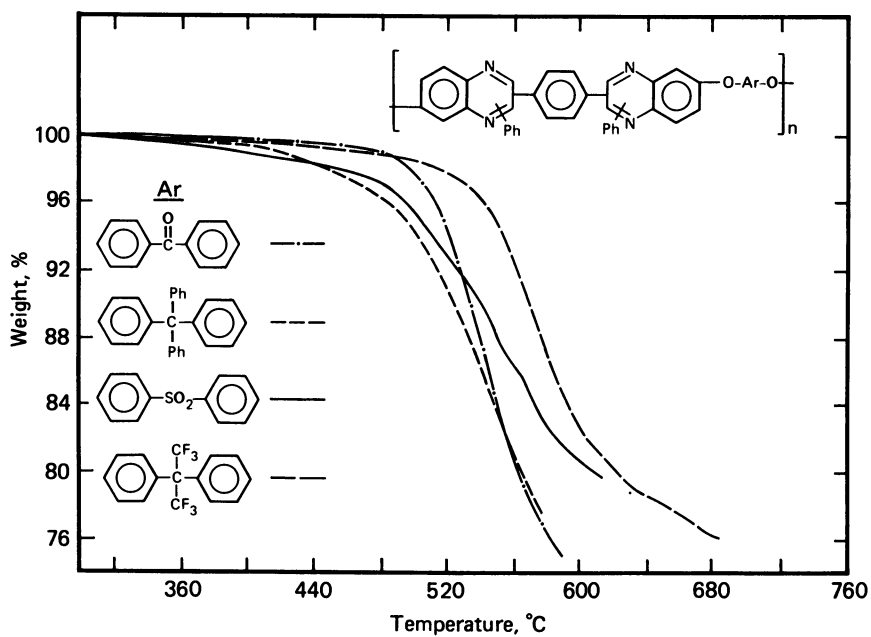
Figure 1. TGA curve for poly(arylene ether phenylquinoxalines).

synthesis. Moreover, heterocyclic activated nucleophilic chemistry should prove effective with monomers derived from other ring systems, providing a general synthetic methodology to high temperature, high T_g arylene ether-heterocyclic polymers.

References

1. Hergenrother, P. M. J. Appl. Polym. Sci. 1974, 18, 1779.
2. Wrasidlo, W.; Augl, J. M. J. Polym. Sci.: Part A-1 1969, 7, 3393.
3. Hergenrother, P. M. J. Macromol. Sci.-Revs. Macromol. Chem. 1971, C6, 1.
4. St. Clair, A. K.; Johnston, N. J. J. Polym. Sci.: Polym. Chem. Ed. 1977, 15, 3009.
5. Hergenrother, P. M., Polym. Preprints 1988, submitted.
6. White, D. M.; Takekoshi, T.; Williams, F. J.; Relles, H. M.; Donahue, P. E.; Klopfer, H. J.; Loucks, G. R.; Manello, J. S.; Matthews, R. O.; Schluenz, R. W. J. Polym. Sci.: Polym. Chem. Ed. 1981, 19, 1635.
7. Hergenrother, P. M.; Kiyohara, D. E. Macromolecules 1970, 3, 387.
8. Johnson, R. N.; Farnham, A. G.; Clendinning, R. A.; Hale, W. F.; Merrian, C. N. J. Polym. Sci.: Part A-1 1967, 5
9. Atwood, T. E.; Barr, D. A.; Faasey, G. G.; Leslie, V.J.; Newton, A. B.; Rose, J. B. Polymer 1977, 18, 354.
10. Hedrick, J. L.; Labadie, J. W. Macromolecules, accepted, 1988.
11. Hedrick, J. L.; Mohanty, D. K.; Johnson, B. C.; Viswanathan, R.; Hinkley, J. A.; McGrath, J. E. J. Polym. Sci.: Polym. Chem. Ed. 1986, 23, 287.
12. DeSchryver, F.; Marvel, C. S. J. Polym. Sci.: Part A-1 1967, 5, 545.

Chapter 19

High-Performance Silicone Gel as Integrated-Circuit-Device Chip Protection

Cure Study and Electrical Reliability

C. P. Wong

AT&T Bell Laboratories, Princeton, NJ 08540

Recent advances in IC device encapsulants and polymeric materials have made high reliability VLSI plastic packaging a reality. High performance silicone gels possess excellent electrical and physical properties for IC protection. With their intrinsic low modulus and soft gel-like nature, silicone gels have become very effective encapsulants for the delicate larger chip size and wire-bonded VLSI chips. Recent studies indicate that adequate IC chip surface protection with high performance silicone gels in plastic packaging could possibly replace conventional ceramic hermetic packaging. This paper reviews some potential IC encapsulants. It focuses on the high performance silicone gels, their cure chemistry, and their application as VLSI device encapsulants.

The rapid advances in integrated circuit (IC) technology have had a profound technological and economic impact on the electronics industry. The exponential growth of the number of components per chip, the exponential decrease of device dimensions (1) and the steady increase in IC chip size have imposed stringent requirements not only on IC physical design and fabrication, but also on the IC encapsulants. The increase of integration in Very Large Scale Integration (VLSI) technology has resulted in a large increase in chip size. The effectiveness of high performance encapsulants, such as silicones (elastomers and gels), polyimides, epoxies, silicone-polyimides, and polyxylylene (Parylene) in protecting these large IC devices has been reviewed. (2-3) High performance silicone gels possess excellent electrical, chemical, and physical properties for this type of IC protection. With their high purity, intrinsic low modulus and soft gel-like nature, silicone gels have become very effective encapsulants for the delicate larger chip size and wire-bonded VLSI chips. Recent studies indicate that adequate IC chip surface encapsulation with these high performance silicone gels in plastic packaging could possibly replace conventional ceramic hermetic packages. (4-5) This paper reviews some potential encapsulants with special focus on the high performance silicone gel, its cure chemistry and Temperature Humidity Bias (THB) accelerated electrical testing as a VLSI device encapsulant.

The purpose of encapsulation is to protect electronic IC devices and prolong their reliability. Moisture, mobile ions, (eg., sodium, potassium, chloride, fluorides), UV-VIS and alpha particle radiation, and hostile environmental conditions are some of the possible causes of degradation or interaction which could negatively affect device performance or lifetime. Silicon dioxide, silicon nitride and silicon-oxy-nitride, commonly used as passivation layers have excellent moisture and mobile ion barrier properties and are, therefore, excellent encapsulants for devices. As for the

sodium ion barrier, silicon dioxide is inferior to silicon nitride. However, the use of phosphorous-doped (a few weight percent) silicon dioxide has greatly improved its mobile ion barrier property. A thin layer (̄1-2μm thickness) of one of these dielectric materials is deposited uniformly on the finished device, except on the bond pad areas. Due to the "edge effect" of passivation of IC devices after wire bonding interconnection, protection to the bond pad area becomes necessary (See Figure 1). In addition, these passivation layers are not 100% pinhole or crack-free. To ensure the device reliability, an organic conformal coating is usually used for
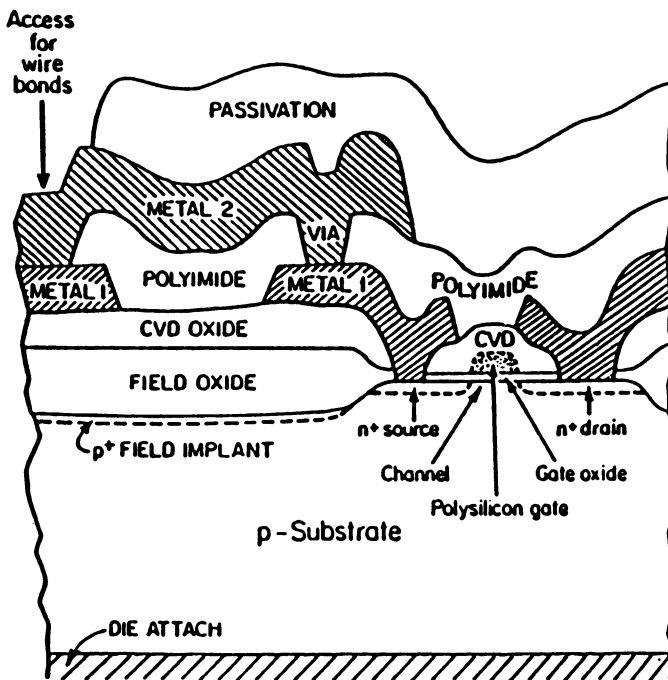
Figure 1 -   Edge Effect of Device Passivation (Due to the exposure of the wire bond pad and the passivation material, this access area for wire bonds must need encapsulation after wire-bonding interconnection).

device encapsulation. Epoxies, polyimides, Parylene, silicone-polyimides, and silicones (elastomers and gels) are typical materials used for this application. Characteristic properties of these potential encapsulants are listed in Table I.

General Chemistry of Silicone Gels. The basis of commercial production of the silicones is that chlorosilanes are readily hydrolyzed to give disilanols, which are unstable and condense to form siloxane oligomers and polymers. Depending on the reaction conditions, a mixture of linear polymers and cyclic oligomers is produced. The cyclic components can be ring-opened to linear polymers, and it is these linear polymers that are of commercial importance. Chlorosilanes, with reactive hydro and vinyl reactive groups, are the intermediates for the synthesis of the silicone gels. These hydro, vinyl reactive functional groups, and the platinum catalyst are essential to the silicone gel chemistry. (6) The reaction mechanism of the hydro, vinyl additional cure system is shown on Figure 2.

EXPERIMENTAL

A Nicolett 7199 FT-IR spectrometer was used to monitor the cure of silicone gel. The decreasing absorption of the Si-H absorption at ⁻2129cm^{-1} was monitored during the cure of the silicone gel (see Figure 3). Silicone gel (Part A and Part B) was freshly mixed at a prescribed ratio prior to the cure study. A NaCl salt plate was used as the IR sample cell. Results of the FT-IR study are shown in Figure 4.

   In addition to the FT-IR cure study, measurements have been made on the silicone gels with a highly sensitive microdielectric apparatus from 0.05Hz to 10KHz. This microdielectrometry, which utilizes the Micromet Instrument's Eumetric System II microdielectrometer with a miniature IC sensor and a wide range of frequencies (from 0.05Hz to 10KHz) to monitor the loss factor (E") of the silicone gels, is a very sensitive technique to detect the final stage of the silicone gel cure. A thin layer of freshly mixed silicone gel (⁻20 mil thickness) was coated on the miniature IC sensor and placed inside a programmable oven. The temperature of the oven was set to the pre-described temperature (i.e., 120°, 150° or 175°C) and the loss factors (E") at various frequencies (0.05, 1, 100, 1000, 10000 Hz) was monitored periodically during the curing time. Results of the microdielectric loss factor measurements are shown in Figure 5.

Temperature Humidity Bias (THB) Electrical Testing of Silicone Gel. The electrical reliability of silicone gels was determined by using a THB test procedure employing an alumina ceramic IC device with a triple track resistor (TTR). The metallization for the TTR is tantalum nitride (Ta_2N). The feature size of this testing device is 75μm metal line-width and spacing. Prior to the silicone gel coating, the TTR was cleaned with Freon TA vapor for 15 min., boiling H_2O_2 for 15 min., deionized water rinsed for 30 min., and oven dried at 120°C for 1 hr. Then, the silicone gel was coated on the freshly cleaned TTR device. These test devices were cured at different curing temperatures (120°C, 150°C, and 175°C) for 2 hrs. The cured test devices were subjected to 85°C, 85% Relative Humidity (RH) and 180 volt-dc bias. The leakage current between the biased center track and the two grounded outer tracks was measured at different intervals to determine the electrical performance of the silicone gel. The difference in the triple track resistance with respect to the initial resistance (ΔR/R) of the biased center track was measured at different intervals during the testing. The electrical performance of different vinyl and hydride mixing ratios (from 1:1 to 10:1 of Part A:Part B) and different curing temperatures (120°, 150°, 175°) of the silicone gels were studied. The results of the THB electrical testing are shown in Figures 6 to 9.

RESULTS AND DISCUSSIONS

Cure Study of Silicone Gel. The chemistry of most silicone gels is based on the reaction of silicon-vinyl (Part A) and silicon-hydride (Part B) addition cure mechanism (see Figure 2). The addition of the hydride functional group from the silicon-hydride (Part B) to the vinyl functional group of the silicon-vinyl (Part A) and the formation of carbon-silicon crosslinking are key steps in the reaction mechanism. A trace amount (a few ppm) of platinum catalyst is needed to

TABLE I

PHYSICAL PROPERTIES OF SOME POTENTIAL ENCAPSULANTS

(Unfilled System)

Encapsulants	TCE* (ppm/°C)	Modulus (psi)
Epoxy	⁻40 - 80	⁻1 - 5 x 10^6
Polyimide	⁻3 - 80	⁻1 x 10^6
Parylene	⁻35 - 40	⁻0.4 x 10^6
Silicone-Polyimide	⁻5 - 100	⁻0.4 x 10^6
Silicone Gel	⁻200 - 1000	⁻0 - 400

*TCE = Thermal Coefficient of Expansion at Room Temperature

$m > n$ (CURED GEL) - (I)
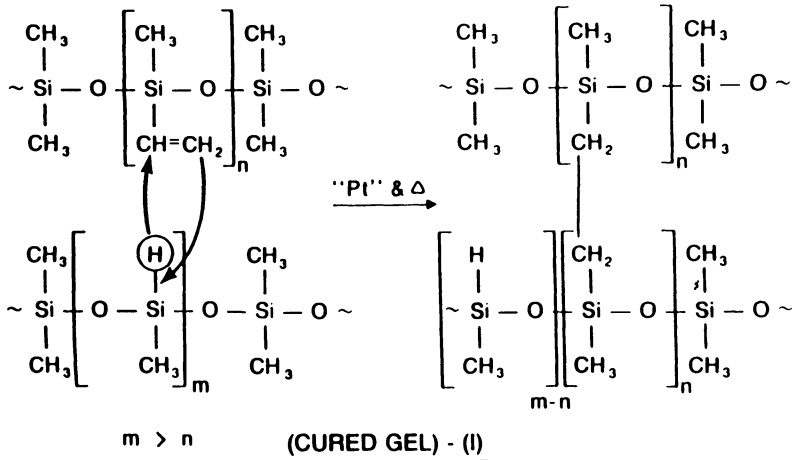
- Excess Hydrides
- Reactive "Pt" Catalyst

Figure 2 -   Silicone Gel Cure Mechanism.
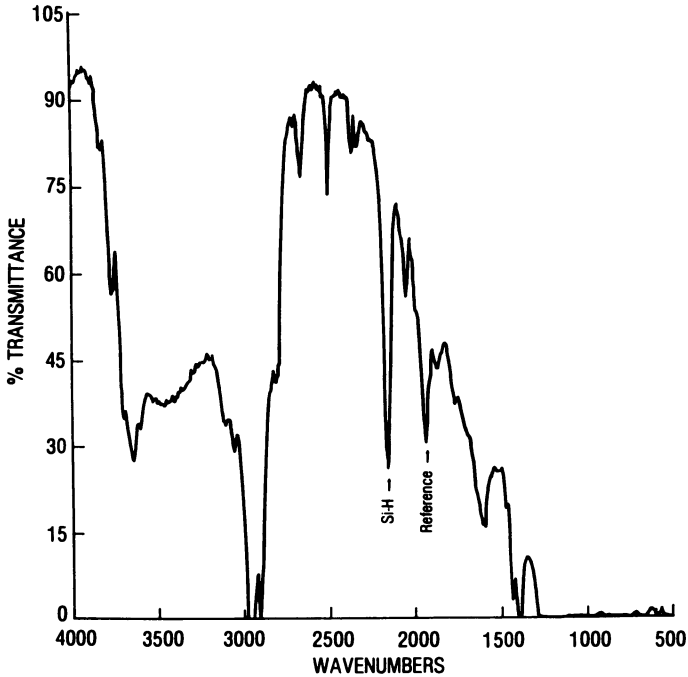
Figure 3 -   Fourier Transform - Infrared Spectrum of a Typical
Silicone Gel .
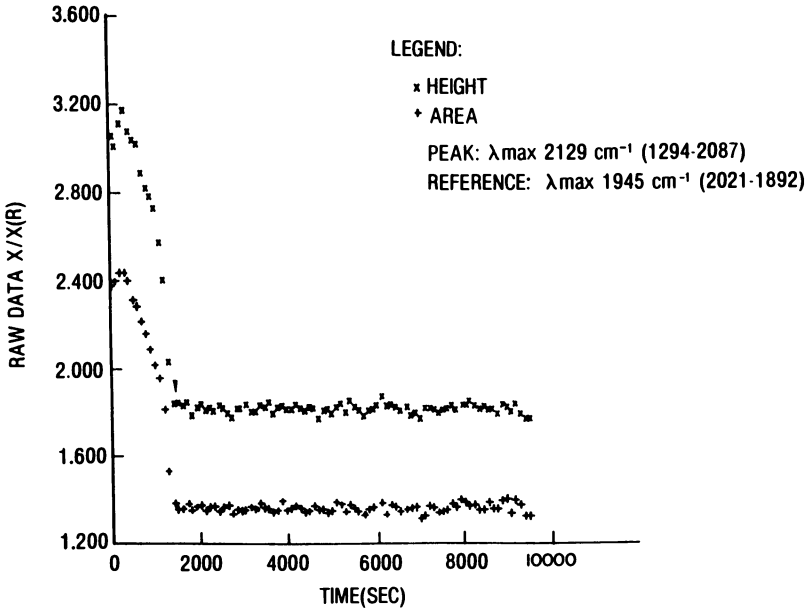
Figure 4 -   Fourier Transform - Infrared Study of Silicone Gel .
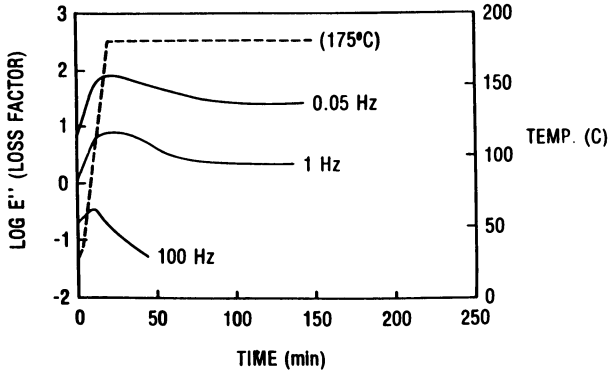
Figure 5 -   Micro-dielectric (loss factor) Measurement of
Silicone Gel Cure Study.

(Silicone Mixing Ratio of Part A: Part B = 1:1—Harder Gels)
(85°C/85%RH/180 Volt·dc Bias)

Legend:

○ —·— Sample 1—Cured at 120°C, 2hr
□ --- Sample 2—Cured at 150°C, 2hr
△ ········· Sample 3—Cured at 175°C, 2hr
▲ —— Control
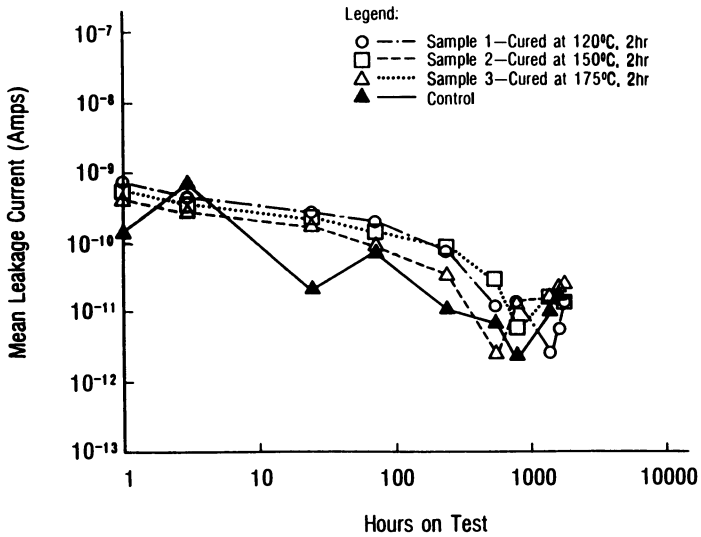
Figure 6 -   Temperature Humidity Bias Testing of Silicone Gels .

(Silicone Mixing Ratio of Part A:Part B = 10:1—Soft Gels)
(85ºC/85%RH/180 Volt-dc Bias)
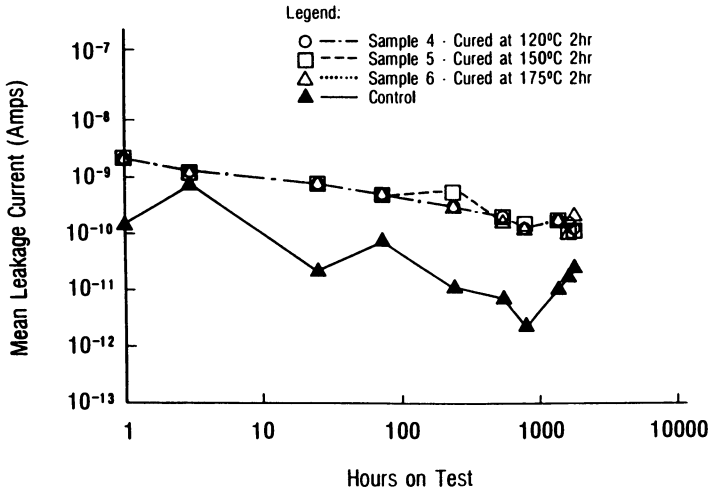
Figure 7 -   Temperature Humidity Bias Testing of Silicone Gels .

(Silicone Mixing Ratio of Part A: Part B = 10:1—Soft Gels)
(85ºC/85%RH/180 Volts-dc Bias)
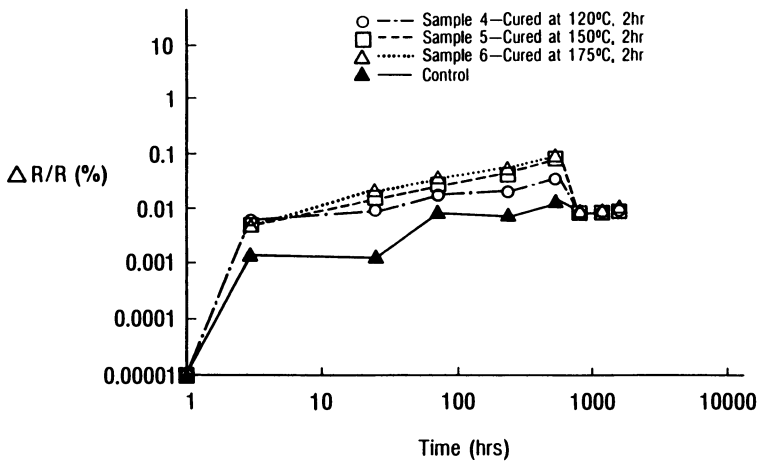
Figure 8 -   Temperature Humidity Bias Testing of Silicone Gels.

(Silicone Mixing Ratio of Part A: Part B = 1:1—Harder Gels)
(85°C/85%RH/180Volt-dc Bias)
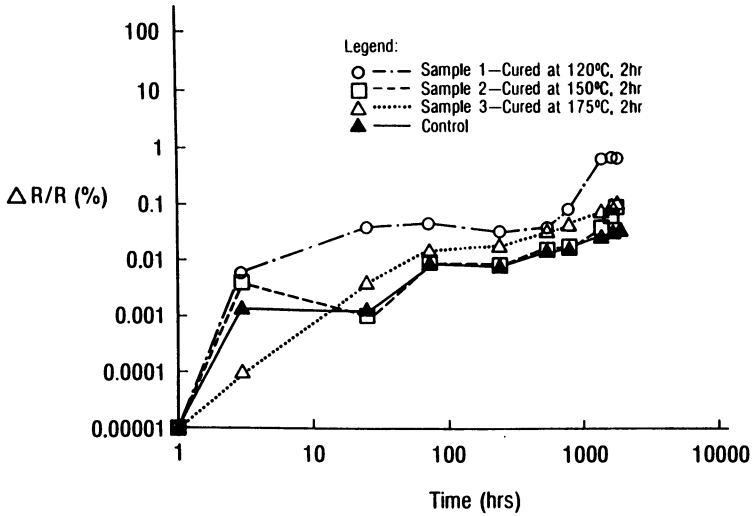
Figure 9 -   Temperature Humidity Bias Testing of Silicone Gels.

facilitate the cure or crosslinking. Fourier Transform-Infrared (FT-IR) provides an excellent tool in detecting the degree of cure of silicone gel. The strong vibration stretch absorption of the Si-H provides a clear indication of the reaction of the silicone gel system. During the curing process, the Si-H concentration decreases as the hydride-vinyl addition takes place (see Figure 4). We follow this curing progress by monitoring the absorption band ratios of Si-H ($^-2129cm^{-1}$) vs. a reference peak ($^-1945cm^{-1}$) either with peak heights and/or the peak areas' measurements. At the beginning of the isothermal cure cycle, a rapid crosslinking takes place. However, the crosslinking rapidly slowed down and gradually stabilized after $^-30$ min. Further heating is mainly to promote better adhesion between the silicone gel resin and the coated substrate. In this study, both the absorption ratios of the peak height and the peak area measurements agree in this study. The results are shown in Figure 4.

A highy sensitive microdielectric measurement is used to define the degree of cure of the silicone gel. (7) In a microdielectric measurement, the loss factors (E") of the silicone gel increase rapidly at the beginning of the cure process (see Figure 5). This rapid E" increase is mainly attributed to the increase in the oven ramping temperature, from room temperature to $^-175°C$, which generates the thermal activation of ionic conductivity within the silicone matrix, as can be seen from the cure temperature profile. However, the loss factors (E") at all frequencies (0.05, 1, 100 Hz) decreased rapidly after the temperature stabilized at 175°C. This decrease in E" can be attributed to the tightening of the silicone gel network and the reduction of the ionic conductivity. (Note the loss factor is in log scale). After $^-80$ minutes heating at 175°C, there is no change in the E" of the material, a good indication of a complete curing of the silicone gel.

Even with silicone gel formulation with excess vinyl functional group vs. hydride functional group, this microdielectric loss factor measurement provides a fast, real-time measurement of the degree of cure of silicone gel.

Temperature Humidity Bias (THB) Testing. In the triple track resistance measurement, we grounded the two outer tracks and biased the center track. Then we measured the resistance change of the center conductor line. The test process measures the degree of "electro-oxidation" of the center track. Leakage current due to impurities can cause the Ta_2N resistor to anodize. The change of the triple track resistance in relation to the original resistance increases with time. This is mainly due to the oxidation process. The smaller the change in resistance and leakage current with time, the better the encapsulant material will be. For the 1:1 vinyl-hydride mixing ratio silicone gel, there is no noticeable change in leakage current ($^-10^{-11}$ Amp) after 1,700 hr. of testing. All the silicone gels (samples 1, 2, and 3) with a 1:1 mixing ratio perform relatively the same as the control RTV sample (see Figure 6). However, the leakage current of the corresponding 10:1 vinyl-hydride mixing ratio of silicone gels (samples 4, 5, and 6) show an order of magnitude higher in leakage current measurement ($^-10^{-10}$ Amp vs. RTV leakage current of 10^{-11} Amp). Furthermore, with leakage current of 10^{-10} Amp after 1,700 hr. of THB testing, we consider these silicone gels to be good device encapsulants (see Figure 7). For the ($\Delta R/R$) resistance change during the initial 800 hr. testing, the 10:1 mixing ratio silicone gels appeared to have an order of magnitude higher resistance change as compared to the RTV silicone control.

However, when the THB testing continued to $^-1000$ hr., the leakage current performances are almost identical to the RTV control (see Figure 8). For the 1:1 mixing ratio of the silicone gel, the $\Delta R/R$ change of the higher temperature cured samples (such as 150° and 170°C) perform better than the 120°C cured sample (see Figure 9). This improvement in $\Delta R/R$ can be attributed to better adhesion because of the higher cure temperature of the silicone gel, which reduces the unreactive cycles or the low molecular weight silicones at the interface of the silicone gel and the coated substrate. Nevertheless, all the silicone gel samples tested show excellent THB electrical performance as IC device encapsulants.

CONCLUSIONS

High performance silicone gels have been shown to have excellent electrical characteristics. With their superior jelly-like (near zero modulus) intrinsically soft, physical property and ultra-high chemical purity, silicone gels are becoming very attractive encapsulants. They are chosen to

provide the essential stress relief on large dies in the post-molded plastic packages and to provide common IC surface protection of the premolded plastic packages. Silicone gels, with higher curing temperature, would improve their adhesion to the coated substrates and increase their reliability as device encapsulants. We strongly believe that these high performance silicone gels offer excellent IC chip protection and have potential for replacing ceramic hermetic packages of IC. However, the poor solvent resistance and the weak mechanical properties of the silicone gels are the main disadvantages of this material as device encapsulants.

ACKNOWLEDGMENTS

LITERATURE CITED

1. In VLSI Technology; Sze, S. M., Ed.; McGraw-Hill: New York, 1983.
2. Wong, C. P. Advances in Polymer Science 1988, 84, 63-83.
3. Wong, C. P. In The Encyclopedia of Polymer Science and Engineering; John Wiley and Sons: New York, 1986; Vol. 5, p. 638.
4. Otsuka, K.; Shirai, Y.; and Okutani, K. IEEE Transactions on Components, Hybrids, and Manufacturing Technology, 1984, CHMT-7, No. 3, 249.
5. Wong, C. P. Material Research Society Symposium Proceedings, Electronic Packaging Materials Science III, 1988, Vol. 108, p. 175.
6. Noll, W. Chemistry and Technology of Silicones; Academic Press: New York, 1968.
7. Wong, C. P. Proceedings of the ACS Division of Polymeric Materials: Science and Engineering, 1986, Vol. 55, p. 803.

Chapter 20

Silicone Gels for Semiconductor Applications

Chemistry and Properties

Gust J. Kookootsedes

Dow Corning Corporation, Midland, MI 48686–0995

The use of soft silicone gels to encapsulate and pro-
tect semiconductor devices is becoming increasingly
important as device complexity increases, greater re-
liability and cost are emphasized and packaging trends
change. In addition, stresses encountered during the
packaging of larger semiconductor chips, and concern
for alpha particle induced errors, in many cases nec-
essitates the use of a protective coating. This paper
reviews the synthesis, chemistry, cure and general
properties of silicone gels. The information provided
is intended for those who may be unfamiliar with this
technology and who are using or contemplating their use.

The escalating complexity and density of circuit elements has in-
creased the lead count and the size of semiconductor chips. At the
same time, there is a growing emphasis on greater reliability and
lower cost. These simultaneous events are prompting the semicon-
ductor industry to investigate moving from costly ceramic packages
to non-hermetic types such as pre-molded plastic chip carriers,
both leaded and leadless, and pin grid arrays. Where post molding
can still be used, stresses induced by the molding material, either
during the molding operation or during thermal stress, and the
threat of alpha particles emitted by fillers in the compound are of
concern. In many instances the solution to these problems is the
use of silicone gels as protective coatings.

In recent years we have read and heard much about the benefits
of silicone gels. For example, Kanji Otsuka of Hitachi (1) and
Rachel Miller of Burroughs (2) described results achieved using
silicone gels as protective coatings for non-hermetic pin grid
arrays. R.E. Thomas of Motorola (3) observed that the deformation
of aluminum metallization of plastic encapsulated semiconductor
chips could be eliminated by coating the chip surface with a soft
gel. Jonathan King of Singer Company (4) reported the use of gels
as particle getters inside hermetic micro-microcircuit packages.

All have stimulated interest in the properties and performance of silicone gels. In addition, in 1986 the IEEE Computer Packaging Committee set up a special task force chaired by Jack W. Balde to investigate the possibility of gaining military approval to use gels for protecting non-hermetic packages.

Recent interest not withstanding, the use of silicone gels to protect micro-circuitry is not new. Silicone gels have been used to protect various automotive electronic modules for a number of years. E. Sailer and A. Kennedy of IBM reported the use of a silicone gel to protect the circuitry of a non-hermetic module used in their IBM System/360 computers as early as 1966 (5). The objective of this paper is to give those unfamiliar with silicone materials a better understanding of the synthesis, chemistry and properties of silicone gels.

Silicone Gels! What Are They?

Silicone gels may be viewed as slightly cross-linked fluids or under cured elastomers. They are unique in their characteristics and their ability to protect both individual integrated circuits and hybrid circuits. Silicone gels may vary from very soft and tacky to moderately soft and only slightly sticky to the touch. In fact, the hardness of a gel as defined can not be measured by the normal methods employed for elastomers and plastic materials. The tensile strength and modulus of silicone gels are very low, which allows their use without unduly stressing small interconnect wires during thermal stress conditions. Historically, firmer high purity silicone coatings, and more recently the gels, have demonstrated their extreme compatibility with most semiconductor devices. In many cases these devices provide improved performance, greater stability and higher yields than their uncoated counterparts.

Several mechanisms for curing gels are possible; however, most have limitations involving either processing or the final gel properties. Condensation type cures form water or alcohol by-products which cause outgassing and voids. Free radical peroxide-activated addition cures make it difficult to control gel consistency from batch to batch. These problems are not evident in the most prevalent cure mechanism used today, the addition of silicon-bonded hydrogen atoms to silicon-bonded olefinic radicals, usually vinyl, in the presence of a few parts per million of a platinum catalyst (I). This system creates no by-products and is easily controlled.

$$\sim\!\!\sim SiCH\!=\!CH_2 + HSi\!\sim\!\!\sim \xrightarrow{\text{Pt}} \sim\!\!\sim SiCH_2CH_2Si\!\sim\!\!\sim + \text{ no by-product} \qquad (I)$$
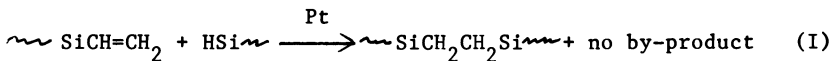
Synthesis

Silicones are unique synthetic polymers that are partially organic and partially inorganic in nature. They have a quartz-like backbone made up of alternating silicon and oxygen atoms rather than the carbon-carbon chain characteristic of organic polymers. Fluid polymers, typically, have two organic groups attached to each silicon atom. They are usually methyl; however, groups such as phenyl and vinyl provide special properties.

The preparation of silicones begins with quartzite which is reduced to silicon metal in an electric arc furnace (II).

$$SiO_2 + 2\ C \longrightarrow Si + 2\ CO \uparrow \quad (II)$$
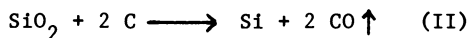
The next step involves the conversion of silicon to chlorosilanes, the basic building blocks for silicones. The most important series of chlorosilanes are those having methyl attached to the silicon atoms. They are produced by reacting the silicon metal in the presence of catalyst and heat with methyl chloride and hydrogen chloride, yielding a family of silanes (III).

$$Si + CH_3Cl + HCl \longrightarrow R_x H_y SiCl_{4-(x+y)} \quad (III)$$
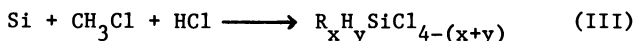
For the purposes of this discussion the most important silane is dimethyldichlorosilane, $(CH_3)_2SiCl_2$. The controlled hydrolysis of dimethyldichlorosilane yields octamethylcyclotetrasiloxane, $[(CH_3)_2SiO]_4$, which is the basic ingredient used to generate dimethyl polymers. Other siloxanes needed to produce the necessary polymers are obtained from the hydrolysis of respective chlorosilanes. Chlorosilanes and siloxanes having substituents on silicon other than methyl and hydrogen are usually prepared by other means, and their syntheses are outside the scope of this discussion. However, their importance will become evident later as we discuss polymer make-up and some low temperature considerations of the final cured gel.

Most polymers used for silicone gels are of two types. In one case the polymer chain is made up of predominantly dimethylsiloxy units with dimethylvinylsiloxy end groups (IV) or a mixture of dimethyl and methylvinylsiloxy units with trimethylsiloxy end groups (V). In some cases methylvinylsiloxy units may be used in the chain and dimethylvinylsiloxy units used as end groups (VI). In all cases the number of vinyl groups present are very small.

(IV)   (V)

(VI)

Polymers of this type are produced by either acid- or base-catalyzed polymerizations of cyclic siloxanes where trisubstituted siloxanes are used to end-cap the polymer chains and control the viscosity (VII).

$$x\ [(CH_3)_2SiO]_4 + y\ [CH_3RSiO]_4 + [(CH_3)_2RSi]_2O \xrightarrow[\text{Base}]{\text{Acid or}}$$

(VII)

$$RSiO\!\left[\!SiO\!\right]_x\!\left[\!SiO\!\right]_y\!SiR \qquad R = CH_3- \text{ or } CH_2=CH-$$

If R is other than methyl on the disubstituted siloxane, they will be distributed randomly in the polymer chain.

The other important type of polymer contains a hydrogen atom attached directly to silicon. These polymers would be very similar in structure to those shown above, (IV), (V), and (VI), if hydrogen groups were substituted for vinyl. These polymers are usually lower in molecular weight and viscosity. Oligomers such as (VIIIa-c) have also been used. The combinations and ramifications are nearly limitless in siloxane chemistry.

$$RSi\!\left[OSiH\atop CH_3\right]_3 \quad \text{(VIIIa)} \qquad Si\!\left[OSiH\atop CH_3\right]_4 \quad \text{(VIIIb)} \qquad HSi\!-\!O\!-\!SiH \quad \text{(VIIIc)}$$

$$R = CH_3- \text{ or } C_6H_5-$$

The viscosity of the vinyl functional polymers used to produce gels may run from approximately 200 to 7000 centipoise, which relates to molecular weights of approximately 7500 to 35000. The hydrogen functional oligomers or polymers are usually much lower in viscosity, 2 to 100 centipoise for molecular weights of 134 to 5000. In formulated systems the hydrogen-functional polymer is usually blended with some of the higher viscosity vinyl functional polymers to make mixing of the two components easier. One-component systems have no problems in this respect. (The reader is directed to "Organosilicon Compounds" by C. Eaborn, Butterworths, London, 1960 and "Chemistry and Technology of Silicones" by W. Noll, Academic Press, New York and London, 1965, for a comprehensive review of the synthesis and chemistry of silicone materials.)

Cure Mechanism

As stated before, the predominant cure mechanism used today is the addition of silicon-bonded hydrogen atoms to silicon-bonded olefinic radicals (I). For gelation or cure to take place, either the vinyl-containing polymer or the hydrogen-containing polymer, or both, must contain more than two reactive groups per polymer chain. A very simplified example is shown below (IX). As can be seen, silethylene cross-links are formed which serve to gel the structure. If the polymers contain two or fewer reactive groups per chain, one would obtain only chain extension with an increase in viscosity but no cross-linking.

```
      Me  ⎡Me⎤  Me  ⎡Me⎤  Me           Me  ⎡Me⎤  Me
2 MeSiO—⎢SiO⎥—SiO—⎢SiO⎥—SiMe  + 3 HSiO—⎢SiO⎥—SiH  ——————→
      CH  ⎣Me⎦x CH  ⎣Me⎦y CH          Me  ⎣Me⎦x Me
      CH₂       CH₂       CH₂
```

$$Me = CH_3 -$$ (IX)

```
      Me  ⎡Me⎤  Me
   MeSiO—⎢SiO⎥—SiH  ——————→  To another vinyl containing polymer chain.
      CH₂ ⎣Me⎦x Me
       |
      CH₂ ⎡Me⎤  Me  ⎡Me⎤  Me            Me  ⎡Me⎤  Me
   MeSiO—⎢SiO⎥—SiO—⎢SiO⎥—SiCH₂CH₂SiO—⎢SiO⎥—SiMe
      Me  ⎣Me⎦x CH₂ ⎣Me⎦y Me            Me  ⎣Me⎦x CH₂
                 CH₂                              |
                MeSiMe                           CH₂ ⎡Me⎤  Me
                  O              Me  ⎡Me⎤  CH₂ ⎡Me⎤  Me
              [Me₂SiO]ₓ—SiMe  MeSiO—⎢SiO⎥—SiO—⎢SiO⎥—SiCH=CH₂ ——————
                         H       CH  ⎣Me⎦x Me  ⎣Me⎦y Me
                                 CH₂
```

To another hydrogen
containing polymer
chain.

To another vinyl containing
polymer chain.

The ideal mixture would have an equal molar amount of silicon-
bonded vinyl and silicon-bonded hydrogen so that the desired con-
sistency is obtained at cure without excess vinyl or hydrogen re-
maining. Unfortunately, this idealized situation is very difficult
to achieve. Without exception, some of one or both will remain
unreacted. Even in the idealized case, not all vinyl and hydrogen
groups would be in a position to react with each other once cross-
linking began to restrict mobility of the polymer chains.

Uncured Properties

Many of the currently used products are two-part systems that re-
quire mixing to activate the cure mechanism. Some are mixed one-
to-one while others are mixed ten to one. Generally speaking, the
mixing ratio may be by weight or by volume. In the past few years
one-part gels which eliminate the need for mixing but make heat
curing mandatory have made their way into the market.
     All currently available systems are free flowing liquids
having viscosities as low as 300 and as high as several thousand
centipoise. In some cases high viscosity may cause interconnect
wire deformation, poor coverage under closely spaced flip chips,
and entrapment of air bubbles. On the other hand, the use of very
low viscosity products may lead to rapid creep of the fluid onto
land areas which will be used for lid sealing.

Cure Time and Temperatures

Room temperature curing two-part systems require from as little as twenty-four hours to as long as seven days to reach ultimate properties. In most cases heat is used to accelerate cure and to speed up the manufacturing process.

Cure times from a few minutes to hours are used at temperatures of 100° to 175°C. Times and temperatures are predicated on coating thickness as well as device type. Work reported by K. Otsuka et al. indicates that high temperature cures may improve device performance (6). In some instances, however, temperatures are limited by device construction; e.g., use of low temperature solders.

Purity And Cleanliness

Silicone gels intended for direct application to active semiconductor devices, especially VLSI's, are controlled for sodium, potassium and chloride content. Values range from one to two parts per million each, to as little as 0.1 part per million. Test methods can have an impact on the value quoted.

Needless to say, purity can affect device performance. If the coating is pure then it only stands to reason that the surface to which it will be applied must also be pure and clean. Anything coming between the coating and the surface will lead to poor performance. This is especially true when adhesion, whether physical or chemical, determines performance.

It is well known that most structures will have at least a monomolecular layer of moisture on their surfaces and in many cases, i.e., silicon, silicon dioxide, and aluminum, will also form surface hydroxides. K. Otsuka and co-workers observed that devices which were coated with gel and then cured at temperatures above the normally used 150°C had less corrosion of the chip pads and aluminum bonding wires when subjected to a pressure cooker cycling test. (6) An explanation for the observed finding is that at the elevated temperatures the silicon hydride groups had sufficient energy to react with the hydroxyl groups, thus dehydrating the surface and possibly forming some covalent bonds with the coated surface (X).

$$\sim\!\!\sim\!\!\sim MOH + HSi \sim\!\!\sim \longrightarrow \sim\!\!\sim\!\!\sim MOSi \sim\!\!\sim + H_2$$
$$\sim\!\!\sim HOH + 2HSi \sim\!\!\sim \longrightarrow \sim\!\!\sim SiOSi \sim\!\!\sim + H_2 \qquad (X)$$
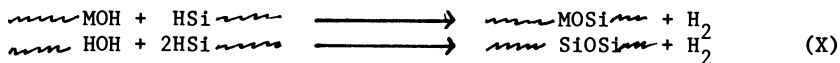
For this to take place, the surface presented to the gel must be clean and free of foreign matter so that the gel can attach itself to the primary surface. Recently reported work by P.R. Troyk, J. E. Anderson and V. Markovac further emphasizes the need for clean surfaces if ultimate performance is to be expected. (7)

Physical Properties

Cured Consistency. The hardness of these gels can not be measured by the normal methods used for elastomeric materials. Test methods for characterizing their physical properties are in various stages of development. The most commonly used technique to describe the gel's softness is the penetration test, which is emerging as a

standard. The method involves the use of a grease penetrometer, which is described in ASTM D217, modified by replacing the normal plunger mechanism with one weighing 19.5 grams. The plunger end is 3/16 inch long and 1/4 inch in diameter. To perform the test, the instrument is carefully lowered until the plunger tip just touches the top surface of the cured sample. The plunger is released and allowed to fall into the sample for five seconds. A reading is then made to tenths of a millimeter. The higher the reading, the softer the gel. Most gels have values of 3.0 to 8.0 millimeters, although some as soft as 20.0 millimeters are possible. Gels having values above 20.0 are edging close to becoming fluid at elevated temperatures.

Tests for other physical properties are more difficult to devise because of the sticky nature of gels. With great resolve we were successful in determining the tensile strength and elongation of a few gels having penetration values of less than 7.2 mm. Our objective was to determine if gels of approximately equal penetrations would yield similar tensile strength and elongation values. The determinations where made at 25°C using a Model 1122 Instron tester with a 500 gram load cell. Pull rate was two inches per minute. Apparent tensile strengths averaging 144 to 420 grams per square inch were found with elongations of 85 to 408 percent. (Table I) As can be seen by the results there is no clear relationship between penetration values and tensile strength or elongation. The differences in tensile strength and elongation noted between some samples may be due to the difficulty in preparing and handling the specimens; however, the high and low values must be considered real, and the difference due to formulation.

Continuing the search for other methods of characterizing gels using simple and easily available tools, we examined the utility of T pins used by upholsterers. The pins are T shaped and made of 44 mil diameter wire. They are available in various lengths; however the one used was 1.75 inches long. The T pin was centered and suspended in a 10 ml beaker which was then filled with a given volume of gel and cured. By means of a Model 4202 Instron tester, operating at a withdrawal rate of one inch per minute, the maximum force required to pull the pin through the gel was determined. In this case two other softer gels were also tested. The results, (Table I), ranged from 88 to 645 grams of force required to extract the pin. As can be seen, the gel having a penetration of 10.6 mm actually had more tenacity than two of the firmer gels. Again, this can be attributed to formulation. The values seem to follow reasonably well the determined tensile strengths.

While these tests contribute to our understanding of the physical properties of silicone gels, their significance is unknown. The use of the T pin test as a means of characterizing gels is uncertain. Its precision and reproducibility as well as the effect of pull rate have yet to be determined. The ultimate method of characterizing gels may be by using today's sophisticated precision rheometers. This work is in the planning stages.

Low Temperature Formulations. In some applications temperatures below -40°C may be encountered. Here it is important that the gel

TABLE I: PROPERTIES OF SOME SILICONE GELS

GEL NUMBER	PENETRATION mm	TENSILE STRENGTH GRAMS/SQ INCH	ELONGATION %	T PIN PULL NUMBER GRAMS
1	5.2	144	85	220
2	5.9	219	117	202
3	6.0	420	408	645
4	7.2	283	150	265
5	10.6	–	–	237
6	16.3	–	–	88

not crystallize and exert undue stress on small wire bonds. Gels
are available with crystallization temperatures below -65°C. This
is accomplished by interrupting the symmetry of the polydimethyl-
siloxane chain by preparing random copolymers of dimethyl and
methylphenyl or diphenyl siloxanes. Temperature transitions can be
readily measured by differential scanning calorimetry (DSC). Fig-
ures 1 and 2 show the observed differences between an all-dimethyl
polymer and one which is a dimethyl copolymer. As can be seen in
Figure 2 the all dimethyl polymer undergoes crystallization around
-43°C while the copolymer of Figure 1 only exhibits a glass
transistion at approximately -120°C.

Moisture Absorption. The water vapor permeability of silicone gels,
like silicone elastomers, is rather high. However, their moisture
absorption is quite low compared to many other polymeric materials.
We have measured water absorptions of 0.01 to 0.05% after 100 hours
at 65°C and 100% relative humidity. After 16 hours at 15 psi steam
while immersed in water, the up-take was found to be only 0.3 to
0.5%; again, low compared to other materials.

Electrical Properties. The electrical properties of silicone gels
are essentially the same as those of most clean, unfilled silicone
elastomers and fluids. Typical values for dielectric constant and
dissipation factor when tested at 25°C and 100 Hz are 2.7 to 2.9
and 0.001 to 0.002 respectively. Volume resistivity values, usu-
ally, fall in the 10^{15} ohm- centimeter range.

Conclusions

The use of soft silicone gels to protect non-hermetic as well as
some hermetic semiconductor devices is actively being pursued by
many investigators. The chemistry of silicone gels, which allows
alterations of physical characteristics to be made easily, along
with their electrical properties and purity make them prime candi-
dates for these investigations. Results to date would indicate
that gels may offer a reasonable way of achieving the desired re-
liability while holding down packaging costs.
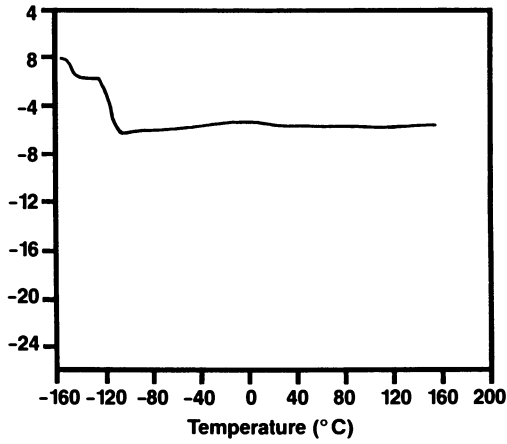
FIGURE 1:   DIMETHYL COPOLYMER.
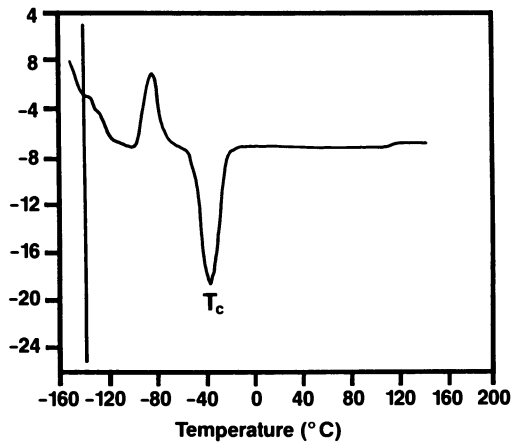
FIGURE 2:   ALL DIMETHYL POLYMER.

Literature Cited

(1) Otsuka, K.; Shirai, Y.; Okutani, K. IEEE Transactions on Components, Hybrids and Manufacturing Technology, 1984, CHMT-7, No. 3, 249.
(2) Miller, R. VLSI Packaging Workshop, 1985.
(3) Thomas, R. E. Proceedings of the 35th Electronic Components Conference, 1985, pp. 37 – 45.
(4) King, J. Proceedings 1985 International Symposium on Microelectronics; ISHM: Montgomery, AL, pp. 322 – 325.
(5) Sailer, E.; Kennedy, A., Electronic Packaging and Production, November 1966.
(6) Otsuka, K.; Takeo, Y.; Tachi, H.; Ishida, H.; Yamada, T.; Kuroda, S. IEPS Proceedings, 1986, pp. 720 – 726.
(7) Troyk, P. R.; Anderson, J. E.; Markovac, V. 1st International SAMPE Electronics Conference, 1987, pp. 590 – 601.

Chapter 21

Advantages of Silicone Gel for Packaging of Devices with Very Large Scale Integration (VLSI)

Kanji Otsuka, Hisashi Ishida, Yasuyuki Utsumi, Takashi Miwa, and Yuji Shirai

Device Development Center, Hitachi Ltd., 2326 Imai, Ome-shi, Tokyo 198, Japan

A silicone gel provides very good adhesion without any stress, with reliability of the VLSI package being very high. A coarse network structure with soft characteristic of the gel allows the less solibility, higher diffusion rate and higher temperature dependence of water molecules in it. In this report, the conditions which induce the water condensation in the silicone gels were investigated during a particular dynamic temperature change. Water immersion with saturated water in high temperature and steep cooling were the water condensation conditions. Any natural environmental changes in air were no problem.

Plastic molded packages have difficultly in achieving high reliability, because molded plastics induce stresses in the structure due to their hardness. In contrast to this, a silicone gel which is a methyl-phenyl siloxane group polymerized by a vinyl group inherently provides very good adhesion without any stress, with subsequent reliability of the VLSI package being very high. The adhesion is made by forming cross-linked molecules even in the presence of water adsorbed on the wafer surface (1). The significant characteristic of silicone gel is its ability to stay soft from temperatures as wide as minus 60 to plus 150° C. The structure of this soft gel has been found to be a coarse network structure impregnated with fluid silicone oil, a mixture with a wide variety of molecular weights and which includes a phenyl-group as reported in a previous paper(2). An earlier investigation (3) also reported that sufficient bond strength between the silicone gel and the surface of the chips or packages could be obtained during a gel curing process of 175°C for 1 hour (3). The interfacial structure would change from a hydrogen bond to a covalent like bond. Water and contaminants cause no attack on the interface because of the strong bond.

In general, to predict LSI field life, preliminary accelerated environment tests have been made such as temperature cycles, pressurized cooker test, soldering test, centrifuge test etc. Dynamic changes during these tests cause some phase separation in the gel due to the coarse network structure. The changing rates of change of field conditions are less than those of accelerated tests. Consequently, the accelerated tests do not represent the field life, because accelerated tests induce failures due to different mechanisms. In order to investigate degradation of the interface due to void formation throughout the gel caused by dynamic environment change, the water absorbance, degas characteristics and penetration rate of water have been examined by specific methods (4).

The full relationship between the reliability and the encapsulation mechanism need to be clarified for better understanding. The goal of these investigations was to further explore the effects of subjecting the system to a dynamic changing environment through which possible external water or swelling reagents get into the gel and migrate through the gel to the interface.

Absorption and Diffusion Constant of the Gel.

First of all, the study must clarify the behavior of the gel in liquid materials during temperature changes. Figure 1 shows the liquid absorbing rate of the gel. A significant weight increase was observed in freon immersion. However, only a slight weight gain was observed for samples with water immersion. Our interpretation is that the segments of the gel network have a lot of oil attracting groups, but are only slightly water attracting. These interpretations are supported by results which show that the gel oligomer is soluble in the freon and fluorinert, but is insoluble in water.

Diffusion constants were obtained from the profiles of Figure 1 using the following equations derived from Fick's law for the case of the plate shape

$$\frac{Qt}{Qs} = \sum_{n=0}^{\infty} \frac{8}{(2n+1)^2 \cdot \pi^2} \left(1 - \exp\left(\frac{-(2n+1)^2 \cdot \pi^2}{d^2} \cdot D\, t\right)\right) \tag{1}$$

Approximations are as follows:

$$\frac{Qt}{Qs} = \frac{2}{\sqrt{\pi}} \cdot \sqrt{\frac{Dt}{d^2}} \quad , \qquad \frac{Dt}{d^2} < 0.555 \tag{2}$$

$$\frac{Qt}{Qs} = 1 - \frac{8}{\pi^2} \exp\left(-\pi^2 \cdot \frac{2\,Dt}{4\,d^2}\right) \quad , \qquad \frac{Dt}{d^2} > 0.555$$

Here Qt is absorbed weight of water at a time t, Qs is the weight of water at saturation, d is gel thickness, and D is the diffusion constant. Figure 2 shows diffusion constants and their temperature dependence. Many data are plotted on this graph. Fluorinert and freon immersion samples were significantly swelled by their liquids. Swelling behavior would have an effect on the diffusion coefficients due to induced stresses on the gel networks. These test values contained relatively large errors. The immersion tests at 44°C for freon and at 140°C for fluorinert were also done.
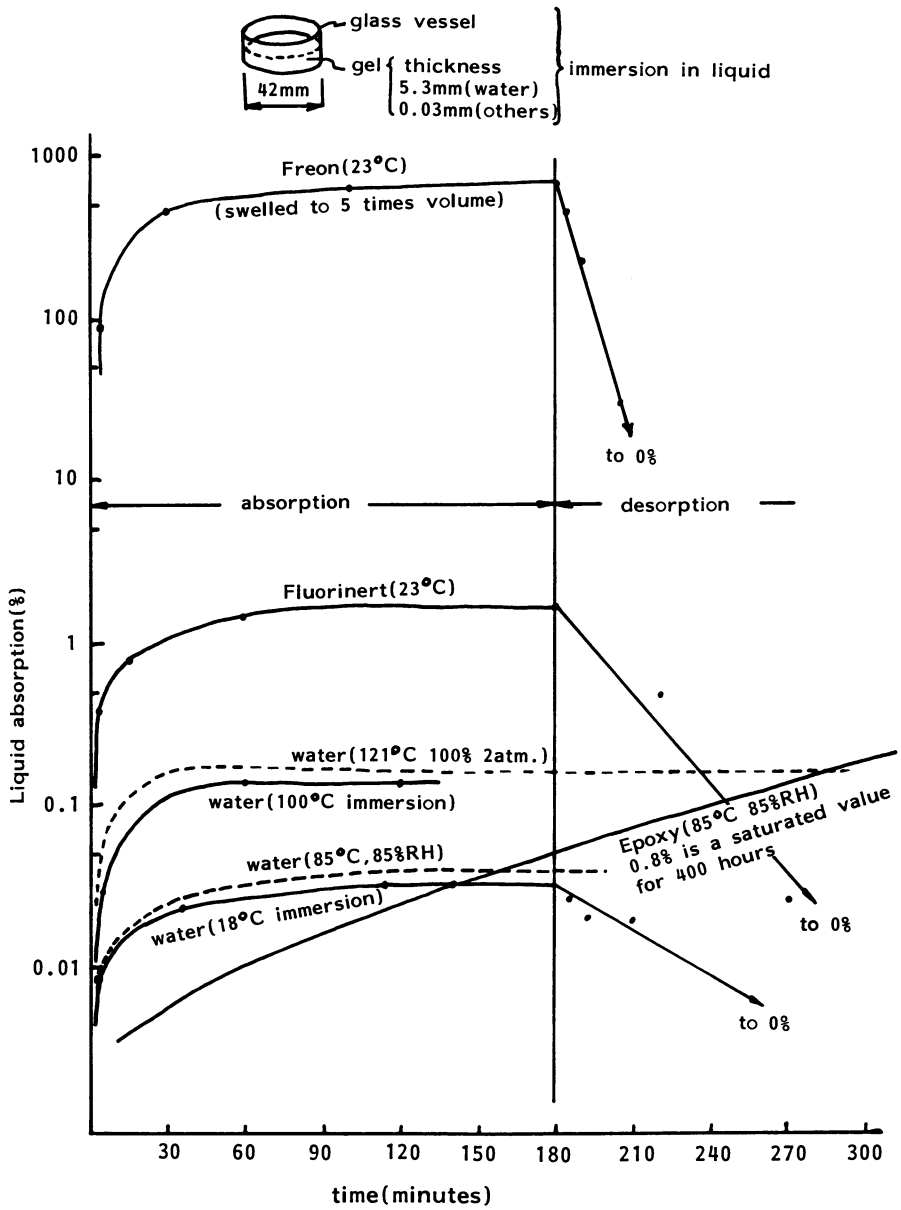
Figure 1.   Relation between the Liquid Absorbance of the Gel
and Soaking time .
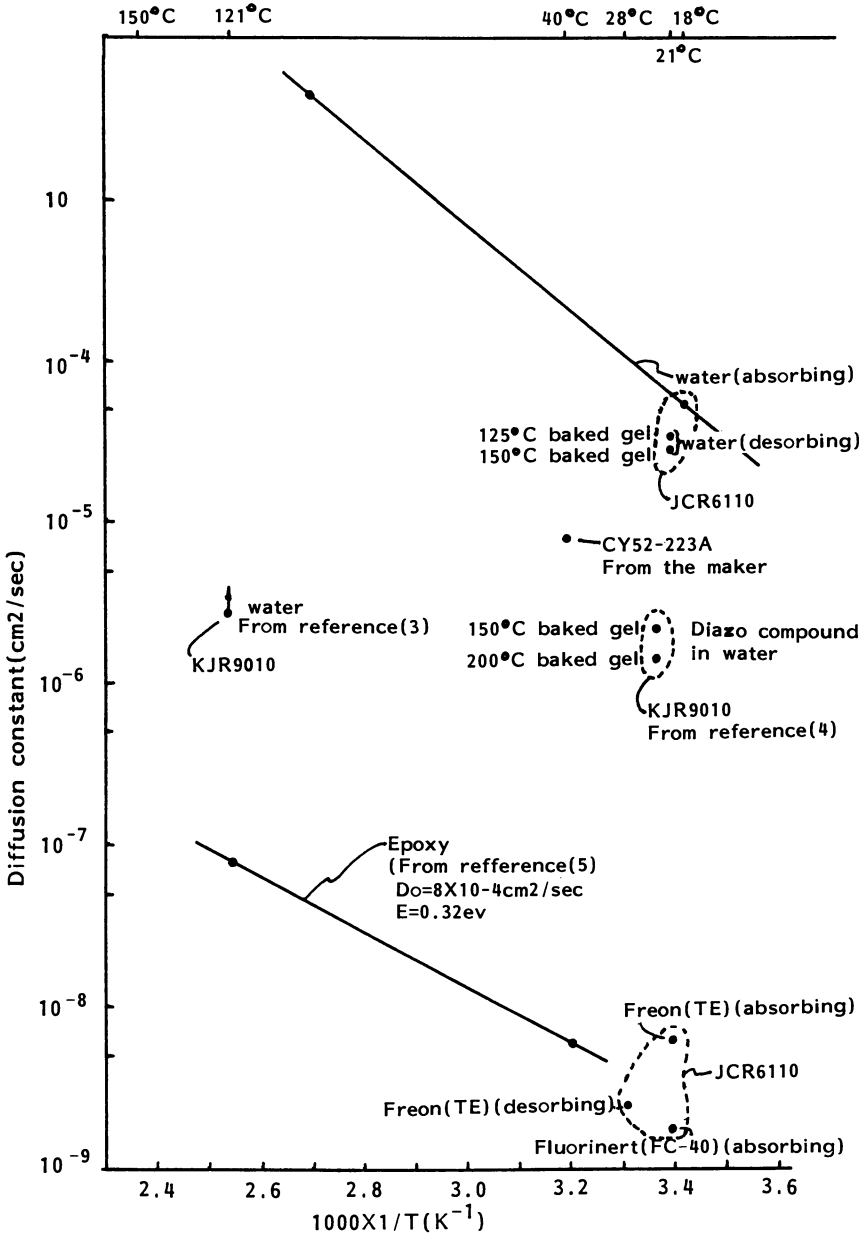
Figure 2. Diffusion Constants and the Temperature Dependence for the Silicone and Epoxy Systems.

However, these data were rejected from Figure 2 because of the dissolving of gels in the liquids.

The activation energy determined from water absorbing rates at 18°C and 97°C could be derived by following equation.

$$D = Do \exp(-E/RT)$$

$$Do = 4 \times 10^4 cm^2/sec \qquad E = 0.51 ev \qquad (3)$$

The water diffusion constants in silicones were much higher than in the other solid. Diffusion in the silicone elastomer was five orders of magnitude greater than that in the epoxy(5). Liquid molecules diffused easily into silicones, and the desorbing rates were also high. The solubility of water in the silicones was less than that in the epoxies. An activation energy of the silicone was higher than that of the epoxy in water, which means higher temperature dependence. The less solubility, higher diffusion rate and higher temperature dependence of water in silicones can possibly lead to a saturation condition during a particular dynamic temperature change, which induces the water condensation or water vapor voids in the silicones and interfaces.

Effects of Steep Temperature Changes on the Gel

Diffusion depth x is given by a typical solution of Fick's law as shown in follows:

$$Qt = Qs \, erfc(x/2\sqrt{D \cdot t}), \quad t \to 0, \quad Qto = Qo = 0$$

$$x = 2\sqrt{D \cdot t} \, erfc^{-1}(Qo/Qs) = 2\sqrt{D \cdot t} \qquad (4)$$

Equivalent time (τ)(sec) of water penetration through the gel coating thickness (d) (cm) is obtained by combining Equations (3) and (4).

$$\tau = \frac{d^2}{4Do \exp(-E/RT)} \qquad (5)$$

where d is diffusion path length (cm). If the cooling time (t) for a change in ΔT(differential temperature) is shorter than the time (τ) of diffusion through the gel coating thickness at the temperature, namely, $\quad t < \tau$

water in the gel becomes over-saturated and condenses in the gel. Therefore, a non-condensation condition should be that

$$t > \tau \qquad (6)$$

Thinking about the equation (6) on differential temperature change,

$$\frac{T}{t}\bigg|_{T \to T - \Delta T} < \frac{T}{\tau}\bigg|_{T \to T - \Delta T} \qquad (7)$$

$$\frac{dT}{dt} < \frac{\Delta T}{\Delta \tau} = -\frac{1}{d\tau(T)/dT} = \frac{RT^2}{E} \cdot \frac{1}{\tau}$$
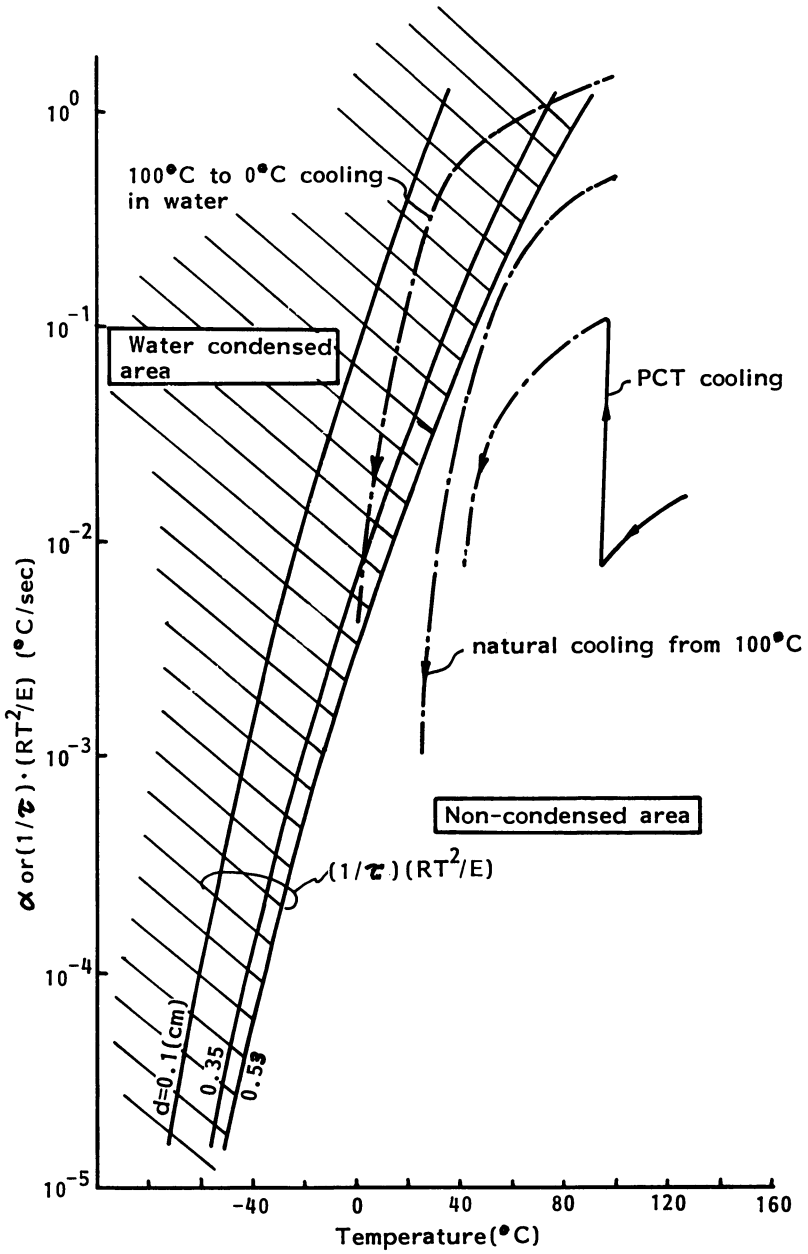
Figure 3. Water Condensation Condition in the Gel under Dynamic Temperature Change.

After 24 hours

After 10 minutes
(the grid again
can oe seen)

Gel changing to milky
(Condensed water bubbles
make it milky)

Quenched
from 100°C
to 0°C in
water

Natural cooling from 100°C

Gel in glass vessel after
30 minutes in boiling water
=

The grid under the vessel
can be seen through the
transeparency gel
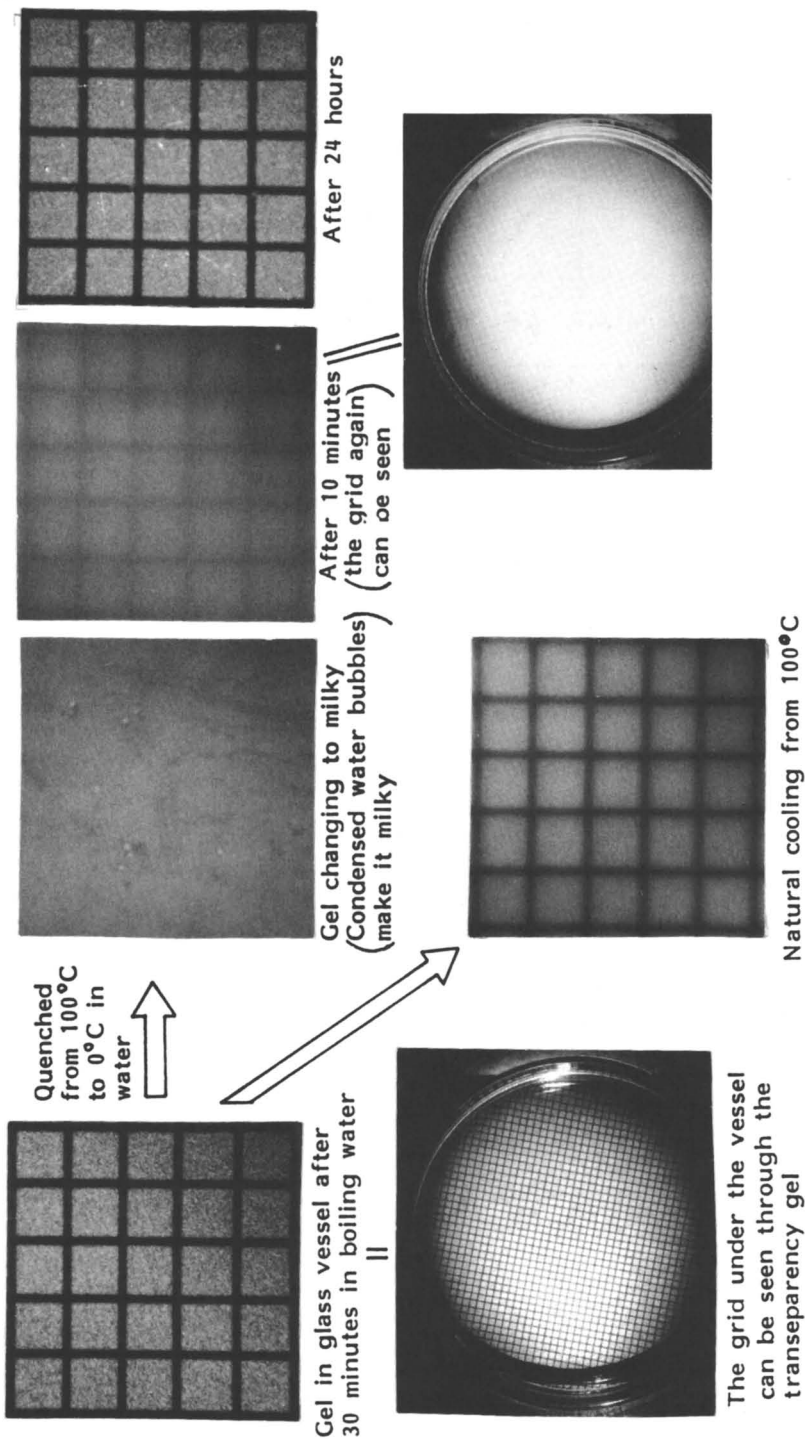
Figure 4.   Changing appearance of gel at quenching.

$$\left[\begin{array}{l}\text{Rearranging Equation (5) gives:} -\dfrac{E}{RT} = \ln\dfrac{d^2}{4D_o} - \ln \tau \\[2mm] \text{Differentiating the above equation} \\ \text{with respect to temperature gives:} \dfrac{E}{-RT^2} = \dfrac{1}{\tau} \cdot \dfrac{d\tau}{dT}\end{array}\right]$$

The most severe condition requires:

$$\left(\frac{dT}{dt}\right)_{max} = \alpha_{max} \ < \ \frac{RT^2}{E} \cdot \frac{1}{\tau} \tag{8}$$

where α is a cooling rate(K/sec).

Figure 3 shows the relation between $1/\tau$ or α and T . The hatched area is the water condensed condition for a gel 5.3 mm thick. The same region for an epoxy is positioned five orders of magnitude lower than that of silicone gel. Silicone gels easily reach a saturation condition of water; it is important to change temperature slowly to avoid saturation. The 3.5 mm thickness silicone gel was immersed in boiling water for 30 minutes which was a saturation condition. After that it was transfered to the $0\,^\circ$C water reservoir, the subsequent gel temperature decreased $2\,^\circ$C in 5 minutes. The cooling rate α is shown in Figure 3. The α for the entire temperature range lies in the area for the water condensation condition. Our test resulted in water bubbles in the gel, as shown in Figure 4. Pressure cooker test also caused bubbles. This α does not lie in the water condensation area, as shown in Figure 3. However, the pressure change had a maximum changing rate of 0.1 atm/sec. From any temperature cycle tests in air (such as $150 \leftrightarrow -55\,^\circ$C, max rate $0.8\,^\circ$C/sec) no water bubbles were found in the gel, because the gel was not in the saturation condition in any temperature range. From these results, any nearly natural environmental changes would not induce any problems of condensation.

Conclusion

Silicone elastomer has characteristics of softness that originate from the coarse network structure. This allows for high diffusion rates of several different liquid molecules. As the saturated absorption of the liquids changes with the environmental changes, the environmental changing rate should be kept less than the diffision rate of the liquid molecules in the elastomers, especially gels, to prevent liquid condensation. In the temperature changes, a $1/\tau$ relation was derived in this study. Borderline conditions occurred for pressurized cooker test cooling with saturated water in $121\,^\circ$C and steep cooling to room temperature, and water immersion test with saturated water in $100\,^\circ$C and steep cooling to room temperature. Any natural environmental changes in air were no problem.

Acknowledgment

Literature Cited

1. White, M.L. *Proc. IEEE*, 1969, *57*, pp 1610-15.

2. Otsuka, K.; Shirai, Y.; Okutani, K. *IEEE Transaction on CHMT, 1984, CHMT-7*, pp 249-56.

3. Otsuka, K.; Takeo, Y.; Ishida, H.; Yamada, T.; Kuroda, S.; Tachi, H. *IEEE Transaction on CHMT*, 1987, *CHMT-12*, pp 666-71.

4. Ishida, H.; Nakata, K.; Otsuka, K. *Proceedings of 38th Electronic Components Conference*, 1988, pp 452-6.

5. Nishimura, A.; Tatemichi, A.; Miura, H.; Sakamoto, T. *Proceedings of 37th Electronic Components Conference*, 1987, pp 477-83.

Chapter 22

Modeling of Triple-Track and Comb-Pattern Leakage Current Measurements

Philip R. Troyk[1], David Conroy[1], and James E. Anderson[2]

[1]Illinois Institute of Technology, Chicago, IL 60616
[2]Ford Motor Company, Dearborn, MI 48121

This research investigates the theoretical predic-
tion of electrical leakage currents for tempera-
ture-humidity-bias (THB) tests. An electrostatic
finite element model was developed for triple-
track and comb patterns. Using known values for
volume resistivity combined with a specific test
pattern geometry, a prediction of leakage currents
can be made. The model can be used to compute the
leakage current for samples in which polymer-
substrate interfacial currents are negligible thus
predicting leakage currents for samples which
would be expected to pass THB testing.

Electrical leakage currents as measured on interdigitated-comb and
triple-track patterns are frequently used to estimate failure rates
for polymeric-encapsulated integrated circuits (1-8). The geometry
of the patterns enhances the opportunity for corrosion of the metal-
lization. Corrosion occurs as the result of electrochemical reac-
tions between the two halves of the patterns. The rate of corrosion
is usually estimated by the measurement of electrical current flow-
ing between the oppositely biased halves of the pattern. The sam-
ples are exposed to environmental conditions of high humidity and
temperature designed to accelerate the deterioration of the inter-
face between the polymer and the substrate, subsequently resulting
in corrosion of the unprotected circuitry.
    The measured value of D.C. leakage current under accelerated
temperature-humidity-voltage-bias (THB) conditions is a function of
the volume resistivity of the substrate and the volume resistivity
of the polymer as well as the surface resistivity at the polymer-
substrate interface. Frequently used THB conditions are 85° C, 85%
RH. In previous work it has been assumed that the lower the meas-
ured leakage current demonstrated by a particular polymer, the
longer the time-to-failure. Reported values of initial leakage
currents under "dry" conditions range from <0.5pA to as high as
100nA. It has been commonly regarded that the volume resistivity of

the polymer, being an indication of its ionic impurity level, can influence leakage currents under wet conditions and that it is desirable to use a polymer with as high of a volume resistivity as possible. Typical values of volume resistivity might range from 10^9 ohm-cm (low) to 10^{15} ohm-cm (high). Comparisons of data between different studies have been difficult due to the use of a variety of different comb and track geometries as well as different bias conditions.

It is theorized that electronic encapsulants function by preventing the condensation of water on the surface of the coated device. The precise mechanisms by which water is prevented from condensing at the polymer-substrate interface are not known. Based, in part, upon the initial theories by White (9) electronic encapsulants are assumed to function by reacting with substrate hydrophilic surface sites, thus preventing interfacial water condensation. Water diffusing through the polymer finds no available sites with which to react, and the electrical leakage currents flowing between the metallization paths are restricted to the active circuit, the substrate, or the bulk polymer coating. Keeping the substrate surface "dry" and free from an electrolytic solution prevents electrochemical reactions from corroding the metallization. Strong interfacial bonding is required between the polymer and the substrate, and none of the measured leakage current is assumed to flow along the polymer-substrate interface. The precise relationship between leakage currents and polymer substrate bonding are not known. However, the onset of a sudden increase in the value of the measured leakage current implies that the bond between the polymer and the substrate has been lost, and that failure is imminent. Materials which perform poorly in THB testing are assumed to fail as a result of interfacial water-induced electrochemical reactions. Ionics present at the interface as a result of poor pre-encapsulation cleaning, or polymer contamination are assumed to participate in this process by providing an "ionic-pool" at the interface which accelerates the electrochemical attack.

From the standpoint of measurements of leakage currents it would be desirable to be able to predict the value of total leakage current which would flow in an encapsulated sample with a given electrode geometry and known material volume resistivities. Assuming that an encapsulant indeed protects a substrate according to the interfacial bonding theory and that little to no interfacial current flows, then the measured value of leakage current should be predictable from a knowledge of the substrate and polymer volume resistivities and the specimen geometry. For an encapsulated sample, with good interfacial bonding, the leakage current should be restricted to flowing through the insulating substrate and the polymer coating. Leakage current predictions could be accomplished by solving Laplace's equation for the geometry of interest, using appropriate values of substrate and polymer volume resistivities.

Modeling Techniques

The theoretical prediction of the leakage current requires the solution of Laplace's equation and a closed-form solution for an arbitrary geometry is not straight-forward. The finite-element method (10) can be used to obtain a numerical solution to Laplace's

equation for complex geometries and varying materials constants. A
model of a triple-track or comb pattern can be developed using a
number of available finite-element software packages. A computer
graphic-generated region duplicating the geometry of the metalliza-
tion pattern is created, and a mesh of elements, square or triangu-
lar, is then superimposed over this region. By setting known volt-
age constraints at the fingers of the computer model for the comb or
triple-track, a solution for the electric field can be obtained over
each element within the region. The current flowing between the two
halves of the pattern can be computed by defining an appropriate
contour and performing vector calculus operations on the mesh volt-
age nodal points.

     The PC-AT-based version of MAGNET (Infolytica) was used to
develop a finite-element model of triple-track and comb patterns.
The model used two infinitely-long strips, which correspond to a
section of the sample through the substrate (Figure 1). This per-
mitted accurate modeling in the direction perpendicular to the
substrate. Thus, the effects of substrate thickness and resistivi-
ty, as well as encapsulant thickness and resistivity could be mod-
eled. In addition, the effect of a layer of condensed water on the
surface of the encapsulant could be investigated. Computer "meas-
urements" of leakage current were made by defining a 128-point
contour of integration (Figure 1, line A-A) through which the cur-
rent normal to the contour was computed. This computation was made
using the powerful MAGNET vector-calculus post-processor, after
computing the electric field distribution. For this study, values
of constant material resistivity were used. However, the program
readily accepts material constants which are voltage sensitive.
Physical measurements on samples which closely approximated the
computer models were made using a Keithley 617 electrometer con-
trolled by an HP Vectra computer.

     The region and mesh were made versatile enough to permit
adaptability to several different pattern geometries and voltage
constraints. Each of the electrode strips was divided into 10
segments in order to examine the effects of pattern spacing and line
widths. By constraining the voltage of different segment combina-
tions, the effective width of the comb lines as well as their spac-
ing could be easily modified. The "encapsulant" portion of the
region was also predivided into smaller sections so that the effects
of different encapsulant thicknesses could be investigated. By
changing the volume resistivities of the individual sections, the
effective encapsulant thickness could be made thicker or thinner,
and the outer medium could be changed from air to water.

     The mesh, shown in Figure 2, consisted of 5395 elements, and
2784 nodes. The need for a large number of elements was a conse-
quence of the use of a first-order solver. Presently we are inves-
tigating the use of high-order (up to 4th order) solvers and possi-
ble mesh size reductions. The density of the mesh is highest in
those areas which require the finest detail, and consequently the
largest number of nodes: along the current contour, and around the
metal electrodes. For this model, the electrodes were assumed to be
of zero thickness. There are two reasons for this simplification:
First, comparisons between zero and finite thickness electrodes
produced near identical results; second, for the modeling of inte-
grated circuits with metallization thicknesses on the order of tens
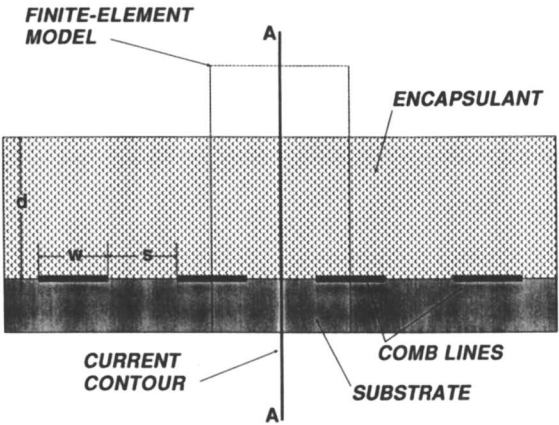
Figure 1. Finite-element model for comb pattern.
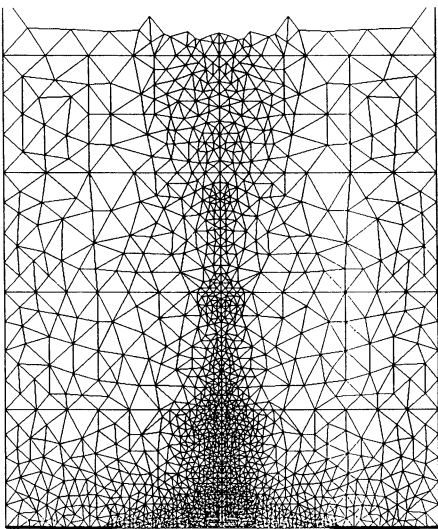
Figure 2. Finite element mesh.

to hundreds of angstroms, the approximation seemed valid, and re-
sulted in a simpler mesh containing fewer elements.

Leakage current normal to the contour A-A was computed, re-
sulting in a prediction of the total current, the current distribu-
tion, and the running current integral throughout the substrate,
encapsulant, and within the surrounding medium. The total current
for any portion of the contour was found by integrating along seg-
ments of the contour. In this way the percentage of leakage current
flowing within the substrate, encapsulant, or outer medium could be
determined.

Postprocessing of the MAGNET data was done using a spreadsheet
which permitted greater data manipulation flexibility. Scaling of
the results from simulations which used relative dimensions, produc-
ing curves useful for absolute dimensions, was quick and accurate.

Experimental Results

The initial model used a large encapsulant-thickness (d) to pattern-
line-spacing (s) ratio (d/s >20). The area of the model correspond-
ing to the encapsulant was assumed to be of uniform volume resistiv-
ity. This was done to minimize the effects of encapsulant thickness
on the solution. Total currents were best expressed as
amperes/centimeter of pattern line length, a consequence of our
cross-sectional model. A comparison was made between the absolute
value of leakage current measured for a triple-track configuration
as opposed to an interdigitated comb.   The currents per cm of line
length for the triple-track were within computation error of the
values found for the comb in several test cases.   Therefore, we used
the comb configuration for most of our computations. A typical
equipotential plot is shown in Figure 3.

The effects of constant line-width (w) with increasing line-
spacing (s) were examined. Resistivity values for the substrate and
encapsulant were 1×10^{17} and 1×10^{15} ohms-cm respectively. These
values were chosen to be representative of typical electronic mate-
rials. The outer environment was assumed to be dry air with a
resistivity of 1×10^{15} ohms-cm and the bias voltage was 1 volt.
Figure 4 shows a non-linear relationship between leakage current and
the line-spacing-to-width ratio (s/w). As the line-spacing (s) was
increased, while keeping the line-width (w) constant, the total
computed current decreased. The points were fitted to an inverse-
power relationship of the form: $I=(A)((s/w)^{-b})$ with I being equal to
the current in pA/cm line length. This fitting produced constants
of $a=5.33 \times 10^{-4}$ pA/cm and $b=0.323429$, and this equation is also
plotted in Figure 4. In contrast, the constant value of 5.36×10^{-4}
pA/cm was found for all computer runs with s/w=1. For s/w=1, the
line-spacing was equal to the line-width, as both were increased.
This shows that for s/w=1 that total leakage current is independent
of the track or comb spacing.

An experimental verification of this "constant-current" concept
was accomplished by measuring the leakage current for IPC-25 combs
of spacings and line-widths of 150um, 300um, and 600um. The combs
were submersed in uncured polysiloxane (with a volume resistivity
significantly lower than that of the cross-linked polymer) which
permitted current measurements in the range of 100 to 500 pA.
Allowing for geometrical differences in the combs caused by edge
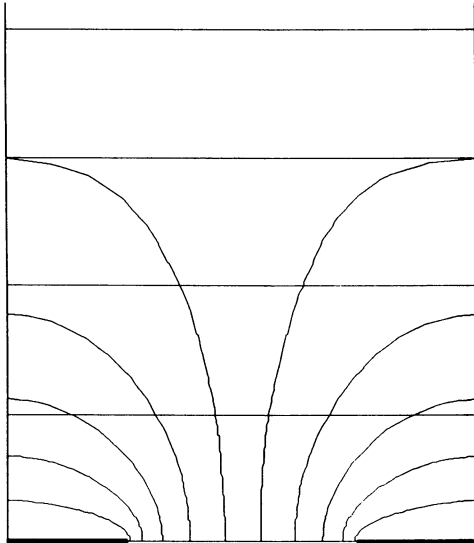
Figure 3. Typical equipotential plot.
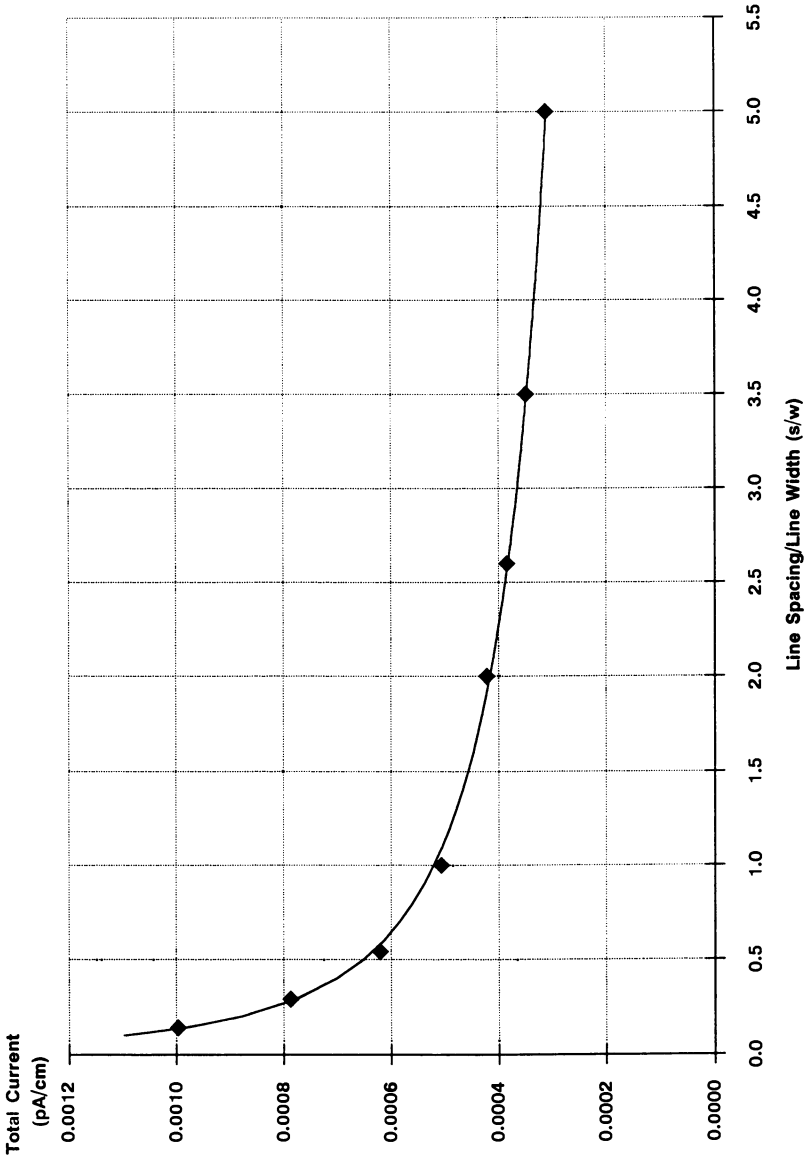
Figure 4. Total current vs. line spacing/line width for p = 1E15, bias = 1 VDC.

effects the ratios of currents for the different combs matched the predicted values by greater than 90%.

Next we examined the profile of current within the encapsulant and the effect of volume resistivity. As expected for a non-voltage dependent value of volume resistivity, the leakage current linearly scaled with encapsulant volume resistivity. The effect of the substrate was minimal in our model since its resistivity was at least 100 times greater than that of the modeled encapsulants. The profile of the leakage current and its running integral for s=10 mils, s/w=1, as computed along the contour A-A, from 0 (the polymer-substrate interface) to d/s=5 is shown in Figure 5. Note that for s/w=1, as the spacing (s) between the comb lines is increased, the current distribution becomes more diffuse in the encapsulant. This can be seen more clearly in Figure 6 which shows a running integral of the current as a function of the distance from the substrate for different line-spacing/widths. Note that for 75um line-width and spacing, that 99% of the current is contained within the 200um of encapsulant which is closest to the polymer-substrate interface. This also suggests that for encapsulant thicknesses less than 200um, the condition of the polymer-environment interface, i.e. the outer medium, may affect the predicted leakage current.

This effect of the outer medium upon the leakage current was investigated by setting the resistivity of selected portions of the region to that of pure water. Since the resistivity of water is more than 7 orders of magnitude lower than that of the encapsulant, virtually no electric field lines leave the sample. However, due to the relatively low value of the water's volume resistivity, significant amounts of current may flow within the water. Figure 7 shows the electric field distribution for a thin encapsulant (s/d=2.00) with external water. Figure 8 qualitatively shows the distribution of current within the encapsulant and the water , compared with that of a thick encapsulant layer (Figure 9). The arrows depict the magnitude and direction of current flow, with the size of the arrow related to the magnitude. Figure 10 shows the computed distribution of current along the contour A-A for a sample with an encapsulant (d) of 5 mils, and a line spacing (s) of 10 mils. Note that for this case the majority of current flows within the water layer. Figure 11 shows the percentage of the total current contained within the outer water for a range of 0.5< d/s > 2.5. Although not seen on this plot, the magnitude of the total current did not significantly change, however for d/s<0.8, less than 1/2 of the total current actually flows in the encapsulant.

Discussion

The most striking feature of all of the plots in Figures 4-10 is the magnitude of the leakage currents. The model predicts leakage currents which are significantly lower than those frequently reported. For example, the 75um triple-track used by previous investigators ($\underline{1-3}$) has a total track length of approximately 40 cm. For DC-648 (Dow Corning) the manufacturer reports a volume resistivity of 191×10^{15} ohms-cm, or 200 times the value used in our model. This suggests a total leakage current of $(5.36 \times 10^{-4}$ pA/cm)$\times$(40 cm)/200 which equals approximately 1×10^{-4} pA/volt. For the 180 volts used for the bias, a total current of approximately 0.018pA should be

All Silicone Insulation
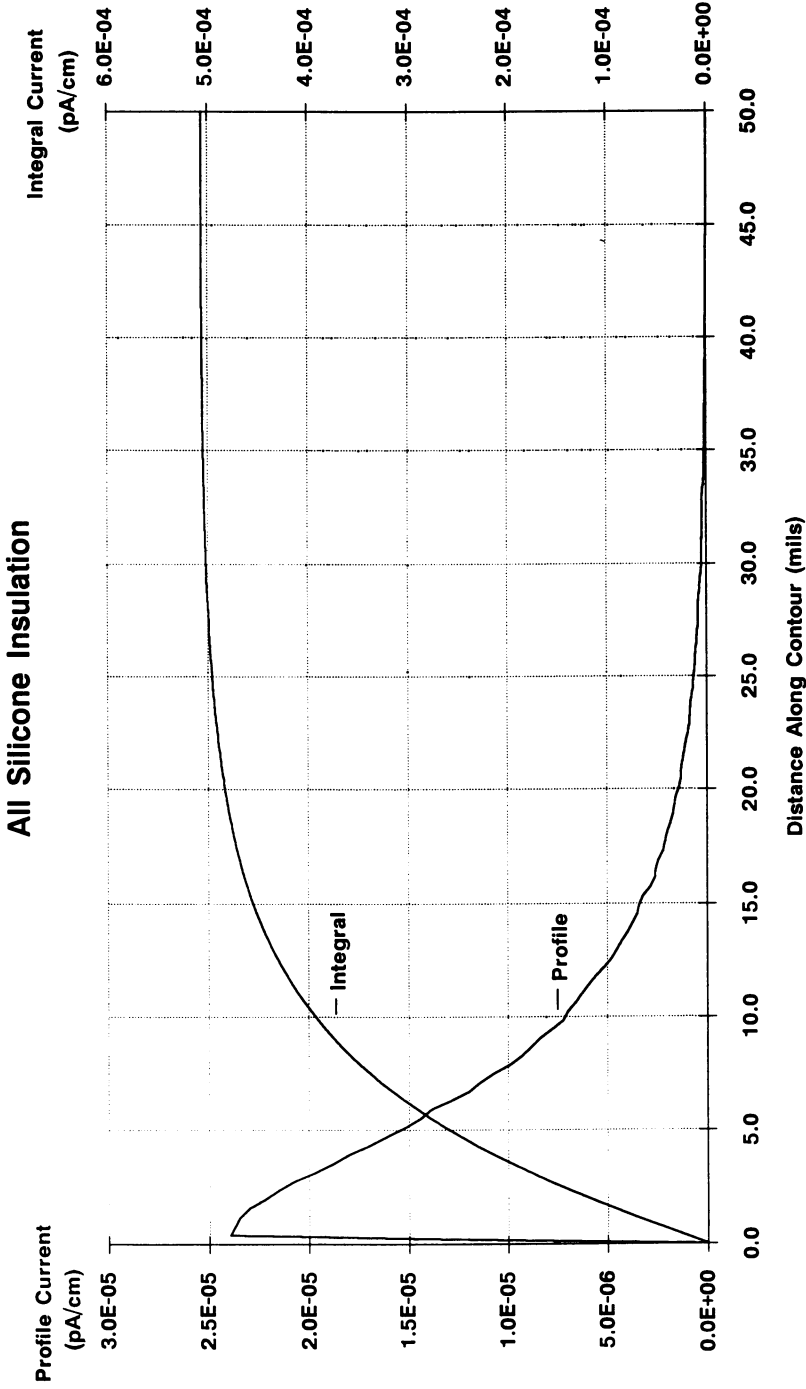
Figure 5. Polymer current profile and running integral of current for s/w = 1.
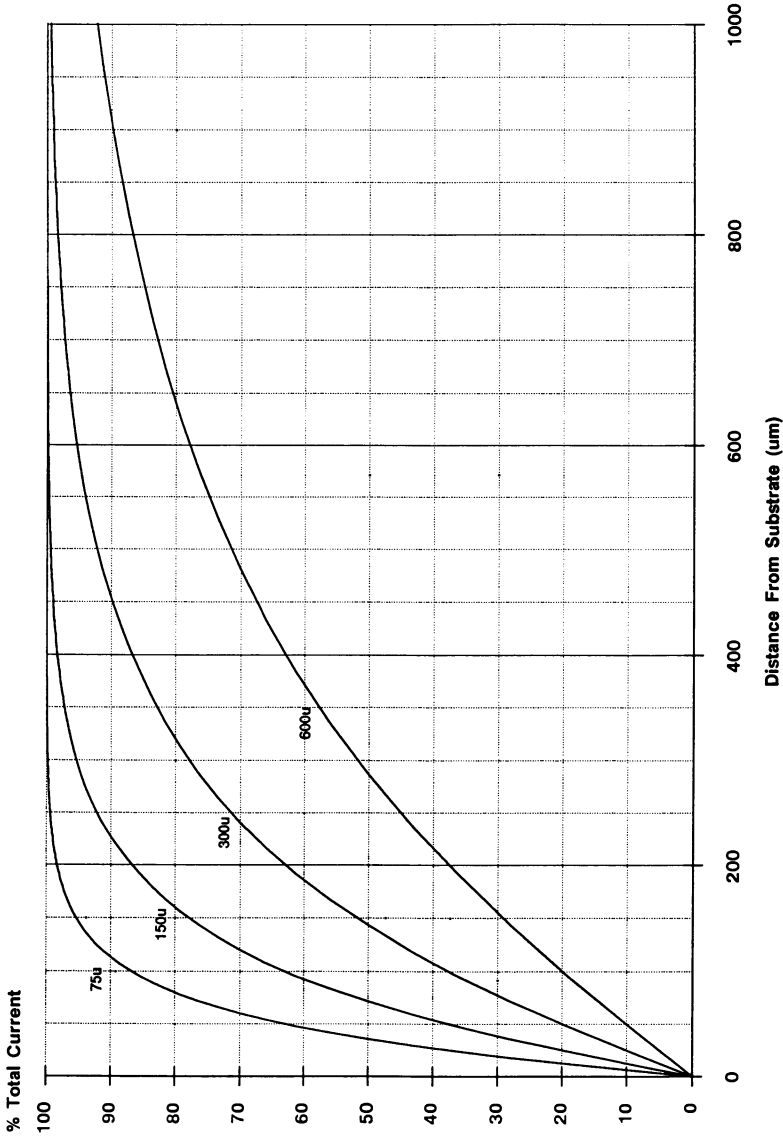
Figure 6. Percent total current vs. distance from substrate for different s.
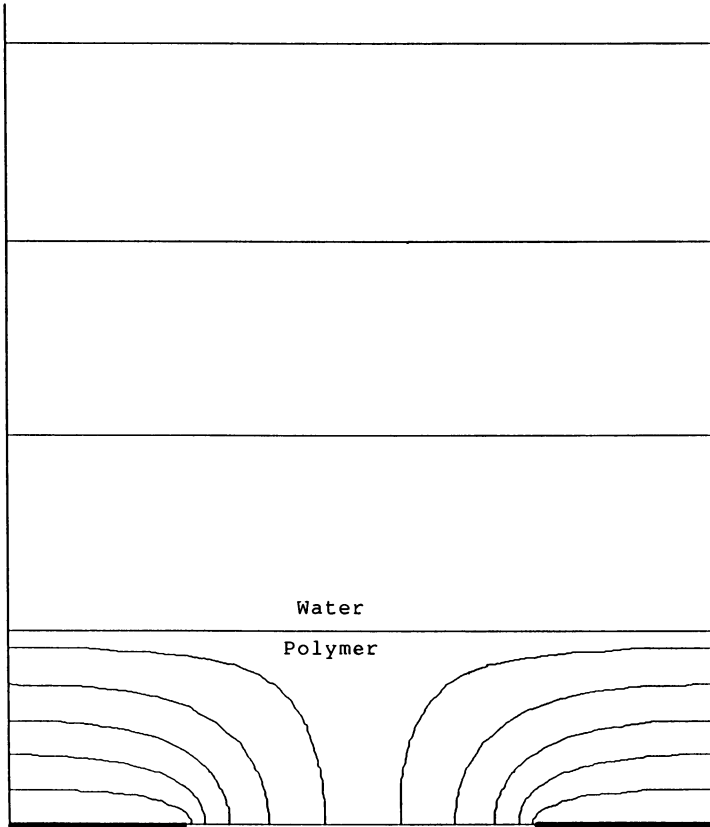
Figure 7. Electric field distribution for a thin encapsulant covered with an outer layer of water.
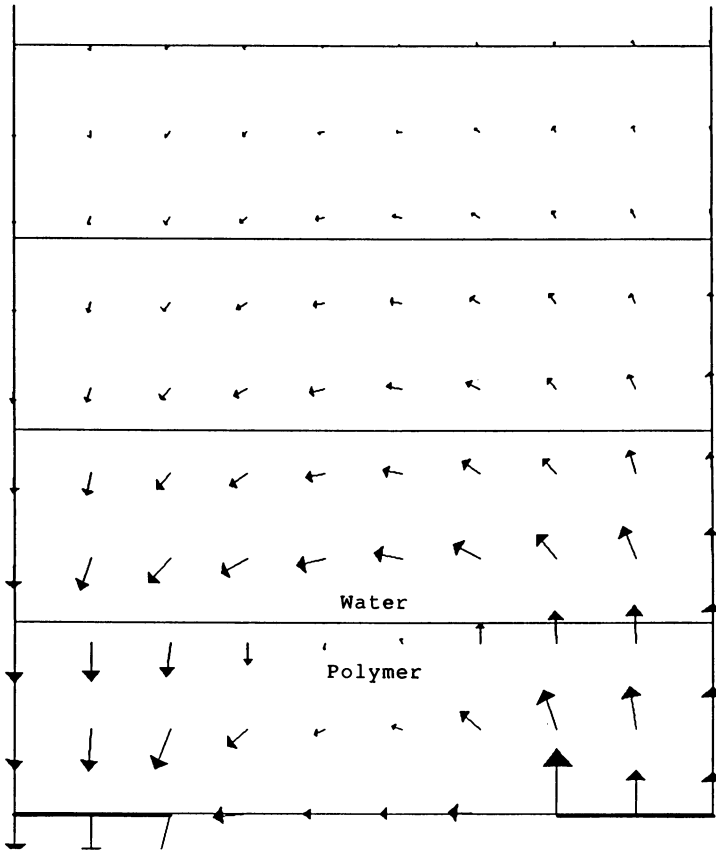
Figure 8. Distribution of current for the sample of Figure 7.
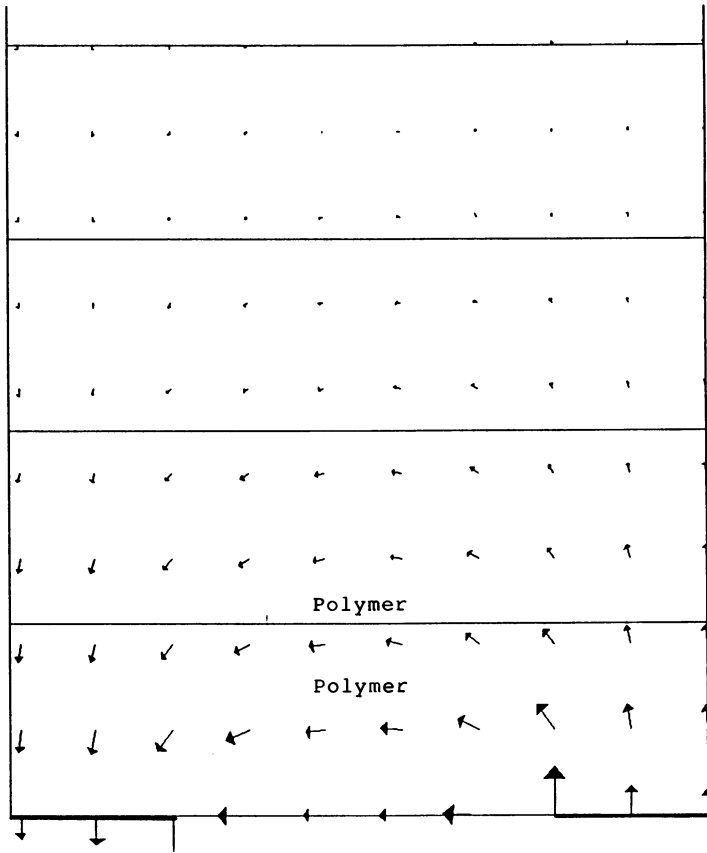
Figure 9. Distribution of current for a thick layer of encapsulant.

s/d=2.00
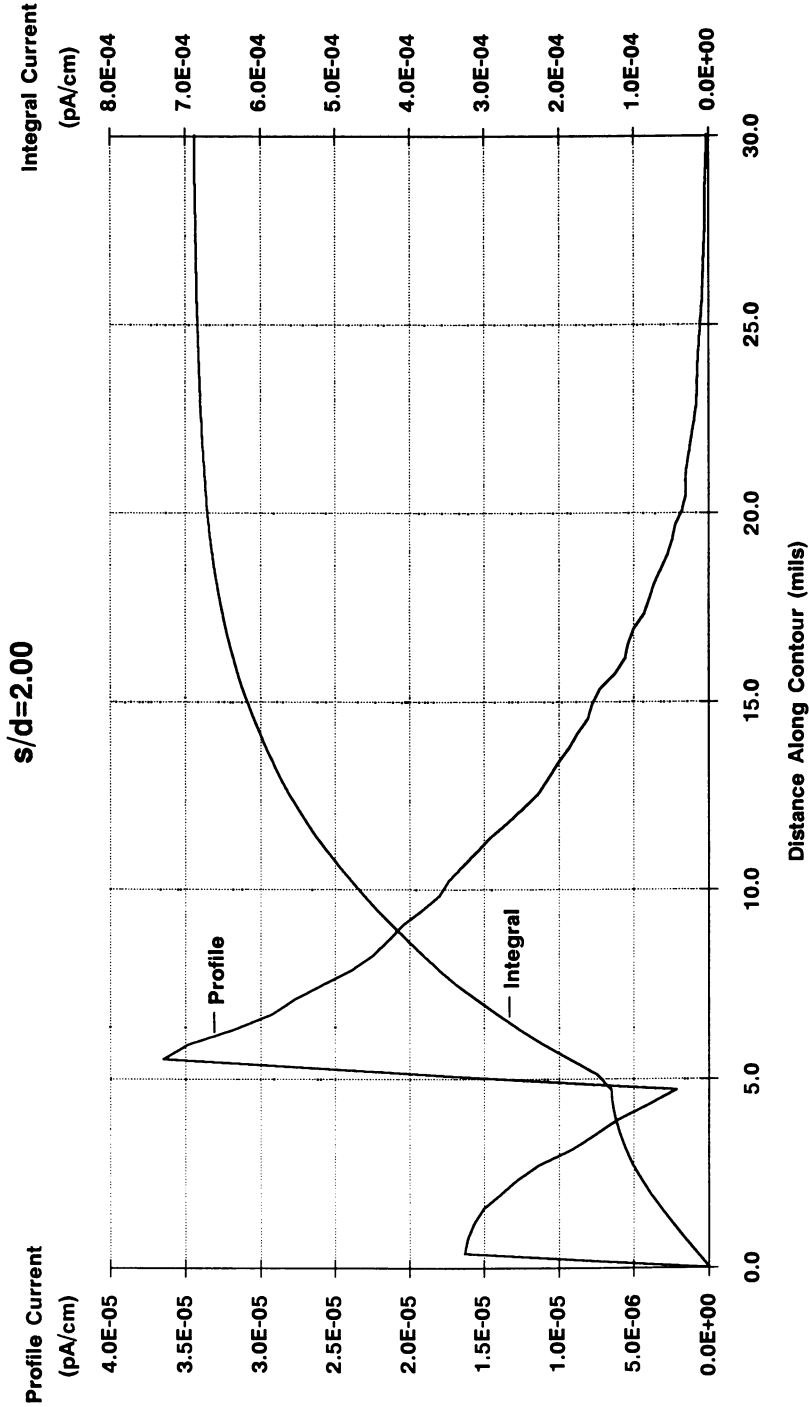
Figure 10. Current integral and profile for sample of Figure 7.
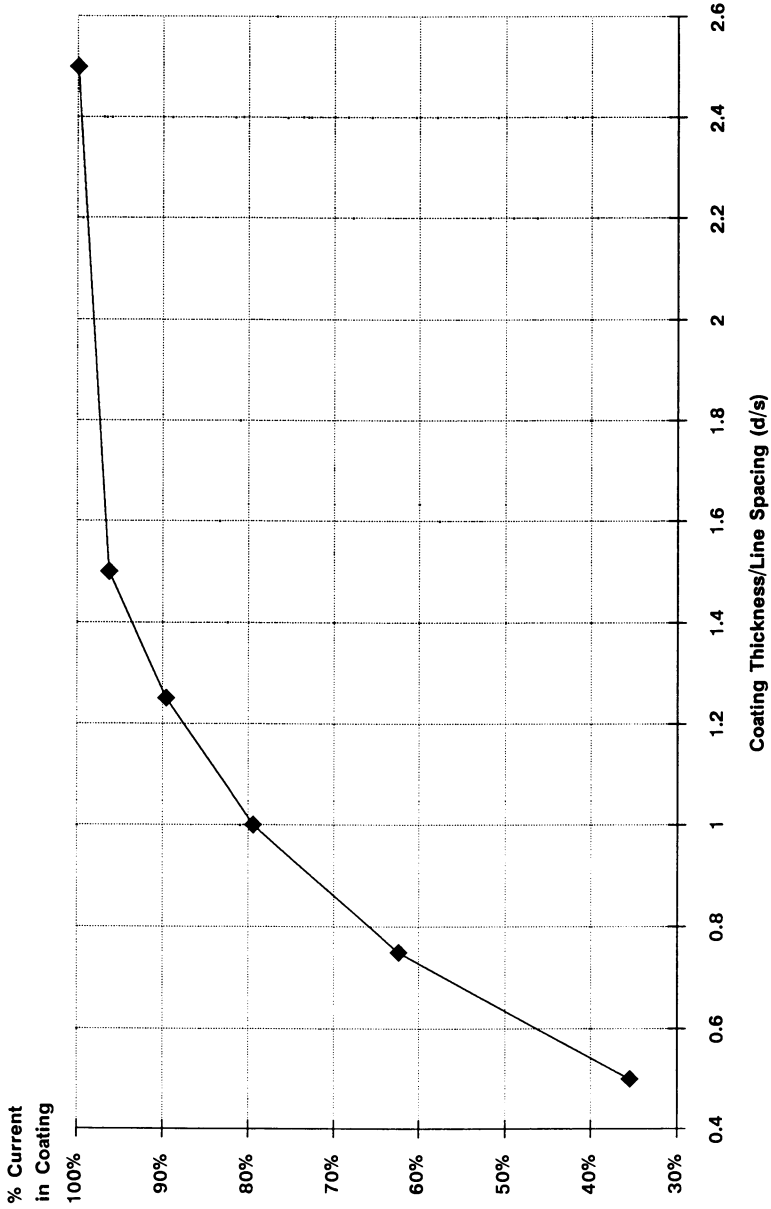
Figure 11. Percent total leakage current contained within an insulating coating vs. d/s.

measured. This value is 3-4 orders of magnitude lower than the previously reported measurements (1-3). The triple-track pattern used has a geometry with s/w=1, and the expected value, as well as the current distribution is easily predicted by our model. This suggests that previous data might be reexamined to determine the location and distribution of the leakage current in addition to its absolute value.

In some cases the measured value may have been influenced more by the shunt error currents or system lower-limits rather than actual sample leakage currents. It is difficult to prevent shunt currents from flowing between the pins of test samples which plug into in-line sockets. A system which switches a large number of samples must also use low-leakage switching elements such as glass encapsulated magnetic reed switches in a TREE switching arrangement (11). This technique minimizes the shunt errors even for a large number of samples. Before using a system, and periodically during use, a check should be made of the shunt error. In our laboratory we use a system of our own design which can test 100 samples in hot water baths with less than 0.02pA of shunt error. In our previous work (4) the lowest practical limit of our measurement system was 0.5 to 0.1 pA, and this limitation was reflected in our data.

Values of "dry" leakage currents for encapsulated samples which are presumed accurate and measure in the 100pA-1nA range, should be easily verifiable by a volume resistivity measurement of the polymer, since the polymer's resistivity would have to be less than approximately 1×10^{12} ohms-cm.

Based upon our model, leakage currents under "wet" conditions, should not appreciably increase over those measured "dry" unless there are significant polymer-substrate interfacial changes, the formation of continuous water pathways within the bulk polymer, or significant reductions (from dry to wet) in the polymer volume resistivity. Even with water absorption as high as 1%, a drop in resistivity from 10^{17} to 10^{13} ohms-cm does not seem likely. Data from our laboratory on electronic grade silicones shows a drop in resistivity of approximately 40% for unfilled, or lightly filled silicones when exposed to 100% RH. More bulk properties measurements need to be made, thus refining the model.

One method of determining the location (at the interface, or within the bulk polymer) of the measured current within a sample might be to increase the line-spacing with s/w=1. In the case of bulk current, no change would be seen for greater spacing. However, for interfacial current a noticeable change in total current would result. Current flowing along the interface, between two lines would be very sensitive to line-spacing since the dominant parameter would be the sheet resistance of the interface. One might expect an inverse relationship following an R=p*l/A equation (p=sheet resistance, l=length, A=area). This concept might be extended to examine early deterioration of the interface by using a sample which contained two different line-spacings on the same substrate.

Figure 12 shows the leakage current integral for three different test patterns. Pattern A (s=1, s/w=1) shows a curve identical in shape to Figure 4, however the current and distance scales have been normalized to "s". Pattern B (s=0.54 that of Pattern A, s/w=0.14) shows a curve which is very similar to that of Pattern A particularly with respect to the current distribution. This is a
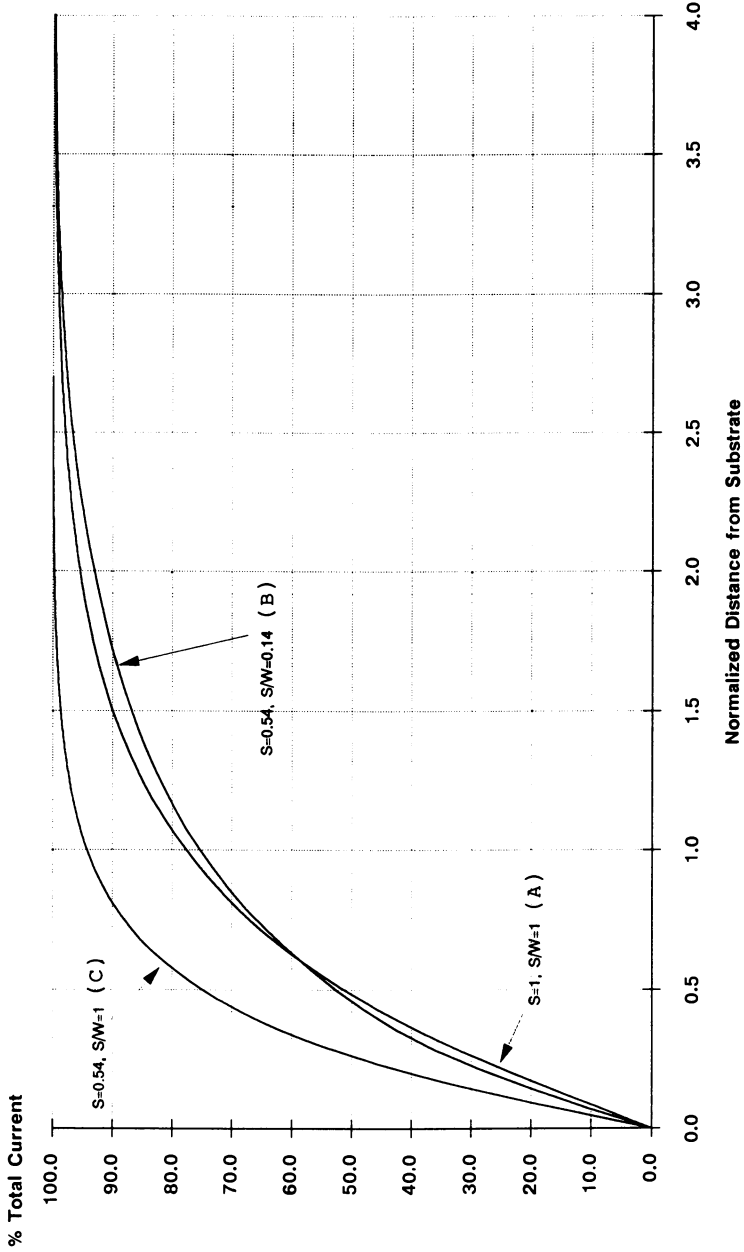
Figure 12. Leakage current integral for three patterns with different line widths and spacings (see text).

consequence of the larger line width (w) relative to the line spac-
ing (s). For Pattern B, the wider lines compensate for the closer
line spacing. This has the effect of doubling the electric field
concentration in the region of the polymer-substrate interface,
without changing the current distribution within the bulk polymer.
In contrast, the analysis of Pattern C (s=0.54 that of Pattern A,
s/w=1), results in a significant change in the current distribution
within the polymer. Therefore, electric field strength, and corre-
spondingly the effect of bias, can be varied independently by chang-
ing the relationship between s and w. Manipulation of the pattern
geometry can be used to determine the location of the measured
leakage current: along the interface, or within the bulk polymer.
     The significance of the model with the outer layer of water is
such that a critical d/s value can be found for which the current
flow and electric field strength are not influenced by the outer
medium. It is reasonable to expect that in a humidity chamber,
water may condense on the surface of the coating. For our model,
the critical d/s is approximately 2.3. The implications of this for
triple-track testing is that when using 75um lines and spacings, the
encapsulant must be at least 200um thick to ensure that 99% of the
measured current flows in the bulk encapsulant and not in the outer
water. Although the _total_ current does not significantly change
with an outer layer of water, the distribution of the current and
the gradient of the electric field within the encapsulant can dra-
matically change, especially as d/s becomes <0.5. The higher volt-
age gradients might magnify the effect of the bias so as to more
quickly accelerate any bias-induced failure mechanisms. To study
coating thicknesses of 25um, a line-spacing of 10um would have to be
used.
     The volume resistivity of the substrate was not an important
effect in any of our models. This was a consequence of selecting
the substrate material to have a resistivity significantly greater
than that of the polymer in all cases. For substrates with resis-
tivities which approached that of the polymer, the model can easily
be modified. One would then expect that the substrate current would
contribute to the total current by approximately the ratio of the
substrate to polymer resistivity.

Conclusions

Finite-element modeling can be used to predict the value of leakage
currents for encapsulated triple-track and comb samples. The data
presented in this paper can be applied to a variety of geometries
and bias conditions. The value of this technique lies in the abili-
ty to differentiate between bulk and interfacial current. Voltage
dependent values of volume resistivities under dry and wet condi-
tions can readily be measured and used in the models to predict
acceptable leakage currents for samples in which the interfacial
current is insignificant - a desirable condition. Values of leakage
current which exceed the predicted levels may be caused by water
collection at the polymer-substrate interface. The use of different
line-spacings may help to differentiate between bulk and interfacial
current. For a given line-spacing, coatings must be roughly twice
as thick as the line-spacing so as to prevent the conditions at the
outer surface of the encapsulant from affecting the measurements.

Values of leakage current which are unusually high and which cannot be correlated to changes in volume resistivity may be caused by shunt error currents. The background leakage of current-measurement systems should be determined and monitored.

Literature Cited

1.   Iannuzzi, M. 33rd Electronics Components Conf. 1983, 591-601.
2.   Iannuzzi, M. 32nd Electronics Components Conf. 1982, 391-400.
3.   Iannuzzi, M. 20th Ann. Proc. Reliabil. Physics. 1977 16-26.
4.   Troyk, P.R.; Watson, M.J.; Poyezdala, J.J. In Polymeric Materials for Corrosion Control; ACS Symposium Series 322, American Chemical Society: Washington, DC, 1986; p 299.
5.   Comizzoli, R.B.; Frankenthal, R. P.; Milner, P.C.; Sinclair, J.D. Science 1986, 234, 340.
6.   Koelmans, H.; Kretschman, H.J. J. Electrochem. Soc. 1978, 125, 1715.
7.   Anderson, J.E.; Markovac, V.; Troyk, P.R. IEEE Trans. Comp. Hybrids and Manuf. Technol. 1988, CHMT-11, 152-158.
8.   Troyk, P.R.; Anderson, J.E.; Markovac, V. 1st Intern. SAMPE Electron. Conf. 1987, 1, 590-601.
9.   White, M.L. Proc. IEEE. 1969, 57, 9, 1610-1615.
10. Silvester, P.P.; Ferrari, R.L. Finite Elements for Electrical Engineers; Cambridge University Press, Cambridge, U.K., 1983.
11. Switching Handbook, A Guide to Signal Switching in Automated Test Systems, Keithley Instruments, Inc, Cleveland, OH, 1987.

Chapter 23

Silicone Gels and Coatings for Integrated-Circuit Packaging

Justin C. Bolger

Emerson & Cuming/W. R. Grace and Company, 25 Hartwell Avenue, Lexington, MA 02173

This chapter describes the use of very soft (Shore 00 scale) silicone gels and coatings for use in hybrid and monolithic IC's for:
1. Stress relief on large dies in post-molded plastic packages.
2. Passivation/corrosion protection in pre-molded plastic packages.
3. Prevention of silver migration in hybrid circuits.
The mechanism for each of these effects is explained. Rules are provided for selecting silicones with optimum hardness, rheology, cure temperature and other properties needed in production.

Dielectric grade silicone gels are now being used in increasing quantities for packaging hybrid and monolithic integrated circuits. These gels are now used either in the form of thin coatings on dies or on hybrid circuits, or in thicker sections as encapsulants for hybrid circuits used in automotive electronics. Silicone gels are also used to encapsulate dies packaged in pre-molded plastic packages and have been suggested for use as "blob top" coatings for low cost, localized protection of dies on PC boards.

Compared to epoxies and other resin-types used in the IC industry, silicones have several unique advantages:

1. Flexibility. Silicone gels have hardness measured in the low end of the Shore 00 scale. They retain useful elongation at temperatures far below 0°C.

2. Excellent thermal stability. No out-gassing or decomposition up to 200°C.

3. Cleanliness. No chlorides or other potentially corrosive contaminants. This provides good semiconductor compatibility.

Silicones have, however, several unique disadvantages vs. other encapsulants such as epoxies, which must be taken into account for proper performance:

   1.   They have a very high thermal expansion coefficient at ambient temperatures.   This creates a large potential thermal mis-match in contact with silicon, alumina, and other surfaces. This expansion mis-match can cause wire breakage and other damage during temperature cycling.

   2.   Low mechanical strength. Silicone gels must be protected by some sort of cover or outer shell against mechanical damage. They also have very low resistance to attack or swelling in cleaning solvents.

   3.   Until recently, most silicone gels provided inadequate adhesion to coated or encapsulated parts.   Modern silicone encapsulants and coatings contain, however, silane "coupling agents", which are able to form a permanent water proof covalent bond to most substrates and therefore avoid failure associated with loss of adhesion to the substrate.

   Other chapters in these proceedings discuss the electrical and mechanical properties of silicone elastomers.   This chapter describes the use of silicone gels to provide stress relief, passivation and corrosion protection, and for the prevention of silver migration.

Stress Relief on Large Dies in Post-Molded Plastic Packages

An increasingly serious reliability problem, for large dies packaged in post-molded plastic packages, involves the possibility of die breakage or other damage, due to compressive surface stresses on the die surface (Fig. 1).   These compressive stresses were a minor consideration when IC dies were relatively small, but are now becoming a very serious cause of failure as dies are approaching 400 mils in length and the lead count is increasing to 100 leads per die or more.

   Figure 1 depicts use of a thin coating of silicone elastomer or gel, which can be a very effective way to avoid localized surface stresses on the die in post-molded plastic packages.   The thickness of the silicone coating need only be ten microns or so to be effective.   Thin silicone coatings apparently can delocalize the stresses and prevent die damage during molding or thermal cycling.

   Applying a uniform coating on the surface of the die, while keeping the coating away from the gold wires, is a difficult production problem.   It would be easier to apply a thicker coating. The question is, therefore, if a ten micron coating is effective in reducing stress, why not use a thicker, more easily applied coating?

   The answer involves the high expansion coefficient of silicone elastomers.   The epoxy molding compounds, used to encapsulate the chip in the post-molded package of Figure 1, do not break the fragile (1 mil diameter) gold wires because of their low expansion coefficient below Tg and because their Tg value is high enough to prevent transition into the rubbery state at all anticipated service temperatures.   Typical values for these epoxy encapsulants, and for the silicone gels, as measured by TMA(thermo-mechanical-analysis) are:

	Wt % Filler	Tg °C	α_1	α_2
Epoxy Encap.	60 to 70% SiO$_2$	140 to 160	20 to 30	150 to 200
Silicone Gel	unfilled	-30 to -40	40 to 60	180 to 300

Here α_1 is the average linear coefficient of thermal expansion in the glassy state, in parts per million per °C. α_2 is the value in the rubbery state. At or near room temperature therefore, the silicone gel is in its rubbery state, and the high α_2 value may cause wire breakage if the silicone die coating is thick enough to extend onto the wires of Figure 1. If the silicone gel is soft enough, however, such that expansion does not apply any significant force to the gold wire, then this wire breakage can be avoided.

The rule, therefore, is that silicone coatings are a very effective way to avoid damage to die surfaces encapsulated in epoxy transfer molding compounds provided that:

a)   The silicone coating is thick enough (ten microns or more) to delocalize the stress, but not thick enough to extend above the tops of the gold ball bonds, or,

b)   if a thicker silicone coating is used, the silicone must be a very soft gel which can expand without breaking the wires.

Passivation in Automotive Hybrids and PCC Packages

One way to avoid the thermal stresses on dies shown in the post-molded package of Fig. 1 is to use a pre-molded plastic package for IC's or hybrids. This involves using a plastic box which contains the die or hybrid in a cavity, and then sealing the cavity by bonding a plastic lid as shown in Fig. 2. Pre-molded plastic packages, frequently called plastic chip carriers (PCC's), have long been proposed for monolithic IC's[1], but because of higher costs relative to post-molded plastic packages, did not sell in volume until the recent increases in die size and in lead count made pre-molded packages more attractive for stress and tooling-cost reasons.

One long established use of silicones has been in the pre-molded plastic packages used in automotive hybrids of Fig.2. Delco first pioneered the use of hybrid circuits[2] in a plastic cavity package over 20 years ago, and virtually all automotive circuits now use this packaging method. The key to reliability has been the use of a silicone gel within the package, which completely encapsulates all components. For reasons noted elsewhere, this silicone is very effective in providing passivation and corrosion protection, and in avoiding silver migration problems. Clearly, the silicone does not function as a barrier coating and does not exclude moisture, oxygen or other ions. Rather, the silicone provides this long-term protection in the very hostile under-the-hood automotive environment, by retaining long-term flexibility, even after extended exposures to high temperatures, and by retaining adhesion to the hybrid substrate and all encapsulated surfaces.

As used above, "adhesion retention" means that the silicone gel must retain a sufficient degree of intimate interfacial contact such that the transport of electrons, as well as liquid water, ions and other reagents, must take place through the bulk polymer, rather than through gaps or along an adsorbed aqueous phase at the substrate surface. Moreover, this interfacial contact must be maintained after thermal cycling, mechanical shock and/or exposure to high humidities.

A detailed discussion of this protection mechanism (3,4) is

beyond the scope of this chapter, other than to note that the displacement mechanism differs for a <u>rigid</u> polymer, where very high tensile and shear forces can be generated at the polymer-substrate interface, versus the present case of very soft silicone gels where interfacial separation is caused primarily by chemical (rather than mechanical) displacement effects. Thermodynamics always strongly favors the displacement of a silicone resin, by water, at an oxide surface, whenever the only interfacial bonds are secondary valence forces (3,4). The best present silicone gel encapsulants retain adhesion because they contain small (ca 1% by wt) additions of silane coupling agents. These are mobile, surface-active, molecules which are able to form covalent bonds to the bulk silicone phase, and also to form hydrolysis-resistant siloxane bonds to silica and other oxide surfaces. Plueddemann (5) and others have described these silane coupling agents in detail.

The least expensive way to package an I.C. chip, on a PC board, is the "Chip-On-Board" method shown in Fig. 2. This method, using epoxy "blob top" coatings, is now widely used in electronic watches, games, pocket calculators, and other low-cost consumer products, but has not yet been accepted for use in higher value, higher reliability circuits, primarily because of stresses generated when the epoxy blob top is cured or temperature cycled. <u>Very</u> soft silicone gels can avoid these stresses, and also provide the ionic purity and other properties needed for long-term passivation, but are too soft to provide mechanical protection or to withstand the solvents used in PC board production. Hence, silicone gels are used only under a plastic shell or cover, or in one of the enclosures shown in Fig. 2.

Silver Migration

Silver migration will occur whenever a silver-filled adhesive, coating or ink is in close proximity to another conductor in a circuit, provided that a DC voltage potential (the silver-filled polymer being the anode), and a film of liquid water, exist on the surface separating the silver compound from the other conductor.

Licari, et al. (6) showed that by placing a drop of deionized water across a 20 mil gap between a conductor and a silver-filled adhesive, and then applying a one volt DC potential, silver dendrites began to grow across the gap within 30 seconds. Bridging, causing an electrical short, occurred within 3-4 minutes. Within eight minutes, silver particles had completely filled the gap.

Licari tested specimens with water droplets bridging the gap between the two conductors as well as with other specimens exposed to relative humidities up to 100% at a constant 80°C. He showed that even with applied voltages over 20 volts, and time periods up to two weeks, silver migriation did <u>not</u> occur unless there was a film of liquid water on the surface.

Licari's conclusion was that water in the vapor phase is not sufficient to induce silver migration. Silver migration is therefore possible only when packages are operating below the dew point of the atmosphere within the package.

Recent work (7) which repeated Licari's tests used a large number of commercially available conductive inks and adhesives to determine the effect of resin-type, of Tg, of ionic purity and of

filler type on silver migration.   The results are summarized in Table I, and lead to the following important conclusions:

1.   Ionic purity and chloride content. One might suppose that clean epoxies or other resins, containing silver fillers, would perform better in migration tests than epoxies containing large quantities of chlorides or other extractable ionic impurities. Table I shows, however, that there is no significant difference between a very clean epoxy adhesive, a clean polyimide, and an epoxy containing over 300 ppm extractable chloride.

2.   Glass transition temperature. One might also expect that high Tg inks and adhesives would perform better, because of slower extraction rates for silver ions. Table I also shows, however, that conductive epoxies with a Tg below 100°C performed almost as well as the high Tg silver-filled polyimide (Tg=180 °C) or the epoxy adhesives with TG=115°C or 130°C. Conductive glass adhesives, in which the glass binder was fired at temperatures of 430°C, also showed rapid failure due to silver migration.

3.   Filler type. The most widely used way to avoid silver migration is to avoid silver. Gold filled epoxies are specified in many military specifications, but are impractical for most commercial applications because of cost. Silver-palladium filled inks and adhesives are therefore frequently used to avoid migration. Table I shows that using a silver-palladium filler, in place of pure silver, can improve the time to failure by metal   migration, although by a surprisingly small degree.

Silver-palladium powders which are now used in conductive products are of two different types. One type is co-precipitated powders, wherein silver and palladium are both precipitated from solution to form a powder in which the two metals are intimately associated but do not form a true alloy. Another, more expensive filler, involves first forming a true silver-palladium alloy, and then pulverizing this to a fine powder.

Table I shows that the silver-palladium alloys do indeed perform better than the co-precipitates. Silver ions are obviously extracted more rapidly from the physical mixture of silver and palladium in the co-precipitate than from the alloy, but that this improvement is still not enough for a high level of security in critical hybrid circuits.

The best technique found (7) for avoiding silver migration is to coat the circuit with a thin coating of silicone or silicone gel. Table I shows that even in the worst case (the low Tg, high chloride silver-filled epoxy, which, in the absence of a silicone coating fails via migration within 45 seconds,) the application of a thin (4 mil thick) silicone coating over this same circuit, essentially eliminates silver migration at these voltages and test conditions.

The fact that silicone coatings are able to prevent silver migration has, of course, been known for over ten years. But the mechanism for this has not been understood. Silicones, as a general polymer class, have a very high permeability to water vapor. Hence, silicones cannot be considered as "barrier coatings" which function by excluding water from the region between the conductors.

The explanation depends on Licari's observation that liquid water, rather than water vapor, is necessary between the silver containing polymer and the nearby cathode. As long as the silicone

COMPRESSIVE STRESS

Thin coating. Below
top of ball bonds.

Thick coating. Use
soft silicone gel.
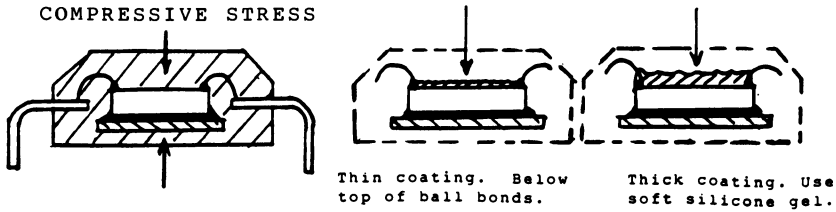
Figure 1. Silicone die coatings can be used to protect the die against damage from the compressive stresses generated during cure and thermal cycling of the transfer molding compound in post-molded plastic packages.
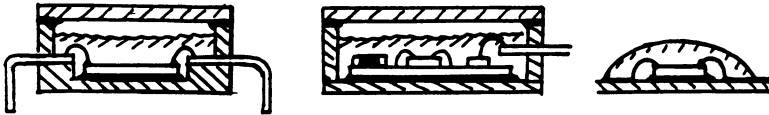
Figure 2. Very soft silicone gels are preferred for encapsulation in post-molded plastic chip carriers (left) and in automotive hybrid packages (center) but are too soft for use as "blob top" coatings (right) for chip-on-board encapsulation.

Table I. Time to failure by electrical short due to silver migration. DC voltage = 5V at 25 °C (data from ref. 7)

RESIN TYPE	FILLER TYPE	Tg	Cl⁻ CONTENT(1)	SILICONE COATING	TIME TO FAILURE
Epoxy A	Silver	95°C	300	NO	45 seconds
Epoxy B	"	115°C	10	"	50 "
Epoxy C	"	130°C	10	"	45 "
P'imide A	"	180°C	5	"	60 "
Glass (2)	"	>200°C	3	"	80 "
Epoxy A	Pd-Silver(3)	95° C	300	"	5 minutes
Epoxy A	" " (4)	95° C	300	"	30 "
Epoxy A	Silver	95° C	300	Yes (5)	2 hrs(7)
Epoxy A	"	95° C	300	Yes (6)	2 hrs(7)

(1) Extractable chloride ion content, ppm
(2) Silver glass mixture. Fired at 430°C
(3) 70% silver. 30% palladium. Co-precipitated powder
(4) 70% " " " True alloy powder
(5) Same as Epoxy A above with 4 mil silicone coating Amicon SC-3613
(6) " " " " with 20 mil silicone gel coating Amicon SC-2650
(7) Test discontinued after 2 hrs. No failure

coating can retain adhesion to the substrate, and to the conductors, a liquid water path cannot form.

As noted above, the best modern silicone gels now contain special organo-functional silane "coupling agents", which are able to form a strong, water resistant, chemical bond to the alumina and conductive surfaces, thereby preventing the formation of a liquid film on the adhesive which could provide a path for migration.

Hence, the best present silicone coatings provide a very reliable method to prevent silver migration in hybrid circuits by preventing the formation of a liquid water path between closely spaced conductors. The effectiveness of these silicones does not depend on hardness. That is, very soft gels are as effective as harder elastomers, as long as adhesion to the substrate is retained. These silicone coatings are therefore more cost effective than previous solutions to the migration problem which require the use of gold-filled, or silver-palladium filled, inks or adhesives.

Literature Cited

1. Rose,A.; Fischer,M. Proc. 32nd Electronic Components Conf., 1982, pp 87-90.
2. Bolger,J.C. Proc. 1984 International Symposium on Microelectronics; ISHM: Montgomery, AL, pp 90-94.
3. Bolger,J.C.; Michaels,A.S. In Interface Conversion; Weiss,P.; Cheevers,S.D., Eds.; Elsevier: New York, 1969; Chapter 1.
4. Bolger,J.C. In Adhesion Aspects of Polymeric Coatings; Mittal,K.L., Ed.; Plenum: New York, 1983 pp 3-19.
5. Plueddemann,E.P. idem., pp 363-379.
6. Licari,J.J.; Perkins,K.L.; Caruso,S.V. Guidelines For The Selection of Electrically Conductive Adhesives for Hybrid Microcircuits, NASA CR-161978, 1981.
7. Bolger,J.C.; Herberg,M.J.; Mooney,C.T. SAMPE Electronic Materials Conf., 1987.

RECEIVED January 18, 1989

Chapter 24

Ultraviolet-Curable Silicones for Integrated-Circuit Protection

Michael A. Lutz and Kristen A. Scheibert

Dow Corning Corporation, Midland, MI 48686–0995

Technology which couples fast ultraviolet (UV) cure
response with silicone performance characteristics
suitable for integrated circuit protection has been
developed. One-part silicones which can be cured in
several seconds to provide products of excellent
purity, stress relief, thermal stability, and pro-
tection against harsh environments are the result.
The new UV curable silicones afford an attractive
alternative to standard heat activated materials for
integrated circuit protection where high speed auto-
mated fabrication and assembly processes are desired.
Additionally, the photosensitivity of these materials
present other convenient processing opportunities.
Included among these would be photobarrier processing,
which involves 'in-situ' generation of flow barriers
during material application, and photoimaging to allow
wafer stage application of permanent, protective
coatings.

Integrated circuits are delicate devices which require protection
to preserve desired electrical performance characteristics over
their intended service life. Although hermetic packaging techni-
ques provide the ultimate in protection against adverse mechani-
cal, thermal, and chemical environments, polymeric materials can
provide acceptable performance levels for a number of applica-
tions at a significantly lower cost. Key properties for mater-
ials targeted for protection of integrated circuits include easy
processing, high ionic purity, good adhesion, moisture and chemi-
cal resistance, acceptable temperature performance, and good
electrical performance. The last two properties are certainly
becoming more prominent as chips trend toward smaller features,
higher speeds, and larger dimensions. Materials which combine
good stress relieving characteristics with excellent dielectric
properties over extended frequencies and temperature ranges will
therefore be in greater demand for protection of integrated
circuits.

Silicones have long been recognized as attractive materials
for protection of integrated circuits. Their excellent electri-
cal properties, elasticity, low moisture uptake, ionic purity,
low temperature performance, and thermal stability provide the
combination of properties necessary for protection of semicon-
ductor devices.(1) Of increasing importance will be the excel-
lent dielectric properties (2) and stress relieving potential of
silicones. Although silicones are available with several cure
systems, only two find widespread use in silicones for integ-
rated circuit protection. The first is a one-part system that
cures upon exposure to atmospheric moisture according to the
following sequence of reactions (3):

$$-SiOMe \ + \ H_2O \ ---> \ -SiOH \ + \ MeOH \qquad\qquad (1)$$

$$-SiOH \ + \ MeOSi- \ ---> \ -Si-O-Si- \ + \ MeOH \qquad (2)$$
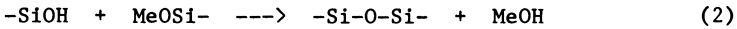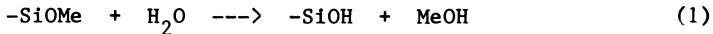
Although handleable properties can normally be achieved in one to
three days at room temperature, depending in part on the thickness
of the coating, full cure typically requires greater than one
week.

The second cure system uses a hydrosilylation reaction for
crosslink formation, and is typically supplied as a two-part
product. In the crosslinking reaction, a silicon hydride group
adds to a vinyl group, typically using a platinum catalyst.(4-6)

$$-SiH \ + \ H_2C=CHSi- \ ---> \ -SiCH_2CH_2Si- \qquad (3)$$
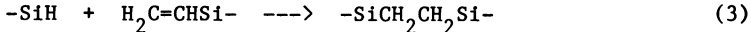
Hydrosilylation cure can be obtained either at ambient or elevated
temperatures, with two hours at 150 C representing a typical ele-
vated temperature cure.

Although silicones used on semiconductor devices have perfor-
mance characteristics that lead to devices with excellent reli-
ability and service life, their processing characteristics are
less than ideal. In particular, emphasis on fast speed automated
fabrication and assembly processes to reduce manufacturing costs
has pressed current heat-activated silicones to their limit.
Ultraviolet (UV) curing is a process which is ideally suited to
meet these fast speed curing requirements. The process uses UV
light to initiate chain reactions which convert fluid materials to
crosslinked products, ideally in just a few seconds.(7) Energy
contained in the UV radiation is readily absorbed by special
molecules, called photoinitiators, causing them to become activa-
ted. The activated photoinitiator subsequently undergoes react-
ions resulting in the formation of reactive species, typically
free radicals or Lewis acids. These, in turn, initiate chain
reactions in the bulk of the composition resulting in crosslink
formation.

UV curable silicones are not new.(8-9) The most common
functionalities incorporated into the system to allow photocross-
linking are thiol/ene, oxirane, or reactive unsaturation such as
acrylate. However, the thiol functionality is corrosive to sub-
strates of interest for integrated circuit applications. Addit-
ionally, the resultant sulfide crosslink has a limited thermal

stability, making this system unattractive. In the oxirane sys-
tem, an onium photoinitiator is used which, upon irradiation,
liberates a Lewis acid to cure the oxirane functionality cationi-
cally. Since the halogen containing Lewis acids are corrosive,
and the cure response is somewhat slow, the oxirane system also
appeared unattractive to use in compositions targeted for protec-
tion of integrated circuits. The last system, based on free rad-
ical polymerizable reactive unsaturation, can provide rapid photo-
cure in addition to useful properties.(10) It thus appeared to
be the most attractive functionality to incorporate into sili-
cone compositions targeted for evaluation as protective materials
for integrated circuits.
     The major ingredients for a UV curable silicone intended for
protection of integrated circuits would therefore consist of a
photosensitization system to facilitate the conversion of light
energy to chemical energy and a polysiloxane containing reactive
unsaturation, such as acrylate functionality, to provide the
elastomeric network. Useful properties for the photosensitiza-
tion system include solubility, pot stability, fast UV cure res-
ponse, absence of odor before and after cure, minimal color of
the resultant cured composition, and no adverse physiological
effects. Selection of the polysiloxane polymer would depend upon
the particular requirements of the application, such as viscosity,
modulus, toughness, low temperature performance, etc. Excellent
low temperature performance can be readily obtained through in-
corporation of small amounts of sidegroups along the polymer
chain in order to disrupt crystallization.(11) In this manner,
it is possible to retain excellent flexibility at temperatures
below -60 C. Optional ingredients would include materials such
as reinforcing agents to increase the strength of the cured elas-
tomeric network, adhesion additives, and rheology modifiers.

Experimental

Formulations were prepared for evaluation by making a simple
physical blend of the desired components. Viscosity was measured
according to ASTM D 1084B. Sodium and potassium levels were de-
termined on uncured samples using flame photometry following sam-
ple preparation consisting of an acid ash and silica removal by
treatment with hydrofluoric acid. The deaired compositions were
subsequently cured by exposure to UV light emitted by medium
pressure mercury vapor arc lamps housed in either a UVEXS Model
750A or 850C Ultraviolet Curing Unit manufactured by UVEXS Inc.
of Mountain View, CA. The irradiation dose represents the light
available for cure as measured with an IL 390 Light Bug manufac-
tured by International Light.
     Water absorption of the resultant cured materials was mea-
sured after immersion for 24 hrs at room temperature and reported
as % weight gain. The modulus was measured according to ASTM D
2240, and the dielectric constant and dissipation factor were
measured using a method similar to ASTM D 150. Glass and melting
transitions were measured by differential scanning calorimetry
(DSC). The thermal stability was determined in a forced air oven

at 150 C for a total time of 1000 hrs, and autoclave stability
was measured for 100 hrs at 121 C and a pressure of 2.1 kg/cm^2.
In both aging tests the modulus was monitored as a function of
time, with less than 15% change considered good performance.

Results and Discussion

Typical physical properties obtainable with UV cured silicones are
provided in Table I. Incorporation of reactive unsaturation into
the silicone polymer backbone in combination with a photosensiti-
zation system provided the photocure capability. Properties of a
standard heat-cured encapsulant developed for use on semiconduc-
tor devices, Dow Corning HIPEC R-6103, are provided for compara-
tive purposes. Clearly, introduction of a photocrosslinking
mechanism into a siloxane type composition has afforded the de-
sired result. The one-part, solventless, UV curable silicone
composition cured rapidly upon exposure to UV radiation, provid-
ing a cured composition which has retained the typical properties
that make silicones so attractive for protection of semiconductor
devices.

Variation of structural and compositional parameters allow
modification of the physical properties to tailor performance to
specific application needs. For example, the effect of ingredi-
ents added to control the modulus of two UV curable silicone
polymers is presented in Figure 1. Both Polymer A and Polymer B
were polydiorganosiloxanes which contained terminal reactive un-
saturation. Admixture with a photosensitization system and sub-
sequent cure afforded soft, elastomeric products. Modifier A was
incorporated into Polymer A to soften the system further. As the
concentration of Modifier A increased, the modulus decreased, and
the resultant composition became more 'gel-like'. In a contrary
fashion, Modifier C was added to Polymer B to provide reinforce-
ment. As the concentration of Modifier C was increased, the mod-
ulus of the resultant cured film increased, the elongation de-
creased, and the tensile strength went through a maximum.

The cure response of silicones containing reactive unsatura-
tion was examined by measuring the effect of irradiation dose on
the modulus (Figure 2) and the cured thickness (Figure 3). When
cured in thick section (0.5 cm), maximum hardness was achieved
with about 2 J/cm^2 for formulations containing Polymer A (Fig-
ure 2). Although the formulation containing Polymer B and Modi-
fier B also attained a major portion of it's modulus after 2
J/cm^2, it continued to harden upon additional irradiation.
Apparently, either the formulation continued to cure, at a much
slower rate, or the resultant, fully cured composition was under-
going a UV initiated degradation resulting in formation of cross-
links. Of course, the required irradiation dose depends upon the
thickness of the material being cured in addition to the specific
composition (Figure 3). The ability to photocure certain sili-
cone compositions in deep section is a consequence of their tran-
sparency to the wavelengths required for photoinitiator excita-
tion and represents a distinct advantage. Even though the maxi-
mum cured thickness was formulation dependent, the UV curable
silicones could be cured in depths sufficient for most applica-

Table I
Typical Physical Properties of UV Curable
Silicone for Integrated Circuit Protection

	Dow Corning HIPEC R-6103	UV Cured Silicone Encapsulant
Package Type	Two-Component Solventless	One-Component Solventless
Viscosity (cps)	3200	2000
Pot Life	< 24 hrs	> 6 months
Na, ppm max	2	2
K, ppm max	2	2
Cure	2 hrs @ 150 C	< 2 J/cm(2)
Hardness	35 Shore A	30 Shore 00
Water Absorption	0.14%	0.3%
Glass Transition	-120 C	-113 C
Melting Transition	None	None
Thermal Stability	> 1000 hrs @ 150C	> 1000 hrs @ 150 C
Autoclave Stability	> 100 hrs	> 100 hrs
Dielectric Constant, at		
10(2) Hz	2.69	3.0
10(5) Hz	2.67	3.0
Dissipation Factor, at		
10(2) Hz	0.0008	0.006
10(5) Hz	0.0011	0.002
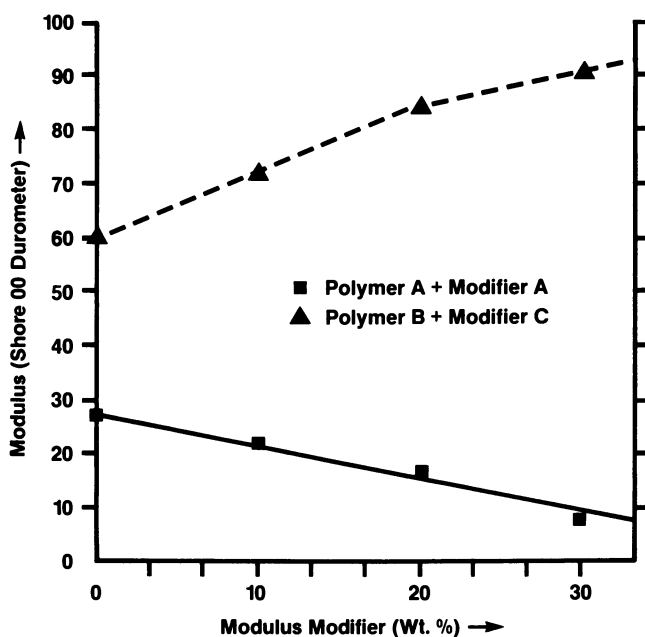
Figure 1. Effect of modifier concentration on modulus of resultant silicone encapsulant.
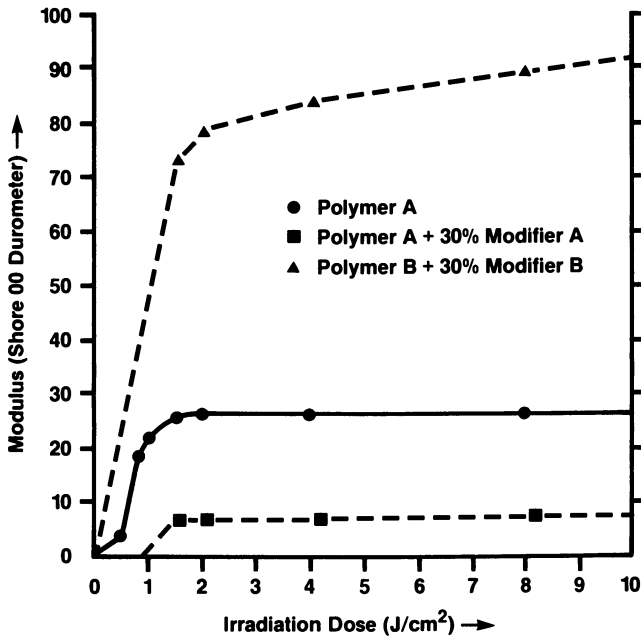
Figure 2.   Modulus of UV curable silicone vs irradiation dose.
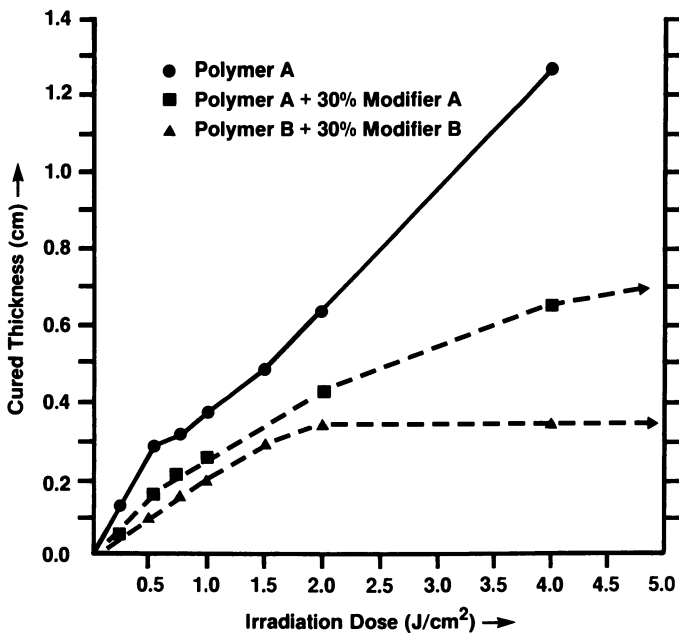
Figure 3.   Cured thickness of UV curable silicone vs
irradiation dose.

tions involving protection of integrated circuits. Finally, since 2 J/cm^2 equates to an 11 second exposure dose in the UV equipment used in the current study, as opposed to days at room temperature for moisture curing systems or hours in the case of heat cured systems, the one-part UV curable silicones do indeed provide a significant processing advantage.

The photosensitivity of these materials could provide additional processing advantages. Similar to the microlithography techniques used to develop patterned images in photoresists (12), a photopatterning process could present a convenient method for application of UV curable silicones to integrated circuits while still at the wafer stage.(13) An example of such a process is depicted in Figure 4. The photopatterned areas not containing cured silicone would allow the bonding pads, probe points, and 'streets' to remain open while the remainder of the surface would obtain a protective coat of silicone. Such a process may provide an attractive alternative to the typical encapsulation and drop-on application methods in current use today.

Another processing option made possible with UV curable materials would be the 'in-situ' development of a barrier to retard flow of coatings and encapsulants during application.(Lutz, M. A.; Eckstein, M. H. U.S. Patent Pending) A simple schematic illustrating the process is provided in Figure 5. In essence, a collimated source of UV light is focused on a region where it is desired to have the flow of material end. Upon entering this zone the fluid material cures to form a solid barrier which retards the flow of material beyond the cured barrier. The height of the barrier increases as additional material enters the barrier zone until the desired depth is reached. The bulk of the material can then be cured by exposure to UV light. In practice, the photo-barrier process could be used to contain a fluid material within a certain boundary or to keep a fluid material out of a region in applications such as Plastic Pin Grid Arrays (PPGA), Tape Automated Bonding (TAB), Chip on Board Encapsulation, and coating of circuit boards.

Conclusion

In conclusion, one-part silicones which can be cured in a matter of seconds upon UV exposure to provide networks of high ionic purity, low moisture uptake, excellent electrical properties, and good stress relieving characteristics, even at low temperatures, have been developed. The excellent stress relieving characteristics and electrical properties of the resultant cured elastomers suggest these materials are suited for protection of semiconductor devices. Thus, these new UV curable silicones afford an attractive alternative to standard heat activated materials for integrated circuit protection where rapid processing, such as in automated production lines, is desired. Additionally, the photosensitivity of these materials present convenient processing opportunities. Included among these would be photobarrier processing, which involves 'in-situ' generation of flow barriers during material application to contain the fluid in the desired regions,

Spin Coat

Pre-bake

Light

Mask

Coating

Wafer

Expose

Cured Coating

Wafer

Develop

Post-bake

**Wafer Stage Applied
Photopatterned Coating**
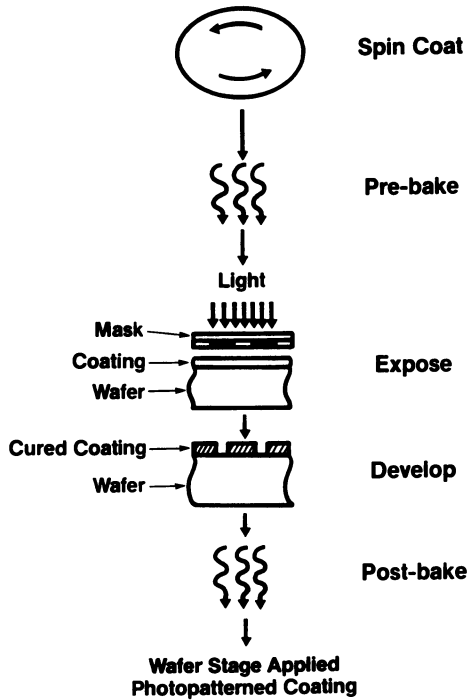
Figure 4. Photopattern process for wafer stage applied UV curable silicone coating.

Collimated UV Light

Dispenser

Fluid Dispensing

Fluid Material

Substrate

Cured
Material

Dispensing
Completed

Bulk Cure
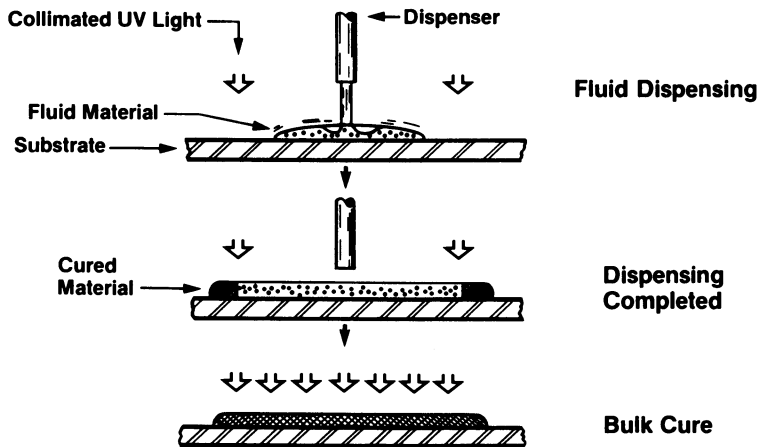
Figure 5. Photobarrier processing example for 'in situ' generation of flow barriers during processing of UV curable materials.

and a wafer stage application option wherein a permanent, photo-defined, protective coating could be used to supplant typical en-capsulation and drop-on application methods in current use today.

Acknowledgments

Literature Cited

1. Noll, W. Chemistry and Technology of Silicones; Academic Press: New York, 1968; pp 437–438.
2. Ibid; pp 507–511.
3. Polmanteer, K. E. Rubber Chem. Technol. 1981, 54 (5), 1051.
4. Stone, F. G. A.; et al. In Transition Metal Hydrides; Bau, R., Ed.; ACS Symposium Series; American Chemical Society: Montreal, Quebec, 1978; p 111.
5. Stone, F. G. A.; et al. J. Chem. Soc., Dalton Trans. 1977, p 1519.
6. Chalk, A. J.; Harrod, J. F. J. Amer. Chem. Soc. 1965, 87, 1133.
7. Roffey, C. G. Photopolymerization of Surface Coatings; John Wiley and Sons: New York, 1982.
8. Eckberg, R. P. Proc. 8th Int. Conf. Radiat. Curing, 1984, p 2/1.
9. Varaprath, P. J.; Wright, A. P. Polymer Preprints 1988, 29, 534.
10. Lutz, M. A. Proc. 2nd Int. SAMPE Electronics Conf., 1988, 2, 236.
11. Polmanteer, K. E.; Hunter, M. J. J. Appl. Polymer Sci. 1959, 1, 3.
12. Thompson, L. F.; Bowden, M. J. Introduction to Microlitho-graphy; Thompson, L. F.; et al., Eds.; ACS Symposium Series; American Chemical Society: Washington, DC, 1983; p 161.
13. Cagan, M.; Ridley, D. Proc. IEEE CHMT International Electronic Manufacturing Symp., 1987, p 154.

Chapter 25

Moisture Transport Phenomena in Epoxies for Microelectronics Applications

D. J. Belton[1], E. A. Sullivan, and M. J. Molter

Philips Research Laboratories, Sunnyvale, CA 94086–3409

In epoxy materials for microelectronic encapsulation, moisture is known to have a deleterious effect upon device reliability. In this paper we are concerned with moisture uptake as a function of relative humidity. The effects of temperature, sample thickness, and processing history were systematically examined for a single commercially important material via conjugate moisture sorption experiments. As temperature or penetrant activity was increased the transport behavior was observed to change in character. The change was in the direction from diffusion to Case II control. The overall character appeared dominated by the diffusion contribution. Post mold curing a sample led to an increase in both the diffusion coefficient and total moisture uptake. This result was explained in terms of both volume recovery during aging, and an increase in sample defect volume.

The effects of temperature and relative humidity on the kinetics of moisture sorption in epoxy materials for microelectronics encapsulation are not generally known. In a previous paper (1) we examined moisture sorption as a function of temperature under conditions of 100 percent relative humidity. Conjugate sorption measurements were combined with mechanical, dielectric and thermal methods of analysis to examine moisture related microstructural alterations.

Exposure of a polymer to a liquid or gaseous pene-

[1]Current address: Signetics Korea Company, Ltd., Seoul, Korea

trant results in a sorption of that penetrant within the
polymeric matrix. The generally accepted transport
mechanism for small molecules in polymers above their
glass transition temperature involves simple solution
followed by diffusion (2,3). Here, solution is
described by Henry's law, and diffusion is Fickian in
nature. The transport of penetrants in glassy polymers
cannot be described by such a simple model. Generally,
anomalous behavior is observed, and has been ascribe to
such phenomena as dual mode sorption (4-10),
fluctuations in the surface boundary conditions (11,12),
polymer relaxation controlled kinetics (13-15),
penetrant clustering (16), a history or time dependent
diffusion coefficient (2), crazing (2,17), or stress and
orientation effects (3).
In the absence of structural defects and
orientation effects, anomalous penetrant transport is
largely the result of a concentration gradient
controlled diffusion superimposed upon a relaxation con-
trolled swelling. The relative contributions of these
effects vary with the system, and within a given system
as a function of temperature, penetrant activity, and
sample geometry to yield a wide range of behaviors
(15,18,19). Fickian diffusion defines the net transport
of a penetrant under ideal circumstances, and as such
represents a limiting case for glassy polymers. Fickian
behavior has been designated, therefore, as Case I
transport (13). If one examines moisture uptake versus
the square root of time, certain criteria must be ful-
filled to characterize the kinetics as Fickian. These
are:

1. Absorption and desorption curves are initially
   linear.
2. Beyond the linear region the curves are concave to
   the abcissa.
3. Reduced curves do not display a dependence on
   sample thickness.

In some cases deviations from Fickian behavior in
glassy epoxy polymers (19-25) have been adequately
described using dual mode sorption theory (22-24). This
theory is based upon the premise that the sorbed
penetrant exists in two thermodynamically distinct
populations. These populations consist of molecules
adsorbed in "holes", and species simply dissolved in the
polymer matrix.
A second limiting transport process finds the
weight gain of penetrant a linear function of time over
the entire sorption range. This process has been termed
Case II Transport, and is mechanistically quite differ-
ent from Fickian diffusion. The rate controlling
phenomena are penetrant induced polymeric relaxations.
A combination of Case I and Case II processes has been

invoked in a number of instances to provide a description of the observed kinetics (1,14,18-21,25). Separation of diffusion and relaxation parameters has been presented for a case where diffusion is considered as Fickian (15). Such an analysis has also been applied to moisture uptake by an epoxy system (25).

In this paper we examine moisture sorption in an epoxy molding compound formulation used for semiconductor encapsulation. In particular, we will be concerned with moisture uptake as a function of relative humidity. The effects of temperature, sample thickness, and processing history will be systematically examined for a single commercially important material.

Experimental

All samples were prepared from a commercially available epoxy cresol novolac-phenol formaldehyde novolac-tertiary amine based molding compound. Pelletized preforms were heated to 85°C in a RF preheater prior to being transfer molded at 180°C/68 atm. for 90 sec. Molded samples were cooled in air to room temperature and stored in a desiccated environment until testing or subsequent thermal treatment. Post mold curing, PMC, was accomplished in a gravity oven at 175°C for a period of 4 hours. Samples without post mold curing are designated by NPMC.

Gravimetric sorption measurements were conducted using a Mettler analytical balance accurate to 0.02 mg. Moisture uptake was monitored as a function of post mold curing schedule, sample thickness, relative humidity, and temperature. For each experimental condition the average of five samples was used in the weight gain/loss determination. The samples were exposed to a series of conditions in order to construct conjugate sorption isotherms. A conjugate sorption isotherm is defined as a set of data encompassing a sorption test followed in sequence by a desorption test and a resorption test. Samples for the sorption and resorption tests were exposed to water immersion (100% R.H.) or the vapor above equilibrated salt solutions in sealed vessels at the appropriate temperature. Temperatures ranged from 25°C to 100°C, and relative humidity from 31% to 100%. Each sample set was removed from its vessel, the surface water blotted away, and then weighed. Desorption measurements were taken at appropriate time intervals on samples stored in convection ovens at the temperature of interest.

Results

A Fickian description for the amount of penetrant taken up by a plane sheet of thickness l in a time t, M_t, is given by (3):

$$\frac{M_t}{M_\infty} = 4\sqrt{\frac{Dt}{\pi l^2}} + 4\sqrt{\frac{Dt}{l^2}}\left(2\sum_{n=0}^{\infty} (-1)^n \ \mathrm{ierfc}\left(\frac{nl}{2(Dt)^{0.5}}\right)\right) \quad (1)$$

M_∞ is the moisture uptake at equilibrium, and D is a constant diffusion coefficient. For short times, Equation 1 can be approximated by (3):

$$\frac{M_t}{M_\infty} = 4\sqrt{\frac{Dt}{\pi l^2}} \quad (2)$$

Reduced conjugate sorption data can therefore be obtained by examining moisture uptake as a function of $t^{0.5}/l$. Moisture uptake is plotted in the form of M_t/W_o, where W_o is the original dry weight of the polymer (19). This approach will allow a comparison of sorption and resorption data for experiments where desorption does not result in a complete loss of sorbed moisture (1).

Classic Case II transport behavior finds weight gain a linear function of time (18). A constant rate of absorption will be the result of a constant rate relaxation process if diffusion of penetrant to the relaxing boundary is rapid when compared to penetrant induced relaxations. A relation describing penetrant uptake as a function of time has been given (26):

$$\frac{M_t}{M_\infty} = 1 - \left[1 - \frac{k_0 \, t}{C_0 \, a}\right]^n \quad (3)$$

where k_0 is a relaxation constant, C_0 is the equilibrium solubility parameter, and a is the half thickness. For a slab the exponent n is unity, and a linear dependence on time is predicted.

Moisture Sorption Under Conditions of 100% Relative Humidity. Conjugate sorption data are given in Figure 1 for NPMC samples conditioned at 100% relative humidity, (R.H.), 25°C. The PMC counterparts are given in Figure 2. The conjugate data sets deviate from Fickian criteria in that there is a crossover in the sorption-desorption curves. Otherwise the curves for sorption and desorption appear initially linear, and become concave toward the abcissa with time. It is apparent from these data that not all of the moisture gained during a sorption cycle is lost during desorption. The moisture uptake during the resorption cycle is observed to increase beyond that experienced during the absorption cycle.

In Figure 3 we present only the first sorption
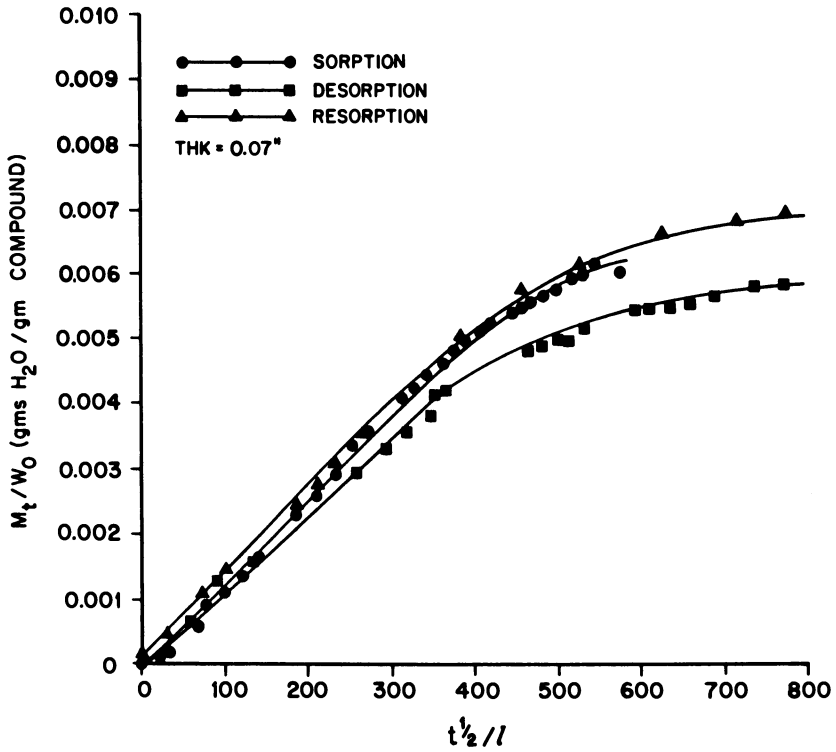
Figure 1:   Conjugate sorption data for samples without post mold cure and exposed to water immersion at 25°C.

(Abscissa units are hours$^{1/2}$/inch.)
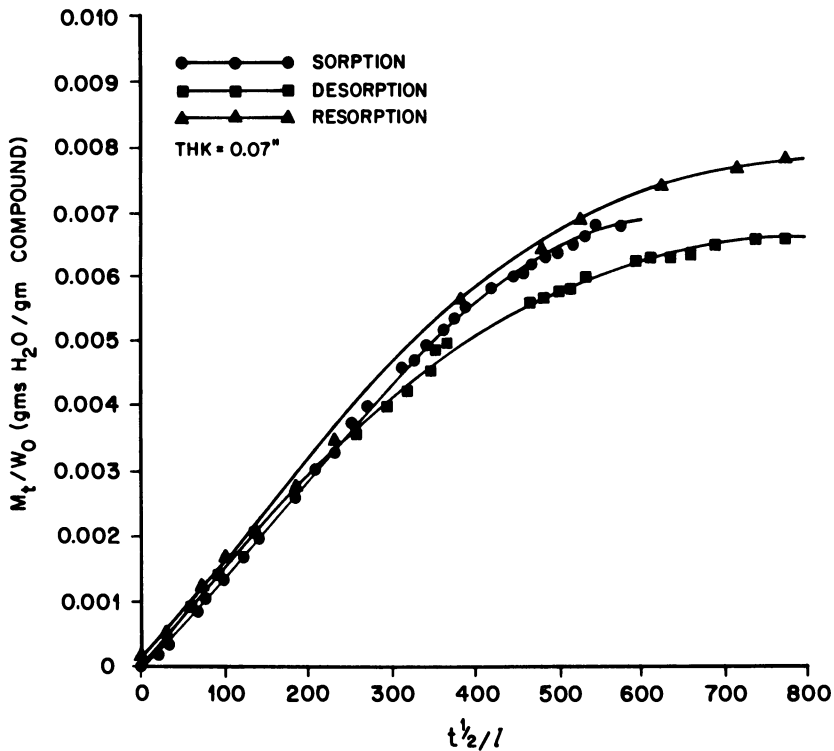
Figure 2: Conjugate sorption data for samples with a post mold cure cycle and exposed to water immersion at 25°C.

(Abscissa units are hours$^{1/2}$/inch.)
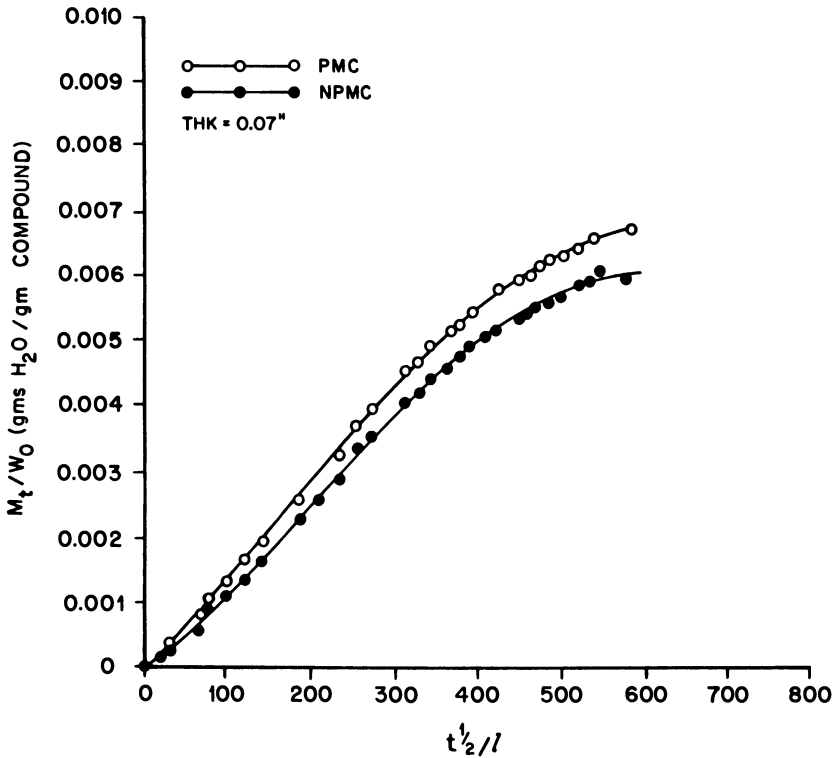
Figure 3:   Comparison of absorption cycle for samples
with and without post mold curing and exposed
to water immersion at 25°C.

(Abscissa units are hours$^{1/2}$/inch.)

cycle as a function of post mold treatment.   It is
apparent that the moisture uptake is increased for
samples that have been post mold cured.   These same
features are observed for samples exposed to 100% R.H.
at each temperature examined.   Consider the data sets
presented in Figures 4-6 for samples exposed to 100%
R.H. at 100°C.   The initial linear portions of the
curves comprising the conjugate data sets allow one to
calculate an average diffusion coefficient for each
experiment.   The results of these calculations are sum-
marized in Table I.

Table I. Average Diffusion Coefficient for Samples of
Thickness 1.78mm

CURE	T(°C)/R.H. (%)	$D(cm^2/sec. \times 10^{-8})$		
		Absorption	Desorption	Resorption
NPMC	25/100	2.26	2.32	2.25
PMC	25/100	2.56	2.63	2.56
NPMC	50/100	4.82	5.23	5.23
PMC	50/100	5.59	6.26	6.09
NPMC	66/100	7.14	8.31	7.87
PMC	66/100	7.91	9.60	8.50
NPMC	100/100	14.50	17.90	17.50
PMC	100/100	15.10	18.80	17.90

The average diffusion coefficient increase with
increasing temperature irrespective of thermal
treatment.   The diffusion coefficient scales according
to Desorption > Resorption > Absorption.   Finally, D for
the post cured sample appears greater than D for the
sample without post cure.   In Figure 7 we summarize
moisture uptake for sorption, resorption cycles as a
function of thermal treatment.   The data in Figure 7 and
in Table I coupled with the fact that the desorption
curve always crosses over the absorption curve summarize
the salient features for each conjugate data set at each
temperature.   That is, conjugate sorption curves are
initially linear with respect to $t^{0.5}/l$, then become
concave to the abscissa.   Desorption is initially faster
than absorption but becomes slower as the moisture loss
proceeds.   The desorption cycle does not result in a
complete loss of moisture.   Resorption proceeds to
higher levels than absorption.
    The criteria that sorption data must scale accord-
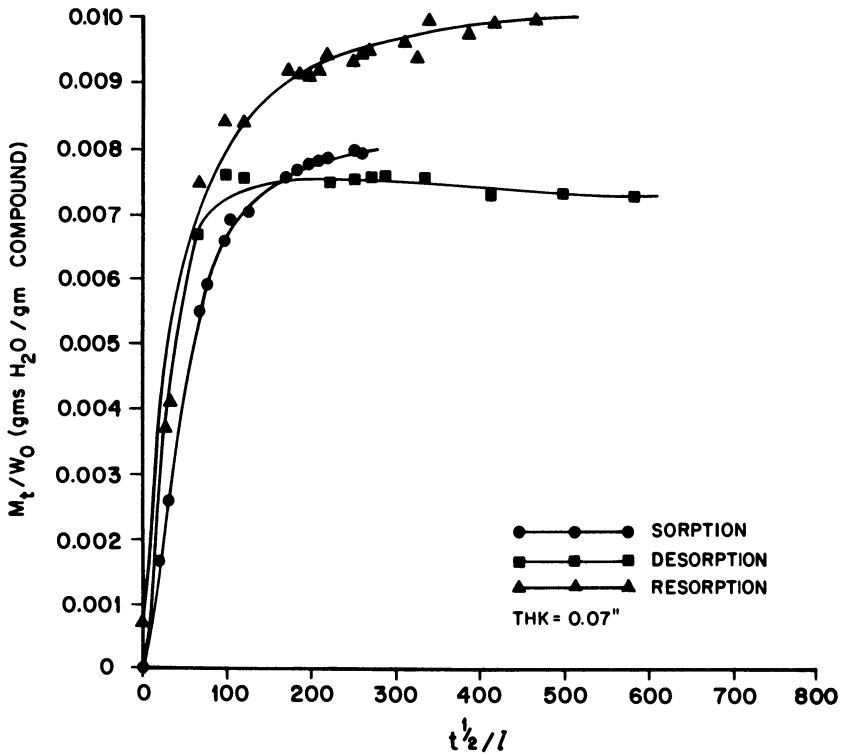
Figure 4:   Conjugate sorption data for samples without post mold cure and exposed to water immersion at 100°C.
(Abscissa units are hours$^{1/2}$/inch.)
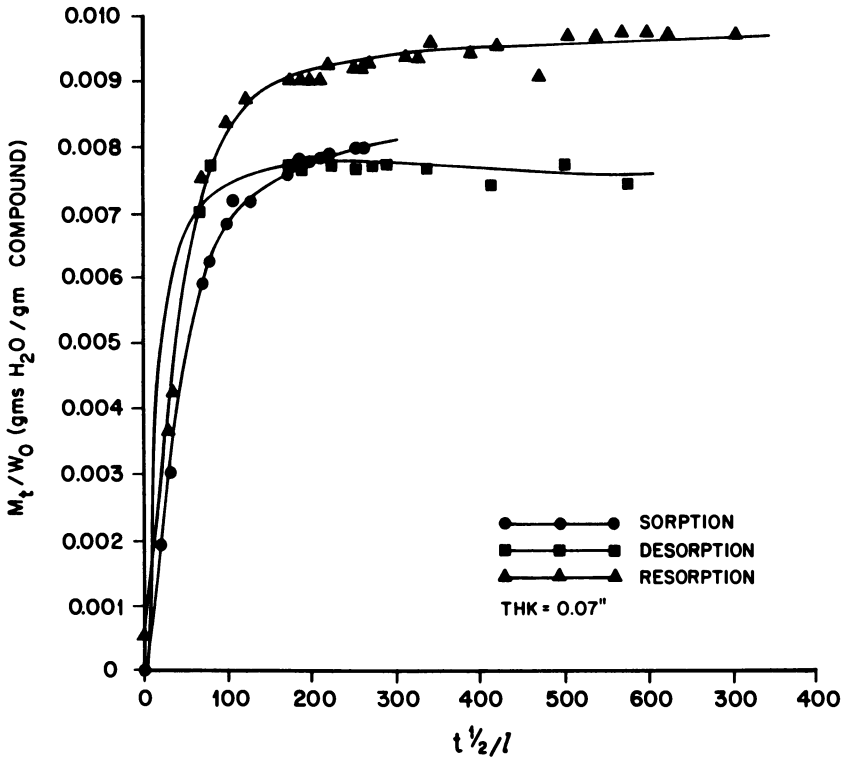
Figure 5: Conjugate sorption data for samples with a post mold cure cycle and exposed to water immersion at 100°C.

(Abscissa units are hours$^{1/2}$/inch.)
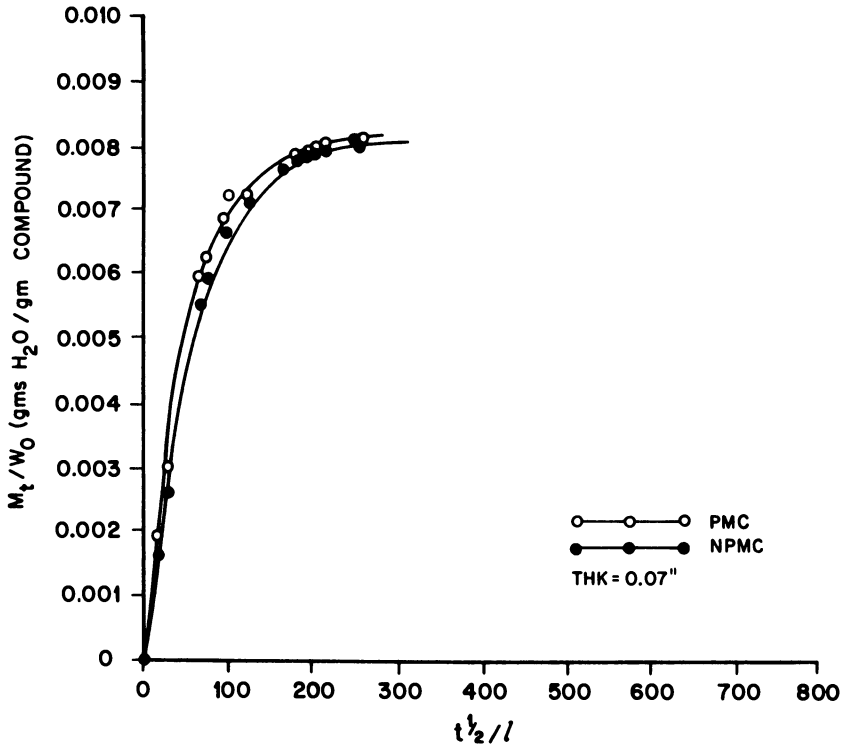
Figure 6: Comparison of absorption cycle for samples with and without post mold curing and exposed to water immersion at 100°C.
(Abscissa units are hours$^{1/2}$/inch.)
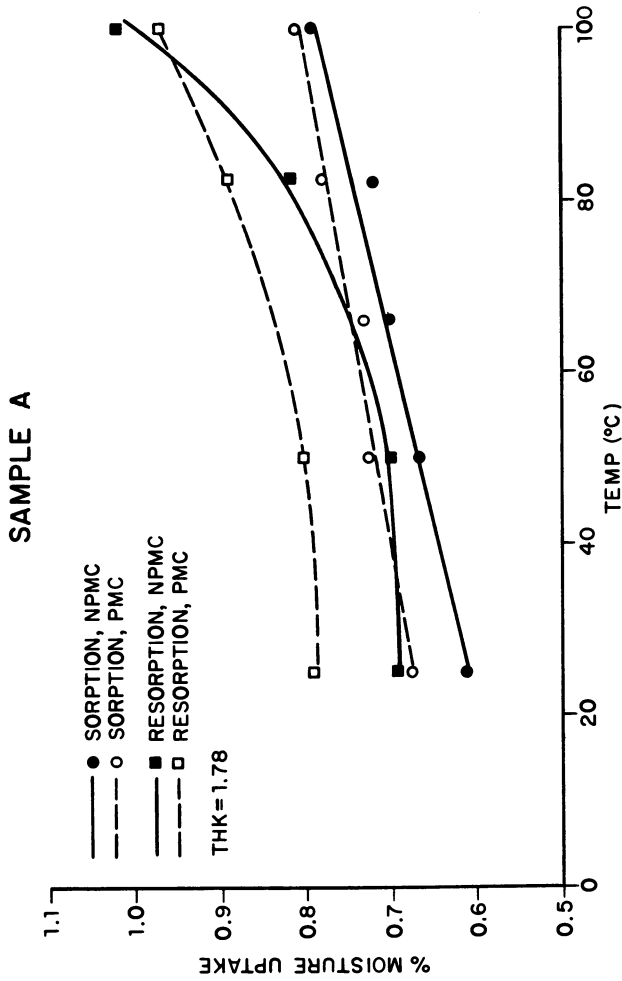
Figure 7: Moisture uptake as a function of temperature for samples with and without a post mold cure during absorption and resorption cycles. (Abscissa units are hours$^{1/2}$/inch.)

ing to thickness are examined in Figures 8 and 9. It can be seen that the data for samples of differing thickness do not lie on the same curve. The correspondence, however, becomes better as temperature increases. This trend was observed at all intermediate temperatures for all samples.

<u>Moisture Sorption as a Function of Relative Humidity</u>. Exposure conditions other than total sample immersion lead to moisture transport kinetics that are devoid of certain anomalies presented above. Figures 10-13 depict conjugate sorption data for samples with and without post mold cure exposed to two different R.H. environments at 25°C. The desorption curve lies below the absorption data in all cases. In addition, the moisture uptake during resorption does not surpass that observed during the first sorption cycle. Samples exposed to 31% and 75% relative humidity, but different temperatures are represented by the data shown in Figures 14 and 15. During desorption complete moisture removal was ensured through the use of a vacuum cycle. All cycles of the conjugate plot now appear to overlap. The percent moisture uptake as well as values of D for absorption cycles as functions of relative humidity and temperature are given in Table II. It can be seen that both moisture uptake and D increases as R.H. increases for either temperature. Both parameters are observed to increase with temperature. Finally, both parameters are increased for the post mold cured sample.

The appearance of the conjugate sorption data presented so far qualitatively indicates a shift from a more to a less Fickian character as the initial surface moisture content increases. That is, the appearance of the conjugate sorption isotherms obtained by totally immersing the samples violate two of the criteria by which Fickian behavior is defined. The same cannot be said for those samples exposed to less than 100% R.H., particularly at 25°C. This qualitative trend for PMC is further demonstrated by Figures 16 and 17. Here M_t/W_0 is presented as a function of time. For both the thick and the thin sample, as either temperature or relative humidity is increased, the character of the curves progresses towards pure Case II description. That is, the moisture uptake becomes linear with time up to the point where a plateau is achieved in the behavior.

<u>Discussion</u>

<u>Moisture Sorption Under Conditions of 100% Relative Humidity</u>. Sorption of moisture in glassy polymers and
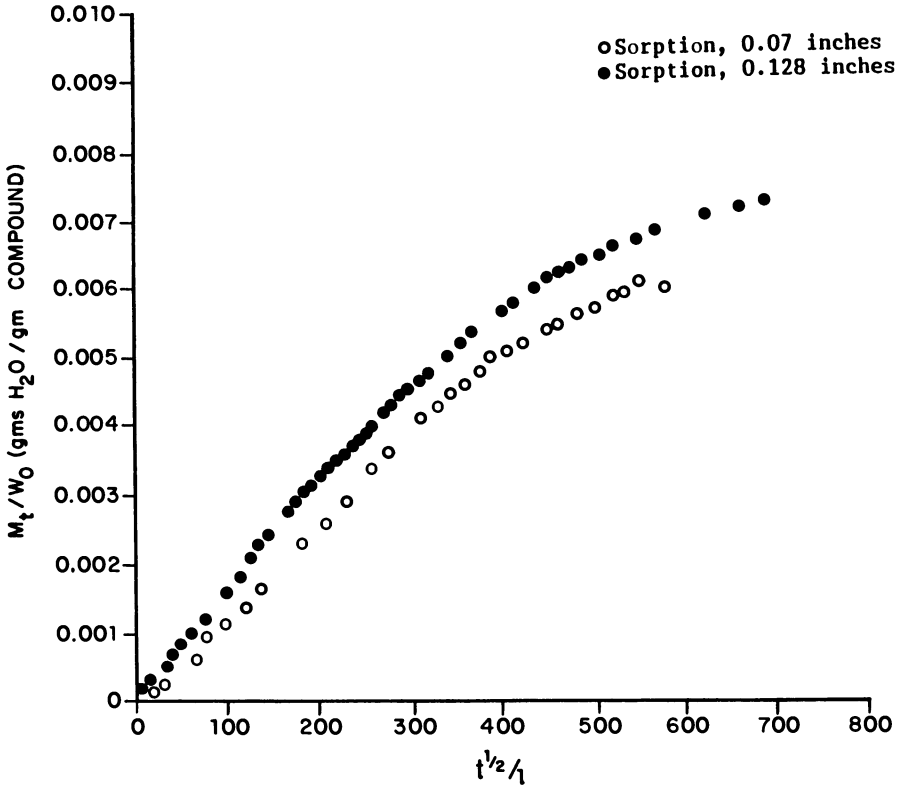
Figure 8:   Thickness scaling for samples without a post
mold cure and exposed to water immersion at
25°C.   (Abscissa units are hours$^{1/2}$/inch.)
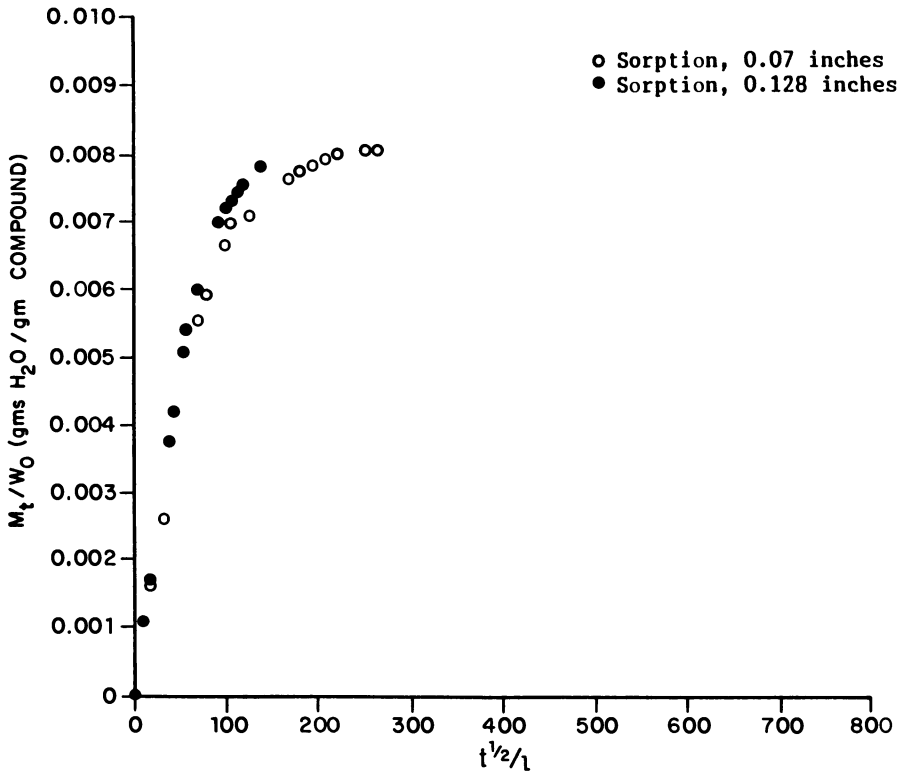
Figure 9:   Thickness scaling for samples without a post mold cure and exposed to water immersion at 100°C.   (Abscissa units are hours$^{1/2}$/inch.)
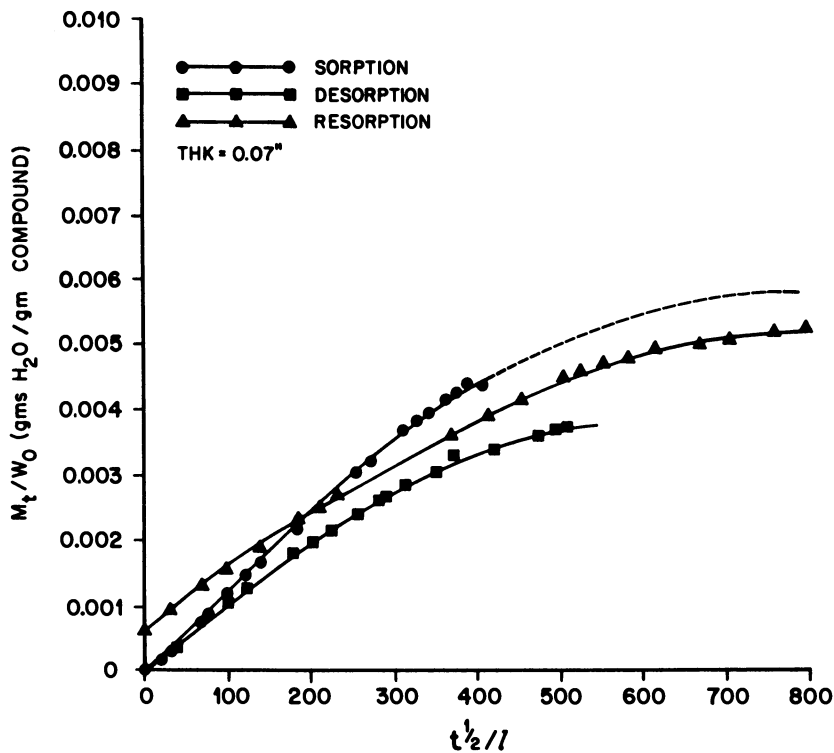
Figure 10: Conjugate sorption data for samples with a post mold cure and exposed to 31% R.H. at 25°C. (Abscissa units are hours$^{1/2}$/inch.)
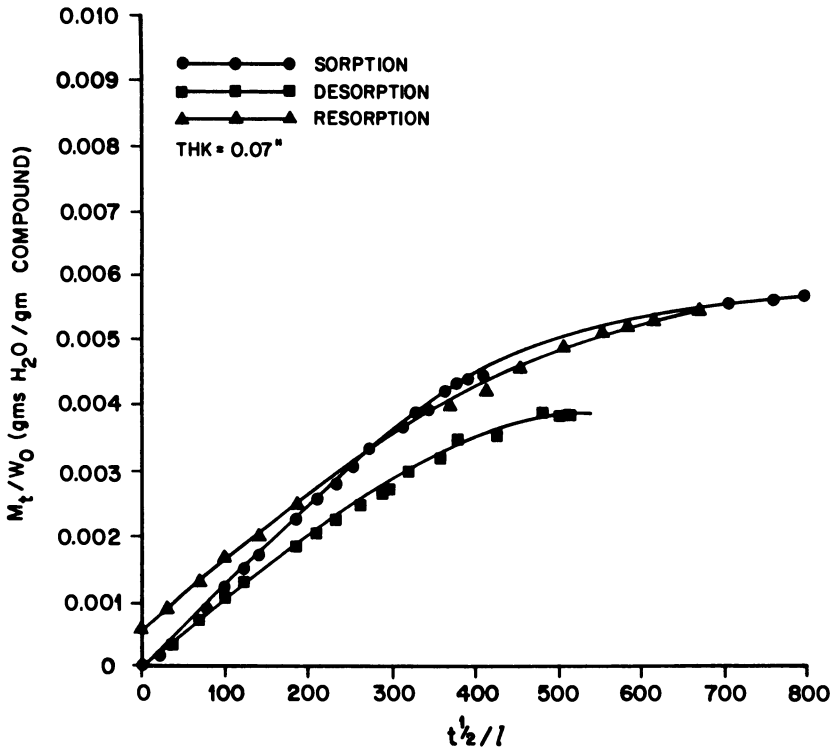
Figure 11: Conjugate sorption data for samples with a post mold cure and exposed to 75% R.H. at 25°C. (Abscissa units are hours$^{1/2}$/inch.)
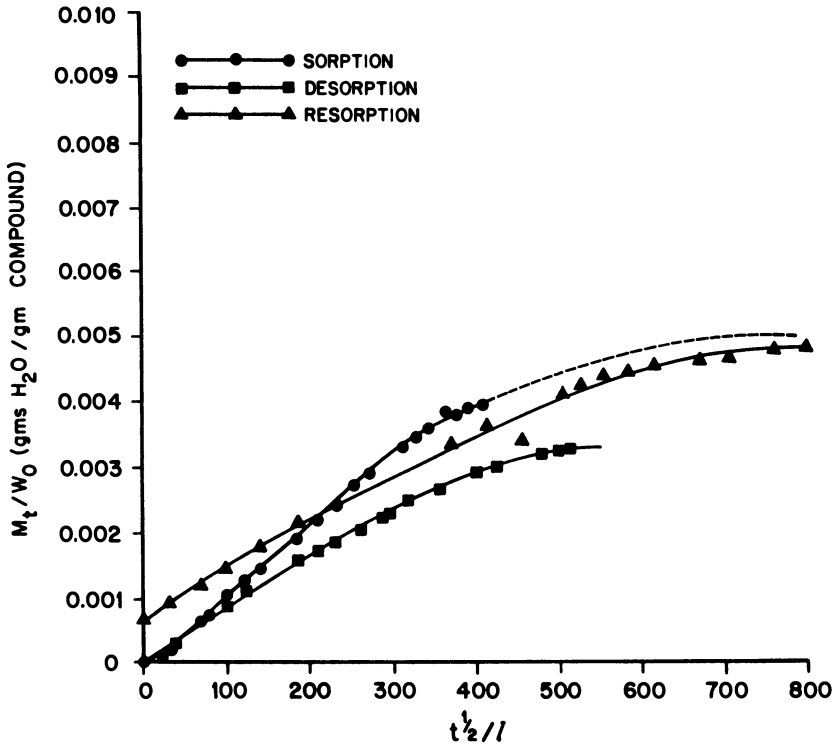
Figure 12: Conjugate sorption data for samples without a post mold cure and exposed to 31% R.H. at 25°C. (Abscissa units are hours$^{1/2}$/inch.)
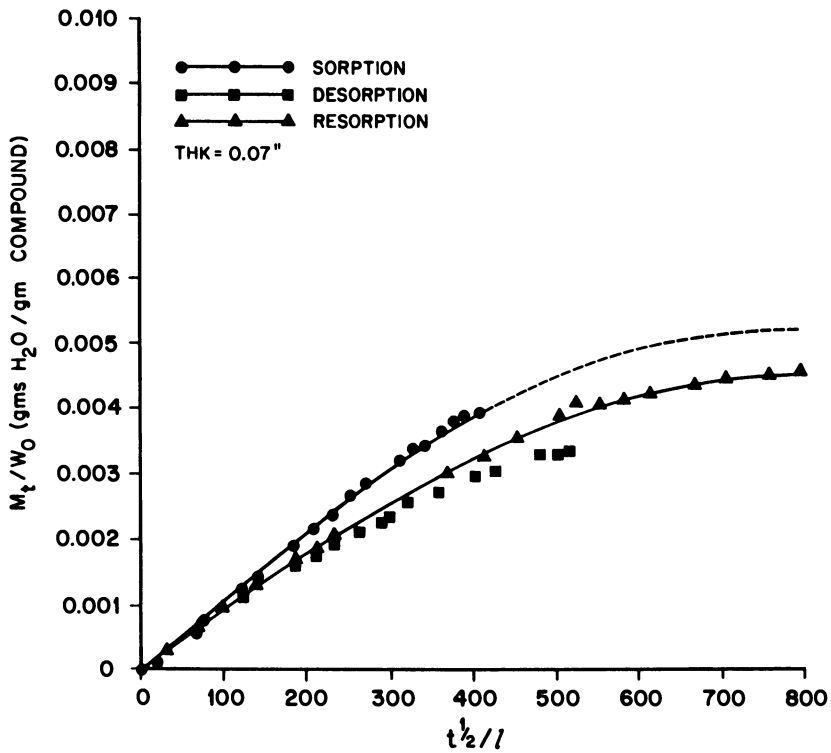
Figure 13: Conjugate sorption data for samples without a post mold cure and exposed to 75% R.H. at 25°C. (Abscissa units are hours$^{1/2}$/inch.)
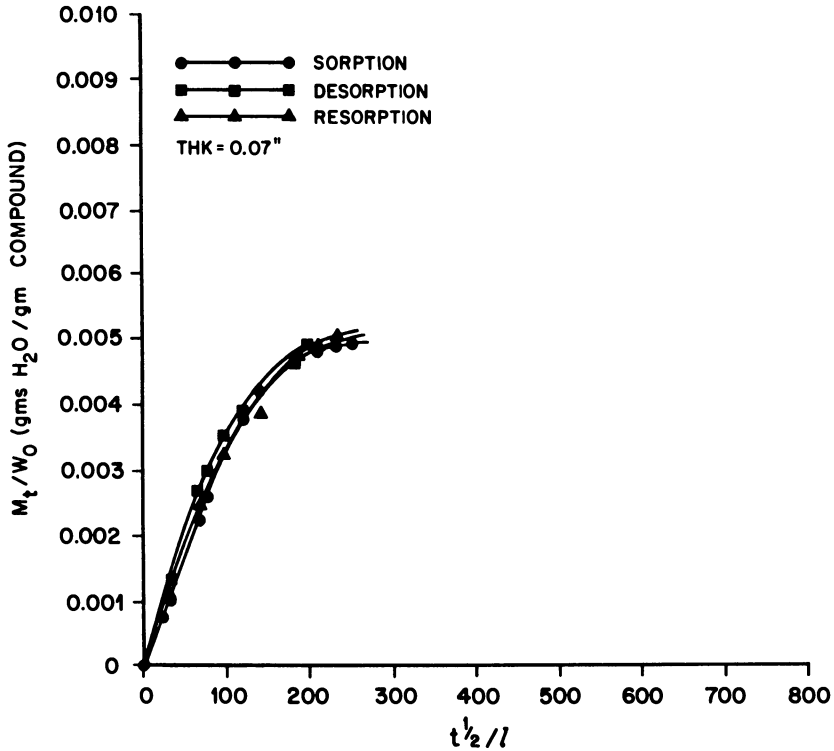
Figure 14: Conjugate sorption data for samples without a post mold cure and exposed to 31% R.H. at 66°C. Desorption conducted under vacuum. (Abscissa units are hours$^{1/2}$/inch.)
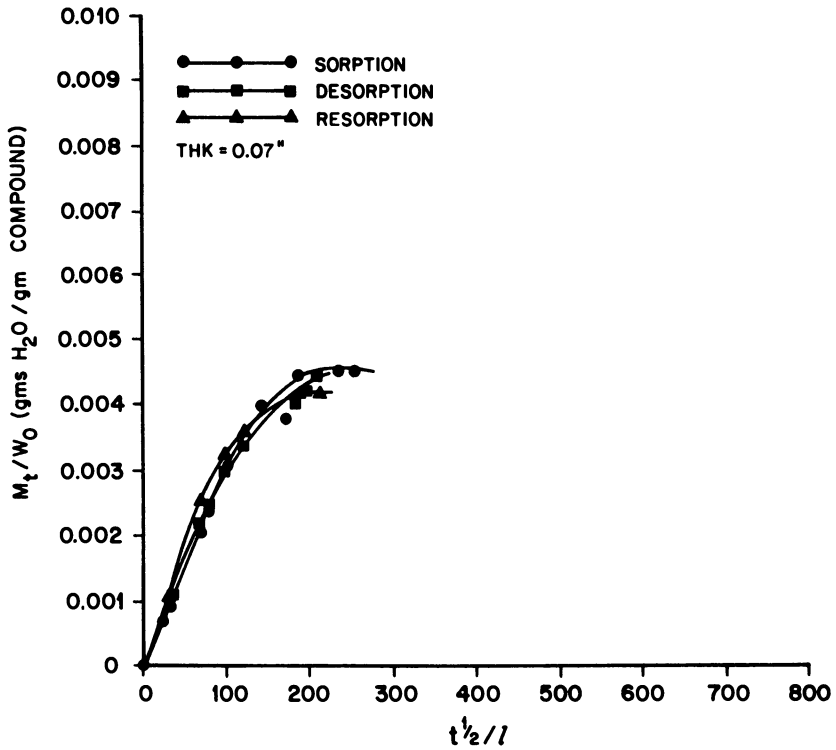
Figure 15: Conjugate sorption data for samples with a post mold cure and exposed to 75% R.H. at 66°C. Desorption conducted under vacuum. (Abscissa units are hours$^{1/2}$/inch.)
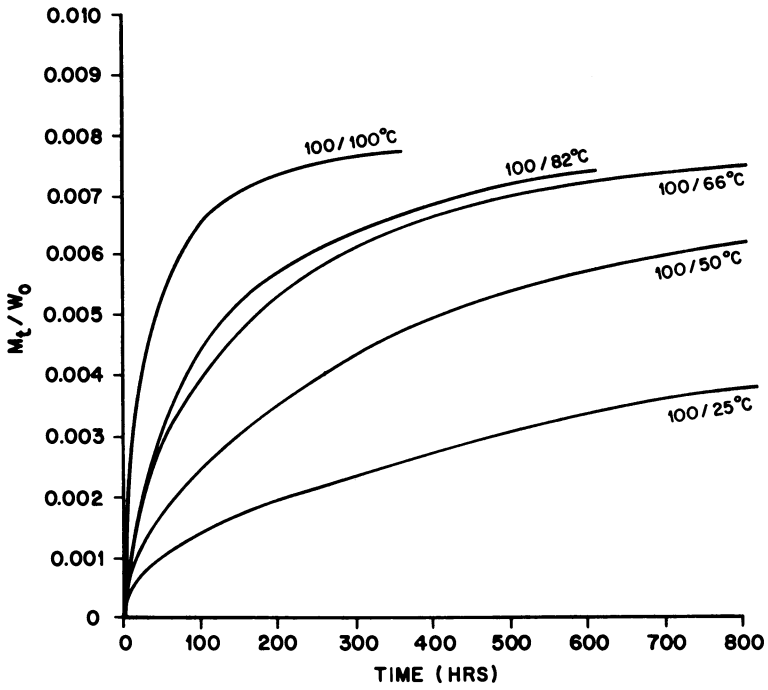
Figure 16: Percent moisture uptake versus time. Sample thickness is 0.07 inch.
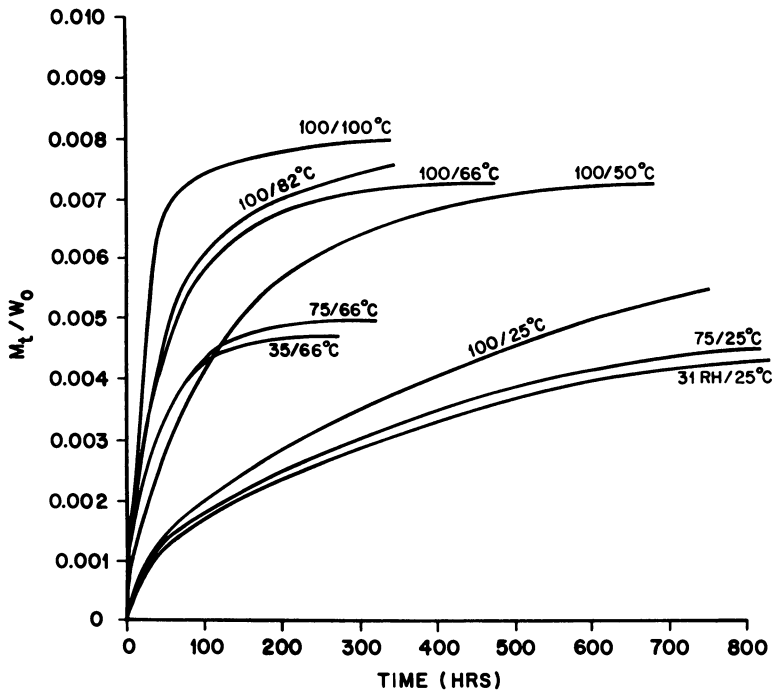
Figure 17: Percent moisture uptake versus time. Sample thickness is 0.128 inch.

Table II. Percent Moisture Uptake and Diffusion Co-
efficient for Samples with and without Post
Mold Curing as Functions of Relative Humidity
and Temperature

SAMPLE	TEMPERATURE (°C)	R.H. (%)	% MOISTURE UPTAKE	$D(cm^2/sec \times 10^{-8})$
PMC	25	31	0.44	2.20
NPMC	25	31	0.40	1.96
PMC	25	75	0.45	2.27
NPMC	25	75	0.40	1.96
PMC	25	100	0.56	2.56
NPMC	25	100	0.50	2.26
PMC	66	31	0.48	6.49
NPMC	66	31	0.46	5.56
PMC	66	75	0.50	5.92
NPMC	66	75		
PMC	66	100	0.75	7.91
NPMC	66	100	0.70	7.14

their composites is a complex process which can be
further complicated by the presence of structural,
stress, and orientational effects. Initially we will
consider conjugate moisture sorption kinetics to be
described by contributions from a concentration gradient
controlled diffusion, and relaxation controlled swell-
ing. The data presented herein are concerned with inte-
gral sorption as well as incremental sorption experi-
ments. Integral sorption kinetics describe transport in
a sample originally penetrant free, while in incremental
sorption there is an initial penetrant concentration
(15). These two cases correspond to the absorption and
resorption cycles of the conjugate data sets. During
the initial sorption cycle transport will always
commence by a diffusive process into the previously
unoccupied polymer matrix. Diffusive motion will occur
when a penetrant molecule jumps from its own position to
an adjacent location, and its previous position is

filled before it can return. When the penetrant has a molecular size much smaller than the monomer unit of a given polymer, and the thermodynamic interaction is weak, a limited movement of only one or two monomer units would be sufficient to provide the cross section required for a diffusive jump. In this limiting case diffusive motion can be described by Fick's law, with Henry's law describing the penetrant-polymer equilibrium. Fickian behavior may persist throughout the time scale of sorption to equilibrium within the proper regimes of the temperature-penetrant activity plane. A generalized diagram of the temperature-penetrant activity plane is given for organic penetrants in glassy polymers in Figure 18 (14). Areas of concentration independent, and concentration dependent diffusion are considered regions of Fickian behavior. At higher penetrant activities (for a range of temperatures below the effective T_g) structural rearrangements become necessary in order to accommodate the equilibrium moisture content. This is the regime of Case II transport depicted in Figure 18. As moisture sorption progresses under Case II conditions a sharp boundary will develop between an inner glassy core of essentially zero penetrant concentration, and a swollen outer shell of uniform concentration. The structural changes accompanying swelling are determined by time dependent relaxations, characterized by a spectrum of relaxation times. Sorption of increasing quantities of moisture can therefore lead to extensive structural rearrangements and can alter the mass transport process from a diffusion controlled to a relaxation controlled process. During Case II sorption, the final picture that emerges is rapid diffusion of penetrant to a boundary separating the swollen shell from the glassy core. This boundary progresses through the sample at a rate proportional to time. If the sample thickness is increased to a critical value, a transition from Case II to another transport mode may occur. As Case II transport progresses, the boundary separating the swollen shell from the glassy core may move to a distance where the time required for a diffusing species to reach that boundary is no longer negligible with respect to the relaxation times. Beyond this point significant diffusional resistances may begin to develop, impeding the otherwise rate determining Case II relaxations. Finally, there is a region labeled anomalous diffusion where both Fickian diffusion and Case II behavior combine to determine the transport kinetics. Samples thickness will serve to induce transport transitions in this region also.

As described earlier, samples immersed in water, regardless of curing history or temperature, exhibited two deviations from the criteria defining Fickian behavior. These are: 1) the initial higher value of D
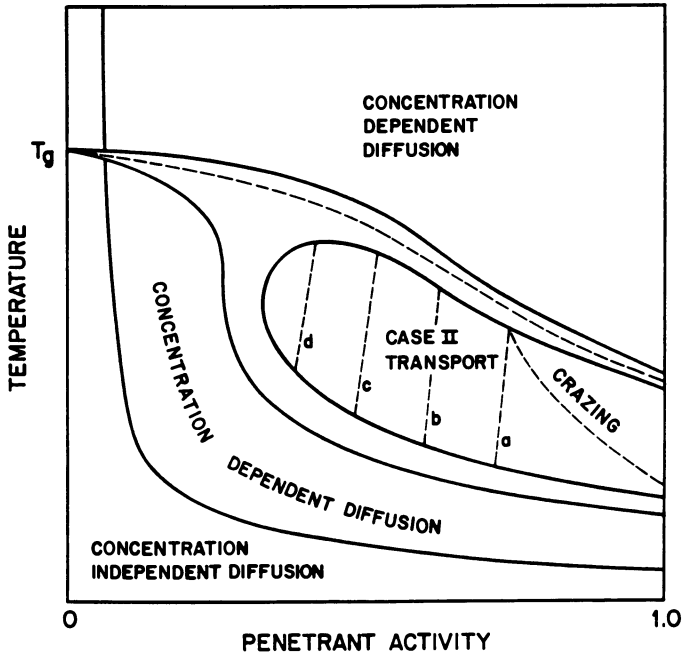
Figure 18: Generalized temperature - penetrant activity plane. (Reproduced with permission from ref. 14. Copyright 1969 Wiley.)

during desorption when compared to absorption, and the crossover of the curves, and 2) the inability of the data to scale with thickness. Deviations from Fickian behavior in glassy epoxy polymers have been described, in some cases, using dual mode sorption theory. This theory is based upon the premise that the sorbed penetrant exists in two thermodynamically distinct populations. These populations are: molecules adsorbed in "hole", C_H' and species simply dissolved in the polymer matrix, C_D. The total concentration of sorbed penetrant is given by:

$$C = C_H + C_D \qquad (4)$$

Simple solution is described by Henry's law, therefore:

$$C_D = kp \qquad (5)$$

where k is the Henry's law constant, and p is the equilibrium pressure. The concentration adsorbed is described by a Langmuir isotherm:

$$C_H = \frac{C'_H \, bp}{1 + bp} \qquad (6)$$

where C_H' is the hole saturation constant, b is the hole affinity constant, and p is the equilibrium pressure. Substitution of Equations 5 and 6 into Equation 4 yields the dual mode sorption model:

$$C = kp + \frac{C'_H \, bp}{1 + bp} \qquad (7)$$

Variation of the hole affinity constant of Equation 7 permits prediction of sorption-desorption curve shapes that match those of Figures 1,2,4 and 5 (22). Moisture diffusion in this system can be given the following interpretation: During a sorption cycle moisture is undergoing ordinary dissolution in the polymer matrix, with a concurrent adsorption at specific sites. (One does not expect a continuous void phase.) Those molecules interacting at specific sites will diffuse further into either population depending upon the adsorption reversibility. At equilibrium the voids and the matrix will be saturated. Void saturation will have an immediate effect upon the desorption characteristics. A high reversibility will speed desorption, an effect opposite to that for sorption. A finite reversibility will give rise to a finite quantity of irreversibly sorbed moisture at reasonable experimental times, hence the crossover in the curves. Dual-mode sorption theory per-

mits interpretation of our conjugate sorption data, but does not resolve the inability of the data to scale according to thickness.

Relaxation controlled moisture sorption can help to explain both of the anomalies observed in the data. At sorption equilibrium polymeric relaxations will have defined a matrix structure through which diffusion is greatly enhanced. Therefore, during an ensuing desorption cycle D initially will be enhanced. Later the curves will cross since some of the moisture is irreversibly sorbed. At intermediate times, a moisture concentration profile should indicate a trend toward reduced diffusivities. A proposed series of profiles is given in Figure 19. As the moisture desorbs, a number of phenomena must occur. During the initial stages of moisture loss the still plasticized matrix will have shorter relaxation times than those in the unplasticized state. Volume collapse can occur more rapidly under these conditions. After a certain moisture loss, contraction of the previously swollen matrix will be hindered because of increasing relaxation times, thereby preventing a complete collapse. During this series of events D should decrease. Continued desorption will further decrease the concentration gradient, again retarding moisture removal and driving the sorption-desorption profiles in the experimentally observed directions. Finally, as mentioned above, moisture loss will not be total, causing the desorption curve to ultimately reside below the absorption curve.

The inability of the data to scale according to thickness can be resolved by considering the effect of matrix relaxations. For specimens of differing thickness, at equivalent fractional distances through a sample, the concentration of moisture will change more slowly for a thicker sample. This will provide more time for those molecular relaxations necessary to accommodate equilibrium amounts of moisture. The moisture induced confirmational time dependence will therefore differ for equivalent locations within such samples. Since more time is available for molecular relaxations at equivalent locations in a thicker sample, one will observe an increase in moisture uptake as demonstrated in Figures 8 and 9. The transport behavior observed in this system has been varied over a wide range by temperature changes. The anomalies observed indicate that the behavior cannot be described as Fickian.

We can speculate, however, on the diffusion or Case II contributions to the character of the observed profiles as a function of temperature. At the lowest temperature-penetrant activity plane, one would expect Fickian transport. At low temperatures the relaxation time is much greater than the time for diffusion. In this situation there is no possibility that the struc-
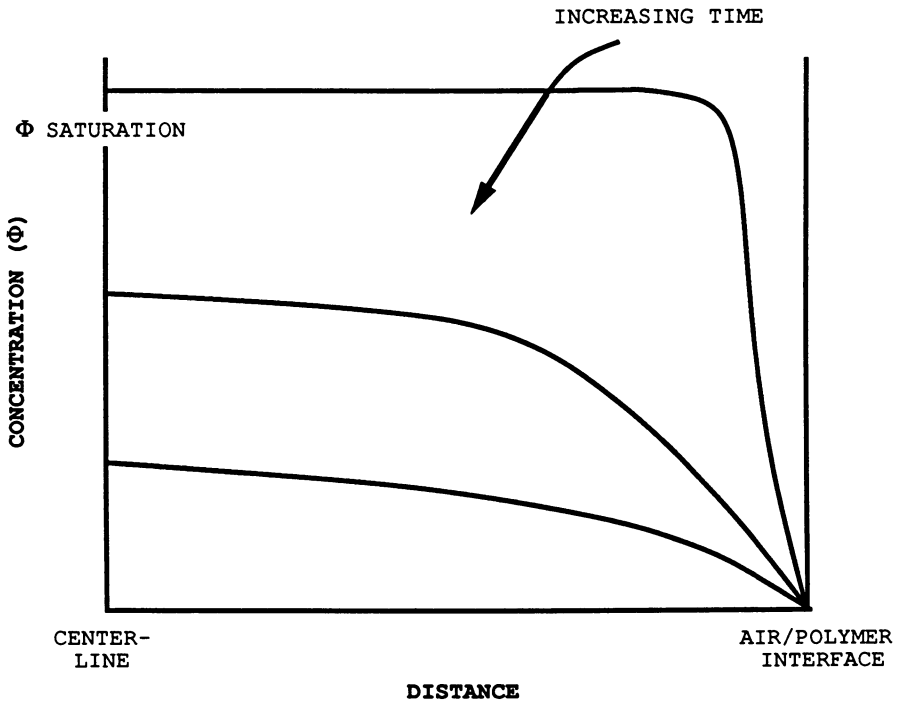
Figure 19: Schematic desorption profiles as a function
            of time.

tural rearrangements necessary to increase the volume of sorbed moisture will occur.   Therefore, moisture enters into the available free volume by a diffusive motion. As the temperature increases, the relaxation times will become comparable to the diffusion time.   The transport behavior will shift from a diffusion to a relaxation control.   The mode does not change abruptly, but is a gradual change that will define a region of behavior where both modes are operative.   Finally, as the temperature increases to values greater than the effective T_g of the material, the mode will return to diffusion control. This is because the relaxation times are now less than the times required for diffusion.

From this discussion and an examination of Figures 16 and 17, we conclude that the character of the transport mode demonstrates an increased Case II contribution as temperature is increased.   Even though the character is shifting, the overall transport behavior is believed to be dominated by diffusion.   This statement is supported by examining the magnitude of the activation energy calculated from the average diffusion coefficients.   Since the diffusion coefficient is given by:

$$D = D_0 \exp\left(\frac{-E}{RT}\right)$$

(8)

the activation energy is easily calculated from a plot of log D vs. 1/T.   The value calculated was 5.61 kcal/gm mole.   This is typical of values characterizing Fickian diffusion of small molecules in other systems (2).

The moisture uptake following a desorption cycle is considered to be an example of an incremental sorption experiment.   This is not strictly true however, since the initial penetrant concentration is present in a matrix structure that may be considerably altered from that present during the initial sorption cycle.   For samples that had been totally immersed, the desorption cycles do not lead to a complete loss of moisture.   A subsequent resorption cycle has moisture uptake increasing with temperature.   The moisture uptake, when compared to the absorption cycle, also increases with increasing temperature.   This behavior is demonstrated in Figure 7.   Relaxations during desorption may not lead to a total collapse of the previously swollen matrix. Therefore, the volume available for moisture uptake may be different during resorption than during absorption. One could expect, however, that the frozen-in volume would relax more rapidly at higher temperatures leading to a trend the opposite of that observed.   The frozen in volume is considered to be a minor effect, and we consider the increased uptake to be the result of an increase in the total defect volume.   The nature of the defect volume will be elaborated upon more below.

<u>Moisture Sorption as a Function of Relative Humidity</u>.
Distinct variations were seen in the conjugate sorption
data at 25°C as the penetrant activity was decreased
below 100% relative humidity (Figures 10-13).   In
particular, the crossover in the absorption-desorption
curves was no longer exhibited, and the moisture uptake
during resorption no longer surpassed that during
absorption.   Certain   criteria   describing   Fickian
diffusion are followed, therefore, for PMC and NPMC
samples at relative humidities of 31% and 75% at 25°C.
The thickness scaling factor has not been investigated
under these conditions.   At lower penetrant activities
more diffusion control is expected in the transport
process.   The polymer matrix does not require structural
rearrangements in order to accommodate the equilibrium
moisture content.   Consider   Figure   20;   this   is   a
schematic representation of sorbed penetrant plotted as
a function of penetrant partial pressure.   Henry's law
behavior is given by the dashed line.   Predictions of
dual mode sorption theory will deviate, as shown, from
those of Henry's law.   The data of Table II demonstrate
a deviation from linear behavior.   In fact, the data
appear to be best described by the region defined by
points A and B of the dual mode sorption theory.   The
transport behavior at R.H. values of 31% and 75% can be
described as dominated by diffusion phenomena, which can
in turn be best described by dual mode sorption theory.
Further support for these ideas is given by considering
the resorption behavior displayed in Figures 10-13.
Structural   rearrangements   will   be   reflected   in   a
resorption   cycle.   That   moisture   uptake   following
resorption   does   not   surpass   moisture   uptake   during
absorption   suggests   no   structural   changes.   Complete
removal of sorbed moisture during vacuum desorption
finds an overlap of all conjugate data at 66°C as shown
in Figures 14 and 15.   Again this can be interpreted as
resulting from a lack of structural alterations during
the initial sorption cycle, and a dominance of diffusive
transport at penetrant activities less than 100% R.H.
Finally,   if   the   moisture   uptake   is   examined   as   a
function of time (Figure 17) it can be seen that the
behavior at activities less than 100% R.H. is distinctly
non-linear,   as   should   be   the   case   during   diffusion
controlled transport.
     The resorption behavior as a function of penetrant
activity up to and including total immersion can now be
discussed   in   more   detail.   As   penetrant   activity
increases   at   a   sufficient   temperature,   the   form   of
transport kinetics can vary from Fickian to Case II to
Case II accompanied by crazing (<u>2</u>).   This progression
appears to be applicable under the conditions cited in
this   paper   for   moisture   sorption   in   epoxy   molding
compounds.   For penetrant activities of 31% and 75%
R.H., transport appears to be dominated by diffusion.
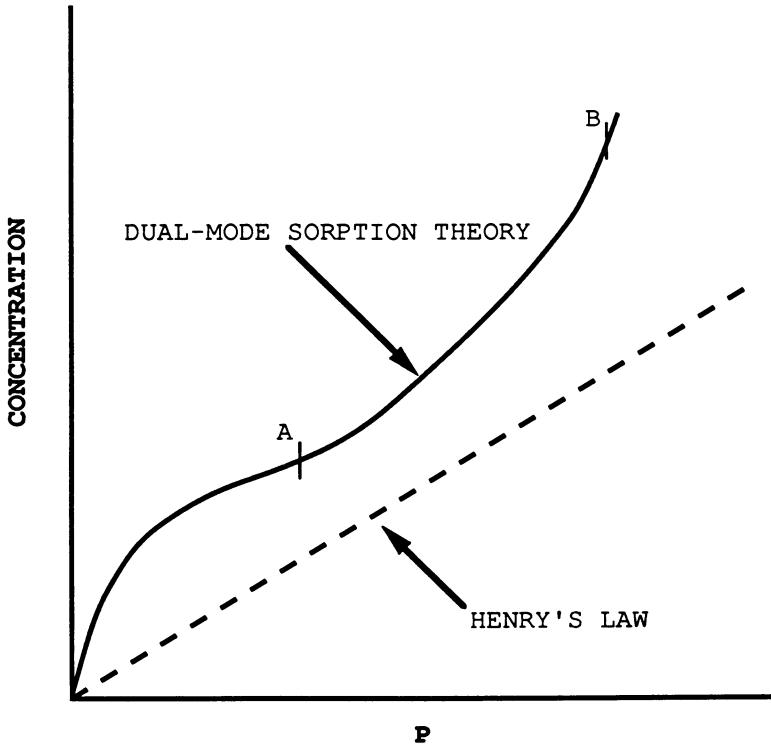
Figure 20: Schematic representation of the dependence of concentration on partial pressure illustrating predications of Henry's law and dual mode sorption theory.

As the activity increases to 100% R.H. the character of the transport begins to illustrate some relaxational contribution. This contribution becomes stronger with increasing temperature. The possibility of crazing also increases with temperature. The nature of the defect volume alluded to earlier could, therefore, in part be due to crazing. Certainly, contributions from matrix-filler breakdown cannot be neglected.

The Effect of Post Mold Curing. In the system studied here, the percent moisture uptake and the diffusion coefficient have been observed to increase for both absorption and resorption cycles following a post mold curing cycle. During the bulk of the post mold curing cycle the aging temperature is less than the sample's Tg, and the effects of both physical and chemical aging must be considered (27,28). This subject of sub-Tg aging in thermosets and its effects upon moisture sorption is interesting and has not been examined to date. Both the diffusion coefficient and the equilibrium moisture uptake are believed to depend upon the free volume in glassy polymers (2,3,20,22,23). An increase in free volume is necessary for an increase in both moisture uptake and D. An alternative explanation could reside in an increase in the defect volume (micro-voids or polymer-filler interfacial breakdown) providing a less tortuous path and an increased volume for moisture sorption. Arguments based upon each of these ideas are examined next.

Moisture has been observed to accelerate physical aging at temperatures well below T_g of the dry sample (1,29). For those samples without post mold curing and exposed to 100% R.H. at 100°C, it has been observed that T_g is initially depressed quite significantly (1). The depression for the post mold cured samples is far less. Following depression of T_g for the NPMC samples, continued moisture exposure leads to an increase in T_g indicating residual cure. The initial depression brings the effective T_g of the moisture exposed NPMC sample close to the experimental temperature. Under such conditions physical aging in the presence of low level cure is enhanced, thereby causing both D and moisture uptake to be a decreasing function of time. In the post mold cured sample T_g is continually depressed; however it remains quite high (quite far above the experimental temperature) suggesting low levels of volume contraction. This explanation assumes more importance at higher temperatures. At the low temperatures, however, the NPMC sample still exhibits lower values of D and moisture uptake. It seems likely, then that an additional mechanism is operative. The volume recovery associated with the post mold curing cycle is synonymous with a contraction of the polymeric matrix. It can be

envisioned that such a contraction could lead to a pulling away of the matrix material from the rigid filler particles. The generation of defects by such a process would drive both D and moisture uptake in the observed directions.

Conclusions

1. Anomalous transport was observed in this system at 100% R.H. As temperature was increased under such conditions the nature of the transport mode was observed to exhibit an increasing Case II character. Even though the character is shifting in such a manner, the overall transport is believed to be dominated by diffusion.
2. Increased moisture uptake under conditions of 100% R.H. during a resorption cycle was ascribed to an increase in defect volume.
3. It appears that moisture transport in conditions of less than 100% relative humidity is largely dominated by diffusion. The diffusion phenomenon is best described using dual mode sorption theory.
4. Resorption with penetrant activities less than 100% R.H. results in behavior which superimposes with that of the initial sorption cycle. This indicates little structural rearrangement or degradation.
5. Post mold cured samples exhibit a greater moisture uptake, and a larger diffusion coefficient. This has been ascribed to the generation of a significant defect volume, as well as to physical aging effects.

Acknowledgments

Literature Cited

1. Belton, D.J.; Sullivan, E.A.; Molter, M.J. *Proc. IEEE/CHMT Int. Elect. Manuf. Tech. Symp.*, Anaheim, 1987, p 158.
2. Hopfenberg, H.B.; Stannett, V. In *The Physics of Glassy Polymers*; Haward, R.N., Ed.; J. Wiley and Sons: New York, 1973; Chapter 9, p 504.
3. Crank, J.; Park, G.S. *Diffusion in Polymers*; Academic Press: New York, 1968; Chapter 1,3,5.
4. Meares, P. *J. Am. Chem. Soc*. 1954, 76, 3415.
5. Michaels, A.S.; Vieth, W.R.; Barrie, J.A. *J. Appl. Phys*. 1963, 34, 1.
6. Vieth, W.R.; Sladek, K.J. *J. Colloid Sci*. 1965, 20, 1014.
7. Petropolous, J.H. *J. Polym. Sci*. 1970, A-2, 8, 1797.

8. Paul, D.R.; Koros, W.J. J. Polym. Sci., Polym Phys. ed. 1976, 14, 675.

9. Fredrickson, G.H.; Helfand, G. Macromolecules 18(11), 1985, 2201.

10. Chern, R.T.; Koros, W.J.; Sanders, E.S.; Chen, S.H.; Hopfenberg, R.B. In Industrial Gas Separations; Whyte, T.E.; Yon, C.M.; Wagener, E.H., Eds.; ACS Symposium Series No. 223; American Chemical Society: Washington, DC, 1983; pp 47-73.

11. Crank, J.; Park, G.S. Trans. Faraday Soc. 1951, 47, 1072.

12. Long, F.A.; Richman, D.J. J. Am. Chem. Soc. 1960, 82, 513.

13. Alfrey, T. Chem. and Eng. News 1965, 43, 64.

14. Hopfenberg, H.B.; Frisch, H.L. J. Polym. Soc. 1969, B7, 405.

15. Berens, A.R.; Hopfenberg, H.B. Polymer 1978, 19, 489.

16. Zimm, B.H. J. Chem. Phys. 1953, 21, 934.

17. Kambour, R.P. J. Polym. Sci. 1966, A2, 4(1), 17.

18. Hopfenberg, H.P. J. Membrane Sci. 1978, 3, 25.

19. Wong, T.C.; Broutman, L.J. Polym. Eng. and Sci. 1985, 25(9), 521.

20. Wong, T.C.; Broutman, L.J. Polym. Eng. and Sci. 1985, 25(9), 529.

21. Moy, P.; Karasz, F.E. Polym. Eng. and Sci. 1980, 20(4), 315.

22. Gupta, V.B.; Drzal, L.J. J. Appl. Polym. Sci. 1985, 30, 4467.

23. Aronhime, M.T.; Peng, X.; Gillham, J.K. J. Appl. Polym. Sci. 1986, 32, 3589.

24. Majerus, M.S.; Soong, D.S.; Prausnitz, J.M.; J. Appl. Polym. Sci. 1984, 29, 2453.

25. Garcia-Fierro, J.L.; Aleman, J.V. Polym. Eng. and Sci. 1985, 25(7), 419.

26. Enscore, D.J.; Hopfenberg, H.B.; Stannett, V. Polymer 1977, 18, 1105.

27. Belton, D.J.; Molter, M.J. Polym. Eng. and Sci. 1988, 28(4) 1.

28. Belton, D.J. IEEE Trans. CHMT 1987, CHMT-10(3S), 358.

29. Ellis, T.S.; Karasz, F.E. Polym. Eng. and Sci. 1986, 26(4), 290.

Chapter 26

Heterogeneous Conduction Processes in Integrated-Circuit Encapsulation

D. A. Hoffmann[1], James E. Anderson[2], L. J. Bousse[3],
and Curtis W. Frank[4]

[1]Department of Materials Science and Engineering, Stanford University,
Stanford, CA 94305
[2]Ford Motor Company, Dearborn, MI 48121
[3]Center for Integrated Systems, Stanford University, Stanford, CA 94305
[4]Department of Chemical Engineering, Stanford University,
Stanford, CA 94305

Microelectronic encapsulation failure mechanisms have been studied using a combination of electrical measurements and *in situ* fluorescence microscopy and imaging. DC resistance and AC impedance measurements were made on a commercial silicone encapsulant on aluminum interdigitated comb test structures. AC impedance measurements were made over a frequency range of 0.1-1000 Hz. In some experiments, controlled levels of ionic impurities were introduced to simulate surface contamination effects. Voltage dependent DC resistances indicate electrochemical conduction with a 1.25-1.5 V threshold. In the presence of ionic contamination, super-threshold conductivity increased by 100X. A proposed interpretation is that conduction occurs via local aqueous pathways near the IC-encapsulant interface. Direct visual evidence of pathway formation was obtained using fluorescence microscopy/imaging. Fluorescent patterns spanning metal lines and local fluorescence oscillations were observed in sinusoidal electric fields. These images are believed to represent local aggregations of surface moisture and electrolytically induced pH swings, respectively.

A number of integrated circuit (IC) failure mechanisms are related to the presence of water and impurities at device surfaces. The most catastrophic failures are open or short circuits resulting from electrochemical attack on substrate metallization. Other, more subtle maladies include increased capacitive coupling between conductors (1), reduced bipolar current gain (2), shifted MOS threshold voltages (3,4), and parasitic MOS devices (5,6). These problems arise from spurious electrical conduction processes in the presence of moisture and ionic contaminants. Polymer encapsulants, such as silicone rubber, provide barriers that prevent the formation of conductive water films on IC surfaces.

DC leakage current measurements are among the most widely accepted methods for monitoring encapsulant performance (6-12). Measurements are made on encapsulated IC test structures under various temperature, humidity and bias (THB) conditions. Exposure to environmental stresses generally causes a leakage current increase which is attributed to water or ionic contamination at the IC surface. Consequently, leakage currents serve as a measure of encapsulant effectiveness as barriers to moisture and contamination. Owing to the availability of good commercial instrumentation, the simple experimental configuration, and a broad base of published data, this technique has been applied in many studies of microelectronic encapsulation.

It is our hypothesis that the observed leakage currents flow in localized conduction pathways consisting of aqueous films or vacuoles that occur heterogeneously throughout the bulk encapsulation or at the IC surface. Further, the formation of these pathways may be related to the presence of structural defects or impurities in the encapsulation or IC surface layers. It was our goal to evaluate alternative experimental techniques to probe mechanisms of conductive pathway formation. We employed a "contamination by design" strategy (9,12) to produce artificial pathways in electrical test specimens. To gain additional insight into failure mechanisms, DC leakage current measurements were extended to AC impedance spectroscopy (ACIS). Finally, a fluorescence microscopy/imaging technique was developed to probe the local chemistry and structure of the conduction pathways causing the observed electrical response.

Contamination by Design. In "contamination by design" experiments (9,12), artificial conduction pathways are introduced deliberately at the IC surface to exaggerate electrochemical failure. To this end, surfaces IC test samples were purposely contaminated with $CaCl_2$ prior to encapsulation. Under conditions of greater than 29% relative humidity (RH), the $CaCl_2$ dissolves, forming aqueous vacuoles spanning adjacent metal lines at the IC surface. These vacuoles function as small electrolytic cells wherein localized reactions occur. Surface loadings were massive from the standpoint of IC practice, perhaps 10,000 to 100,000 times larger than those of cleaned specimens. Since fundamental electrochemical processes should be unaffected by the quantity of contamination, light and heavy surface loadings are expected to produce similar effects, differing in magnitude, with heavy loadings easier to characterize by electrical measurements and microscopy.

AC Impedance Spectroscopy. ACIS is essentially the AC analog of DC leakage current measurements. This technique has been used in studies of corrosion kinetics of coated metals (13-15). While DC leakage currents reveal the rate of the slowest step in the conduction mechanism, ACIS measurements probe the rates of all processes. The principle is that processes with rates closest to the AC measurement frequency dominate electrical impedance. ACIS measurements usually involve small-amplitude voltages relative to those used in DC leakage current measurements. This is advantageous in minimizing system perturbation, but it also can result in poor signal-to-noise ratios, especially at low frequencies. Although ACIS

is a potentially powerful technique for defining the presence and rates of conduction processes, results must be viewed with the usual caveat that electrical measurements provide no direct information about the chemical or physical identity of localized processes. ACIS is therefore most useful in studying systems for which qualitative models of the conduction mechanisms exist.

Fluorescence Microscopy and Imaging. Fluorescence microscopy and imaging provide a means of visualizing local chemical events related to the observed electrical response of an encapsulated IC. While electrical measurements reflect values of current flow averaged over an IC surface area of 10-100 mm^2, regions 1000 times smaller can be resolved with a fluorescence microscope. The contrast and resolution of local fluorescence images are enhanced using new pseudocolor imaging techniques. Chemical and structural properties of both polymers and oxides have been studied extensively using fluorescence. In addition, defects in IC surfaces have been identified with fluorescence microscopy (16,17). In our initial experiments, we introduced fluorescein in the region of the encapsulation/IC interface. The emission intensity of fluorescein is sensitive to pH, polarity and dielectric constant of the surroundings. Based on these properties, fluorescein molecules serve as chemical probes at the IC surface. The presence of water at the interface increases the local polarity and dielectric constant resulting in higher fluorescence intensity. Similarly, local shifts in pH caused by electrochemical reactions cause fluorescence fluctuations. Therefore, the formation of conductive pathways and electrochemical reactions can be observed as local regions of intense fluorescence. This technique provides a critical connection between average electrical properties and their local chemical origins.

EXPERIMENTAL

Sample Preparation. Electrical test specimens were interdigitated aluminum combs, consisting of metallization lines 6600 μm long x 140 μm wide, separated by 114 μm. The combs were patterned photo-lithographically in a 1 μm thick layer of aluminum metallization sputter deposited onto a 1 μm thick layer of SiO_2 thermally grown on a silicon substrate. Specimens were mounted on Airpax ADI-140-0059 chip carriers with electronic-grade epoxy cement. Gold wires, 25 μm in diameter, established electrical contact between comb pattern and chip carrier. Prior to encapsulation, specimens were cleaned with methanol and dried in a 120° C oven. Specimens were encapsulated in Amicon SC-120-8 polysiloxane. This is a hybrid grade (<10 ppm ionic impurities) polydimethylsiloxane crosslinked by addition cure with a platinum catalyst. Specimens were encapsulated by coating with uncured polysiloxane, evacuating under vacuum to remove dissolved air, and curing at 120-150° C. The cured encapsulant was 0.40 ± 0.05 cm thick. These samples had been used in previous DC leakage current measurements as a function of temperature and RH (12).

Some specimen surfaces were "contaminated by design" by evaporating aqueous droplets of .01 M $CaCl_2$ solution. $CaCl_2$ is an hygroscopic salt that readily forms aqueous vacuoles under the polysiloxane at ambient humidities above 29.3% RH (12). It is important to note that surface impurity levels in our experiments can be traced entirely to deliberate contamination, as noted above, or to inadequate surface cleaning prior to encapsulation. To the best of our knowledge, the Amicon silicone encapsulant was free of contamination.

Electrical Measurements. DC leakage current measurements were made as a function of applied bias voltage over a range of -10 to +10 V. Data were obtained with a Keithley Model 616 Digital Electrometer. The voltage source was a battery-regulated potentiometer.

ACIS measurements were performed at frequencies between 1 mHz and 1 kHz using a Solartron Model 1250 Frequency Response Analyzer. Output from the comb specimens was amplified with a Keithley Model 427 Current-to-Voltage Converter before waveform analysis. Reference electrodes were not used owing to the geometry of the encapsulated test specimens. The data reported herein were obtained with a 0.1 V rms amplitude sinusoidal excitation waveform. In one experiment, DC bias was superimposed on this waveform.

Fluorescence Microscopy/Imaging. Figure 1 shows a schematic diagram of the fluorescence microscopy/image processing system. Test specimens on the microscope stage were epi-illuminated with UV/visible light and viewed through a Leitz fluorescence microscope. Fluorescence images were examined either through the microscope ocular or with a Hamamatsu Model C100 Vidicon camera. Camera output, in turn, was viewed directly on a Sony PVM 1271 RGB Monitor and/or after digitization by an Imaging Technologies Incorporated Model FG100 board. This board, whose 512 x 480 pixel output spans 256 grey levels, was housed in an IBM PC AT computer.

Test specimens consisted of parallel gold conductor tracks patterned on FR-4 epoxy glass substrates using conventional PC board technology. The line widths and spacings were 250 μm. Prior to encapsulation, a layer of dilute fluorescein-in-water solution was evaporated on the specimen surface leaving a residue of crystalline fluorescein. Specimens were then encapsulated and subsequently equilibrated with liquid water which dissolved the fluorescein. External voltage, derived from an HP Model 3310A function generator, was applied to the specimens mounted on the microscope stage. Fluorescence intensity changes, caused by the external bias, were observed. To improve contrast, it proved useful to create difference images by subtracting the average pixel intensity of a series of images from the corresponding pixel intensity in each image. This differencing procedure was applied to each of the (512 x 480) pixel locations. It also proved useful to construct a 512 x 480 array consisting of the rms pixel intensity fluctuation over one cycle of external voltage (results not shown).

RESULTS

DC Leakage Current. Under 0% RH, DC leakage currents on clean and contaminated specimens were indistinguishable. Leakage currents of 10 pA were measured under 10 V DC bias, corresponding to a resistance of 10^{12} ohms. Resistances were independent of bias between -10 and 10 V.

Figure 2 shows I-V curves for clean and contaminated samples at 100% RH. Within a range of $\pm$ 1.25 volts, the resistances of both samples were ~10^9 ohms. Above a threshold of 1.25-1.5 V, the contaminated sample exhibited a sharp leakage current increase, and the resistance dropped to 10^7 ohms. The clean specimen exhibits a similar, but much smaller leakage current increase, corresponding to a super-threshold resistance of 10^8 ohms. At positive bias levels from 8 to 10 V, the current reaches a plateau of 600 nA.

AC Impedance Spectra. Figures 3 and 4 show ACIS for a clean specimen at 0% and 100% RH, respectively. Under dry conditions, the signal-to-noise ratio was too low for reproducible low frequency impedance measurements, and only a few data points are shown. These results suggest essentially capacitive behavior. An equivalent circuit consists of a large resistor (~10^{12} ohms) in parallel with a small capacitor (~ 200 pF). Considerably more structure can be seen in the 100% RH data where the impedance is reduced by several orders of magnitude over the entire frequency range. The high frequency semicircle, or capacitive loop, is characteristic of parallel resistive and capacitive conduction processes. An equivalent circuit would consist of a 270 pF capacitor in parallel with a 6 x 10^7 ohm resistor. The low frequency impedance dispersion can be described by a second parallel RC circuit with a 10^5 pF capacitor and a 5 x 10^8 ohm resistor. This resistance is found by extrapolating an arc to the right from the low frequency dispersion to intersect the real impedance axis, and matches the DC leakage current result.

The effect of DC bias on a contaminated sample at 100% RH is shown in Figure 5. At bias levels corresponding to threshold and super-threshold levels for electrochemical reactions, the impedance spectrum shows the capacitive loop that intersects the real axis at low frequency (.1 Hz). Zero-DC-bias data, which are not shown, form a similar arc that is large compared to the scale of this plot. This behavior is modelled by a parallel RC circuit, whose resistance decreases from 1 x 10^9 to 1.6 x 10^7 and whose capacitance remains constant at approximately 30000 pF, as DC bias is raised from 0 to 3.0 V. The resistances agree with those measured in DC leakage current experiments. The capacitances are 100 times larger than those measured on the clean sample at 100 % RH.

Fluorescence Microscopy/Imaging. Fig. 6 shows representative data obtained in a localized region of high fluorescence intensity. External AC voltage was applied to the specimen, and images were captured at various phase-angles, Φ. The fluorescence of large regions of the specimen did not change in time in response to AC bias. However, all local time-dependent fluorescence changes that did occur were reproducible and periodic with the external field. In order to delineate regions where fluorescence changes took place,
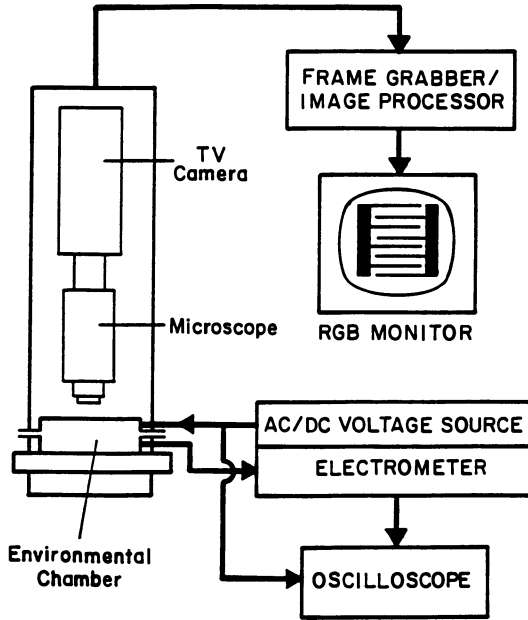
Figure 1   Fluorescence Microscope / Imaging System.

D.C. Response: Contamination
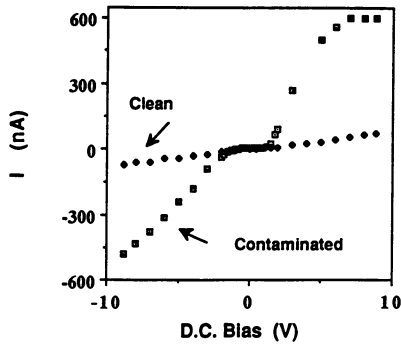
Figure 2   DC Leakage Currents at 100% RH.

A.C. Response: Dry
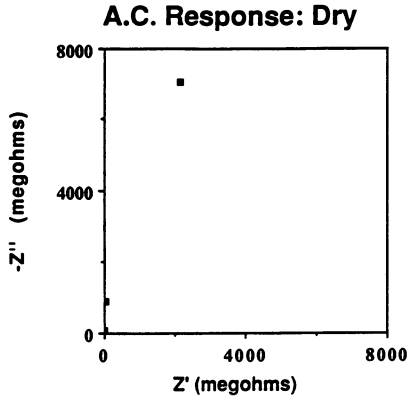
Figure 3   AC Impedance of Clean Specimen at 0% RH.

A.C. Response: Wet
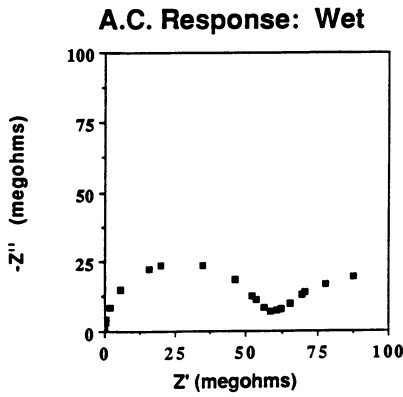
Figure 4   AC Impedance of Clean Specimen at 100% RH.

A.C. Response: D.C. Bias
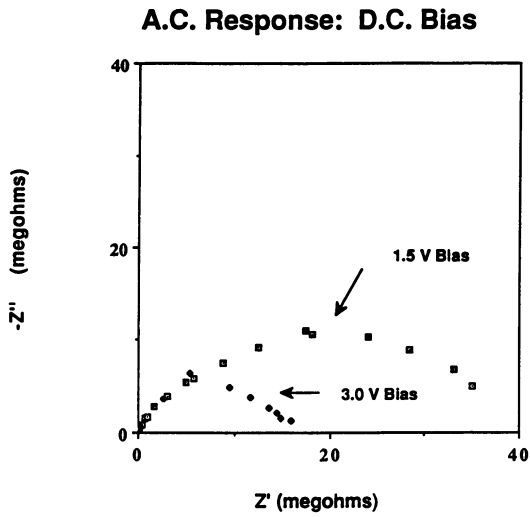
Figure 5   AC Impedance of Contaminated Specimen at 100% RH.
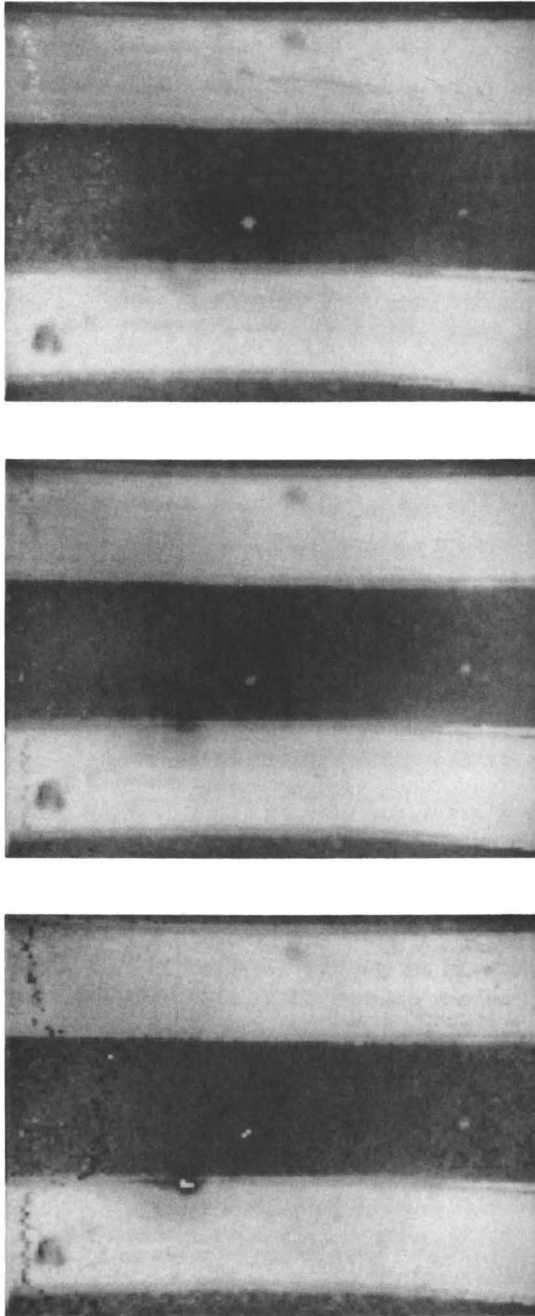
Figure 6   Localized fluorescence during application of a
Sinusoidal Electric Field. Top, Φ = 0°; middle,
Φ = 90°; bottom, Φ = 180°.

sixteen images obtained at Φ-increments 22.5° apart, were averaged. This image-average, which emphasized fluorescence regions that were insensitive to the AC field, was then subtracted from images obtained at specific phase-angles. Fig. 7 shows two difference-images taken 180° apart: For clarity in this black-and-white reproduction, Fig. 7 shows only those areas where fluorescence intensity is <u>greater</u> than its average value. At Φ = 0°, fluorescence over one metallization line is greater than its average while fluorescence near the other metallization line is less than its average. The reverse is true at Φ = 180°.

As the AC frequency was increased, or the voltage amplitude decreased, the time-dependent fluorescence change decreased at all pixel locations. At sufficiently high frequencies, changes became indistinguishable from the camera shot-noise observed in a series of images derived from a static specimen. Conversely, lowering the AC frequency or increasing the voltage amplitude, increased rms fluorescence variations.

In other situations, external voltage changed the spatial location of fluorescence regions. These motions were most pronounced at high voltage amplitudes. Fig. 8 shows a fluorescent pattern that has grown from one metallization line toward another. The region between the metallization lines exhibited no appreciable fluorescence before application of external bias.

<u>DISCUSSION</u>

<u>DC Conduction.</u> Adsorbed water increases DC conductivity, even at low bias levels, and introduces a new conduction mechanism, which is enhanced by surface impurities. Transitions in DC current-voltage measurements (c.f. Fig. 2) are consistent with the onset of an electrochemical reaction, such as water electrolysis or corrosion of the aluminum metallization, with an EMF threshold near 1.25 V. The presence of these transitions in both clean and contaminated samples suggests that the dominant reaction is the same in both cases. The relatively large super-threshold currents in the contaminated specimen are evidence that calcium and chloride ions increase the magnitude of this reaction. At 100% RH, contaminants dissolve to form aqueous droplets on the surface beneath the encapsulation (<u>12</u>). Owing to the high impurity levels, some of these vacuoles are large enough to span adjacent metallization lines of the comb patterns. Consequently, heavily-contaminated specimens containing these low-resistance shunts might be expected to exhibit lower resistance than clean specimens at sub-threshold voltages. In contrast, we measured the same sub-threshold resistance in clean and contaminated specimens. This suggests that charge transfer at the metallization surface, rather than conduction between metallization lines, is the rate controlling step under these conditions. Finally, the reduction of dI/dV slope at super-threshold voltages (8-10 volts) is interpreted as a limiting-current behavior induced by polarization of the aqueous electrolyte.
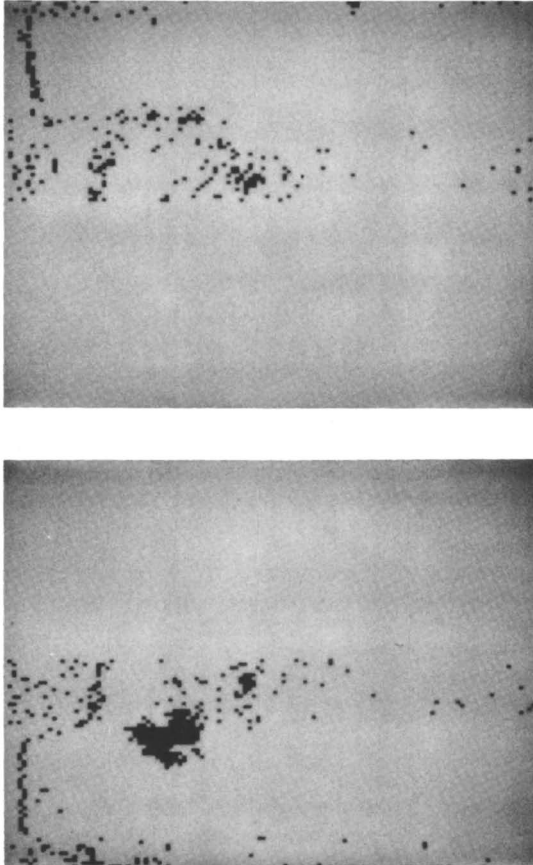
Figure 7   Difference images showing regions where local fluorescence is greater than the average. Top, $\Phi = 0^\circ$; bottom, $\Phi = 180^\circ$.
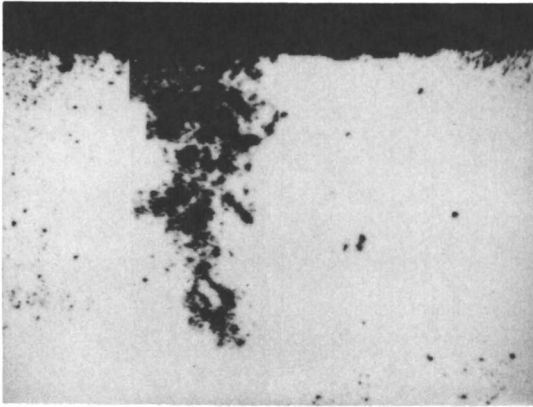
Figure 8   Localized fluorescence response to a 10 V step DC field. The central tree-like pattern is a fluorescein-stained water pathway extending from the top metallization line toward a bottom line not shown in the photograph.

<u>AC Impedance of Clean Specimens.</u> ACIS for clean specimens bear a general resemblance to recent impedance studies of organic coatings (<u>14,15,18</u>). Dry samples exhibit large imaginary (capacitive) impedances. In comparison, spectra from wet samples are semicircular in shape due to relatively low real (resistive) impedances at low frequencies. One possible interpretation of our preliminary data follows. The encapsulation behaves essentially as a dielectric insulator; i.e., a capacitor, at 0% RH. In the presence of moisture, the system exhibits lower resistance and higher capacitance, as shown by the high frequency arc, which is commonly ascribed to bulk coating properties (<u>14</u>). However, the experimental resistance values are inconsistent with the resistance of the bulk encapsulant. Silicone rubber absorbs about .15 weight % water when equilibrated at 100% RH. This sorbed water reduces the bulk resistivity of the dry polymer by 2X - 10X (Anderson. J.E.; Troyk. P.R., unpublished results). Bulk resistivities of other non-porous materials exhibit similar insensitivity to adsorbed water (<u>19</u>). In contrast, clean combs show a 100X-1000X resistivity reduction in going from dry to wet conditions. The applied waveform amplitude of 100 mV rms is well below the electrochemical threshold voltage observed in the DC measurements. Therefore, the impedance reductions cannot be attributed to chemical reactions. Although this topic requires further study, the possibility of a high concentration of water at the silicone/SiO_2 interface is suggested.

The high frequency capacitance (270 pF) is attributed to the 1 μm thick oxide layer acting as an insulator between the metallization and the silicon substrate.

<u>Low Frequency AC Response.</u> The low frequency impedance dispersion in the clean specimen at 100 % RH indicates a second conduction process in series with those described above. Either interfacial or Maxwell-Wagner polarization are reasonable explanations. Maxwell-Wagner polarization (<u>20-23</u>) arises in heterogeneous specimens containing domains of different conductivity and/or dielectric constant. This phenomenon can be distinguished by low-frequency impedance dispersions that extend over several decades of frequency. In addition, the magnitude and frequency dependence of Maxwell-Wagner polarization is related to spatial fluctuations of dielectric constant and conductivity within test specimens along with the aspect ratio of different domains. The visual observation of cloudiness in the silicone encapsulant exposed to 100% RH suggests the presence of heterogeneities in the bulk material, related to the presence of water, and presumably possessing different conductivities and dielectric constants than the bulk silicone. Interfacial polarization would involve the presence of ionic species at the interface that are swept back and forth by the sinusoidal field, while coated metallization acts as a blocking electrode. It should be noted that our test samples differ geometrically from those used in metal coating studies. In our system, charge may flow not only through the coating and across the coating/metal interface, but also along the coating/SiO_2 interface between metal conductors. The same kinds of conduction processes may occur in the bulk and along this interface, but at different rates.

AC Impedance of Contaminated Specimens. The ACIS of the contaminated sample under DC bias at 100% RH is consistent with a corroding system (15) in which a fixed number of aqueous pathways have formed, resulting in a constant area of metallization exposed to the electrolyte. In this case, the parallel capacitance corresponds to an electrical double layer of ions on the metallization. The capacitance of the contaminated sample is > 100 times larger than that of the clean sample at 100% RH due to the relatively larger concentrations of ions and water at the IC surface, which overwhelms the oxide capacitance described earlier. The reduction in the parallel resistance with increasing bias arises from the voltage dependent charge transfer process (i.e. electrochemical reaction).

Fluorescence in Sinusoidal Electric Fields. Fluorescein is an indicator whose fluorescence intensity changes with pH. Consequently, it is reasonable to interpret fluorescence response to applied AC voltage in terms of electrochemical reactions that alter the local pH. This AC-response of local fluorescence intensity exhibits classic relaxation behavior. At high frequencies, electrochemical reactions do not proceed long enough during each half-cycle to produce any appreciable pH change; consequently, specimens exhibit time-independent fluorescence patterns. At lower frequencies, the processes of electrochemical reactions at the metallization lines and mass transport combine to produce periodic time-varying fluorescence.

The fluorescence pattern that grew from one metallization line to the next under low frequency excitation is believed to represent an aqueous pathway. Although the formation mechanism has not been identified, in light of the AC experiment, a chemical attack of the polymer leading to delamination at the interface may create an area for water to aggregate. The observed growth from one metallization line to another of opposite bias is consistent with chemical attack related to a local extreme in pH arising from an electrochemical reaction at a metallization defect.

We are aware of possible similarities between Fig. 8 and water-treeing phenomena in dielectric breakdown (24).

CONCLUSIONS

DC and AC electrical measurements, contamination by design and fluorescence microscopy/imaging are feasible, complementary techniques for the study of microelectronic encapsulation failure mechanisms. In this approach, DC leakage current measurements are important for several reasons. As a starting point, DC I-V plots verify the presence of electrochemical conduction mechanisms. In relation to ACIS, DC resistance represents the low frequency impedance limit, which is difficult to measure with AC techniques. Finally, DC results provide evidence that artificial contamination of the IC surface accelerates existing corrosion mechanisms rather than producing new ones. ACIS data contain more fine structure than DC data and potentially yield more information. In this light, the sensitivity of the ACIS technique to humidity, DC bias and contamination level is encouraging. If features of these spectra can be attributed unambiguously to chemical events near the IC surface, quantitative kinetic data can be extracted. However, it is apparent

that AC results alone are insufficient to determine either the chemistry or location of failure mechanisms. For these reasons, the fluorescence microscopy/imaging experiments are especially intriguing. The development of localized fluorescent regions, whose position and intensity change in response to humidity and applied fields, supports the hypothesis of conduction pathway formation.
Future efforts will center on development of methods for collecting spectral fluorescence data and measuring electrical response simultaneously. This development will involve combined spectro-chemical and electrical interrogation of conduction pathways, leading to clearer understanding of their formation and composition.

ACKNOWLEDGMENTS

LITERATURE CITED

1. Gunther, H.; Muller, H.; Goetz, J.R.; Kantz, D. Electronic Components Conference Proceedings, 1983, p 344.
2. Mizugashira, S.; Higuchi, H.; Ajaki, T. 25th Ann. Proc. Rel. Phys., 1987, p 212.
3. Noyori, M.; Ishihara, T.; Higuchi, H. 20th Ann. Proc. Rel. Phys., 1982, p 113.
4. Noyori, M.; Nakata, Y.; Kuninobu, S. 21st Ann. Proc. Rel. Phys., 1983, p 60.
5. Wakashima, Y.; Inayoshi, H.; Nishi, K.; Nishida, S. 14th Ann. Proc. Rel. Phys., 1976, p 223.
6. Comizzoli, R.B.; Frankenthal, R.P.; Milner, P.C.; Sinclair, J.D. Science 1976, 234, 340.
7. Troyk, P.R.; Watson, M.J.; Poyezdala, J.J. ACS Div. Polym. Mat. Sci. Eng. 1985, 53, 457.
8. Koelmans, H.; Kretschman, H.J. J. Electrochem. Soc. 1978, 125, 1715.
9. Der Marderosian, A.; Murphy, C. 15th Ann. Proc. Rel. Phys., 1977, p 92.
10. Cerofolini, G.F.; Rovere, C. Thin Solid Films, 1977, 47, 83.
11. Ianuzzi, M. IEEE Trans. Comp. Hybr. Manuf. Tech. 1983, CHMT-2, 191.
12. Anderson, J.E.; Markovac, V.; Troyk, P.R. IEEE Trans. Comp. Hybr. Manuf. Tech. 1988, CHMT-11, 152.
13. Kendig, M.; Leidheiser, H. J. Electrochem. Soc. 1976, 123, 982.
14. Hubrecht, J.; Vereecken, J.; Piens, M. J. Electrochem. Soc. 1984, 131, 2010.
15. Scantlebury, J.D.; Ho, K.N.; Eden, D.A. In Electrochemical Corrosion Testing, ASTM STP 727; Mansfeld, F.; Bertocci, U., Eds.; American Society for Testing and Materials: Phildelphia, 1981; p 187.
16. White, L.K.; Comizzoli, R.B.; Deckert, C.A.; Schnable, G.L. J. Electrochem. Soc. 1981, 128, 953.

17. Cipollini, N.E. <u>J. Electrochem. Soc.</u> 1982, <u>129</u>, 1517.
18. Doblhofer, K; Eiselt, I. <u>Corrosion Science</u> 1987, <u>27</u>, 947.
19. Curtis, H.L. <u>U.S. Bureau of Standards Sci. Paper No. 234</u>, 1915.
20. Landauer, R. In <u>Electrical Transport and Optical Properties of Inhomogeneous Media</u>; Garland, J.C; Tanner, D.B. Eds.; Amer. Inst. Phys.: New York, 1978; p 2.
21. Bruggeman, D.A.G. <u>Ann. Physik (Leipz.)</u> 1935, <u>24</u>, 363; 1935, <u>24</u>, 665; 1936, <u>25</u>, 645; 1937, <u>29</u>, 160.
22. Springett, B.E. <u>Phys. Rev. Lett.</u> 1973, <u>31</u>, 1463.
23. Sillars, R.W. <u>J.I.E.E.</u> 1937, <u>80</u>, 378.
24. Dissado, L.A.; Wolfe, S.V.; Filippini, J.C.; Meyer, C.T.; Fothergill, J.C. <u>I.E.E.E. Trans. Elect. Insulation</u> 1988, <u>EI-23</u>, 345.

Chapter 27

Novel Coatings That Maintain Low Surface-Water Concentrations

James E. Anderson[1], V. Markovac[1], I. Kim[2], and Philip R. Troyk[2]

[1]**Ford Motor Company, Dearborn, MI 48121**
[2]**Pritzker Institute, Illinois Institute of Technology, Chicago, IL 60616**

This research concerns desiccant coatings that limit surface water concentrations. The coatings are useful in protecting microelectronic devices that operate in high humidity environments. The physicochemical basis for these coatings can be understood in terms of a three-layer sandwich structure. A bottom layer, applied to the microelectronic device surface, functions as a chemical barrier. A second layer, deposited over the bottom layer, contains hygroscopic material which ties up water. A top layer, deposited above the hygroscopic layer, minimizes water permeation into the composite coating. Simple calculations, validated by experiments, show that this geometry can restrict surface water for times of several years.

It is well known that the combination of surface water and surface impurities leads to high failure rates for microelectronic devices (1-6). Under high humidity conditions, solid surface contaminants take up water from the environment and dissolve to form liquid droplets, or vacuoles. These vacuoles exhibit high conductivity, relative to dry surface impurities, and facilitate electrochemical attack on metallization, which, in turn, leads to device failure.

For this reason, encapsulation is used to isolate devices from their external surroundings. Encapsulants comprise a variety of materials; viz., metals, inorganic glasses, and conformal organic polymer coatings. Each has the same function, to act as a protective molecular barrier.

In previous work (1), we examined the impact of surface impurities on electrochemical reactions beneath polysiloxane encapsulant coatings. Test specimens consisted of aluminum combs prepared on SiO_2 by photolithography. Leakage currents were measured as functions of temperature, surface impurity levels, and relative humidity. In all cases, increasing relative humidity, RH, produced a monotonic rise in leakage current, corresponding to increased water

concentrations at the polymer/substrate interface. Thoroughly-cleaned combs showed a 50X leakage current increase in going from dry (<1% RH) to moist (>99% RH) conditions. Surface impurities caused much larger increases; for example, we observed 10^5-10^7 fold changes when specimen surfaces were deliberately contaminated with $CaCl_2$ or NaCl prior to encapsulation.

The present research began as an extension of this earlier study. We had examined effects of impurities actually on the polymer-substrate interface. Now it was our intention to explore impurity transport from an external environment through the encapsulant to this interface.

Our work led instead to a novel method for maintaining low water concentrations at polymer-substrate interfaces. Although our experiments are directed at encapsulated microelectronics, the underlying chemical principles apply to other coating applications.

Experimental Results

The test specimens, encapsulant materials, and experimental methods were described in previous work ([1]). However, the present experiments involved direct contact between liquid aqueous solutions and the outer encapsulant surface (cf., Figure 1). Previously, specimens were equilibrated with N_2-water vapor combinations of controlled RH.

Initial experiments were performed under what appeared to be "worst case conditions"; i.e., encapsulated specimens in contact with saturated solutions of $CaCl_2$ or NaCl. The encapsulation consisted of a uniform polysiloxane layer. Measured leakage currents increased from 0% RH values to values previously observed in wet N_2 having a RH corresponding to equilibrium water vapor pressure over NaCl or $CaCl_2$ saturated solutions [76% and 29% RH, respectively]. Agreement between gas phase and solution phase results was expected since the chemical potential of water is the same in both situations, and this chemical potential dictates water sorption by the polymer/encapsulant. When saturated solutions were replaced with pure water, leakage currents increased further to values previously measured at 100% RH ([1]). These changes appear reversible over many cycles (Figure 2).

Two other experiments were performed in an external gas phase maintained at >99% RH. In the first case, the external encapsulant surface was kept in direct contact with a $CaCl_2$ or NaCl solution containing excess solid salt (Figure 1). In the second case, crystalline $CaCl_2$ or NaCl was encapsulated in an interlayer above the surface encapsulant (Figure 3). In both cases, leakage currents rose to values corresponding to saturated solution RH, and went no higher.

Finally, comparison experiments were performed, with and without a $CaCl_2$ interlayer, on specimens whose polymer-substrate surface was contaminated by evaporation of a liquid droplet containing 0.01 M $CaCl_2$. Previous studies ([1,5]) have shown that the leakage current of surface-contaminated $CaCl_2$ combs increases by several orders of magnitude at 20% RH, the location of the solid to saturated solution transition. Consequently, surface contamination provides a convenient method for increasing specimen sensitivity to surface water. In one experiment, the contaminated specimen was coated with a bottom layer of polysiloxane; a layer of solid $CaCl_2$ was placed on top of this coating; and the whole structure was encapsulated with a second
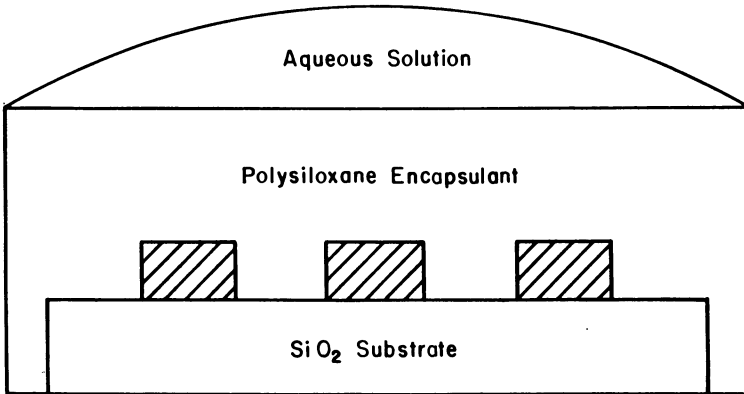
Figure 1. Schematic representation of the test specimen geometry used in the first set of experiments. The cross-hatched regions represent aluminum metallization lines.
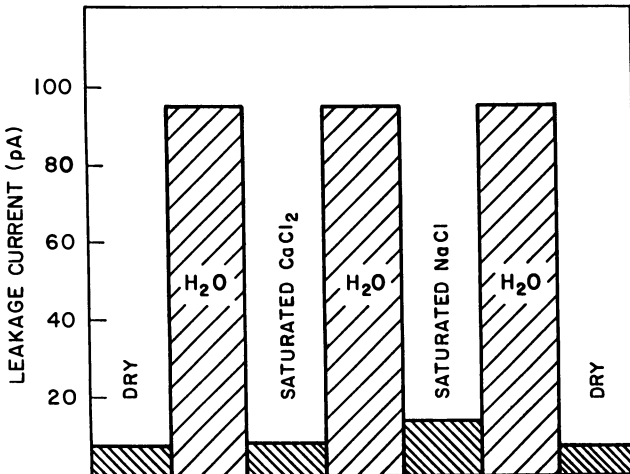
Figure 2. Experimental leakage currents measured in the first set of experiments using the specimen geometry shown in Figure 1.
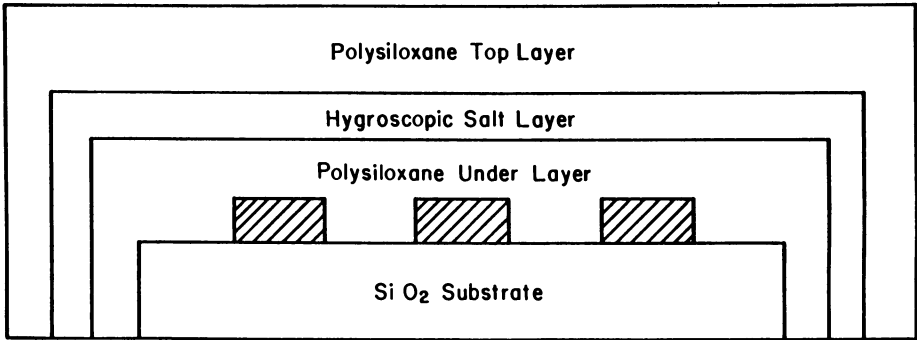
Figure 3.   Schematic representation of specimens used in final
set of experiments.   Corresponding leakage   currents are given
in Table I.

polysiloxane layer (Figure 3). Representative data on this sample are compared with a second specimen which did not contain the $CaCl_2$ interlayer (Table I). Both specimens were submerged in 85°C water under continuous 20 Vdc bias. The sample containing the $CaCl_2$ interlayer did not exhibit a characteristic leakage current increase, even after water immersion for 16 days, and showed no visible corrosion at the end of this time. In contrast, the companion surface-contaminated specimen without the $CaCl_2$ interlayer exhibited higher leakage currents and clear visual corrosion.

Table I. Leakage Currents [nA] During Underwater Immersion at 85°C [Samples were Surface-Contaminated by Evaporation of 0.01 M $CaCl_2$ Droplet Before Polysiloxane Encapsulation]

	With Interlayer	Without Interlayer
Dry, before immersion	.056	.034
After 30 hr immersion	.72	2.5
After 389 hr immersion	.50	80000.

Discussion

These experiments suggest that multilayer coatings can maintain low surface water concentrations. A bottom polymer layer is applied directly to the surface. This layer isolates the surface from an interlayer consisting of a hygroscopic material, such as $CaCl_2$. The interlayer, in turn, is covered with a top layer of polymer, whose function is to minimize water transport into the interlayer.

During exposure to high external relative humidity, water from the surroundings diffuses through the top layer, producing an interlayer consisting of a solid $CaCl_2$ and a $CaCl_2$ saturated solution. Until all salt dissolves, the water chemical potential of the saturated solution defines the water content of the bottom layer and at the polymer-surface interface.

Of course, water concentrations throughout the coating and at the polymer-substrate interface eventually must reach thermodynamic equilibrium with the relative humidity of an infinite external reservoir irrespective of the presence or absence of a salt interlayer. The essential point is that very long times are required to reach thermodynamic equilibrium. Using reasonable estimates of (a) water permeability through polymers, (b) coating dimensions, and (c) the amount of water required to convert an interlayer of solid $CaCl_2$ into aqueous solutions, it is easy to show that equilibration can take years. A sample calculation, given below, illustrates this point.

Heertjes et al. (7,8) reported kinetic studies of water uptake by polymer films containing soluble inclusions that are pertinent to the present research.

Donaldson (9) applied water chemical potential arguments to explain lower leakage currents measured in encapsulated microelectronic devices exposed to sugar-water solutions, relative to devices exposed to pure water. The differences reported by Donaldson are smaller than those reported here, since a saturated sugar solution has less effect on the water chemical potential than a saturated $CaCl_2$ solution.

Throughout this article, the basic concept of using hygroscopic coatings to control interfacial water concentrations has been framed in terms of $CaCl_2$. This is a common laboratory desiccant which should be familiar to a chemical audience. It should be noted, however, that similar arguments apply to any interlayer desiccant material. In order to preclude ionic diffusion from the interlayer to the polymer-substrate interface, it may be preferable to replace inorganic salts with immobile hygroscopic species such as molecular sieves.

A Representative Calculation of Water Uptake Through Coatings

Assume the geometry shown in Figure 3 with an interlayer containing 0.1 gm of anhydrous $CaCl_2$. This corresponds to 9.0×10^{-4} moles of $CaCl_2$. At 20°C, a saturated aqueous $CaCl_2$ solution [6.7 molal] contains roughly 8 moles H_2O per mole $CaCl_2$. It follows that some 0.13 gm [7.2×10^{-3} moles] H_2O must permeate through the outer layer to dissolve all the $CaCl_2$. Until this occurs, water in the interlayer is maintained at the H_2O chemical potential of a saturated $CaCl_2$ solution: This chemical potential corresponds to a 29% RH.

Assume the outer layer has an area of 1 cm^2, a thickness of 0.1 cm, and a water permeability of 10^{-10} gm/cm-sec. At 100% RH, it should take 1.3×10^8 sec [about 3 years] for 0.13 gm H_2O to reach the interlayer.

Literature Cited

1.   Anderson, J.E.; Markovac, V.; Troyk, P.R. IEEE Trans. Components, Hybrids and Manuf. Technol. 1988, CHMT-11, 152.

2.   Troyk, P.R.; Watson, M.J.; Poyezdala, J.J. ACS Div. Polym. Mat. Sci. Eng. 1985, 53, 457.

3.   Koelmans, H; Kretschman, H.J. J. Electrochem. Soc. 1978, 125, 1715.

4.   Der Marderosian, A; Murphy, C. 15th Ann. Proc. Reliabil. Physics 1977, pg. 92.

5.   Cerofolini, G.F; Rovere, C. Thin Solid Films 1977, 47, 83.

6.   Iannuzzi, M. IEEE Trans. Components, Hybrids and Manuf. Technol. 1983, CHMT-2, 191.

7.   Perera, D.Y.; Heertjes, P.M. J. Oil Colour Chem. Assoc. 1971, 54, 777.

8.   van der Meer-Lerk, L.A; Heertjes, P.M. <u>J. Oil Colour Chem.</u>
      <u>Assoc.</u> 1975, <u>58</u>, 79.

9.   Donaldson, P.E.K; Sayer, E. <u>Med. Biol. Eng. Comput.</u> 1981,
      <u>19</u>, 483.

RECEIVED May 30, 1989

Chapter 28

Thermal Stress in Epoxy Molding Compounds and Packaged Devices

W. F. van den Bogert, M. J. Molter, S. A. Gee, D. J. Belton[1], and V. R. Akylas

Signetics Division, Philips Research Laboratories, Sunnyvale, CA 94086–3409

Studies on thermomechanical stresses in plastic pack-
aged integrated circuits after molding and in encap-
sulation materials, show the resulting stress distri-
bution on the surface of the die and clarify the
fundamental mechanism in the generation of thermo-
mechanical stresses in molding compounds.

Use was made of a piezoresistive strain gauge
array to measure the stress distribution on the sur-
face of the die. A beam bending apparatus was used
to study the importance of the thermoviscoelastic
properties of the molding compound. The strain gauge
allowed for the study of the effects of thermal shock
testing.

The largest stresses are observed as shear
stresses at the corners of the die at the lowest
temperature. Three commercially available epoxy-
based molding compounds were studied. Two of these
materials are standard packaging formulations for
smaller devices. Both strain gauge and beam bending
experiments showed comparable stress levels with
these two materials. The third material is a rubber
modified, low stress material. As expected, stress
levels in devices packaged with this material, as
well as stresses observed in the beam bending
apparatus, were considerably lower than those for the
other two materials.

In integrated circuit packaging, thermosetting polymers are import-
ant due to cost considerations in both manufacturing and material
selection. Plastic packaging (1) has therefore become the dominant
method of protecting integrated circuits from the environment. The
manufacturing process involves a transfer molding operation in
which an integrated circuit is encapsulated with a silica filled

[1]Current address: Signetics Korea Company, Ltd., Seoul, Korea

epoxide (approximately 70% filler, 20% polymeric material, and 10% other additives) at elevated temperatures (175°C) and pressures (7 MPa) in 20 seconds or less. The design of the mold (i.e. runner system, cavities, gates and vents), the rheological characteristics of the molding compound, and the process parameters are important to ensure a void-free package with minimal distortion of the wire connections between die and lead frame (wire sweep). Alignment of filler particles and flow patterns in the cavities will lead to a certain amount of anisotropy in the molding material. To ensure some mechanical integrity, a certain amount of cure is necessary, and the parts are kept in the mold at 175°C for approximately 90 seconds. Subsequently they are removed from the mold and quenched to room temperature.

Differences in thermomechanical properties between the silicon die/lead frame assembly and the molding compound, in combination with the manufacturing process, cause residual thermal stresses (2). Furthermore, the increasing complexity of integrated circuits with an accompanying increase in die size leads to larger thermal stresses. At the same time reliability concerns necessitate severe thermal stress testing of packaged integrated circuits in order to evaluate package design, material selection, and manufacturing operations. This accelerated life testing may cause metal shift, top to bottom metal shorts or package cracking (3).

Selection of molding compounds for integrated circuit packaging must be based on the measurement of material properties and an understanding of the relationship between these properties and thermal stresses. To determine this relationship a bilayer beam structure has been utilized. A beam bending apparatus allows for the measurement of the curvature, a direct measure of the stress in the bilayer structure. The time-temperature history of the molding process is important in determining the resulting mechanical properties of the molding compound. The transfer molding operation introduces other stress determining factors as well. Stress measurement should therefore not be limited to the beam bending structure, but should also include the use of a piezoresistive strain gauge device to allow for the measurement of package-related stresses at the die level.

Experimental

Materials. In this study three commercially available molding compounds were studied. Materials A and B are standard packaging formulations. However, material B has a lower chloride content to improve humidity resistance. Material C is a rubber modified version of material B that was developed to reduce stress related problems. All materials are based on an epoxy cresol novolac-phenol formaldehyde novolac resin, a tertiary amine curing agent and the usual additives such as flame retardants, release agent, silica filler, coupling agent and pigment.

Samples were prepared using in-house molding facilities from preforms heated to 85°C prior to molding at 175°C with a process time of 90 seconds and a maximum pressure of 6.9 MPa. All samples were post mold cured at 175°C for 4 hours and were stored in a desiccator until testing.

<u>Thermomechanical properties</u>. Mechanical properties were obtained through Dynamic Mechanical Analysis (Dynastat, Imass) in three point bending over a frequency range from 0.1 Hz to 10Hz and a temperature range from -150°C to 200°C. Time-temperature superposition (4) yielded master curves in the transition range, giving the storage modulus, E', and the loss modulus, E", as functions of reduced frequency. The displacement along the frequency axis, necessary to superimpose the storage and loss moduli curves measured at different temperatures, is equal to log a_T, the logarithm of the shift factor, a_T. The superposition therefore also yielded the shift factor as function of temperature.

Thermal expansion was determined with Thermo Mechanical Analysis (Perkin Elmer TMA-7) over a temperature range from -150°C to 180°C at heating rates that were equivalent to those used in the beam bending experiments.

<u>Bilayer beam analysis</u>. Thermal strains cause a bilayer beam structure to bend as a function of temperature. If both materials are elastic the resulting curvature is determined by Young's moduli, thermal expansion coefficients and temperature difference only (5). Thermosetting polymers behave viscoelastically, and the curvature becomes a function of a more complicated viscoelastic material description, temperature dependent thermal expansion, temperature difference, and rate of change of temperature. Calculation of the resulting curvature is complicated and only possible for thermorheologically simple materials, materials to which time-temperature superposition applies (6). A phenomenological approach, valid for sufficiently small rates of temperature change as experienced in the beam bending experiments (1-5°C/min), has been described elsewhere (7). In that approach the viscoelastic behavior of the molding compound is described by the three parameter, standard linear solid model in combination with a temperature dependent modulus at lower temperatures.

The standard linear solid model consists of a spring parallel to a spring in series with a dashpot (8). To model the temperature dependence of the mechanical properties, the viscosity of the dashpot in the model is assumed temperature dependent. The spring constants are independent of temperature. At lower temperatures the viscosity becomes very high and the model reduces to the equivalent of a single spring, with a spring constant that is assumed to be temperature dependent. The parameter values are based on the measurement of the complex modulus as a function of frequency and temperature. The temperature dependence of the viscosity parameter is obtained from the temperature dependence of the shift factors. The model describes the basic features, i.e. the finite values for the storage modulus at low and high temperatures, of a crosslinked polymer. However, the transition between these two regions is modelled poorly. With the measured thermal expansion data, stresses in the molding compound can be calculated from the model. These stresses are proportional to the curvature 1/R of the bilayer structure. A schematic of the beam bending apparatus is shown in Figure 1. Samples were prepared by coating a polished silicon strip (50.0mm x 6.0mm x 0.5mm) with a layer (0.3mm) of one of the molding compounds in the molding press.

<u>Strain gauge device.</u>   Stress fields, generated in devices during assembly due to differences in thermomechanical properties, are of great importance in integrated circuit packaging. A semiconductor strain gauge array was specifically designed to measure these mechanical stress fields (9). The basic stress sensor is a compact resistor rosette consisting of four resistors oriented at 45 degrees on a planar area of 220x220 μm^2, as shown in Figure 2. The die size used in this study was 4.5x4.5 mm^2, with a total of 64 sensors, situated primarily in one of the corners. The decoding logic, necessary to address each individual resistor, is contained on the die in the opposite corner. The devices are processed using MOS technology on (111) oriented silicon for piezoresistance isotropy. After calibration, using a 4 point bending jig, measured resistance changes can be converted to a stress field on the surface of the die.

For this study individual die were packaged in 28 lead DIP packages (36.195 mm x 13.970 mm x 3.810 mm) using standard assembly technology. After dicing, the devices were attached to copper lead frames with a polyimide adhesive. Based on previous experience stresses introduced during die attach were neglected. After thermosonic gold wire bonding, parts were encapsulated in one of the molding compounds, deflashed, and the leads were trimmed, formed and soldered.

The four measured resistor changes can be converted to a stress field with respect to a coordinate system parallel to the edges of the die. Assuming that stresses perpendicular to the surface can be neglected (10), the stress field is completely determined by these resistor changes, and is given by two normal stresses, σ_x and σ_y, and a shear stress, τ_{xy}. It is often convenient to consider the principal stress field on the surface of the die. This field is characterized by a zero shear stress and is obtained from the original stress field by rotating the coordinate system over an angle θ given by:

$$\tan (2\theta) = \frac{2\tau_{xy}}{\sigma_x - \sigma_y} \tag{1}$$

The principal stresses σ_1 and σ_2 are given with respect to this rotated coordinate system and are equal to:

$$\sigma_{1,2} = \frac{\sigma_x + \sigma_y}{2} \pm \left[\left(\frac{\sigma_x - \sigma_y}{2}\right)^2 + \tau_{xy}^2 \right]^{1/2} \tag{2}$$

With both the two principal stresses and the rotation angle known the stress field is completely determined. At 45 degrees to the principal stress field orientation, one finds the directions of maximum shear stress:

$$\tau_{max} = \frac{\sigma_1 - \sigma_2}{2} \tag{3}$$

This maximum in-plane shear stress can also be used to represent the stress field on the surface of the die.
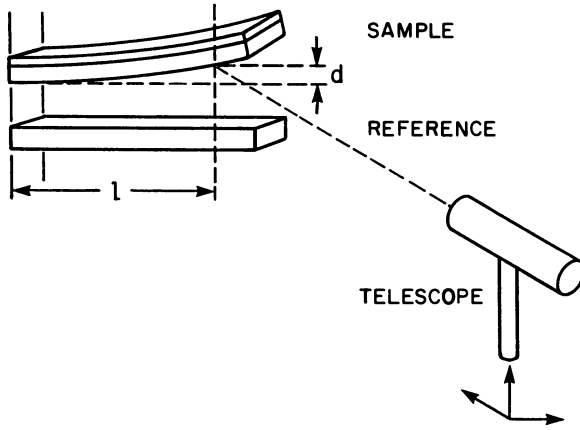
Figure 1: The beam bending apparatus.
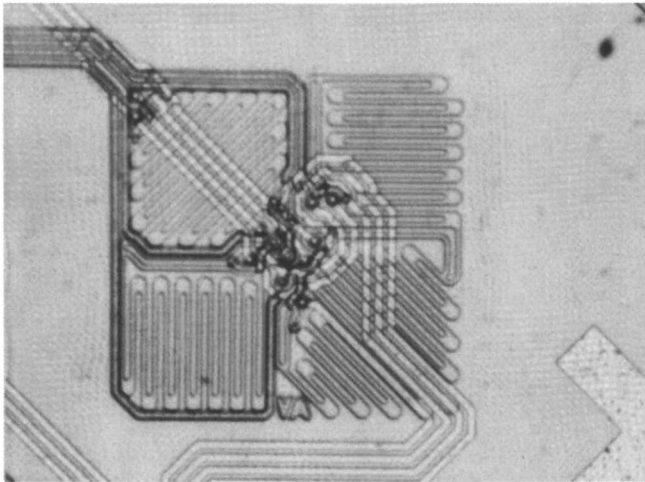
Figure 2: The basic strain gauge.

Thermal shock testing.   One of a large number of methods to test
the reliability of plastic packaged devices is thermal shock (THSK)
testing according to Mil STD-883C, method 1011.4, Condition C.
Samples are exposed to rapidly changing temperatures by immersing
in hot (150°C) and cold (-65°C) inert liquid with a 5 min. dwell
time and less then 10 sec. transfer time.   This is an extremely
severe test on the mechanical compatibility between package and
die.   The rapidly changing temperature also causes additional
mechanical stress due to temperature gradients in the package.   In
device testing, devices will undergo a certain number of cycles and
be tested after exposure.   In this study parts were exposed to 100,
300 and 500 cycles and stresses were measured and compared after
each test.   Bilayer beam samples could not be tested even after 100
THSK cycles due to poor adhesion of the molding compound to the
die.

Results and Discussion

The theoretical stress levels for the three molding compounds A, B,
and C are compared in Figure 3 based on the measurement of their
thermomechanical properties and the calculation of the curvature
for the bilayer beam structure.   The low stress material C has the
lowest calculated stress levels, while material A has stress levels
that are comparable to those of material B.
     As discussed above, these stress levels are determined by the
thermal expansion difference between the molding compound and
silicon, the moduli, and the amount of relaxation that occurs dur-
ing the experiment due to the viscoelastic nature of the molding
compound.   The glass transition temperature, T_g, of a molding
compound is important since the behavior in terms of thermal expan-
sion, moduli and relaxation times changes abruptly in this tempera-
ture region.   By decreasing the glass transition temperature
residual stresses can be reduced but in general such a decrease is
undesirable in view of the required performance of molding com-
pounds at higher temperatures.
     The thermal expansion of materials A and B is comparable over
the temperature range of interest.   However, the storage modulus
values for material A are smaller than those for material B over
the complete range of experimental frequencies and temperatures.
At the same time, the transition range for material A is found to
be shifted to lower reduced frequencies with respect to the same
reference temperature.   This results in considerable longer relaxa-
tion times for material A than for material B at each temperature.
The observed shift is also reflected in a higher glass transition
temperature for material A than for material B.   The influence of
these differences on the theoretical stress levels is predominantly
a combination of higher thermal strain, due to differences in the
glass transition temperature, with smaller modulus values, result-
ing in approximately the same stress levels for materials A and B.
Material C has less thermal expansion and lower storage modulus
values than either of the other two materials, while the relaxation
behavior is comparable to that of material B.   This was somewhat
expected since material C is a rubber modified version of material
B and based on the same resin system.   The glass transition
temperature is therefore almost equal to that of material B.   This

combination of decreased thermal expansion, smaller modulus values, and sufficiently high glass transition temperature, results in the lowest theoretical stress levels for material C.

These theoretical stresses can be compared to the stresses observed in beam bending experiments as a function of temperature. The results of the experiments for the different molding compounds are given in Figure 4. These experiments show good agreement with the theoretical stress levels.

Results of the strain gauge experiments are given in Figures 5 through 8. Figure 5 shows the maximum in-plane shear stress distribution for a strain gauge die encapsulated in material C, immediately after packaging. It is clear that the stresses are a function of position on the die surface and are maximized at the corners. The edge of the die oriented in the length direction of the DIP package, shows the highest stress. The overall distribution resembles the well known pillow shape predicted by Finite Element analysis (11). With an increasing number of cycles in THSK testing one observes a reduction of the highest maximum in-plane shear stress at the corners. The stresses in the center of the die remain almost constant. With respect to the orientation of the coordinate system of the principal stress system on the surface of the die we have observed a change from a strong orientation toward the center of the die to no preference in orientation at all after 500 cycles THSK testing. Both these observations are believed to be related to changes in the integrity of the interface between the molding compound and the surface of the die.

Figures 6 through 8 show results of the strain gauge experiments on the three different molding compounds A, B, and C. Each of these figures gives the principal stresses σ_1 and σ_2 and the maximum shear stress τ_{max} as measured in the center and on the corner of the die. These results were obtained after averaging measurements on at least 10 individual die. The results are given as function of the number of cycles in THSK testing. Except for the measurement after 300 cycles the stress levels at all positions after any number of cycles are smaller for material C than for material B. The stresses for material B are comparable to those for material A. The deviant behavior after 300 cycles observed with material A shows a large reduction in stress, indicative of a loss of adhesion. However, the increase observed after 500 cycles cannot be explained if indeed the integrity of the interface has been compromised.

As observed previously for material C in Figure 5, the maximum shear stress is highest at the corner of the die for all materials. The first measurement after 100 cycles THSK shows the largest decrease in stress level. Subsequent measurements after a larger number of cycles show no significant differences in stress levels. Although this maximum in-plane shear stress is not directly related to the stresses that cause such effects as metal shift, its behavior does indicate that after only a limited number of THSK cycles stress relief, leading to increased movement of materials with respect to one another, has occurred. Damage to the die surface is then inevitable. Further analysis of the parts and stress measurement after a smaller number of THSK cycles, is necessary to gain more insight in the changes in stress levels and orientation
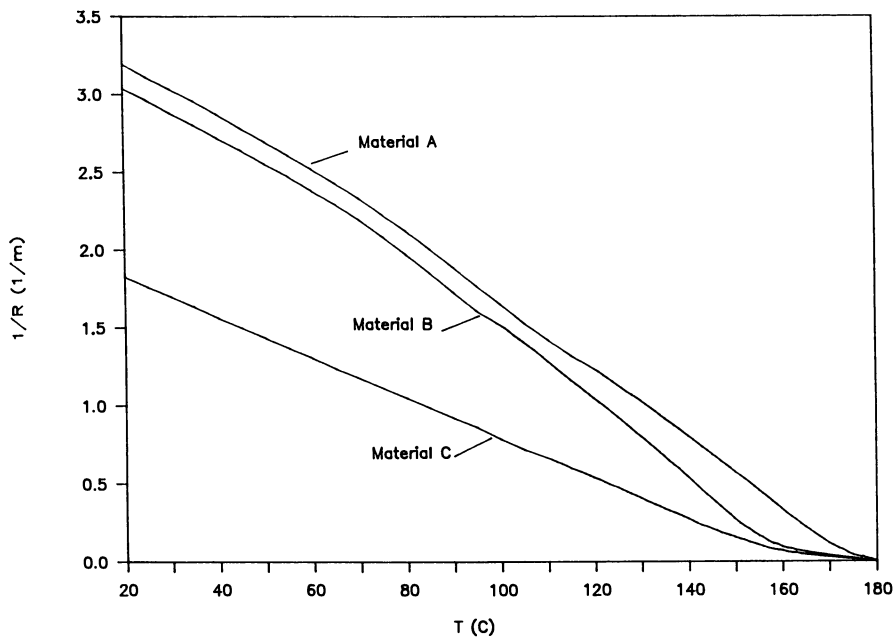
Figure 3:   Calculated stress levels in beam bending experiment.
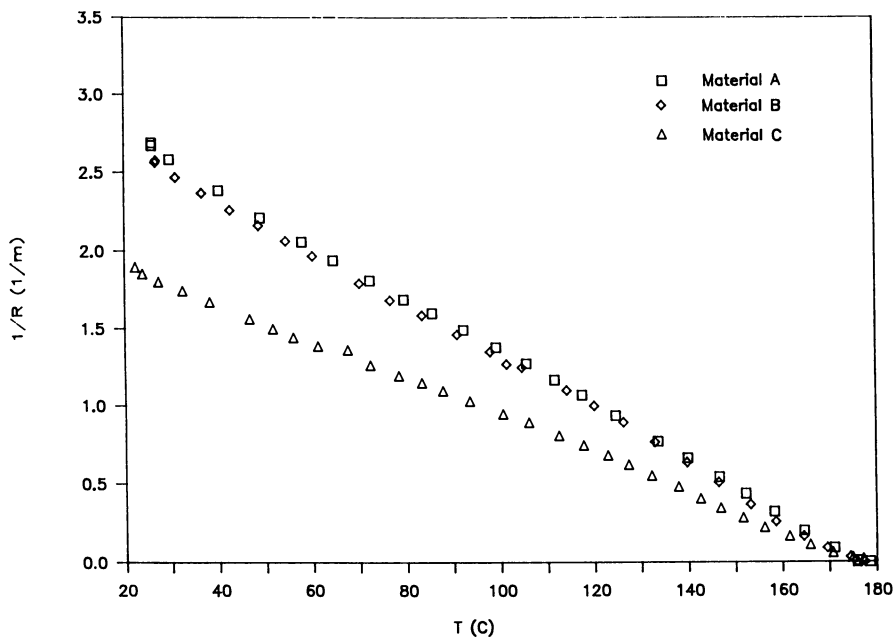
Figure 4:   Measured stress levels in beam bending experiment.
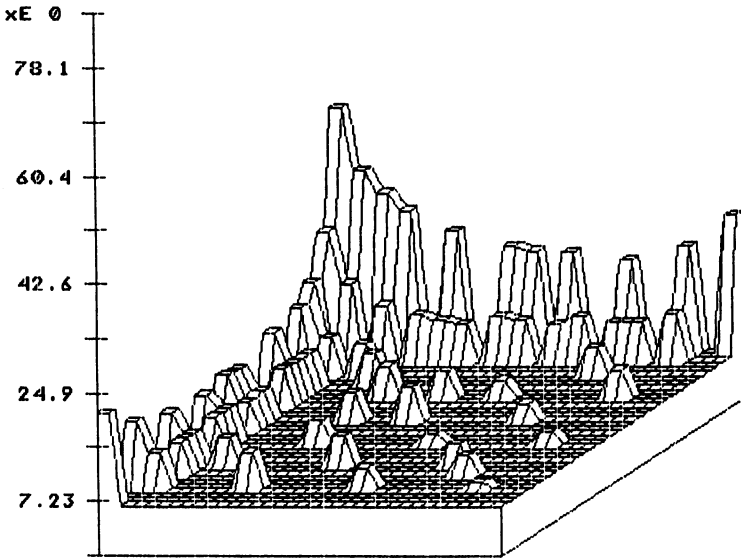
MATERIAL C
0 TMSK CYCLES

Figure 5: Maximum shear stress distribution.
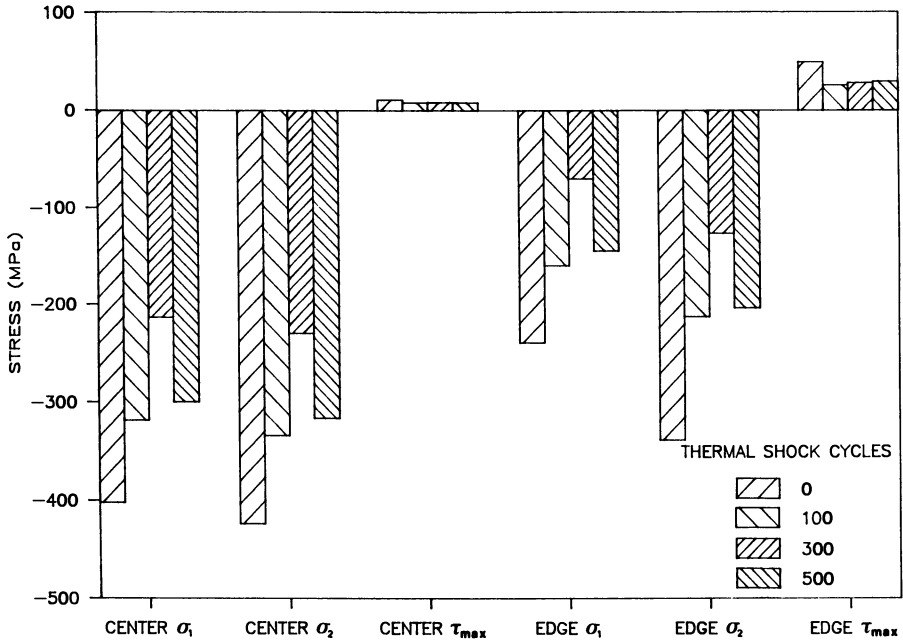
Figure 6: Stress levels for material A.
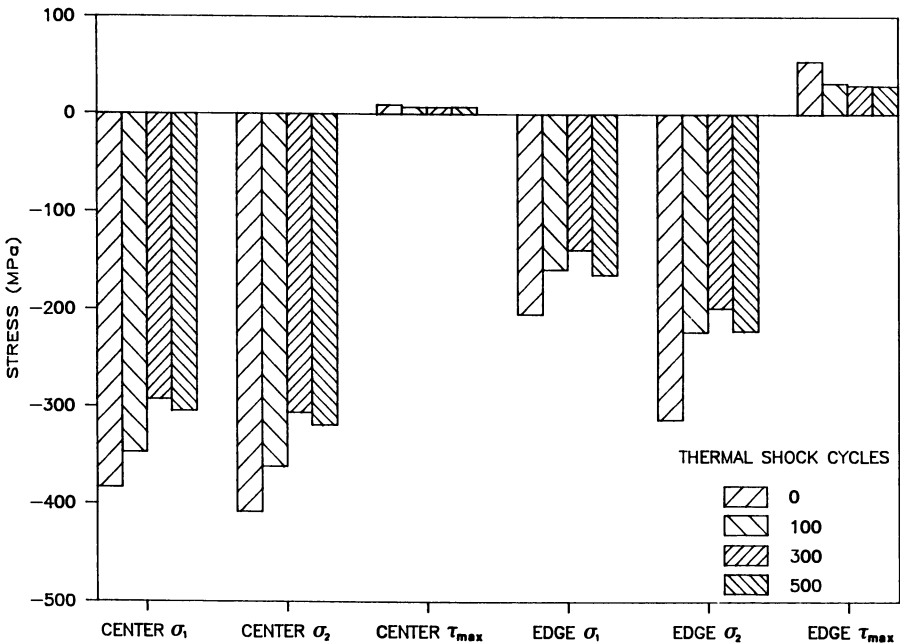
Figure 7: Stress levels for material B.
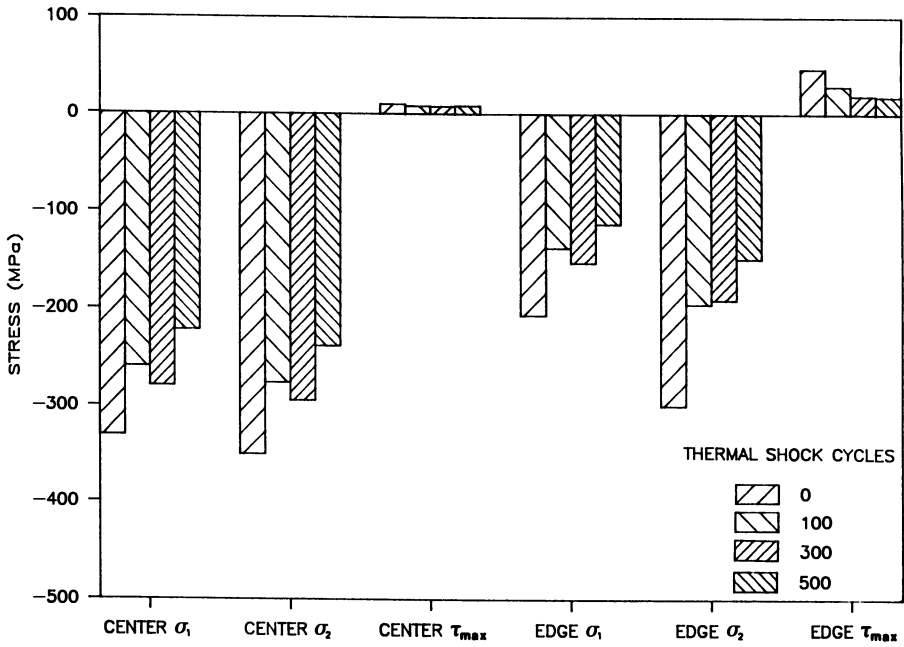
Figure 8: Stress levels for material C.

of the stress field during THSK testing, and to relate the results to observed damage and possible failure.

Since bilayer beam experiments after any number of THSK cycles were impossible, a comparison between strain gauge experiments and these bilayer beam experiments is only possible after molding. Based on the results presented above it can be concluded that strain gauge experiments correlate well with bilayer beam experiments, showing that low stress molding compounds can be characterized as such based on measurement of the fundamental thermo-mechanical properties that determine residual stresses.

Acknowledgment

Literature Cited

1. Goosey, M.T. In Plastics for Electronics; Goosey, M.T., Ed.; Elsevier: London, 1985; Chapter 5.
2. Thomas, R.E. IEEE Trans. on Components, Hybrids, and Manufacturing Technology 1985, 8, 427.
3. Merrett, R.P. In Plastics for Electronics; Goosey, M.T., Ed.; Elsevier: London, 1985; Chapter 6.
4. Ferry, J.D. Viscoelastic Properties of Polymers; J. Wiley & Sons: New York, 3rd ed., 1980; Chapter 11.
5. Timoshenko, S.P. J. Opt. Soc. Am. 1925, 11, 233.
6. Christensen, R.M. Theory of Viscoelasticity: An Introduction; Academic Press: New York, 2nd ed., 1982; Chapter 1-3.
7. van den Bogert, W.F.; Belton, D.J.; Molter, M.J.; Soane, D.S.; Biernath, R.W. IEEE Trans. on Components, Hybrids, and Manufacturing Technology 1988, 11, 245.
8. Ward, I.M. Mechanical Properties of Solid Polymers; J. Wiley & Sons: Chichester, 2nd ed., 1983; Chapter 5.
9. Gee, S.A.; Akylas, V.R.; van den Bogert, W.F. Proc. IEEE International Conf. on Microelectronic Test Structures, 1988, p 185.
10. Natarajan, B.; Bhattacharyya, B. Proc 36th Electronic Components Conf., 1986, p 544.
11. Groothuis, S.; Schroen, W.; Murtuza, M. Proc. 23rd Annual Reliability Physics Symp., 1985, p 184.

Chapter 29

Characterization of Stresses in Polymer Films for Microelectronics Applications

Rolf W. Biernath and David S. Soane

Department of Chemical Engineering, University of California at Berkeley, Berkeley, CA 94720

Experimental results and modeling strategy for
the determination of stresses in thermosets used
in microelectronics are presented. The bending
beam technique for in situ stress measurement is
particularly emphasized. This technique is here
extended to determine the glass transition
temperature, Tg, and the product of the elastic
modulus and coefficient of thermal expansion,
Eα, above and below Tg. Three case studies
illustrate the range of applicability of the
bending beam setup and factors contributing to
the stress state. The first is a comparison of
two polymers for interlayer dielectrics: PMDA-
ODA (pyromellitic acid dianhydride - oxydiamine)
and a bis-benzocyclobutene. The second is of a
neat epoxy resin commonly used for
microelectronics encapsulation (epoxidized
ortho-cresol novolac cured with a phenolic
novolac). The third is a screen-printable
polyimide coating used for protection of the
integrated-circuit chip. An outline of our
stress model is sketched, and example results
are presented.

Polymers are used extensively in the fabrication and
encapsulation of microelectronics (1). They function as
photoresists, intermetallic dielectric layers, passivation
coatings, die attach adhesives, and encapsulants for the
packaging of individual chips. Polymer-impregnated
composites also serve as printed circuit boards for
mounting and interconnection of integrated circuits. Since
polymers generally exhibit different thermal expansion
behavior from other materials commonly employed in
microelectronics, significant stresses are caused by
temperature transients during manufacturing and in use (2).

Even if failures such as chip cracking or spalling are avoided, repeated straining of integrated circuits may alter their electrical characteristics through metallurgical fatigue and geometrical distortion. It is the objective of our research to establish mechanisms by which stresses are created in polymer layers deposited on silicon, quartz, and other substrates. Once the dependence of thermo-viscoelastic stresses on material properties and processing parameters is firmly understood, we plan to develop material design and process optimization guidelines to minimize stresses in packaged integrated circuits.

Stress is related to strain through constitutive equations. Metals and ceramics typically possess a direct relationship between stress and strain: the elastic modulus (3). Polymers, however, may exhibit complex viscoelastic behavior, possessing characteristics of both liquids and solids (4). Their stress-strain behavior depends on temperature, degree of cure, and thermal history; the behavior is made even more complicated in curing systems since material properties change from a low molecular weight liquid to a highly crosslinked solid polymer (5).

When a dimensional change in a polymer coating does not match that of its constraint (such as the substrate to which it adheres), the resulting strain generates stress in both the polymer and the substrate. Strain arises in polymers by thermal expansion and contraction (6), from solvent and by-product evaporation (7), from moisture absorption (8), from cure (9), and from physical aging (10).

Polymer properties are highly sensitive to temperature with transitions between physical states typically occurring over many tens of degrees Celsius (4). Additionally, the properties are sensitive to the rate at which the temperature changes. For example, the apparent glass transition temperature of a given polymer sample increases with the rate of temperature scan. For thermosets (such as epoxies and polyimides) the thermal history is especially important because of its coupled effect on the physical state of the polymer and the reaction kinetics (11).

Other factors having a substantial influence on polymer properties are solvent and by-product concentrations. Here, an increase in solvent concentration decreases the glass transition temperature (12). Repeated thermal cycling also impacts the polymer properties and the state of stress (13).

The conversion of strain mismatch into stress is a function of the stress relaxation modulus exhibited by the polymer. A predictive stress model must incorporate the complex dependencies of the modulus and stress relaxation behavior on temperature, glass transition temperature, degree of cure, crosslink density, solvent-plasticization, and reaction kinetics.

Experimental Method

The stress measurement technique employed in our laboratory
is based on the principle of a bending cantilever beam.
The method was first developed for stress measurement in
metal films (14, 15), but has recently been extended to
polymers (8, 16) due to the availability of ultra-thin
quartz strips (~ 80 μm thick).
     When two material layers adhere to one another and one
layer differentially expands or contracts relative to the
other, the layers bend in order to minimize the strain
energy. Subject to various constraints, such as locally
uniform layer thicknesses, and that the stiffest layer be
linear elastic, the local bending can be described by the
arc of a circle of radius, R. If the constraints are valid
across an entire sample, the entire sample will indeed bow
in the form of an arc of a circle. This is the operating
principle of the bending beam apparatus and is illustrated
in Figure 1.
     Depicted in Figure 1 is a bi-material strip subject to
bending by internal stresses after cooling from its cure
temperature to below the glass transition temperature of
the polymer layer. Layer 1 represents a low modulus, high
thermal expansion polymer; layer 2 represents a high
modulus, low thermal expansion substrate. The polymer
seeks to contract along its length more than does the
substrate because of its greater thermal expansion
coefficient. The substrate resists the contraction of the
polymer, thereby inducing a tensile stress in the polymer
and a compressive stress in the substrate near the
interface. The tensile stress in the polymer layer will
cause the substrate to bow in the direction of the polymer.
The bowing of the substrate induces a tensile stress at its
outside edge. A typical linear elastic stress profile is
superimposed on the diagram; tension is denoted by "+",
compression by "-". As will be shown later, the bowing of
the substrate is directly proportional to the stress felt
by the polymer coating.
     The bending beam apparatus offers several specific
advantages for stress measurement. First, the experiment
measures directly the true average stress in the material
(15, 17). Therefore, results from different laboratories
can be meaningfully compared. Secondly, the stress is
measured during processing, enabling individual factors
contributing to the stress state to be discerned and
quantified. Thirdly, the experiment requires only a
minimal amount of material (less than a gram), and thus can
be very valuable in screening and comparing low stress
resins in a development laboratory environment.
Additionally, several material properties of the resin can
be determined - these include the glass transition
temperature, Tg, and the product of the elastic modulus and
thermal coefficient of expansion, Eα, both below and above

Tg. Effects of stress relaxation, aging, and thermal cycling can also be quantified.

Apparatus Description. A schematic of the bending beam apparatus is given in Figure 2. The polymer being studied is spin-coated onto a thin strip of silicon or quartz (1). The resulting sample is placed in a small environmental chamber, which houses a sturdy reference beam held parallel to the sample beam. This reference beam provides an exact measure of sample displacement due to chamber and holder expansion or contraction, which can then be accounted for in the curvature calculation. The environmental chamber, which has dual quartz windows to allow sample observation, is heated by electrical resistance heaters and cooled by a circulating fluid. A digital ramp temperature controller ensures precise control of heating and cooling rates (up to 10°C/min). The temperature is measured by a thermocouple positioned near the sample, and is uniform to within 3°C across the sample. The thermocouple timelag is accounted for in the data analysis.

The chamber maintains a vacuum and offers a controlled atmosphere. Most experiments are run with the chamber slightly pressurized with an inert gas, although sometimes a humidified or oxygenated atmosphere is employed. The high-temperature limit of the chamber is 280°C.

The deflection of the sample beam is measured by a 200x microscope fitted with a crosshair, and mounted on a precision x-y-z translator. The microscope is designed to achieve high magnification, yet to maintain a large working distance (50 mm). Displacements on the order of 3μm can be readily detected with this system, by using a stepper micrometer. Repeatability of a single deflection measurement (distance between reference beam and sample beam) is on the order of 1 μm.

Typical procedures of the bending beam experiments were as follows. Resin coatings were applied to one side of a clean quartz strip by spin-coating from an appropriate solvent at 2000 to 8000 rpm for about 30 seconds. Coatings were then evaluated for uniformity, and acceptable beams were then inserted into the bending beam apparatus. Stress measurements were taken during temperature ramps and holds. The specific cure schedule followed for each material depended on the manufacturers recommendations or the results of microdielectric cure studies (18). Upon completion of all stress experiments, the beam was removed and the film thickness measured by an Alphastep profilometer. The quartz beams were 82 ± 2 μm thick, 3.8 cm long, and 0.31 cm wide. Their elastic modulus and thermal coefficient of expansion are 74,500 MPa and 5.7×10^{-7} °C^{-1} (19).
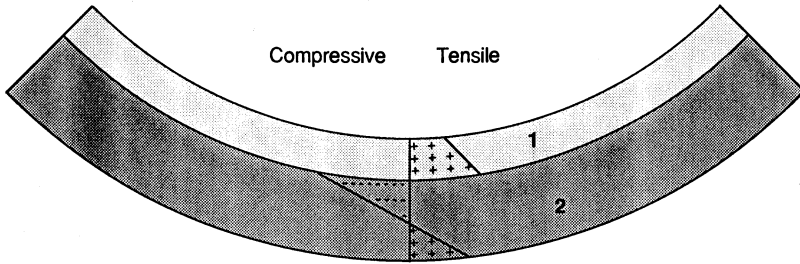
Figure 1. Bi-material strip subject to bending by internal stresses after cooling from its cure temperature to below the glass transition temperature of the polymer layer 1 .
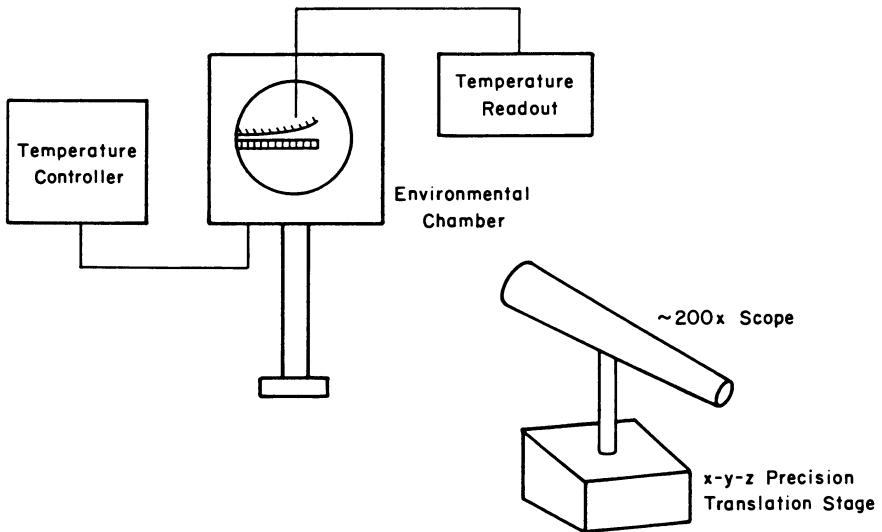
Figure 2. Schematic of bending beam apparatus.

Bending Beam Theory

A well known equation by Timoshenko (14) is employed to
determine the layer stresses from the measured radii of
curvature of a bimaterial strip (Figure 1). The stress in
layer 1 as a function of distance y from the center of the
layer is:

$$\sigma_1 = \frac{1}{R} \frac{E_2 \, t_2}{6 \, (1+m) \, m} \left[\left(1 + \frac{6 \, y}{t_1} \right) n \, m^3 + \frac{6 \, y}{t_1} n \, m^2 + 1 \right] \qquad (1)$$

where t_1, t_2, E_1 and E_2 are the respective layer
thicknesses and elastic moduli of layers 1 and 2, m is the
ratio of the thicknesses (t_1/t_2), n is the ratio of the
moduli (E_1/E_2), and R is the measured radius of curvature.
This relation for stress requires knowledge of the moduli
of both layers. The stress-relation for layer 2 is similar
to that for layer 1, only the subscripts are interchanged.
Also, the highest stress in each layer is felt at the
interface.
    For a thin polymer layer (i.e., $t_1 \ll t_2$), Equation 1
reduces to:

$$\sigma_1 = \frac{1}{R} \frac{E_2 \, t_2^2}{6 \, t_1} \qquad (2)$$

This equation has several important features. The material
properties of layer 1 are absent. Also, the thickness of
the substrate, t_2, is the parameter of greatest sensitivity
- typically this is an easily measured quantity. In
addition, the stress profile in the thin layer is flat for
a linear elastic layer, i.e., the entire film is subjected
to a uniform stress.
    By algebraic manipulation, it can be shown that for a
cantilever beam of length L, the radius of curvature can be
determined from the deflection, δ, of the beam tip:

$$R = \frac{L^2}{2 \, \delta} \qquad (3)$$

when $\delta \ll R$; typical magnitudes for δ and R are in the
micron and meter range. This equation is employed for
obtaining R from deflection data in the bending beam
experiment. Actual experiments are run by measuring the
deflection at a point x < L, in order to avoid edge effects
which are estimated to be operative within an order of two
to three beam thicknesses (20).
    The product of the elastic modulus and thermal-
expansion coefficient for the thin polymer coating, $E\alpha$, can
be calculated from the stress-temperature curve by the

relationship of the thermally induced stress, $\Delta\sigma_1$, in a thin layer to the thermal expansion mismatch and temperature change, ΔT: (21)

$$\Delta\sigma_1 = E_1 \, \Delta\alpha \, \Delta T \qquad\qquad (4)$$

where E_1 is the elastic modulus of the film, $\Delta\alpha = \alpha_1 - \alpha_2$, is the mismatch between the linear thermal expansion coefficients of the film and substrate, and $\Delta\sigma_1$ is the increase in film stress resulting from a temperature decrease ΔT. For most polymers on quartz or silicon, $\alpha_1 \gg \alpha_2$, giving,

$$\frac{\Delta\sigma_1}{\Delta T} = E_1 \, \Delta\alpha \cong E_1 \, \alpha_1 \equiv E\alpha \qquad\qquad (5)$$

Thus, $E\alpha$ of the polymer is proportional to the slope of the stress-temperature curve in thermal-expansion dominated regimes. A decrease in $E\alpha$ results in a lower thermal-expansion-mismatch induced stress. Thus, a lower $E\alpha$ should also endow the material with the ability to sustain a greater number of thermal cycles before fatigue-induced fracture because of a smaller cyclical stress amplitude. The elastic modulus of the polymer can be calculated from $E\alpha$ with knowledge of α_1 from thermal mechanical analysis (TMA), when stress relaxation effects are negligible. It should also be possible to calculate crosslink density from the rubbery modulus (above Tg) by using rubber elasticity theory.

The glass transition temperature, Tg, can also be calculated from the stress-temperature profile. It can be taken as the intersection of two lines drawn from the linear regions of the glassy and rubbery regimes, in a manner similar to Tg determination from TMA. Here, however, the measured Tg corresponds more with those derived from dynamic mechanical methods because of the strong dependence of stress on the modulus transition between the rubbery and glassy states. Other ways to measure Tg would be to take the derivative of the $\sigma(T)$ curve to obtain $E\alpha(T)$; the Tg could then be determined as either the inflection point or the midway point in the transition between glassy $E\alpha$ and rubbery $E\alpha$.

The Timoshenko equation holds only for elastic films on elastic substrates. Polymer layers, however, are viscoelastic, in particular near their glass transition temperatures. The experimental raw data can be deconvoluted to obtain stress measurements, even if the viscoelastic effects are important. This is because we use the thin-film equation, where the viscoelastic modulus of the polymer is not needed for the stress computation. For

the case of thick coatings, indeed, the proper viscoelastic modulus should replace the elastic modulus.

Results and Discussion

Three case studies are examined which illustrate the use of the bending beam stress experiment. The first is a comparison of two polymers for interlayer dielectrics. The second is of a neat epoxy resin commonly used for microelectronics encapsulation. The third is a polyimide coating used for protection of an integrated-circuit chip.

PMDA-ODA and BCB. Stresses induced during processing of a PMDA-ODA polyimide (pyromellitic acid dianhydride - oxydiamine, Dupont Pyralin 2545) and a bis-benzocyclobutene (BCB, Dow proprietary) were studied using the bending beam apparatus. Both materials were used as supplied by the manufacturer: the PMDA-ODA solvated in n-methyl pyrrolidinone and the BCB in xylene. Final coating thicknesses, as measured by profilometry, were 2.8 μm for the PMDA-ODA and 3.2 μm for the BCB on fused quartz strips.
    Both materials were subjected to the same processing conditions. The cure profile consisted of heating from room temperature to 260°C at 5°C/min, holding at 260°C for 2 hours, then cooling to room temperature at 5°C/min. As can be seen in Figure 3, their stress-temperature profiles are quite different. Both films left the spin-coater with approximately zero stress. Upon heating, the polyimide film developed substantial tensile stress due to film contraction from solvent evaporation while the BCB film exhibited only mild tensile stress buildup. The stress in the BCB film relaxed at 260°C while the stress in the polyimide did not.
    The differing behavior can be explained on the basis of their respective chemistries and their initial physical states. The polyimide polymerization occurs via a two step mechanism (Figure 4). First, the PMDA reacts with the ODA to yield a polyamic acid polymer. The polyimide is then formed by a ring closure reaction and yields water as a condensation by-product. Both reactions take place fairly rapidly at the temperatures at which the PMDA-ODA is manufactured.
    The benzocyclobutene reaction also takes place via a two step reaction (Figure 5); however, the polymer is not formed until the second step. First, the cyclobutene ring is destabilized upon heating above 200°C producing highly reactive methylene groups. These, in turn, react with one another to yield linear or network polymer. Unsaturation in the intervening group, X, may also result in its participation in curing via Diels-Alder reactions.
    The polyimide, as supplied, was in a slightly advanced state, a moderate molecular weight polymer, with a distinctly higher viscosity than the BCB. The advanced state of the polyimide is a consequence of the high-
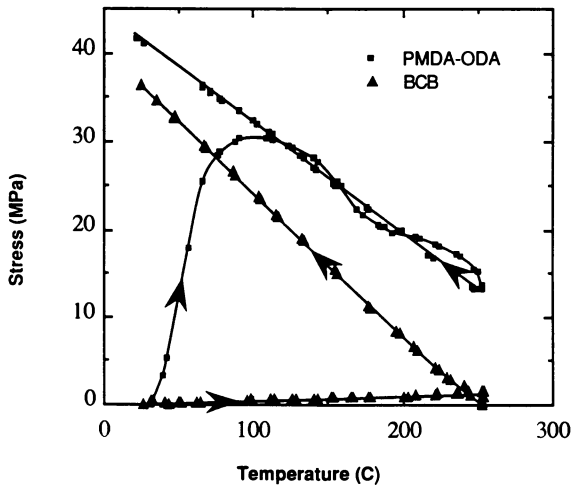
Figure 3. Comparison of stress-temperature profiles for BCB and PMDA/ODA.
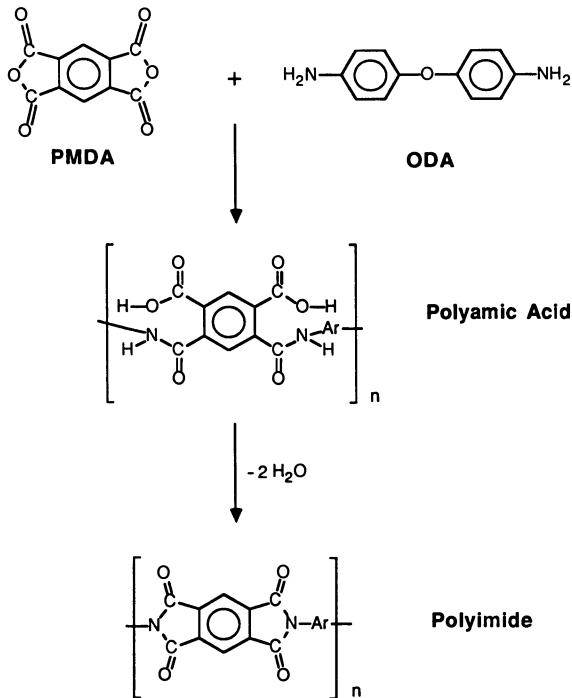
Figure 4. Reaction of PMDA with ODA to form polyimide.

temperature manufacturing process. It facilitates
polyimide processing under spin-coating conditions;
however, it also imparts greater solid-like character to
the polyimide. Consequently, when the film contracts due
to solvent evaporation, the strain does not relax. Rather,
it translates to significant tensile stress in the film.
In order for the polyimide to have such a high modulus
throughout the course of the heating cycle, the Tg of the
polyimide must increase via curing to remain near or above
the sample temperature.

    Note also that a competition exists between film
contraction due to solvent evaporation and film expansion
due to thermal expansion during the heating ramp to the
cure temperature. This competition becomes apparent as the
solvent is driven out of the polyimide film. The slope of
the stress-temperature curve becomes zero as the mechanisms
balance each other (~100°C). It becomes negative as
thermal expansion dominates. At 180°C film contraction due
to water evaporation, the imidization by-product, begins to
compete with thermal expansion. Stress retention at 260°C
indicates that the polyimide has gelled, and possesses a Tg
significantly higher than 260°C. These results appear to
be in agreement with the cure characteristics reported for
a similar polyimide system (22).

    The BCB exhibits minimal solid-like character upon
heating; contraction due to solvent evaporation only
slightly outpaces thermal expansion. The Tg remains
significantly below the sample temperature, resulting in a
low modulus and thus low stress. Upon reaching 260°C, the
tensile stress in the BCB film relaxes because of only
minimal network formation, which would inhibit the
relaxation, during the heating cycle.

    Upon cooling, after a 2 hour cure, both materials
exhibit linear stress-temperature profiles. This indicates
that the glass transition temperature is at or above the
cure temperature, and that measurements have been made in
the glassy elastic regime. The glassy-state Eα can be
calculated from the slopes of these curves. For the
polyimide it is 0.13 MPa/°C and for the BCB it is
0.16 MPa/°C. Note that the polyimide bears a higher
cumulative stress at room temperature because of the stress
induced by solvent evaporation, in spite of its lower Eα.

Encapsulant Resin. Figure 6 shows the stress trace of an
epoxy resin typically used in encapsulant formulations.
The resin consists of epoxidized ortho-cresol novolac
(EOCN, Shell DPS-164) cured with a phenolic novolac (PN,
Borden 1731), catalyzed by triphenyl phosphine (TPP,
Aldrich). It was spin coated onto a quartz strip from a
mixture of methyl ethyl ketone and Dowanol PM yielding a
final coating thickness of 5.3 μm. The cure schedule
consisted of heating to 160°C, holding for 1 hour, cooling
to -30°C, heating to 210°C, holding for 1 hour, then cooling
to room temperature; heating and cooling was done at
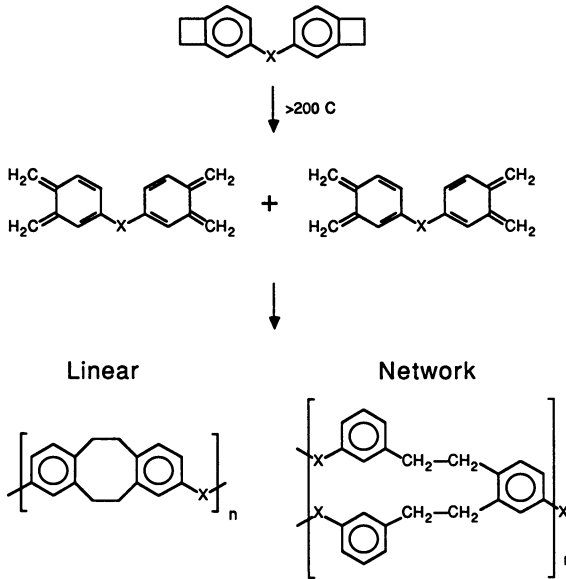
Figure 5. Reaction of bis-benzocyclobutene to form polymer.
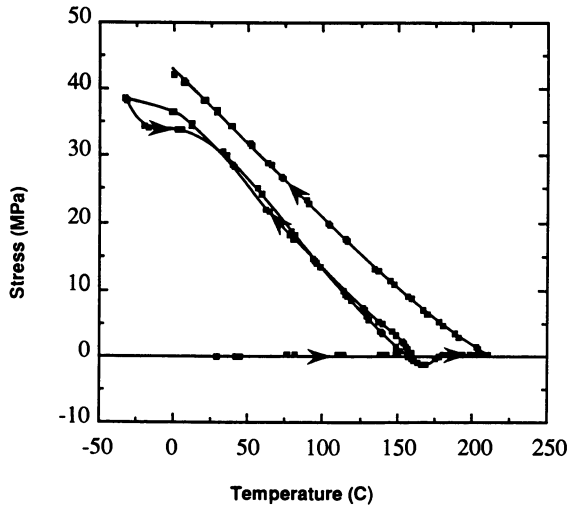
Figure 6. Stress-temperature plot for an EOCN-based encapsulant resin.

5°C/min. Microdielectrometry was used to determine that
the resin had ceased reacting at the cure temperatures
before cooling.

The initial heating is uneventful, as the resin is
insufficiently advanced to sustain stress. Upon cooling
from 160°C, stress increases nearly linearly, indicating
that the glass transition temperature is at or above the
cure temperature, and yielding an Eα of 0.24 MPa/°C. Upon
cooling below 0°C, anomalous behavior due to condensation
of moisture on the sample beam is noted. Such condensation
weighs the beam downward, decreasing the apparent beam
deflection, and thus anomalously decreases the measured
stress. The moisture evaporates during the second heating
cycle, giving normal behavior upon reaching 50°C. This
demonstrates that a substantially moisture-free environment
must be employed in order to use the bending beam technique
at sub-zero temperatures (i.e., the dew point of the
ambient gas must be below the lowest desired temperature).

As the beam is heated towards 210°C, the resin
exhibits a compressive stress above its cure temperature of
160°C. The stress passes through a minimum at 170°C where
the rate of stress induction due to thermal expansion is
balanced by stress relaxation. Stress relaxation is the
dominant mechanism until 210°C. There are no detectable
cure-shrinkage induced stresses during the 210°C cure. The
stress increases non-linearly upon cooling, indicating that
the glass transition temperature is below the cure
temperature. Under 150°C, the stress increases linearly,
yielding an Eα of 0.22 MPa/°C. This Eα is lower than that
following the 160°C cure, and agrees with behavior expected
below Tg from an increase in crosslink density. The Eα
reduction is due to a decreased thermal expansion
coefficient resulting from a more highly crosslinked
network.

Figure 7 shows the behavior of the same sample heated
to 280°C at 5°C/min. The cured sample follows the same
stress-profile as the prior cooling curve, with the point
of zero stress occurring slightly above the cure
temperature at 214°C. The stress becomes mildly
compressive with further heating, and a glass transition
temperature of 190°C is noted. The slope of the linear
region above the glass transition temperature yields a
rubbery Eα of 0.014 MPa/°C upon heating, and 0.026 MPa/°C
upon cooling from 280°C.

The higher rubbery Eα upon cooling is best explained
by the viscoelastic nature of the thermoset coating. The
heating rate of the environmental chamber decreases rapidly
above 200°C because it is nearing its high temperature
limits, such that the final approach to 280°C occurs at
about 0.5°C/min. The cooling, however, occurred at a well
controlled 5°C/min. This ten-fold difference in heating
rates is quite significant, having allowed significantly
more time for viscoelastic stress-relaxation upon heating
than upon cooling. Since Eα is determined from the slope

of the stress-temperature curve, a reduction of stress by
stress relaxation will decrease the apparent Eα.

Screen-Printable Polyimide. Bending beam results for a
screen-printable polyimide used for chip protection are
presented in Figure 8. The EPO-TEK 600 polyimide paste was
applied to a quartz beam, then the beam was spun at 5000
rpm to achieve high uniformity. Results are presented as
inverse radius of curvature, 1/R, because the 50 μm coating
thickness on the 84 μm substrate violates the thin film
criterion of Equation 2. We have no knowledge of the
polyimide's viscoelastic modulus, which is needed in order
to convert 1/R into interfacial stress using Equation 1.
The polyimide is known to bow silicon wafers (~450 μm
thick) very little; it bows the thin quartz strip
significantly because of the lower bending modulus of the
thin strip.
        The polyimide was cured as follows: one hour at 160°C
to drive off the solvent, and 1 hour at 280°C to cure the
polyimide, with temperature ramps of 5°C/min. The EPO-TEK
develops a significant modulus as it is heated to 160°C, as
can be seen from the bowing induced by solvent evaporation.
An inflection in the 1/R curve is noted at 178°C on heating
to 280°C - this corresponds to the glass transition
temperature. Again it is noted that the glass transition
temperature can rise higher than the cure temperature. The
coating sustains a mildly compressive stress as it cures at
280°C; negligible stress induced by cure shrinkage is noted
for this polyimide. Upon cooling, stress increases in
proportion to the temperature change.

Modeling Thermoset Properties During Cure

These studies pointed out that a comprehensive model of
thermoset cure for stress calculations must account for a
large number of processing influences and material
properties. Mass transfer (23), chemical kinetics, network
structure formation, and material property development are
essential ingredients. Induced strains must be accurately
calculated, as must stress relaxation. Properties
dependencies on temperature are significant and must be
accounted for, as must the inter-relationship between
reaction kinetics and diffusion.
        Figure 9 outlines the thermoset cure model being
developed in this laboratory to describe property changes
and stress buildup during processing. The intent of this
model is to develop processing and material guidelines for
minimizing residual stresses. A forthcoming paper will be
devoted to this topic. However, it is instructive to
briefly summarize the modeling strategy employed.
        A cure temperature profile is input into the model.
The physical structure of the polymer is then computed from
knowledge of the chemical kinetics, utilizing the
statistical methods developed by Macosko and Miller (24,
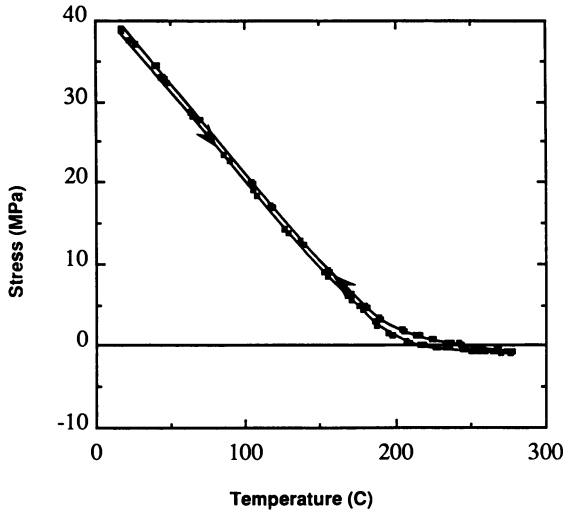
Figure 7. Stress evolution during second heating of cured EOCN encapsulant resin.
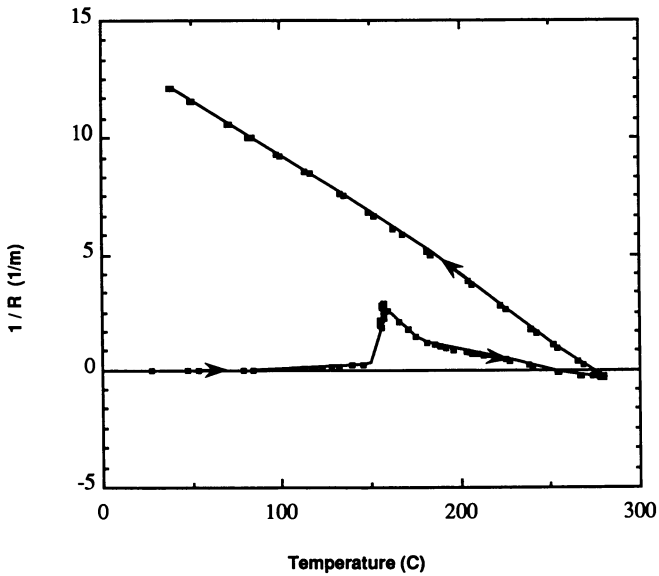
Figure 8. Beam radius of curvature as a function of temperature for 50 μm thick EPO-TEK 600.
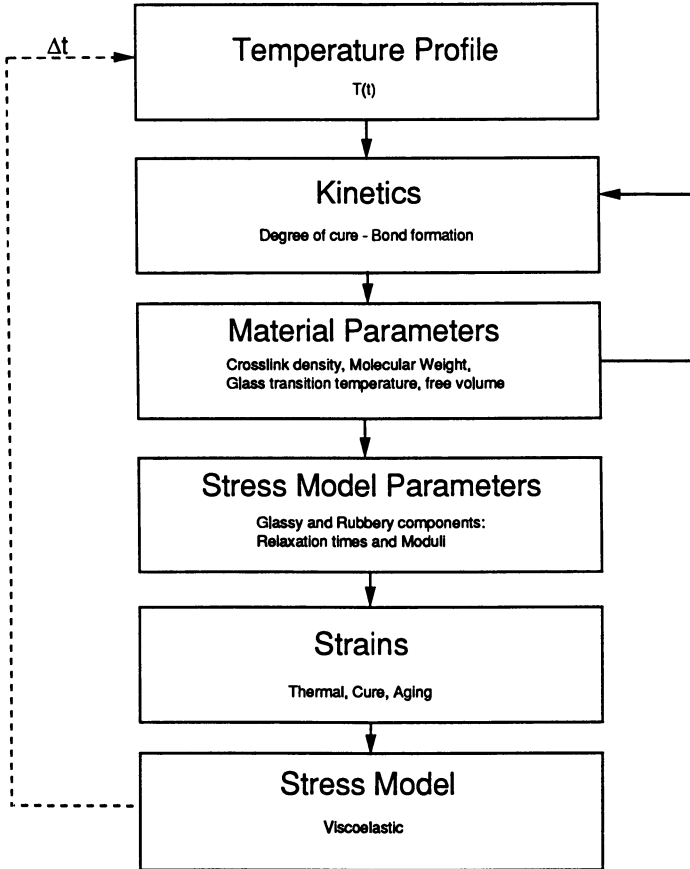
Figure 9. Flowchart of thermoset cure model.

25). The glass transition temperature and resulting free
volume are calculated from the DiBenedetto equation (26) or
by an approach which incorporates the effect of crosslink
density on the glass transition temperature (27). This
part of the model is iterative in order to account for
diffusion-limitations on the reaction rate in the later
stages of thermoset cure (28).

The material properties (moduli and relaxation times)
are then calculated from knowledge of network structure and
free volume. Strains imparted by processing and reaction
are determined. These inputs are then applied to a
viscoelastic bi-Maxwell model, whereby stress in the
polymer is determined. Time is then incremented and the
procedure repeated until the cure profile is complete.

Sample model results are presented in Figure 10.
Realistic model parameters were selected to demonstrate the
model capabilities for a generic thermoset resin similar to
the EOCN-based resin. The cure schedule simulation
consisted of heating to 125°C, holding for 1 hour, cooling
to 60°C, heating to 200°C, holding for 1 hour, then cooling
to room temperature. All heating and cooling was done at
5°C/min.

The model correctly simulates the qualitative behavior
exhibited by the EOCN. Stress retention upon cooling
after both the 125°C and 200°C cures is noted, with a
decreased Eα when more fully cured. A compressive stress
which relaxes out is observed on heating the partially
cured resin to 200°C. Both cool-down curves exhibit
curvature near the cure temperatures due to the dependency
of modulus, thermal expansion, and stress relaxation on
temperature, Tg, and crosslink density.

Solvent and by-product evaporation can be accounted
for in a manner analogous to the methods used previously
(23).

Conclusions

Stresses in polymers for microelectronics are very complex
functions of time, temperature, thermal history, solvent
and by-product evaporation, degree of cure, cure kinetics,
crosslink density, and viscoelasticity. The bending beam
experiment enables these effects to be observed and
quantified. It measures a true stress in the polymer,
allowing the product of the elastic modulus and thermal
expansion coefficient, Eα (both above and below Tg), and
the glass transition temperature, Tg, to be determined from
a small quantity of material. Modeling efforts are
underway to determine processing and materials guidelines
for minimizing residual stresses.
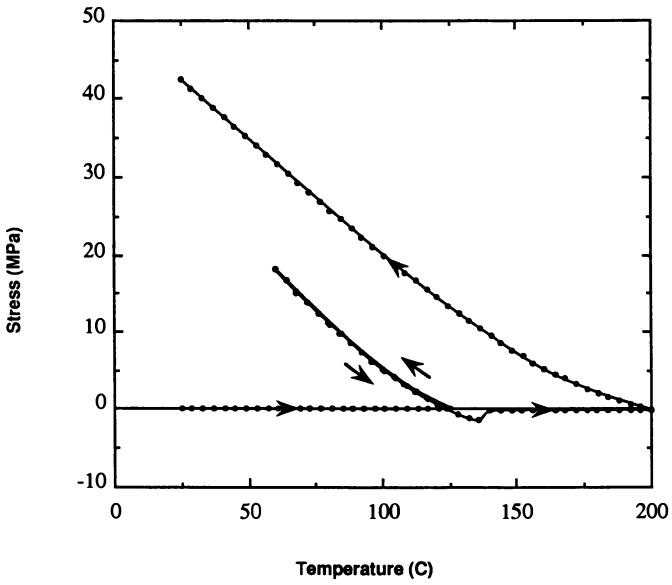
Figure 10. Example model predictions for thermoset curing.

Acknowledgments

Literature Cited

1.   Soane, D.; Martynenko, Z. <u>Polymers in Microelectronics: Fundamentals and Applications</u>; Elsevier: New York, 1989.

2.   Bolger, J. C. In <u>Polyimides: Synthesis, Characterization, and Applications II</u>; Mittal, K. L., Ed.; Plenum: New York, 1984; p 871.

3.   Popov, E. P. <u>Introduction to the Mechanics of Solids</u>; Prentice-Hall, Inc.: Englewood Cliffs, 1968.

4.   Ferry, J. D. <u>Viscoelastic Properties of Polymers</u>, 3rd ed.; John Wiley & Sons, Inc.: New York, 1980.

5.   Aronhime, M. T.; Gillham, J. K. <u>J. Coat. Tech.</u> 1984, <u>56</u>, 35.

6.   Timoshenko, S. <u>J. Opt. Soc. Am.</u> 1925, <u>11</u>, 233.

7.   Croll, S. G. <u>J. Coat. Tech.</u> 1979, <u>51</u>, 64.

8.   Berry, B. S.; Pritchet, W. C. <u>IBM J. Res. Develop.</u> 1984, <u>28</u>, 662.

9.   Srivastava, A. K.; White, J. R. <u>J. Appl. Polym. Sci.</u> 1984, <u>29</u>, 2155.

10.   Chow, T. S. <u>J. Rheol.</u> 1986, <u>30</u>, 729.

11.   Wisanrakkit, G.; Gillham, J. K.; Enns, J. B. <u>Polym. Mat. Sci. Eng.</u> 1987, <u>57</u>, 87.

12.   Duda, J. L.; Vrentas, J. S.; Ju, S. T.; Liu, H. T. <u>AIChE J.</u> 1982, <u>28</u>, 279.

13.   van den Bogert, W. F.; Molter, M. J.; Belton, D. J.; Gee, S. A.; Aklas, V. R. <u>Polym. Mat. Sci. Eng.</u> 1988, <u>59</u>, 642.

14.   Timoshenko, S. <u>J. Opt. Soc. Am.</u> 1925, <u>11</u>, 233.

15.   Wilcock, J. D.; Campbell, D. S. <u>Thin Solid Films</u> 1969, <u>2</u>, 3.

16.   Hu, C.-K.; Tong, H. M.; Feger, C.; Ho, P. S. In <u>IEEE V-MIC Conf.</u>, 1985, p 280.

17.   Scherer, G. W. <u>Relaxation in Glass and Composites</u>; Wiley-Interscience: New York, 1986.

18.   Senturia, S. D.; Jr., N. F. S. <u>Adv. Polym. Sci.</u> 1986, <u>80</u>, 1.

19.   Hibshman Corp. 1988.

20.   Scherer, G. W. <u>J. Am. Cer. Soc.</u> 1982, <u>66</u>, 135.

21.   Mahrenholtz, O.; Johnson, W. <u>Int. J. Mech. Sci.</u> 1962, <u>4</u>, 35.

22.   Feger, C. <u>Polym. Mat. Sci. Eng.</u> 1988, <u>59</u>, 51.

23.   Biernath, R. W.; Soane, D. S. In <u>Polymeric Materials for Electronic Packaging and High Technology Applications</u>; The Electrochemical Society: Honolulu, 1987; p 147.

24. Macosko, C. W.; Miller, D. R. <u>Macromolecules</u> 1976, <u>9</u>, 199.
25. Miller, D. R.; Macosko, C. W. <u>Macromolecules</u> 1976, <u>9</u>, 206.
26. Nielsen, L. E. <u>J. Macromol. Sci.</u> 1969, <u>C3</u>, 69.
27. Hale, A. Doctoral Dissertation, University of Minnesota, 1988.
28. Chern, C.-S.; Poehlein, G. W. <u>Polym. Eng. Sci.</u> 1987, <u>27</u>, 788.

Chapter 30

Stress Factors in Molding Compounds

A. A. Gallo

Dexter Electronic Materials Division, Dexter Corporation, 211 Franklin Street, Olean, NY 14760

Particulate elastomer additives to semiconductor molding compounds can lower stress in the molded part by reducing modulus and coefficient of thermal expansion and possibly by reducing dimensional changes when the part cools from the molding temperature. A designed experiment, including the effect of two elastomers and of filler content, has shown that one elastomer is effective at reducing the coefficient of thermal expansion of the cured molding compound, while another elastomer is effective at reducing the modulus. Molding compounds containing mixtures of these two elastomers have performed well in commercial evaluations.

As the size and complexity of plastic encapsulated semiconductor devices has continued to increase, the need for "low-stress" molding compounds has become apparent. Mechanical stresses in large complex packages result mainly from the mismatch in thermal expansion rates between the silicon chip/lead frame and the plastic encapsulant. This mismatch can lead to deformation of the die metallization, passivation cracking or even package cracking under thermal cycle loads. Low-stress molding compounds have been developed as one method of lowering these stresses in the package; redesign of the structure of the entire package is another. The strategy behind the design of low-stress molding compounds has centered mainly on lowering the coefficient of thermal expansion of the plastic (CTE, 20-30 ppm/°C) to more closely match that of the die (2-3 ppm/°C), and the lead frame (5-17 ppm/°C), and by making the encapsulant more yielding to stress by reducing the elastic modulus (1).

Other stress factors that have been considered, are the degree of adhesion between the die and the plastic encapsulant, the resistance to crack propagation (or fracture toughness) of the plastic, and reduced dimensional changes with thermal cycling, through increased glass transition temperatures, Tg (2). While increased adhesion has been seen by some as an advantage (3),

others find the most effective encapsulant formulations as behaving
in a way that is equivalent to a reduction in adhesion (4,5).
Elastomer addition to the plastic to increase fracture
toughness has been generally seen as an advantage (6), while
increases in Tg values, may or may not be seen as an advantage.
     In this work, we have investigated one aspect of this problem;
i.e. the effects of adding two types of particulate elastomeric
additives and of filler content on two recognized stress factors
(coefficient of thermal expansion and modulus) of a model molding
compound. From this work, we have concluded that particulate
elastomer additives can not only lower stress by modulus reduction
but also by CTE reduction and possibly by reduced dimensional
changes when the part cools from the molding temperature.

EXPERIMENTAL

Thermal mechanical analysis (Dupont 990/942 TMA), and dynamic
mechanical analysis (Dupont 1090/982 DMA) curves for a designed set
of model formulations were evaluated for CTE and tensile storage
modulus as a function of filler level and elastomer additive type
and level. Fifteen formulations were prepared with 68-75% filler,
0-4% silicone elastomer A, 0-4% non-silicone elastomer B and the
balance 17-32%. Both elastomers have Tg's below room temperature.
An extreme vertices formulation design was generated by computer
(Table I).

Table I
Extreme Vertices Design

Run #	Filler	Elast. A	Elast. B	Resin
1	0.750	0.000	0.000	0.250
2	0.750	0.040	0.040	0.170
3	0.680	0.000	0.040	0.280
4	0.680	0.000	0.000	0.320
5	0.750	0.040	0.000	0.210
6	0.750	0.000	0.040	0.210
7	0.750	0.020	0.000	0.230
8	0.680	0.020	0.020	0.280
9	0.680	0.040	0.040	0.240
10	0.722	0.040	0.024	0.214
11	0.722	0.024	0.040	0.214
12	0.750	0.000	0.020	0.230
13	0.715	0.000	0.000	0.285
14	0.715	0.000	0.040	0.245
15	0.680	0.040	0.000	0.280
1	0.750	0.000	0.000	0.250

     Runs 1,2,3,4,5,6,9,&15 are the vertices of the factor space
(Figure 1).
     Based on a standard deviation for our DMA determinations of
0.55 GPa (Storage Modulus), it was determined that a 16 trial
design (15 formulations + 1 replicate, see above) would be
sufficient and yield a resolution of 0.84 GPa (i.e. the smallest

practical difference in modulus which can be significantly differentiated by this design).

In order to ensure that the design formulations would have practical molding parameters (e.g. reasonable gel times and good release), the catalyst levels were varied according to the epoxy resin and phenolic novolac hardener levels, while the other minor components, such as release agents and coupling agents (gamma-glycidoxypropyl trimethoxysilane), were kept constant in each formulation. The stoichiometric relationship between the resins and hardener was kept constant in each formulation.

DMA bars (1/8"x½"x5") were molded from each formulation. Samples for the DMA runs were cut from the center of the molded bars and the end pieces were used for TMA. In most cases, duplicate bars were molded and run (14 replicates, 29 observations in all), and all measurements were run in a randomized order. Both the DMA and TMA experiments were run at 5°C/min. The CTE below Tg was determined between 80-100°C; the CTE above Tg was determined between 220-240°C and the Tg was determined by the intersection of the extrapolations from these two expansion regions. Tg was also determined from the peak of the DMA-loss modulus curve. The DMA storage modulus was determined at 40°C. This temperature was chosen because a more stable reading can be obtained than at room temperature.

RESULTS

The CTE data below Tg were analyzed in a linear model and an "Effects Table" was generated (Figure 2). The values in the first column represent the average CTE value, and the "factor effects" for filler, elastomer A, elastomer B, and resin. That is, for each percent of added filler, CTE (below Tg) is lowered 0.17 ppm/°C, elastomer A lowers CTE by 0.35 ppm/°C, elastomer B lowers CTE by 0.09 ppm/°C, and resin raises CTE by 0.54 ppm/°C. The statistical significance of each factor effect is shown by the number of stars in the second column. The increasing number of stars correspond to significance levels 0.05, 0.01 and 0.001, respectively. The numerical value in the significance column indicates the resolution of the data with respect to particular effects. That is, the larger the numerical value is, relative to the size of the effect, the lower the significance of that effect. If the numerical value is very large, it is flagged with "!" as an extraneous term. Thus, the factor effect for elastomer B is statistically not significant and, as an extraneous term, might be eliminated from the model. The replicate standard deviation (REP SD) is calculated from the replicated observations and measures "pure" experimental error. The residual standard deviation (RESD SD) is calculated from the difference between the observations and the values calculated from the model. A model that fits the data well will have a RESD SD which is similar to the REP SD. By this criterion, a linear model fits the CTE (below Tg) data well.

The effect of filler and resin on the composite CTE of the molding compound is well understood and is a reflection of the low and high CTE values, respectively, that these two components have as intrinsic properties (Figure 3). On the other hand, elastomer A
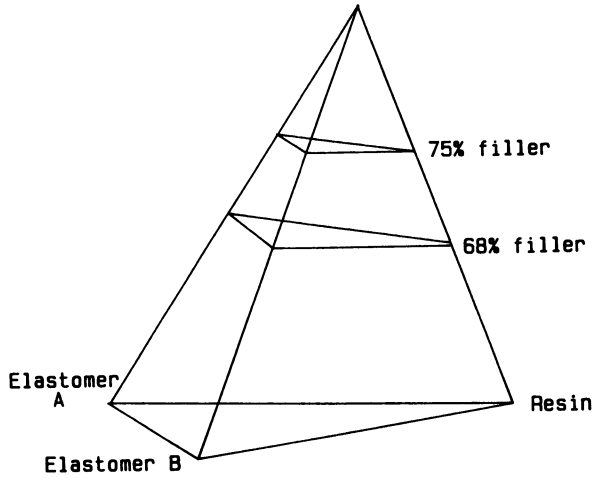
Figure 1.   Factor Space.

EFFECTS TABLE

CTE (BELOW Tg)

ppm/ $^{\circ}$C

		SIGNIFICANCE
AVERAGE	18.20	
FILLER	−17.13	* * *
ELASTOMER A	−35.02	*
ELASTOMER B	− 9.20	42.45!
RESIN	53.74	* * *

RESD	SD	1.499
REP	SD	1.461

Figure 2.   Effect of Elastomers on CTE (below Tg).

CTE

PPM/oC

SILICA FILLER	3
COMPOSITE	18
RESIN	60
ELASTOMER A (SILICONE)	300

Figure 3.   Representative CTE Values (below Tg).

has an even larger effect than the filler in reducing CTE (below Tg), yet its intrinsic CTE is larger than the composite. A hypothesis for the effect of elastomer A is as follows: During molding, the elastomer A particles are trapped in the glassy resin/filler matrix. As the part cools, the elastomer particles separate from the matrix as a result of their poor adhesion to the matrix and their high CTE relative to the matrix, leaving gaps. As the temperature is raised during the subsequent TMA measurements, the gaps are filled by the expanding elastomer without contributing to the overall bulk expansion, which is measured by the TMA instrument (Figure 4). In effect, the elastomer acts as a low expansion filler since it is decoupled from the bulk matrix expansion. A test of this hypothesis would be the observation of a high composite rate of expansion (TMA) above the molding temperature (near Tg) associated with elastomer A, since no gaps would be present at or above this temperature and the elastomer would be expected to contribute to the overall bulk expansion. This is, indeed, the case (Figure 5). In this case, both elastomers A and B show positive factor effects for CTE (above Tg) which are greater than that for the resin. Increased filler levels, as expected, show a reduction in CTE both above and below the Tg.

The TMA curves can also be used to estimate Tg. When this is done, a strong positive correlation is found between each of the elastomers and Tg (Figure 6). Each elastomer is found to increase Tg by 3°/percent, while no significant correlation with filler or resin is found. When the TMA curves are examined in more detail, it is noticed that the transition range between low and high expansion rates is broadened when elastomers are part of the formulation (Figure 7). As a result the Tg extrapolated from the low and high expansion regions appears to shift to higher values. Another estimate of Tg can be obtained from the peak of the DMA loss-modulus curve. In this case, the Tg's varied from 168-176° with no apparent correlation with elastomer content. It is concluded that there is no significant change in Tg. Although the broadened transition from low to high expansion rates, with elastomer addition, may not lead to true Tg increases, it does lead to lowered dimensional changes when the part cools from the molding temperature (Figure 8). In this case, elastomer A has a much stronger effect on reducing this dimensional change than the filler.

Using the linear factor model with the coefficients generated from the experimental modulus data, a contour plot of the predicted moduli at 73% filler is generated (Fig. 9). This contour plot is a slice of the factor space shown in Figure 1 with the modulus values coded between 7 and 16 GPa as letters A-I. As expected, both elastomers appear to have a strong effect on reducing the modulus of the molding compound. However, the mixture region with high amounts of elastomer B and low-to-moderate amounts of elastomer A and resin, shows the lowest modulus.

DISCUSSION

One type of elastomer additive (A) is effective at reducing the
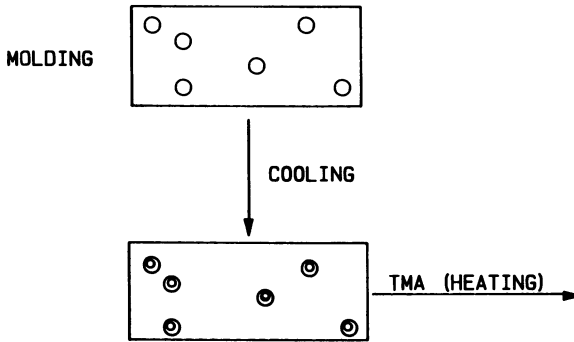
Figure 4. Elastomer Effect on CTE.

EFFECTS TABLE

CTE (ABOVE Tg)

ppm/ °C

		SIGNIFICANCE
AVERAGE	75.7	
FILLER	−73.3	* * *
ELASTOMER A	319.5	* * *
ELASTOMER B	324.3	* * *
RESIN	166.0	* * *
RESD SD	7.185	
REP SD	6.720	

Figure 5. Effect of Elastomers on CTE (above Tg).

EFFECTS TABLE

Tg, °C

		SIGNIFICANCE
AVERAGE	167.4	
FILLER	−13.9	34.8
ELASTOMER A	317.4	* * *
ELASTOMER B	305.3	* * *
RESIN	−7.3	61.3!

RESD SD	5.63
REP SD	5.25

Figure 6.   Effect of Elastomers on Tg as measured by TMA.
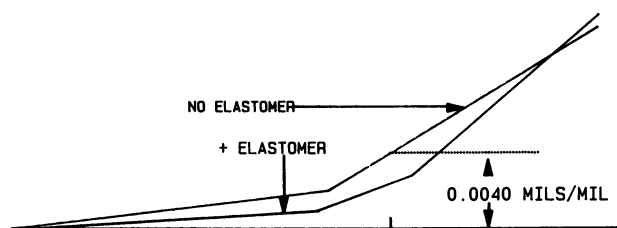
Figure 7.   Elastomer Effect on Dimensional Changes During Part Cooling.

EFFECTS TABLE

DIMENSIONAL CHANGE (180-25 °C)
MILS/MIL

		SIGNIFICANCE
AVERAGE	0.00389	
FILLER	-0.00174	*
ELASTOMER A	-0.01111	*
ELASTOMER B	-0.00198	0.01131!
RESIN	0.00608	**

RESD	SD	0.00042
REP	SD	0.00043

Figure 8. Effect of Elastomers on Dimensional Changes.

```
                    ECHIP                      SMOD
                0.00 *B* 0.10
                    /BB.\                   A =   7.00
                    /BBB.,\                  . =   7.56
                    /BBB.,,C\                B =   8.13
                    /.BBB,..CC\              , =   8.69
        B    0.02 *.BBB..,:CC.* 0.07   E     C =   9.25
        -         /..BBB,,.:CC..\        L    . =   9.81
        T         /..BBB,,,CCC....\       A   D = 10.38
        S        /...BBB,,,.CCC...DD\       S  , = 10.94
        A       /...BBB,,,CCCC...DDD\        T  E = 11.50
      L.  0.05 *A...BBB,,,CCC...DDD,,* 0.05  -   . = 12.06
      E       /A...BBB,,,,CCC...DDD,,,\       A  F = 12.63
            /AA...BBB,,,CCC...DDD,,,EE\          , = 13.19
           /AA...BBBB,,,CCC...DDD,,,EEE\         G = 13.75
          /AAA...BBB,,,CCC...DDD,,,EEE..\        . = 14.31
    0.07 *AAA....BBB,,,CCC...DDD,,,EEE...* 0.02  H = 14.88
         /<AAA...BBB,,,CCC...DDD,,,EEE...FF\     . = 15.44
        /<AAAA...BBB,,,CCC...DDD,,,EEE...FFF\    I = 16.00
       /<<AAA...BBB,,,CCC...DDD,,,EEE...FFF,\
       /<<<AAA...BBB,,,CCC...DDD,,,EEE...FFF,,,\  FILLER = 0.730
  0.10 *<<<AAA...BBB,,,CCC...DDD,,,EEE...FFF,,,,G* 0.00
       **---------*---------*---------*---------**
     0.17      0.19      0.22      0.24      0.27
                        RESIN
```

Figure 9. Contour Plot of DMA Storage Modulus.

coefficient of thermal expansion of the molding compound below Tg, while another type (B) is more effective at reducing the modulus. Combined CTE and modulus reduction is efficiently accomplished by using mixtures of these two elastomers. Molding compounds with this type of mixed particulate elastomer additives, have shown excellent results on package cracking tests and have also performed well on thermal stress-preconditioning tests in commercial evaluations.

Part of the effectiveness of particulate elastomer additives may also result from the reduced dimensional changes which they bring about during cool down from molding. Reduced stress during moderate thermal cycling of IC packages during their normal life would also benefit from these reduced dimensional changes. On the other hand, thermal cycling well above Tg (e.g. during vapor phase soldering of IC packages) may not benefit as much, from elastomer additives as from high filler levels.

LITERATURE CITED

1. Thomas, R.E., IEEE Transactions on Components Hybrids and Manufacturing Technology, 1985, Vol. CHMT-8, No. 4.
2. Sumitomo Product Bulletin, Sumikon EME-6300/9300 Series for VLSI, Sumitomo Bakelite Co. Ltd., 1986, Tokyo, Japan.
3. Suzuki, H.; Tabata, H.; Inamura, N.; Oizumi, I; Proc. ACS Polymeric Mater. Sci. and Eng., 1986, Vol. 55, 811-815.
4. Thomas, R.E., IEEE Transactions on Commponents, Hybrids and Manufacturing Technology, 1985, 0569-5503/85/0000-0037.
5. Shoraka, F.; Kinsman, K.; Notarajan, B.; Gealer, C.; Proc. Sixth Annual International Electronics Packaging Conference., 1986, 294-312.
6. Nishimura, A.; Tatemichi, A.; Miuri, H.; Sakamoto, T., Life Estimation for IC Plastic Packages under Temperature Cycling Based on Fracture Mechanics, 1987, Hitachi Ltd., Ibaraki, Japan.

Chapter 31

New Transfer Molding Compounds

E. W. Walles[1], John H. Lupinski[1], S. Bandes[2], and M. Rosenfield[2]

[1]General Electric Company, Corporate Research and Development Center, Schenectady, NY 12301
[2]The Harris Corporation, Somerville, NJ 08876

An advanced epoxy molding composition for encapsulation of integrated circuitry has been developed. It is characterized by a latent catalyst system containing an iodonium compound and a copper derivative. Prior to molding, the material is characterized by excellent stability at ambient temperatures, eliminating the need for refrigerated storage and shipping. After molding and curing it has a high glass transition temperature and a high heat deflection temperature. Encapsulated IC devices were tested under bias in accelerated life tests. Properties, process conditions and performance are described in detail.

Due to their small feature sizes, microelectronic circuits need protection from environmental hazards such as mechanical damage and adverse chemical influences from moisture and contaminants. Several approaches are currently in use, for example, hermetic encapsulation of the device in sealed metal or ceramic enclosures, application of soft silicone gels as a cover over integrated circuitry, and encapsulation by transfer molding, which is the topic of this report. Both silicone resins and epoxy resins are used for this purpose. As the quality and performance of the epoxy encapsulants improved, the need for the generally more expensive silicone resins diminished. The present work is exclusively devoted to epoxy transfer molding compounds.

Generally these compositions contain an epoxy-novolac, a hardener, a catalyst, silica fillers, and an internal lubricant/mold release compound. Brominated epoxies and antimony trioxide are included to provide the required flame retardant characteristics. Other, unspecified additives are used to promote adhesion or to reduce corrosion rates. Because of their superior thermal capabilities and electrical properties, epoxidized novolacs are preferred over epoxy homopolymers. Near stoichiometric amounts of hardeners such as novolacs (Equation 1), anhydrides, and primary amines can be used to cure the resins in the presence of a catalyst. The linkages which are formed include ethers, esters, or secondary amines, respectively.

NOVOLAC

EPOXY NOVOLAC

(1)
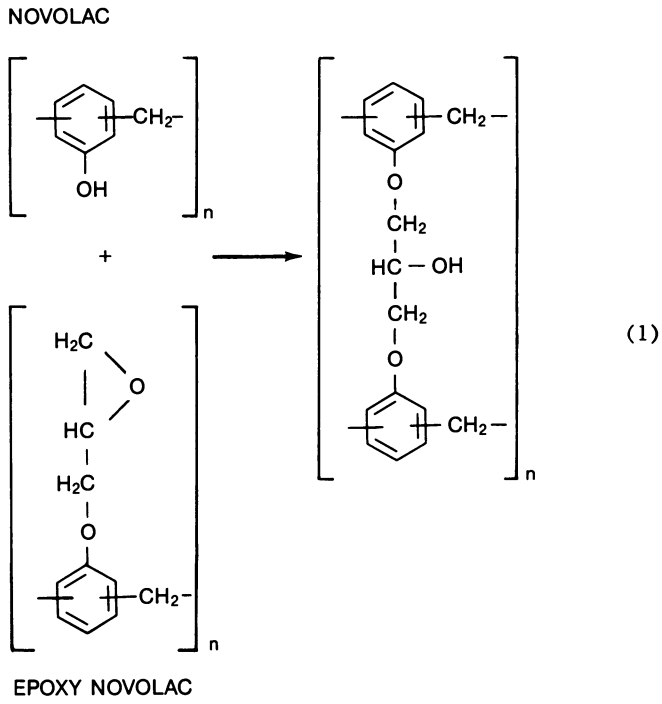
Frequently used catalysts include triaryl phosphine and tertiary amines. Since such compositions will slowly cure at ambient temperatures, they are normally kept refrigerated at 4°C during shipment and storage.

These molding compounds have to meet rather stringent requirements in order to produce highly reliable encapsulated devices. For example, the resin has to provide a good melt flow for rapid filling of the mold holding the IC's in its cavities. The viscosity of the melt should be sufficiently low to permit easy flow around the 1 mil (.025mm) diameter wires which connect the IC to the leadframe. Too high a viscosity will displace the wires (wire sweep), resulting in shorts or open connections. Once the mold is completely filled, the resin should harden rapidly so that the devices can be removed from the mold after a short time without damage or deformation. After molding, the encapsulated devices are usually given a post bake to complete the cure of the resin (1). Great progress has been made, for instance, in the solvent resistance of the cured resins. While earlier devices could easily be freed from the encapsulant by prolonged immersion in N-methylpyrrolidone (NMP), modern encapsulants can be removed only by treatment with very hot (~300°C) concentrated sulfuric acid.

Typical properties of both "conventional" and new molding resins are listed in Table I.

Novel Epoxy Transfer Molding Compounds

Although epoxy novolac resins are used in the present work, there is a fundamental difference from conventional encapsulant resins in that onium compounds in combination with copper acetyl(acetonate) are used in our materials as catalyst systems (2). These catalyst systems promote epoxy/epoxy polymerization and eliminate the need for hardeners.

Crivello has published extensively on onium compounds and their function as catalysts (3,4). Generally, such compounds are photocatalysts, but are stable in the absence of light. Irradiation at the proper wavelength leads to a complex photodecomposition of the onium ion in which reactive cation radicals and neutral radicals are formed as short lived intermediates. Also formed are acids, corresponding to the anion of the onium compound, which catalyze the epoxy polymerization. Equations 2 and 3 show the decomposition of iodonium cations.

$$Ar_2I^+ \ X^- \rightarrow [Ar_2I^+ \ X^-]^* \rightarrow ArI^{\cdot +} \ X^- + Ar\cdot \tag{2}$$

$$ArI^{\cdot +} \ X^- + R\text{-}H \rightarrow ArI + R\cdot + HX \tag{3}$$
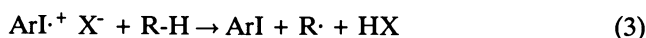
R-H represents a proton source (e.g., solvent). The radicals Ar· and R· may dimerize or give ArR type products.

Crivello (5) also found that these photocatalysts could be activated thermally when used in combination with copper compounds. For those conditions, Crivello has proposed a cationic polymerization mechanism which does not

Table I. Properties of Molding Compounds

Properties	Molding Compound	
	Conventional	New
a) Properties during molding		
at 1000 psi (7MPa)		
Flow length at 180°C:* (inches/cm)	25/63.5	25/63.5
Flow length at 150°C: (inches/cm)	23/58.4	43/109
Curing time at 180°C: (seconds)	19	8
Curing time at 150°C: (seconds)	85	48
Percent decrease in flow length:		
*i) After 5 days at 43°C/40%RH:	100 (no flow)	2
ii) After 2 preheat cycles to 100°C:	100 (no flow)	0
b) Properties after molding		
at 1000 psi (7MPA):		
Hot Hardness, Shore D:*		
After 1.5 min at 180°C	95	97
After 2.0 min at 150°C:	75	75
Glass Transition Temperature:**		
After 16 hrs at 180°C:	180°C	195°C
Linear coefficients of		
Thermal expansion:** at 50°C:	19	19
(x 10^{-6}mm/mm/°C) at 150°C:	27	33
at 200°C:	65	47
Heat Distortion Temp.:***	240°C	315°C

*ASTM method D3123; 0.12 to 0.14 inch (.30-.36 cm) cull; 12 sec transfer time.

**Thermomechanical analysis; heating rate 2.5°C/min; ASTM method D696.

***ASTM method D648-56; 264 psi (1.8 MPa) test.

involve the formations of acids, HX. It is based on the presence of alcohols in commercial epoxy resins and it can be represented by Equations 4-7.

$$R\text{-}OH + 2Cu(II)L_2 \rightarrow R{=}O + 2Cu(I)L + 2HL \qquad (4)$$

$$ArI^+ \ X^- + Cu(I)L \rightarrow ArI + [ArCuLX] \qquad (5)$$

$$[ArCuLX] + M \rightarrow ArM^+ \ X^- + Cu(I)L \qquad (6)$$

$$ArM^+ \ X^- + nM \rightarrow Ar(M)_n \ M^+ \ X^- \qquad (7)$$
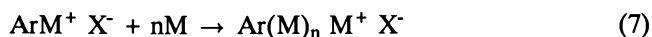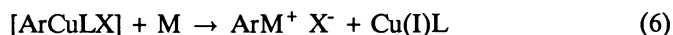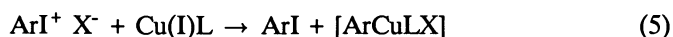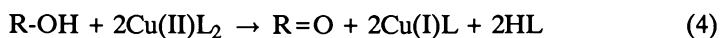
in which R is a hydrocarbyl group, L is an organic ligand, [ArCuLX] is an inter-mediate complex and M is a monomer. The molding compounds described in this paper are based on such catalyst systems.

During the development of the molding composition it was noted that the surface treatment and the particle size of the silica filler had a large influence on the flow characteristics of the resin. Table II shows that filler particles with a complete hydrophobic surface gave molding compounds with lower melt flow than filler particles with a partial hydrophobic surface. Untreated particles with a large hydrophilic surface gave molding compounds with even larger melt flow. Further improved melt flow was realized when the silica filler with 100% <40μm particle size was replaced by a similar filler with a particle size 100% <90μm.

Table II. Influence of Silica Filler Conditions on Flow Characteristics

Particle Size	Surface Treatment	Catalyst System(%)	150°C Flow,Inches	T_g °C[a]
100% <40μm	$(H_3C)_2Si(OCH_3)_2$			
"	complete	.3	4	
"	partial	.3	9	
	$(CH_3)_3SiNSi(CH_3)_3$ H			
"	complete	.3	4	
"	no treatment	.15	23	135
100% <90μm	no treatment	.3	35	180

a) Glass transition temperature was determined by dilatometry at a heating rate of 2.5°C/min. The samples were post-cured for 16 hrs at 180°C.

The molding compound chosen for this work has the composition as shown in Table III.

Table III. Molding Compound Composition in Weight Percent

Epoxy Resin	27.6
Silica Filler	68.3
Catalyst System	.3
Carnauba Wax	.4
Flame Retardants	3.3
Carbon Black	.1

The flame retardants give the required V-0 flammability characteristics; the wax functions as an internal lubricant and mold release compound, and the carbon black provides the uniform black color. After 90 secs in the mold at 150°C the Shore D hot hardness is 78, sufficient to push the device from the mold without damage.

Encapsulant powders are generally compacted into pellet-like preforms for ease of handling. These preforms are then dielectrically preheated to 100°C prior to molding. Figure 1 is a plot of spiral flow length (inches, 100 psi/150°C) versus preheating cycles at 100°C of a standard preform (30 grams, 1.25" (3.18 cm) diameter). At 150°C and 1000 psi (7MPa) this formulation showed an initial spiral flow length of 34" (86.4 cm). At 180°C and 1000 psi (7MPa) the initial spiral flow length is 25" (63.5 cm) and remains stable at 18-20" (46-51 cm) for about 60 days while the sample was kept at 43°C (see Figure 2). This flow length was sufficient to completely fill the mold during transfer molding. The new material can be molded at a temperature as low as 150°C, while 180°C is required for commercial materials. Typically, the new resin shows a T_g of about 150°C after molding and post baking at 150°C for 16 hours, while a T_g of about 180°C is obtained after molding at 180°C followed by a 16 hour post bake at the same temperature. For temperatures below T_g the linear coefficient of thermal expansion is approximately constant at 21×10^{-6} mm/mm/°C up to nearly 180°C (see Figure 3).

The new encapsulant could be preheated to 100°C at least fifteen times while still maintaining excellent flow length. Clearly the catalyst is inactive below 100°C but at 150°C and above it is very active and it causes rapid cure of the resin. The onset of exotherm is 145°C for the new encapsulant vs. about 170°C for conventional encapsulants. This is consistent with the fact that the 63.5 cm flow length at 180°C is considerably shorter than the 109cm flow length observed at 150°C. Because of this demonstrated stability at ambient temperatures, the material was kept in closed containers at ambient temperatures throughout this work and during shipping and storage. It was never refrigerated as is required for all the current commercial molding compounds used in microelectronic applications.

Selection of Test Devices

Recognizing that the performance of a particular molding composition may depend on the type of test vehicle chosen, it was decided to evaluate the new molding compounds with different devices. Test vehicles selected included linear amplifiers with four independent high-gain amplifiers per chip and two digital devices: a CMOS nandgate and a hexbuffer/converter. Not only is the circuitry of the test vehicle important, but also the way it is protected with inorganic passivation layers. Other characteristics which influence the test results are the leadframes to which the IC's are connected by wire bonds. In some parts of this work two different metals were used for leadframes, namely A-42 (42% Ni; 58% Fe) and a copper alloy (CuA).

Finally, the actual shape of the leadframe is important. Under certain conditions, ionic impurities, under the influence of electric fields and high humidity, are considered to migrate along the leads of the leadframe toward the thin electrical conductors, which are very vulnerable to corrosion. To make this migration along the leads as difficult as possible, the lead is given the character of a tortuous path. In some designs there are holes in the leads. These holes serve a dual purpose: they make migration of ionic impurities more difficult and they also allow for "a better grip of the resin" on the leadframe. All devices in this work were
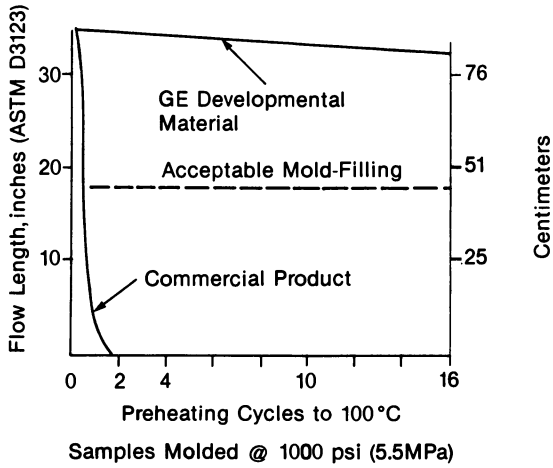
Figure 1. Ability of GE development material to be reheated.
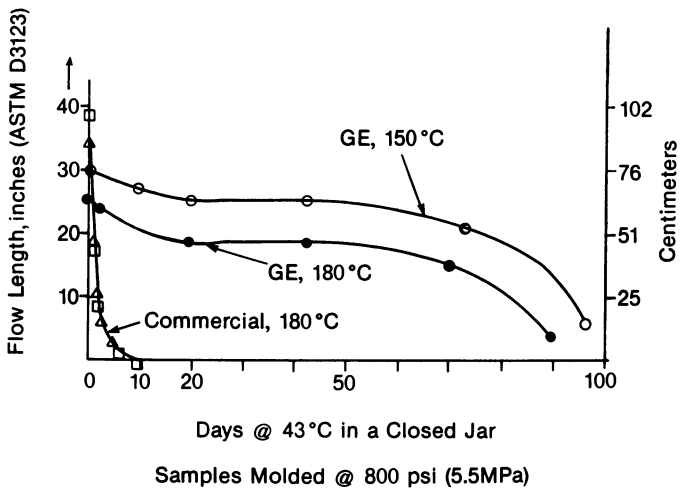
Figure 2. Shelf stability of encapsulants stored at 43°C in a closed jar.

mounted on leadframes with locking holes. Three leadframe designs are illustrated in Figure 4.

Device encapsulation conditions are summarized in Table IV. Upon completion of the encapsulation, the devices molded at 150°C were post baked for 16 hours at 150°C, and those molded at 175°C were post baked at that temperature. After trimming, clipping, and forming, the IC's had their final dual in-line package shape. The leads were dipped in 63/37 Sn/Pb solder using a halide-containing flux (Alpha 200).

Table IV. Device Encapsulation Conditions (336 Cavity Mold)

Devices	Digital 1	Digital 2	Linear	Digital 1	Digital 2	Linear
Leadframes	A-42	A-42	A-42	A-42	A-42	A-42
Transfer Temp. (°C)		175			150	
Transfer Time (secs)		12-15			18-20	
Transfer Pressure (MPa)		7.2			7.2	
Cure Time (secs)		90			150	
Post Mold Cure (Hrs/°C)		16/175			16/175	
Moldability/1344		2			8	
Wire Sweep/336	6			7		
Internal Voids/336	83			66		
Resin Bleed/336	0			4		
Test Yield (%)	99.1	99.3	99.1	98.7	99.0	98.8

The moldability/1344 indicates the number of samples which, upon visual inspection, show flaws such as surface voids and rounded corners. Wire sweep and internal voids were determined by x-ray screening. These data may reflect a somewhat greater reactivity of the new molten resin. A further increase in resin viscosity may lead to wire sweep and other imperfections such as internal voids. A low resin bleed count supports this idea. (Resin bleed is resin material protruding onto leadframes beyond the rectangular shape of the resin mass). Linear devices were also molded over CuA leadframes at 175 and 150°C. The test yields were 98.0 and 98.8% respectively. These yields, as well as those obtained with A-42 leadframes (Table IV) are identical to the yeilds observed when commercial encapsulants are used.

Device Testing

Testing of encapsulated devices was done by thermal cycling and by accelerated moisture testing at elevated temperatures, high humidity and bias (6).

All devices made with both copper alloy (CuA) and A-42 leadframes and encapsulated with the developmental resin were subjected to thermal cycling between -65°C and 150°C. Samples were kept for 5 min. at each temperature,
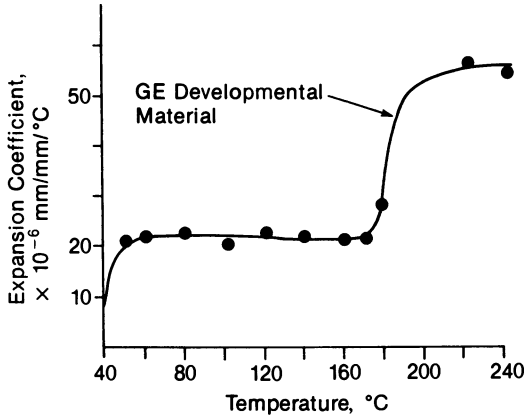
Parts Were Molded @ 1000 psi (7MPa) 90 secs, 180 °C
and Post-cured 16 hrs @ 180 °C. TMA: 2.5 °C/min

Figure 3. Expansion coefficient vs. temperature. (Reproduced with permission of Reference 2. Copyright 1988 Cahners Exposition Group.)
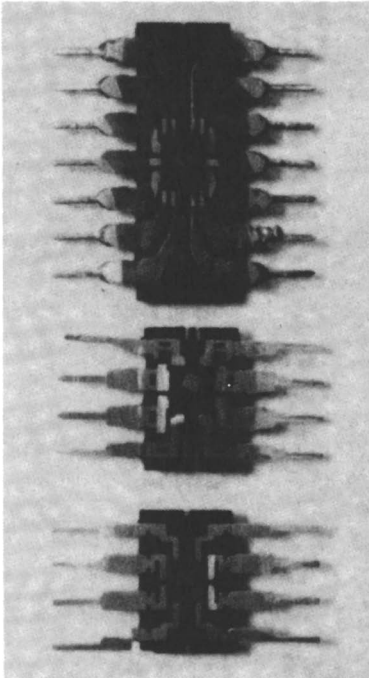
a) Simple design leadframe

b) Leadframe with locking holes

c) Leadframe with tortuous path

Figure 4. Simple and advanced leadframe designs.

while the time for switching between the two temperatures was approximately 10 secs. After 1000 cycles, there were no failures for any of the devices.

Highly accelerated moisture tests (HAST) were performed in a two-zone Hirayama pressure chamber in which samples were exposed to 145°C, 85% R.H. and 18V bias. Periodically, the devices were removed from the pressure chamber and the linear devices were tested for electrical performance in a Gen Rad 1731M Linear IC Test System. This instrument monitors several device parameters. All of these parameters remained within specifications until the devices failed due to open circuitry resulting from corrosion. Earlier tests were performed at 131°C, 85% R.H. and 30V bias (2). Under these conditions the test requires long times. Short test times are readily achieved at 145°C (6).

Failures as a function of pressure chamber time for the linear amplifiers made with alloy A-42 and copper alloy (CuA) leadframes are given in Table V. Even though the resin can be molded at 150°C, the test results indicate that devices encapsulated at 175°C out-perform all others.

Table V. Accelerated Moisture Testing of Linear Devices at 145°C/85%RH/18V

Molding Temp (°C) Leadframe	150 CuA	175 CuA	150 A-42	175 A-42
40 hrs	3/25	0/25	0/25	0/25
80 hrs	22/25	21/25	22/25	7/25
120 hrs	-	4/25	3/25	5/25
Failures (120 hrs)	25/25	25/25	25/25	12/25

In addition to the linear devices, accelerated moisture tests under identical conditions were also performed on the digital devices on A-42 leadframes. The results are given in Table VI.

Table VI. Failures* Upon Accelerated Life Testing of Devices Encapsulated with GE's Developmental Molding Compound. Digital Devices on A-42 Leadframes

Devices	Digital 1	Digital 2
Molding Temps. (°C)	175	175
Hours of Testing		
120	0/25	0/25
200	0/25	5/25
300	15/25	23/25

*All failures are open circuits caused by corrosion

Summary

Latent catalysts consisting of onium compounds and copper compounds have been shown to be excellent curing agents of epoxy-novolac transfer molding compounds for encapsulation of electronic devices. Since these catalysts initiate the epoxy polymerization only at elevated temperatures, the formulations show long-term stability at ambient temperatures, whereas current commercial materials require refrigeration during storage and shipping. Another difference with commercial transfer molding compounds is that the composition described here does not contain hardeners such as novolac resins.

Both CMOS and bipolar devices encapsulated with the new transfer molding compositions performed well under thermal cycling between -65°C and +150°C and also under accelerated life testing at 145°C, 85% RH and 18V bias. Further optimization of this type of molding composition is expected to improve its performance as a protective material for integrated circuitry.

Acknowledgments

Literature Cited

1. Burggraaf, P. *Semiconductor International*, December 1984, p 60.
2. Walles, E. W.; Lupinski, J. H. *Proc. of the Technical Program*, Nepcon West '88, Anaheim, CA; 1988, p 854.
3. Crivello, J. V.; Lee, J. L. *Polymer Journal* 1985, *17*, 73.
4. Crivello, J. V. US Patents 4,173,551, 1979; 4,216,288, 1980; 4,238,587, 1980; 4,239,725, 1980; 4,283,312, 1981.
5. Crivello, J. V.; Lockhard, T. P.; Lee, J. L. *J. Pol. Sci. Polymer Chemistry Edition* 1983, *21*, 97-109.
6. Gallace, L.; Rosenfield, M. *RCA Review* 1984, *45*, 2249.

Chapter 32

Chemistry of Stable Brominated Epoxies

C. S. Wang, D. B. Fritz, and A. Mendoza

Dow Chemical Company, Freeport, TX 77541

In electronic encapsulation applications, epoxy derivatives of
novolacs containing meta-bromo-phenol have exhibited
substantially better physical and performance properties
compared to the conventional tetrabromobisphenol-A or
brominated phenol novolac epoxies which are either ortho- or
para-brominated phenolics. The instability of ortho- or para-
brominated phenols is due to the formation of an unstable
cyclohexadienone structure via Keto-enol tautomerization. Upon
heating, this unstable cyclohexadienone structure generates free
radicals •(BR) which in turn abstract proton from a neighboring
molecule to form HBr. An intermediate which is used as an
alkylating agent to incorporate the stable meta-bromo-phenol
moiety into a variety of novel materials has been synthesized.
The meta-bromo-phenol moiety contributes the expected
improvements in thermal and hydrolytic stability to the molding
formulation while providing fire retardancy properties.

Epoxy resins are widely used for semiconductor device encapsulation in the
microelectronic industry. The major criteria for measuring quality of epoxy resin
in microelectronic applications are the level of total leachable halide and the
epoxide content. Both factors have a great influence on the reliability of an
encapsulated semiconductor device.

   One of the most frequent failures encountered in the encapsulated micro
devices is the so-called open circuit, which results from a break of the bonding
wire between circuitry. The breakage is primarily due to corrosion. This is
initiated by the impurities in epoxy resins, such as halogen, which upon exposure
to heat and moisture generate a corrosive acid.

With the consistent increase in computer memory capacity (from 16K to 4 MM) the requirement of higher purity epoxy resins becomes essential since the circuitry of high capacity memory chips has to be much denser and finer which will render it more susceptible to corrosion failure. Table I indicates the resin purity requirement over recent years. Figure 1 demonstrates the relationship between resin purity and device reliability; the higher the purity the longer the expected device life. Inorganic halides of resins are less than 5 ppm.

TABLE I. Resin Purity Development

Prior to	1981	Hydrolyzable Chloride	2500 ppm
	1982	Hydrolyzable Chloride	1000 ppm
	1983	Hydrolyzable Chloride	100 ppm
	1984	Hydrolyzable Chloride	20 ppm
	1985	Total Chloride	1200 ppm
	1986	Total Chloride	900 ppm
	1987	Total Chloride	<750 ppm

Effect of Bromine on Device Reliability

In order to provide the required flame retardancy to the molding compound, an encapsulated formulation usually contains brominated resins and antimony oxide. The brominated resins used in the encapsulated formulation are mainly tetrabromobisphenol A (TBBA) based epoxy resin or brominated epoxy novolac. These bromine-containing additives were reported to cause bond degradation at high temperature through accelerated void formation in the gold-aluminum intermetallic phases (1-4).

For the purpose of identifying the cause of this detrimental effect of the brominated resins on the wirebond reliability, the diglycidyl ether of tetrabromobisphenol A (TBBA) was exposed to 150° or 180° C for two hours, and the resultant resins were analyzed for the hydrolyzable halide content. A hydrolyzable halide is the halogen adjacent to a hydroxyl group and hence can be easily dehydrohalogenated (Table II).

TABLE II. Thermal Stability of TBBA Epoxy Resin

		Hydrolyzable (ppm)	
Temperature (° C)	Time (hr)	Bromide	Chloride
Start	0	95	18
150°	2	105	21
180°	2	286	35

The results strongly indicate that at 180° C, bromine is coming off from the aromatic ring and opening up the glycidyl ether to form hydrolyzable bromide. To further prove this possibility, TBBA was mixed with the diglycidyl ether of bisphenol-A (D.E.B.) in an equal weight and then immersed in an oil bath at 180° overnight. Results in Table III indicate that the bromine not only came off from the ring, but also that the total chloride in D.E.B. was converted partially to hydrolyzable chloride. Total chloride is the combination of hydrolyzable and bound chloride in an epoxy resin where the bound chloride is the chlorine not adjacent to a hydroxyl group. At 180° C, part of the bound chloride has come off and opened the glycidyl ether of D.E.B. to form the hydrolyzable chloride.

FAILURE RATE, Percent

Low Purity CEN
(1800 ppm total Cl)
——*——

Medium Purity CEN
(1000 ppm total Cl)
——⊖——

High Purity CEN
(250 ppm total Cl)
——▭——

TESTING TIME, Hours
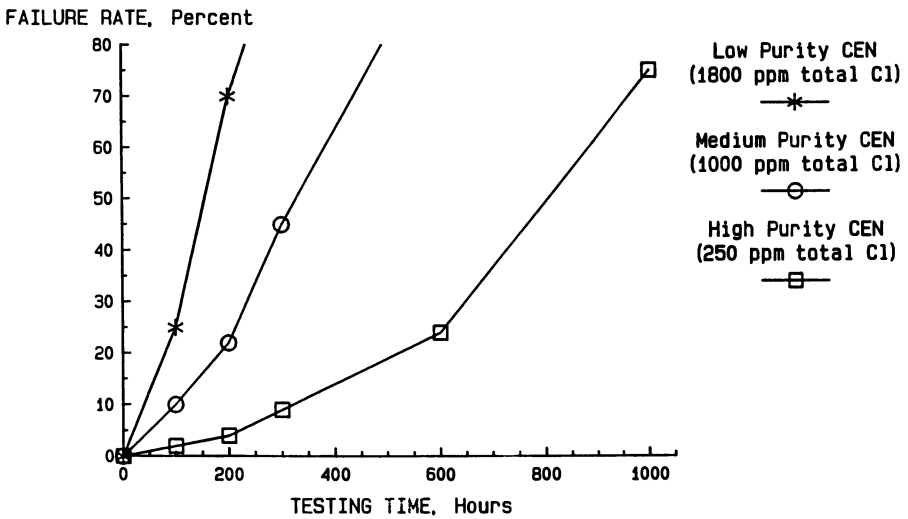
LM324 Quad Op Amp (Single Passivation)
Conditions=> 110 deg C, 100% RH, 20 Volts DC

Figure 1. Bias pressure cooker-device reliability test, cresol-epoxy-novolac-based molding compounds.

TABLE III. Temperature Aging of TBBA/D.E.B.

Material	ppm HyBr	HyCl
TBBA	183	9
TBBA + D.E.B. (1:1)	88	12
TBBA + D.E.B. 180° C overnight	599	136

With the introduction of low total chloride epoxy resins (chlorine content <700 ppm), the wire bond failure due to the chlorine impurities in the resin has become much less prominent than that due to the bromine from the fire retardant additives in the molding compound. The chlorine content in a typical molding compound is less than 150 ppm while the bromine content is 0.75-1.25% (12,500 ppm). A release of bromine upon heating from resin, as experienced above, certainly will have a great detrimental effect on device reliability.

Stable Bromine Containing Resins

It is reported in the literature (5-7) that m-bromo-phenolic compounds are more stable than their o- or p-brominated counterparts. An o- or p-Brominated phenol forms an unstable cyclohexadienone structure via keto-enol tautomerization. Upon heating, this unstable cyclohexadienone structure generates free radicals which, in turn, abstract a proton from a neighboring molecule to form HBr.
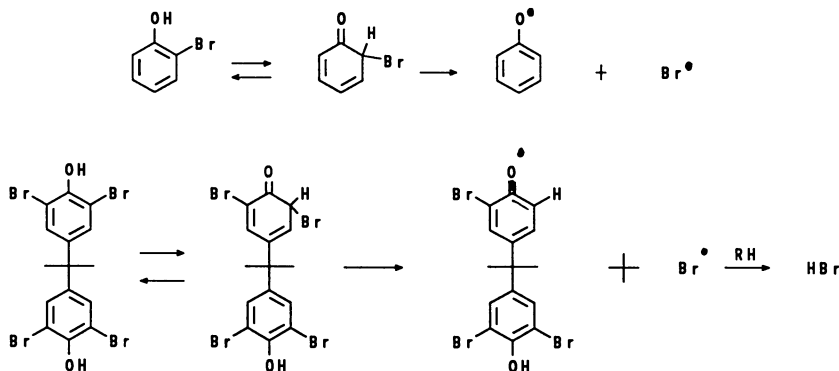
Electron Spin Resonance (ESR) measurements further demonstrated the instability of TBBA at high temperature (250° C for one hour), showing a relative radical concentration of 960 for TBBA compared to <10 for the metabrominated mesitol.

Bromination

The simplest method for the synthesis of m-brominated phenolics is the bromination of o- and p-substituted phenolics. As shown in the following equations, mesitol was brominated to give 3-5 dibromomesitol (8). The o-substituted tetramethyl bisphenol gave tri- and tetra-brominated compounds (9). Similar substitution occurs with the o-substituted tetramethyl bisphenol ethane (10).
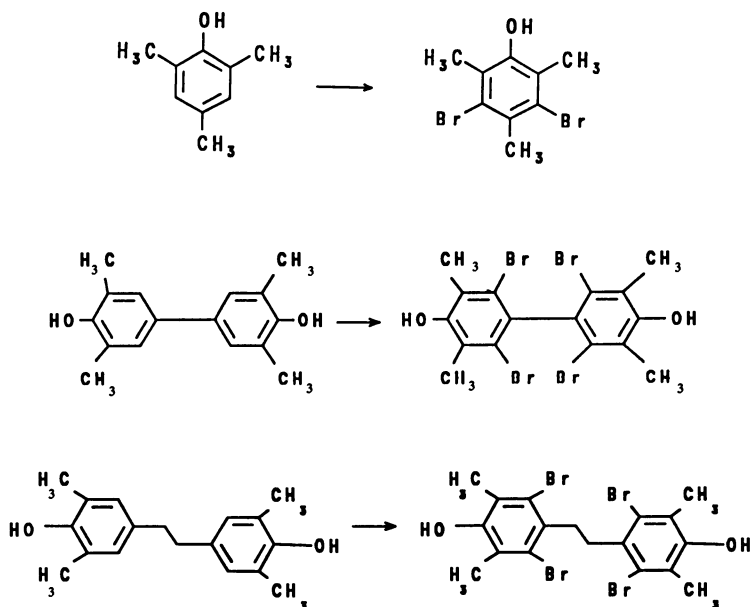
Incorporation of the above m-brominated phenolics into epoxy resin was accomplished either by the thermally catalyzed phenolic hydroxyl - epoxy reaction or by the caustic catalyzed reaction (11). The reactions are depicted as follows:
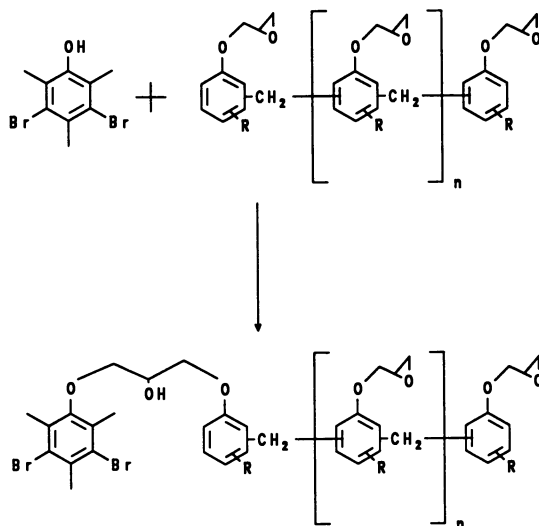
For difunctional phenolics, such as biphenol and bisphenol ethane, two moles of epoxy resins are reacted with the difunctional phenolics to form an adduct.
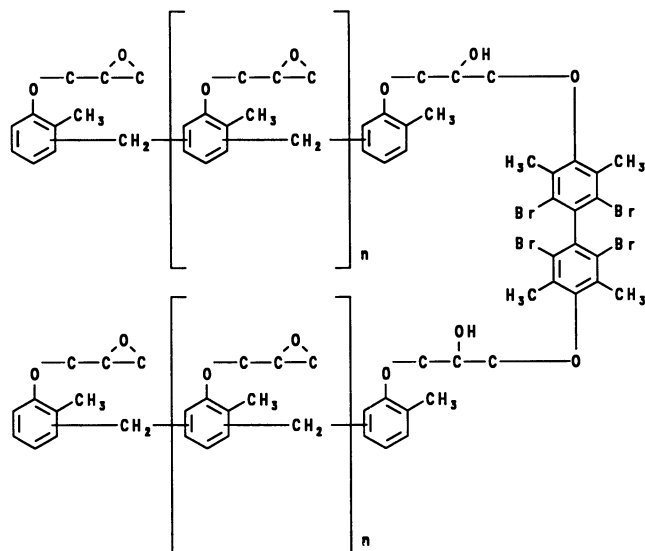
Chemical stability of the m-bromo phenol containing epoxy resin was compared with commercially available brominated resins. Epoxy resins were refluxed in N-methyl-pyrrolidinone with 1 N KOH for 15 minutes. Results in Table IV clearly demonstrated the extraordinary chemical stability of the m-bromo-phenol containing epoxy resin over the commercial product.

TABLE IV. Comparison of Commercial and m-Br Phenol Epoxy Resin

Formulation	ppm Br	ppm Cl
*Commercial I	863	157
*Commercial II	526	229
Dow (o-Brom)	313	339
Dow (m-Brom)	52	130

* Commercial resins may contain aliphatic bromine

Although the m-bromo phenol containing epoxy resin exhibits unusual stability, the chemistry for the incorporation of these phenolics into epoxy resin involves opening of the epoxy ring which eventually reduces the epoxy content of the final resin. Reduction of the glass transition temperature by 15-20° C was observed.

Both reductions in the glass transition temperature and the epoxy content are not acceptable. A new chemistry was developed to correct this problem.

Meta-Bromo-Phenolic Alkylating Agents

Bromination of mesitol with excess bromine produced 4-bromomethyl-3,5-dibromo-2,6-dimethylphenol as a major product which on hydrolysis produced 4-hydroxymethyl-3,5-dibromo-2,6-dimethylphenol (8). Both 4-bromomethyl- and 4-hydroxymethyl-3,5-dibromo-2,6-dimethylphenol are excellent alkylating agents. With or without catalyst, in a solvent or without solvent, they react readily with other phenolics to form alkylation products (12). The following equations exemplify these reactions:

X = Br OH
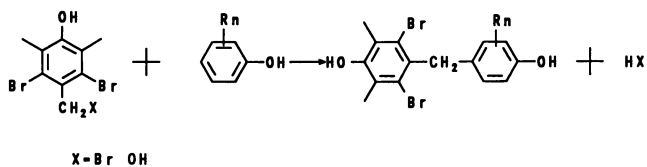
Meta-Bromo Phenol Containing Epoxy Resins

For electronic applications, 4-hydroxymethyl-3,5-dibromo-2,6-dimethyl-phenol was reacted with cresol novolac to form the m-bromo phenol containing cresol novolac which is then epoxidized to the corresponding epoxy resin (12):
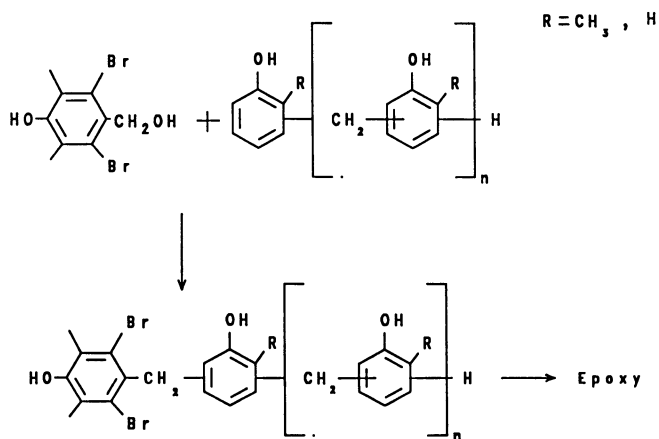
The chemistry was extended to phenol-formaldehyde novolac, trisphenol novolac and dicyclopentadiene-phenol novolac (12). Structures of these products are shown as follows:
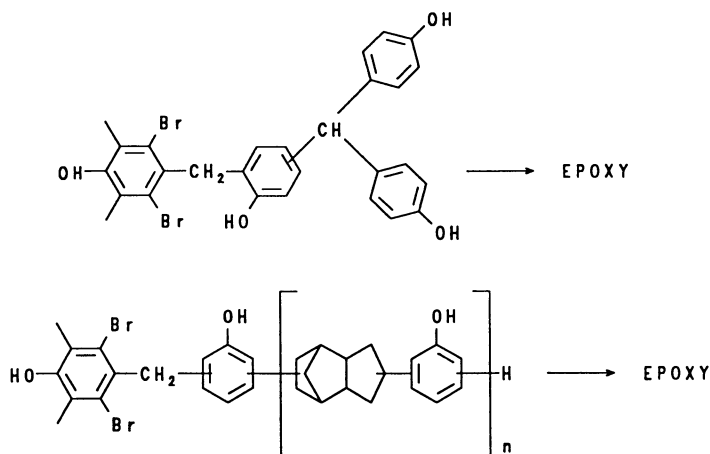
Conclusion

Meta-halogenated phenols are generally known to be more chemically and thermally stable than their o- or p- halogenated counterparts. A reactive intermediate, produced by the brominated 2,4,6-trimethylphenol is being used as an alkylating agent to incorporate this stable m-bromo-phenol moiety into a variety of novel materials.

In electronic encapsulation applications, epoxy derivatives of novolacs containing meta-bromo phenol have exhibited substantially better physical and performance properties compared to the conventional tetrabromo bisphenol-A epoxies and brominated epoxy novolacs. The meta-bromo phenol moiety contributes the expected improvements in thermal and hydrolytic stability to the formulation while providing fire retardancy properties (13).

Literature Cited

1. Khan, M. M.; Fatemi, H., Proc. Int. Symp. Microelec. 1986, p 420.
2. Gale, R. J., Proc. IEEE Int. Reliability Physics Symp., 1984, p 37.
3. Ahmad, S.; Blish, R.; Corbett, T.; King, J.; Shirley, G., Comp. Hybr. Manuf. Technol., 1989, 9 (4), 379.
4. Ritz, K. N.; Stacey, W. T.; Broadbent, E. K., Proc. IEE Int. Reliability Physics Symp., 1987, p 28.
5. Factor, A., J. Polymer Science, Polymer Chem. Ed. 1973, 11, 1691.
6. Nara S.; Matsuyama, K., J. Macromol. Sci. Chem. 1971, A5 (7) 1205.
7. Zaks, Y.; Lo, J.; Raucher, D.; Pearce, E. M., J. Appl. Poly. Science 1982, 27, 913.
8. Mendoza, A. U.S. Patent 4 684 752, 1988.
9. Orlando, C. M.; Lavallee, F. A. U.S. Patent 3 929 908, 1975.
10. Mendoza, A. U.S. Patent 4 705 901, 1987.
11. Berman, J. R.; Wang, C. S. U.S. Patent 4 727 119, 1988.
12. Mendoza, A.; Wang, C. S.; Fritz, D. B. U.S. Patent 4 731 423, 1988.
13. Fritz, D. B.; Wang, C. S. 196th ACS National Meeting, Division of Polymeric Materials Science and Engineering, 1988, Abstr. No. 161.

Chapter 33

Performance of Stable Brominated Epoxies in Encapsulants for Microelectronic Devices

D. B. Fritz and C. S. Wang

Dow Chemical Company, Freeport, TX 77541

Epoxy molding compounds, used to encapsulate microelec-
tronic devices, contain bromine to provide flame
retardancy to the package. This bromine, typically
added as tetrabromo bisphenol-A or its epoxy derivative,
has been found to contain many hydrolyzable bromides.
These bromides, along with the presence of chloride
impurities, are detrimental to the life of the elec-
tronic component. Bromine especially has been suspected
(proven) to cause wire bond failure when subjected to
moisture and/or high temperatures. With the addition of
a more thermally and hydrolytic stable bromine compound,
flame retardancy does not have to be compromised to
increase the device reliability. Stable brominated
cresol epoxy novolac, when formulated into a
microelectronic encapsulant, increases the reliability of
the device without sacrificing any of the beneficial
properties of present-day molding compounds.

Cresol Epoxy Novolac (CEN) and the epoxy derivative of tetrabromo-
bisphenol-A (TBBA) are the resins typically employed to encapsulate
microelectronic devices in molding compounds. The brominated resin,
which is utilized as a flame-retardant additive to impart a degree of
ignition resistance to the encapsulant, contains many unstable
hydrolyzable bromides. These bromides, along with the presence of
chloride impurities, are detrimental to the life of the electronic
component. Specifically, bromine has been suspected and proven to
cause wire bond failure (1-3).
    Brominated compounds, where the bromine is in the meta position
to the phenolic hydroxyl, have been shown to be more hydrolytically
and thermally stable than ortho-brominated compounds such as TBBA
(4). These stable bromine compounds can be incorporated in the CEN
molecule and formulated into a molding compound. These molding
compounds provide increased device reliability without sacrificing
any of the beneficial properties of present molding compounds.

Table I shows the typical analytical properties of stable brominated CEN and the standard high purity resin blend of CEN (QUATREX* 3430) and the epoxy of TBBA (QUATREX 6410). This resin blend of CEN and the epoxy of TBBA was mixed in a ratio that corresponds with what is typically used in microelectronic encapsulants. The stable bromine CEN was synthesized to match the bromine content of the resin blend. The total bromine content of the resin blend and the stable bromine CEN is 7%; however, the hydrolyzable bromide impurities of the stable bromine CEN is much lower than that of the standard resin blend. This low content of hydrolyzable bromide, along with the low chloride content, contributes to an increase in device reliability

TABLE I. Typical Analytical Properties Based on Resin(s)
at 7% Bromine

Property	Stable Bromine Cresol Epoxy Novolac	QUATREX 3430 + QUATREX 6410
Bromine, wt. %	7.0%	7.0%
Viscosity @ 150°C, cks	300-600	300-600
Epoxide, wt. %	20.5%	20.3%
Epoxide Equivalent Weight (EEW)	210	212
Hydrolyzable Chloride, ppm	<25	<50
Hydrolyzable Bromide, ppm	<25	300+
Total Chloride, ppm	650	700
Ionic Chloride, ppm	<1	<1

Because the analytical properties of the two resin systems are similar, the stable bromine CEN can be substituted into the formulation without significant component modifications.

Molding Compound Technology

Table II shows the ingredients used in this comparison between the stable bromine CEN and the standard high purity resins. These ingredients are found in standard molding compounds for use in microelectronic encapsulation.

Table III shows the reactivity properties of the molding powder and the physical properties of the cured compound. This table indicates there are virtually no differences in gel times, flow properties, flexural properties, moisture absorption, flame retardancy, and glass transition temperatures between the compound based on stable bromine CEN and the compound based on the standard system of CEN and the epoxy of TBBA.

Figures 1 and 2 show the bulk electrical properties of the two cured molding compounds. The dielectric constant and dissipation factor were determined before and after moisture exposure. For moisture exposure, the samples were placed in an autoclave at 100% relative humidity, 15 psig, and 250°F for 500 hours. Measurements

TABLE II.   Molding Compound Ingredients Approximately 1.3%
by Weight of Bromine in Each Total Formulation

	Stable Bromine CEN Molding Compound	Standard Molding Compound
QUATREX 3430, EEW-195	---	16.0%
QUATREX 6410, EEW-450, Bromine-50%	---	2.5%
Stable Bromine CEN, EEW-210, Bromine-7%	18.5%	---
Phenolic Novolac-Hardener	9.1%	9.1%
Triphenylphosphine-Catalyst	0.2%	0.2%
Fused Silica-Filler	70.0%	70.0%
Antimony Trioxide-Synergistic FR Agent	1.0%	1.0%
Carbon Black-Pigment	0.4%	0.4%
Refined Montan Wax-Mold Release Agent	0.4%	0.4%
Silane Coupling Agent	0.4%	0.4%
TOTAL	100.0%	100.0%

TABLE III.   Reactivity, Physical, and Thermal Properties
Based on Molding Compound

Property	Stable Bromine CEN Molding Compound	Standard Molding Compound
Reactivity:		
Gel Time @ 170°C	40 seconds	42 seconds
Spiral Flow @ 175°C	46 inches	49 inches
Spiral Flow @ 175°C after 6 days @ 40°C	22 inches	25 inches
% Retention of Flow	48%	51%
Physical:		
Moisture Absorption, wt. % 500 hours @ 1 ATM Steam	+0.93%	+0.97%
UL 94 Flame Retardance Rating, based on 1/16 inches thick	VO	VO
Flexural Strength	20,100 psi	19,250 psi
Flexural Modulus	2,053,000 psi	2,027,000 psi
Thermal:		
Glass Transition Temperature, by Thermomechanical Analysis	154°C	153°C
Coefficient of Thermal Expansion		
Below glass transition	20 um/m°C	22 um/m°C
Above glass transition	62 um/m°C	68 um/m°C

DIELECTRIC CONSTANT   Sample=> 3 inch by 1/16 inch molded disc
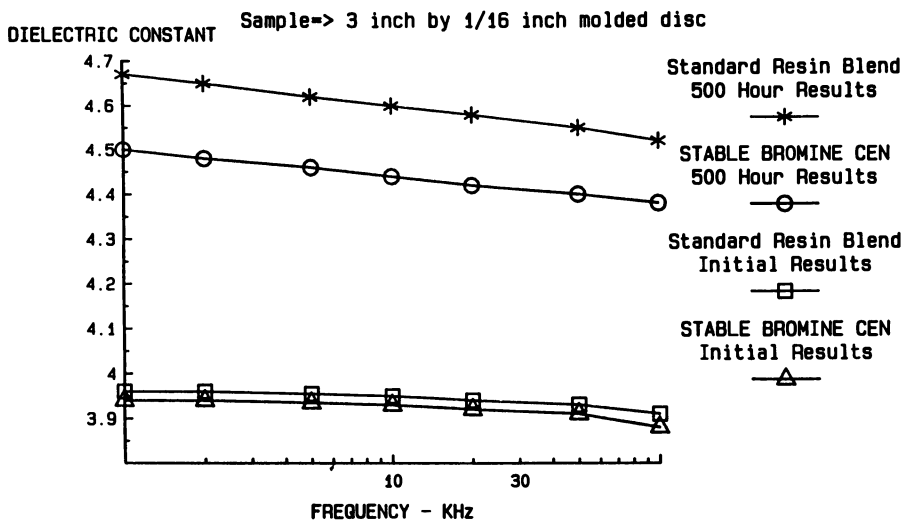
Figure 1.   Dielectric Constant - Molding Compound
Initial and 500 Hours at 1 Atmosphere Steam

DISSIPATION FACTOR   Sample=> 3 inch by 1/16 inch molded disc
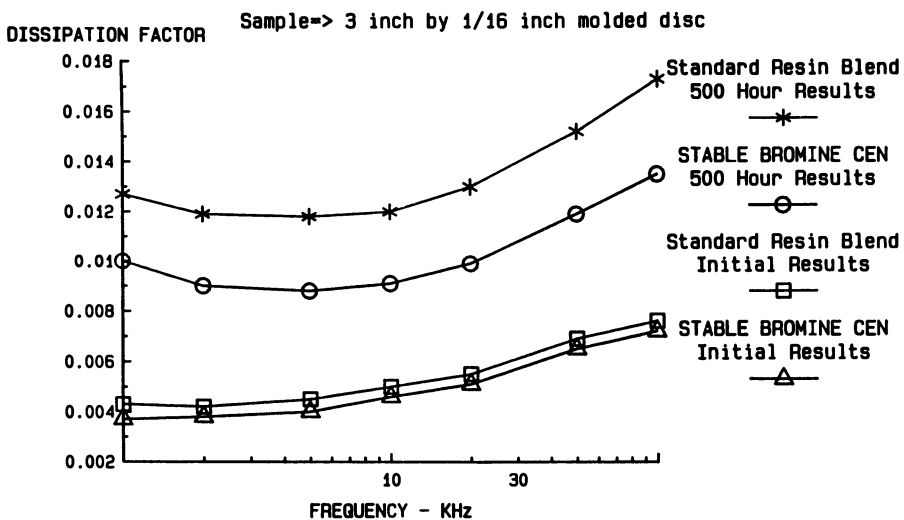
Figure 2.   Dissipation Factor - Molding Compound
Initial and 500 Hours at 1 Atmosphere Steam

indicate that the incorporation of the stable bromine CEN into the molding compound does not adversely affect the bulk electrical properties. Lower dielectric constant and dissipation factor results of the stable bromine CEN compound after 500 hours of exposure are seen because it does absorb less moisture than the standard, but the differences should not be considered significant.

Figure 3 shows a thermogravimetric analysis performed on the two molding compounds. The scans show that the molding compound based on the stable bromine CEN has a 15-20°C increase in thermal degradation temperature over the standard compound. Even though the stable bromine CEN is more thermally stable than standard resins, it still supplies the bromine necessary to achieve the desired flame retardancy properties.

Device Reliability Testing

These molding compounds were also used to encapsulate electronic devices for reliability testing. In Figures 4, 5, and 6, stable bromine CEN outperformed "state-of-the-art" resins in the bias pressure cooker device test (BPC), high temperature storage device test (HTS), and the highly accelerated stress test (HAST). In each test the stable bromine CEN-based molding compound took a significantly longer time to achieve incremental failure rates than the standard high purity resins.

Figure 4 shows the performance of encapsulated devices under the standard bias pressure cooker device test. The conditions of this test are as follows: 100% relative humidity, 15 psig, 250°F, and electrical bias. In this test, the encapsulant based on stable bromine CEN took more than 1000 hours to achieve 50% cumulative failure while the encapsulant based on the standard high purity resins took about 700 hours.

Figure 5 shows the performance of encapsulated devices under the high temperature storage device test. The conditions of this test are as follows: storage in standard convection oven @ 200°C, no induced humidity, and no bias. Test results indicate that the encapsulant based on the stable bromine CEN took greater than 52 weeks to reach 50% failure; that is, 50% of the initial number of devices have failed, in contrast to the standard high purity resin encapsulant which failed at 14 weeks.

Figure 6 shows the performance of encapsulated devices under the highly accelerated stress test which utilizes the following conditions: 145°C, 85% relative humidity, 37 psig, and electrical bias. The bias on this test is cycled; specifically, the bias is initially off to allow for full moisture penetration and then turned on. These cycles are repeated throughout the test. The stable bromine CEN compound took 2500 hours to reach 50% failure rate, compared to the standard resin compound at 1900 hours.

Another advantage of this stable bromine epoxide is that it can be incorporated into a wide variety of epoxy resins. Figure 7 shows a BPC curve where an experimental moisture resistant stable bromine epoxy novolac outperformed stable bromine CEN by a substantial margin.
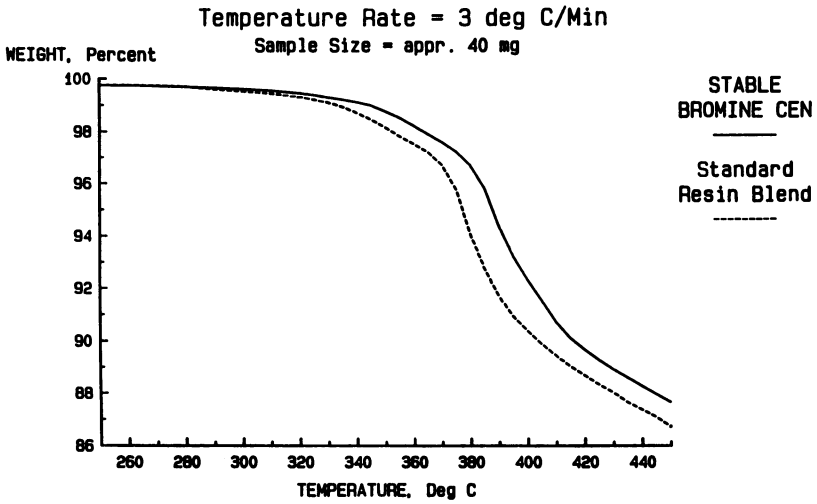
Figure 3.   Thermal Gravimetric Analysis on Molding Compound
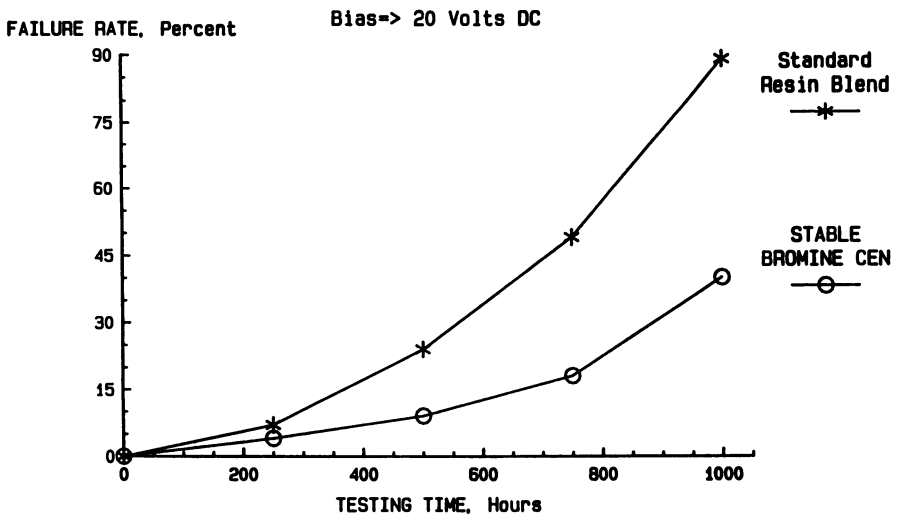
Figure 4.   Bias Pressure Cooker - Device Reliability Test
LM324 Quad Op Amp, 121°C, 100% RH, and Bias

FAILURE RATE, Percent   LM324 Quad Op Amp
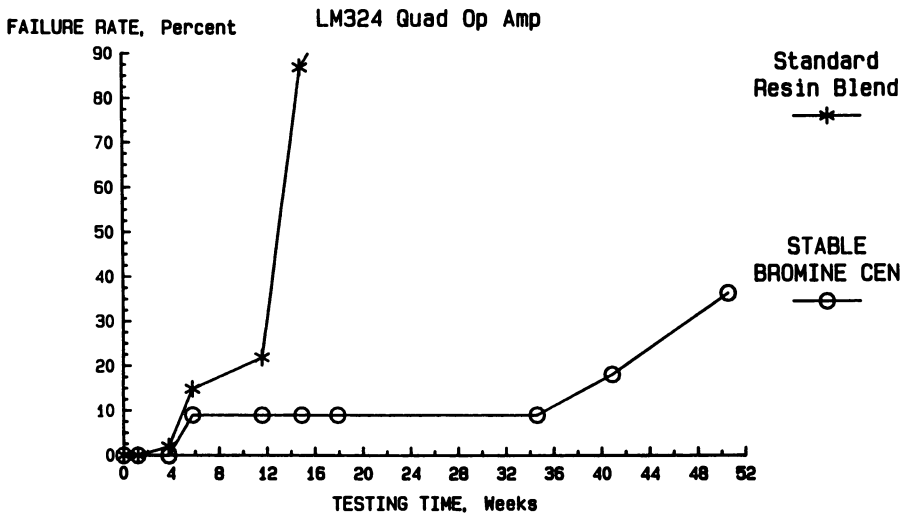
Figure 5. High Temperature Storage Device Test
200°C, No Induced Humidity, and No Bias

FAILURE RATE, Percent
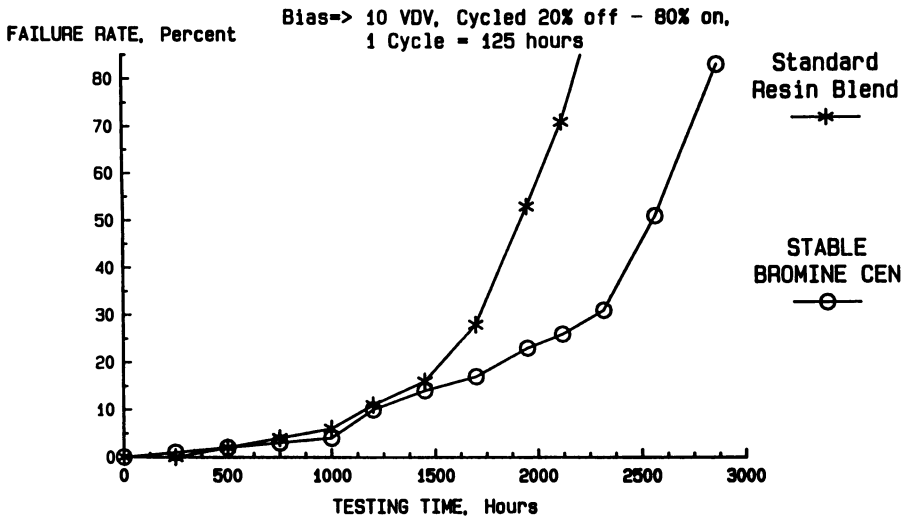
Figure 6. Highly Accelerated Stress Test - Device Test
LF412 Dual Op Amp, 145°C, 85% RH, and Bias

Failure Rate, Percent

Moisture Resistant
Epoxy + QUATREX*6410
—*—

QUATREX*3430/6410
—○—

Stable Bromine CEN
—□—

Stable Bromine Moist
Resistant Epoxy
—△—

Time in Autoclave, Hours
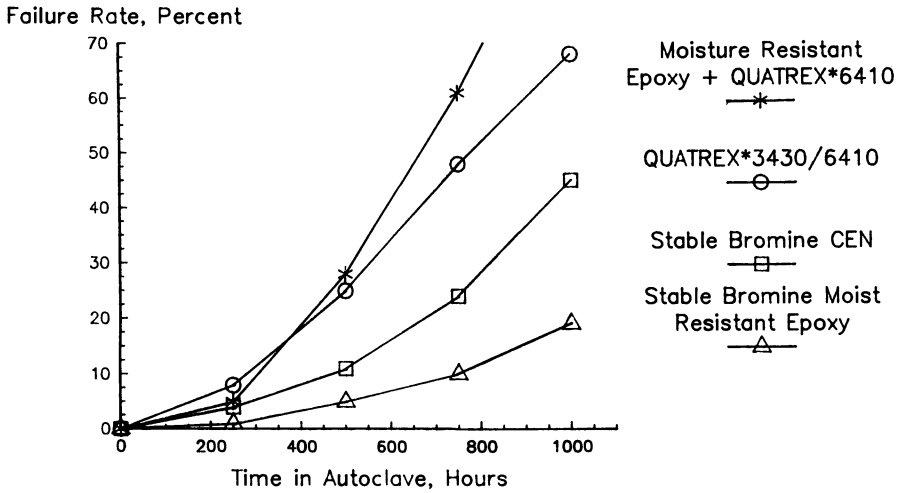
StBr9
*Trademark of The Dow Chemical Company

Figure 7.   Bias Pressure Cooker - Device Test
1 ATM Steam (250°F & 15 psig) + 25 Volts DC
LM 324 Quad Op Amp (Single Passivation)

Conclusion

The electronics industry desires improved flame suppressant additives for microelectronic encapsulants due to bromine induced failure. Epoxy derivatives of novolacs containing meta-bromo phenol have exhibited exceptional hydrolytic and thermal stability in contrast to standard CEN resins with conventional TBBA epoxy resins. When formulated into a microelectronic encapsulant, this stable bromine epoxy novolac contributes to significant enhancements in device reliability over standard resins. The stable bromine CEN encapsulant took about 30% more time to reach 50% failure than the bias pressure cooker device test. In the high temperature storage device test, the stable bromine CEN encapsulant took about 400% more time to reach 50% failure than the standard compound. Finally, the replacement of the standard resins with stable bromine CEN does not adversely affect the desirable reactivity, mechanical, flame retardance or thermal properties of standard molding compounds.

Literature Cited

1. Khan, M.; Fatemi, H. <u>Proc. Int. Symp. Microelec.</u>, 1986, p 420.

2. Ahmad, S.; Blish, R.; Corbett, T.; King, J.; Shirley, G. <u>Comp. Hybr. Manuf. Technol.</u> 1986, <u>9</u>, 379.

3. Khan, M.; Fatemi, H.; Romero, J.; Delenia, E. <u>Proc. IEEE Int. Reliability Physics Symp.</u>, 1988, p 40.

4. Factor, A. <u>J. Polym. Sci: Polym. Chem. Ed.</u> 1973, <u>11</u>, 1691.

Chapter 34

New Polymeric Materials for Electronics Packaging

H. Hacker, K.-R. Hauschildt, J. Huber, H. Laupenmühlen, and D. Wilhelm

Siemens AG, Research and Development Center, D–8520 Erlangen, Federal Republic of Germany

Low pressure moulding compounds for the encapsulation of electronic devices are usually polyepoxide/polyphenol based. We report on the base compounds of an accelerator-free system based on aromatic polyepoxide and a recently developed hardener, containing highly heat resistant structural units of the isocyanurate type. Due to this chemical structure, outstanding properties of the moulded material can be realized, such as glass transition temperatures > 200°C, low coefficient of linear thermal expansion, high impact strength, reduced combustibility without using bromine, long shelf-life at room temperature and rapid curing at elevated temperatures. A survey will be given on the synthesis of the hardener, the influence of the chemical structure on the reaction behavior of low pressure moulding compounds, different preparation methods of moulding compounds, and the thermomechanical performance of the moulded materials.

Semiconductor components for the electronics industry are sensitive to mechanical stresses and corrosive influences.

In the early seventies, the first epoxide resin moulding materials, developed especially for the encapsulation of electronic components, appeared on the market (1). A packaging technology developed parallel to a semiconductor technology, where epoxide resin moulding materials outstripped other substances by far. Packaging technology based on these materials can, on the one hand, meet high demands and, on the other hand, keep costs low.

Worldwide consumption was estimated at approx. 40.000-50.000 tons in 1987. Depending on the development of the electronic market, predictions of the growth rate up to 1991 vary between 3 % and 15 % (2).

Today the epoxide-resin base is almost exclusively epoxidized cresol-novolak, especially when performance at elevated temperatures is important. Hardened by an aromatic amine, the cured material has a heat destortion temperature 50-60°C higher than found for similar cured bisphenol A based systems.

Flame resistant thermosets frequently use brominated bisphenol-A-bisepoxides as co-component. Due to the increasing demands made on electronic components, the purity of resins, especially with regard to the concentration of sodium and chlorine ions (or rather bonded chlorine), is particularly important. The purity question also applies to curing agents.

Criteria for moulding materials are:

Storage stability at ambient temperatures > 6 months
Easy processing and rapid curing
High mechanical strength
High glass transistion temperature
Low coefficient of thermal expansion
Low combustibility
Moisture resistance

Commercially available packaging materials meet almost all these demands, except storage stability and high glass transistion temperatures. At room temperature or slightly elevated temperatures their storage life retention is poor. The storage temperature must be kept below 10°C or the flowability continually decreases. Within a period of a few weeks at storage temperatures between 20°C and 30°C a significant flow variation down to 1/10 of the initial flowability can very often be observed.

The glass transition temperature of the moulded substances must be higher than the expected operating temperatures in the electronic component. This avoids excessive shear stress between electronic component and moulded substances caused by change of the CTE (coefficient of thermal expansion) in the Tg range. The mould-release rigidity is also improved if a high Tg is obtained in the mould.

Most of the commerically available high-performance moulding materials use epoxidized cresol-novolak/novolak (especially phenolic novolak) as a base. Systems with amine curing agents, for instance 4,4'-diaminodiphenyl-sulfone (3) or 4,4'-diaminodiphenylmethane, do provide high-quality moulding substances with a thermo-mechanical performance comparable to our system. They are, however even less stable under storage.

Curing Component

Using suitable basic catalysts like sodium benzoate, al-
kyldiisocyanates (I) can be trimerized to polyisocyanato-
arylisocyanurates with > 95 % of the theoretical yield of
1,3,5-tris (3-isocyanato-4-alkylphenyl)-2,4,6-trioxohexa-
hydrotriazine (II). The corresponding polyamines (III)
are obtained in a single-step process using an excess of
water in the presence of unsoluble, basic magnesium sili-
cate-gel as catalyst and water soluble solvents like di-
oxane or dimethylacetamide at elevated temperatures
(4,5). (See Figure 1.)
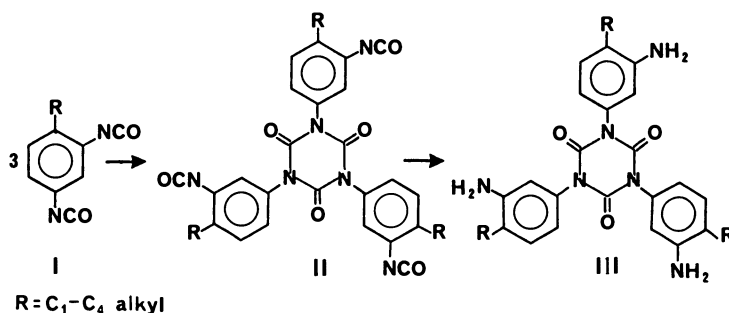
Figure 1. Synthesis of the curing component (schematic).

There are two structural features of this Polyamine
III that are of particular interest:

1.   The aromatic-heterocyclic moiety has a high C:H
      ratio. This improves the combustion resistance (6)
      of systems compounded therefrom, and

2.   The alkyl groups ortho to the NH₂-groups exert a
      shielding effect which effectively slows down the
      - otherwise continued - reaction with epoxide groups
      at room temperature.

Packaging Materials, Production and Properties

Resin. Polyglycidyl compounds with at least two epoxide
groups per molecule, such as polyglycidylether on a base
of novolak, bisphenol A, bisphenol F etc., are generally
suitable as EP-resin components. Our tests were carried
out with epoxidized novolaks (epoxide number between 0.5
and 0.6) and total halogen contents < 0.1 % by weight.

Curing Agent. The curing agent used was a polyaminoaryl-
isocyanurate with approximately 50 % content of 1,3,5-
tris-(3-amino-4-methyl-phenyl)-2,4,6-trioxo-hexahydro-
triazine with an amine content of 6.8 %. The initial
ratio between epoxide function and amino-hydrogen (NH)
was 1:1. Quartz powder (Silbond ᴿ, Quarzwerke Frechen)
served as filler in our experiments.

Production of Moulding Materials. The moulding materials
were prepared by two different methods.

Method A (wet preparation)
By weight, 450 parts of an epoxidized novolak with an
epoxide number of 0.57 were dissolved in 450 parts by
weight of acetone. To this solution were added 300 parts
by weight polyaminoarylisocyanurate (amine content
6.8 %), dissolved in 300 parts by weight of acetone.
    The solution of 50 % resin/curing agent was then
compounded with 1630 parts by weight quartz powder and
mixed intensively. Subsequently, the mixture was dried
for 30 minutes at 60°C/1 mbar. The material obtained pos-
sesses granularity and flowability.

Method B (dry preparation)
By weight, 600 parts of an epoxidized novolak with an
epoxide number of 0.57 and 400 parts by weight poly-
aminoarylisocyanurate (amine content 6.8 %) as well as
2170 parts by weight quartz powder were mixed together in
a roller mill (roll temperature 60°C) for a period of 30
minutes. The material obtained possesses granularity and
flowability.

Test Pieces. The moulding materials produced with methods
A and B (filler content 70 %) were processed to test
pieces according to the normal transfer moulding tech-
nique without processing aids, such as mould lubricants,
coupling agents, etc. The moulding temperature was 175°C,
moulding pressure was 100 bar and moulding period was 5
minutes.

Properties

Spiral Flow (according to test method EMMI 1-66) - For
method A and B materials, 60-80 cm were found.

Storage Stability. The storage stability is longer than
1 year. The moulding materials were stored in polyethy-
lene bags under normal room conditions. After one year
they were processed to test pieces. Neither a difference
in their flowability nor in the thermo-mechanical perfor-
mance of the moulded material was found. This is an ex-
cellent result, regarding the storage stabilities of
other moulding compounds.

Glass Transition Temperature. The glass transition tem-
peratures are based on torsion modulus curves according
to DIN 53445. Table I shows the dependence of the glass
transition temperature on the post-curing of the moulded
substances.
     No difference in Tg was found between test samples
prepared from method A and B materials after opening the
mould. Additional post-curing, i.e. 2 hours at 190°C,
plus 2 hours at 210°C, plus 2 hours at 220°C causes the
Tg rise shown in Table I.

Table I: Influence of the Post-Curing Conditions on the
         Glass Transition Temperatures Tg

Test Sample (60x10x1 mm)	Post-Curing Time (h)	Temp. (°C)	Glass Transition Tg (°C)
Method A or	–	–	210
	2	190	220
Method B	+ 2	210	233
	+ 2	220	240

In contrast to Tg evaluations, a slight decline of the
flexural strength after post-curing of test samples pre-
pared from method B materials was observed. Considering
the permissible variation this is of no significance
(Table II).

Table II: Flexural Strength (DIN 53452) and Impact
          Strength (DIN 53453) in Dependence on Curing
          Conditions

Test Sample (60x6x4 mm)	Flexural Strength (N/mm^{-2})	Impact Strength (Nmm•mm^{-2})
Method A		
post-cureless	169 ± 20	6,0 ± 1,5
post-cured *	162 ± 18	6,1 ± 1.1
Method B		
post-cureless	168 ± 17	5,7 ± 1,4
post-cured *	134 ± 30	6,2 ± 1,0

* up to 220°C

Coefficient of Thermal Expansion. The linear thermal ex-
pansion coefficient was determined by TMA measurement ac-
cording to VDE standard 0304, part 1.
    In the range from room temperature up to tempera-
tures exceeding 200°C a constant value of $23 \cdot 10^{-6} K^{-1}$ was
found.

Combustibility. The moulded material shows self-extin-
guishing properties without using halogenated components
due to the partially heterocyclic structure of the resin
component. The stage of combustibility conforms with UL
94 V-1, using test specimens of 3 mm thickness.

Water Absorption. The water absorption was tested accor-
ding to ISO 62-1980, method 1 (immersion in water of 23°C
for 24 ± 1 hours), using a test specimen of 50 mm in dia-
meter and a thickness of 3 mm. The water uptake was 0,05
%. Comparable novolak hardened systems have slightly
smaller water absorptions in the range of 0,03 to 0,04 %.

Evaluation

The basic system using EP-novolak/polyamino-aryl-
isocyanurate provides an interesting base for electronic
packaging. The system combines a whole range of desirable
properties, such as:

Processing technology

- High storage stability at room temperature because of
  the chemical structure of the curing agent (shielding
  effect of the - CH_3-groups).

- Cost effective preparation of moulding materials, since
  the thermomechanical and mechanical values of the
  moulded materials obtained by "wet preparation" do not
  differ significantly from the values of moulded
  materials obtained by the less costly "dry
  preparation", so that the latter method can be applied.

- Good flowability.

- Good adhesion to metal surfaces.

- Low cost of raw products for the hardener synthesis.

- Easy and clean synthesis in the sense of pollution
  control, i.e. solventless synthesis in the first step
  and reuse of solvents of the second step.

Thermal/mechanical Properties

- Glass transition temperatures > 200°C are attainable in
  the mould. This leads to the advantages mentioned at

the beginning with respect to mould release and shear stress of the electronic component.

- The basic system using normal silanized silica powder as a filler already shows a low linear thermal expansion coefficient ($\alpha_{lin} = 23 \cdot 10^{-6} K^{-1}$), which is constant up to temperatures exceeding 200°C.

- Good mechanical properties, flexural strength > 130 Nmm^{-2}, impact strength > 6 $Nmm \cdot mm^{-2}$.

- Highly reduced combustibility due to the chemical structure of the resin matrix.

<u>Literature Cited</u>

1. Salinsky, G. <u>Insulation/Circuits</u> 1972, <u>5</u>, 19-25.

2. <u>Modern Plastics</u>, 1986, <u>12</u>, 44-47.

3. Heißler, H.; Scheer, W. German Patent 3 210 746, 1986.

4. Hacker, H.; Hauschildt, K.-R.; Huber, J.; Laupenmühlen, H.; Wilhelm, D. European Patent 0 271 772, 1988.

5. Raßhofer, W. European Patent 0099537; US Patent 4 525 534, 1986.

6. V.Krevelen, D. <u>Chem.-Ing. Techn.</u> 1975, <u>47</u>, 739 ff.

Chapter 35

Degradation of Brominated Epoxy Resin and Effects on Integrated-Circuit-Device Wirebonds

M. Nakao, T. Nishioka, M. Shimizu, H. Tabata, and K. Ito

Nitto Denko Corporation, 919 Fuke-cho, Kameyama-shi, Mie, Japan

The gases that are emitted when an encapsulant resin is exposed to a high-temperature were analyzed by GC-MS. The effect of these gases on IC devices were studied using a Teflon vessel. The result showed that large amounts of bromides and organic acids are emitted from the encapsulant resin and that these gases are generated by the accelerated decompositions of the brominated epoxy resin by amine and silicone in the resin. The addition of certain ion trapping agents to the resin was found to solve this problem and to increase the high-temperature durability several fold.

Semiconductor devices are being used in an ever increasing number of applications and under very severe environmental conditions. These applications have brought about the use of new evaluation methods. One such method is the high-temperature stress test, and many reports have been published discussing this topic (1-3). According to these reports, a semiconductor device fails during high temperature exposure when the brominated resin contained in a resin forms intermetallic alloys at the gold-aluminum interface, thereby increasing resistance (2).

However, there are still unanswered questions about the mechanism leading to the generation of intermetallic alloys, and an explanation is yet to be provided for the difference in degradation rates among IC devices containing like amounts of brominated resin.

Objectives

The gases that are generated when an encapsulant resin is exposed to a high temperature were analyzed by GC-MS to disclose the cause for resin degradation and chip failure. This paper describes the cause for chip failure, and also presents a method for controlling the formation of intermetallic alloys.

Experimental and Results

Corrosion of IC Devices by Decomposition Gases of Encapsulant Resin and Formation of Intermetallic Alloys. To study the effects on IC devices of gases that are generated by the thermal decomposition of encapsulant resin, encapsulant resin in powder form and wire-bonded IC devices were placed inside a Teflon vessel (Figure 1). The vessel was left standing for 20 hours in an oven heated to 225°C to observe the change in the IC device. The chip that was used is shown in Figure 2. Aluminum patterns were formed on a silicon substrate. No passivation film was formed. Corrosion of aluminum pads and formation of intermetallic alloys near gold balls were observed, indicating the strong effects of the discharged gases (Figure 3).

Analysis of Thermal Decomposition Gases of Encapsulant Resin. The gases which were collected as shown in Figure 4 were analyzed by GC-MS (using model QP-1000 manufactured by Shimazu Seisakusho). The components are shown in Table I. The Table shows emission of large amounts of bromides and other highly corrosive gases which are know to degrade IC chips.

The accelerated decomposition of brominated epoxy resin by other materials contained in the encapsulant resin was studied by GC-MS from the amount of methylbromide that was emitted from the resin. The Teflon vessel used in the previous experiment was again used to study the corrosion of the device. The results are shown in Table II. The results show that the decomposition of brominated epoxy resin is significantly accelerated by amine and silicone.

Effects of Ion Trapping Agents. The effects of ion trapping agents were studied in experiments that used a Teflon vessel and gas analysis by GC-MS. Table III shows the results. The ion trapping agents that were used in this experiment were bismuth hydroxides.

Actual encapsulant resins were exposed to high temperature tests to measure the generation of intermetallic alloys and the degradation of the device. The results are shown in Table IV. The generation of intermetallic alloys was measured by the cross section of the gold balls (Figure 5). The lifetime was determined from the time when an open failure in resistance was observed with the device. The results showed that the resin properties are greatly improved by the addition of ion trapping agents.

Discussion

Degradation of the Brominated Resin. From past studies, it is believed that the generation of intermetallic alloys is triggered by methylbromide (or hydrogen bromide) (1-3). The generation of these substances from brominated epoxy resin is discussed below.

The thermal decomposition of the brominated epoxy resin depicted in Figure 6 occurs in the following manner (Figure 7).

Because the reaction is a radical reaction, significant amounts of energy are required. However, if a nucleophilic reagent such as amine is present in this system, bromide ion easily separates and forms bromide complexes as shown in Figure 8.

Furthermore, silicone undergoes an oxidation decomposition at high temperature, and generates formic acid and formaldehyde (Figure 9). Formic acid
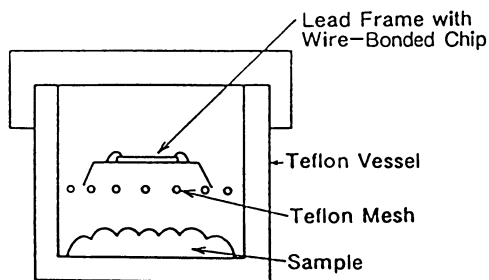
Figure 1. Experimental setup.

CHIP SIZE 2×3.5MM
AL PATTERN DISTANCE
(A)10μm
(B)20μm
(C)50μm
AL PATTERN WIDTH
    30μm
AL PATTERN THICKNESS
    1.2μm
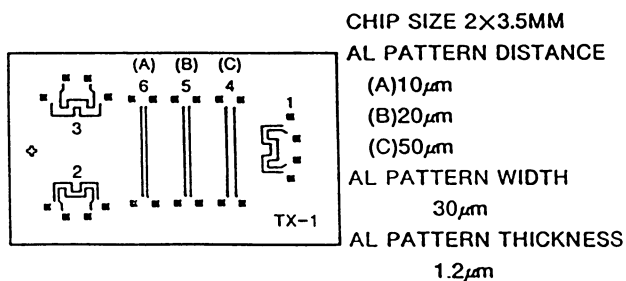
Figure 2. Test chip specimen.
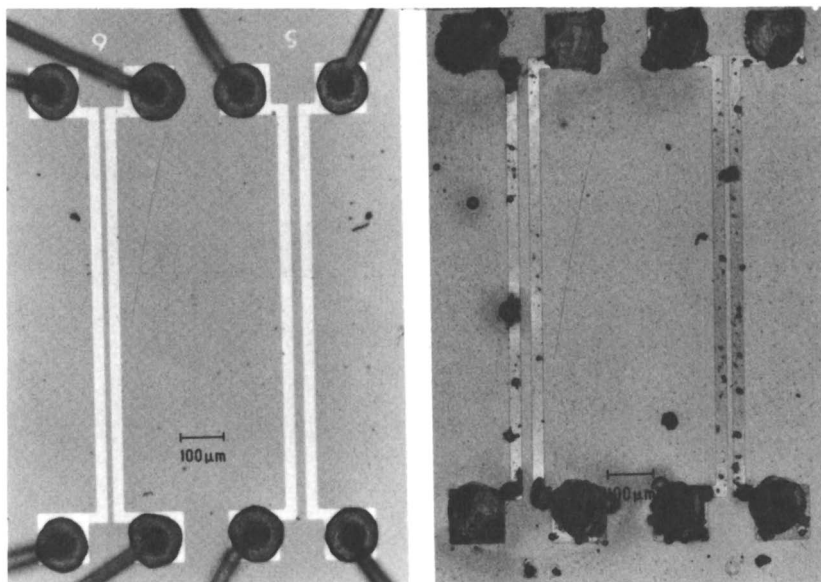
(without Encapsulant Resin)   (with Encapsulant Resin)

Figure 3. Chip surface after high-temperature exposure test.
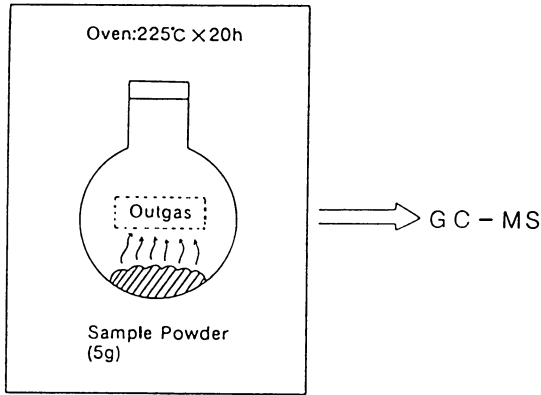
Figure 4. Analysis of outgas from specimen with GC–MS.

Table. I   Components of Outgas
from Molding Compound(dy GC–MS)

Component	Strength
Cardon Dioxide	W
1–Propene & other Hydrocarbons	W
Methyl Chloride & other Cl–Complexes	W
Methyl Bromide & other Br–Complexes	S
Acetaldehyde & other Aldehydes	S
Formic Acid & other Organic Acids	W
Methanol & other Alcohols	M
Methyl Formate & other Esters	M

S:Strong   M:Medium   W:Weak

Table. II   Effects of Ingredients in Molding Compounds
on Degradation of Br−Epoxy

RESULT ⟍ SAMPLE	Outgassed CH₃Br (ppm)	Effect of Gas Al−pad	Au−Ball
Br−Resin	120	M	M
Br−Resin+ Epoxy−Resin	100	M	M
Br−Resin+ Phenolic−Resin	110	M	M
Br−Resin+Silicone	1200	S	S
Br−Resin+Amine	1800	S	S
Br−Resin+Filler	50	W	W
Br−Resin+Sb₂O₃	30	W	W

S:Strong   M:Medium   W:Weak

Table. III   Effects of Ion Trapping Agent
on the Degradation of Br−Epoxy Resin

RESULT ⟍ SAMPLE	Outgassed CH₃Br (ppm)	Effect of Outgas Al−Pad	Au−Ball
Br−Resin	120	M	M
Br−Resin+Silicone	1200	S	S
Br−Resin+Amine	1800	S	S
Br−Resin+Silicone +X	30	No	No
Br−Resin+Amine +X	20	No	No

S:Strong   M:Medium   W:Weak   X:Ion Trapping Agent

Table. IV Effects of Ion Trapping Agents
on Wire−Bond Degradation

RESULT ⟍ SAMPLE	Intermetallics Layer Ratio (b/a) (%) 50h	100h	10%−Fail Time (h) 225°C	200°C
Compound A	40	75	95	960
Compound B	70	100	70	340
Compound C	0	0	310	>2000
Compound D	5	10	220	>2000

Compound A:Silicone-less Resin
Compound B:Silicone-Modified Resin
Compound C:Comp.A+X
Compound D:Comp.B+X
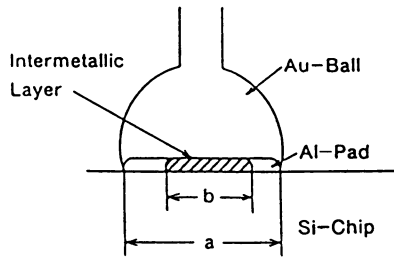
Figure 5. Intermetallic layer ratio in the bonding pad area.

Figure 6. Br–epoxy resin.

$$RH \quad +Br\cdot \longrightarrow R\cdot \quad +HBr$$
$$R\cdot \quad +O_2 \longrightarrow ROO\cdot$$
$$ROO\cdot +RH \longrightarrow ROOH+R\cdot$$
$$ROOH \longrightarrow RO\cdot \ + \cdot OH$$
$$R'Br \ +R\cdot \longrightarrow R'\text{-}R \ +Br\cdot$$
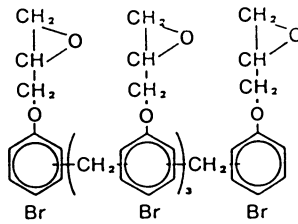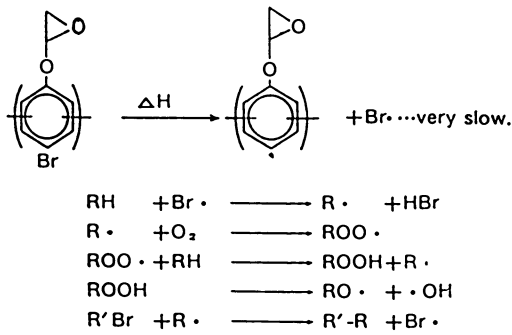
Figure 7. Br–epoxy degradation process.

...very fast.
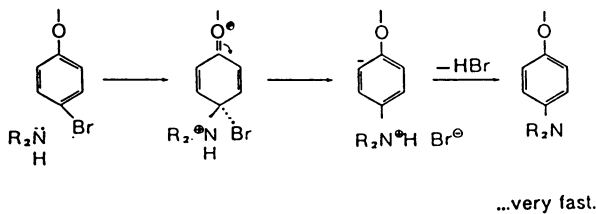
Figure 8. Reaction acceleration mechanism of amine (nucleophilic reaction of amine).

that is generated in the reaction is a strong nucleophilic reagent, and accelerates the degradation of brominated epoxy resin and generation of methylbromide as shown in Figure 8.

Intermetallic Alloy Formation Reaction. Intermetallic alloys such as Au_2Al or $AuAl_2$ are formed at the gold aluminum interface as early as when gold balls are wirebonded to aluminum pads. However, this is not a problem at room temperature, because the rate of formation of the intermetallic alloys is very low at room temperature (4-6).   But if bromide ions (Br⁻) are present in this system, many different intermetallic alloys are formed very quickly following the reaction shown in Figure 10.   The generation of intermetallic alloys increases the interatomic distance (Au,Al :   4.0 Angstroms; Au-Al complex :   6.0 Angstroms) (5). This increases the volume of the intermetallic alloys. The shear force generated by the expansion is transmitted to the gold ball/aluminum pad interface, generating the voids.   Because aluminum bromide, which is formed by this reaction, has a low melting point, and the boiling point is near the storage temperature (Table V), the aluminum bromide volatilizes and diffuses immediately as it is generated.   The above described reactions occur simultaneously, resulting in void growth.

Effect of Ion Trapping Agents. Ion trapping agents react with hydrogen bromide (Figure 11) and fix the bromide ion.   Because the bismuth bromide that is formed in the above reaction has a higher melting point and a higher boiling point than the storage temperature, bromide ions cannot separate from the complex.   This reduces the formation of intermetallic alloys and extends the device's life.

$$CH_3-Si-CH_3 \ +O_2 \longrightarrow HCHO + HO-Si-CH_3$$

$$HCHO \xrightarrow{\ O_2\ } HCOOH$$
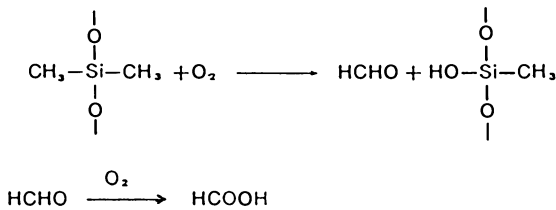
Figure 9. Silicone oxidation mechanism.

$$AuAl_2 \ + 6Br^- \rightarrow Au+Al_2Br_6+6e^-$$
$$2Al \quad + Au \quad \rightarrow AuAl_2$$
$$AuAl_2 \ + Au \quad \rightarrow 2AuAl$$
$$AuAl \quad + Au \quad \rightarrow Au_2Al$$
$$2Au_2Al + Au \quad \rightarrow Au_5Al_2$$
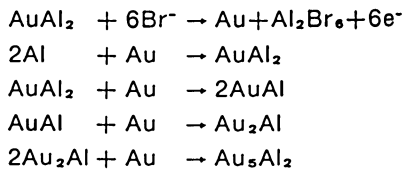
Figure 10. Au/Al intermetallic alloy formation reaction.

Table. V   Melting Point and Boiling Point
of Metal Bromide

Metal Bromide	m.p.	b.p.
$AlBr_3$	97.5°C	225°C
$BiBr_3$	218°C	453°C

$$Bi(OH)_3 + HBr \rightarrow Bi(OH)_2Br + H_2O$$

$$\vdots$$

$$Bi(OH)Br_2 + HBr \rightarrow BiBr_3 + H_2O$$
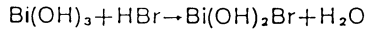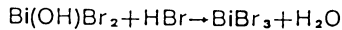
Figure 11. Ion trapping reaction.

Conclusion

The study of high temperature exposure of encapsulant resin has disclosed the following points:

1. GC-MS analysis of the gases emitted during high temperature exposure of the encapsulant resin disclosed the emission of many bromides and organic acids.

2. These gases are formed by the degradation of the brominated epoxy resin.

3. Amine and silicone contained in the encapsulant resin accelerated the degradation of brominated epoxy resin.

4. Bromide ions that separate from bromide compounds accelerate the degradation at the gold aluminum junction.

5. The addition of certain inorganic ion trapping agents to the encapsulant resin improves the high temperature exposure durability of encapsulant resin.

Literature Cited

1. Gale, R. J. IEEE Int. Reliab. Phys. Symp. 1984, p 37.
2. Blish II, R.C.; Parobek, L. IEEE Int. Reliab. Phys. Symp. 1983, p 142.
3. Khan, M.M.; Fatemi, H. Proc. Int. Symp. Microelec. , 1986, p 420.
4. Philofsky, E. Solid-State Electronics ; 1970, 13 , 1391.
5. Tomioka, H.; Kitamura, H.; Ueda, S. J. Metal Fin. Soc. Jpn. 1987, 38 , 199.
6. Plunkett, P. V.; Salporto, D. F. IEEE Proc. 32nd. Elec. Comp. Conf. 1982, p 421.

Chapter 36

Enhancement of Gold–Aluminum Wirebond Reliability in Plastic Encapsulated Very Large Scale Integration (VLSI) Devices Through C–Br Bond Stabilization

Muhib M. Khan, Homi Fatemi, Jeremias Romero, and Eugene Delenia

Materials Technology Development, Advanced Micro Devices, 901 Thompson Place, Sunnyvale, CA 94088

Cresolic epoxy novolac resins brominated by specially tailored brominating agents to impart a high C-Br bond energy remarkably enhanced thermal stability of the encapsulants and gold-aluminum wirebond reliability. At 190- to 250°C, decomposition times of these encapsulants were three to four times longer than a state-of-the-art commercial material. Halogenated organic residues among some of the experimental materials caused increased gold-aluminum wirebond failure through degradation of the intermetallic. These residues were by-products of resin synthesis, which were eliminated by modification of the chemistry and processing. After such modification, the halogen induced failure time was found to be prolonged by as much as eighty percent compared to a commercial resin. The apparent activation energy of wirebond failure was 18 kcal/mole, which was found to equal that of diffusion of organic halide through the polymer matrix in an aqueous environment.

In light of an increasing demand for plastic encapsulated high power dissipating VLSI devices for use under severe environmental conditions, development of newer encapsulation materials with superior thermal stability has become a major goal for the plastic packaging technology. While significant progress is underway toward that end, the issue of gold-aluminum wirebond corrosion due to the presence of brominated additives should be emphasized. The mechanism of wirebond degradation at high temperature through accelerated void formation in the gold-aluminum intermetallic phases in the presence of bromine containing additives and other halogenated impurities has been fairly well established (1-4). In a detailed account of this mechanism, the activation energy of wirebond failure was correlated with that of bromide ion release by aqueous extraction of the cured molding compound (1). While the link between halide ion release and wirebond failure has been recognized, the mode(s) of ion release that is detrimental to the wirebond still requires further investigation.

For an epoxy encapsulating material, the thermal stability of the brominated resin is crucial for wirebond pad metallization and wirebond reliability. In an earlier work, (1) it was found that even in the total absence of free ionic bromide, brominated organic compounds could release bromine by thermal activation, causing accelerated wirebond failure. If that were true, then the use of a thermally stable organic bromide as a fire retardant in the epoxy molding compound would reduce, if not eliminate, the bromine induced corrosion problem. The key to stabilization of the organic bromide is an increased C-Br bond energy in the brominated epoxy resin.

This was achieved through a proprietary process developed by a US resin manufacturer. The process involved bromination of cresolic epoxy novolac (CEN) with a brominating agent specially tailored to render a high bond energy to the C-Br bond. Commercial epoxy resins, on the other hand, are made flame retardant by providing brominated epoxy resin as an additive to CEN. A set of four resins were synthesized through variations of process conditions, chemistry, and brominating agents. These resins as well as molding compounds formulated therefrom were used in this study.

The purpose of this work was to study the role of the organic bromide in causing failure at the Au-Al bimetallic junction, and to establish any possible relationship between thermal stability of the brominated resin and wirebond failure. Special emphasis was placed on the identification of any contaminants other than inorganic ionic species that might be responsible for accelerated failure.

EXPERIMENTAL

MATERIALS

Resins. A standard commercial resin called resin Q was used as the control for comparison with the experimental resins: X_0, X_1, X_2, and X_3. Resin Q was a cresolic epoxy novolac (CEN) with a brominated epoxy additive based on tetrabromobisphenol-A (TBBPA) and its diglycidyl ether. All of the experimental resins were also CEN, but brominated with proprietary brominating agents designed to enhance thermal stability. This was made possible by tailoring the brominating agents to impart a high activation energy of C-Br bond scission to the experimental resins.

In synthesizing the experimental resins, the process as well as the brominating agent was varied. Resin X_0 was prepared by a standard process using a proprietary brominating agent. For resin X_1, a modified chemistry of synthesis and a different brominating agent were used. Resins X_2 and X_3 were made with the same brominating agent as resin X_0, but with two different modifications of the standard process.

Molding Compounds. A host of commercial as well as experimental molding compounds were included in this study. The commercial molding compound HC used as the control was a state-of-the-art, low stress, CEN based material. The experimental compounds, HC-M_0, HC-M_1, HC-M_2, and HC-M_3, were variations of compound HC. Experimental resins X_0, X_1, X_2, and X_3 respectively were used to formulate HC-M_0, HC-M_1, HC-M_2, and HC-M_3. The bromine content of resins and molding compounds were respectively 7.0- and 1.3 percent by weight. Epoxide equivalent weight of the resins was approximately 210.

Test Device. The test vehicle for the wirebond failure study was a 200 × 200 mil^2 silicon die uniformly metallized with Al-1%Si-.5%Cu and assembled in an open ceramic flatpack package. Dice were rinsed with Freon-TF and thoroughly washed in deionized water to remove all traces of ionic and organic contaminants, as verified by Auger spectroscopic analysis. The level of detection by Auger is about 1 mole percent within first 20 Å of the surface. Sixteen wirebonds per package were made thermosonically and coated with an approximately 20 μ layer of the resin. The resin was dispensed as two-percent solution in THF (tetrahydrofuran) using a 10 μL syringe.

EXPERIMENTAL METHODS

Thermal Stability Measurements. Cured molding compound samples were given isothermal bake at various temperatures ranging from 190- to 310°C in a thermogravimetric analyzer (TGA) to determine their thermal stability. All measurements were carried out using 20 mg portions of ground samples in 50 ml/min flowing air. Times to two- and five-percent weight loss were determined from the respective isothermal TGA curves.

High Temperature Ion Extraction. Halide and alkali metal ions were extracted from 0.75 g of 100- to 200-mesh ground samples of resins with 15 ml volumes of deionized water in Teflon-lined Parr bombs. Extractions were carried out for 16 h at various temperatures ranging from 120- to 250°C. Ions were quantitatively determined by analyzing the aqueous extracts with a Dionex 2020i ion chromatograph. Concentrations thus determined in the water extracts were normalized with respect to the weight of the solid samples and expressed as parts per million (PPM).

Wirebond Degradation Studies. The coated specimens were baked at temperatures of 175-, 190-, 200-, 225-, and 250°C, and were periodically examined for resistance increase across the gold-aluminum junction. The resistance measurements on individual wirebonds were carried out with a Kelvin probe with the device placed on a hot stage set to the respective experimental temperature. The input measuring current was 15 μA. Packages with uncoated specimens were included as controls. Two test devices containing a total of 32 wirebonds were used per experiment. The time to fifty-percent failure of the 32 wirebonds was determined by a lognormal plot of the cumulative percent failure versus the failure time.

Molecular Weight Distribution Analysis. Two-percent solutions of resins in THF were prepared for the molecular weight distribution analysis. Analysis was done by size exclusion chromatography (SEC) with a *Hewlett-Packard 1090* high performance liquid chromatograph (HPLC). The bank of SEC columns consisted of one 1000 Å, two 500 Å, and one 100 Å pore diameter polystyrene-divinyl benzene (PLGEL) connected in series and equilibrated at 45°C. The eluent was THF at a flow rate of one ml/min. Samples were detected with a differential refractive index (DRI) detector. The hydrodynamic volume, which is a product of viscosity and molecular weight, was determined from the SEC retention times based on a calibration using polystyrene standards under identical experimental conditions. The resulting SEC chromatogram provided a measure of the molecular weight distribution of the polymer sample and of the polystyrene equivalent molecular weight of its components.

RESULTS

THERMAL STABILITY

High-Temperature Storage. Cured mold materials formulated with the experimental brominated CEN resins were found to have remarkably superior thermal stability to that of the commercial mold materials. By isothermal bake at various temperatures ranging from 190- to 310°C, times to two- and five percent weight loss of the experimental materials were found to be significantly longer than those of the commercial materials. The data are summarized in Table I. At 240°C or below, HC-M_1 was found to be approximately two to three times more thermally stable than HC-M_0, which was in turn about forty- to ninety-percent more stable than the standard material HC. At higher temperatures, however, no difference in stability among these materials could be observed. It is clear from these data that bromination of the CEN resin with the stable brominating agent indeed enhanced the thermal stability of the molding compound.

Table I. Weight Loss Times of Cured Molding Compounds
Under High-Temperature Storage

Molding Compound	Temperature,°C					
	190	210	225	243	270	310
2% Weight Loss Time, Hour						
HC	27.0	6.7	2.67	0.77	0.08	0.01
HC-M_0	37.0	12.5	5.42	1.42	0.50	0.04
HC-M_1	*	32.5	14.8	2.83	0.29	0.06
HC-M_2	*	*	*	1.30	0.30	0.05
HC-M_3	*	*	*	2.78	0.33	0.04
5% Weight Loss Time, Hour						
HC	–	–	16.0	5.73	0.92	0.14
HC-M_0	–	–	25.0	8.08	3.20	0.42
HC-M_1	–	–	61.7	13.3	2.93	0.67
HC-M_2	–	–	*	5.3	2.90	0.52
HC-M_3	–	–	*	18.2	2.65	0.63

* Data are not available.
 Source: Reproduced with permission from ref. 7. Copyright 1988 IEEE.

AQUEOUS ION EXTRACTION

Aqueous extractions of bromide and chloride ions were done at various temperatures ranging from 120- to 250°C. This was done to verify the thermal stability of brominated resins in aqueous medium at elevated temperatures. The total level of alkali metal ions and NH_4^+ combined was nearly an order of magnitude lower than either bromide or chloride; this indicated that the halides were mostly derived from organic sources. Arrhenius plots of bromide

and chloride ion extraction data are shown in Figures 1 and 2 respectively. While chloride levels at various temperatures were comparable, there were some distinctive features of bromide extraction data, as discussed below.

Bromide. Experimental resins X_0 and X_1 had two orders of magnitude lower level of bromide released at 250°C than the standard resin Q. This is shown in the Arrhenius plots of bromide extraction amounts presented in Figure 1. As will be discussed later, this steep rise in bromide was due to thermal cracking of brominated additives in resin Q; resins X_0 and X_1 being thermally more stable did not exhibit such trends. Between 160- and 225°C, there was no difference in the levels of extracted bromide. The bromide level reached a plateau around 300- to 500 PPM within this range after a monotonic linear increase between 120- and 160°C.

The linear portion of the Arrhenius curves in Figure 1 showed some significant differences among the resins. Within the temperature range of 120- to 160°C, resin X_0 released about an order of magnitude more bromide ion than resin Q. At 150°C, 53 PPM bromide was extracted from resin X_0; this could be compared with three PPM from Q and nine-, four-, and five PPM from resins X_1, X_2, and X_3 respectively. The Arrhenius plots of bromide concentrations extracted from experimental resins X_2 and X_3 showed trends almost identical to X_1. The activation energy determined from the slope in the lower portion was 69 kcal/mole for resin Q. As will be discussed later, this represented the activation energy for hydrolysis of low molecular weight brominated organic species.

Chloride. Aqueous chloride ion extraction data over the temperature range of 120°C to 250°C are presented in Figure 2. The amount of extracted chloride was less than 15 PPM at temperatures below 150°C. It increased to about 600- to 700 PPM around 200°C and leveled off. Unlike the data for bromide, Arrhenius plots of chloride concentration data were linear at all temperatures below 175°C for all of the resins. Besides, there was no enhancement of chloride release at temperatures above 225°C caused by thermal cracking of resin Q. The activation energy calculated from linear segments of the curves was about 46 kcal/mole. According to the kinetic model proposed later, this activation energy data could be ascribed to hydrolysis of organic chlorides present as impurities in the resin.

MOLECULAR WEIGHT DISTRIBUTION

Residual By-Products. Resins X_1, X_2, and X_3 were found to contain significantly lower levels of low-molecular-weight residues than resins X_0 and Q. This was determined by molecular weight distribution analysis. As shown in Figure 3, the SEC peak at molecular weight of 190 was much stronger in resin X_0 than in the other three: X_1, X_2, and X_3. In an SEC study of epoxy novolac polymers, such a low molecular weight peak was assigned to a phenol- or cresol-like residue (5). Considering the molecular weight for this peak, a bromophenol- or bromocresol-like residue or an epoxy derivative would be a likely assignment in this case.

WIREBOND RELIABILITY

Effects of Brominated Resins. Wirebonds under high-temperature bake endured a remarkably longer life when coated with the experimental resins as compared to the standard. Uncoated wirebonds, of course, still had longer
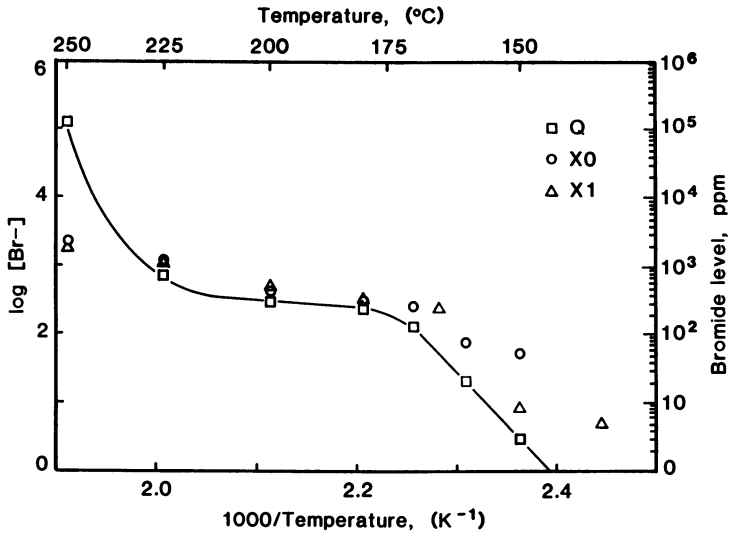
Figure 1. Arrhenius plots of bromide levels determined by aqueous extraction of standard resin Q and experimental resins X_0 and X_1. (Reproduced with permission from ref. 7. Copyright 1988 IEEE.)
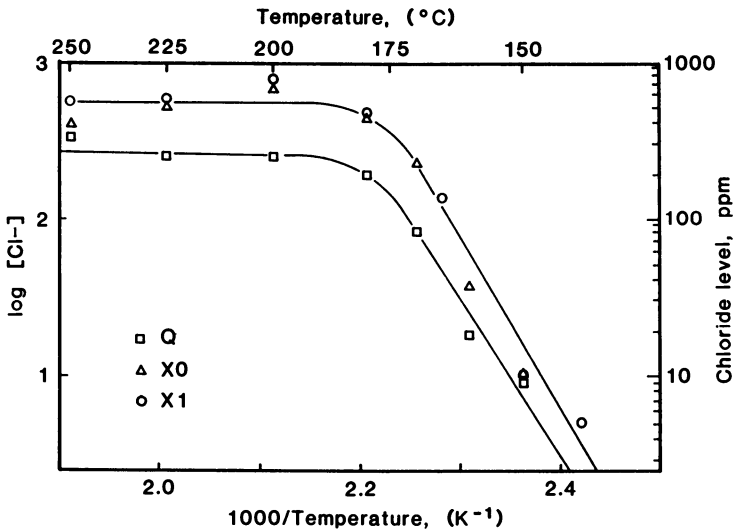
Figure 2. Arrhenius plots of chloride levels determined by aqueous extraction of standard resin Q and experimental resins X_0 and X_1. (Reproduced with permission from ref. 7. Copyright 1988 IEEE.)
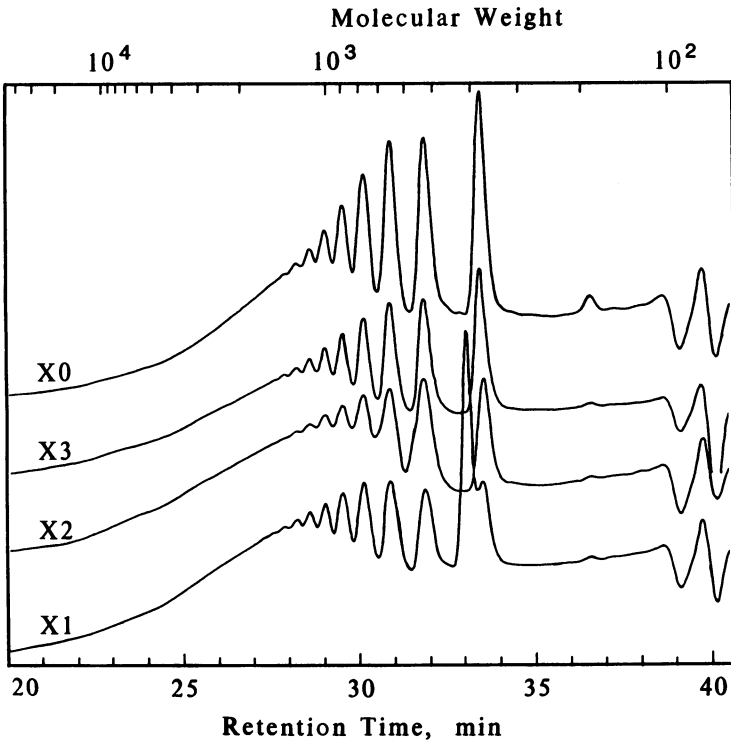
Figure 3. Molecular weight distribution of experimental resins X_0, X_1, X_2, and X_3 determined by SEC analysis. (Reproduced with permission from ref. 7. Copyright 1988 IEEE.)

time to failure than either group. The cumulative failure of wirebonds coated with various resins and aged at 175°C is shown as lognormal plots in Figure 4. Similar data were also obtained at 200- and 225°C. At all of these temperatures, wirebonds coated with resins X_1, X_2, and X_3 had longer failure times than wirebonds coated with resins X_0 and Q. Resin X_1 had the least detrimental effect on the wirebond life. The effects of resins X_2 and X_3 were between those of resins X_1 and Q. The poor performance of resin X_0 compared to control resin Q was an anomalous deviation from the effects shown by the other experimental resins. Differences in their effects on the wirebond life were traced to the chemistry and process of their synthesis, as will be discussed later.

A more quantitative comparison of the effects of resins on wirebond failure can be obtained from the time to fifty percent failure data tabulated in Table II. At 200°C, while uncoated wirebonds remained intact even after 700 h, coated wirebonds had times to fifty-percent failure (t_{50}) of 125 h or less. Among the coated wirebonds, those coated with resin X_1 had the longest time to failure, and with resin X_0 the shortest. By comparison, resin Q was slightly better than resin X_0, and resins X_2 and X_3 were between resins Q and X_1. These data definitely suggest that the chemistry of resin synthesis had a significant effect on the wirebond reliability. The unique features of resin X_1 that make for such an improvement deserve extensive exploration, and will be investigated further. Such studies could provide valuable insights into the molecular processes that lead to degradation of the gold-aluminum intermetallic.

Table II. Time in Hours to Fifty-Percent Failure
of Wirebonds Coated with Various Resins

Coating Resin	Temperature,°C				
	175	190	200	225	250
None	a	a	>700[b]	a	100[c]
Q	292	146	94	39	19
X_0	242	139	92	39	19
X_1	901	a	125	72	a
X_2	582	a	115	43	a
X_3	489	a	112	44	a

Notes:
(a) Data are not available.
(b) All of the wirebonds remained intact.
(c) All of the wirebonds failed at this point.
Source: Reproduced with permission from ref. 7. Copyright 1988 IEEE.

The activation energies of wirebond failure due to high temperature storage of wirebonds coated with resins were determined from the Arrhenius plots based on times to fifty-percent failure. Arrhenius plots are shown in Figure 5. Wirebonds coated with resins X_1, X_2, and X_3 failed with a slightly higher activation energy (21 to 23 kcal/mole) than with resins x_0 and Q (16 kcal/mole). It was interesting to note that while for wirebonds coated with resins X_0, X_2, X_3 and Q the Arrhenius plots were linear over
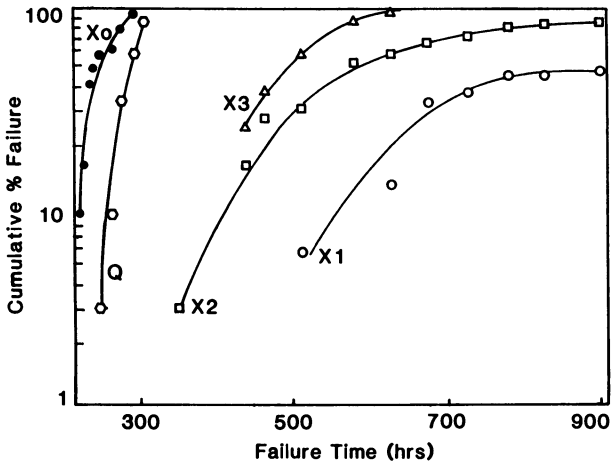
Figure 4. Lognormal plots of cumulative percent failure versus period of aging at 175°C of gold-aluminum wirebonds coated with standard resin Q and experimental resins X_0, X_1, X_2, and X_3. (Reproduced with permission from ref. 7. Copyright 1988 IEEE.)
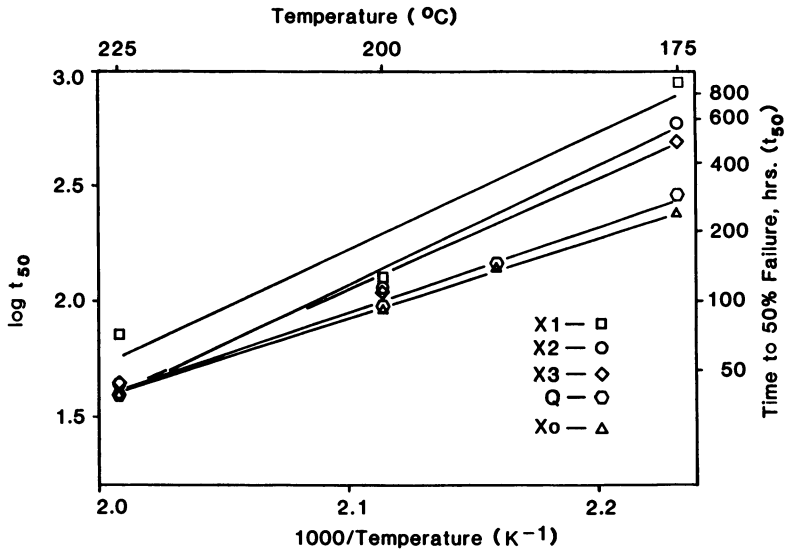
Figure 5. Arrhenius plots of times to fifty-percent failure of high temperature aged wirebonds coated with standard resin Q and experimental resins X_0, X_1, X_2, and X_3 . (Reproduced with permission from ref. 7. Copyright 1988 IEEE.)

the entire temperature range of 175-to 225°C, there appeared to be a change in slope around 200°C in the case of resin X_1-coated wirebonds. More data will be required to confirm this observation.

DISCUSSION

Results thus far have shown that properties such as thermal stability and aqueous ion extraction characteristics of various resins and their molding compounds are not direct indications of any predictable effects on high temperature storage life of the wirebond. The most intriguing features of the findings are: (a) comparable levels of water-extractable halides in resins and yet a remarkable difference in their effects on resistive wirebond failure, and (b) higher wirebond failure with experimental resin X_0 in spite of its superior thermal stability. In order to find answers to these observations one must try to understand the thermal stability and aqueous ion extraction data from a perspective of molecular processes.

AQUEOUS ION EXTRACTION RESULTS

A Kinetic Model. The shapes of the Arrhenius curves in Figure 1 are indicative of the mechanism of aqueous ion extraction. A closer examination of the shapes entails a detailed mathematical analysis of the kinetics of the elementary steps comprising the aqueous bromide extraction process. A rate equation will be derived here in order to interpret the experimental data in terms of a simplified kinetic model. The case study specifically involves bromide extraction from the resins because of the particularly complex shapes of the Arrhenius curves in Figure 1, but it is applicable to all aqueous ion extraction processes with suitable modifications.

The elementary processes are as follows:

$$\text{Resin} \xrightarrow{k_c} \text{RBr (bulk)} \qquad \text{Thermal cracking} \qquad (1)$$

$$\text{RBr (bulk)} \xrightarrow{K} \text{RBr(aq)} \qquad \text{Partition equilibrium} \qquad (2)$$

$$\text{RBr (aq)} + H_2O \xrightarrow{k_h} \text{ROH} + Br^- \qquad \text{Hydrolysis} \qquad (3)$$

In the above process steps, RBr represents a low molecular weight brominated organic residue in the bulk of the resin that may either be *initially present* or be produced from thermal cracking represented by Step 1. This process, however, is not expected to kinetically control the overall mechanism at temperatures lower than 200°C. The term k_c is the rate constant of thermal cracking. The residual RBr is diffused to the aqueous phase and a diffusion equilibrium is established. The equilibrium amount of RBr dissolved in the aqueous phase is controlled by the diffusion equilibrium process represented by Step 2. The partition coefficient K is the ratio of forward and reverse diffusion coefficients, k_d and k_{-d} respectively, which are determined by the molecular size of RBr and its solubility in water. The dissolved RBr is then hydrolyzed in the aqueous phase as shown in Step 3; k_h is the rate constant for this step.

According to the preceding kinetic model, the rate of ion release at the *initial stage* of extraction is equal to the rate of hydrolysis, R_h, which may be expressed as:

$$R_h = \frac{d[Br^-]}{dt} = k_h[RBr]_a = [RBr]_a A_h exp(-E_h/RT) \tag{4}$$

where, A_h and E_h are respectively the Arrhenius pre-exponential term and the activation energy of hydrolysis of RBr. $[RBr]_a$ is the concentration of RBr dissolved in the aqueous phase. The kinetics of hydrolysis has been assumed to be of first order with respect to aqueous RBr. Assuming the amount of RBr in the bulk ($[RBr]_b$) to be at a steady state at a very slow cracking rate at the lower temperature range, a quantitative expression for $[RBr]_a$ may be worked out in the following manner: The net rate of growth of RBr in bulk is given by the balance of formation through cracking and consumption through a net diffusion into the aqueous phase. The change in the level of $[RBr]_b$ is therefore expressed by Equation 5 below.

$$\frac{d[RBr]_b}{dt} = R_c - k_d[RBr]_b + k_{-d}[RBr]_a \tag{5}$$

where, R_c is the rate of cracking of polymer. However, at low temperatures where R_c is negligibly small, the steady-state approximation for RBr in the bulk can be invoked whereby R_c as well as $d[RBr]_b/dt$ may be set to zero. Equation 5 may then be rearranged to obtain an expression for $[RBr]_a$.

$$[RBr]_a = \frac{k_d}{k_{-d}} [RBr]_b = K[RBr]_b \tag{6}$$

by substituting for $[RBr]_a$ from Equation 6 into Equation 4, one may obtain the following expression for the rate of hydrolysis:

$$R_h = K[RBr]_b A_h exp(-E_h/RT) \tag{7}$$

Taking the logarithm of bromide concentration in the water extracts (normalized to the weight of resin) for the Arrhenius plots in Figure 1 was based on the following assumption: the level of Br^- ions accumulated over the period of extraction was proportional to the rate of RBr hydrolysis. This assumption would hold if the rate of hydrolysis (and hence ion release), R_h, were constant over that period of extraction. Under that assumption the following equation would apply:

$$[Br^-] = \int_0^t \frac{d[Br^-]}{dt} dt = \int_0^t R_h dt = R_h \int_0^t dt = R_h t \tag{8}$$

By substituting for R_h from Equation (7),

$$[Br^-] = tK[RBr]_b A_h exp(-E_h/RT) \tag{9}$$

Equation 9 above is the empirical formulation of the Arrhenius rate law. Among the factors within its pre-exponential term, t, the period of extraction; $[RBr]_b$, the steady-state concentration of RBr in bulk; and K, the partition coefficient, are all fixed. Within the experimental range of temperature, K will be a weak function of temperature, since enthalpy of partition is usually very small. With all of the preceding approximations assumed, E_h may be estimated from slopes of Arrhenius plots as in Figure 1.

The preceding kinetic model was designed to provide a systematic basis for abstracting useful information out of aqueous ion extraction data. It helped isolate the rate limiting process under a given set of experimental conditions so that a sound interpretation of the acquired data could be made. In the present case, the apparent equality of halide contents among various resins was dismissed by comparing the trends in the Arrhenius curves at the low temperature tail. It also helped elucidate the mechanism of aqueous digestion of halogenated resins.

Bromide Extraction from Resins. It is now possible to analyze the shapes of the Arrhenius plots in Figure 1. The onset of nonlinearity at 160°C was due to glass transition of the resin, which caused K to be substantially increased and thus attainment of the hydrolysis equilibrium to be proportionately accelerated. Under such conditions, the assumption of unidirectionality of Step 3 and the deduction of Equation 4 become untenable. In more simple terms, if accumulation of $[Br^-]$ in the digestion bomb is linear with time, the constancy of R_h is maintained, and hence, validity of Equations 8 and 9 is preserved. As the hydrolysis process approaches equilibrium, $[Br^-]$ growth assumes a non-linear trend, thus causing the rate measured through accumulated $[Br^-]$ determination to be underestimated. The Arrhenius curves in Figure 1, as a result, levels off at this point. The plateau regime between 160- and 225°C resulting from this phenomenon has a small slope. It represents the activation energy of diffusion of RBr through the resin melt, estimated to be about 3- to 5 kcal/mole.

At temperatures above 225°C, polymer cracking defined by Step 1 becomes extremely rapid and takes control of the overall ion extraction process. This was reflected in the bromide extraction data of resin Q in Figure 1, where the level of extracted bromide rose precipitously at temperatures above 225°C. Because of their higher thermal stability, none of the experimental resins showed such a phenomenon.

The low temperature linear segment in Figure 1 is representative of rate Equation 9. Bromide extraction data of all of the resins, with the exception of resin X_0, showed this sharp linear drop of the Arrhenius plots at the low temperature end. Resin Q data was strictly linear, while that of experimental resin X_1 deviated somewhat. The best estimate of E_h from resin Q data within this linear regime was 69 kcal/mole. The activation energy value was in agreement with a study of thermal degradation of diglycidyl ether of TBBPA reported by Nara, et al. (6) In that study, this activation energy was reported to be representative of C-Br bond energy. Data obtained with resins X_2 and X_3 were very similar to resin X_1, and therefore were not included in Figure 1. Resin X_0 data showed no such linear behavior at the lower temperature range.

Chlorides in Resins. The Arrhenius plots of chloride concentrations extracted from all of the resins followed the same linear trend at temperatures below 160°C. According to the kinetic model discussed earlier, this linear regime with an activation energy of approximately 46 kcal/mole was

representative of hydrolysis of organic chlorides diffused out of the resin matrix. According to the data in Figure 2, the levels of such organic chlorides were the same in all of the resins. The fact that it did not show a sharp increase at temperatures above 225°C indicates the chlorides to be incorporated as organic residues, and not to result from the cracking of the polymer.

RESIDUAL ORGANIC BROMIDES

Aqueous Bromide Extraction. It was observed that deviations from linearity at the low temperature end of the Arrhenius plots in Figure 1 were due to higher levels of extracted bromide. Among the experimental resins, X_0 deviated the most, and had an order of magnitude higher level of Br^- than resin Q and the other experimental resins at low temperatures. This was to be expected if the pre-exponential term in Equation 9 was of larger magnitude for resin X_0 because of a larger K and/or increased level of RBr in *bulk*. Value of K would be higher if RBr was of very low molecular weight and/or more soluble in water. An example of such a low molecular weight brominated species is bromophenol or bromocresol, but it is subject to further chromatographic analysis. It appears that resin X_0 contained a much higher level of low molecular weight brominated organic residue than the standard resin Q and the other experimental resins: X_1, X_2, and X_3. The moderate tailing of the Arrhenius plot for resin X_1 in Figure 1 is also indicative of the presence of low molecular weight brominated organic residues, but in much smaller quantities compared to resin X_0.

Molecular Weight Distribution Results. There was evidence for the presence of low molecular weight residues in experimental resin X_0. Their origin in the resins could be traced to the process of bromination of CEN. That process presumably led to the formation of these by-products. In that case, the process for preparing resin X_1 would be most conducive to eliminating such by-products, closely followed by processes for resins X_2 and X_3. It should be reiterated here that resin X_1 was different from the rest in its chemistry of synthesis and the selection of the brominating agent.

WIREBOND AND PAD DEGRADATION

Effects of Brominated Materials. Failure data presented in Table II shows that even at 250°C, resistive wirebond failure is strongly accelerated by the brominated resin. Uncoated wirebonds at this temperature had a failure time of 100 h, compared to 19- to 20 h for wirebonds coated with brominated resins. This finding confirmed that the rate of degradation of the interface between gold and the intermetallic phase could be accelerated by a brominated resin at any practical design temperature.

Thermal stability of, as well as the presence of low-molecular-weight by-products in the brominated resins had strong influence on wirebond failure characteristics. Even at 225°C such effects were obvious. Resin X_1 was far superior to the other experimental resins in this regard. Resin X_0, on the other hand, was even worse than the standard resin Q. These effects, however, showed a diminishing trend as higher temperatures were approached. More experiments are in progress for finding the limiting temperature.

The origin of residual by-products in the resins was traced to the process of bromination to prepare resin X_0. After modifications of process and chemistry, the amounts of by-products were reduced in resins X_1, X_2, and

X_3. The process for preparing resin X_1 was most effective in rendering thermal stability as well as enhancing wirebond reliability, as concluded from the failure data. Processes for resins X_2 and X_3 were somehow not as effective as for resin X_1 in terms of wirebond reliability. More studies of these materials are needed to elicit any unknown factors that could contribute to metallization and wirebond corrosion.

Mechanism of Wirebond Failure. By considering the apparent activation energy of wirebond failure in the presence of brominated resins, the overall wirebond degradation process appeared to be controlled by a diffusion step. The activation energy values ranged from 21- to 23 kcal/mole for various resins. This closely agreed with the value of 18 kcal/mole reported by Gale, (2) but higher than found earlier (1) with resins containing high amounts of free ionic bromides. In the present case, the materials were all free from contamination by inorganic salts, and as such, effects on failure rate were mostly determined by the presence of residual organic halides. The magnitude of the activation energy is indicative of a possible solid-state diffusion process to be the rate-limiting step.

A series of elementary steps leading to the degradation of the Au-Al junction in the presence of ionic and organic halides was proposed in a mechanistic study earlier (1). In that study, the degradation was found to be initiated at the interface between gold and gold-aluminum intermetallic. The degradation front was found to contain oxides of aluminum, gold-aluminum intermetallic compounds, residual organic species, and brominated materials, as determined by laser ionization mass spectrometry (LIMS) and energy dispersive x-ray (EDX) spectrometry. In a subsequent study by transmission electron microscopy (TEM), the species found at the intermetallic region were oxides of aluminum, traces of brominated species, and precipitated gold crystallites (4). It appears from these facts that gold-aluminum intermetallic compounds, generically represented as Au_mAl_n, are particularly reactive toward halide ions as well as halogenated organic species, and lead to the formation of aluminum oxide and elemental gold as corrosion products. From the foregoing considerations and other relevant facts reported so far in the literature, the following sequence of reactions may be proposed as the possible mechanism of wirebond degradation:

$$RBr \rightarrow R\cdot + Br\cdot \qquad \text{Thermal Dissociation} \qquad (10)$$

$$RH + Br\cdot \rightarrow R\cdot + HBr \qquad \text{Organic} \qquad (11)$$
$$\text{halide}$$
$$HBr + H_2O \rightarrow Br^- + H_3O^+ \qquad \text{release} \qquad (12)$$

$$Au_mAl_n + H_3O^+ \rightarrow mAu + nAl^{+3} \qquad \text{Intermetallic} \qquad (13)$$
$$\text{corrosion}$$

$$Al^{+3} + X^- \rightarrow [AlX_4]^- \qquad (14)$$

$$[AlX_4]^- + H_2O \rightarrow Al(OH)_3 + HX \qquad (15)$$

$$HX + H_2O \rightarrow H_3O^+ + X^- \qquad \text{Halide regeneration} \qquad (16)$$

$$[AlX_4]^- \rightarrow AlX_3 + X^- \qquad \text{Halide regeneration} \qquad (17)$$
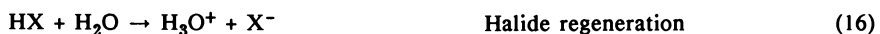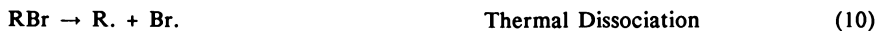
From the polymer matrix, the halide ions are released through thermal dissociation (Equation 10) followed by radical reaction (Equation 11) and

hydrolysis (Equation 12) steps. The hydronium ion H_3O^+ produced in Step 12 is the active species that reacts with the intermetallic phase (Equation 13) to form gold precipitates and aluminum cation. In a recent study by Ritz, *et al.* (4) The Au_4Al and Au_5Al_2 phases were found to undergo oxidation, resulting in Au precipitation and Al_2O_3 formation. This observation can be explained by the reaction sequence given by Steps 13 through 15. Halide and hydronium ions and AlX_3 are regenerated in Steps 16 and 17.

In all reactions involving X, Cl^- as well as Br^- has been assumed. Because of the large quantities of chloride ions determined by aqueous extraction, its role in the wirebond degradation process is considered to be fairly important. From the above discussion, it seems very likely that elimination of low molecular weight organic halides is very crucial to the protection of the aluminum metallization as well as the gold-aluminum intermetallic from halide induced degradation. Lowering of such species will reduce the levels of ions generated in Steps 10 through 12. Thermal stability of the resin is also very important, since a superior thermal stability would mean a slower rate process for Step 10, and thus less halide in the encapsulant.

CONCLUSION

Use of thermally stable brominated CEN resins was found to significantly reduce wirebond failure. Presence of low molecular weight halogenated organic impurities and by-products with labile C-Br or C-Cl bonds in the CEN resin had adverse effects on the Au-Al wirebond reliability, and was found to subvert the beneficial effect brought about by superior thermal stability. Among the current generation of ion-free molding compounds, the interaction of organic brominated species with the Au-Al intermetallic is the predominant failure mechanism. The overall failure rate was found to be controlled by a solid state diffusion step.

It is possible, by manipulating the chemistry of the brominated CEN resin, to make the molding compound more thermally stable. Through proper selection of the chemistry, process and material for brominating the CEN resin, it is possible to enhance the stability of the C-Br bonds in the resin network, minimize the formation of residual organic halides, and thus minimize the Au-Al failure.

LITERATURE CITED

1. Khan, M. M.; Fatemi, H. Proc. Int. Symp. Microelec., 1986, p 420.
2. Gale, R. J. Proc. IEEE Int. Reliability Physics Symp., 1984, p 37.
3. Ahmad, S.; Blish, R.; Corbett, T.; King, J.; Shirley, G. Comp. Hybr. Manuf. Technol. 1986, 9, 379.
4. Ritz, K. N.; Stacey, W. T.; Broadbent, E. K. Proc. IEEE Int. Reliability Physics Symp., 1987, p 28.
5. Dark, W. A. Anal. Purif. 1987, 2, 63.
6. Nara, S.; Matsuyama, K. J. Macromol. Sci.-Chem. 1971, A5, 1205.
7. Khan, M. M.; Fatemi, H.; Romero, J.; Delenia, E. Proc. IEEE Int. Reliability Physics Symp., 1988, pp 40-49. Figures and Tables were reproduced from here with permission from IEEE.

Chapter 37

Ordered Polymers for Interconnection Substrates

Richard Lusignea, Joseph Piche, and Richard Mathisen

Foster-Miller, Inc., 350 Second Avenue, Waltham, MA 02254

Ordered polymer films made from poly benzthiazole
(PBZT) and poly benzoxazole (PBO) can be used as
substrates for multilayer printed circuit boards and
advanced interconnects to fill the current need for
high speed, high density packaging. Foster-Miller,
Inc. has made thin substrates (0.002 in.) using
biaxially oriented liquid crystal polymer films
processed from nematic solutions. PBZT films were
processed and laminated to make a substrate with
dielectric constant of 2.8 at 1 MHz, and a
controllable CTE of 3 to 7 ppm/$^{\circ}$C. The films were
evaluated for use in multilayer boards (MLBs) which
require thin interconnect substrates with uniform
controllable coefficient of thermal expansion (CTE),
excellent dielectric properties, low moisture
absorption, high temperature capability, and simple
reliable processing methods. We found that ordered
polymer films surpass the limitations of fiber
reinforced resins and meet the requirements of future
chip-to-chip interconnection.

The requirements for advanced military MLBs are shown in Table I.
One of the major problems of using leadless ceramic chip carriers
in advanced avionics (VHSIC and VLSI) applications is the mismatch
between the CTE of alumina chip carriers (6.4 ppm/$^{\circ}$C) or silicon
(3 ppm/$^{\circ}$C) and conventional glass/epoxy substrates (12 to
17 ppm/$^{\circ}$C). This mismatch results in work-hardening and cracking
of solder joints which attach the devices to the substrate.
Thermal cycles as extreme as -65 to +125°C may be encountered, and
are known to cause solder failure and other damage. Ordered
polymer films can solve this problem because they can be matched to
the ceramic CTE. Moreover, ordered polymers have excellent

Table I.   Requirements for Surface Mount MLBs

CTE (x-y)	3 to 7 ppm/$^{\circ}$C tailorable
CTE (z)	~17 to 18 ppm/$^{\circ}$C
Dielectric constant	<3.5 (VHSIC <3.0) at 0.01 to 100 MHz
Moisture absorption	<0.5% (saturation)
Single layer thickness	<2.5 mils
Flexural strength	≥graphite/epoxy
Resin-reinforcement adhesion	≥graphite/epoxy
Tg	>200°C
Processing	Compatible with existing modes

dielectric properties, and thin biaxially oriented films can be produced with better impedance control and less crosstalk at finer pitch than with other high performance substrates. Table II compares the current approaches to matched CTE advanced printed wire board (PWB) substrates for high performance avionics applications.

PBZT and PBO are ordered polymers which form long rigid-rod molecules which give rise to a microfibrillar network structure in biaxially oriented films (Figure 1). Such biaxial films have been used in combination with low dielectric constant resins, such as cyanate ester resins, to make circuit substrates for use in MLBs

Table II.   Advanced Substrates for Controllable CTE

Approach	Advantages	Disadvantages
Kevlar fiber reinforced polyimide or epoxy	CTE matched to ceramic, available from DuPont-Howe, dielectric constant = 3.6, moisture absorption reduced	Relatively thick (over 4.5 mil), fiber anisotropy may produce non-uniform strains, microcracking problems
Graphite fiber reinforced polyimide or epoxy	CTE matched to ceramic, patented Boeing process available, can be used as ground plane or heat sink	Poor dielectric constant, anisotropy and micro-cracking problems, relatively thick, vias must be insulated
Copper-Invar-Copper	Matched CTE, readily available, can be used as ground plane or heat sink	Relatively heavy, poor dielectric, vias must be insulated
Polyimide film	Hitachi Corp. reports matched CTE, thin high temperature film, good dielectric (Note: other polyimides have a CTE of 30 to 50 ppm/$^{\circ}$C)	Experimental material, moisture absorption, hygroscopic expansion, bonding problems

(Figure 2). Orientation of the films is used to tailor and control the CTE, and the low dielectric thin film layers provide more controlled impedance and reduced crosstalk than other substrate materials. In addition to MLBs, ordered polymer films can be used to advantage in multichip molecules where silicon chips are directly bonded to the interconnect substrate. The very low permeability of PBO and PBZT films will protect the chips from moisture. Flexible circuitry is another promising application area for these films.

Fiber reinforced substrates (Kevlar and graphite reinforcement) are being developed (1) to match the ceramic CTE, but these materials have drawbacks. Fibers must be woven into a fabric, or cross-plied, resulting in increased thickness and anisotropy at a relatively large scale (fiber tow diameters are about 0.002 in.; minimum fabric thickness is about 0.0045 in.). Additional problems arise from high dielectric constant and costly manufacturing. Copper-Invar-Copper (CIC) laminated foils can provide matched CTE, but these materials are relatively heavy (this precludes their use in avionics applications) and require insulation on the surface and inside vias (holes which connect multilayers). Ceramic substrates are not considered because their brittleness and high dielectric constant rule them out. Recently, Hitachi, Inc., has reported low CTE polyimide film (2), but the material is still in the early development stages and sample quantities cannot be evaluated. Polyimide films also suffer from high moisture absorption (5 percent by weight), which degrades dielectric performance and causes hygroscopic expansion. PBZT or PBO films can be used to provide a thin, homogeneous continuous reinforcement to overcome the disadvantages of current materials. Table III summarizes the properties of biaxially oriented PBZT film.

Table III. Properties of Biaxially Oriented PBZT Film

Property	Value
Tensile modulus of elasticity	10 (10^6) psi
Coefficient of linear thermal expansion (in the film plane)	-7 (10^{-6}) in./in./$^{\circ}$C
Ultimate tensile strength	80 (10^3) psi
Ultimate compressive strength	10 (10^3) psi
In-plane Poisson's ratio (estimate)	0.3
In-plane shear modulus (estimate)	0.1 (10^6) psi
Dielectric constant	2.8 to 3.2 at 1 MHz
Dissipation factor	0.002 to 0.008 at 1 MHz
Maximum use temperature	over 400°C
Moisture absorption	Less than 0.5% by weight
Film thickness	0.0005 to 0.003 in.

Ordered Polymer Film Processing

The processing of ordered polymer (PBO and PBZT) films is based on pioneering work in polymer synthesis and fiber spinning by the U.S. Air Force and their contractors (3-5). Impressive success has been realized in rigid-rod polymer synthesis (6-7) and fiber spinning from anisotropic solutions (8-9). Structure-property relationships

PBO

PBZT

PROCESSING
ROD-LIKE
MOLECULE

ORIENTED MOLECULAR   ORIENTATION
LAYERS WITHIN SINGLE   DIRECTORS
PLY OF PBZT FILM
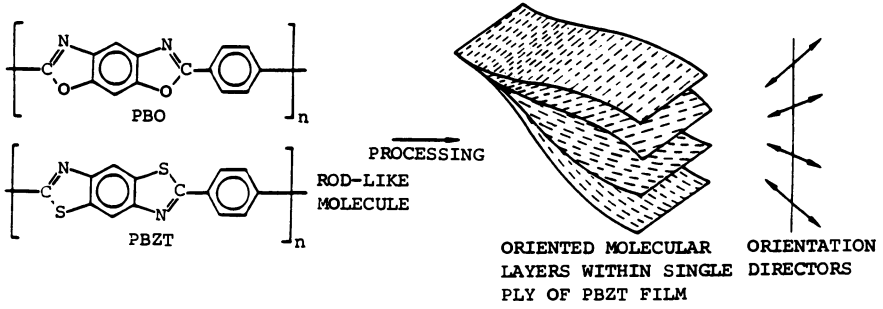
Figure 1.   Rod-like molecules give rise to self-reinforced microstructure within single plies of PBZT film.
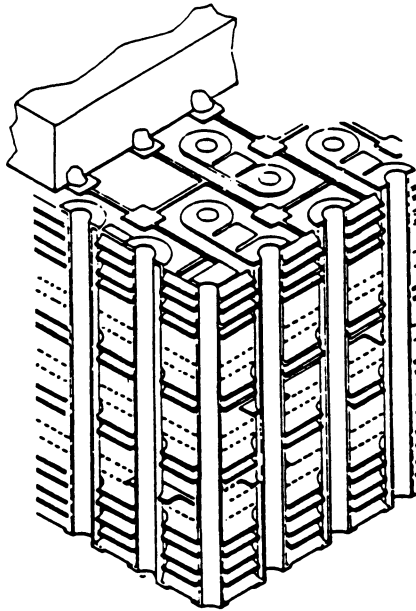
Figure 2.   Multilayer circuit board with surface mounted components.

in fiber and uniaxial tapes have been studied (10-13), specifically with respect to high strength and modulus, and high temperature properties which show service temperatures well above 400°C. Film processing and applications work with poly benzobisthiazole (PBZT) is being conducted (8), and shows that rigid-rod polymer films will play an important role in aerospace structures, electronics, power systems, nonlinear optics, and other high performance applications.

Ordered polymers are processed from their solutions in highly protonated strong acids including polyphosphoric acid (PPA), methanesulfonic acid (MSA), and chlorosulfonic acid (CSA). This begins with de-aeration of the extremely viscous PPA solutions. The next step is extrusion of the solution into an oriented film. The shearing and drawing of the polymer solution in this step are key means to imparting orientation. Then, the formed polymer solution is coagulated, which causes formation of a microfibrillar network (14-16). The coagulated material then is washed in water, resulting in the slow removal of PPA solvents and the eventual formation of a PPA-free, water-swollen film. The final two steps, drying and heat treating, achieve densification, water removal, and mechanical property enhancement.

Drying of the water-soaked films results in a reduction in thickness to 1/5 the thickness of the wet film. For this reason, dimensional constraints are needed during drying to control the stress in the film. Heat treatment refers to very high temperature exposures in inert atmospheres, usually at fairly high tension loadings. The heat treatment process perfects molecular orientation, raises the density and typically results in high tensile moduli and lower breaking elongations.

Rigid-rod polymers PBO and PBZT are highly conjugated heterocyclic aromatic polymers that are sterically constrained to long, straight chain configurations. Physically, they are strong, stiff, rod-like molecules which result in liquid crystal polymer solutions and give rise to self-reinforced fibrillar microstructure. Films produced from these polymers by special solution processing methods consistently show tensile strength over 200 Ksi (1.4 GPa) and tensile modulus over 30 Msi (207 GPa). Combining high temperature capability (over 400°C), chemical resistance and low density, PBO and PBZT films are uniquely suited for a variety of aerospace, electronic and industrial applications.

Rigid-rod polymer films fulfill the promise of "self-reinforced" materials: They surpass the performance of fiber-reinforced composite materials without suffering from the drawbacks of distinct fiber and matrix phases. This is possible because the molecular structure of PBO and PBZT produces a fibrillar microstructure, analogous to continuous fiber reinforcement, but at a physical size about 100 to 1,000 times finer than fiber plies or fabrics (see Figures 3 and 4). The ordered polymer microfibrillar network, or "molecular fabric," is the key to the advantages of these materials. These include controlled coefficient of thermal expansion (CTE), tailorable strength and stiffness, and elimination of interface problems such as microcracking associated with fiber-based composites. A major advantage of rigid-rod polymer films is that they are thin, less than 0.002 in. (less than 0.05 mm), which is difficult or impossible to achieve with fiber composites.

SCHEMATIC REPRESENTATION
OF PBO INTERCONNECTED
MICROFIBRILLAR NETWORK

25 MICRON DIAMETER FIBER OR FIBER
BUNDLE IN A TYPICAL COMPOSITE
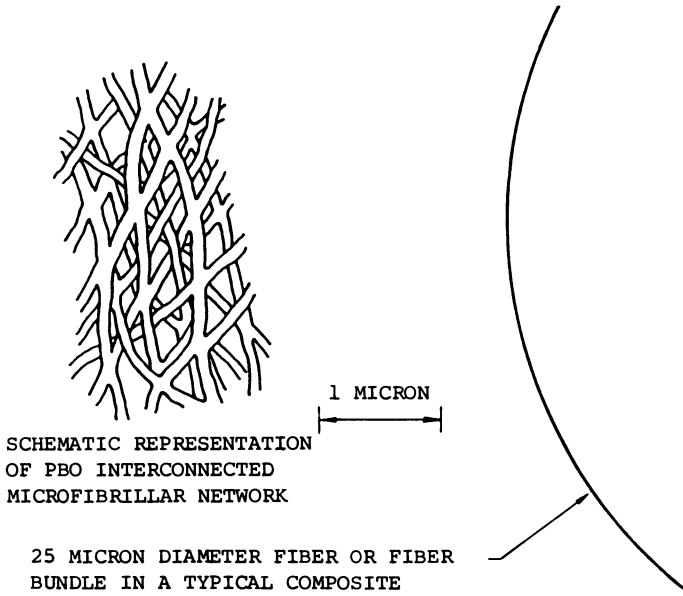
Figure 3.   PBO films provide more efficient reinforcement.
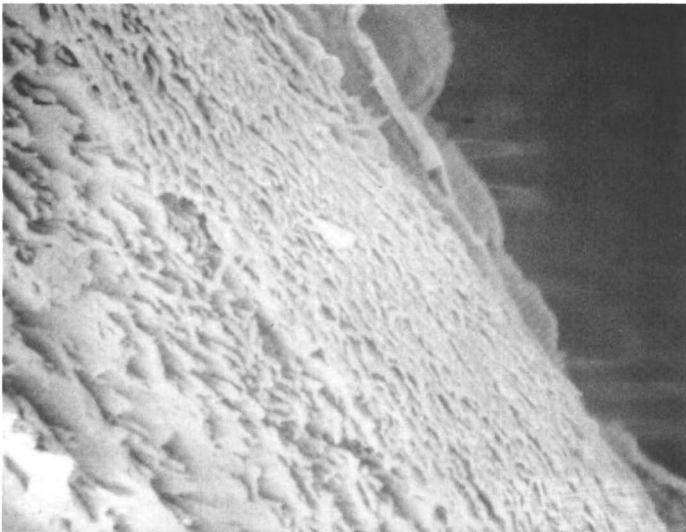
Figure 4.   SEM showing texture in biaxially oriented PBZT film
at the fracture surface.

Rigid-rod polymer films made from PBO and PBZT are being developed because they provide important performance improvements over competing materials such as fiber reinforced composites and metals. Table I summarizes some of the highest payoff applications. Thin PBZT films combined with low dielectric constant resins are being developed for multilayer circuit boards and multichip modules to increase interconnection density and speed with matched circuit impedance and reduced crosstalk.

During processing, rod-like molecules are formed into a microfibrillar network with homogeneity down to a very fine scale, below 0.1 micron ([17]). Thus, the self-reinforced material will appear continuous to the relatively large electronic components, printed conductors and other features of the electronic package. After processing, the mechanical properties of ordered polymer films are consistent and repeatable, and the films show excellent environmental stability including low moisture pickup (less than 0.5 percent by weight after 24 hr immersion at 25°C). The completely processed films cannot be further formed by application of heat and pressure. In fact, tests of tensile strength at 300°C indicate that the materials retain 75 percent of room temperature properties ([18]).

Film Orientation and Properties

The key to achieving engineering utility with rigid-rod polymer films is controlled orientation. The maximum achievable density and the highest degree of order are present in the case of rigid-rod polymers. Figure 5 shows some examples of oriented rigid-rod polymer films. Uniaxial orientation results in very high longitudinal (or machine direction) properties, but little or no transverse strength and stiffness.

Uniaxial films, like fibers, require multiple plies at controlled orientations to build in desired properties. (A major drawback of uniaxial films is that they split apart when handled.) In Figure 5b, films have isotropic in-plane properties, but there is no long-range order (beyond about 0.1 μ). Such films do not achieve high strength and stiffness. The twisted nematic orientation does have long-range order, with continuous microfibrils oriented at various directions through the thickness of the film. Balanced angle biaxial film has two primary directions of orientation at $\pm\theta$ to the machine direction. The strength, stiffness and CTE of balanced angle films can be tailored by controlling the orientation angle. The twisted nematic and balanced angle films have continuous fibrillar layers oriented at specific directions within the film thickness. X-ray diffraction and SEM studies at the University of Massachusetts ([19]) and the Air Force Materials Lab ([20]) have confirmed the balanced angle film orientation and morphology. The two-layer balanced angle model is idealized, as some molecules will be oriented between the two directions, as well as out of the plane of the film. However, this ideal biaxial orientation serves as a good approximation to describe CTE, and is shown in Figure 6. The CTE of the films was measured with a Perkin-Elmer TMS-2 quartz tube dilatometer over the range -50 to 125°C with an experimental error of ± 2 ppm/°C.

The negative CTE of PBZT film in the primary orientation direction is similar to that noted for PBZT fibers as well as other high modulus fibers including graphite, polyaramid (Kevlar) and ultra-drawn polyethylene (21). These high modulus fibers exhibit a negative CTE in the axial direction and positive CTE in the transverse direction. When these fibers are used in conjunction with a positive CTE matrix material (such as epoxy or polyimide), the net thermal expansion can be tailored to the 3 to 7 ppm/^{o}C desired for PWB substrates. This is done by controlling the fiber-to-resin ratio and cross-plying the unidirectional fiber layers. Biaxial ordered polymer films are similar to fiber reinforced substrates, except that the microfibrillar reinforcement is at a much smaller and more homogeneous scale. Ordered polymer films such as PBZT can be used with positive CTE resins to make MLBs. Figure 7 shows how the volume percent of resin can be used to tailor CTE. The data plotted shows the average for 5 measurements on each of the three laminated samples. The measurements were made on free-standing samples 2.5 mm thick, and the experimental error was 0.5 ppm/^{o}C.

Summary

In summary, PBZT and PBO ordered polymer films should eventually lead to PWBs with circuit densities now common to the semiconductor industry. Advanced computer systems are dependent upon very high density circuit boards having a large number of internal planes, many conducting circuit lines, and a multitude of holes formed in close proximity to the internal conductors. Higher density PWBs are needed to meet the increasing density of circuits packaged on semiconductor devices and modules including chip-on-board, multichip modulus and flexible circuitry.

The next generation of electronic packaging will be VLSI/VHSIC (Very Large Scale Integrated/Very High Speed Integrated Circuits). Requirements for fine line wiring, high power density, multilayer board constructions, and many components per board place severe demands on materials. PBZT and PBO are uniquely well-suited for these applications owing to:

1. Dimensional stability and controllable CTE (coefficient of thermal expansion)
2. Low dielectric constant (less than 2.8) for low power loss and high speed circuits
3. High temperature and environmental resistance for compatibility with new fabrication methods including metal spattering and ion plating.

PBO and PBZT films can be made very thin (less than 0.002 in.) and can be impregnated with secondary resins, resulting in a substrate with a dielectric constant less than 2.8, an isotropic planar CTE of 7 ppm per ^{o}C or less, and temperature resistance over 250°C. Copper circuits and ground planes can be added by a variety of additive or substrative means, and multilayer circuit boards can be fabricated using plated through holes. Further development of these thin film dielectric substrates should result in interconnection density over 100 times greater than is currently possible with fiber reinforced epoxy multilayer boards.

ORIENTATION
DIRECTORS

ORIENTATION
DIRECTORS

2

1

+θ

−θ

a) UNIAXIAL
   ORIENTATION

b) PLANAR ISOTROPIC
   (POLYMER RODS LIE
   IN 1-2 PLANE)

c) TWISTED NEMATIC
   (OR CHOLESTERIC)
   ORIENTATION

d) BALANCED ANGLE
   BIAXIAL
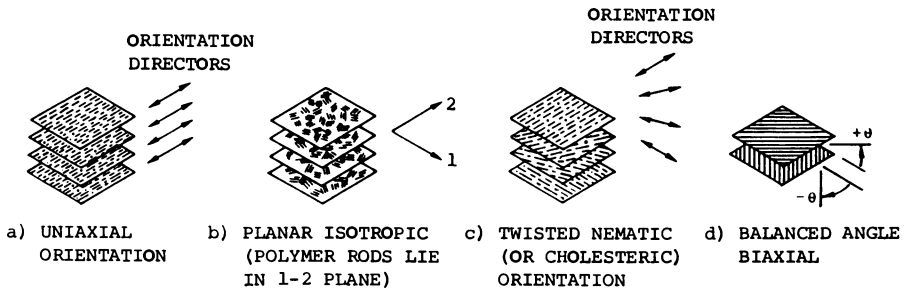
Figure 5.   Morphology of oriented single PBZT film through the
thickness.

SHOWS RANGE OF
EXPERIMENTAL DATA

−θ +θ

BIAXIAL
FILM

±45°

θ

IN-PLANE
ISOTROPIC
ORIENTATION

20

10

0

−10

−20

CTE ppm/°C

TD

MD
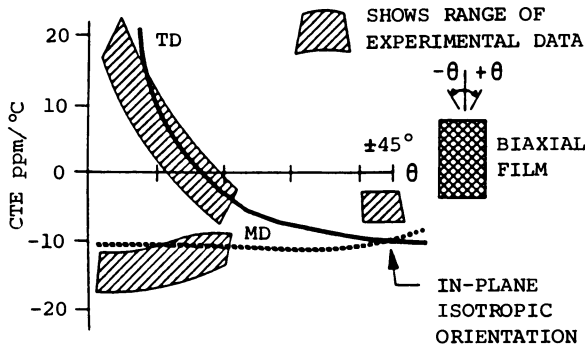
Figure 6.   CTE behavior of pure PBZT films.

50

40

30

20

10

0

−10

PWB CTE, ppm/°C

$\alpha_{RESIN} = 50$

$\alpha_{RESIN} = 30$

O PBZT/XU71787
● PBZT/QUATREX 5010
▲ PBZT/META-ATB

DESIRED CTE

.2   .4

.6   .8   1 V_r
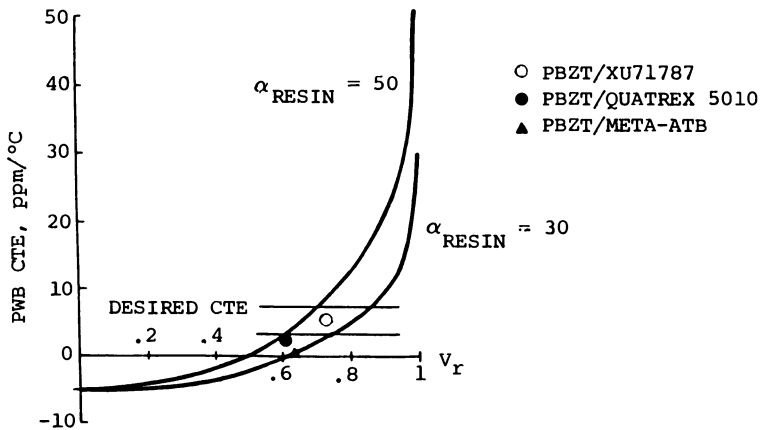
Figure 7.   Relationship between volume fraction of resin (V_r)
to CTE in PBZT/resin substrate.

Literature Cited

1. Packard, D.C. SAMPE Journal, Jan.-Feb, 1984, 6-14.
2. Numota, S. Proc. Second International Conference on Polyimides, 1985, Society of Plastics Engineers, Inc. 492-510.
3. Helminiak, T.E.; Benner, C.L.; Arnold, F.E. Polymer Preprints 1975, 16, (2), 659.
4. Helminiak, T.E. Organic Coatings and Plastics Chem. 1979, 40, 475.
5. Adams, W.W.; Eby, R.K. MRS Bulletin 12, No. 8, 22-26.
6. Wolfe, J.R.; Loo, B.H.; Arnold, F.E. Macromolecules 1981, 14, 915.
7. Wolfe, J.R.; Arnold, F.E. Polymer Preprints 1977, 18, (2), 414.
8. Choe, E.W.; Kim, S.N. Macromolecules 1981, 14, 920.
9. Helminiak, T.E. Proc. National Symposium on Polymers in the Service of Man 1980, 16, 86.
10. Allen, S.R.; Filippov, A.G.; Farris, R.J.; Thomas, E.L.; Wong, C.P.; Berry, G.C.; Chenevey, E.C. Macromolecules 1981, 14, 1135.
11. Allen, S.R.; Filippov, A.G.; Farris, R.J.; Thomas, E.L. J. Appli. Polym. Sci. 1981, 26, 291.
12. Thomas, E.L.; Minter J.R.; Shimamura, K. J. Mat. Sci. 1981, 16, 3303.
13. Thomas, E.L.; Farris, R.J.; Hsu, S.L. AFWAL-TR-85-4151, June 1986.
14. Pottick, L.A.; Farris, R.J. 1985 Nonwovens Symposium, April 1985, 65-71.
15. Cohen, Y. AFWAL Technical Report 87-4030, April 1989.
16. Cohen, Y.; Thomas, E.L. Polym. Engr. and Sci., 25, 1985, 1093.
17. Thomas, E.L.; Cohen, Y. of University of Massachusetts, Polymer Science and Engineering, Personal Communication, 1986.
18. Thomas, E.L.; Farris, R.J. in Vol. II, Technical Report AFWAL TR 80-4045, July 1981.
19. Thomas, E.L. Interim Report, Air Force Contract No. F33615-83-C-5120, 1983.
20. Adams, W.W. Private Communication, 1986.
21. Porter, R.S. J. Thermal Analysis 1975, 8, 547-555.

Chapter 38

Three-Dimensional Circuit Interconnections with Thermoplastic Performance Polymers

David C. Frisch and John F. Rowe

Pathtek, 250 Metro Park, Rochester, NY 14623

This chapter presents an overview of performance plastic polymers in commercial planar and 3-dimensional circuit board products, and describes in detail one approach (two-shot molding) developed as an integrated 3-D circuit manufacturing technology. The distinctions between conventional planar (2-dimensional) circuitry, based on thermoset laminates and "subtractive" etching processes, and the enhanced design flexibility afforded by expanded interconnection capacity in three axes are discussed. Specific examples of 3-dimensional interconnect protoypes and products are described and pictured.

Plastic materials appear in all aspects of everyday life, providing a vast range of protective, insulating and packaging roles. Within the plastics field, the technology of injection molding probably provides the greatest opportunity to capitalize upon the benefits of plastic materials. By "filling" space with a molded material, it is possible to create very complex and sophisticated components which exploit the benefits of the material properties in a 3-dimensional way. Most plastic moldings provide a kind of "structural" or "spatial" customization. They allow a product designer to inclose three dimensional space with a component which either acts as a container or enclosure, or which fixes the relative positions of other components in relation to each other. (1)

Printed circuits are generally planar objects. Usually square or rectangular, they are essentially flat platforms supporting interconnect networks on which are mounted a mixture of electronics or electrical components. These components may be leaded devices (either radial or axial) passing through the board, or mounted components on the board surface. The circuit board acts as a "customizing" device, linking standard or special components to create circuit functionality. (2)

Molded printed wiring boards create revolutionary new dimensions for designing and manufacturing electrical and electronic interconnection products. The commercial value for these new substrates resides not solely in their potential to increase density, but more so in their unique ability to consolidate mechanical and/or electro-mechanical features and structural components into a "one piece" single unit package. The printed circuit board becomes transformed into a multipurpose device supplying both electrical as well as mechanical elements. Using selective additive plating techniques and injection molded thermoplastic resin polymers, circuit boards do not need to be limited to planar or 2-dimensional forms. Instead, by incorporating molded-in 3-D structural features such as; bosses, ribs, stand-offs, and recessed cavities, boards can be transformed into multi-functional devices possessing customized forms and shapes. "Circuits can be:

- Designed to provide mounting points for components

- Shaped to fit into the interior of equipment

- Provided with locating points to "snap into" other
  components

- Designed to provide a dual function, doubling as a
  structural component

- Instrumental in saving "down stream" assembly costs"(2)

In addition, molded holes can be custom designed to aid in insertion of leaded components (entry radii or countersink) or to provide recessed mounting of hardware (counterbore). Furthermore, holes can be oblong, rectangular or parallel to the plane of the molded substrate. Possible hole geometries are illustrated in Figure 1.

Molded 3-Dimensional circuit boards, as shown in Figure 2, can be formed into almost unlimited shapes, sizes and geometries. Conductors can be routed around corners, into deep recesses, along ramps and up nearly 90 degree walls. In addition, depending upon material selection, non-plated areas may be transparent, translucent, or colored to satisfy specific performance objectives.

Multiplanar circuitry and through-hole interconnections enable product or component designers to produce customized "Application specific" multifuctional devices. As shown in Figure 3, circuitry may traverse a horizontal plane and then gradually transit a raised hemisphere molded feature.

Conversely, as shown in Figure 4, circuitry may be predominantly 2-dimensional with non-conductive molded-in structural features simplifying assembly of down-stream assembled components.

The development of a molded interconnect technology has spanned more than a decade of materials and chemistry development and process refinement. What began as a concept in the minds of several entrepreneurial companies and research technologists, has finally achieved true market commercialization. Molded boards and 3-dimensional interconnect devices comprise a new manufacturing industry as opposed to being merely another niche market segment of
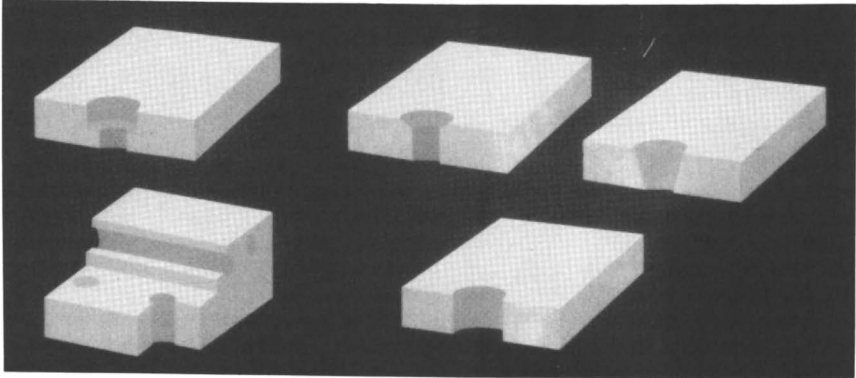
Figure 1.   Molded through-holes offer custom geometries.
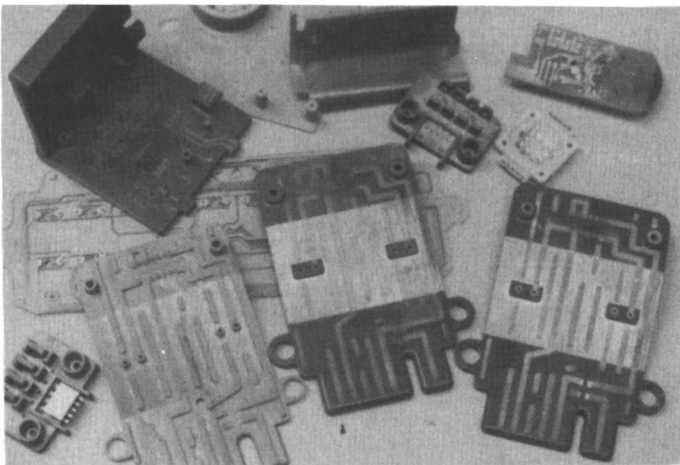
Figure 2.   3-D Molded Interconnects feature unique shapes/forms.
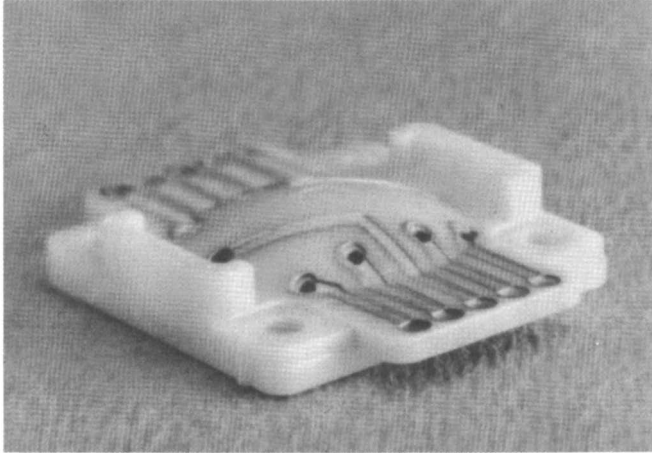
Figure 3. Molded substrate combines circuitry and Mechanical structure.
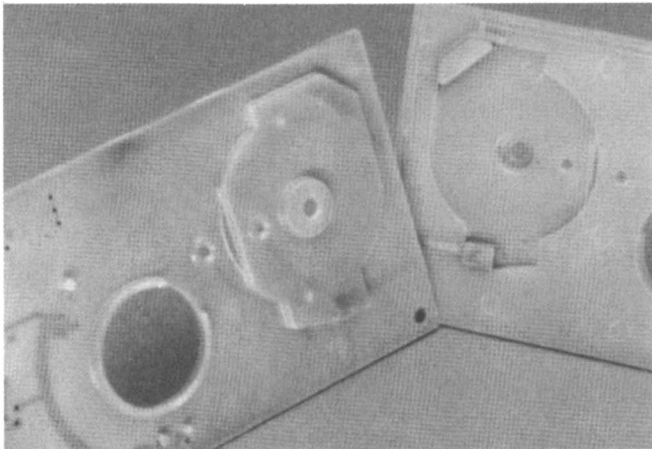
Figure 4. Recessed "Molded-in" features simplify component assembly.

the conventional circuit board industry. While offering benefits of both economy and performance over standard epoxy-glass laminate 2D boards, a molded board achieves far greater value through the 3-dimensional feature-forming capabilities which integrate mechanical support, structure, and custom shapes with highly conducting, readily solderable circuitry patterns. Molded circuits will take interconnection into new areas as they link together the printed circuit industry with the molded component industry. "Additional "value added" will be achieved by augmenting the circuit with extra features. This will cause the molded circuit business to grow outside the hitherto traditional market areas, currently filled by PCBs, into new fields which embrace the structural components market." (3)

As a manufacturing technology, selective metallization of a molded plastic substrate has wide utility in electrical and electronic componentry, connector and receptacle devices, customized IC carriers, electro-mechanical and electro-optical products. "The major benefits which come from a molded circuit board may be grouped under four headings including; structural/mechanical, material, cost and design/aesthetics.

1. Structural/Mechanical

     Create 3-dimensional configurations
     Save space and weight
     Provide an enclosure or rigid structure
     Reduce the number of secondary assembled components
     Minimize assembly complexities
     Integrate functionality of components
     Accuracy and reproducibility of products within desired
     tolerances.

2. Material

     Provide electrical insulation
     Lower weight per unit volume
     Enhanced dielectric properties: Volume and surface-
                                       resistivities
                                       dielectric constant
                                       dissipation factor
                                       arc tracking
     Options for color matching and transparency
     Resistance to corrosion and hostile environmental
     exposure
     Permits liquid retention or exclusion

3. Cost

     Reduce component costs
     Provide a "systems level cost reduction"
     Reduce a product's "net cost to assemble"
     Minimize assembly and/or component tooling costs
     Lessen parts inventory and control costs

4. Design/Aesthetics

Create customized styles
Textured finish options" (4).

MANUFACTURE OF MOLDED INTERCONNECTION DEVICES

MATERIALS. Selection of a base polymer thermoplastic resin from
which a molded substrate is produced is influenced by factors of
price and performance. Secondary considerations include supplier
preference. Given the uniqueness of each product application,
standardization of generic polymers is unlikely. In fact, the
selection possibilities are likely to grow with continued
diversification of application requirements/specifications.
Materials with high temperature properties are desired where flow
soldering assembly operations are involved. In these applications,
material selection includes high-temperature, engineering grade,
thermoplastic polymers characterized by high heat deflection and/or
high glass transition temperatures.
    Conversely where less stringent thermal demands are appropriate.
choices are broadened to encompass materials more commonly referred
to as "commodity resins". Ultimate end product operational
environments will impact the material selection process. Where
in-service temperatures range from room ambient to moderate thermal
extremes, lesser thermally tolerant resins may be considered.
Conversely, for hostile environments such as those encountered in
"under the hood" automotive, down-hole (geothermal), tropical, or
corrosive climatic extremes. enhanced material properties will be
required.
    Plateability or metallization compatibility cannot be overlooked,
as not all resin materials are readily capable of being plated using
currently available commercialized techniques.
    Typical examples of materials now being used are given in Table I
followed by a brief properties description.

Materials For Molding (5)

   -Polyarylate

   -Polysulfone

   -Polyarysulfone

   -Polyethersulfone

   -Polyetherimide

   -Polyphenylene Sulfide

TABLE I

Polyarylate-	Aromatic polyesters having an amorphous molecular structure. Compared with other amorphous engineering plastics in terms of heat resistance, polyarylates are generally positioned between polycarbonate on the low side and sulfone and polyether polymers on the high side. Compared with crystalline and semi-crystalline engineering plastics, polyarylate resins offer better resistance to warping, and generally comparable mechanical properties.
	The HDT of commercial polyarylate-based compounds range from 310F to 345F at 264psi. Polyarylates have inherently good flame retardancy, and generate little smoke during burning. Grades meeting requirements for UL 94V-0 down to 0.062" are available.
Polyetherimide-	Amorphous thermoplastic introduced in 1982. The material is characterized by high strength and rigidity at elevated temperatures, long-term heat resistance, and highly stable dimensional and electrical properties.
	Polyetherimide has a chemical structure based on repeating aromatic imide and ether units. High performance strength characterisitics at elevated temperatures are provided by rigid imide units, while the ether linkages confer the chain flexibility necessary for good melt processing and flow.
	Polyetherimide resins are rated for 338F and 358F continuous-use temperatures by U.L., and are UL94-VO flame listed down to 0.010" (depending upon grade). The HDT of commercial polyetherimide based compounds ranges from 387F to 420F at 264psi.
Polysulfone-	Aromatic amorphous thermoplastic introduced in the mid-1960s. Polysulfone is a transparent, heat resistant, ultra-stable engineering polymer. It possess good electrical properties that remain relatively unchanged up to temperatures near its glass transition temperature (Tg) of 374F.
	Polysulfone is UL listed for continuous service at 320F, although it will withstand higher temperatures intermittently. It offers a good combination of electrical properties: dielectric strength and volume resistivities are high, while dielectric constant and dissipation factor are low.

Polyethersulfone-   Aromatic amorphous engineering thermoplastic.
                      Listed by the UL for continuous service at 356F,
                      operation at higher temperatures up to 400F is
                      feasible.

                      Inherent low flammability meeting UL94-VO
                      requirements at thicknesses of 0.017" and above.
                      Possesses good resistance to most inorganic
                      chemicals, oils, greases aliphatic hydrocarbons
                      and gasoline at ambient and elevated temperatures.

                      Most proprietary cleaning solvents do not attack
                      it unless the components are heavily stressed;
                      known exceptions are esters, ketones, methylene
                      chloride and polar aromatic solvents.

Polyarylsulfone-   Typical characteristics of aromatic, amorphous
                      sulfones. Able to withstand high temperatures in
                      long-term usage as characterized by heat
                      deflection temperature (HDT) values of 399F at
                      264psi, and glass transition (Tg) ratings of 428F.

                      Good ductility and toughness are retained from
                      -148F to 392F.

Polyphenylene
Sulfide -   High performance crystalline aromatic polymer.
                      Exhibits outstanding high-temperature stability,
                      inherent flame resistance, and good chemical
                      resistance. Its structure also promotes a high
                      degree of crystallinity. UL listed for continuous
                      service from 392F to 464F depending upon compound,
                      thickness and end use. Compounds can withstand
                      higher temperature exposure due to heat deflection
                      temperature ratings of over 500F.

                      Nearly chemically inert, it is highly resistant to
                      attack by solvents. In fact, no chemical has been
                      found to dissolve it readily below 400F.

Reinforced PET-   Thermoplastic polyesters based on polyethylene
                      terephthalate. Closely related in terms of
                      chemistry, properties, and areas of application to
                      reinforced polybutylene terephthalate (PBT)
                      compounds. Key distinguishing features are higher
                      strength properties and higher use temperatures.

    The materials shown in Table I are available in varying molecular
weights and filler compositions. For molded circuit applications,
the most commonly used fillers comprise chopped or milled glass
fibers and/or mineral talcs. In addition to these fillers,
additional components may be incorporated to impart flammability
resistance or to promote electroless plating. The latter is achieved
by the addition of a proprietary mineral filler which renders the
polymer "catalytic" to plating.

This additive does not adversely affect the dielectric properties of the base polymer, but merely ensures initiation of the electroless plating process upon exposure of the molded plastic substrate to the plating solutions.

The unique attributes of "catalyzed" resins are that they eliminate the need for secondary (after molding) pre-plate activation or "seeding" operations common to conventional plating-on-plastics (POP) processes. For molded circuit board manufacture, catalytic resins are used in two-shot (two-component) molding processes which form highly complex 3D plastic structures which are capable of being selectively plated without the need for plating masks or resists. Polymers currently available in a "catalytic" composition include only amorphous sulfone and imide based systems.

MOLDING/METALLIZATION. Molded thermoplastic circuit board substrates may be rendered selectively conductive by several additive process techniques including conductive polymeric thick film inks (PTF), and semi and fully additive electroless/electrolytic platings. Of the various chemical process methods developed to produce circuitry on a molded plastic substrate, one method practiced by Pathtek, A Kodak Company, combines both "catalytic" and "non-catalytic" resins in a highly automated commercialized two-shot molding/selective metallization process.

The process starts by injection molding a plastic substrate (or "first shot"). Using a "catalytic" polymer resin, the first shot mold tool cavity produces a plastic substrate containing only those features and component elements which are designed to accept subsequent electroless deposition. Those features formed into the "first shot" plastic molding will produce the metallized through-holes, circuit traces, and other conductive structural elements. As illustrated in Figure 5, molded-in features are formed as raised tracks or traces which allow for subsequent encapsulation with "non-catalytic" resin during the "second shot" molding cycle

The "catalytic" molded plastic part is then inserted, either manually or automatically, into either; (a) a second mold (tool) base or (b) a second cavity within the same mold (tool) base. The second molding cycle injects a non-catalytic (or "non-plateable") resin which overmolds (encapsulates) the non-raised background areas of the first shot plastic part. This second shot cycle completes the molding process. The finished (ejected) plastic substrate, as shown in Figure 6, contains predefined patterned areas of exposed "first shot catalytic" resin and areas of "second shot-non catalytic" resin.

Another way of looking at the two-shot process is to consider the technique to be a derivation of metal insert molding except that the first shot is plastic rather than a stamped or formed metal.

The unique attribute of this process is that upon ejection from the molding machine, two-shot (fully formed) plastic parts are ready for selective electroless plating without the need for imaging, masking or resist application/developing processes. Highly complex 3-D shaped molded substrates containing recessed cavities and multi-axis circuitry may be produced using the "in-mold" imaging techniques of two-shot molding.

The final process step is a chemical plating of "catalytic" resin sites with electroless copper/nickel/tin etc.
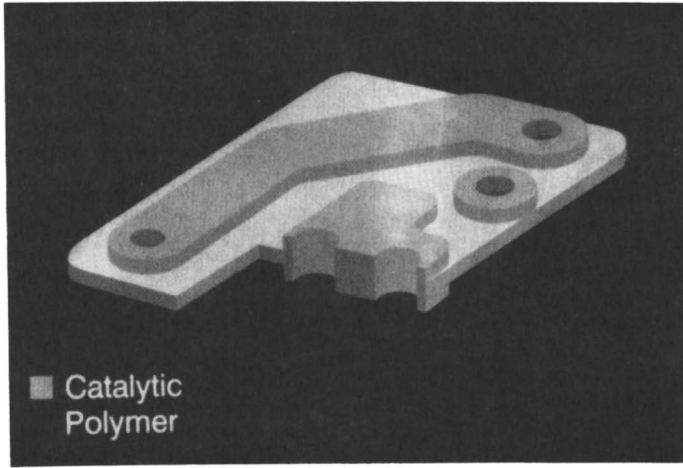
Figure 5. Two-Shot Process: First shot molded insert.
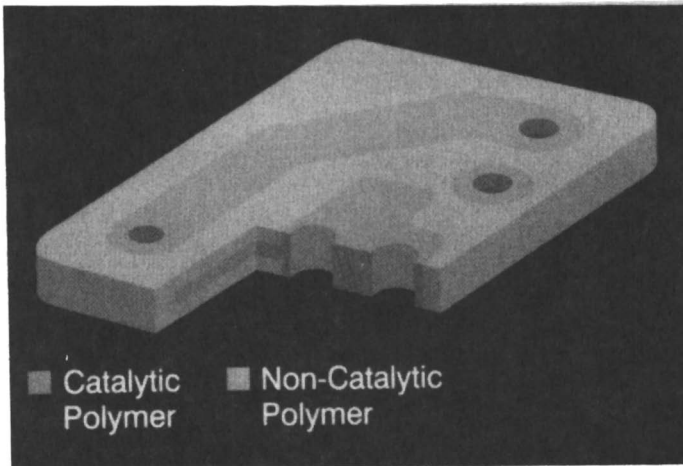
Figure 6. Two-Shot Process: Second shot composite molding.

Deposition initiates only on exposed (non-overmolded) "first shot" catalyzed resin areas. Second shot (non-plateable) material is "non receptive" to electroless plating. The resulting selective metallization is shown in Figure 7.

MOLDED CIRCUIT INTERCONNECT APPLICATION

An example of a multi-functional electro-mechanical interconnect device produced using the two-shot process is shown in Figure 8. This device is used in an new Eastman Kodak Desktop Microfilmer performing functions of document/paper sensing. Electroless copper and nickel platings are deposited on highly irregular surfaces with high consistency and uniformity. Furthermore, through-hole metallization is achieved with plating aspect ratios approaching nearly 8:1; i.e., 0.030" diameter in a 0.230" part thickness.

The 3D molded interconnect is uniquely shaped to provide specific mechanical features. As shown in Figure 8, three individual circuit traces (plated pads) function as three separate switches whose pitch is such that for documents containing holes, even if one or two traces coincided with a hole, at least one circuit trace would still detect a document presence. Trying to package three optical sensors that close together would be difficult or nearly impossible.(6)

The profile of the surface containing the three circuit traces, as shown in Figure 9, is sloped (angled). This slope, prevents edges or corners of a document from getting caught or snagged.

FUTURE OF PERFORMANCE POLYMERS and 3-D MOLDED SUBSTRATES

The driving force behind this emerging technology is the engineering design freedom and creativity developed through three-dimensional component packaging. "The strongest attraction for "moving into molding" occurs when the benefits of structural customization can be synergized with the circuit customization. The molded board industry will grow on the following bases:" (7)

- Some penetration into conventional double-sided, plated through-hole (pth) printed circuit board areas on the basis of pure cost savings in the board cost.

- A degree of penetration in traditional areas on the basis of improved dielectric performance and/or thermal stability under hostile environmental exposure.

- The realization of total system cost savings by designing boards with assembly and other component cost-saving features built-in.

- The creation of molded circuit boards which reduce "down stream" assembly costs.

- The bringing together of 3-dimensional molding skills and interconnection systems to create components which do two jobs in one, acting as a case, cover or some kind of housing, at the same time doubling as a molded circuit boards." (8)
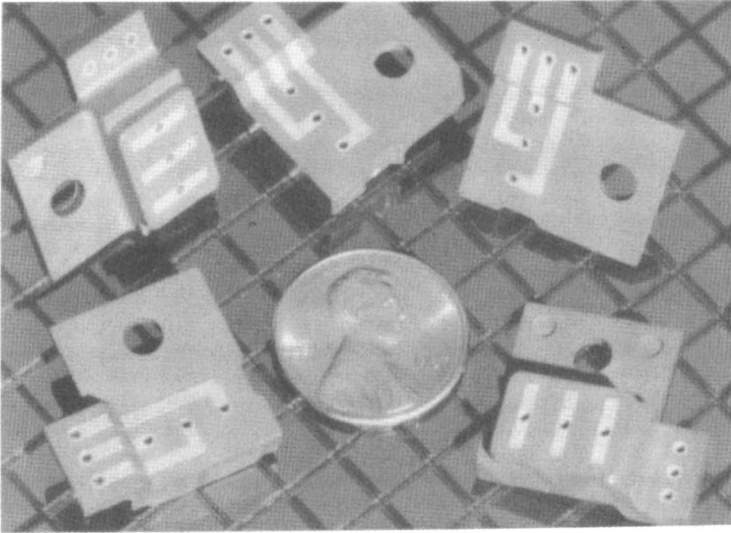
Figure 7. Molded document sensor integrates selective plating and Mechanical/Structural features.
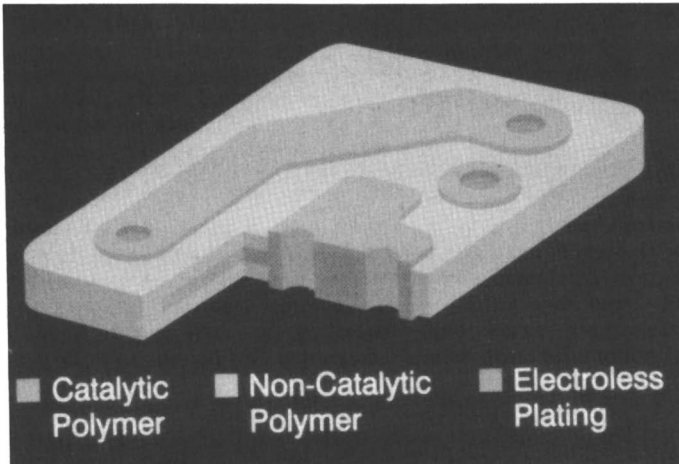
Figure 8. Two-Shot Process: Selective plating completes circuitization process.
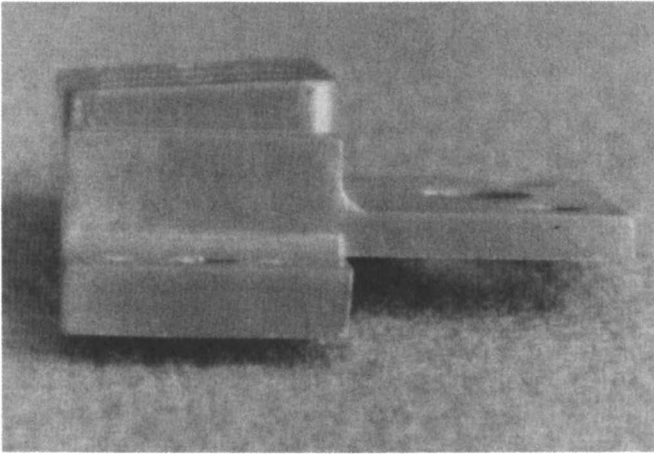
Figure 9.   Molded document-sensor side-view: Circuitry on 5
degree tapered surface assures reliability and product
functionality.

LITERATURE CITED

1. BPA (Technology & Management, Ltd.) <u>Technology Update 8705, Molded Circuit Boards</u>: Surrey, U.K., 1988, p 1.

2. Reference 1, p 3.

3. Reference 1, Preface.

4. Reference 1, pp 1,2.

5. <u>MODERN PLASTICS ENCYCLOPEDIA</u>; McGraw-Hill, Inc.: New York, 1988; Vol. 65, No. 11, pp 34,46-49, 50,84,108-110.

6. Hamlin, R.J.; Romansky, JA. <u>Proc. Technical Program</u>, NEPCON EAST Boston, MA, 1988.

7. Reference 1, p 23.

8. Reference 1, p 26.

Chapter 39

Significance of Developments in New Substrate Materials

Edward Donnelly

BPA (Technology and Management) Ltd., Dorking, Surrey, England

The widespread developments in integrated
circuits have resulted in different
requirements for the substrate materials.
To overcome these problems of cost
pressure, higher density, the move to
surface mounting, increased signal speeds
and more heat, the range of standard
substrates of reinforced polymers or
ceramics have been modified, and a range of
new materials developed. In addition, many
special substrates are now being built up
whilst producing the circuit and mechanical
engineering skills used, rather than wet
chemistry. This paper sets to put these
developments in substrate materials into
context to see their significance.

The test of significance in this case is in a business
sense. Will the developments improve profitability or
clear away problem areas to permit other techniques?
    Circuit substrates are products that are totally
dependent on the electronics industry for their
existence and future. They are the basic raw
materials that the PCB and hybrid industries convert
into carriers which mechanically support active and
passive devices, and which contain the customised
interconnection patterns to link the devices together
in an assembly. Any changes in these products have to
arise from the changes in equipment design,
improvements in the electronic devices themselves, and
modifications to the packages that contain the
devices.

The major driving forces in electronics are lower costs and higher performance. In striving to meet these needs, important developments are occurring such as Very Large Scale Integration (VLSI) and more specialized customization using Application Specific ICs (ASICs). These developments are creating problems for dependent components such as circuit substrates, and also problems in judging the importance of the innovations in electronics. The developments are naturally exciting, and many papers are published and presented at conferences etc. by enthusiasts, which often leads to a perception of topics being much more important than they actually are. This confuses company strategists who have to determine which developments are significant for their products and which will remain small niche markets for specialist companies.

Before looking at the developments we should look at the significance of substrate materials in the context of the whole electronics industry.

ELECTRONIC EQUIPMENT MARKETS

Currently the value of the worldwide electronic equipment production is $476 bn, and this is forecast to grow at 8.5%-9% pa through the next decade. The USA production accounts for about 38% of that figure, and therefore developments in this market must be significant.

However, from the breakdown of this production (Figure 1) it can be seen that the USA is not representative of the world market, because of the strong Military/Aerospace sector which currently accounts for 27% of the USA production.

By 1997 this is forecast to reduce to 14% because of the extraordinary growth in the Electronic Data Processing (EDP) section. The Military sector has traditionally governed the PCB market in America, but it should be noted that what is significant for the USA Military is often not desirable for the rest of the world. Companies who want to sell on a world basis may consider it more significant to be involved with other market sectors that have more universal opportunities.

Many of these markets are now becoming as large as the whole electronics industry was a few years ago, and these sectors are often developing their own unique methods of packaging and interconnection which are leading to specialist substrate materials and techniques.

The most dominant sector is computers, which are a large proportion of the production in all the regions of the world. The developments in computers are of even greater significance than just EDP because they

are also key factors in modern telecommunications, industrial, and even some consumer applications.

The size and growth of the overall equipment market naturally tempts company strategists into planning entry into the "Electronics Market". For chemical companies this usually means entry at the substrate level. However, what is ignored is that much of the added value occurs in the design and final assembly of the finished black box. PCBs and Hybrids account for only 2.5% of the overall electronics market, and the total value of substrates involved in these two sectors only accounts for some 0.8% of the finished equipment value, and therefore appears to be a very insignificant factor.

However, they are vital to the overall systems, and it would be a great mistake to consider them as becoming less important. In fact, the opposite would appear to be the case. When the dual in-line package (DIP) was the most important IC package the other components tended to be in a support or service role. With VLSI, the system designer will have to pay greater attention (not less) to these other components if the advantages inherent in IC technology are to be fully exploited. Already, it is possible to see the growing interdependence between the IC die, its package, and the interconnection substrate.

These developments obviously create problems for the substrate manufacturer, but they can also offer significant opportunities for companies to exploit these demands and produce satisfactory new materials.

Developers, however, must assess their products from the viewpoint of the basically conservative equipment manufacturers. Many new products can be substituted for existing ones, and give an improvement, but often do not succeed because the gain is judged to be marginal. Changing materials for circuitry involves a lot of long term, expensive testing to verify the usefulness, long term reliability, and compliance to specifications.

As a rough rule, products only succeed if they give a four to five fold improvement. This may be a five times price reduction or property improvement, or half the price and a three times property improvement.

SUBSTRATE PROBLEMS RESULTING FROM IC DEVELOPMENTS

The main problems can be summarized as follows:

- Cost reduction pressures.
- Wider range of new IC packages.
- More integration on the chip.
- Need for surface mounting.
- Higher speeds of operation.
- More heat produced.

COST REDUCTION. One of the major trends in the
introduction of ICs has been the rapidly falling cost,
which has not been matched by any other components,
especially by the PCBs where the cost per interconnect
made on a PCB is about 1,000 times that of an
interconnection made on a VLSI chip. There are many
cost reduction developments going on with the standard
substrates, but these are now very mature products and
improvements are limited.

In BPA we are regularly analyzing worldwide prices
of PCBs, particularly those with fines lines (6 mil
and below). The prices are compared against
interconnection density, which covers line and space
dimensions, numbers of holes, number of layers with
allowance made for component areas, etc. At higher
circuit densities the price increases rapidly, and
virtually seems to be hitting a barrier. Much of this
extra cost comes from the rapid reduction in process
yields as the PCB manufacturer tries to get finer
lines. Whilst this is primarily a PCB problem,
assistance in improving PCB yields has to come from
the substrate manufacturer by better control of
consistency, dimensional stability, surface flatness,
copper bond characteristics etc. These developments
are not glamorous, but are significant to the circuit
manufacturer, the OEM and, therefore, ultimately to
the material supplier.

Most of the new materials now being evaluated to
improve the other properties of high speed and heat
all tend to be more expensive, and this is going to
further aggravate the cost situation. Systems
manufacturers therefore are considering whether they
can afford to go for more expensive PCBs, or whether
they should have some intermediate level of packaging
such as multichip modules, which can cope with the
higher density, speed and heat, and permit the usage
of a lower cost, simpler PCB.

A cost reduction area that could have significant
opportunities for chemicals companies is the interest
in cheaper track generation systems such as screen
printed conductive inks and the conductive pastes that
are being used to replace plated through holes (PTH).
Copper-based inks are already being used to form
crossovers and simple circuits, and the use of thick
film techniques of multiple layer printing is being
evaluated to replace some multilayer circuits.

WIDER RANGE OF NEW PACKAGES. Apart from the 3-4% of
chips worldwide that are used "naked", the remainder
are supplied in a package which transforms the silicon
chip into a manageable device and affords it
protection, both mechanical and chemical.

For many years the standard package was the Dual
In Line (DIP) and the plated through hole (PTH) glass

epoxy laminate has proved very successful as a carrier base for this package. However, with increasing complexity and performance of the chip, new packages are being developed which have different requirements for their substrates. At the end of the decade the idea of a standard IC package probably will no longer be valid, and equipment manufacturers will select one of several alternatives to best suit their needs, e.g., pin count, electrical performance, cost or a combination of these factors. Furthermore, advanced sectors like computers, military and telecommunications are evolving their own individual packaging and interconnect solutions accentuating the move away from a single standard package concept.

The BPA forecast of the distribution of these packages in the mid 1990s is given in Figure 2 based on the number of IC packages. This shows a large drop in the proportion of through hole mounted packages. However, it should be noted that the overall market numbers will have trebled over this period.

MORE INTEGRATION ON THE CHIP. This has been a major trend in electronics for a number of years, and is achieved mainly by reducing the dimensions of the devices, usually transistors, on the ICs.

Reducing a device's linear dimensions by a factor of 2 reduces chip area by a factor of 4, doubles operating speed, reduces power consumption by a quarter, and the cost/performance ratio improves by a factor of approximately 8 times. Currently the achievable number of functions in an IC doubles every one to two years. This is having a major effect on the pin counts of IC packages, and already we are seeing a number of packages with more than 100 pins.

The problem that this places on the substrate circuit is that finer conductors and features will be required. Primarily, this is a problem for the PCB and Hybrid manufacturer who has to refine and develop new methods of track generation.

As already stated, the assistance that substrate manufacturers can give for this problem is to improve the mechanical properties of flatness, warp, dimensional stability, and the supply of thinner copper layers with better adhesion to retain the bond of the narrower tracks.

Copper foils of thickness 5 microns are available, but are not popular because of the problems of handling. A newer process "Metclad" can give laminates with 2 microns of copper. In addition, a number of processes that vacuum-deposit a thin layer of metal are being developed. However, versions of these products have been available for some time, but the usage still remains low. Most of the pressure for fine line circuits can be met by PCB producers
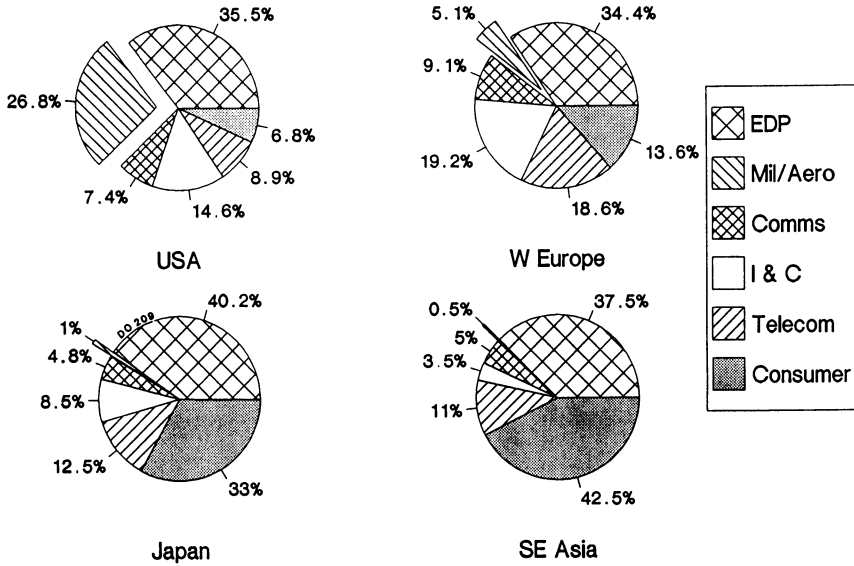
Figure 1. Worldwide Electronic Equipment Production Value by Business Sector and Region: 1987. (Courtesy of BPA Technology and Management Ltd.)

Type	Qty (Bn) 1997
DIPs	15.6
SPs/ZIPs	2.8
PGAs	1.5
Socketed SM	7.0
Flat Packs & Others	0.6
Hermetic CCs	0.9
Plastic SOs	32.0
PLCCs	6.6
PQFPs	16.0
TAB	7.9
COB	7.1
Flip Chip	7.0
Total	105
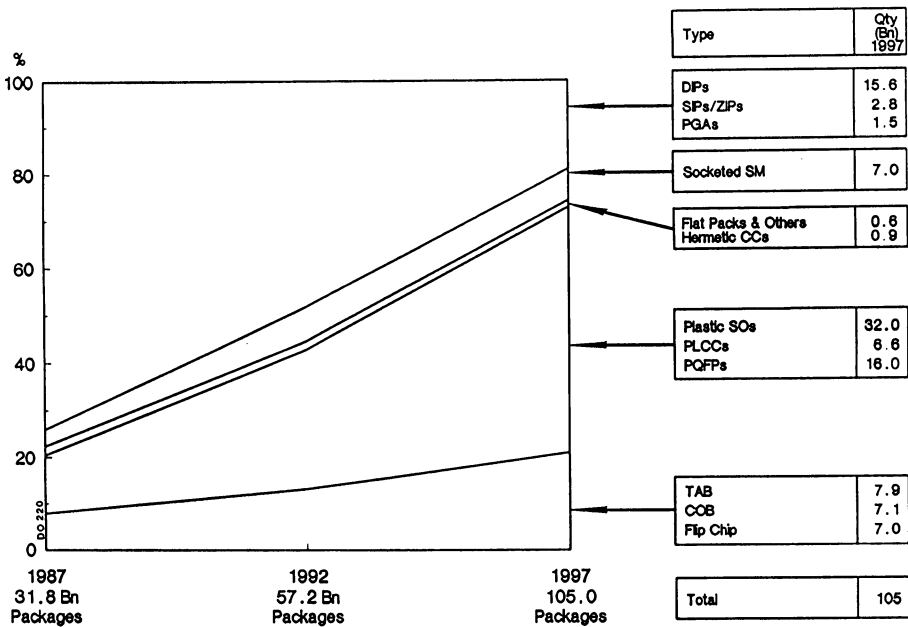
Figure 2. World IC Package Types 1987 - 1997. (Courtesy of BPA Technology and Management Ltd.)

improving their techniques or by using additive
processes. The very thin copper is really for the
very difficult situations.
   In the case of ceramics, developments in the low
sintering temperature, co-fired multilayer materials
will assist in increasing circuit density. A "green"
tape is produced using a mixture of ceramic with
a separate glassy phase to aid densification. Other
ceramics such as mullite and cordierite may be added
to modify other properties such as the dielectric
constant. The tape can be printed and fired using
conventional thick-film equipment, and can be
laminated together in a simple standard press. This
opens up the process to the whole Hybrid industry, and
with the advantages of multilayer circuits obtained at
a cost claimed as half that of conventional cofired
systems this development looks significant.

SURFACE MOUNT TECHNOLOGY (SMT)

SMT has been used in the hybrid industry since the
late 1950s. Nowadays, however, SMT implies the
assembly of surface mountable components onto organic
substrates such as glass epoxy and phenolic paper.
Surface mounting makes more efficient use of substrate
area through the use of smaller components and the
elimination of large PTH's, because only smaller via
holes will be required. As the IC complexity,
customization and pin count increase there will be no
alternative interconnection technology that can cope.

THE TWO APPROACHES TO SMT. There are two approaches
to SMT. The first of these is the "value engineering"
approach which is basically a move to SMT for cost
reduction/miniaturization reasons. The IC often is
very similar to that previously packaged in DIP form,
with the same number of pins, and the customization
still takes place on the PCB.
   By taking this value engineering approach to its
extreme with the total replacement of all through-hole
components by their surface mounting equivalents,
reductions in PCB sizes of between 60% and 70% can be
achieved. However, the performance improvements are
limited and, although a great many of the current SMT
implementations have taken this approach, many have
found SMT a less than satisfactory alternative to
insertion.
   In contrast, large performance/cost improvements
are available from using the second approach. This is
the "designing on silicon" approach whereby
customization occurs at the IC level, and the PCB is
used merely as an interconnection media. Although
this leads to more complex chips, higher pin counts,
and serious packaging problems concerning lead

pitch, heat dissipation, and hermeticity it also leads
to big improvements in cost and performance. SMT is
the only viable way to use these packages, and it is
only by using this approach that the true benefits of
SMT will be seen.

FUTURE TRENDS IN SMT. In the longer term, further
integration on silicon will be the key underlying
drive behind the continued growth of the electronics
industry. It is clear that the adoption of SMT is no
longer an option to be considered only when time
permits; it is an inevitable requirement for
competitive cost/performance design now facing all
moderate and large scale manufacturers.
     By the mid 1990s surface mounting will be an
extremely important method of production throughout
the world, and the rapid switch from the present
through hole mounting systems to surface mounting will
occur in the late 1980s and early 1990s.
     Without doubt, substrates will form an important
part of SMT introduction. In general, improvements
are required in mechanical properties such as
stiffness, dimensional stability, flatness and, above
all, consistent properties.

MISMATCH OF THERMAL EXPANSION. The thermal expansion
mismatch of organic substrates and leadless ceramic
chip carriers has been widely reported, and a great
deal of development work was carried out. However,
the actual number of these packages used worldwide is
small, and many of those overcome the problem by using
clips and sockets.
     It is much more of a problem in the USA, because
of the military influence, but there are now a range
of products designed to cope with this weakness, such
as laminates with polyimide/Kevlar or reinforced
substrates with copper/invar/copper foils, or
alternatively, use of compliant surfaces.
     This situation is now satisfactory for the OEMS,
but whilst a few companies will produce these special
grades it is very doubtful that all the development
time and money spent on this problem will be recouped.
However, this preoccupation with expansion did raise a
lot of interest in the Tg of materials and emphasise
its importance in dimensional stability.
     Generally, some improvement in Tg will be
required, partly because this will help retain the
mechanical properties over a wider temperature range,
and partly because the soldering of surface mounting
components often puts a large heat load on the entire
board and not just on one surface.

SUBSTRATES FOR HIGH SPEED OPERATION

At present the number of IC's that are operating fast
enough to create problems for the substrate is small,
but by the mid 1990's it is estimated that 9%-10% of
IC's will be in this category. Satisfactory operation
at high signal speeds depends to some extent on the
track geometry, but largely on the substrate material.
    Digital processors, which operate by means of a
stream of pulses, are now operating at high speeds
(10-100 MHz clock rates), and at these rates, signals
are propagated as an electrical wave system travelling
through the substrate, the air and the metal
conductor. The substrate now becomes a key factor.
    The dielectric constant of the substrate is the
prime property because the propagation speed of the
signal is inversely related to it. At these speeds
the system has to be designed as a transmission line
which must match the impedance of the devices used.
Impedance mismatch can lead to reflected signals, and
hence to signal distortion. The characteristic
impedance of the line is also dependent on the
dielectric constant, and for the devices now being
used higher impedances are required and, therefore,
low dielectric constant substrates. In addition, it
is also important to have low-loss materials to
prevent distortion of the pulses.
    When designing these high speed interconnection
circuits the dimensions of the copper track, the
separation between tracks and ground planes, and the
dielectric thickness all come into the calculations.
It is therefore vital that the material should be
consistent so that these dimensions remain stable and
uniform and the tolerances can be maintained.
    The dielectric properties of substrates depend
heavily on the chemistry of the constituent raw
materials. The presence of polar chemical groups
within the molecules increases the dielectric
constant. The relatively simple molecular structures
of polyethylene (CH2 - CH2) and polytetrafluorethylene
(CF2 - CF2) would be expected to have low dielectric
constants. Epoxy resins and polyimides have
relatively high dielectric constant values since they
have complex molecular structures.
    The propagation velocities, which are inversely
related to the square root of the dielectric constant,
are shown in Figure 3.
    This Figure shows that the fluorinated polymers
are the best, with inorganic ceramic products having a
low propagation velocity. An interesting product based
on PTFE is "Goretex" from W.L. Gore, a fibre
containing air which reduces the dielectric constant.
The fibres are woven into a fabric which is then
incorporated into the laminate, giving enhanced high

speed characteristics. Other thermoplastic polymers
are good, partly because they are pure and not
reinforced. In the case of flexible films, however,
speed will be decreased because of the adhesive that
has to be used to bond on the copper foil. The new
polycyanurate resins look promising, with much better
speed characteristics than other rigid laminates.
     These are a new range of laminating resins
produced from cyanate ester resins which are
thermosetting monomers which can co-react with epoxy
resins. The cured polymer has a low dielectric
constant (2.8) and high Tg (250°C). When reinforced
with quartz or glass fibres the dielectric properties
fall but are still much better than current standard
laminates. Although the Tg is near that of polyimides,
processing and the properties of toughness, adhesion,
etc. are greatly improved.
     The high speed characteristics of ceramics are
being improved by coating their surfaces with polymers
such as polyimides and newer materials specifically
developed for this purpose such as Dow's bis
(benzocyclobutene) which has a dielectric constant of
2.7 and a low moisture uptake.
     To increase the impedance for device matching,
narrow tracks are desirable, and of course this also
helps with the density of leads from higher functional
devices. However, as tracks get closer the problems
of cross talk get worse, and more ground screening is
required.
     Uniform cross section can also be obtained using
additive or semi-additive techniques, and this method
is becoming very popular for high performance
circuits.   Accurate tracks with widths of 1 to 2 mil
(25 to 50 microns) can be obtained using this
technique.
     Wire also has accurate geometry, having been drawn
through a die, and for high performance systems coated
wire is increasingly being used. The wire is laid on
the surface using computer controlled heads. An
example of this technique is "Microwire" from PCK
which gives very dense circuits with controlled
impedance mounted onto heat sinks to remove the heat.
The original "Multiwire" system has now been adapted
to use a thin coaxial cable with a Goretex dielectric,
giving a very high propagation velocity.

HEAT REMOVAL

The result of higher integration on a chip with faster
processing, leads to the generation of more heat. At
present, it is estimated that 3-4% of all IC's are
running hot enough to create problems for the
substrate. By 1995 this figure is expected to have

risen to 6-7% of all IC's, mainly because of the increasing circuit density. There is a strong move from the Bipolar ECL (Emitter-coupled logic) systems to CMOS, which generates less heat, but this is merely permitting more functions to be included, and the heat problem keeps increasing. As a result, substrates come under pressure because they have to be able not only to withstand the higher temperatures but also to conduct heat away from the chip to prevent the circuitry from reaching temperatures where they cease to function.

In this respect, organic polymers are very poor, as seen in Table I. It can be seen that even the worst ceramic is about 100 times better than most polymers.

The only useful materials for heat removal are metal or ceramics. The ceramics obviously can be used as a substrate material in their own right, and beryllia is the standard for this kind of application. Now, other materials such as Aluminium Nitride and Silicon Carbide are being developed to replace beryllia because of its reputation as a poisonous product.

Table I   Thermal Conductivity of Substrates
Dielectrics and Conductors

Material	Thermal Conductivity (W.m/m2.°C)
Copper	390
Beryllia (95%)	200
Aluminium	200
Aluminium Nitride	180
Alumina (96%)	20
Polyimide Glass	0.35
Epoxy-Glass (FF14)	0.23

Aluminium Nitride is looking very promising, and there are many companies worldwide developing these substrates. This promises well for the OEMs, but as the market for this product is relatively small it is inevitable that many of these potential suppliers will not have commercial success.

Ceramics are also being used in conjunction with resins. Ceramic papers have been developed in Japan, and ceramic fibre reinforced polymers in the USA. Resin impregnated porous ceramic is another Japanese development aimed at high heat resistance and better dielectric properties.

Although metals are good heat conductors, they obviously must have some electrically insulating layer added to make them into a useful circuit substrate. However, as seen from Table I, good electrical insulators are also good thermal insulators. Even a thin layer of insulation greatly reduces the conductivity of the composite structure.

Even with only a few mils of an FR4 or epoxy resin coating, the conductivity of a 62 mil (1.5 mm) thick sheet of copper drops to 5-8 from the 390 for the metal itself. The conductivity of steel (55) is reduced to a value of 12-18 when coated with porcelain.

It is clear, therefore, that if significant amounts of heat have to be removed from a polymer based circuit then the best way is to cut access holes through the polymer to get the package into direct contact with the metal heat sink.

In the future, the very hot IC's will be packaged in a thermally efficient module or in a multichip module, which will then be mounted on a more conventional substrate.

COMBINATION OF PROBLEMS

From the previous sections it is clear that solutions exist for the separate problems arising from IC and Packaging developments.

Fine line circuitry can be obtained from current materials, and particularly with thin copper foils. Additive systems can take this further. In addition, multichip modules may be used for the most severe situations.

Surface mounting of plastic packages is quite feasible with current standard materials, and improvements in mechanical properties will enhance this. Where leadless ceramic chip carriers have to be used there are now satisfactory products available. The real problems with surface mounting are to cope with the placement accuracies and inspection, and as such do not involve the substrate.

Higher operating speeds will require new materials for the substrates, but there are products available to cope with present requirements.

Heat does create problems for substrates, and either ceramics have to be used, or else a metal core with direct access to the hot package or to the chip must be employed, to bypass the extremely high thermal insulation effects of polymers. Therefore where problems occur on their own they can be overcome. However, usually a number of problems occur together and interact with each other.

The two major problems are speed of signal propagation and thermal conductivity. The

relationship between these properties for a number of the substrate solutions is shown in Figure 4.

This Figure shows that whilst ceramics are useful for heat transfer, they have poor speed propagation. This result may seem odd, since silicon is the base for present IC's, but in practice the poor propagation speed is counterbalanced by the very short distances that the signal has to travel on the chip. Polymers have much better speed characteristics, and this is why there is development going on to combine ceramics with polymers such as polyimide.

The poor heat transfer characteristics of polymers has been seen in Figure 4. Combining polymers with metals gives only marginal improvements. Only direct-access through-holes in the insulator can produce improved assemblies. Even then, the conductivity is less than that of the base metal because some attachment material will be used.

The merit of using PTFE for high speed signals is clear. When PTFE has air introduced, as in the Goretex fabric, then the speed properties are greatly enhanced; but, unfortunately, the fabric generally has to have a resin binder, and the position of Goreply shows how severely the epoxy resin degrades the speed.

The development product with Goretex coaxial cable laid down with the Multiwire process shows great promise, as a dielectric constant of 1.3 can be obtained giving a propagation speed of 26 cm/nanosecond, which is 88% of the speed of light.

Other resins may be used, such as the polycyanurates, and developments are in hand combining this with Goretex. The propagation speed of this combination would be near to that of PTFE, and could be a little higher.

Obviously, the most significant factor of all is the potential size of the market for these special substrates. In our definition, these specials include the high speed types and also the high Tg laminates such as Polyimide, BT (Bis maleimide triazine) and the high Tg epoxies. At present, these products account for 4% of the total worldwide value of substrates, but this number is forecast to rise to about 12% by the mid 1990s. These are high-value products, and in area terms this sector will still account for only about 4% of worldwide substrates by the mid 90s.

It is becoming clear that to meet the OEM's requirements which now nearly always have a combination of problems, these problems will be resolved by building up the substrate as the circuit is produced. Different layers will be added to cope with high speed signals, or to stiffen the board or to modify the thermal expansion. Heat removal will be done through heat pillars or openings in the dielectric. In Japan, fibre optical cables are being

Substrate
Materials
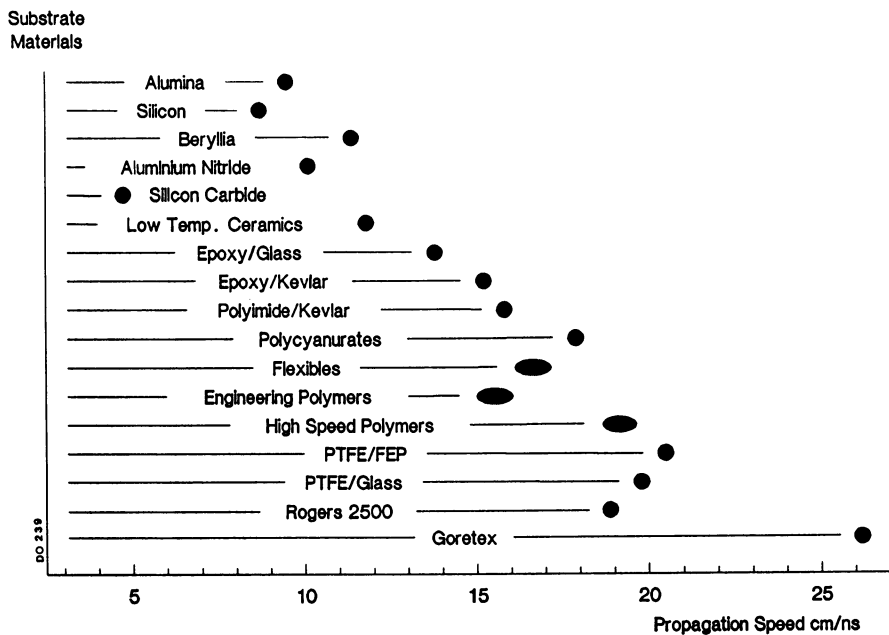
Figure 3. Propagation Speed of Substrate Materials.
(Courtesy of BPA Technology and Management Ltd.)

Thermal Conductivity
$W.m/m^2.°C$
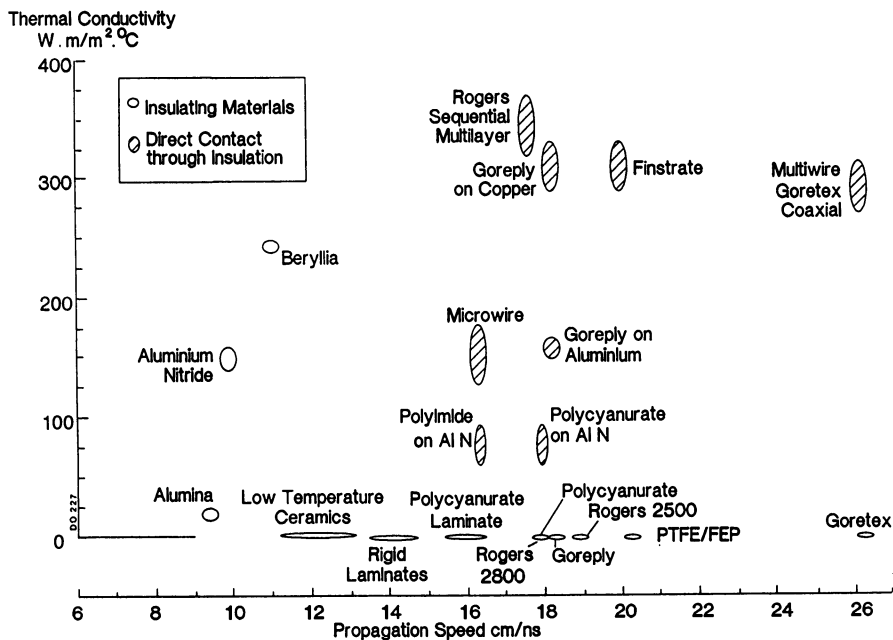
Figure 4. New Development Materials. Heat/Speed
Comparison. (Courtesy of BPA Technology and Management Ltd.)

embedded in the substrates, and it is quite possible that Automated Discrete Wiring (ADW) connections can be made on the surface to enable high speed operation and to permit quick circuit modifications.

Because of speed requirements, the substrate will have to be assembled with tight thickness and physical tolerances. This type of substrate circuit now effectively becomes a component, and the board structure has to be built up as the circuit is produced. The substrate production therefore will take place at the PWB manufacturer, and this is where the added value will occur. Although some new materials will be included, at present their use seems to be restricted to specialised niche areas. In general, however, standard materials can be used, a fact of life which is not advantageous to substrate suppliers.

CONCLUSION

The assembly of the new composite substrate circuits is a market sector that scarcely exists at present. Because it relies on a knowledge of materials, bonding techniques, etc., some materials manufacturers are considering that the most significant move for them could be to move into this sector and actually build the circuits themselves.

RECEIVED April 21, 1989

Author Index

Affiliation Index

Subject Index

A

B

Affiliation Index

Subject Index

A

B

Conduction transients in polyimides—
  Continued
  voltage dependence of transient
    current, 178,179*f*,183,186*f*
Corrosion of integrated-circuit devices by
    decomposition gases of encapsulant resin
  analysis of outgas from specimen with
    GC–MS, 422,424*f*
  brominated epoxy resin
    structure, 422,426*f*
  chip surface after high-temperature
    exposure test, 422,423*f*
  components of outgas from molding
    compound, 422,424*t*
  degradation of brominated resin, 422,426*f*
  effects of ion-trapping agent, 422,425*t*
  effects of ion-trapping agent on wire-bond
    degradation, 422,425*t*
  effects of molding-compound
    ingredients, 422,425*t*
  experimental setup, 422,423*f*
  intermetallic alloy formation
    reaction, 427*f*
  intermetallic layer ratio in bonding pad
    area, 422,426*f*
  ion-trapping reaction, 427,428*f*
  melting point and boiling point of metal
    bromide, 427,428*t*
  reaction acceleration mechanism of
    amine, 422,426*f*
  silicone oxidation mechanism, 422,427*f*
  test chip specimen, 422,423*f*
Cresol epoxy novolac, use as microelectronic
    encapsulants, 405
Cure of polyimides by fluorescence
    spectroscopy
  analysis of supported films, 30*t*,31*f*,32,33*f*
  analysis of unsupported films, 32*t*,35*f*
  Arrhenius plots of emission intensity of
    supported films, 32,33*f*
  assignment of spectral features, 39–45
  effect of stress on electronic
    transitions, 46–47
  emission spectra
    model compounds, 34,38*f*,39*t*
    supported films, 30*t*,31*f*,32
  excitation spectra
    model compounds vs. concentration,
      34–40
    supported films, 30*t*,31*f*,32
    unsupported films, 32*t*,35*f*
  fluorescence analysis, 29–30
  molecular ordering, 44,46
  normalized intensity vs. normalized
    reciprocal distance, 44,45*f*
  sample preparation, 27–28
  structural effects, 34*t*,35*f*

Curing of binary mixture of polyimides
  curing behavior
    BTDA–ODA–MPDA film, 116,118*f*,119
    fast-mixed blend, 119,120*f*,121
    mixture equilibrated for 141 h, 121,122*f*
    PMDA–ODA films, 116,117*f*
    slow-cured, fast-mixed blend,
      121,122*f*,123
    slow-cured, long-equilibrated blend,
      123,124*f*
  preparation of materials, 116
  thermogravimetric analysis, 119,120*f*

D

Decomposition gases of encapsulant resin,
    corrosion of integrated-circuit
    devices, 421–428
Degree of cure, determination, 26–27
Diamic acid effect on polyimide dielectric
    constant
  characterization procedure, 88
  diamic acid additive, preparation, 87,88*f*
  improvement in polyimide
    processability, 86–87
  polyamic acid resin preparation, 87
  polyimide film preparation, 88
  preparation of experimental materials, 87
  properties of films containing amic acid
    additives, 89,90*t*
  properties of films containing diamic acid
    additives, 88,89*t*,90,91*t*
  structures of experimental materials, 87*f*
  variability of dielectric constant
    data, 89,90*f*
Dielectric characterization of water in
    polyimide and poly(amide–imide) thin
    films
  calculation of effective
    polarizability, 72,74*f*,75
  calculation of number of water dipoles per
    unit volume, 72
  calculation of polarizability, 71–72
  dielectric measurements, 69,71,73*f*
  dipole moment of absorbed water vs.
    polymer dielectric constant, 72,74*f*
  molecular weight gain, 69,71,73*f*
  polarization of amide group, 74*f*,75
  preparation of experimental films, 69
  properties of polymer film, 69,70*t*
  structures of experimental films, 68–69
  water dipole moment vs.
    concentration, 72,73*f*
Dielectric constant of polyimides, effect of
    diamic acid additives, 86–91